

The Handbook of Electrical Resistivity

New materials and pressure effects

Edited by
G. Dyos

The Handbook of Electrical Resistivity

Other volumes in this series:

- Volume 8 **Physics and technology of heterojunction devices** D.V. Morgan and R.H. Williams (Editors)
- Volume 9 **Electrical degradation and breakdown in polymers** L.A. Dissado and J.C. Fothergill
- Volume 12 **Handbook of microlithography, micromachining and microfabrication, 2 volumes** P. Rai-Choudhury (Editor)

The Handbook of Electrical Resistivity

New materials and pressure effects

**Edited by
G. Dyos**

The Institution of Engineering and Technology

Published by The Institution of Engineering and Technology, London, United Kingdom

The Institution of Engineering and Technology is registered as a Charity in England & Wales (no. 211014) and Scotland (no. SC038698).

© 2012 The Institution of Engineering and Technology

First published 2012

This publication is copyright under the Berne Convention and the Universal Copyright Convention. All rights reserved. Apart from any fair dealing for the purposes of research or private study, or criticism or review, as permitted under the Copyright, Designs and Patents Act 1988, this publication may be reproduced, stored or transmitted, in any form or by any means, only with the prior permission in writing of the publishers, or in the case of reprographic reproduction in accordance with the terms of licences issued by the Copyright Licensing Agency. Enquiries concerning reproduction outside those terms should be sent to the publisher at the undermentioned address:

The Institution of Engineering and Technology
Michael Faraday House
Six Hills Way, Stevenage
Herts, SG1 2AY, United Kingdom

www.theiet.org

While the authors and publisher believe that the information and guidance given in this work are correct, all parties must rely upon their own skill and judgement when making use of them. Neither the authors nor publisher assumes any liability to anyone for any loss or damage caused by any error or omission in the work, whether such an error or omission is the result of negligence or any other cause. Any and all such liability is disclaimed.

The moral rights of the authors to be identified as authors of this work have been asserted by them in accordance with the Copyright, Designs and Patents Act 1988.

British Library Cataloguing in Publication Data

A catalogue record for this product is available from the British Library

ISBN 978-1-84919-149-4 (hardback)

ISBN 978-1-84919-117-3 (PDF)

Typeset in India by MPS Limited

Printed in the UK by CPI Group (UK) Ltd, Croydon, CR0 4YY

Contents

Preface	vii
1 Introduction	1
1.1 Continuation of the <i>Electrical Resistivity Handbook</i>	1
1.2 Explanation of the graphical format	1
1.3 Material classification	1
1.4 Electronic conduction in solids	2
1.5 Pure metals	5
1.6 Metallic alloys	6
1.6.1 Dilute alloys	6
1.6.2 Concentrated alloys	7
1.7 Semiconductors	9
1.8 Summary	9
1.9 Abbreviations	10
2 Measurement techniques	11
2.1 Introduction	11
2.2 Four probe methods	13
2.3 Temperature variation of resistivity	14
2.4 Eddy current methods	15
2.5 Step function methods	16
2.6 Periodically varying fields	17
2.7 Inductive techniques	20
2.7.1 Self-inductance	20
2.7.2 Mutual inductance	20
2.7.3 Inductive techniques and temperature variations	22
3 Explanation of graphs	25
3.1 Data analysis	25
3.2 Catalogue system for materials	25
3.3 Material composition	25
4 Text references	27
5 Index of materials	29

6	Material resistivity graphs	39
6.1	Electrical resistivity as a function of temperature	39
6.2	Electrical resistivity as a function of temperature and pressure	380
6.3	Resistance measurements as a function of temperature and pressure	427
7	Resistivity references	461

Preface

Since the publication of the *Electrical Resistivity Handbook* by the IET, edited by G.T. Dyos and T. Farrell in 1992, interest in high-temperature superconductivity has grown. I was approached and commissioned by the Institution of Engineering and Technology to produce a further volume covering the electrical resistivity of new materials produced in the last two decades and the effects of pressure on resistivity.

I would be pleased to receive any copies of original referenced papers describing the resistivity of materials which might be of interest for inclusion in a further volume at a later date.

I would like to thank my wife Muriel who has supported me during this project, often only seeing me when I emerged from the study at mealtimes. Also I would like to thank Professor J. Lawton for his support and helpful discussions and IET staff for sorting out problems in the INSPEC searches.

Gordon T. Dyos
GT Innovations
Ysgubor Newydd
Llandrillo, Corwen, UK LL21 0SY

Chapter 1

Introduction

G. Dyos and T. Farrell

1.1 Continuation of the *Electrical Resistivity Handbook*

This volume incorporates two sections dealing with the resistivity of elements, compounds and alloys as a function of temperature and pressure and a third section dealing mainly with the resistance of various materials.

The compilation of this volume was made easier by the search facilities of the IET's INSPEC database containing some 13 million papers. From which the leading authors of approximately 3000 papers were contacted by email and postal services. It was very disappointing that only 35% bothered to reply and some 30 authors wanted a free copy of the book! It was very much appreciated by the editor for the plaudits received from university professors for undertaking this work.

1.2 Explanation of the graphical format

The vast majority of the data presented here has been gathered from technical papers published in the last two decades. Some graphical data, which were included in the *Electrical Resistivity Handbook*, have been included in this volume, where they cover a larger temperature range.

The data has been obtained from copies of the pertinent paper, either in graphical or in tabular format. In the case of the graphical format, the graphs have been scanned into the computer and the axes calibrated and the data coordinates used to produce a graph based on a standard graphical format. The resistivity data is expressed in units of ohm metre ($\text{ohm m}) \times 10^{-8}$, temperature in kelvin (K), pressure in gigapascals (GPa) and resistance in ohms.

1.3 Material classification

The catalogue system used in this volume is the same as that used in the *Electrical Resistivity Handbook*. First, the materials are listed in alphabetical order. Where

2 The handbook of electrical resistivity: new materials and pressure effects

a compound has several elements they are listed in order of decreasing atomic percentage. Should a compound have elements all having equal atomic percentage, then they are listed in alphabetical order.

Data which has been presented in the original paper in graphical form and then extracted by scanning and replotting is indicated by an asterisk (*) against the reference number for that graph. It should be noted that only data obtained from bulk and crystalline materials has been evaluated. No data from thin films has been used.

It should be noted that the majority of authors of papers do not indicate whether an allowance for thermal expansion has been applied to the resistivity of the compound.

All the compounds in this handbook are expressed in terms of atomic percentages, that is, the number of atoms of an element present in the compound expressed as a percentage of the total number of atoms present in one molecule of the compound. Where compounds have been listed in the original reference as weight percentages, these have been converted into atomic percentages.

1.4 Electronic conduction in solids

To aid the understanding of the electrical resistivity data on the materials presented in this handbook and to assist with its estimation for materials whose exact composition is not listed, some fundamental concepts of electronic conduction in solids are required. These concepts are presented at the descriptive level; the reader who requires a more detailed quantitative approach should consult the standard text books [1–5] or the cited references.

Electronic conduction is concerned with the motion of electrons within the solid under the influence of an applied electric field. Of necessity, therefore, the electrons must be free to move; experience shows that metals are good conductors of electricity and thus some of the electrons in the metal can be regarded as ‘free’. The earliest approach to quantifying the electrical conduction in metals, recognising that electrons were responsible for the transport of charge, was that of Drude [6], who treated the metal as an electron gas. When an electric field, E , is applied to the metal, the electrons of charge $-e$ are accelerated by the electrostatic force eE . After they have travelled for a certain average time, τ , the electrons suffer a collision with the atoms of the solid and are effectively arrested, transferring their kinetic energy to the solid. From simple mechanics, the mean drift velocity of the electrons, v_D , is given by

$$v_D = \frac{Ee\tau}{m}$$

where m is the mass of the electron. If the volume density of the electrons is n , then the electrical current per unit area, J , is given by

$$J = nev_D = \frac{ne^2\tau E}{m} \quad (1.1)$$

This is a statement of Ohm's law, where the electrical conductivity ρ is defined as $J = \sigma E$.

The electrical resistivity $\rho = 1/\sigma$ is therefore

$$\rho = \frac{m}{ne^2\tau} \quad (1.2)$$

To obtain an estimate of ρ from (1.2), the values of n and τ are required. Taking the 'relaxation time' τ to be given by λ/v_0 , where λ is the electron mean free path and v_0 the thermal velocity of the electrons, then from the equipartition law $mv_0^2/2 = 3k_B T/2$ and

$$\rho = \frac{(3k_B m T)^{1/2}}{n \lambda e^2} \quad (1.3)$$

If it is assumed that each atom contributes one electron to the conduction process, n is the number density of atoms in the solid, and if λ is taken to be the interatomic spacing, then (1.3) gives values of ρ in the 10^{-6} to 10^{-7} ohm m range, which covers the room temperature experimentally observed resistivities for most metals.

Although this simple classical Drude theory gives Ohm's law and taking the power dissipation to be approximately mv_D^2/τ is consistent with Joule heating (it can also be used to derive the relationship between the electrical and thermal conductivities of metals – the Wiedemann–Franz law), it cannot readily explain the differences in the electrical resistivity upon alloying, nor does it predict the correct variation of resistivity with temperature. The Drude theory is restricted to metals; it cannot explain the electrical resistivity of semiconductors. However, the important point to emerge from this approach is the concept of collisions or scattering of electrons and the significance of τ , the 'relaxation time'.

The quantum mechanics approach pioneered by Sommerfeld [7] assumes the free electrons of the metal to be moving in a constant internal potential and that the electrons in this potential well obey the laws of quantum mechanics rather than the laws of classical mechanics. Essentially, this well consists of a quasi-continuum of energy levels and when the valence electrons are 'poured' into the well they progressively fill these levels up to a certain energy, E_F , known as the Fermi level. This value of E_F varies from metal to metal but is typically a few electron volts ($1 \text{ eV} = 1.6 \times 10^{-19} \text{ J}$). In this quantum Fermi gas model, the number of electrons which take part in the conduction is restricted to those lying within the energy range $k_B T$ of the Fermi level, where k_B is Boltzmann's constant. Thus, at room temperature, for a monovalent metal with $E_F \approx 5 \text{ eV}$, the number of electrons is only 5×10^{-3} times the total number of valence electrons. The average drift velocity of the classical mechanics is replaced by the Fermi velocity, $v_F \approx (2E_F/m)^{1/2}$, which for $E_F \approx 5 \text{ eV}$ is about $1.3 \times 10^6 \text{ m/s}$. If these mean values are substituted into (1.3), and the mean free path, λ , is again taken to be the interatomic spacing, then the Sommerfeld model predicts a resistivity which is several orders of magnitude larger than the experimental values. However, the Fermi gas model derives the Wiedemann–Franz law with remarkable agreement with experiment and successfully accounts for electronic specific heat. Thus, the difficulty it encounters in describing conductivity must lie in the

definition of the mean free path. In order to reconcile the prediction of the Fermi gas model with experiment, the electron mean free path must be larger than interatomic spacings.

The Fermi gas model, in its simplicity, treated the electrons as being in a constant potential well. Solids are comprised of crystals, the sizes of which are large compared with atomic dimensions (with the exception of amorphous metals). Each ion within the crystal lattice has its own potential well, and as the ions are arranged periodically, there is a periodic arrangement of potential wells.

If one atomic potential well is considered in isolation, then there are discrete electron energy levels such as those that are encountered in the hydrogen atom. If two such wells are brought into close proximity, then from the Pauli exclusion principle which forbids any two electrons from occupying the same energy level (neglecting electron spin), the isolated discrete energy levels split into two levels. When a large number, N , of such wells are brought into close proximity, which is the case in a crystal lattice, then the original discrete energy level is broadened into a quasi-continuous energy band (actually comprising N energy levels). The gaps between the original isolated discrete energy levels may be preserved, but are smaller; in some cases the gaps no longer exist and the energy bands overlap. This ‘Band Theory of Solids’ provides the framework for understanding the classification of solids into metals, semiconductors and insulators.

If the electron is considered to be a wave travelling perpendicular to a set of lattice planes, then Bragg reflection will occur at certain wavelengths. For these wavelengths, λ_F , the wave is not propagated through the crystal and therefore they are forbidden to the conduction electrons of the crystal. The wave vectors, k , corresponding to the wavelengths ($k = 2\pi/\lambda_F$) occur at the boundaries of the Brillouin zone (the unit cell of the reciprocal lattice) and constitute energy gaps.

The Brillouin zone model relates the electron energy levels to the crystal structure. In regions close to the zone boundaries the variation of electron energy with its wave vector deviates from that where the periodic potential can be treated as constant, as a direct result of energy gaps. One consequence is that the mass of the electron is no longer that of the free electron; if the Fermi level occurs in such a region, the mass of the electron should be replaced by an effective mass, m^* , and this can be quite different from m .

The quantum mechanical approach provides the basis for the understanding of solids in terms of their conduction behaviour. The band theory and Brillouin zone model are primarily concerned with electronic structure, whereas electron conduction is concerned with the motion of the electrons under the influence of an externally applied electric field within that structure. The solution to the vexing problem of the mean free path being considerably larger than atomic dimensions was provided by Bloch [8], who considered, via a Fourier analysis, the propagation of electron waves in the lattice structure. If the structure is perfectly periodic, no scattering occurs, whereas deviations from periodicity give rise to scattering and hence to electrical resistance.

If the potential wells at the lattice sites are identical and the lattice sites themselves are regularly spaced, then the electron wave propagates almost undisturbed; in other words, very little scattering occurs, which is equivalent to a mean free path

which is much longer than interatomic distances. In fact, in a perfectly periodic structure, the electron wave is not disturbed at all and in such a structure the resistivity would be zero (this is not to be confused with superconductivity, where the resistivity is zero in non-periodic structures). A perfectly periodic structure is never realised in practice although it is approached in very pure single crystal solids at temperatures close to absolute zero.

Thus, in normal solid electronic conductors, the electrical resistivity arises from departures from periodicity in the lattice potential wells and there are many ways in which this can occur. These include

- (i) displacement of the atoms due to their thermal motion;
- (ii) imperfections in the crystal lattice, such as dislocations, vacancies and grain boundaries in polycrystalline solids;
- (iii) the substitution of foreign atoms at the lattice sites.

The departures from periodicity arising from (i) and (ii) are characteristic of pure metals whilst all three sources contribute to the resistivity of metallic alloys.

1.5 Pure metals

In a well-annealed pure metal at low temperature, the density of the imperfections is low and their contribution to the electrical resistivity is small. Dislocations, which arise for example by cold working, give rise to a temperature-independent resistivity which is usually negligible in comparison with the resistivity at high temperatures where phonon scattering dominates (see below) but may contribute significantly to the resistivity at cryogenic temperatures. For this reason, when studying pure metals it is preferable to use well-annealed specimens. On the other hand, vacancies are thermally activated; their number density increases with temperature. At room and cryogenic temperatures, the vacancy contribution to the resistivity is negligibly small and only starts to become significant at temperatures approaching the melting point. However, this is somewhat academic in the sense that the vacancy contribution to the resistivity is inherent to the metal and temperature.

At finite temperatures, the atoms vibrate about their mean positions. Effectively, the interatomic spacing is no longer constant; as the temperature increases, so does the amplitude of the vibrations, giving rise to greater changes in the interatomic spacing and hence larger departures from periodicity. The result is a temperature variation of the mean free path and hence of the electrical resistivity.

The vibration of the atoms can be regarded as waves propagating through the crystal lattice. By treating the lattice vibrations as being quantised (the quantum of energy is known as a phonon), it can be shown that there is a cut-off phonon frequency; phonons of frequency larger than the cut-off frequency are not allowed. The temperature corresponding to this frequency is known as the Debye temperature (usually denoted by θ_D).

Now the scattering of the electrons is essentially the interaction of the electron waves (which are defined by the periodicity of the lattice) and the displacements of

the lattice sites which can be described by lattice waves. The characteristic electron energy E_F (the Fermi energy) is equivalent to many thousands of degrees kelvin, whilst the Debye temperature is typically a few hundred degrees kelvin. Thus, the effect of temperature on the electronic structure of a solid is small compared with its effect on the lattice and, consequently, for scattering purposes, the effect of temperature on the lattice only need be considered.

At temperatures above θ_D , all lattice modes are excited and contribute to the scattering of the electrons. The phonon occupancy of the excited lattice modes increases linearly with temperature and consequently, as the mean free path is inversely proportional to the number of scattering centres, the resistivity increases linearly with temperature. At temperatures much lower than θ_D not all lattice modes are excited; only those with frequency v less than $k_B T/h$ (where h is Planck's constant) will be excited, and at very low temperatures the number of excited modes falls off as $(T/\theta_D)^3$. Thus, for temperatures lower than θ_D , the resistivity varies more rapidly than linear, and it was shown by Bloch [9] that at these very low temperatures the resistivity varies as the fifth power of temperature. Gruneisen [10] later developed the Bloch analysis to give an expression for the resistivity which covered the entire temperature range.

Some pure metals can exist with different crystal structures known as allotropes. Each allotrope has its own Brillouin zone and thus its own characteristic resistivity, which may exhibit a different temperature dependence. Such phase changes are more often encountered in metallic alloys and these are discussed later.

Whilst electron scattering by phonons is the dominant process in determining the temperature variation of the resistivity of most metals, other temperature-dependent scattering processes, such as electron-electron scattering, which gives a T^2 dependence for the resistivity at low temperatures, occur, and these are often seen in the magnetic and transition metals. Magnetic phase transformations occur in the ferromagnetic metals at the Curie temperature, T_c . These transitions are associated with a continuous decay in long-range magnetic order, which vanishes at T_c . As the temperature is increased and T_c is approached, the resistivity rises at an increased rate reflecting the increase in disorder. At T_c , where magnetic disorder is complete, there is a change in slope of the resistivity/temperature curve.

The abrupt increase in the electrical resistivity of many metals at the melting point in passing from the solid to the liquid state, and its steady increase with temperature in the liquid state, is associated with the absence of long-range crystal structure and the increase in disorder in the liquid state.

1.6 Metallic alloys

1.6.1 Dilute alloys

When a 'foreign' atom is substituted for an atom of the host metal, the potential well at the substitution site is changed. The contributions to the change in the potential well due to the substitution arise from the change in valency and change in atomic

volume. The valence electrons from the foreign atom merge with the conduction electron number of the host with the result that the potential well at the substitution site has a different charge from that which exists at the host sites; in the mathematical treatment, the potential well has a different depth. The change in atomic volume causes the spatial dimensions of the impurity potential well to differ from that of the host.

When foreign atoms are randomly substituted into the host lattice and the crystal structure of the host is preserved, then provided that the foreign atoms do not interact with each other, the electrical resistivity increases in proportion to the number of foreign atoms added. Such a situation is realised in practice in dilute alloys where the alloy addition is typically less than 5%. Moreover, with such dilute alloys, the foreign atoms vibrate as though they were host atoms and consequently the additional contribution to the resistivity is temperature independent. This was first recognised experimentally in the 1860s by Matthiessen and Vogt and a simple rule, known as Matthiessen's rule, which applies to many dilute alloys, can be stated:

$$\rho_a(T) = \rho_p(T) + \rho(c) \quad (1.5)$$

where $\rho_a(T)$ and $\rho_p(T)$ are the temperature variations of the resistivities of the dilute alloy and the host and $\rho(c)$ is the concentration dependent resistivity of the foreign atoms, which is almost linear in concentration. There are deviations from this rule even for very dilute alloys, but with the exception of transition metal alloys involving the magnetic metals, the deviations are very small and for practical purposes can often be regarded as negligible.

1.6.2 Concentrated alloys

When the number of substitutional foreign atoms becomes large, for example when their concentration is greater than 5%, the assumption that they do not interact with each other is no longer valid and Matthiessen's rule breaks down. The distinction between host and foreign atom becomes obscure (with a 50 atomic percent binary alloy there is no distinction) and thus the $\rho_p(T)$ term of (1.4) loses its original significance. That is not to say the resistivity is temperature independent but rather the temperature dependence is not necessarily that of the major constituent of a concentrated alloy. As the concentration of foreign atoms increases, then so does $\rho(c)$ of (1.4) although it is no longer linear with concentration, and the result is that the contribution from the foreign atoms dominates.

To complicate matters further, according to the equilibrium phase diagram the alloy may exist as a single or multiphase, ordered or disordered solid solution depending on concentration and temperature. The data is presented in this handbook in terms of resistivity against temperature. Whilst this is the preferred means of presentation, it is sometimes easier to discuss the resistivity at a given temperature as a function of concentration.

The simplest situation in concentrated alloys is that of a binary system which exhibits complete solid solubility series at a given temperature. For such a disordered alloy, Nordheim [11] showed that the resistivity was of the form $\rho \propto c(l - c)$, which

can be written more generally as $\rho = A + c(1 - Bc)$, where A and B are constants which depend on the alloy series and c is the concentration of one of the components of the alloy. The Nordheim rule specifically relates to the impurity resistivity of concentrated alloys. With such alloys, impurity resistivity normally dominates and the rule can be applied to the total resistivity, especially for room temperature and below.

The above account relates to substitutional impurities which are randomly distributed in the host lattice. There are some alloy systems where for certain compositions the impurity atoms are located at distinct lattice positions, creating a long-range ‘ordered’ state with a degree of periodicity which is absent in the random state. At these compositions, where such a ‘superlattice’ exists, the resistivity of the ordered state is somewhat less than that of the random state. Generally, the random state is preferred at high temperatures and the long-range ordered state only occurs below a critical temperature. Thus, care should be exercised when using Nordheim’s rule to estimate the resistivity of an alloy.

Phase-equilibrium diagrams of alloy systems indicate that the crystal structure of the alloy often changes with temperature. As mentioned above, these allotropes have different electronic structures which give rise to differences in the electrical resistivity, and this is manifest as a discontinuity in the resistivity/temperature plot, the discontinuity occurring at the boundary of the phase field. In a particular phase field, Nordheim’s rule can in principle be applied, but the constants A and B will differ from phase to phase.

Alloy systems do not necessarily exist in a single phase. Indeed the mechanical properties of many engineering alloys depend on the coexistence of two or more phases. Each phase has its own characteristic resistivity which may exhibit a different temperature variation. For the binary two-phase systems, the resistivity may be regarded as lying between two limits corresponding to the two phases being elongated and aligned parallel to the current flux and where the two phases are platelets perpendicular to the current flow. If the volume fractions of the phases are known together with the characteristic resistivities of the individual single-phase alloys which bound the two phase fields, then the limits can be evaluated by regarding them as parallel and series networks. There is no general rule which governs whether the series or parallel configuration will exhibit the greater resistivity and in any case it is highly unlikely that these two somewhat idealised situations will be encountered in practice; likewise, there is no general rule to indicate whether or not the resistivity of the two-phase alloy will be greater or less than that of one of the individual bounding single-phase alloys; however, it might be anticipated that the resistivity would be less than that of the single-phase disordered alloy of the same composition and this is often observed.

In alloy systems where magnetic transformations occur, the change in long-range order is reflected in the resistivity and is often manifest as a change in slope of the resistivity/temperature curve at the critical or transition temperature. In general, the magnitude of the effect of long-range order on the resistivity is difficult to estimate. Ferromagnetic alloys usually contain one of the ferromagnetic pure metals whilst anti-ferromagnetic long-range ordering can be found in many of the alloy systems involving transition and rare-earth metals.

1.7 Semiconductors

As mentioned above, the band theory of solids provides a framework for classifying solids into metals, semiconductors and insulators, the last of which are not relevant to this handbook. In metals, there are continuous energy states above the Fermi energy due either to the bands not being completely filled or to the bands overlapping in energy, whereas in semiconductors there exists an energy gap, E_g , between the valence and conduction bands with the Fermi energy lying in the gap. In the pure elemental semiconductors such as germanium and silicon, electrons must be thermally excited into the conduction band (and as a result an equal number of holes created in the valence band) for these materials to behave as intrinsic conductors. At temperatures of around room temperature and below, the thermal energy, $k_B T$ (<0.03 eV), is small compared with E_g (≈ 0.7 eV for germanium, ≈ 1.1 eV for silicon), and as the number of carriers varies according to $\exp(-E_g/2k_B T)$, these materials are poor conductors; at absolute zero no thermal excitation can occur and they behave as insulators. Increasing the temperature causes the number of carriers to increase exponentially and hence the resistivity to fall. Small amounts of impurities can give rise to donor and acceptor levels within the energy gap which are very close, in energy terms, to the conduction band and valence band, respectively; the energy separation, E_i , may be comparable to the room temperature thermal energy ($k_B T = 0.026$ eV). As the number of carriers now varies as $\exp(-E_i/2k_B T)$, the result is that many more electrons are excited from the donor level into the conduction band (or correspondingly many more holes created in the valence band) at lower temperatures, leading to *n*-type (electron) and *p*-type (hole) conductivity. This conductivity, which is proportional to the concentration of impurities, can be several orders of magnitude larger than the intrinsic conductivity. On the other hand, the addition of some impurities to an already impure semiconductor can reduce the total number of carriers via compensation. Thus, the influence of impurities on the resistivity is in marked contrast to the case of metals. Because impurity concentration is usually very low and these materials are normally used in single crystal form where the defect concentration is low, phonon scattering is dominant, but the variation of resistivity with temperature is most strongly influenced by the variation in the number of carriers. For these reasons only the high temperature resistivity of the elemental semiconductors is given in the handbook.

1.8 Summary

To summarise these fundamental concepts, the resistivity of the pure metals is well understood. Reliable experimental data exists over a wide range of temperature and this in general conforms to theoretical expectations. For dilute alloys (less than 5 atomic percent), provided the increase in residual resistivity per atomic percentage impurity addition is known, the resistivity can be estimated with reasonable confidence from Matthiessen's rule. This rule holds remarkably well for many alloy systems although there are exceptions, notably when the host metal is one of the ferromagnets.

In concentrated alloys the situation is much more complicated. While Nordheim's rule can be used to obtain a fair estimate of the resistivity of some concentrated binary alloys, it has limited applicability. This is due to the many factors which influence the resistivity; these include atomic and magnetic long-range order, changes in crystal structure (or phase) as the alloy composition and temperature vary and coexistence of two or more phases. All these factors together make it almost impossible to make even a fair estimate of the resistivity of a given alloy, let alone its temperature dependence. If the resistivity of an alloy of near composition and similar heat treatment is known, then by using the principles outlined above, a reasonable estimate of the resistivity of the alloy in question may be obtained.

The purpose of this handbook is to provide a comprehensive compilation of experimental data in graphical form of resistivity versus temperature which we hope will be of assistance in this respect. Failing this, one must resort to the experimental determination of the resistivity; chapter 2 deals with some of the experimental methods of measuring resistivity.

1.9 Abbreviations

The graphical data presented in this book is based on either single crystals, bulk characteristics or alloy format. Some materials incorporate unusual resistivity characteristics when pretreated and these have been annotated with the abbreviations listed below.

AP	As prepared
MSG	Monoclinic space group
n/a	Data not available
OA	Oxygen annealed
OSG	Orthoclinic space group
Q	Quench temperature, K
δ	Thermal correction factor

Chapter 2

Measurement techniques

T. Farrell

2.1 Introduction

There are many techniques available for the determination of electrical resistivity. The simplest and most widely used is the so-called four probe method in which the resistance of a portion of the sample is measured when a direct current passes through the sample. This technique involves two current contacts and two voltage contacts attached to the sample. The four probe technique is applicable to the vast majority of metals and alloys and a variation of the method, the Van der Pauw technique, is widely used for the determination of the resistivity of semiconductor wafers. The technique is applicable over a wide range of temperature. However, difficulties may be experienced with contacts if, for example, the material is brittle or chemically reactive (as it may be in the molten state). For such materials, methods which do not rely on making physical contact to the sample are preferable; the most widely used non-contacting techniques are those based on eddy currents induced in the sample when it is placed in a magnetic field which varies with time. In the following paragraphs, the four probe technique and some of the eddy current techniques are briefly described.

The theoretical background to the four probe and eddy current methods can be demonstrated by the application of two of Maxwell's equations:

$$\text{curl } \mathbf{E} = -\frac{\partial \mathbf{B}}{\partial t} = -\mu \mu_0 \frac{\partial \mathbf{H}}{\partial t} \quad (2.1)$$

$$\text{curl } \mathbf{H} = \mathbf{J} + \frac{\partial \mathbf{D}}{\partial t} = \frac{\mathbf{E}}{\rho} + \varepsilon \varepsilon_0 \frac{\partial \mathbf{E}}{\partial t} \quad (2.2)$$

In these equations, \mathbf{E} is the electric field, \mathbf{D} is the electric displacement, \mathbf{H} is the magnetic field, \mathbf{B} is the magnetic induction, ε_0 and μ_0 are the permittivity and permeability of free space, ε and μ are the relative permittivity and permeability of the sample and \mathbf{J} is the current in unit cross-sectional area of the sample of resistivity ρ .

For a conducting sample, the displacement current $\partial \mathbf{D} / \partial t$ is negligible in comparison with \mathbf{J} and thus (2.2) becomes

$$\text{curl } \mathbf{H} = \mathbf{J} = \frac{\mathbf{E}}{\rho} \quad (2.2a)$$

Equation 2.2a is the basis for the four probe method. The expression $\mathbf{J} = \mathbf{E}/\rho$ is simply a statement of Ohm's law. Thus, writing $\mathbf{J} = I/A_S$ where I is the current in the sample of uniform cross-section A_S and V the voltage measured by two impedance probes separated by a distance L , the resistance R is

$$R = \rho \frac{L}{A_S} \quad (2.3)$$

If the sample is cylindrical of radius a , the resistance is

$$R = \left(\frac{\rho}{a^2} \right) \frac{L}{\pi} \quad (2.3a)$$

The basis for the eddy current methods is seen by substituting (2.1) into (2.2a):

$$\operatorname{curl} \operatorname{curl} \mathbf{H} = \nabla^2 \mathbf{H} = \frac{1}{\rho} \operatorname{curl} \mathbf{E} = -\frac{\mu\mu_0}{\rho} \frac{\partial H}{\partial t} \quad (2.4)$$

For a sample having isotropic magnetic and electrical properties, which is true of most polycrystalline materials, and where the magnetic field is aligned along the principal sample dimension (for example, along the axis of a cylinder, say the z direction), the vector equation (2.4) becomes scalar, and since $B = \mu\mu_0 H$ and the magnetic flux, ϕ , in the sample is $\phi = A_S B$, we have

$$\frac{\partial \phi}{\partial t} = -\frac{\rho}{\mu\mu_0} \frac{\partial^2 \phi}{\partial z^2} \quad (2.4a)$$

Equation (2.4a) is the standard diffusion equation where the flux diffusivity (which has the dimensions of (length)²/time) is $\rho/\mu\mu_0$. It governs how the magnetic flux in the sample changes with a time-dependent magnetic field. Solutions to the diffusion equation for various geometrical arrangements and different boundary conditions (for example, the time dependence of the magnetic field) are given in standard texts [12]. By way of illustration, consider a cylindrical sample of radius a which experiences a uniform magnetic flux, ϕ_0 , which is suddenly removed at time $t = 0$; the average flux at time t is given by

$$\phi = \frac{4\phi_0}{a^2} \sum_{n=1}^{\infty} \frac{1}{\beta_n^2} \exp \left(-\beta_n^2 \left(\frac{\rho}{\mu\mu_0 a^2} \right) t \right) \quad (2.5)$$

where the coefficients β_v are the positive roots of $J_0(\beta) = 0$, J_0 being the zero-order Bessel function. Thus, by observing the time dependence of the flux decay, the resistivity can be deduced. Details of this method along with other diffusion eddy current based methods involving periodic magnetic fields are discussed below. It is seen that in both (2.3) and (2.5) a term involving ρ/a^2 appears. The same term appears in other eddy current methods, which being diffusion based must have a term involving (length)² – or cross-sectional area – and this is important when considering the accuracy of the determination of ρ .

2.2 Four probe methods

These methods rely on the measurement of the resistance of the portion of the sample between the two voltage probes. For (2.3) to be applicable, the cross-sectional area of the sample should be uniform and the voltage probes should be connected to the sample in such a way that the length, L , can be accurately determined.

The preferred method of measuring the resistance is to use a Wheatstone bridge, which compares the unknown resistance of the sample with that of three standard resistors, one of which is a variable standard. As the bridge is a null method, calibration of the detector is not necessary. The accuracy with which the null point can be determined depends not only on the sensitivity of the detector but also on the relative magnitudes of the resistances of the arms of the bridge. A good general rule for optimum bridge operation is that the resistances in the four arms should be of the same order. With a well-designed bridge and sensitive detector, the bridge sensitivity can be very high and errors in the determination of resistivity arising from the resistance measurement can be regarded as being negligible.

Alternatively, the sample resistance can be measured using a constant current and measuring the probe voltage difference using a potentiometer or digital voltmeter; the latter has the advantage that it can be calibrated to give a direct reading of the resistance. To avoid zero errors it is usual practice to incorporate current reversal and take the average value of the two readings. Zero errors can arise not only from an incorrectly adjusted voltmeter but also from thermoelectric effects if a temperature gradient exists along the sample and the voltage leads, usually copper, have a different thermoelectric power from that of the sample being measured.

The accuracy with which the resistivity is determined from the resistance measurements can be dominated by the errors involved in the measurements of the sample cross-section and the separation of the voltage probes. This depends on the magnitude of A_S and L , which in turn is influenced by the magnitude of the resistivity through the need to have an accurate measurement of the resistance. For a pure metal with a resistivity of 5×10^{-8} ohm m, through which a current of 1 A passes and where the voltage is determined to an accuracy of 10 nV, then for a resistance measurement to an accuracy of 0.01%, the voltage between the probes should be 100 μ V, giving a resistance of 10^{-4} ohm. From (2.3), L/A_S should be 2×10^3 /m and thus can be satisfied realistically with a cylindrical sample of diameter 8 mm and with $L = 100$ mm. The power dissipated in the sample is 0.1 mW and this will not cause any significant heating.

Thus, for the majority of metals and alloys, the resistivity at temperatures above room temperature, cylindrical samples measuring about 10 mm in diameter and with L of about 50 to 100 mm are ideal shapes. Clearly, if this demands too large a quantity of material, the sample dimensions should be scaled down accordingly, but this will have the effect of increasing the errors in the measurement of L and A_S . At lower temperatures, particularly with annealed pure metals, the resistivity can be as low as 2×10^{-11} ohm m and this usually requires the sample to be in the form of a thin wire.

The measurement of L usually presents no problems. If mechanical clamps embodying ‘knife-edge’ contacts are used as the voltage probes, then the separation of appropriate datum marks on the clamps can be determined to plus or minus 0.02 mm with a travelling microscope; thus, the error introduced in the measurement of L is less than 0.1%.

The determination of A_S is more demanding. First, A_S should be uniform, and this can be checked by measuring the sample diameter (for the cylindrical sample) at various positions along L . It is preferable to use a non-contacting method for this measurement (if a micrometer is used, the contact pressure can lead to an erroneously low value for the diameter). Optical projection techniques and photographic enlargements can be used to get an accuracy of better than 0.1% in A_S , provided, of course, the sample is prepared to this accuracy.

Thus, provided care is taken in the measurement of L and A_S , the resistivity can readily be determined with an absolute accuracy of around 0.1% at and above room temperature. At cryogenic temperatures, in particular at liquid helium temperatures and with pure metals, the error in the determination of the resistance is maintained at negligible proportions by employing voltage detection equipment which involves superconducting elements and has much higher sensitivity.

2.3 Temperature variation of resistivity

With the four probe technique, the temperature variation of the resistivity can be determined quite simply by thermally attaching the sample to a heat sink, the temperature of which is controlled. The sample temperature can be measured using a suitable thermocouple attached to one of the voltage probes and any temperature gradients can be measured using a differential thermocouple with its two junctions thermally anchored to the two voltage probes; in this way, the mean sample temperature can be determined. The design of the furnace is not considered here, but for high-temperature work, a vacuum furnace is usually used to reduce the thermal load and prevent oxidation.

To overcome problems with thermoelectrically generated voltages, the voltage leads should be continuous to the wall of the vacuum vessel; likewise, for accurate temperature measurements it is preferable to use continuous thermocouple leads.

When varying the temperature, the change in sample dimensions due to thermal expansion should be taken into account, especially since L and A_S are usually carefully determined at room temperature. To illustrate the magnitude of the error which may be introduced by the neglect of thermal expansion, consider a cylindrical sample to which (2.3a) applies. At any temperature T , the resistance is

$$R_T = \rho_T \frac{L_0}{\pi a_0^2} \frac{(1 + \alpha \Delta T)}{(1 + \alpha \Delta T)^2} = \rho_T = \frac{L_0}{\pi a_0^2} (1 + \alpha \Delta T)^{-1}$$

where α is the thermal expansion coefficient, R_T is the measured resistance and ρ_T is the resistivity. Thus, the percentage error introduced is $\alpha \Delta T \times 100$. Taking a representative value of $\alpha = 15 \times 10^{-6}$ for most metals and alloys, it is readily

appreciated that the error can be comparable to the accuracy in the determination of the resistivity for a ΔT of 100 K.

2.4 Eddy current methods

Several techniques which rely on induced eddy currents for the determination of resistivity have evolved, the simplest of which correspond to the situations where the applied magnetic field is periodic, for example varying sinusoidally with time, and where the field is a step function being suddenly switched from zero to a preset constant value or conversely switched from a steady value to zero. Whilst these elegant techniques overcome the need for electrical contact to the sample, they do have characteristic features which can give misleading results.

First, it is important to recognise that the eddy currents are not uniformly distributed throughout the sample when a periodic magnetic field is applied. They decay exponentially from the sample surface with a measure of the decay being the ‘skin depth’. The skin depth, δ , is given by

$$\delta = \left(\frac{\pi f \mu \mu_0}{\rho} \right)^{-1/2}$$

and is the depth at which the eddy currents have fallen to $1/e$ of their surface value. If the whole of the sample is to be examined, then, in the case of the periodically varying magnetic field, the frequency, f , should be chosen so that δ is not significantly less than the sample dimension, which, in the case of a cylinder with the magnetic field parallel to the cylinder axis, is the cylinder radius. If δ is significantly less than the sample dimensions, then surface features such as roughness and contaminant films can affect the resistivity measurements. It must be emphasised that the only situation where uniform current density occurs is in the direct current measurements on uniform cross-section samples as discussed in the four probe method.

Second, the magnetic field can directly influence the motion of the electrons within the sample (in addition to ‘indirect’ influence via induction which gives rise to the eddy currents), leading to additional resistance over that caused by scattering. This ‘magnetoresistance’ is dependent on the magnitude of the applied magnetic field and its occurrence can be checked by varying the field strength.

These techniques are well suited to the determination of the resistivity of weakly magnetic materials where the relative permeability, μ , can safely be regarded as unity. However, some caution should be exercised when dealing with ferromagnetic and strongly paramagnetic materials or materials which exhibit magnetic transformations where μ is neither constant nor unity.

The most convenient means of applying a magnetic field is to place the conducting sample in a coil. With the step function methods, the resistivity is determined by observing the change of flux in the sample as a function of time after the field has suddenly been applied or removed; this is described for the case of field removal by (2.5). For periodically varying fields, the difference between the impedance of the loaded and empty coil is measured.

2.5 Step function methods

The basis of this method has already been mentioned. A convenient arrangement is to insert the sample into a coil, apply a direct current to the coil for sufficient time to ensure complete flux penetration into the sample and then de-energise the coil by opening a switch. A simple circuit is shown in Fig. 2.1. The flux decay is detected by a secondary coil wound over the central region of the energising coil. The time dependence of the average flux, ϕ , in a cylindrical sample after removing the magnetic field is given by (2.5). If there are N turns on the second coil then the voltage induced in that coil is

$$-N \frac{\partial \phi}{\partial t}$$

Using the relationship between ϕ and magnetic field H

$$\phi = \pi a^2 \mu \mu_0 H$$

and differentiating (2.5) with respect to time and multiplying by N , the secondary coil voltage is obtained:

$$V = 4\pi N \rho H_0 \sum_{n=1}^{\infty} \exp \left(-\beta_n^2 \left(\frac{\rho}{\mu \mu_0 a^2} \right) t \right)$$

The voltage decays as a sum of exponential factors. The first three coefficients β_n^2 have the values 5.784, 30.470 and 74.892; thus, for longer times, the decay is a simple exponential governed by β_1^2 . To illustrate this, consider the exponential term involving β_2 to contribute a maximum of 0.1% of the contribution from β_1 . For this condition to apply:

$$\exp \left(-\left(24 \cdot 676 \left(\frac{\rho}{\mu \mu_0 a^2} \right) t \right) \right) \leq 10^{-3}$$

Thus, for a material with $\rho = 5 \times 10^{-8}$ ohm m, $a = 5 \times 10^{-3}$ m and $\mu = l$, the time should be greater than 1.75×10^{-4} s in which case the sum of the exponential

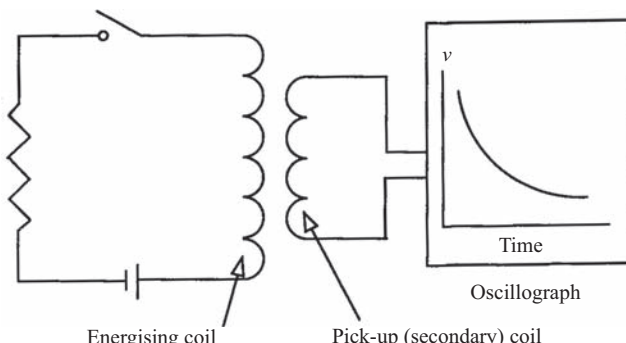


Figure 2.1 Simple circuit for the step function method

factors is approximately 0.2. The measured voltage at this time is $1.25 \times 10^{-5} H_0$ V and after $t = 5 \times 10^{-4}$ s the voltage has decayed to $6.25 \times 10^{-7} H_0$ V. The voltage/time variation can be measured and stored using a suitable oscilloscope.

2.6 Periodically varying fields

The impedance, Z_L , of a magnetic field coil into which a conducting sample is placed (a loaded coil) comprises resistive and reactive components:

$$Z_L = R_L + iX_L$$

The resistance R_L and reactance X_L of the loaded coil are given by

$$R_L = R_0 + R_1$$

$$X_L = X_0 + X_1$$

where R_0 and X_0 refer to the empty solenoid and R_1 and X_1 are the resistive and reactive contributions from the eddy currents induced in the sample. In fact, R_1 and X_1 measure the out-of-phase and in-phase flux in the sample.

In general

$$R_1 = A'X_0F_R(y)$$

$$X_1 = A'X_0F_X(y)$$

$$\text{or } \frac{X_1}{R_1} = \frac{F_X(y)}{F_R(y)} = F_{XR}(y)$$

where the constant A' is a measure of the ratio of the cross-sectional area of the sample to that of the coil and y is a parameter involving the skin depth and the dimension of the sample. Analytical expressions of the coil functions $F_X(y)$, $F_R(y)$ and hence $F_{XR}(y)$ can be derived for the simpler geometrical shapes such as ‘infinite’ cylinders, in which case y is given by

$$y = \frac{\sqrt{2}a}{\delta} = (2\pi\mu\mu_0)^{1/2} \left(\frac{fa^2}{\rho} \right)^{1/2}$$

where a is the radius, as before, and the coil ‘filling factor’, A' , is simply A_S/A_C , where A_C is the cross-sectional area of the coil. The coil functions for cylindrical geometry are shown in Figs. 2.2 and 2.3 and for such a geometry these figures can be used directly to obtain ρ once X_0 , X_1 and R_1 have been measured.

Samples of irregular geometry, for which analytic expressions cannot be derived, can be used but the coil/sample system should be calibrated over a range of frequencies using a ‘standard’ specimen of known resistivity, ρ_S , having identical shape to that to be determined. The experimentally determined R_S/X_0 , X_S/X_0 and X_S/R_S give $A'F_R(y)$, $A'F_X(y)$ and $F_{XR}(y)$, respectively (X_S and R_S refer to the calibration with the standard resistivity specimen). There are advantages in using $F_{XR}(y)$ as this eliminates the need to know the coil filling factor which, for non-simple geometries, is difficult to calculate.

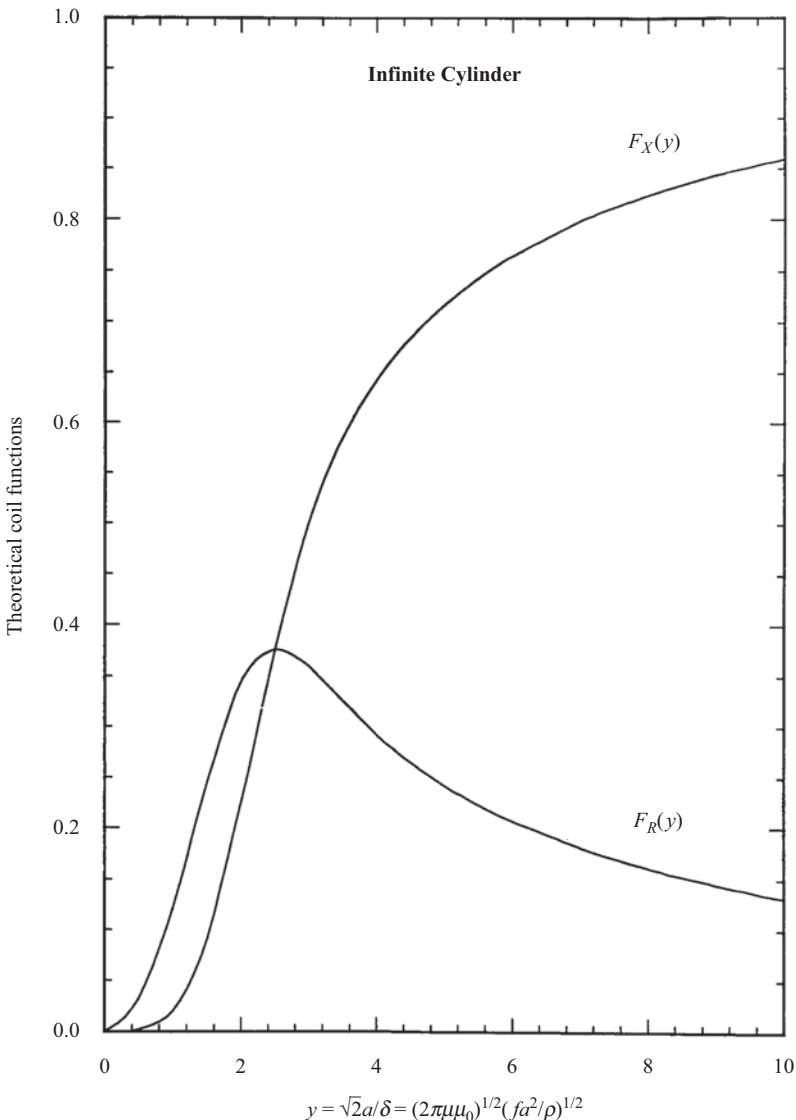


Figure 2.2 Coil functions $F_R(y)$ and $F_X(y)$ for an infinite cylinder

Having determined the empty coil parameter and obtained the coil functions, a single frequency measurement is sufficient to determine the resistivity of the unknown sample. The choice of frequency is important for two reasons. First, as mentioned beforehand, it is desirable that $\delta > a$, and second, since the resistivity determination involves the subtraction of the unloaded coil measurements from the

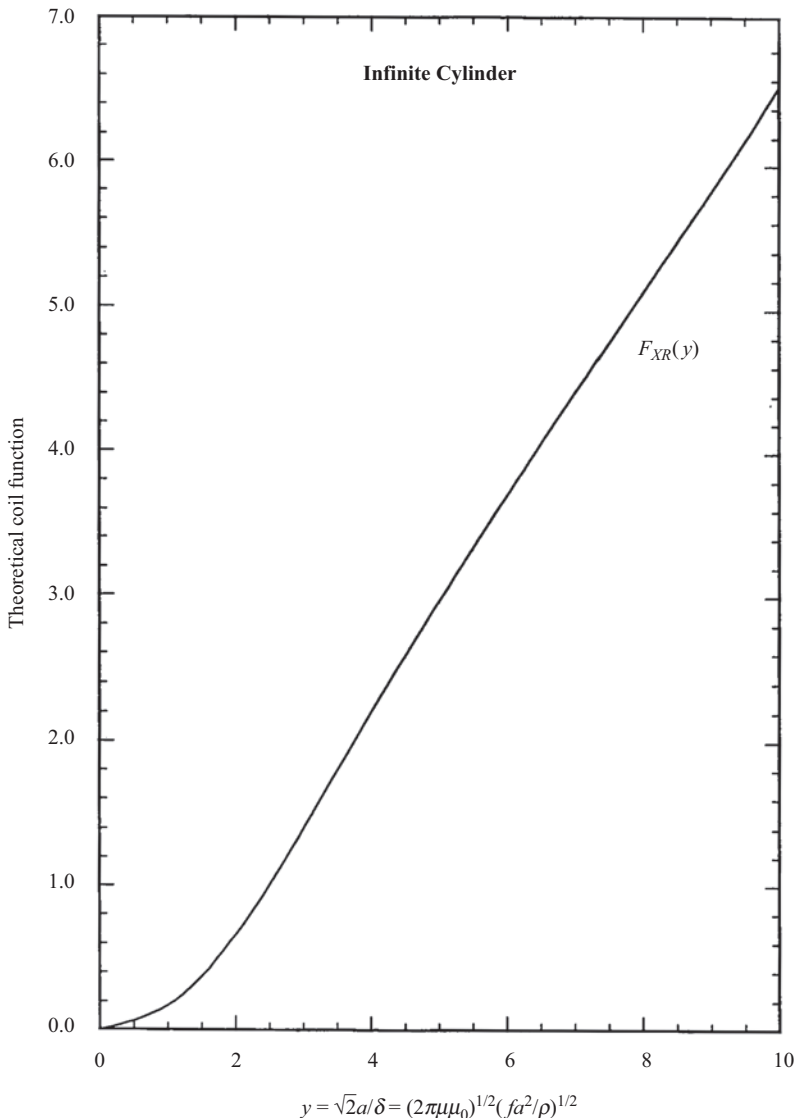


Figure 2.3 Coil function $F_{XR}(y)$ for an infinite cylinder

loaded coil measurements, it is desirable to have a large difference between the two sets of measurements. This can be illustrated by reference to Fig. 2.2 and again taking a cylindrical sample of radius 5 mm and resistivity of 5×10^{-8} ohm m. $F_X(y)$ and $F_R(y)$ are both greater than 0.2 in the range from $y = 2$ to 5.5 and this corresponds to $f = 1$ to 7.5 kHz. At $f = 1.0$ kHz, the skin depth in the above material

is 3.6 mm, whilst at $f = 7.5$ kHz, the skin depth is 1.3 mm. If the criterion of $\delta = a = 5$ mm is used, the frequency is 500 Hz giving $y = 1.4$; $F_X(y)$ and $F_R(y)$ are reduced to 0.07 and 0.22, respectively. This implies that the maximum value of X_L/X_0 is 1.07 (taking $A' = 1$), which imposes a more stringent demand on the experimental determination of X_L and X_0 . At higher frequencies (7.5 kHz), the experimental demands are relaxed but skin depth considerations may affect the result.

2.7 Inductive techniques

2.7.1 Self-inductance

The coil should be longer than the sample to avoid end effects, thus ensuring uniformity of the magnetic flux in the sample. Coil design details are beyond the scope of this account, but taking into consideration such factors as low thermal dissipation, maximum coil filling factor, small magnetic fields, etc., then for a cylindrical sample of diameter about 10 mm, R_0 and $2\pi f X_0$ ($f = 10^3$ Hz) can each be a few ohms, giving a coil impedance of around 10 ohms.

The loaded and unloaded coil impedances are measured using an appropriate variable frequency bridge. Two self-inductance bridge networks are shown in Fig. 2.4. The Anderson bridge, Fig. 2.4b, has the advantage that it avoids the use of variable standard inductors or capacitors. Taking the coil current to be in the milliampere range (for low thermal dissipation and low magnetic fields) and following the general rule for optimum bridge operation, the driving voltage of the audio-frequency oscillator is in the 0.1 to 1.0 V range. Using a tuned detector, the sensitivity of the bridge can be higher than 0.005%, and with an appropriately chosen frequency and good coil filling factor, R_1 and $2\pi f X_1$, can be around $0.15 \times 2\pi f X_0$ implying that R_1 and X_1 can be measured to an accuracy of 0.05%. The error in y is that associated with the accuracy to which a can be measured and this has been discussed in connection with the four probe method.

The uncertainty in ρ arises from the uncertainties in y^2 (and hence a^2) and if $F_X(y)$ and $F_R(y)$ are used the uncertainties in A' , which involve both a^2 and d^2 (d is the coil diameter); if $F_{XR}(y)$ is used the uncertainties are reduced as A' is not required. If a non-simple shape is used which necessitates experimental determination of $F_X(y)$ and $F_R(y)$, the errors are compounded by the dimensions of both the standard and unknown samples. Taking all these factors into consideration the accuracy in ρ when determined using the self-inductance technique is likely to be in the region of 0.1% with the lowest uncertainties being achieved with a uniform cross-section cylindrical sample.

2.7.2 Mutual inductance

The use of a secondary coil wound over the central region of the primary coil has the advantage of eliminating end effects and offers the prospect of examining regions of the sample along its length. The analysis of the coils for mutual inductance is quite complex. As an approximation, the reactance and resistance of a suitable unloaded

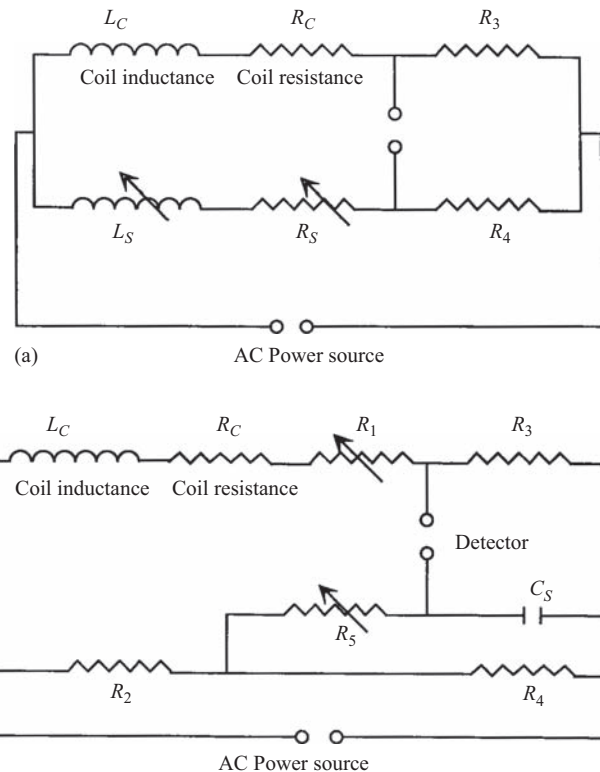


Figure 2.4 Typical bridges for the determination of self-inductance. (a) Typical bridge using standard inductors; (b) Anderson bridge

coil system is scaled down from the self-inductance and resistance of the primary coil by the turns ratio. Thus, a typical system will have a mutual inductance in the region of $100 \mu\text{H}$ (as opposed to a few millihenries for the single-coil self-inductance).

The determination of mutual inductance is most readily achieved by making a direct comparison with a variable standard mutual inductance, connecting the primary windings of both standard and unknown in series to an audio-frequency oscillator and connecting the secondary windings in series opposition so that the induced voltages oppose each other. In principle, the detector which is in series with the secondaries shows a null reading when the mutual inductances and unknown inductors are equal. In practice, because a resistance element exists, it is almost impossible to obtain a balance. The so-called Hartshorn bridge, shown in Fig. 2.5, overcomes this difficulty. The technique requires a balance to be obtained in the unloaded system by adjusting M_S and R . The sample is then inserted and the balance is restored by varying M_S and R by ΔM_S and ΔR from the unloaded condition. Recognising that R_1^+ and X_1^+ are measures of the out-of-phase and in-phase flux associated with the eddy currents, R_1^+ is given by ΔM_S and X_1^+ by $\Delta R/2\pi f$. As with the self-inductance technique,

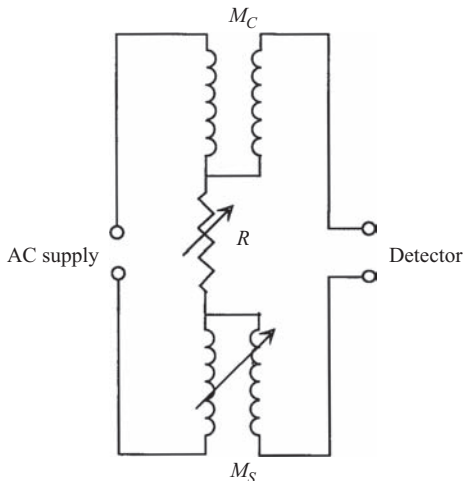


Figure 2.5 The Hartshorn mutual inductance bridge. M_C = mutual inductance of the coil, M_S = variable standard mutual inductance

the value of y is then obtained from the calibrated coil function or, if cylindrical samples are used, from the theoretical coil functions shown in Figs. 2.2 and 2.3.

The mutual inductance technique relies on exactly the same parameters as the self-inductance method; the uncertainties involved are again those associated with the measurement of sample and coil dimensions and hence the achievable accuracy in the determination of the resistivity is similar.

2.7.3 Inductive techniques and temperature variations

The primary purpose of using eddy current techniques is to avoid physical contact with the sample. When determining the resistivity as a function of temperature, the sample should be in an isothermal enclosure with the temperature of the enclosure monitored with an appropriate thermometric device such as a thermocouple, resistance thermometer or pyrometer. The use of an isothermal enclosure virtually eliminates thermoelectrically generated voltages.

When the highest accuracy is sought, the effects of thermal expansion must be taken into account and these effects enter through expansion of the sample and the coils (in the four probe method only the expansion of the sample needs to be considered).

The reactance of the unloaded coil is related to its dimension via $X_0 = \text{constant} \times d_c^2/l_c$, where d_c and l_c are the coil diameter and length, respectively. The effect of an increase in temperature, ΔT , is to increase X_0 by $\alpha\Delta T \times 100\%$ where α may be taken to be the coefficient of expansion of the coil windings. The magnitude of the change is similar to that discussed in connection with the variation of resistance with temperature in the four probe method.

Neglecting the lead resistances, R_0 is proportional to l_w/d_w^2 , where l_w and d_w are the wire length and diameter. Assuming the coil is tightly wound then $d_w \approx B_c l_c$ and $l_c \approx C_c l_c$ where B_c and C_c are constants involving the number of turns on the coil and the number of layers of windings. R_0 is therefore proportional to d_c/l_c^2 and the effect of a temperature increase of ΔT is to decrease R_0 by $\alpha\Delta T \times 100\%$. Again, the magnitude of the effect can easily exceed the accuracy with which the resistivity can be determined and corrections for thermal expansion should be made.

The sample dimensions enter through the parameter y which is proportional to $(r/a^2)^{1/2}$; thus, if the thermal expansion behaviour of the sample is known, a simple correction can be applied for y .

However, it is not just a simple matter of correcting the impedance measurements for thermal expansion as is the case with the resistance measurements in the four probe method. Since R_0 and L_0 change with temperature, the bridge balance conditions also change. Thus, for the most reliable results, the implication is that the equipment should have provision for withdrawing the sample from the coil to enable R_0 and L_0 as well as R_L and X_L to be measured at each temperature.

The coil filling factor is also affected by thermal expansion. If F_X, F_R are used to determine the resistivity, then a simple correction for thermal expansion (sample/coil) can be applied; this is not necessary if F_{XR} is used.

This account of experimental techniques concludes with a few remarks about an interesting method of resistivity measurement which involves induced eddy currents and as such avoids the use of electrical contact. Unlike the eddy current techniques discussed above, it does not rely on electrical measurements. The technique involves a rotating uniform magnetic field such as that produced by the stators of a polyphase induction motor. When a cylindrical sample is placed in the field, the induced eddy currents interact with the flux causing the sample to experience a torque, Γ , given by

$$\Gamma = \frac{\pi \omega_r \mu^2 \mu_0^2 l a^4 H^2}{4\rho}$$

where ω_r is the relative angular velocity of H and the sample. If the sample's motion is restrained by a torsion wire, it will rotate to a fixed position where Γ is balanced by the reaction in the torsion wire, enabling the above expression to be used with ω_f , the angular velocity of the field, replacing ω_r . Measurement of the deflection by the incorporation of a mirror into the torsion wire suspension and the use of optical levers gives an accurate measurement of Γ . The resistivity, ρ , is then determined using the above expression. This technique is more sensitive to the sample dimensions than the electrical techniques and is thus inherently less accurate. Furthermore, when using this method to determine the temperature variation of the resistivity, it is important that corrections for thermal expansion be applied.

Chapter 3
Explanation of graphs
G. Dyos

3.1 Data analysis

The majority of the data presented in this handbook has been gleaned from material published over the last two decades. The data has been extracted from the original published paper or book. The interpretation of the data is that of the original author except where an obvious error has occurred in the publishing of tabular material. Otherwise, every effort has been made to ensure the accuracy of the transcribed original data.

3.2 Catalogue system for materials

The catalogue system used in this book is based on two levels. First, the materials are listed in alphabetical order; where a material has several elements, they are listed in order of decreasing atomic percentage. Should a material have elements all having equal atomic percentage then they are listed in alphabetical order.

Data which has been presented in the original paper in graphical form and extracted is indicated by an asterisk (*) against the reference number in question. Data presented, in the original form, in tabular format is indicated by the absence of an asterisk against the reference number. Data from various sources which has been surveyed by an author to determine a best fit of that data is indicated by an 'R' after the reference. Data included in that survey is not represented in this handbook.

If the material is a disordered crystalline compound, the letter 'D' is placed after the reference number and similarly the letter 'A' is used if the material is amorphous. It should be noted that the vast majority of authors do not indicate whether an allowance for thermal expansion has been applied to the resistivity of the material. Where the purity of an element has not been stated in the original paper, but the information greatly extends the range of resistivity, this has been denoted by '%na'.

3.3 Material composition

The purity of the elements in this book is expressed in terms of the weight percentage of the elements present.

All the compounds listed in this handbook are expressed in terms of atomic percentages, that is, the number of atoms of an element expressed as a percentage of the total number of atoms present in one molecule of the material.

Where compounds have been listed in the original reference as weight percentages, these have been converted into atomic percentages.

Chapter 4

Text references

- [1] Pollock D.D. *Electrical Conduction in Solids: An Introduction* (Ohio, American Society for Metals, 1985)
- [2] Rossiter P.L. *The Electrical Resistivity of Metals and Alloys* (Cambridge, Cambridge University Press, 1987)
- [3] Schroder K. *Handbook of Electrical Resistivities of Binary Metallic Alloys* (Florida, CRC Press, 1983)
- [4] Meaden G.T. *The Electrical Resistance of Metals* (London, Heywood Books, 1963)
- [5] Kittel C. *Introduction to Solid State Physics* (New York, John Wiley & Sons, 1976)
- [6] Drude P. ‘Zur elektronentheorie der metalle’. *Ann. Phys.* 1900, vol. 1, p. 566
- [7] Sommerfeld A. ‘Zur elektronentheorie der metalle auf grund der Fermischen statistik’. *Z. Phys.* 1928, vol. 47, p. 1
- [8] Bloch F. ‘Über die quantenmechanik der elektronen in kristallgittern’. *Z. Phys.* 1928, vol. 52, p. 555
- [9] Bloch F. ‘Zum elektrischen widerstandsgesetz bie tiefen temperaturen’. *Z. Phys.* 1930, vol. 59, p. 208
- [10] Gruneisen E. ‘Die abhangigkeit das elektrischen widerstandes reiner metalle van der temperatur’. *Ann. Phys.* 1933, vol. 16, p. 530
- [11] Nordheim L. ‘Zur elektronentheorie der metalle’. *Ann. Phys.* 1931, vol. 9, no. 5, pp. 607–78
- [12] Carslaw H.S., Jaeger J.S. *Conduction of Heat in Solids* (Oxford, Oxford University Press, 1959)

Chapter 5

Index of materials

Aluminium Ytterbium	39
Antimony	40
Antimony Cobalt Titanium - 1	41
Antimony Cobalt Titanium - 2	42
Antimony Cobalt Titanium Indium	43
Antimony Cobalt Titanium Iron	44
Antimony Cobalt Titanium Manganese	45
Antimony Cobalt Titanium Nickel	46
Antimony Cobalt Titanium Niobium	47
Antimony Cobalt Titanium Platinum	48
Antimony Cobalt Titanium Tellurium	49
Antimony Cobalt Titanium Tin	50
Antimony Cobalt Titanium Vanadium	51
Antimony Cobalt Vanadium	52
Arsenic Barium Iron	53
Arsenic Calcium Fluorine Iron - 1	54
Arsenic Calcium Fluorine Iron - 2	55
Arsenic Calcium Fluorine Iron Chromium	56
Arsenic Calcium Fluorine Iron Cobalt - 1	57
Arsenic Calcium Fluorine Iron Cobalt - 2	58
Arsenic Calcium Fluorine Iron Copper	59
Arsenic Calcium Fluorine Iron Manganese	60
Arsenic Calcium Fluorine Iron Nickel	61
Arsenic Cerium Iron Oxygen	62
Arsenic Cerium Iron Oxygen Fluorine	63
Arsenic Cerium Nickel Oxygen	64
Arsenic Cerium Nickel Oxygen Fluorine	65
Arsenic Cerium Rhodium	66
Arsenic Dysprosium Iron Oxygen	67
Arsenic Europium Fluorine Iron	68
Arsenic Fluorine Iron Neodymium Strontium	69
Arsenic Fluorine Iron Strontium	70

Arsenic Fluorine Iron Strontium Neodymium	71
Arsenic Fluorine Iron Strontium Samarium	72
Arsenic Gadolinium Iron Oxygen	73
Arsenic Gadolinium Iron Oxygen Fluorine	74
Arsenic Holmium Iron Oxygen	75
Arsenic Iron Barium	76
Arsenic Iron Barium Lanthanum	77
Arsenic Iron Barium Potassium - 1	78
Arsenic Iron Barium Potassium - 2	79
Arsenic Iron Calcium	80
Arsenic Iron Calcium Sodium	81
Arsenic Iron Europium Sodium	82
Arsenic Iron Gadolinium Oxygen	83
Arsenic Iron Lanthanum Oxygen	84
Arsenic Iron Lanthanum Oxygen Fluorine	85
Arsenic Iron Lanthanum Oxygen Fluorine Sodium	86
Arsenic Iron Lanthanum Oxygen Fluorine Ytterbium	87
Arsenic Iron Lithium	88
Arsenic Iron Neodymium Oxygen	89
Arsenic Iron Neodymium Oxygen Fluorine	90
Arsenic Iron Oxygen Cerium Gadolinium Fluorine	91
Arsenic Iron Oxygen Gadolinium Cerium Fluorine	92
Arsenic Iron Oxygen Gadolinium Thorium	93
Arsenic Iron Oxygen Lanthanum Ytterbium Fluorine	94
Arsenic Iron Oxygen Praseodymium	95
Arsenic Iron Oxygen Samarium	96
Arsenic Iron Oxygen Terbium	97
Arsenic Iron Oxygen Thulium	98
Arsenic Iron Oxygen Yttrium	99
Arsenic Iron Potassium	100
Arsenic Iron Praseodymium Oxygen	101
Arsenic Iron Praseodymium Oxygen Fluorine	102
Arsenic Iron Samarium Oxygen	103
Arsenic Iron Samarium Oxygen Fluorine - 1	104
Arsenic Iron Samarium Oxygen Fluorine - 2	105
Arsenic Iron Strontium	106
Arsenic Iron Thulium Oxygen Fluorine	107
Arsenic Lanthanum Oxygen Iron Nickel	108
Arsenic Nickel Barium	109
Arsenic Oxygen Praseodymium Iron Cobalt	110
Barium Cobalt Germanium	111
Bismuth Antimony	112
Bismuth Antimony Nickel	113
Bismuth Cerium Platinum	114

Boron Aluminium	115
Boron Aluminium Magnesium	116
Boron Aluminium Zinc Magnesium	117
Boron Cadmium Magnesium	118
Boron Carbon Silicon	119
Boron Erbium	120
Boron Magnesium	121
Boron Magnesium Aluminium - 1	122
Boron Magnesium Aluminium - 2	123
Boron Magnesium Aluminium Lithium	124
Boron Magnesium Aluminium Zinc	125
Boron Magnesium Carbon	126
Boron Nickel Carbon Holmium	127
Boron Niobium	128
Boron Silicon Erbium	129
Boron Silicon Gadolinium	130
Boron Silicon Terbium	131
Boron Silicon Ytterbium	132
Boron Ytterbium	133
Boron Yttrium	134
Boron Ytterbium Carbon	135
Bromine Thallium	136
Carbon Hydrogen Nitrogen Selenium Sulphur Chlorine	137
Carbon Selenium Hydrogen Nitrogen Chlorine	138
Carbon Silicon	139
Carbon Silicon Boron	140
Carbon Silicon Germanium	141
Carbon Silicon Nickel	142
Carbon Sulphur Hydrogen Nitrogen Chlorine	143
Carbon Ytterbium	144
Chlorine Thallium	145
Chromium Gallium	146
Chromium Gallium Vanadium	147
Chromium Vanadium Gallium	148
Copper - 1	149
Copper - 2	150
Copper Nickel	151
Copper Tin	152
Dysprosium	153
Gadolinium	154
Gadolinium Lanthanum	155
Germanium Cobalt Europium	156
Germanium Cobalt Praseodymium	157
Germanium Platinum Lanthanum	158

Germanium Platinum Praseodymium	159
Germanium Silicon	160
Indium Selenium	161
Indium Selenium Holmium	162
Iodine Thallium	163
Iron - Linear - 1	164
Iron - Logarithmic - 2	165
Iron - Crystalline - 3	166
Iron Lanthanum Oxygen Phosphorus	167
Iron Lanthanum Phosphorus Oxygen Fluorine	168
Iron Phosphorus Thorium	169
Iron Phosphorus Uranium	170
Iron Selenium	171
Iron Tellurium	172
Iron Tellurium Sulphur	173
Lanthanum Nitrogen Boron Nickel	174
Lanthanum Rhodium Tin	175
Lead Tellurium	176
Lithium Aluminium - 1	177
Lithium Aluminium - 2	178
Magnesium Silicon Tin	179
Magnesium Silicon Tin Antimony	180
Magnesium Silicon Tin Bismuth	181
Molybdenum	182
Nickel	183
Nickel Bismuth Antimony	184
Nickel Boron Magnesium	185
Nickel Carbon Magnesium	186
Nickel Chromium	187
Niobium	188
Niobium Indium Carbon	189
Niobium Titanium	190
Oxygen Barium Tin Bismuth Antimony	191
Oxygen Barium Titanium Lanthanum	192
Oxygen Barium Titanium Silicon Lanthanum	193
Oxygen Bismuth Niobium Lanthanum Strontium	194
Oxygen Bismuth Niobium Strontium	195
Oxygen Bismuth Niobium Strontium Lanthanum	196
Oxygen Bismuth Strontium Calcium Bromine	197
Oxygen Bismuth Strontium Copper	198
Oxygen Cadmium Rhenium	199
Oxygen Calcium Titanium Arsenic Iron Magnesium	200
Oxygen Chromium Lanthanum Calcium	201
Oxygen Chromium Lanthanum Calcium Manganese	202

Oxygen Cobalt Lanthanum Strontium	203
Oxygen Cobalt Lanthanum Strontium Iron	204
Oxygen Copper Barium Beryllium Calcium Tellurium Cobalt	205
Oxygen Copper Barium Calcium Magnesium Tellurium Cobalt	206
Oxygen Copper Barium Calcium Magnesium Thallium - 1	207
Oxygen Copper Barium Calcium Magnesium Thallium - 2	208
Oxygen Copper Barium Calcium Tellurium	209
Oxygen Copper Barium Calcium Tellurium Cobalt	210
Oxygen Copper Barium Calcium Tellurium Scandium	211
Oxygen Copper Barium Calcium Thallium	212
Oxygen Copper Barium Europium	213
Oxygen Copper Barium Europium Manganese	214
Oxygen Copper Barium Gadolinium	215
Oxygen Copper Barium Gadolinium Calcium Molybdenum	216
Oxygen Copper Barium Gadolinium Molybdenum	217
Oxygen Copper Barium Gadolinium Molybdenum Calcium	218
Oxygen Copper Barium Gadolinium Praseodymium - 1	219
Oxygen Copper Barium Gadolinium Praseodymium - 2	220
Oxygen Copper Barium Neodymium	221
Oxygen Copper Barium Neodymium Lanthanum	222
Oxygen Copper Barium Praseodymium	223
Oxygen Copper Barium Praseodymium Silver	224
Oxygen Copper Barium Praseodymium Yttrium	225
Oxygen Copper Barium Yttrium	226
Oxygen Copper Barium Yttrium Gallium	227
Oxygen Copper Barium Yttrium Nickel	228
Oxygen Copper Barium Yttrium Phosphorus	229
Oxygen Copper Barium Yttrium Praseodymium	230
Oxygen Copper Barium Yttrium Scandium	231
Oxygen Copper Bismuth Calcium Strontium	232
Oxygen Copper Bismuth Calcium Strontium Bromine	233
Oxygen Copper Calcium Barium Magnesium Thallium	234
Oxygen Copper Calcium Barium Thallium	235
Oxygen Copper Rhodium	236
Oxygen Copper Rhodium Magnesium	237
Oxygen Copper Strontium	238
Oxygen Copper Strontium Cobalt	239
Oxygen Copper Strontium Erbium Niobium Cerium	240
Oxygen Copper Strontium Gadolinium Ruthenium	241
Oxygen Copper Strontium Gadolinium Ruthenium Niobium	242
Oxygen Copper Strontium Gadolinium Ruthenium Tin	243
Oxygen Copper Strontium Holmium Niobium Cerium	244
Oxygen Copper Strontium Ruthenium Gadolinium Dysprosium	245
Oxygen Copper Strontium Ruthenium Gadolinium Yttrium	246

Oxygen Copper Strontium Terbium Niobium Cerium	247
Oxygen Europium Zirconium	248
Oxygen Iron Barium	249
Oxygen Iron Barium Antimony	250
Oxygen Iron Cobalt Lithium Antimony	251
Oxygen Iron Lithium Antimony	252
Oxygen Iron Lithium Cobalt Antimony	253
Oxygen Lanthanum Chromium Manganese Calcium	254
Oxygen Lanthanum Copper	255
Oxygen Lanthanum Copper Magnesium Strontium	256
Oxygen Lanthanum Copper Nickel	257
Oxygen Lanthanum Copper Strontium	258
Oxygen Lanthanum Copper Strontium Magnesium	259
Oxygen Lanthanum Copper Strontium Nickel	260
Oxygen Lanthanum Copper Strontium Titanium - 1	261
Oxygen Lanthanum Copper Strontium Titanium - 2	262
Oxygen Lanthanum Copper Strontium Zinc	263
Oxygen Lanthanum Copper Zinc	264
Oxygen Lanthanum Manganese Calcium Chromium	265
Oxygen Lanthanum Nickel Antimony	266
Oxygen Lanthanum Rhodium	267
Oxygen Lanthanum Rhodium Nickel	268
Oxygen Lanthanum Strontium Copper Titanium	269
Oxygen Manganese Calcium Lanthanum	270
Oxygen Manganese Lanthanum	271
Oxygen Manganese Lanthanum Barium Calcium	272
Oxygen Manganese Lanthanum Calcium - 1	273
Oxygen Manganese Lanthanum Calcium - 2	274
Oxygen Manganese Lanthanum Calcium Aluminium	275
Oxygen Manganese Lanthanum Calcium Barium	276
Oxygen Manganese Lanthanum Calcium Chromium	277
Oxygen Manganese Lanthanum Calcium Gallium	278
Oxygen Manganese Lanthanum Calcium Iron	279
Oxygen Manganese Lanthanum Calcium Silver Barium	280
Oxygen Manganese Lanthanum Calcium Tellurium	281
Oxygen Manganese Lanthanum Calcium Titanium - 1	282
Oxygen Manganese Lanthanum Calcium Titanium - 2	283
Oxygen Manganese Lanthanum Lead	284
Oxygen Manganese Lanthanum Lead Silver	285
Oxygen Manganese Lanthanum Lithium	286
Oxygen Manganese Lanthanum Potassium	287
Oxygen Manganese Lanthanum Rubidium	288
Oxygen Manganese Lanthanum Silver Calcium Barium	289
Oxygen Manganese Lanthanum Sodium	290

Oxygen Manganese Lanthanum Zinc	291
Oxygen Manganese Silver Lanthanum Barium Calcium	292
Oxygen Manganese Silver Lanthanum Calcium Barium	293
Oxygen Manganese Strontium Lanthanum	294
Oxygen Manganese Strontium Lanthanum Praseodymium	295
Oxygen Manganese Strontium Praseodymium	296
Oxygen Manganese Strontium Praseodymium Chromium	297
Oxygen Manganese Strontium Praseodymium Lanthanum	298
Oxygen Neodymium Copper Cerium	299
Oxygen Osmium Potassium	300
Oxygen Palladium Calcium Copper Sodium	301
Oxygen Rhodium Calcium Sodium	302
Oxygen Rhodium Sodium Calcium	303
Oxygen Rhodium Strontium	304
Oxygen Samarium Copper Cerium	305
Oxygen Samarium Copper Cerium Selenium	306
Oxygen Samarium Copper Selenium Cerium	307
Oxygen Strontium Arsenic Chromium Iron	308
Oxygen Strontium Arsenic Iron Scandium	309
Oxygen Strontium Arsenic Nickel Scandium	310
Oxygen Strontium Iron Phosphorus Scandium	311
Oxygen Strontium Nickel Phosphorus Scandium	312
Oxygen Strontium Rhodium	313
Oxygen Strontium Titanium	314
Oxygen Titanium Barium Calcium Silicon Lanthanum	315
Oxygen Titanium Barium Erbium	316
Oxygen Titanium Barium Lanthanum	317
Oxygen Titanium Barium Silicon Lanthanum	318
Oxygen Titanium Barium Strontium	319
Oxygen Titanium Barium Strontium Manganese	320
Oxygen Titanium Copper Calcium	321
Oxygen Titanium Strontium Yttrium	322
Oxygen Tungsten Phosphorus Molybdenum Potassium	323
Oxygen Tungsten Phosphorus Potassium Cobalt	324
Oxygen Tungsten Phosphorus Potassium Molybdenum - 1	325
Oxygen Tungsten Phosphorus Potassium Molybdenum - 2	326
Oxygen Tungsten Phosphorus Potassium Molybdenum - 3	327
Oxygen Tungsten Phosphorus Potassium Rubidium	328
Oxygen Tungsten Phosphorus Potassium Tin	329
Oxygen Tungsten Phosphorus Potassium Tin Iron	330
Oxygen Vanadium Tungsten	331
Oxygen Zinc	332
Oxygen Zinc Calcium Barium Copper Thallium	333
Oxygen Zinc Iron	334

Oxygen Zinc Nickel	335
Platinum	336
Platinum Uranium	337
Platinum Uranium Gadolinium	338
Platinum Uranium Yttrium	339
Rhenium	340
Rhodium Sulphur	341
Rhodium Sulphur Iridium	342
Samarium	343
Selenium Bromine	344
Selenium Chromium Mercury Copper	345
Selenium Copper Aluminium Cadmium	346
Selenium Copper Aluminium Zinc	347
Selenium Copper Germanium	348
Selenium Copper Germanium Manganese	349
Selenium Iodine	350
Selenium Molybdenum Lanthanum	351
Silicon Carbon Copper	352
Silicon Chromium	353
Silicon Chromium Aluminium	354
Silicon Germanium	355
Silicon Lanthanum Rhenium	356
Silicon Manganese Ruthenium	357
Silicon Rhenium Ruthenium	358
Silicon Rhenium Ruthenium Aluminium	359
Silicon Ruthenium Rhenium	360
Silicon Zirconium	361
Silicon Zirconium Copper	362
Silver Chromium	363
Sulphur Iron	364
Sulphur Iron Nickel	365
Sulphur Molybdenum Lanthanum	366
Sulphur Tantalum Copper	367
Sulphur Tungsten	368
Sulphur Tungsten Rhenium	369
Sulphur Vanadium Iron	370
Sulphur Yttrium Aluminium	371
Tantalum	372
Tellurium Hafnium	373
Tellurium Lead Europium	374
Tellurium Zirconium	375
Tin Copper	376
Titanium	377
Titanium Vanadium Aluminium Chromium Tin	378
Tungsten	379

Resistivity – pressure effects

Aluminium Ytterbium	380
Arsenic Iron Barium - 1	381
Arsenic Iron Barium - 2	382
Arsenic Iron Barium Potassium	383
Arsenic Iron Europium	384
Arsenic Iron Lanthanum Oxygen	385
Arsenic Iron Lanthanum Oxygen Fluorine - 1	386
Arsenic Iron Lanthanum Oxygen Fluorine - 2	387
Arsenic Iron Neodymium Oxygen	388
Arsenic Rhodium Lanthanum	389
Beryllium	390
Erbium	391
Gadolinium - 1	392
Gadolinium - 2	393
Iron - 1	394
Iron - 2	395
Iron Lithium Phosphorus	396
Iron Selenium Tellurium	397
Nickel - 1	398
Nickel - 2	399
Nickel - 3	400
Nickel - 4	401
Oxygen Copper Barium Praseodymium - 1	402
Oxygen Copper Barium Praseodymium - 2	403
Oxygen Copper Barium Praseodymium - 3	404
Oxygen Copper Barium Yttrium Nickel	405
Oxygen Germanium	406
Oxygen Manganese Lanthanum	407
Oxygen Manganese Lanthanum Strontium Scandium	408
Oxygen Manganese Lanthanum Zinc	409
Oxygen Silver Sulphur - 1	410
Oxygen Silver Sulphur - 2	411
Oxygen Silver Sulphur Thallium - 1	412
Oxygen Silver Sulphur Thallium - 2	413
Oxygen Silver Sulphur Thallium - 3	414
Ruthenium Silicon Uranium - 1	415
Ruthenium Silicon Uranium - 2	416
Silicon Cerium Iridium	417
Tantalum	418
Thorium	419
Uranium - 1	420
Uranium - 2	421
Ytterbium	422

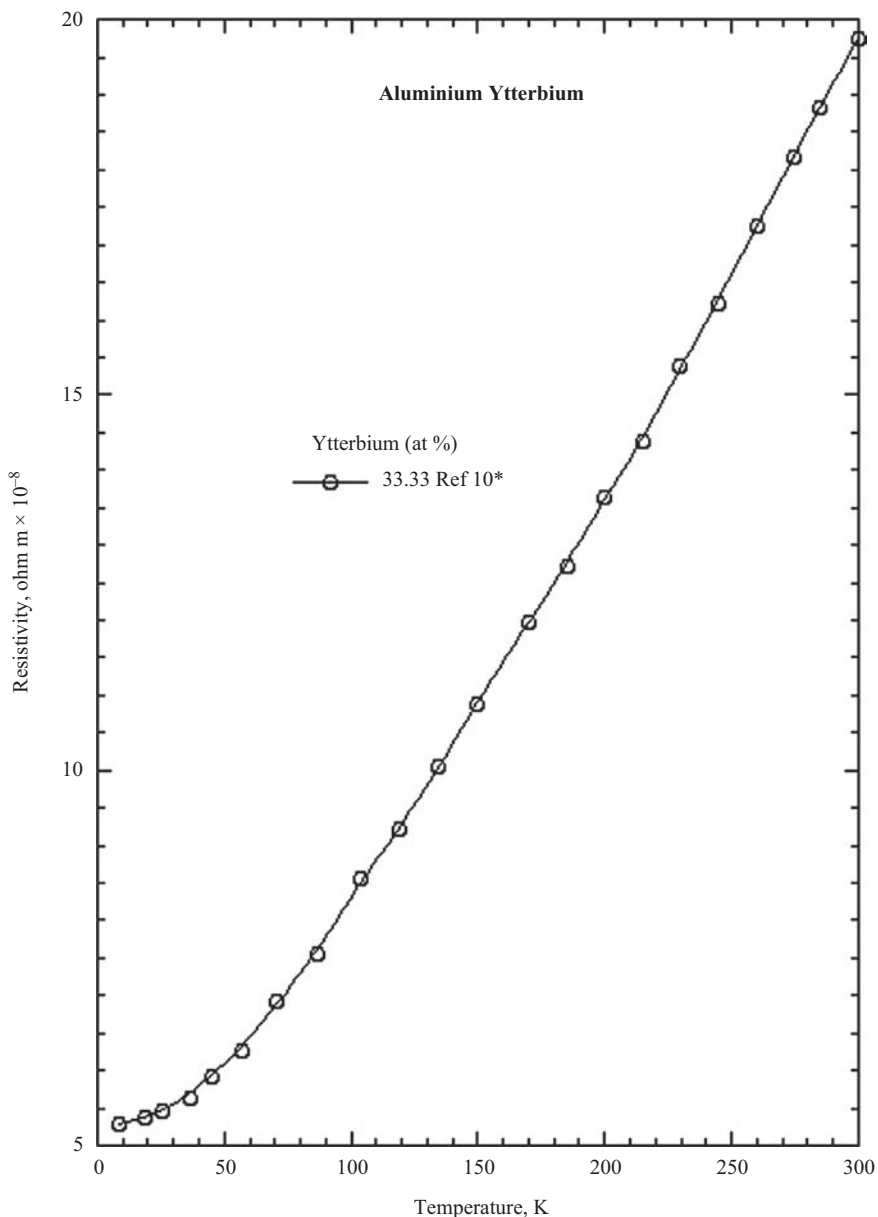
Zinc Cobalt Ytterbium	423
Zinc Iridium Ytterbium	424
Zinc Rhodium Ytterbium	425
Zirconium	426

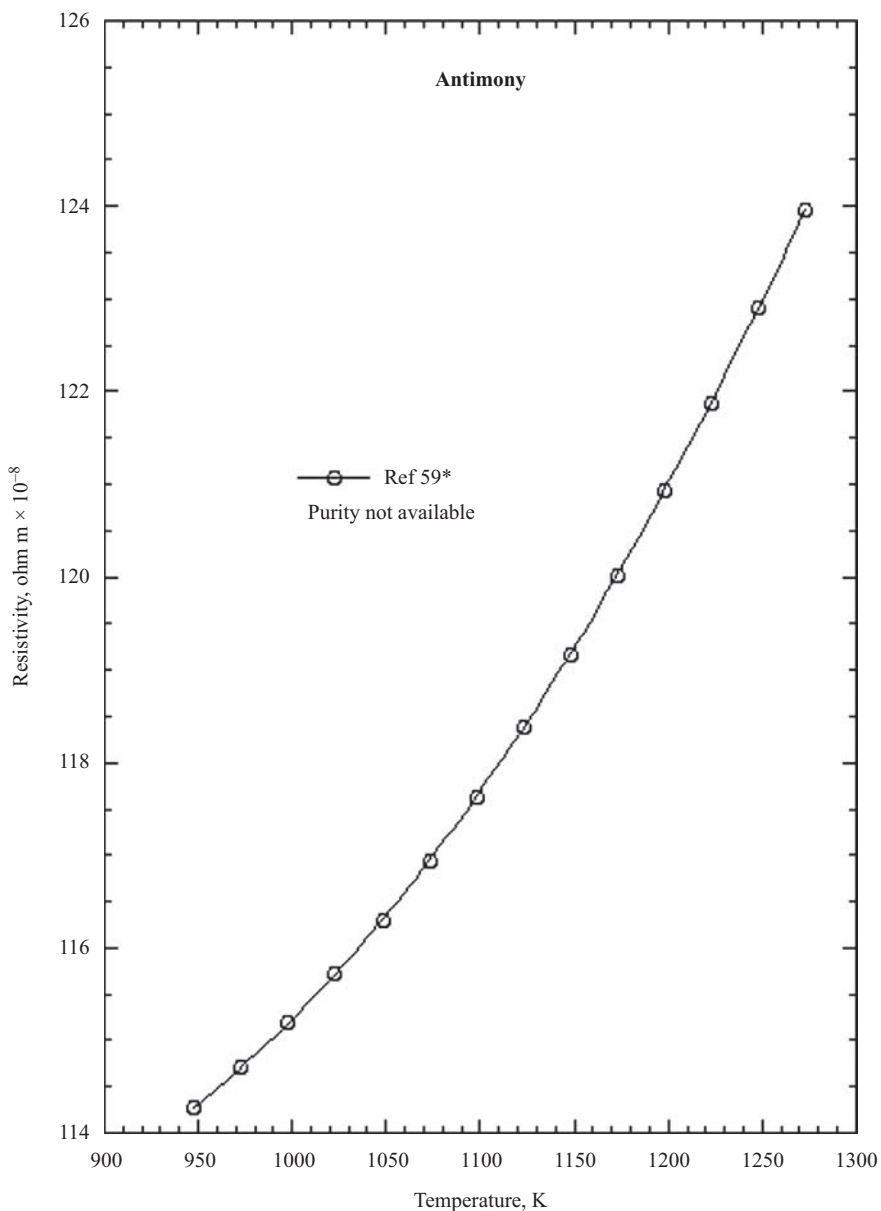
Normalised resistance, pressure and resistance effects

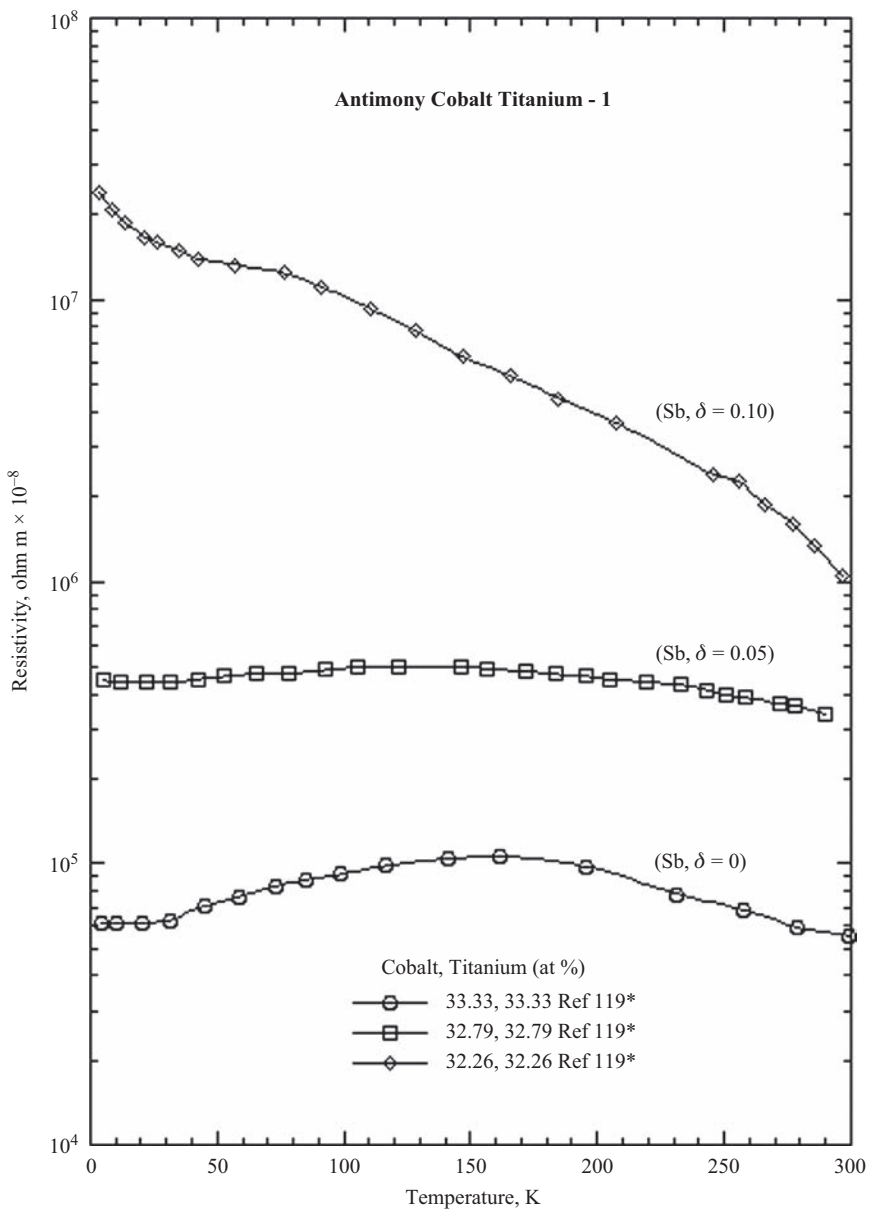
Barium	427
Bismuth	428
Calcium - 1	429
Calcium - 2	430
Calcium - 3	431
Deuterium, Hydrogen	432
Dysprosium - 1	433
Dysprosium - 2	434
Europium	435
Gadolinium	436
Nickel - 1	437
Nickel - 2	438
Nickel - 3	439
Oxygen Copper Barium Gadolinium Strontium	440
Oxygen Copper Barium Gadolinium Strontium Calcium	441
Oxygen Copper Barium Gadolinium Strontium Nickel	442
Oxygen Copper Barium Gadolinium Strontium Zinc	443
Oxygen Copper Barium Yttrium	444
Oxygen Copper Barium Yttrium Calcium Nickel	445
Oxygen Copper Barium Yttrium Calcium Zinc	446
Oxygen Copper Barium Yttrium Cobalt	447
Oxygen Copper Barium Yttrium Cobalt Gallium	448
Oxygen Copper Barium Yttrium Gallium	449
Praseodymium	450
Selenium - 1	451
Selenium - 2	452
Selenium Niobium	453
Selenium Niobium Vanadium	454
Silicon	455
Tellurium	456
Tellurium Bismuth Tin Iodine Antimony	457
Titanium	458
Zirconium	459

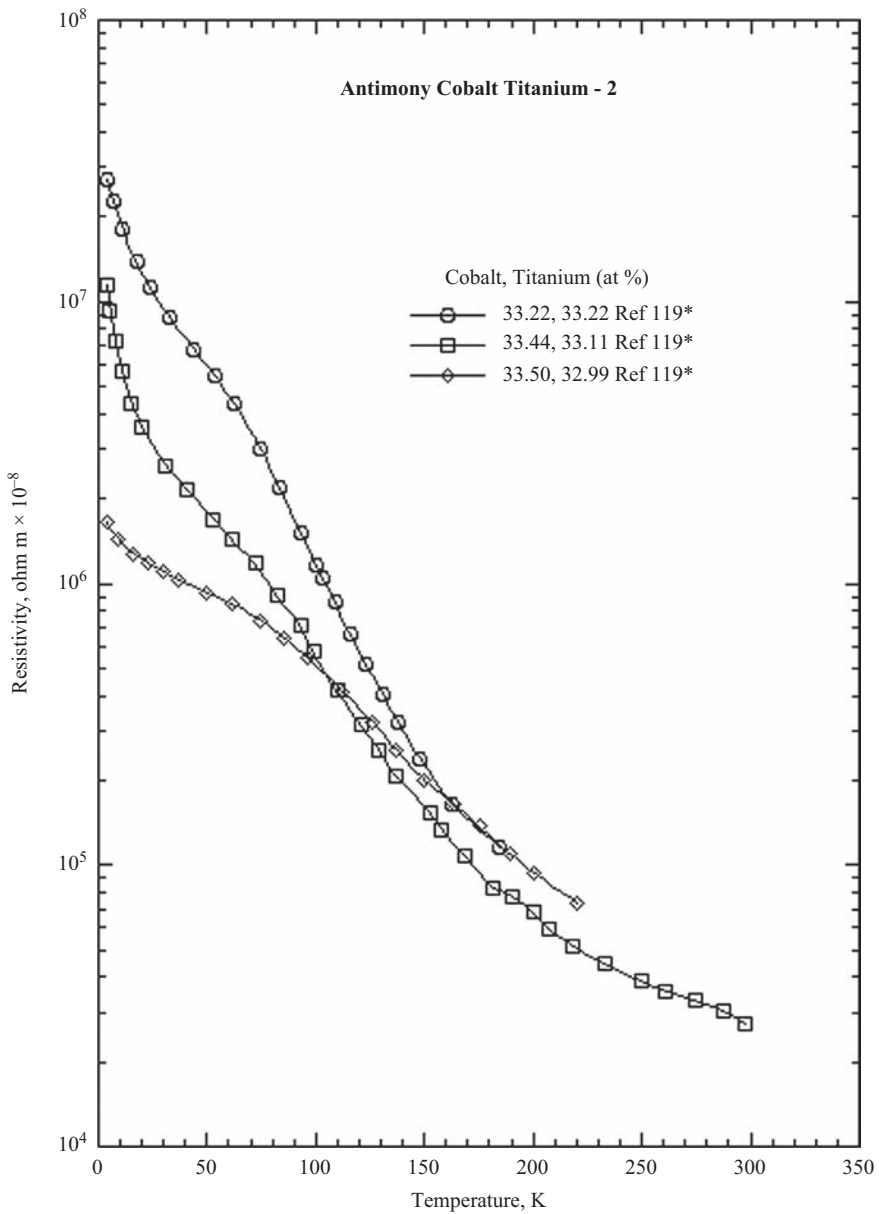
Chapter 6
Material resistivity graphs

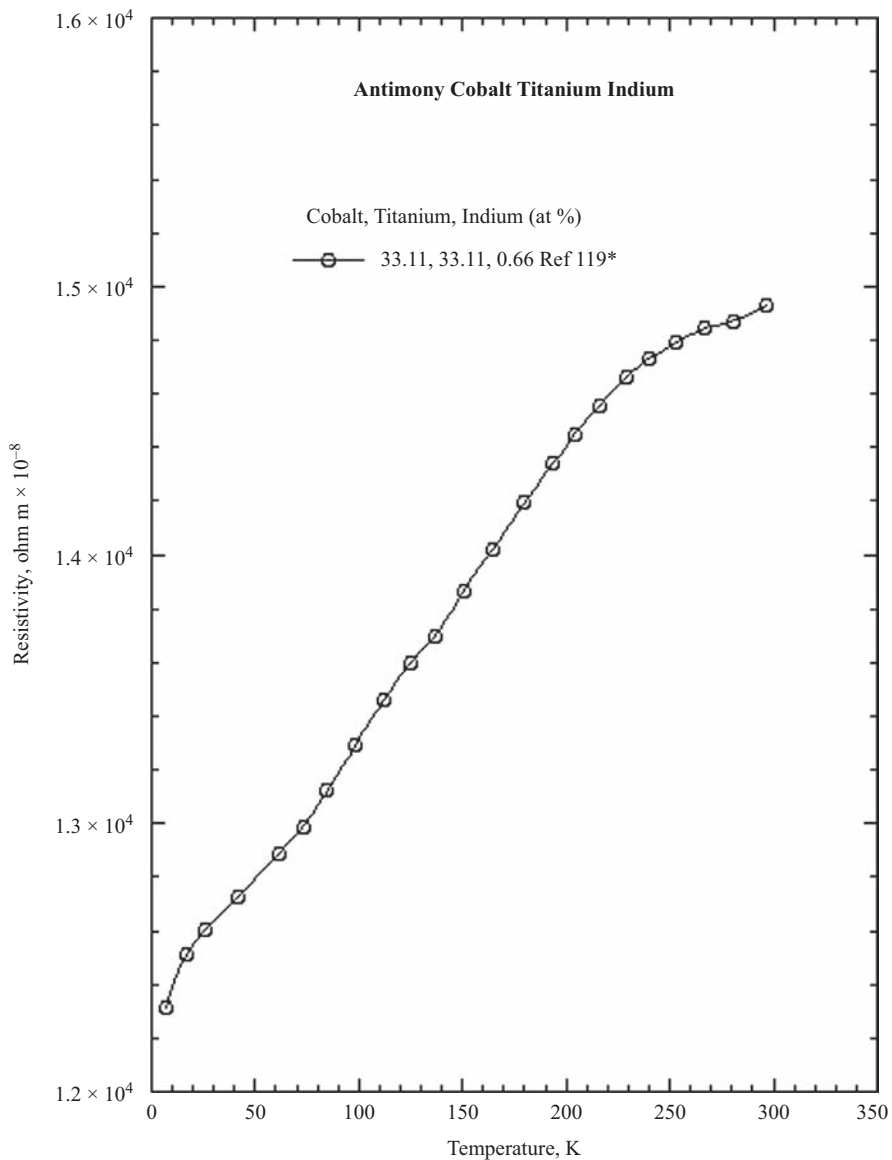
6.1 Electrical resistivity as a function of temperature

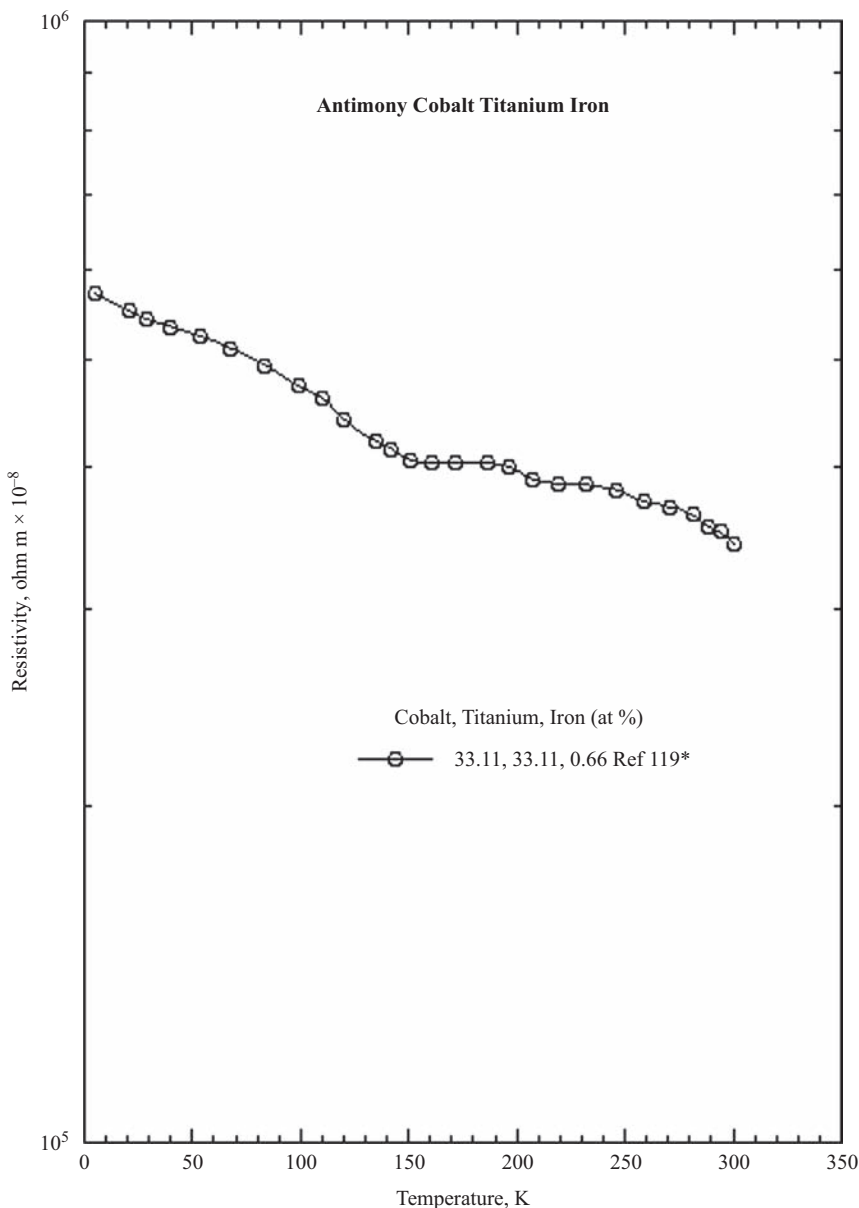


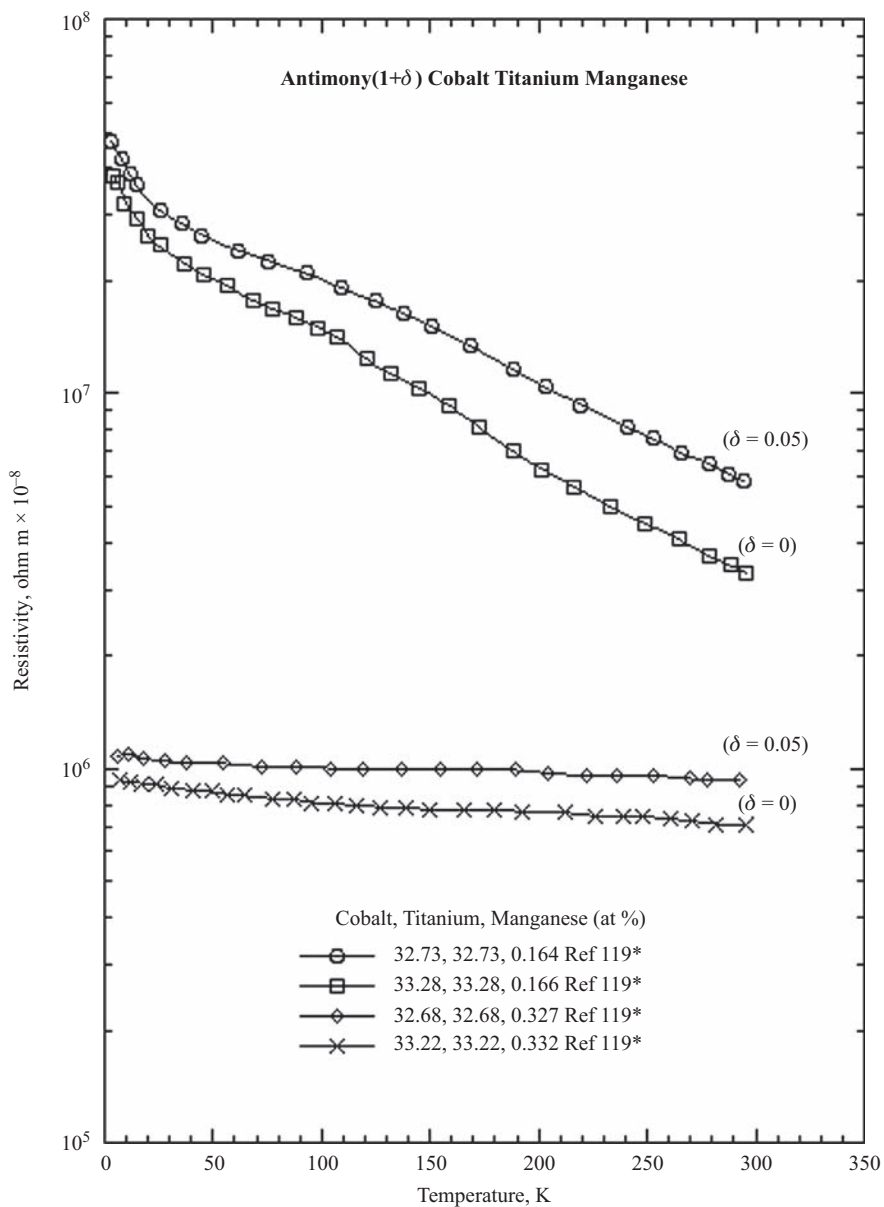


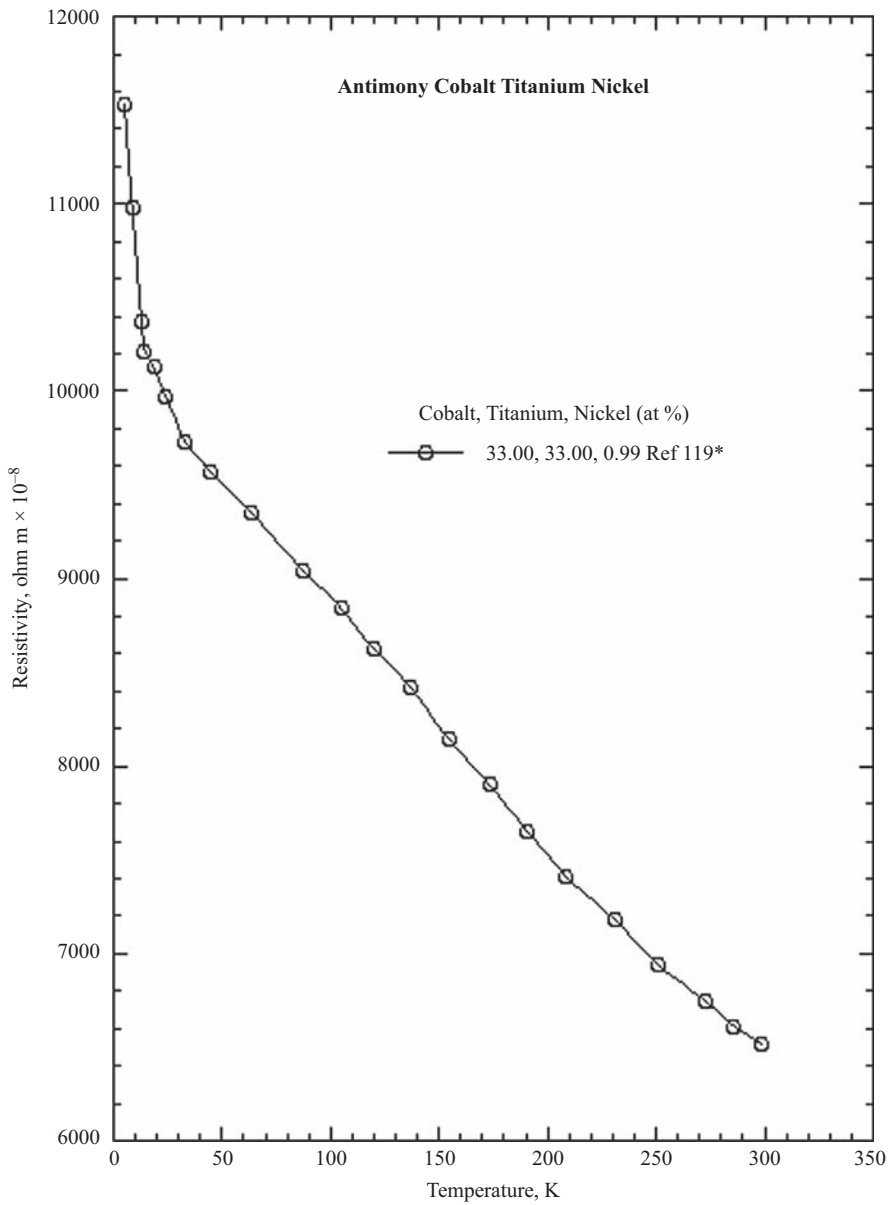


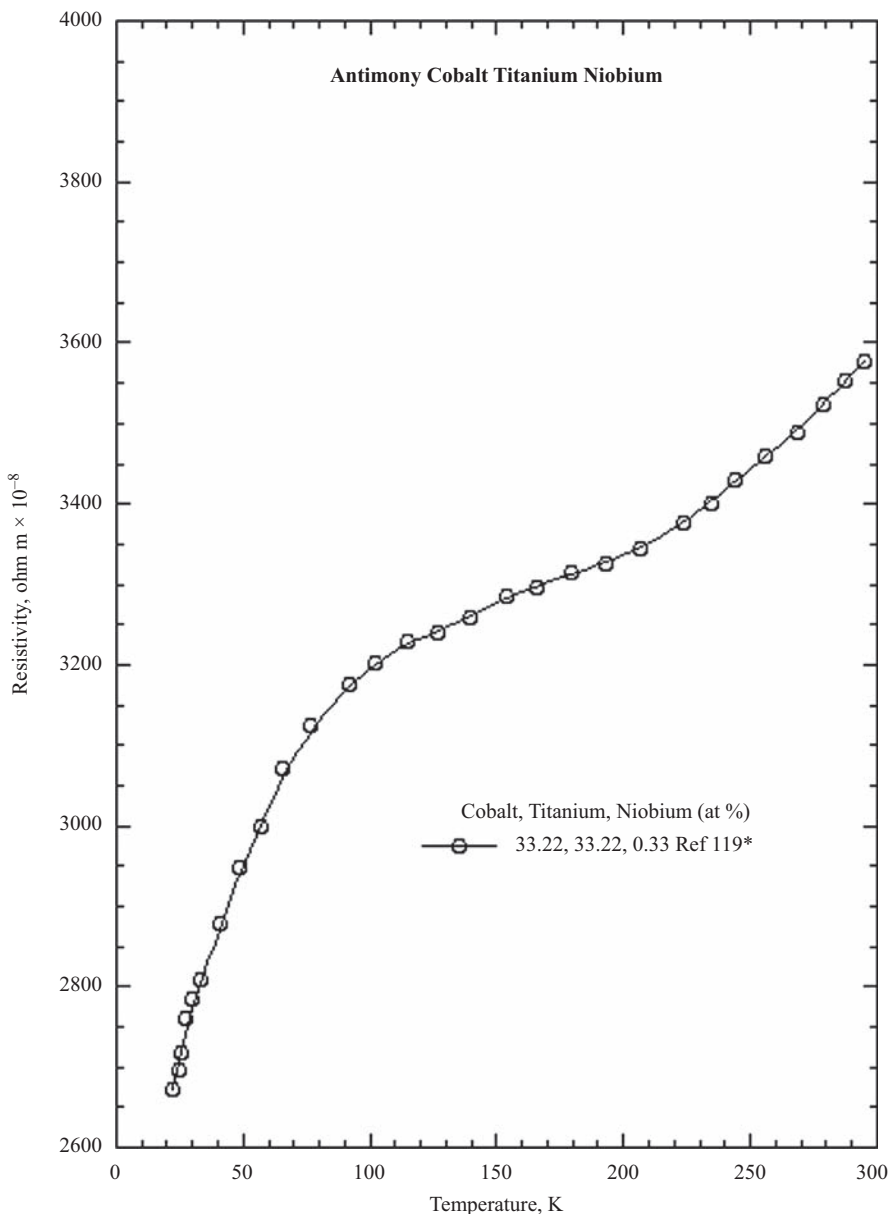


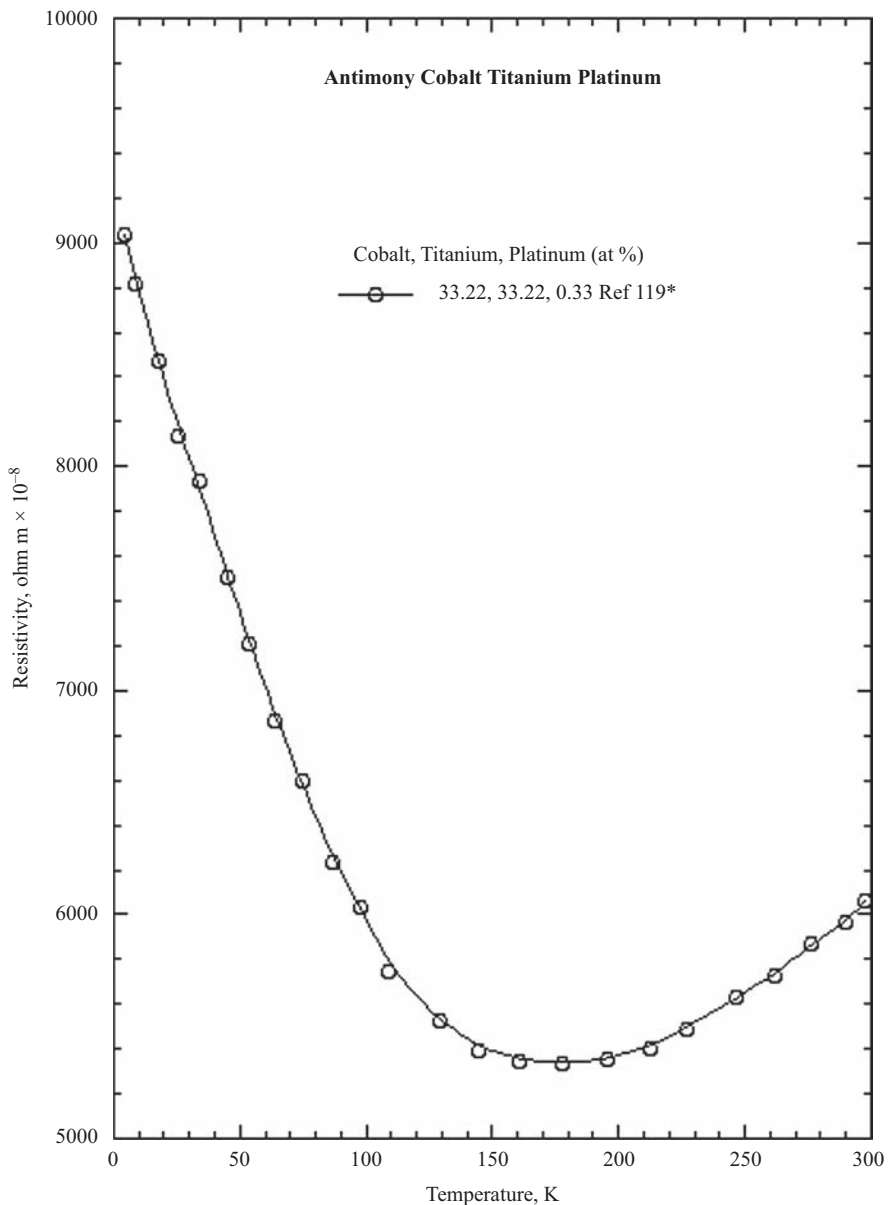


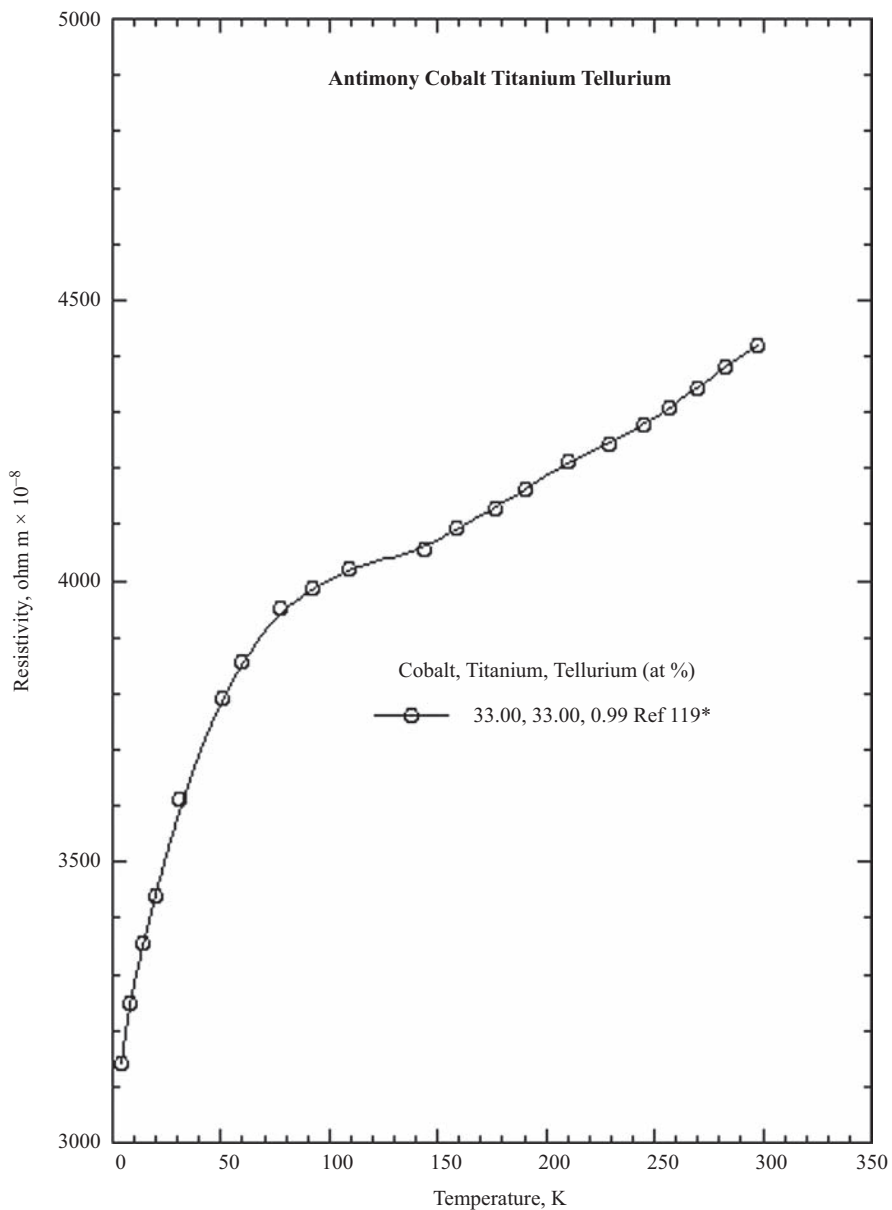


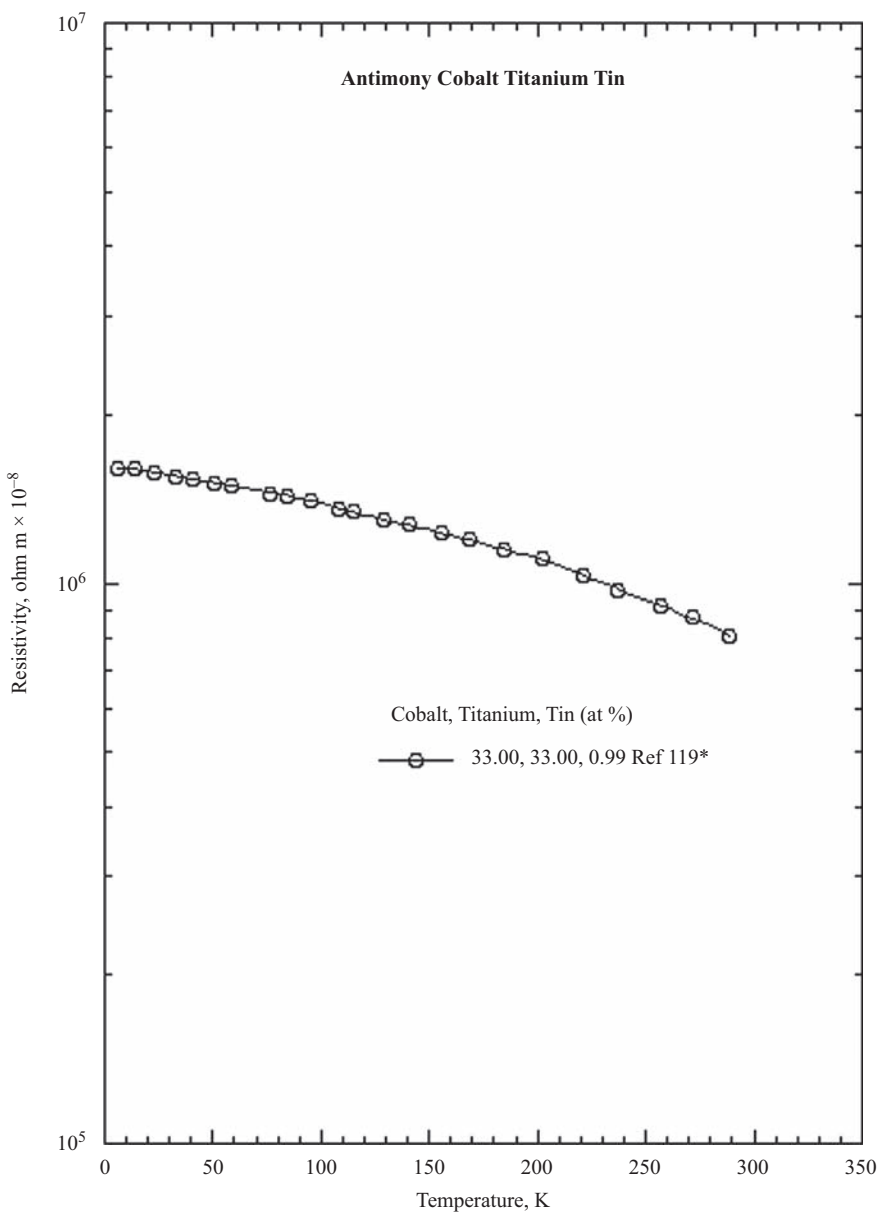


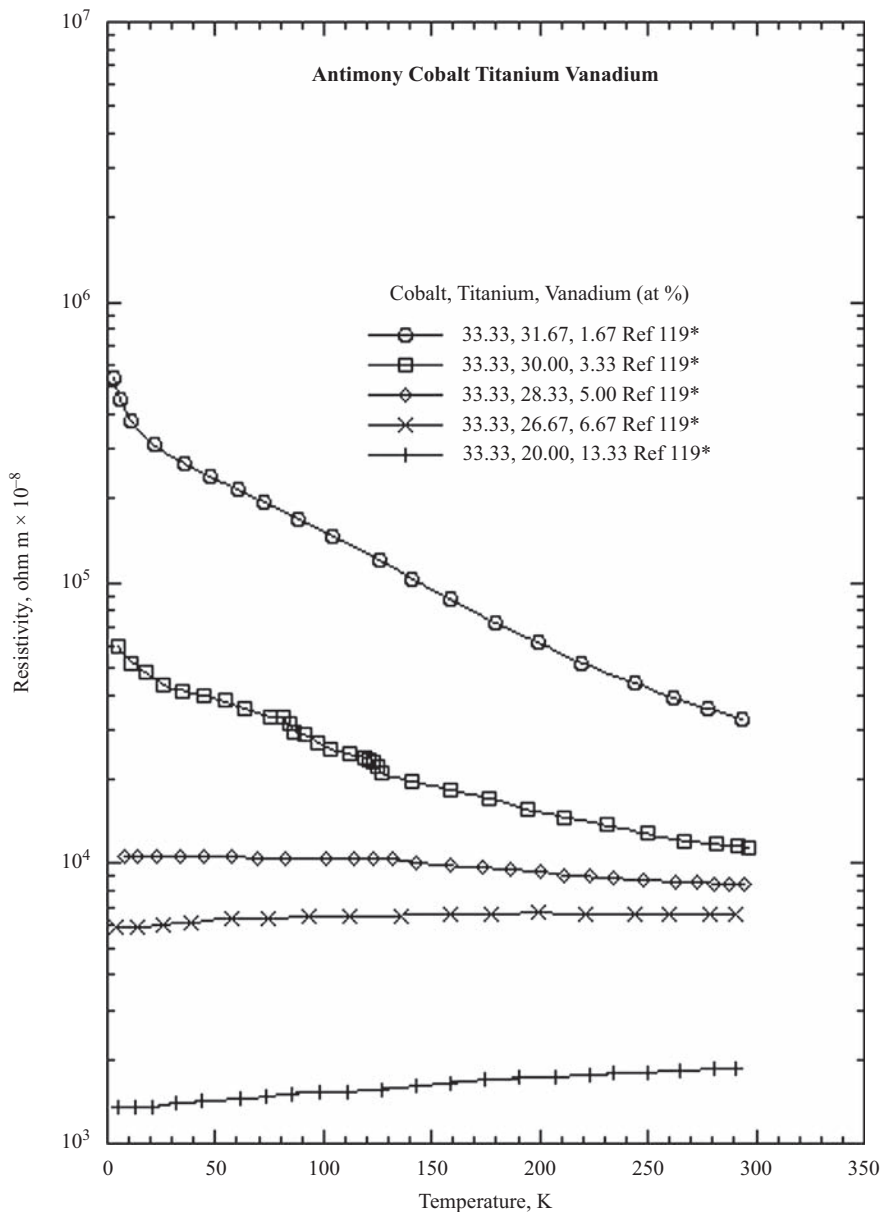


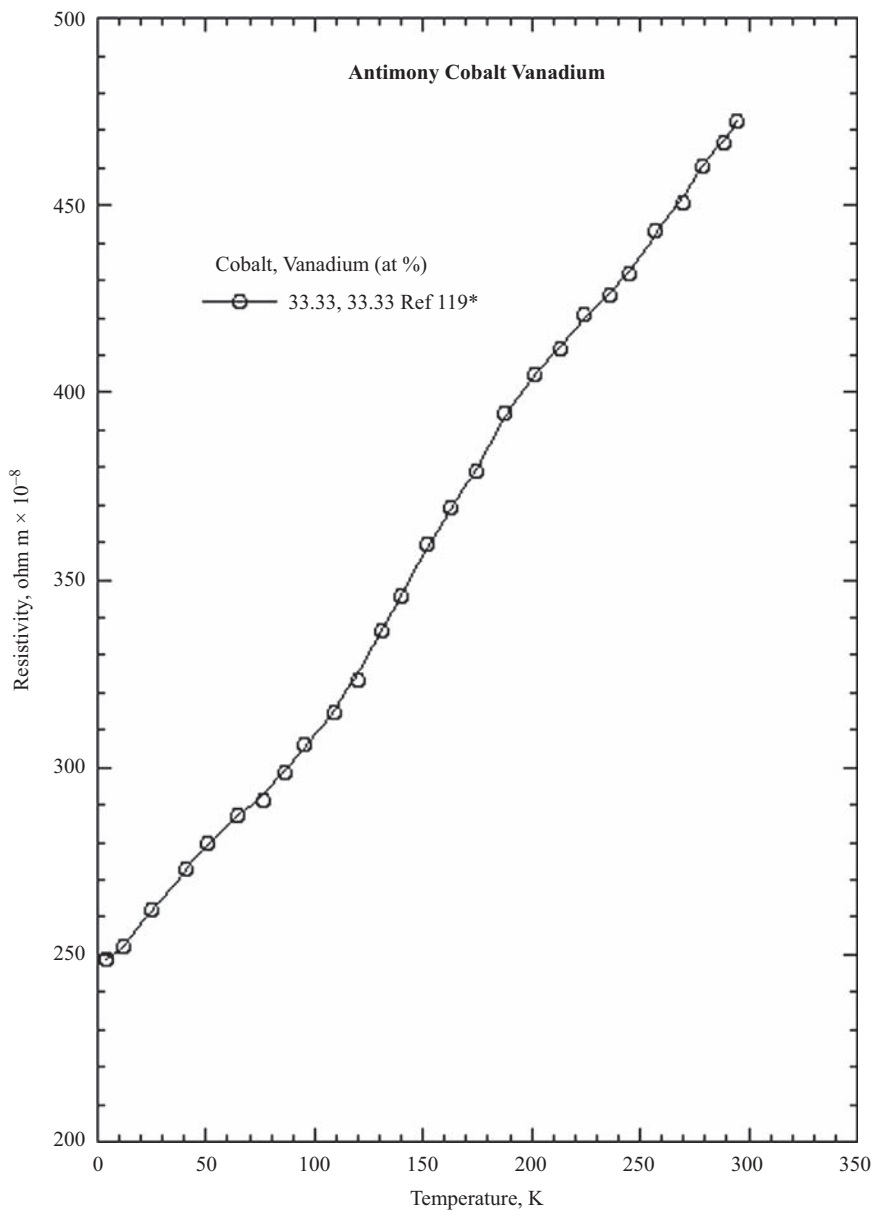


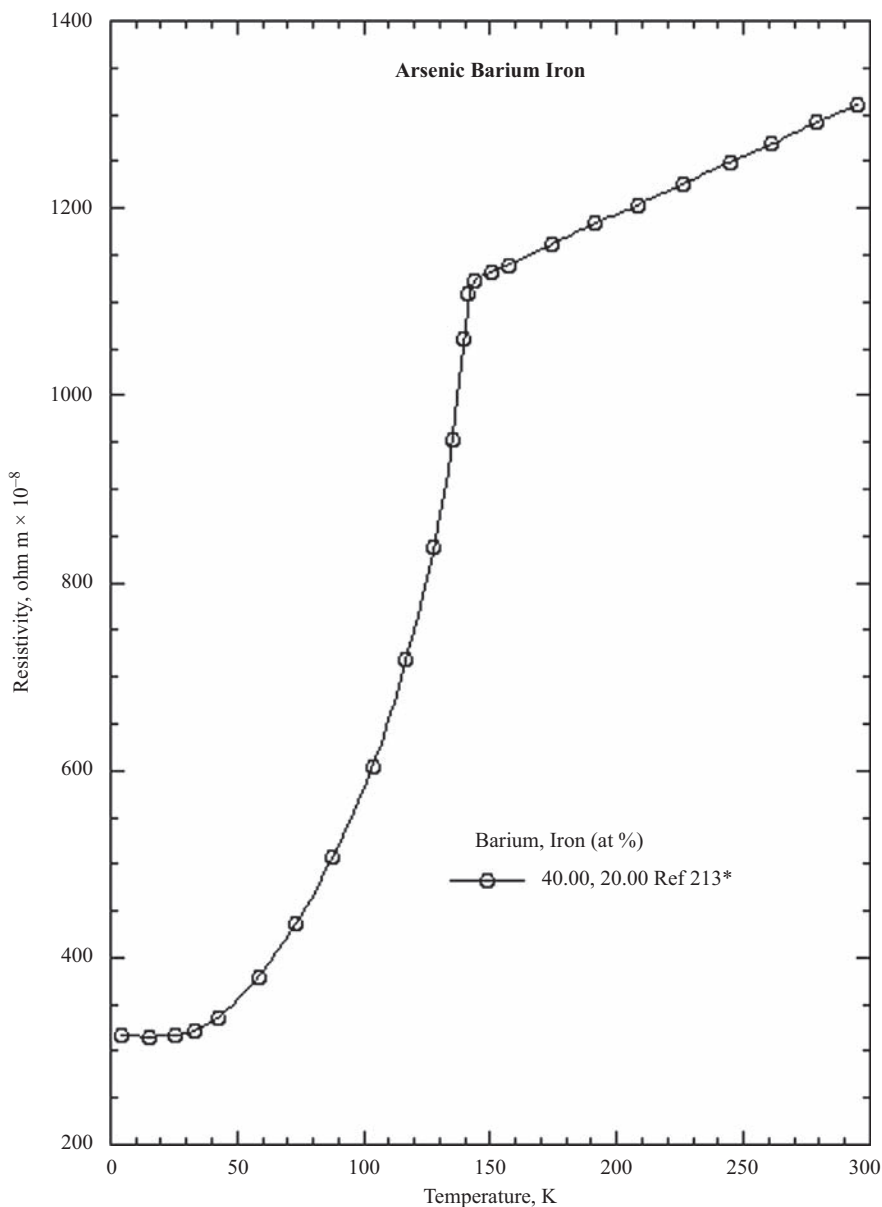


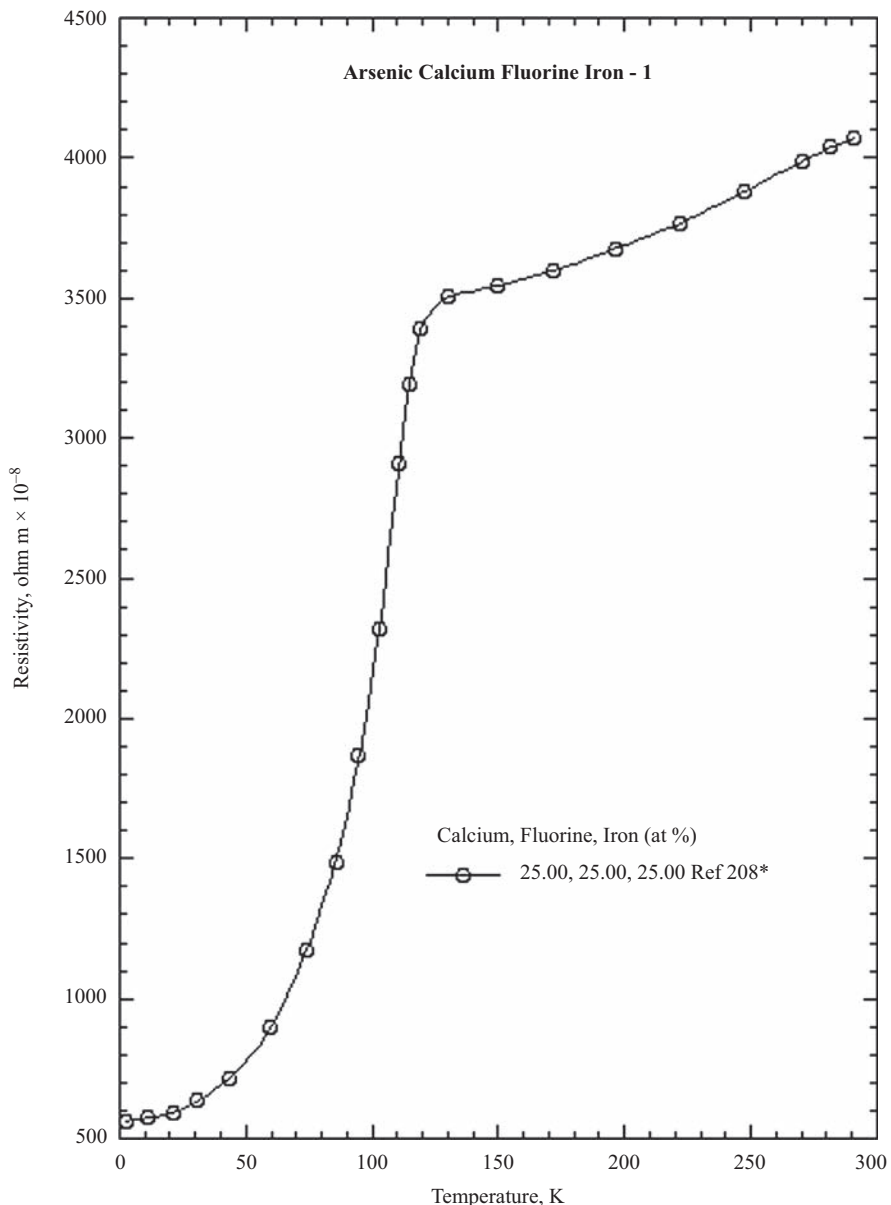


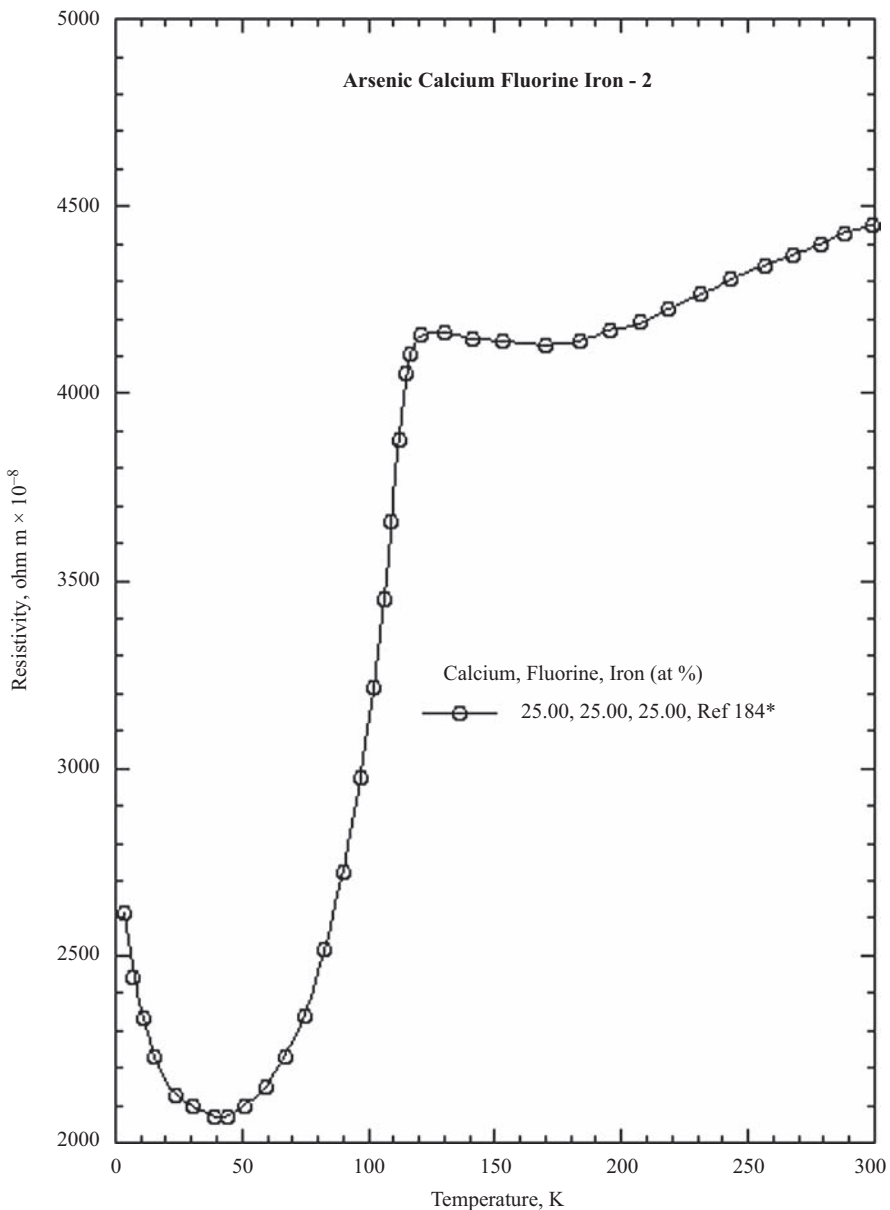


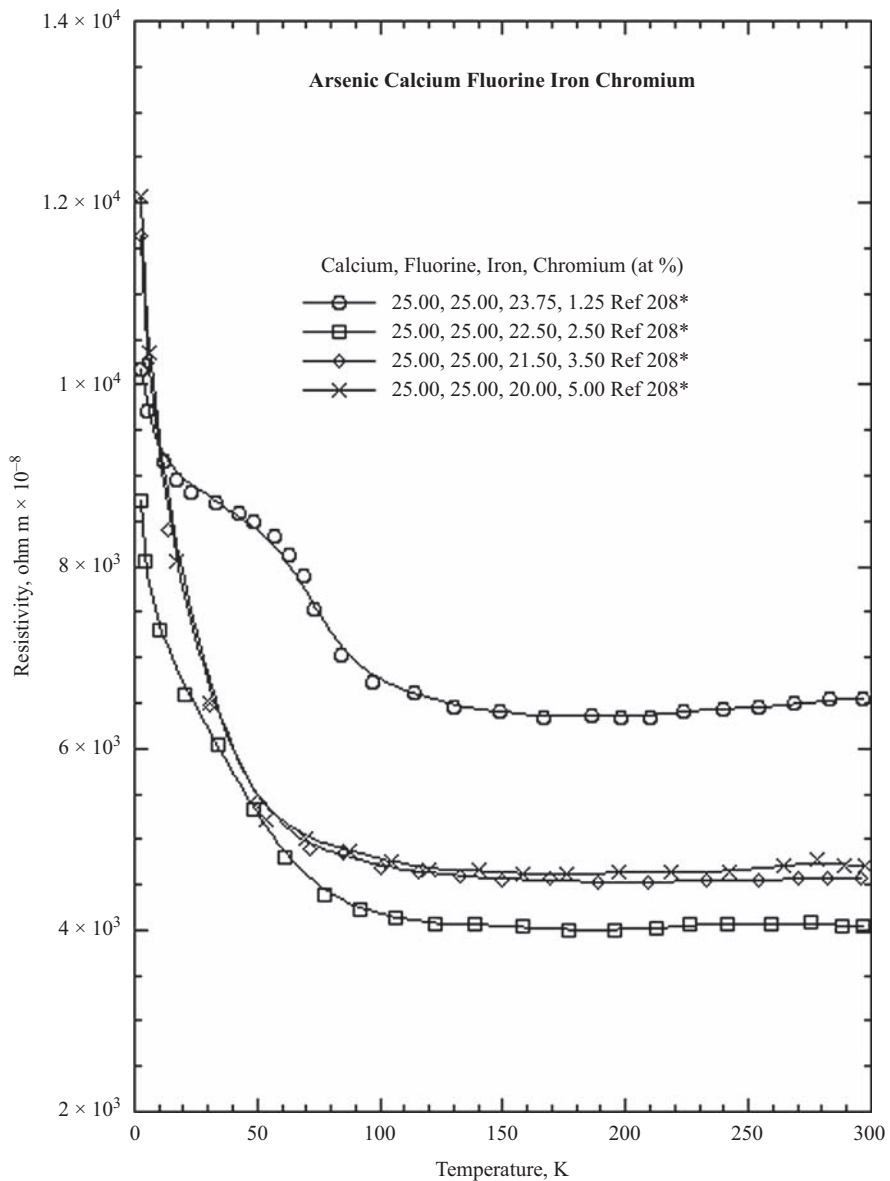


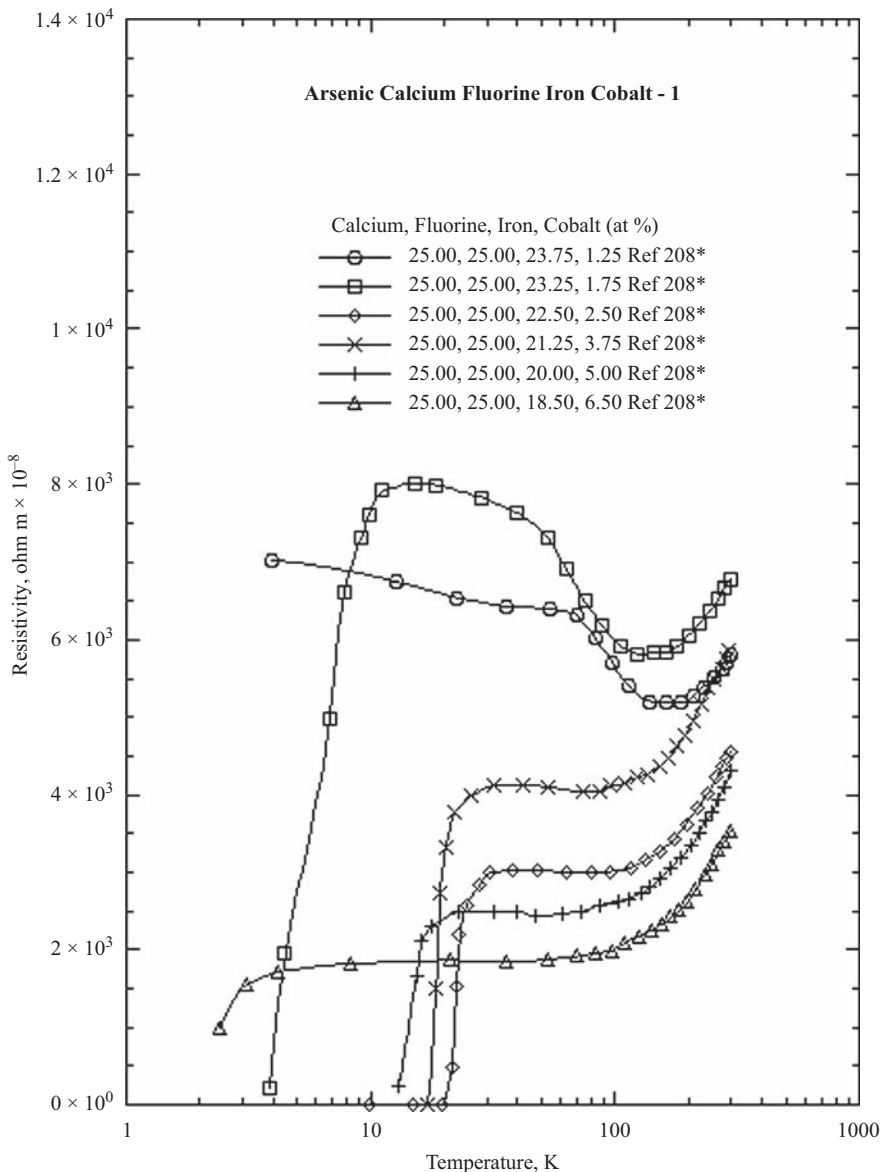


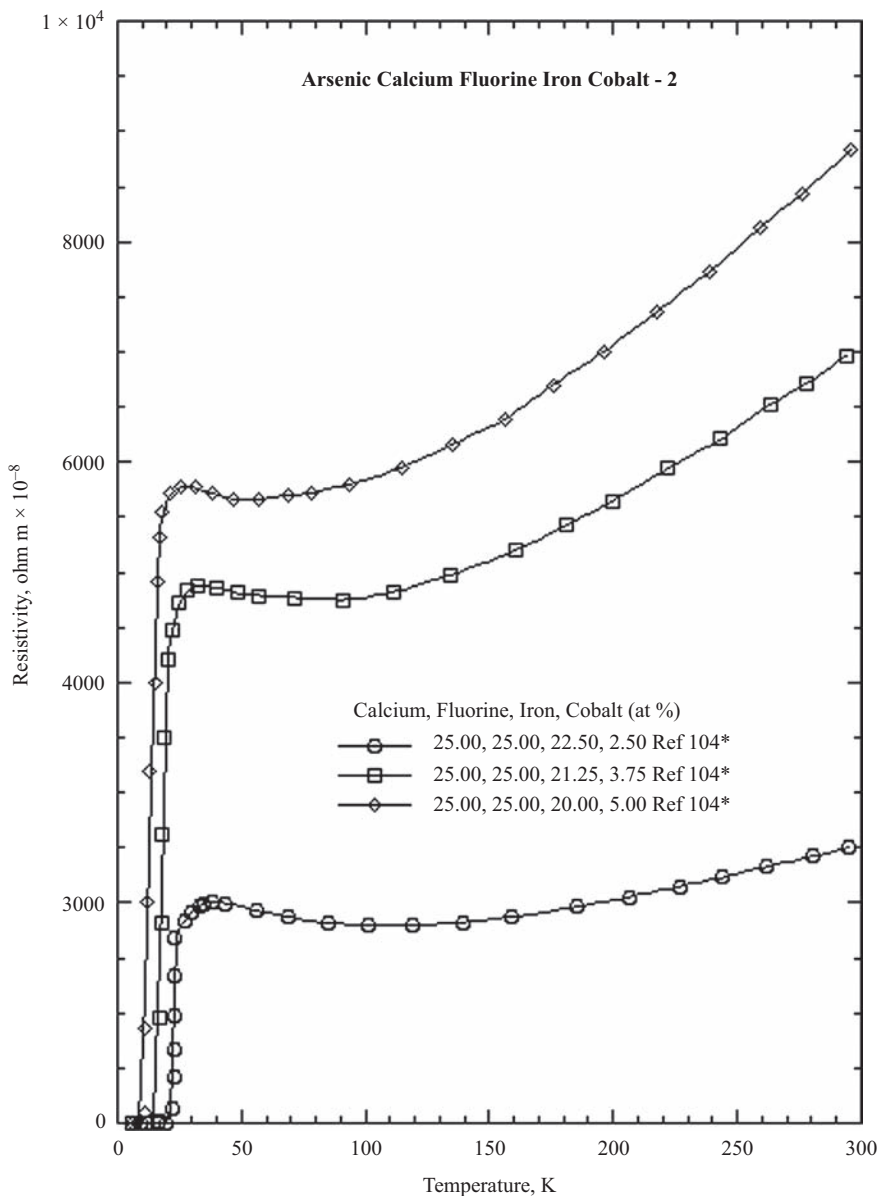


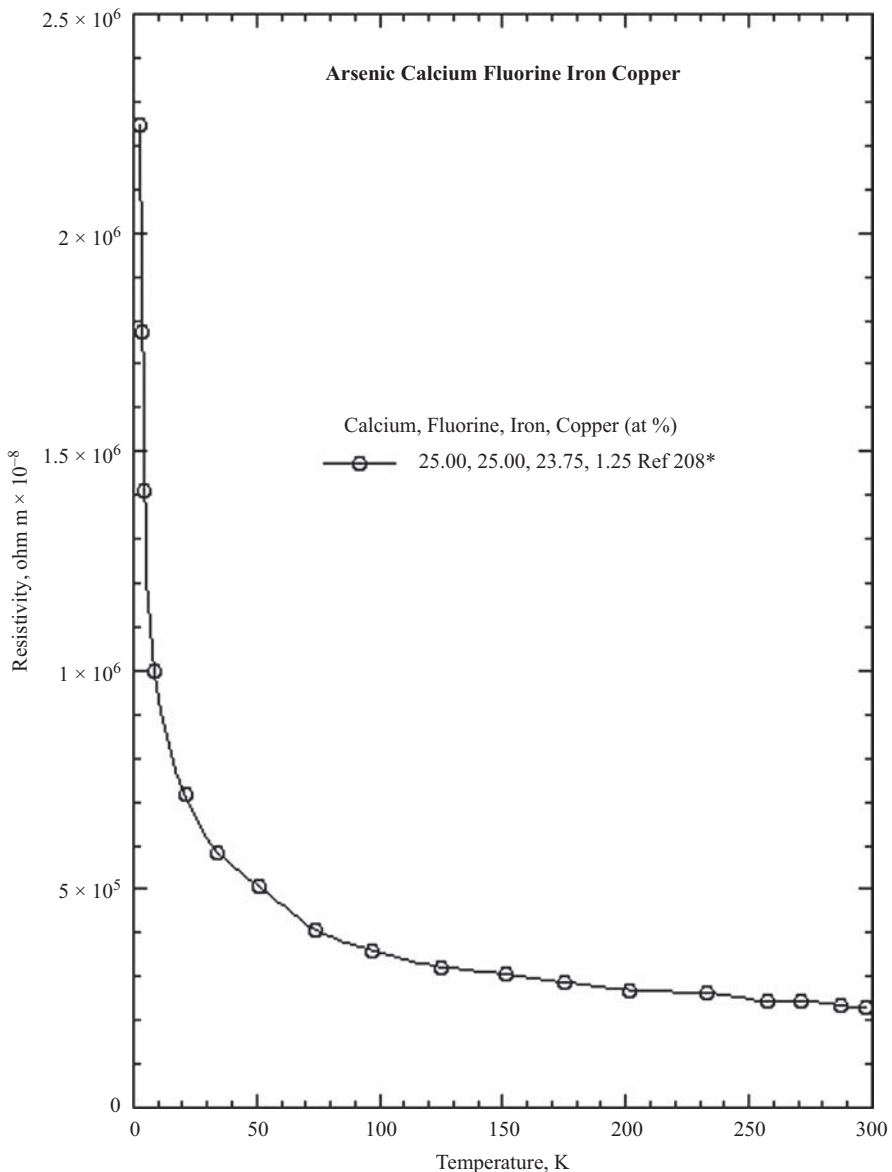


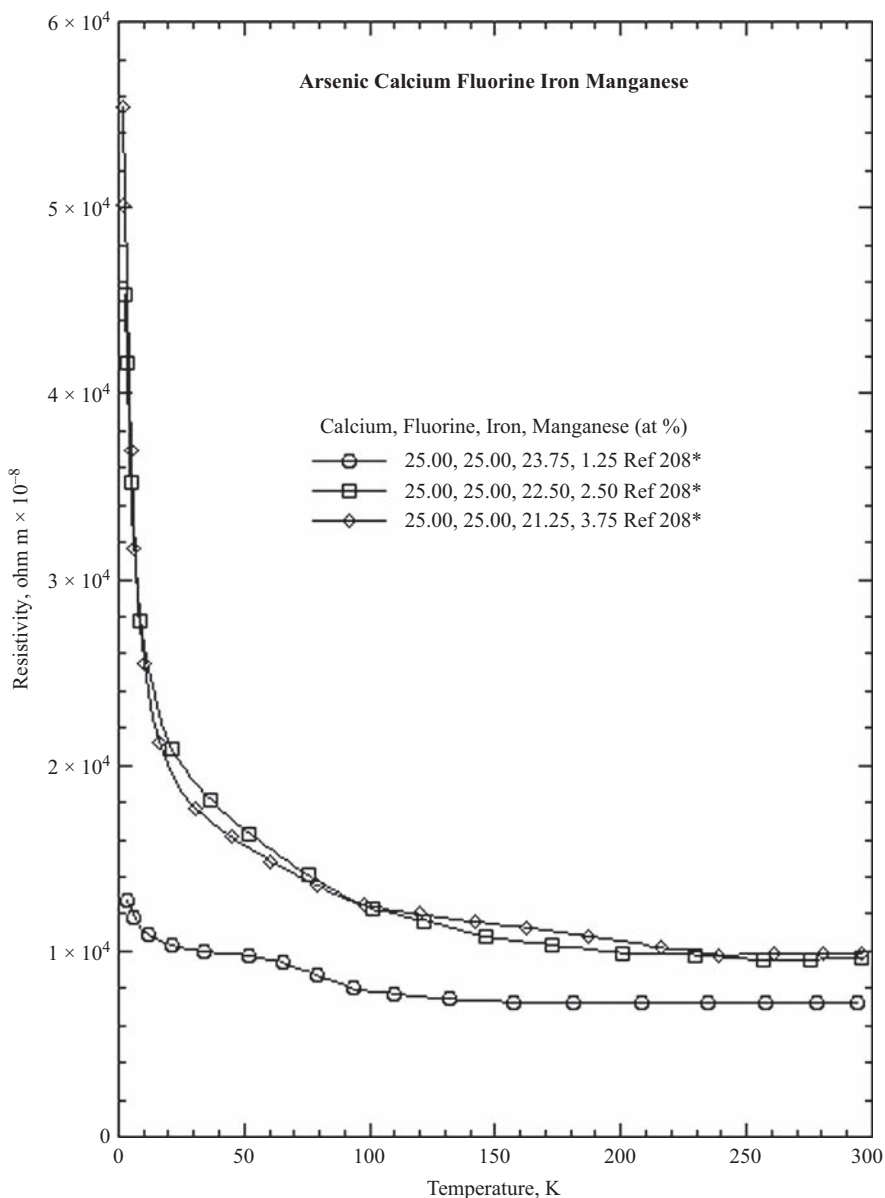


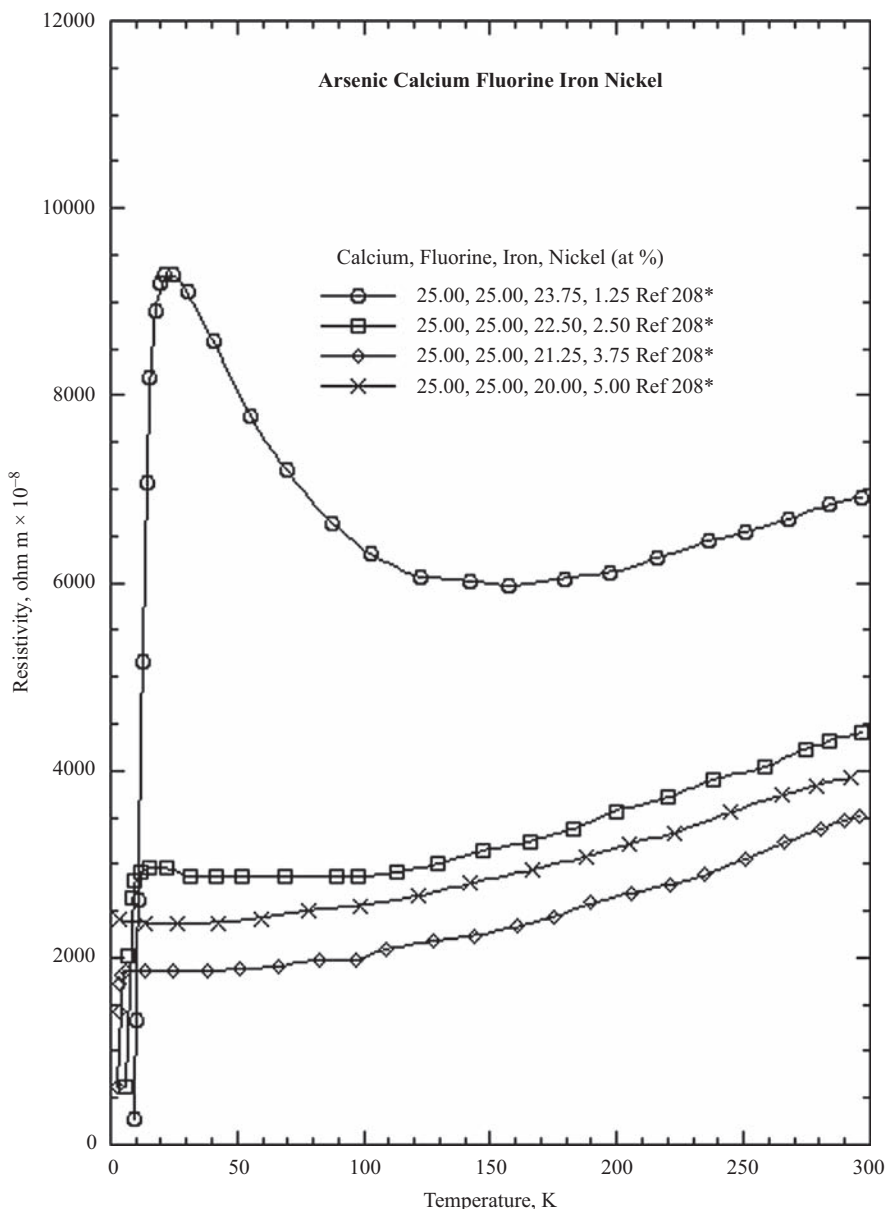


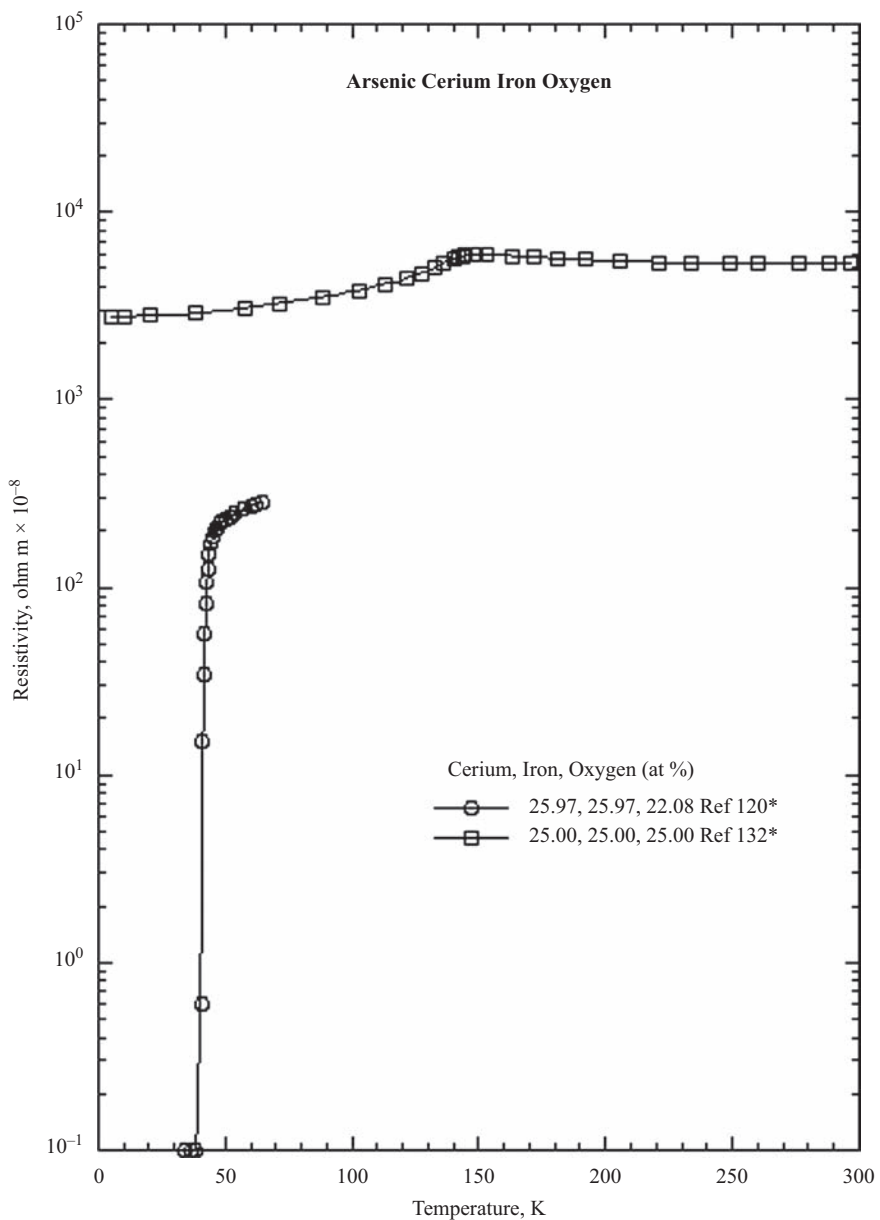


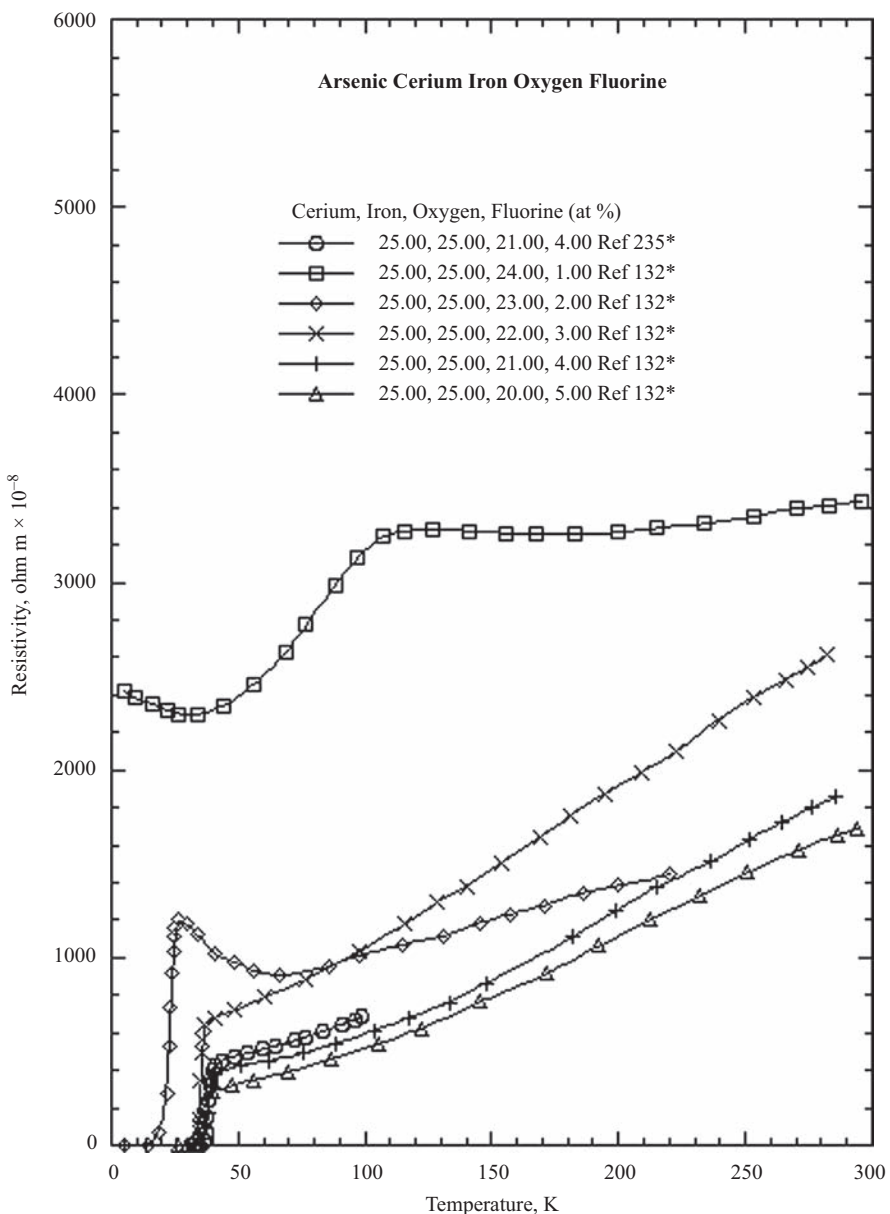


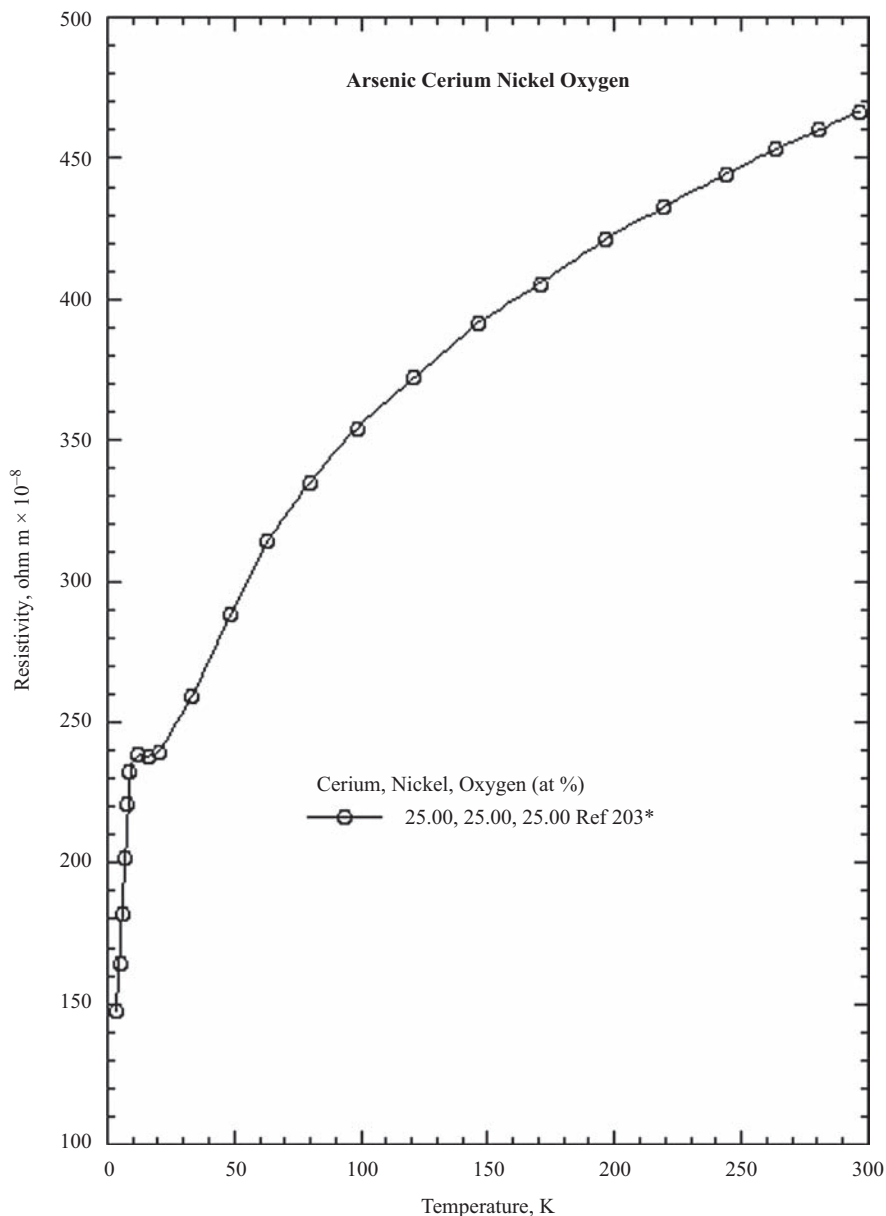


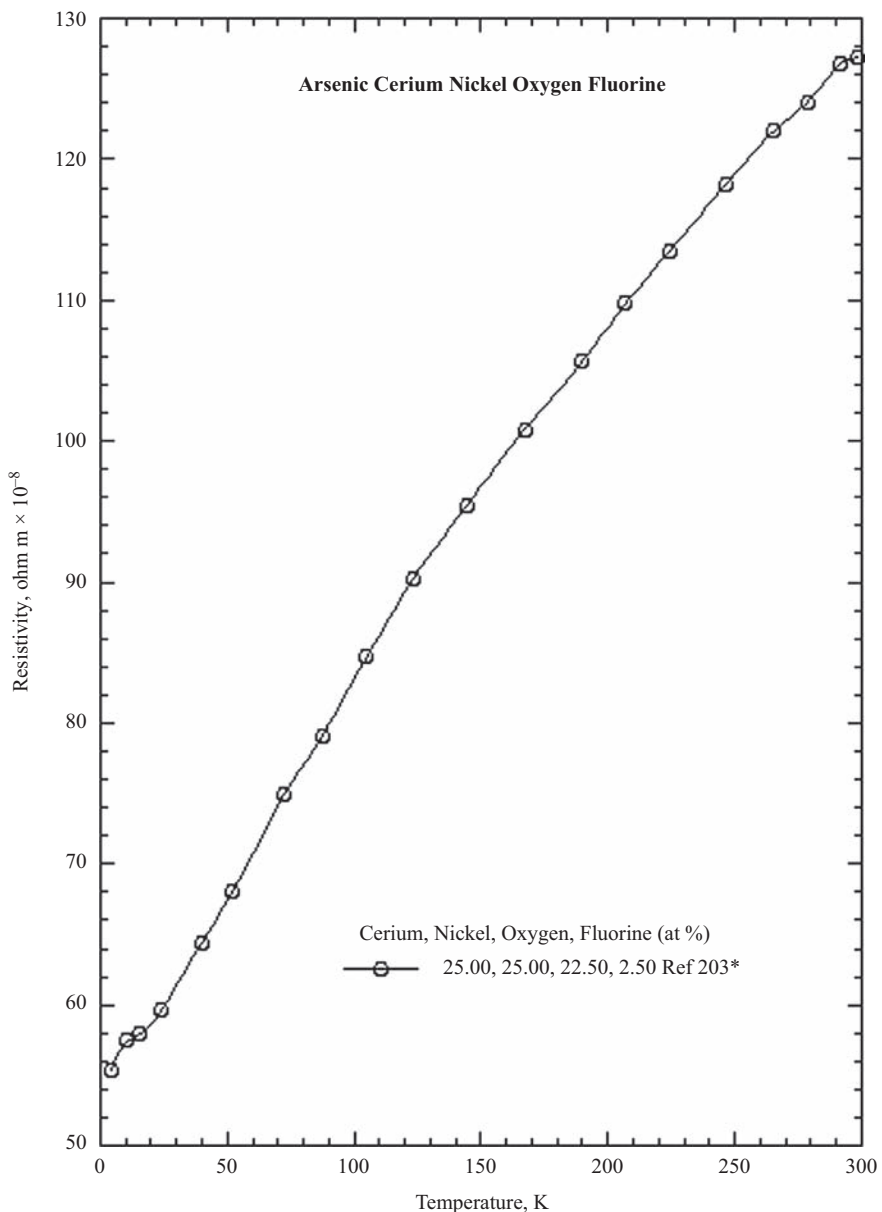


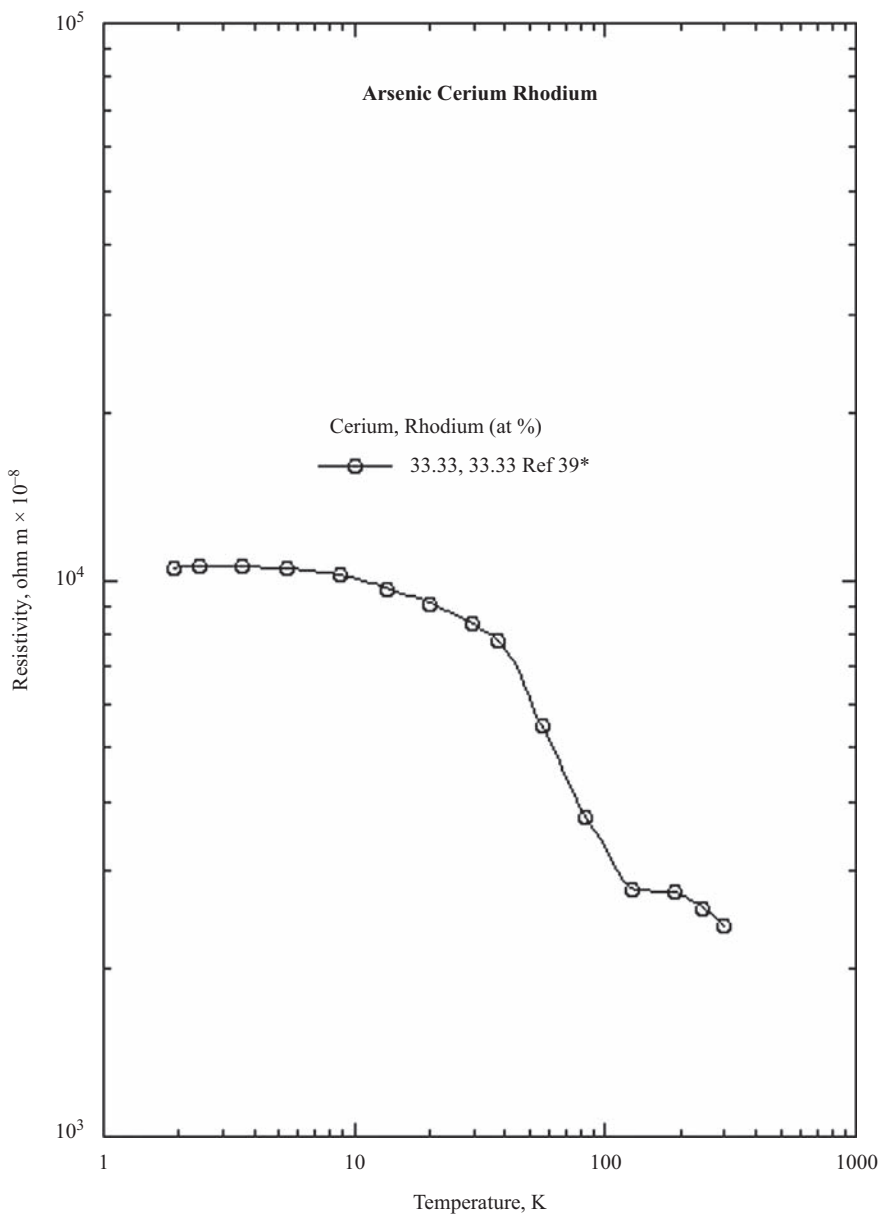


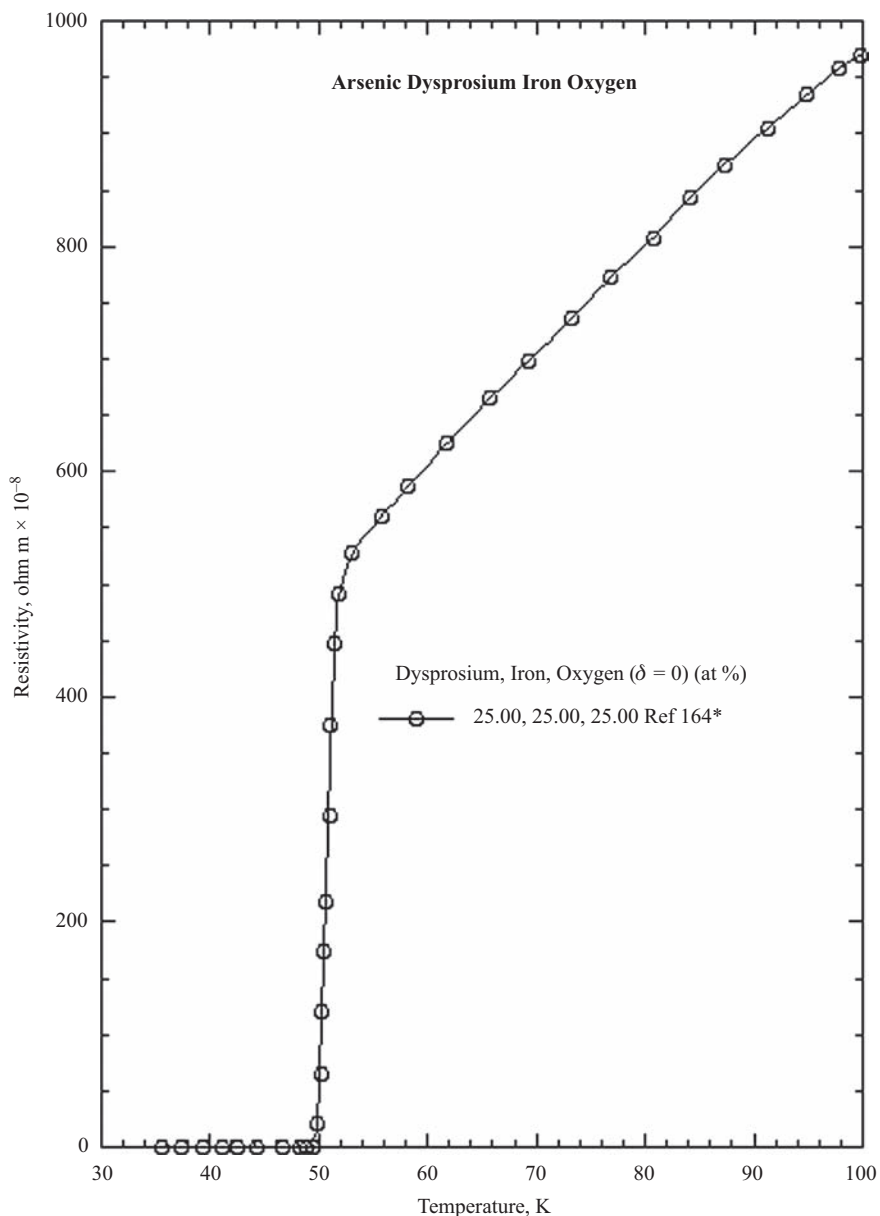


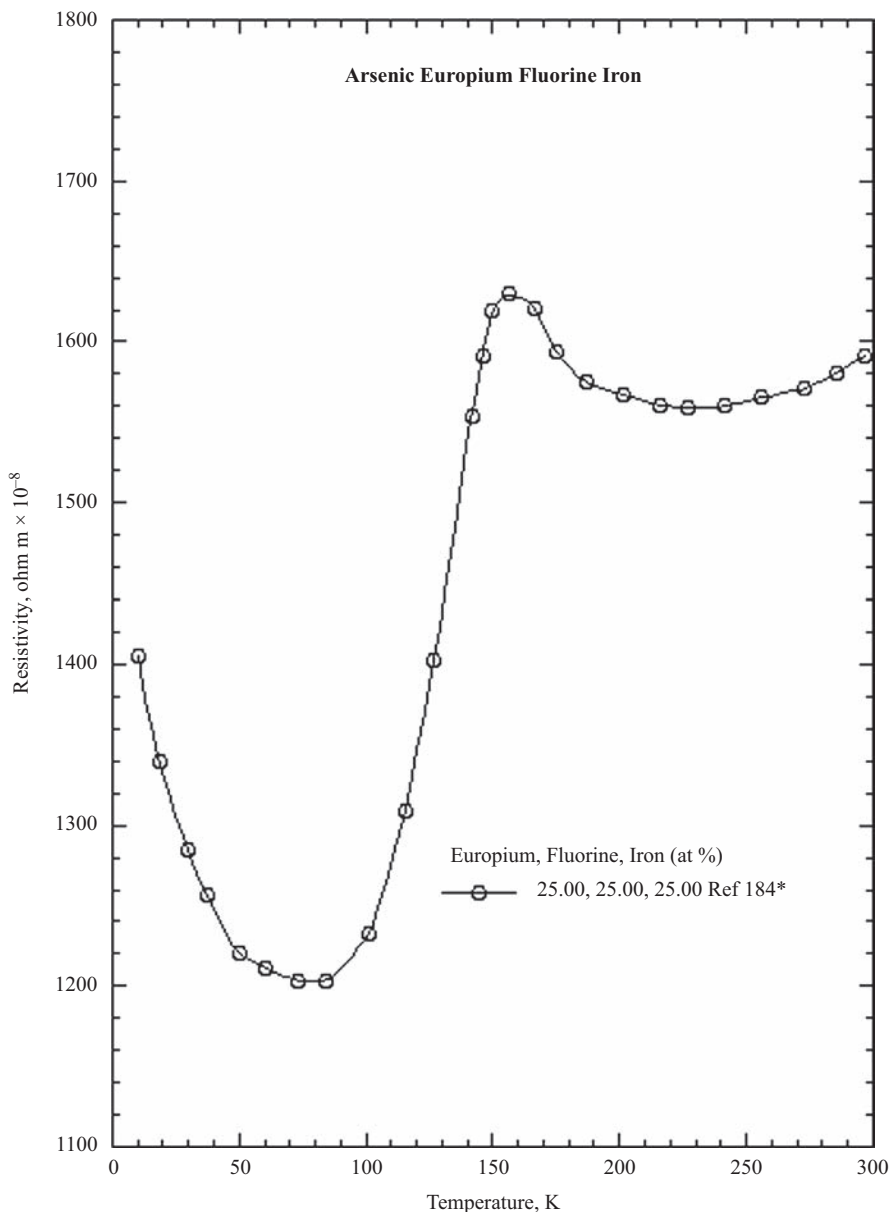


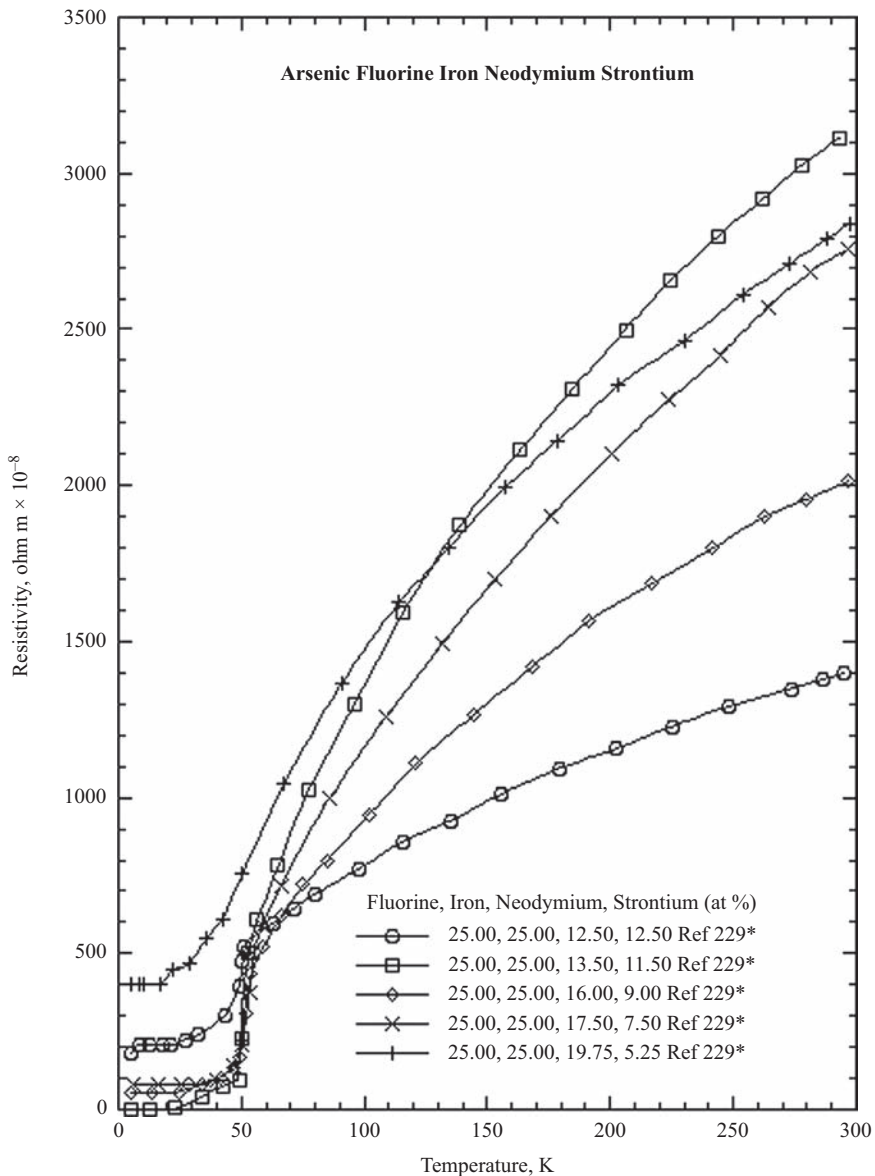


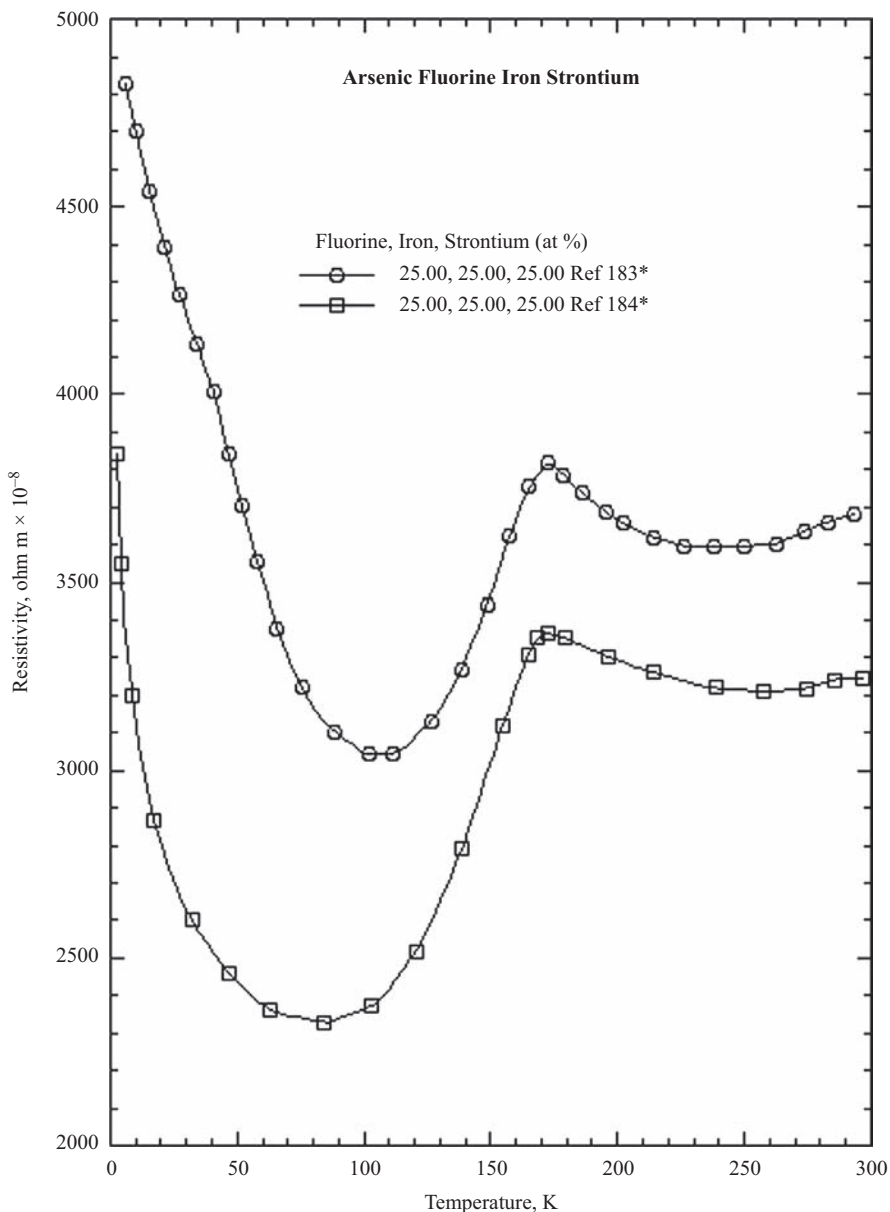


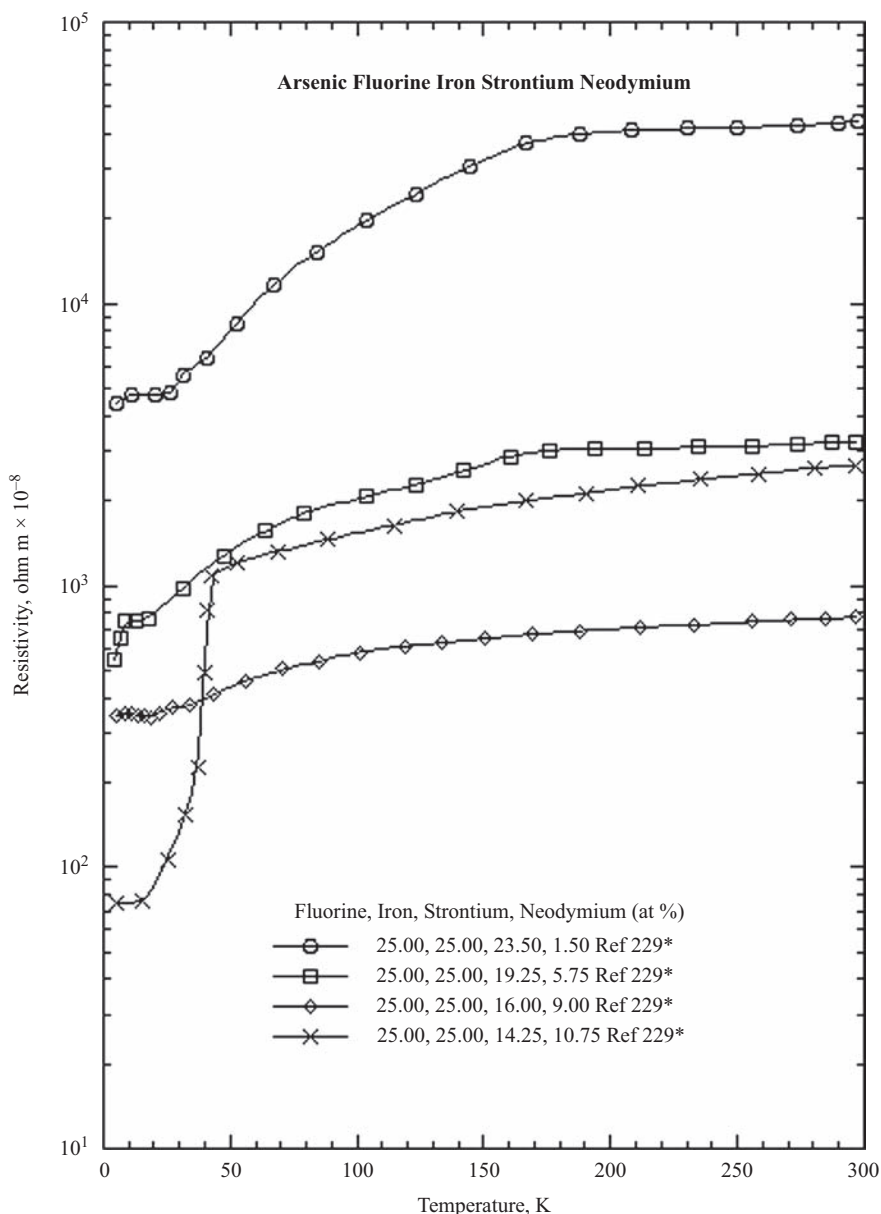


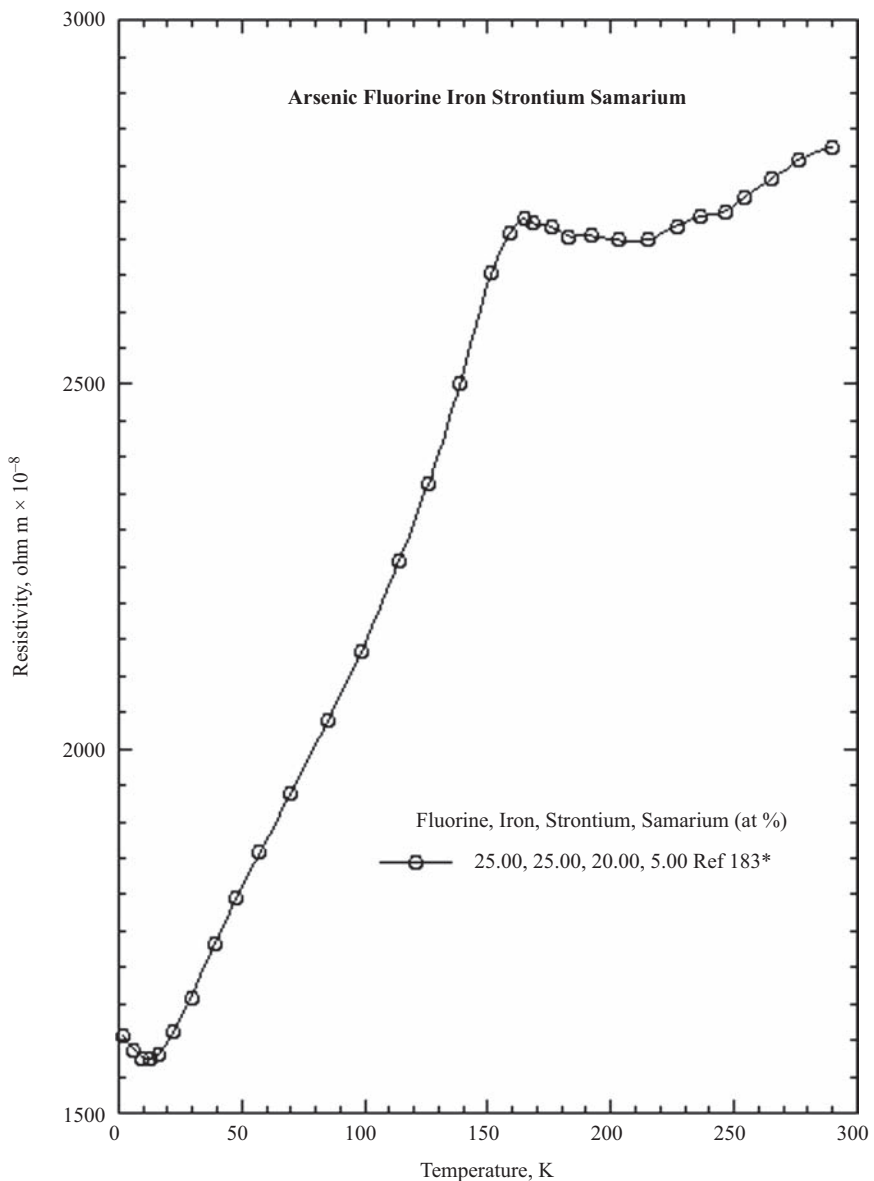


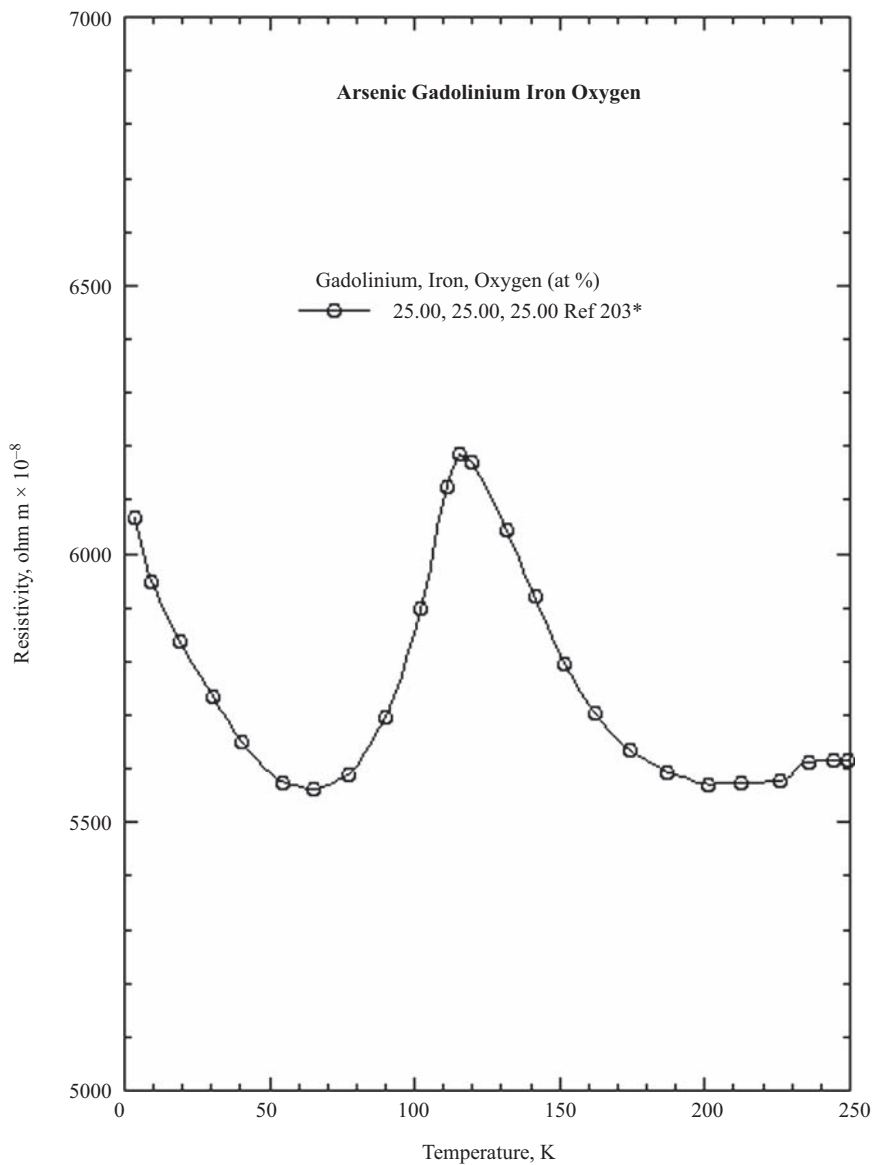


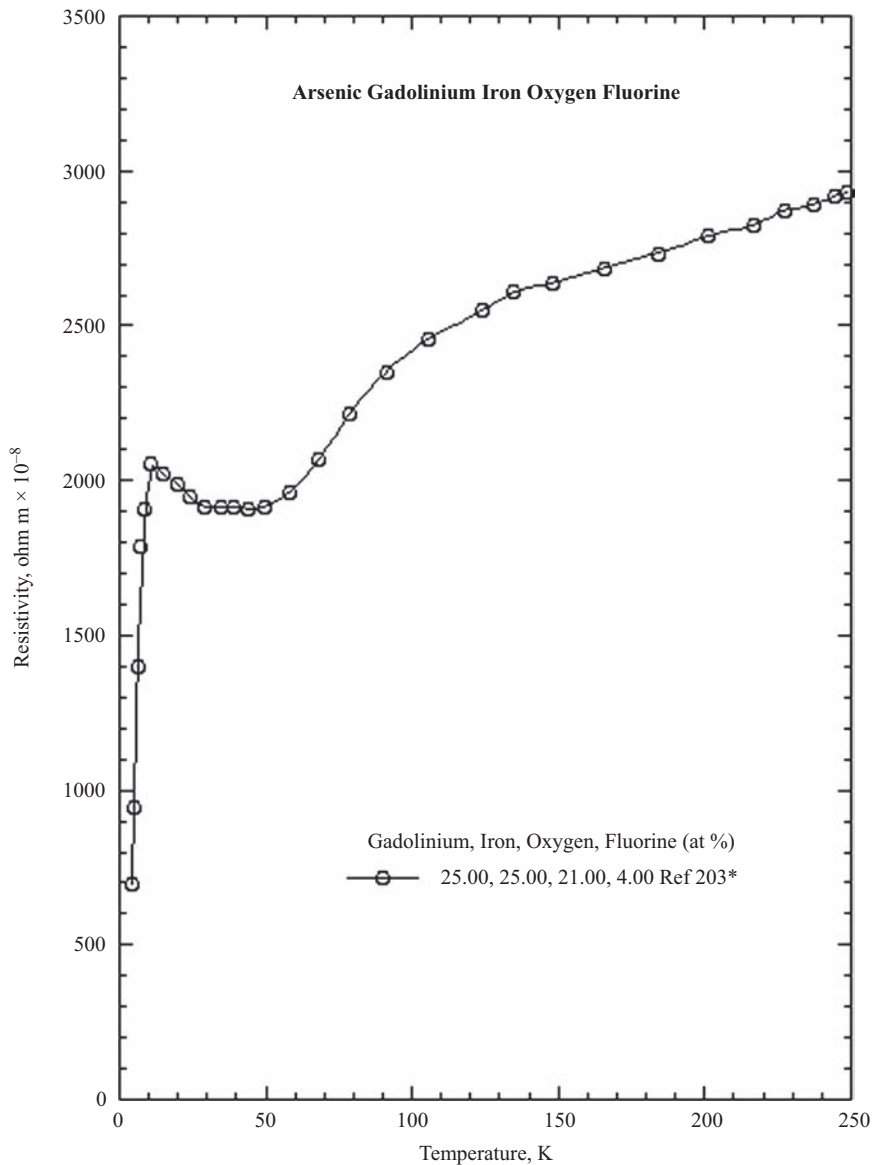


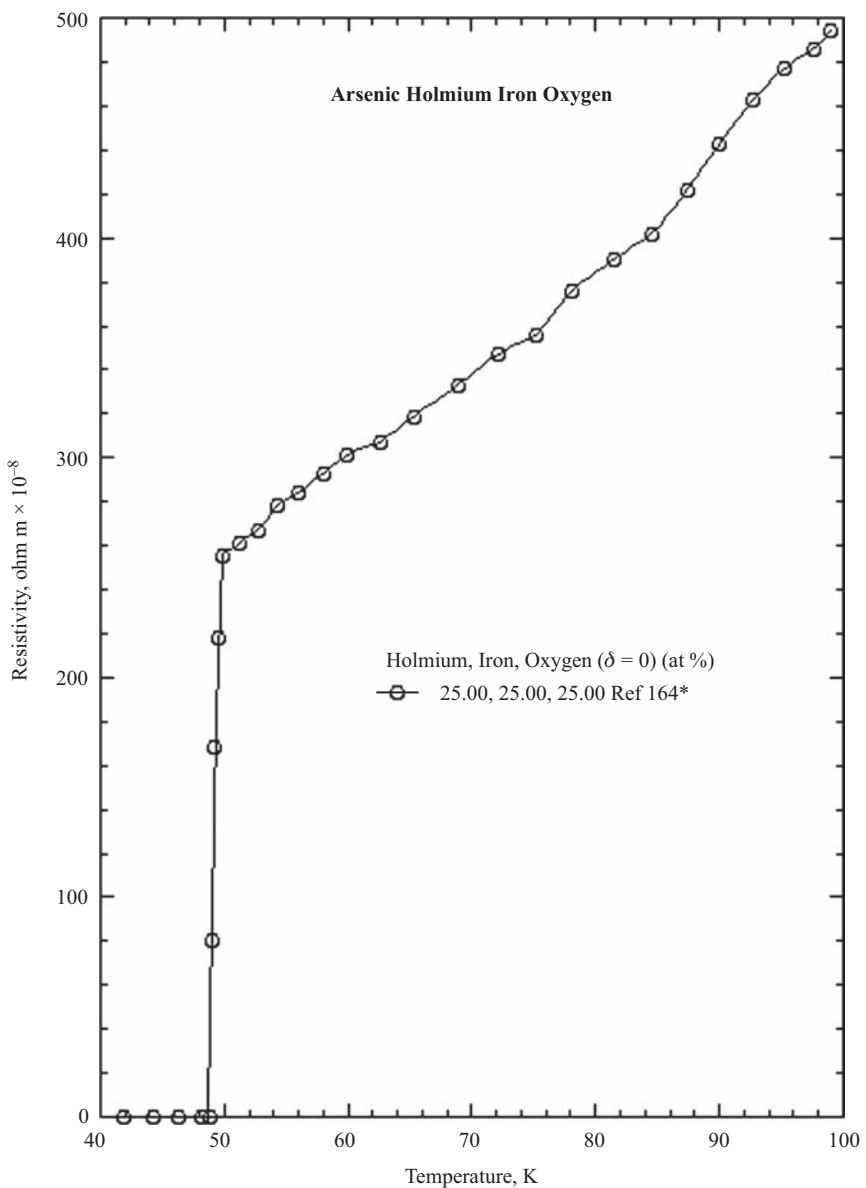


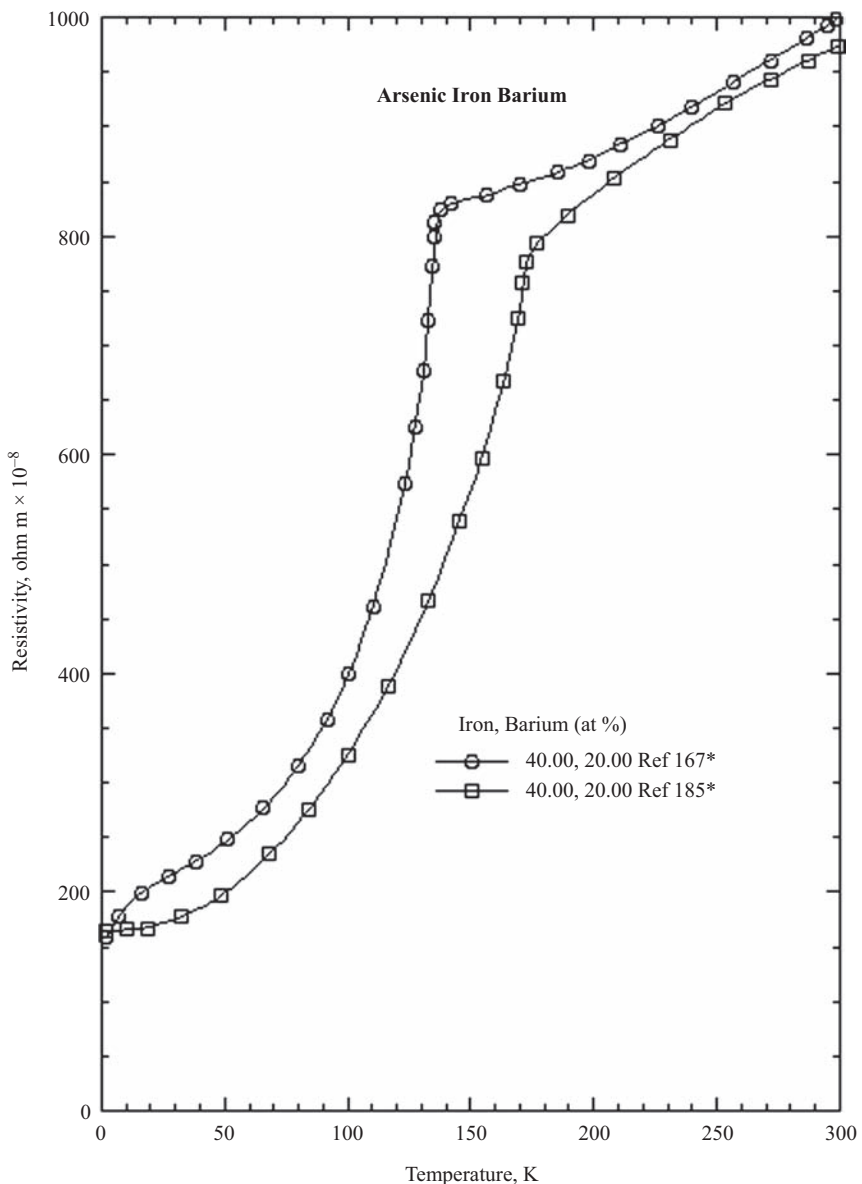


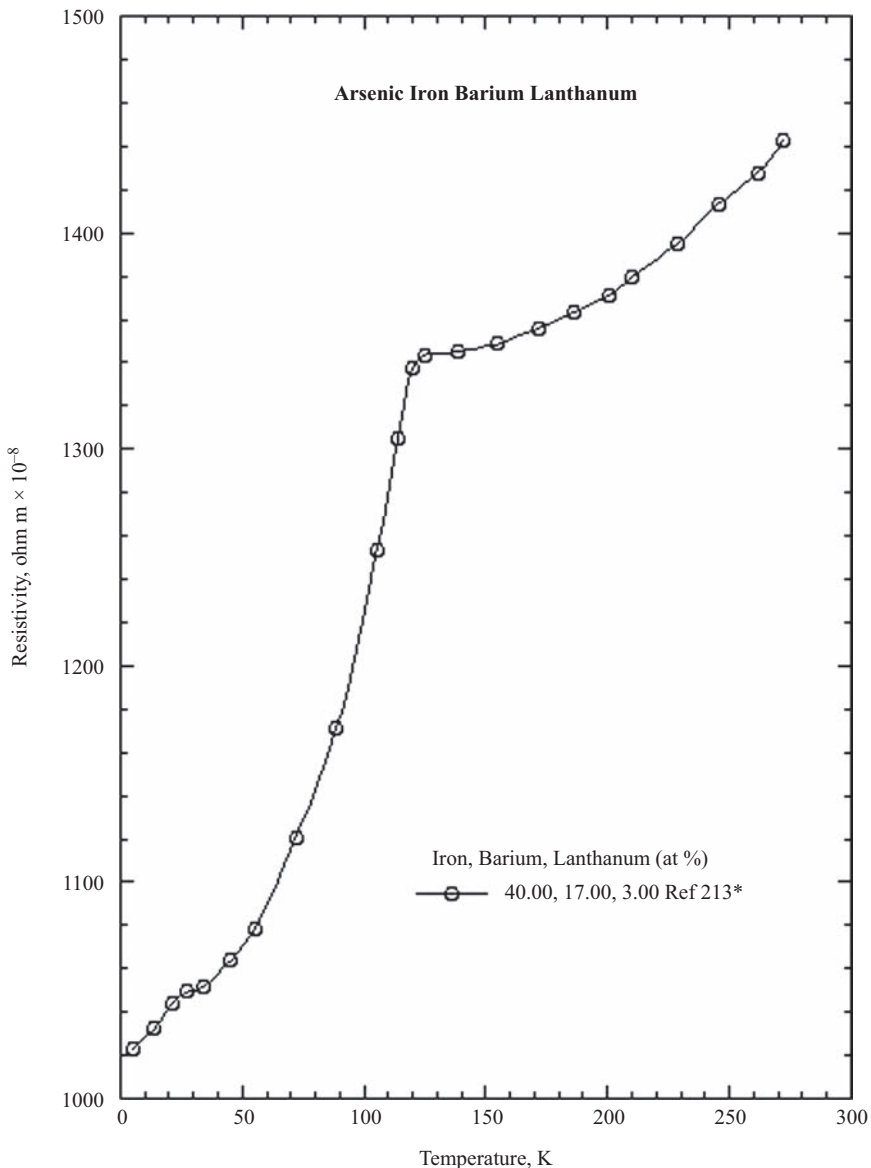


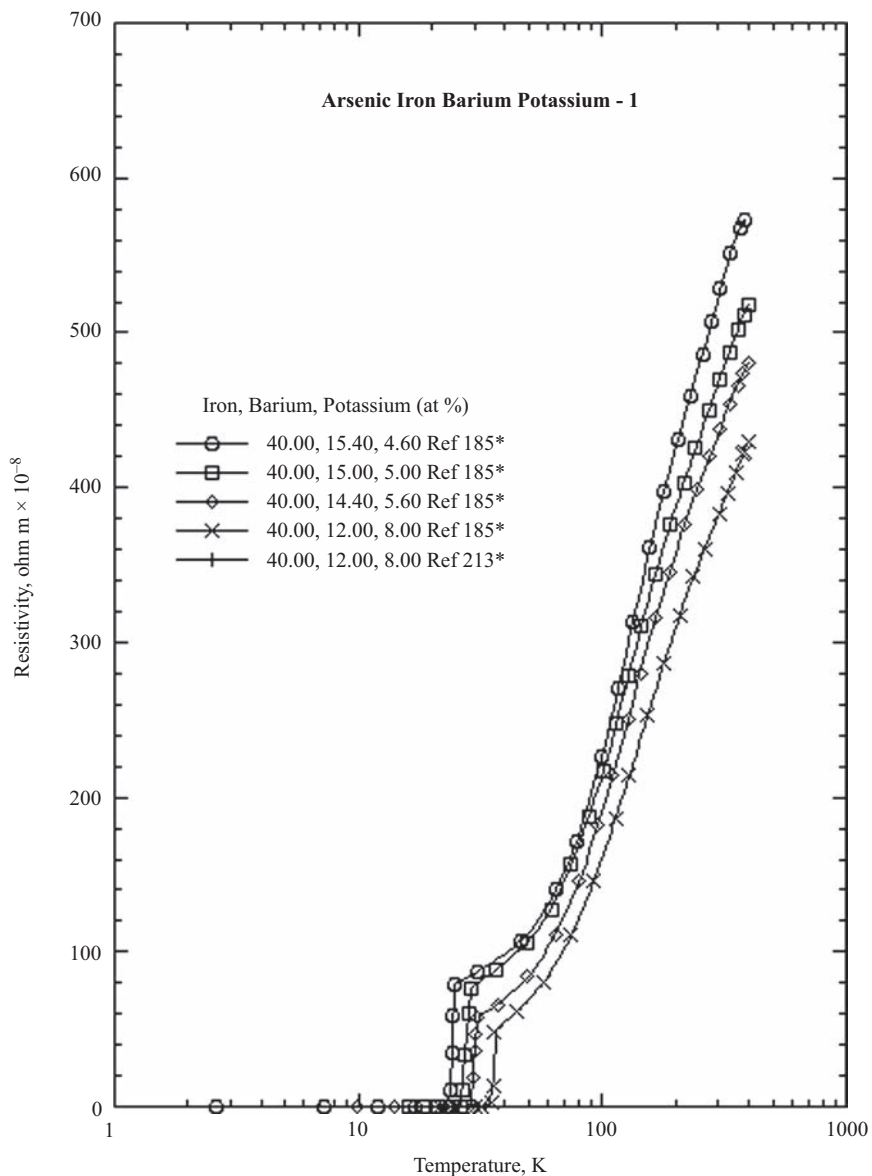


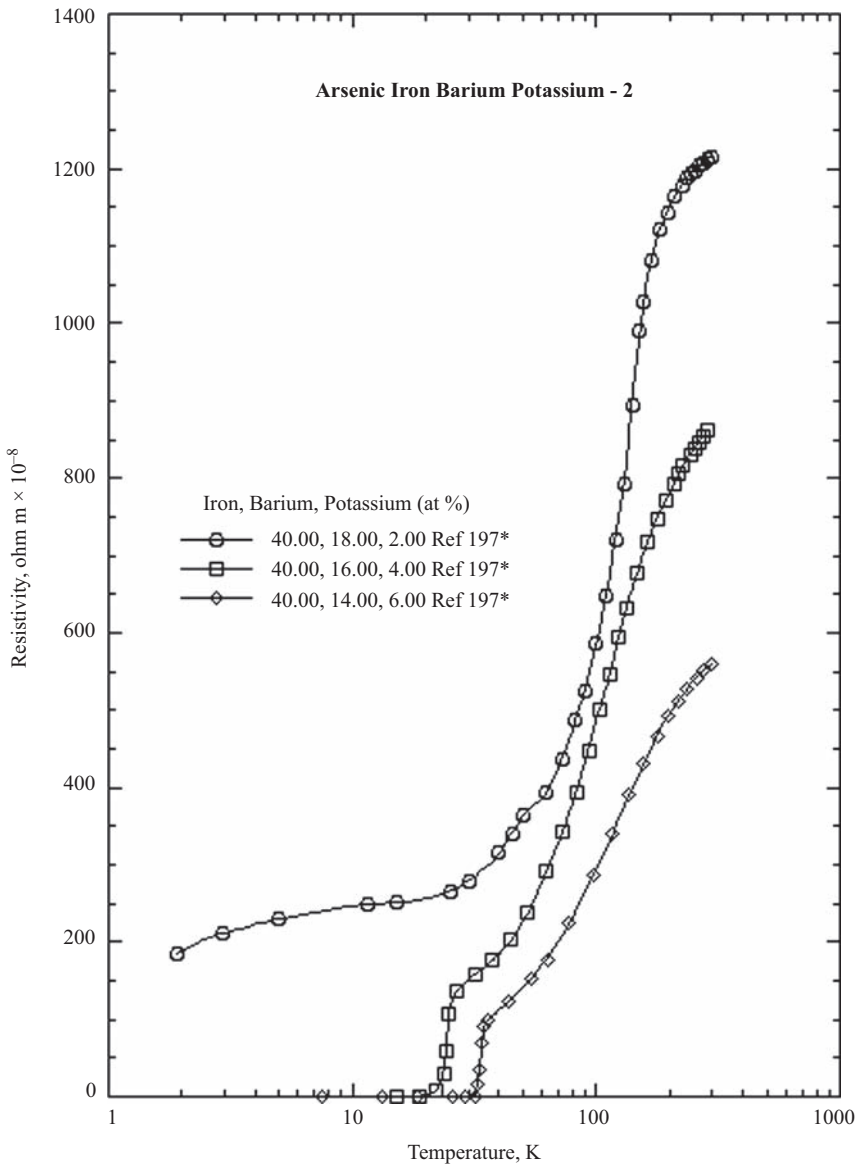


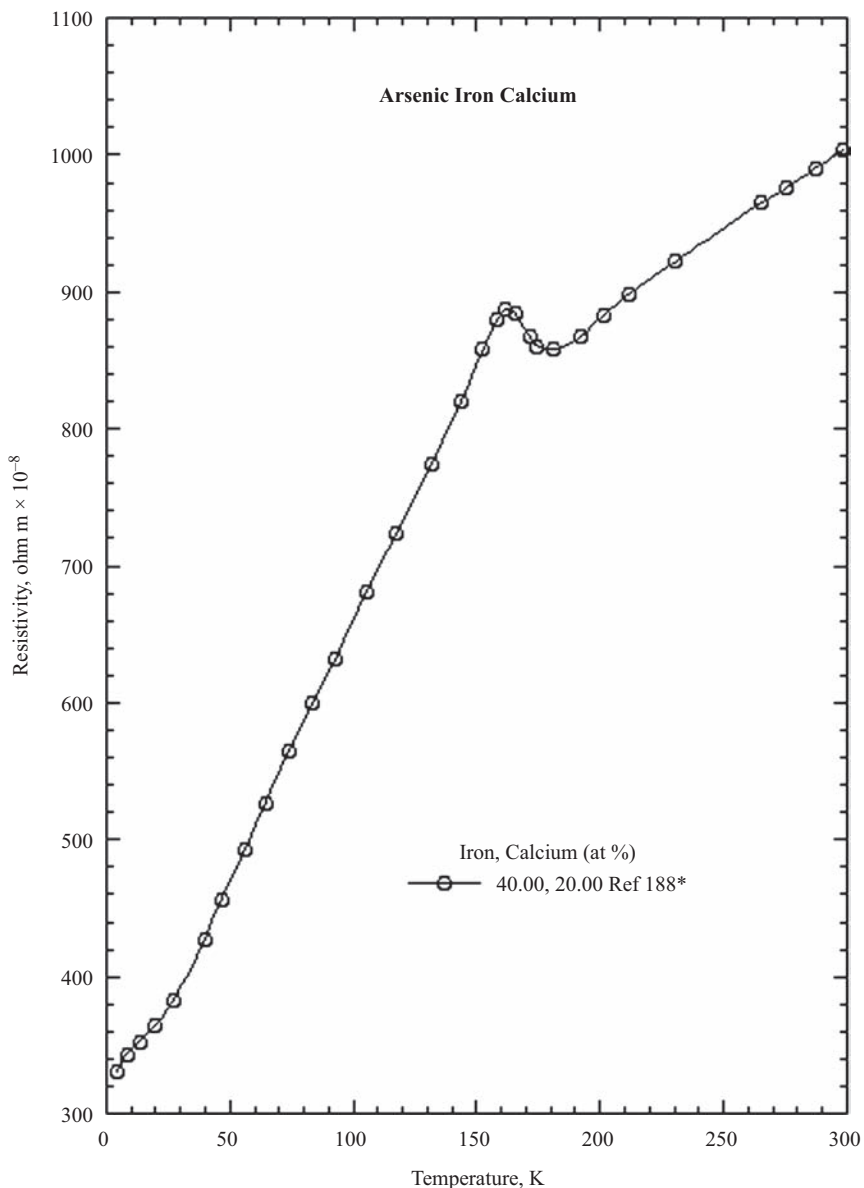


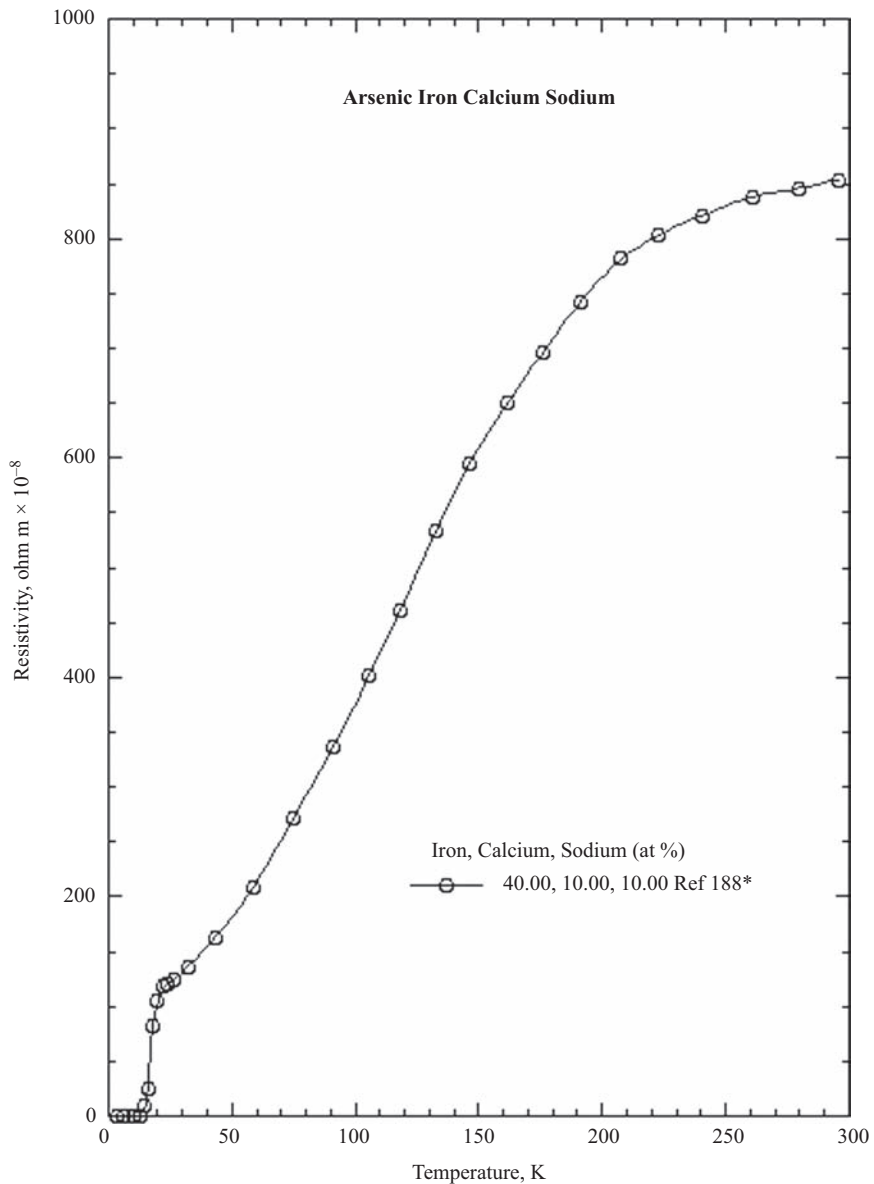


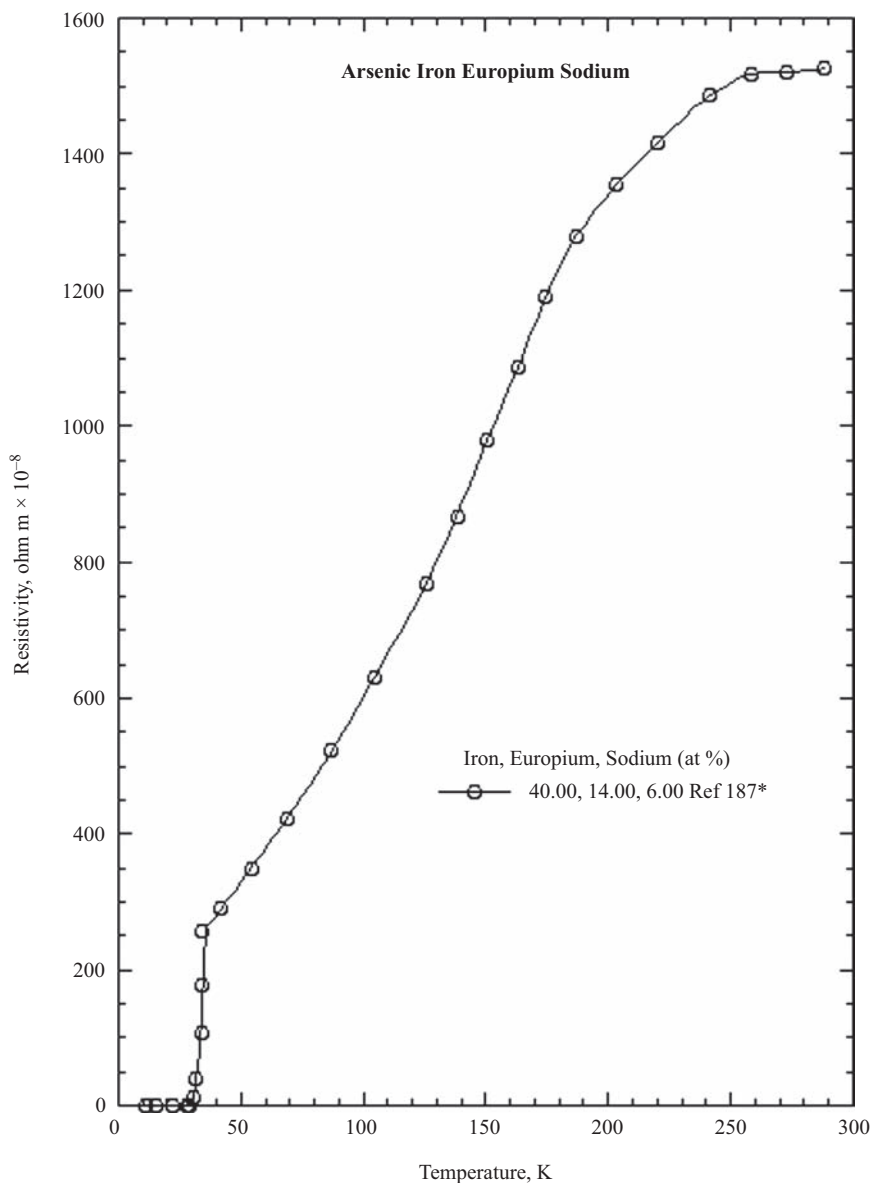


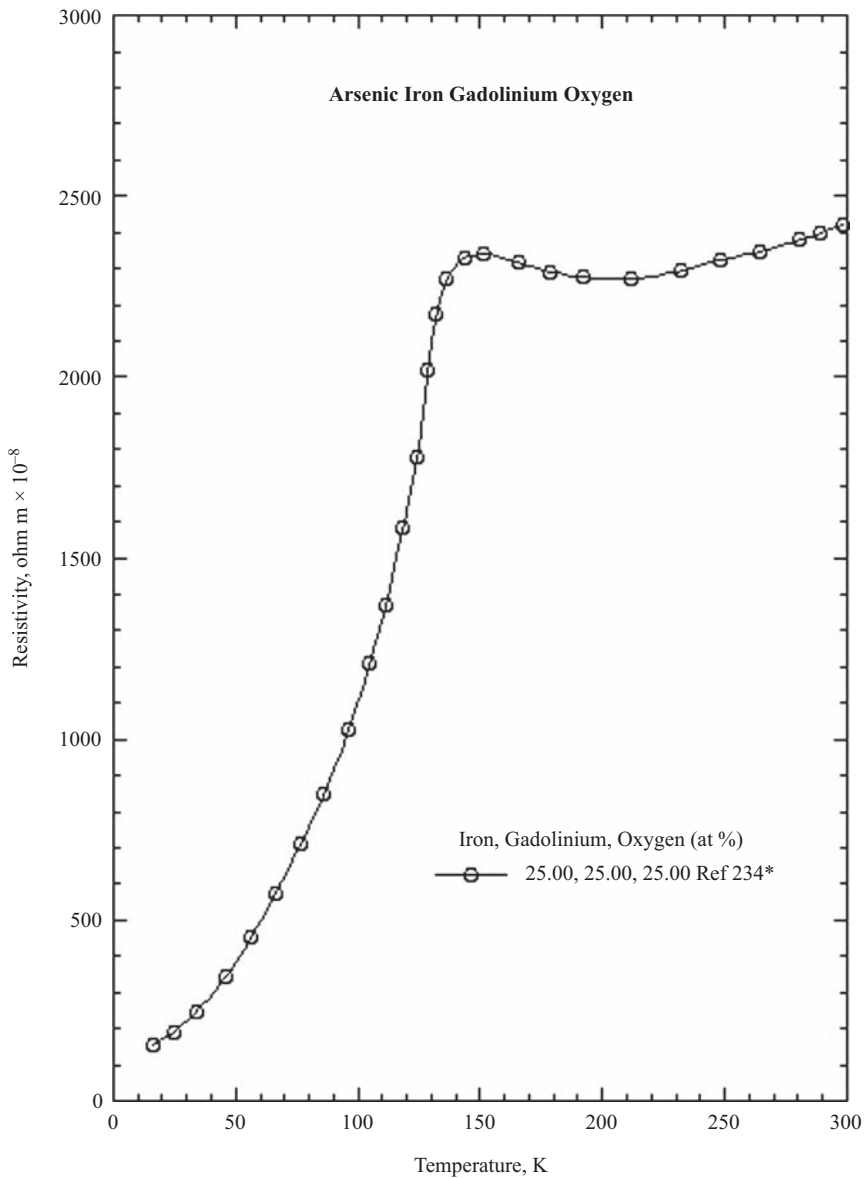


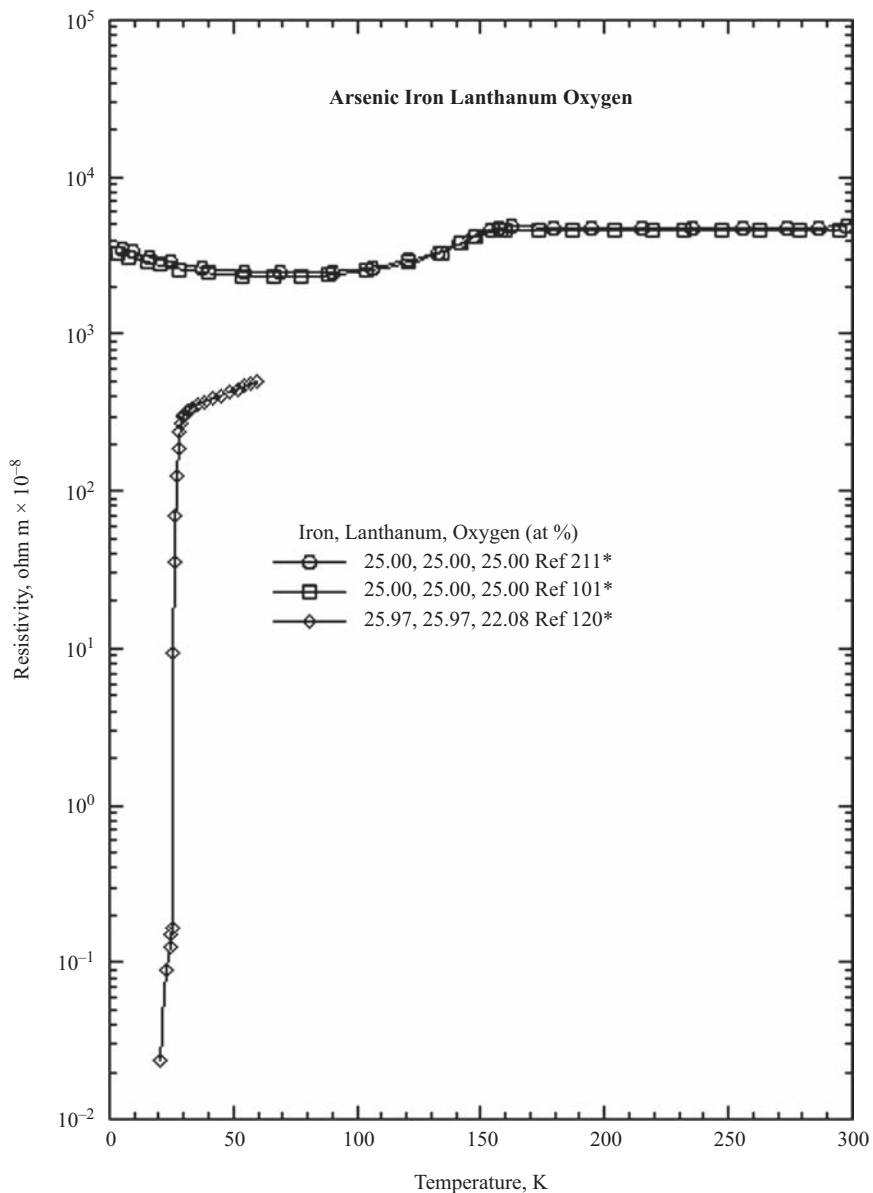


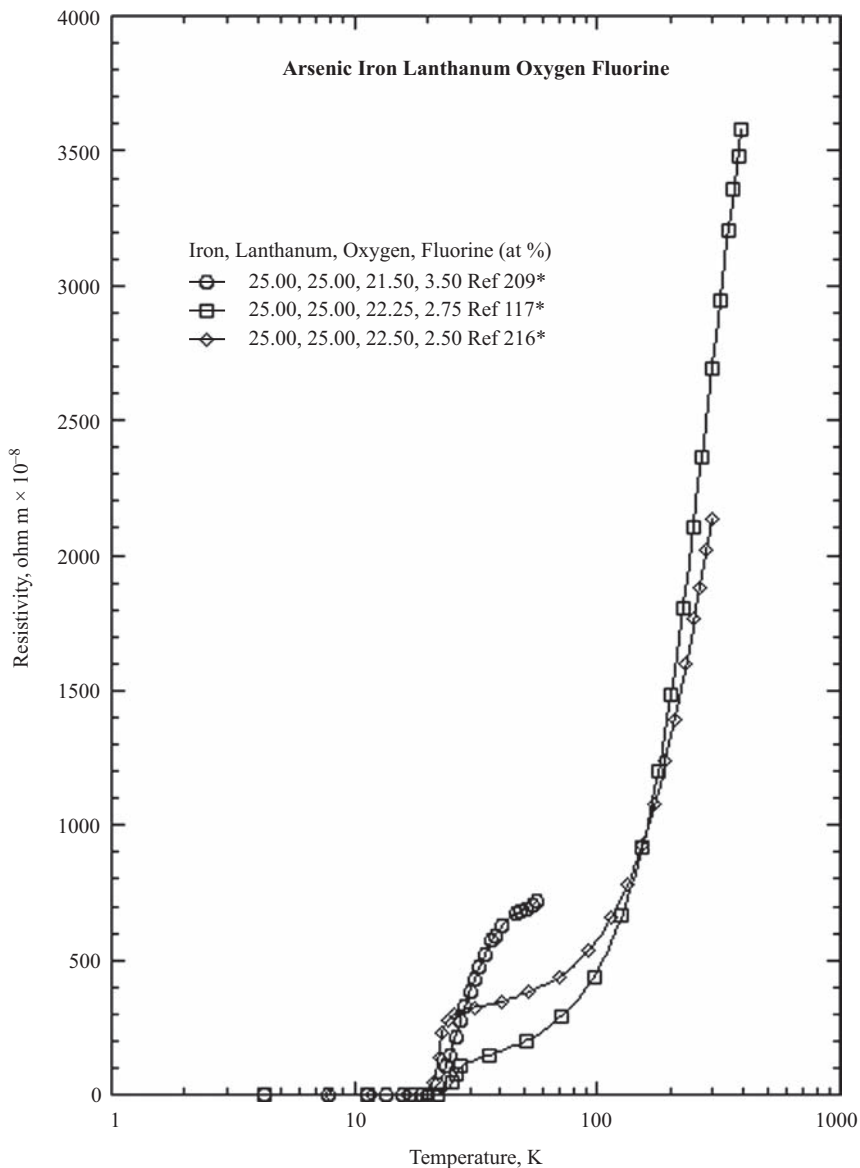


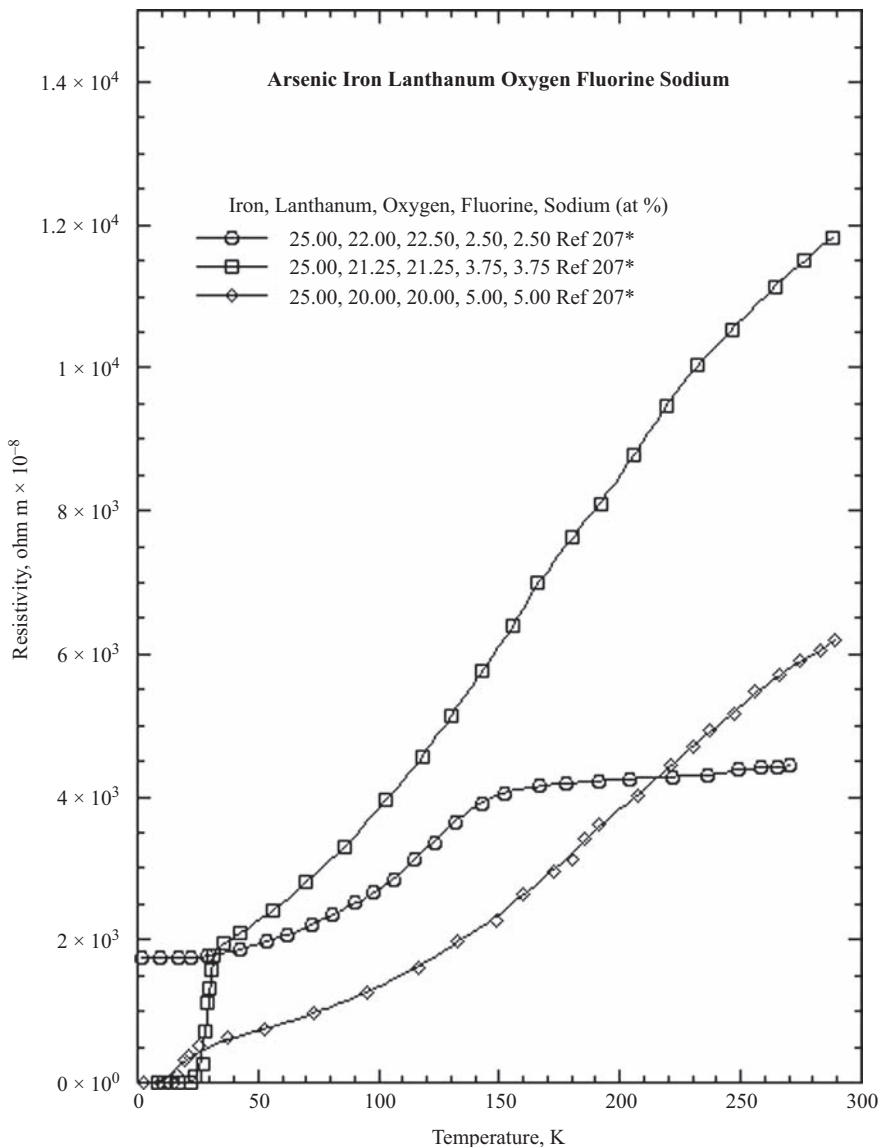


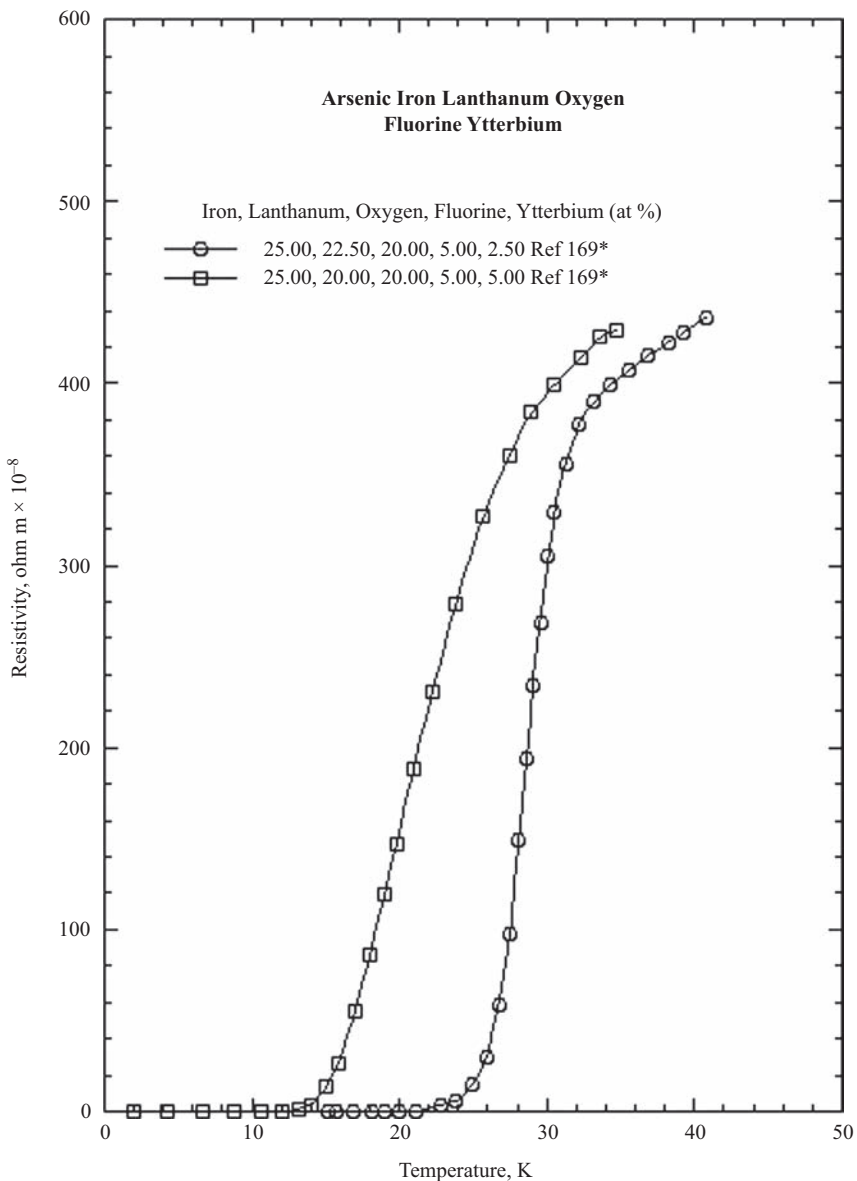


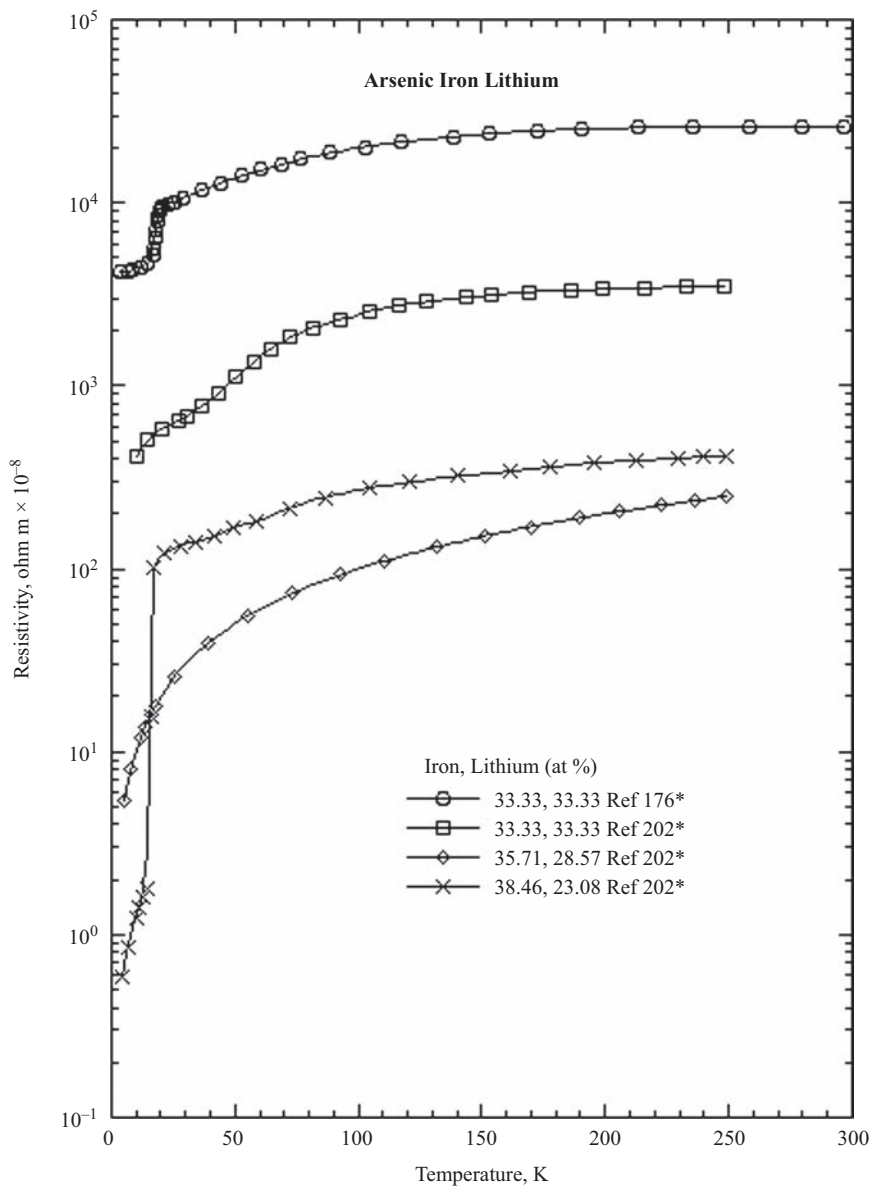


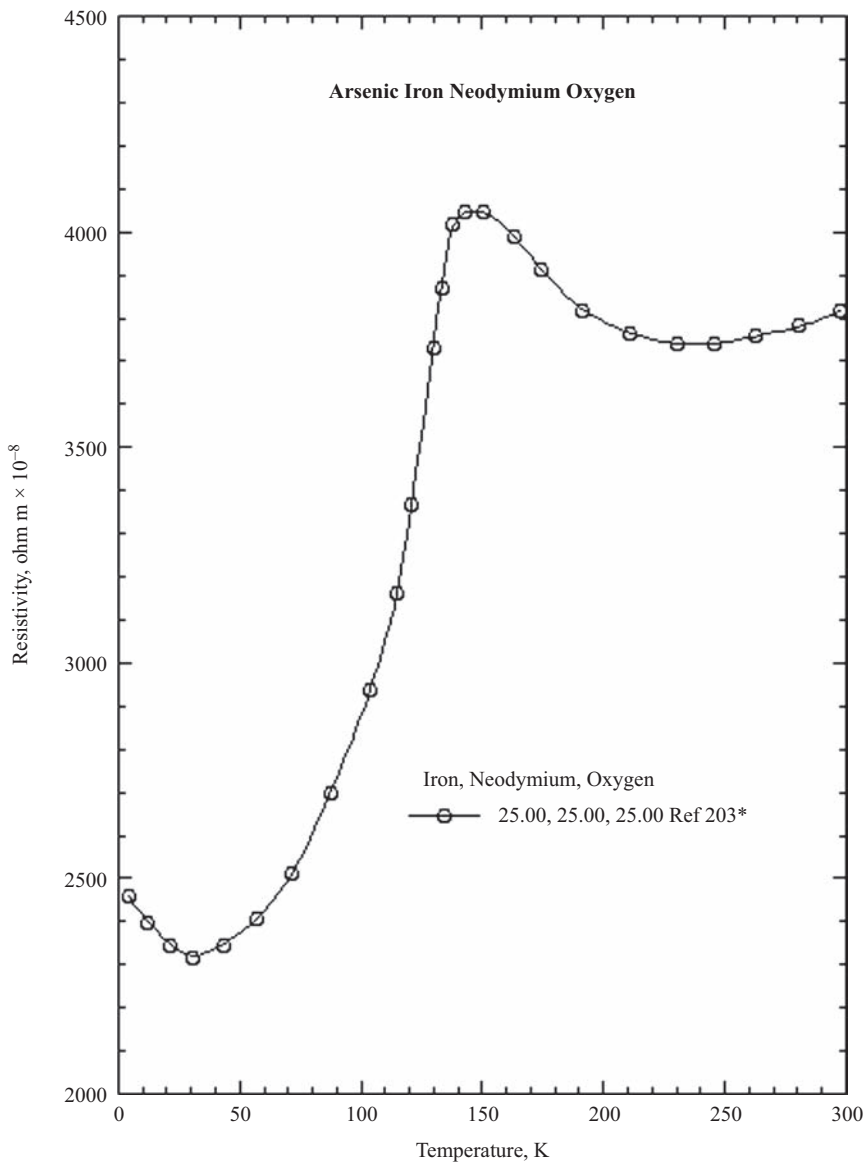


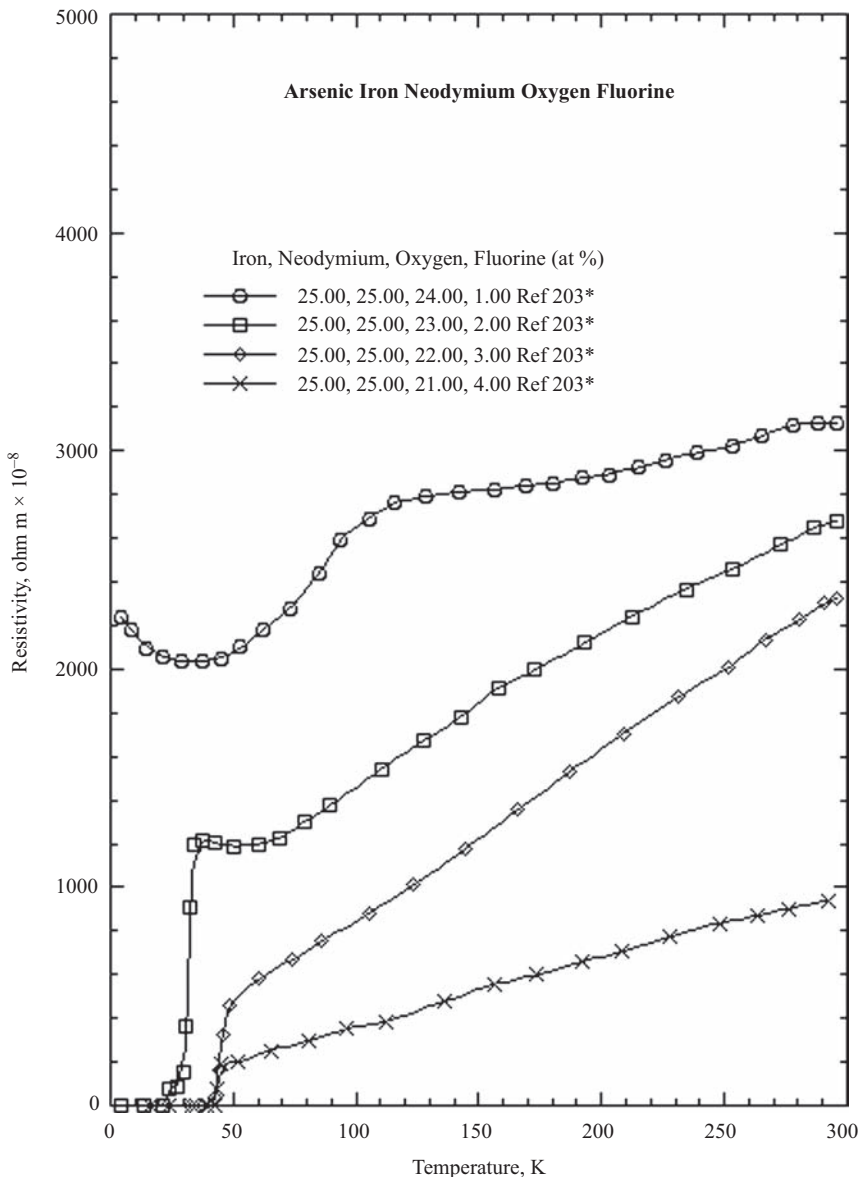


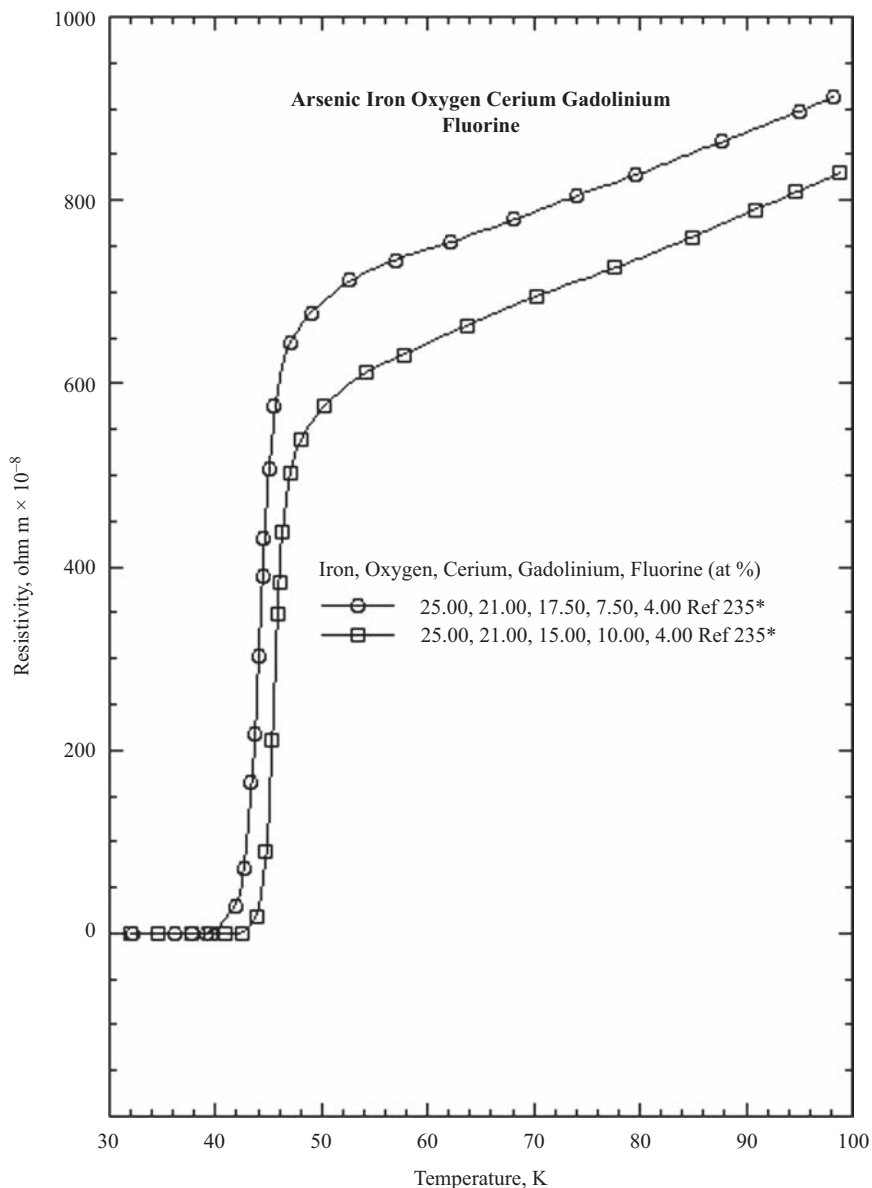


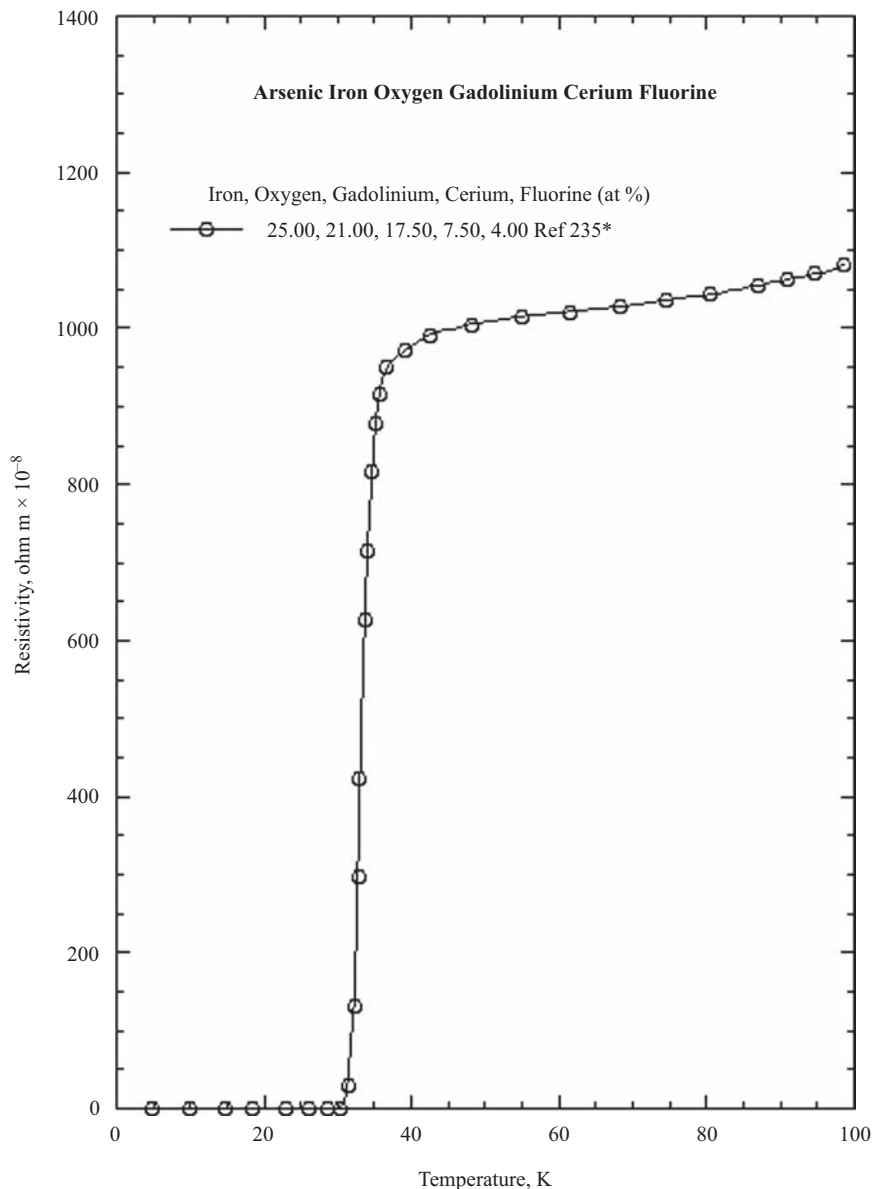


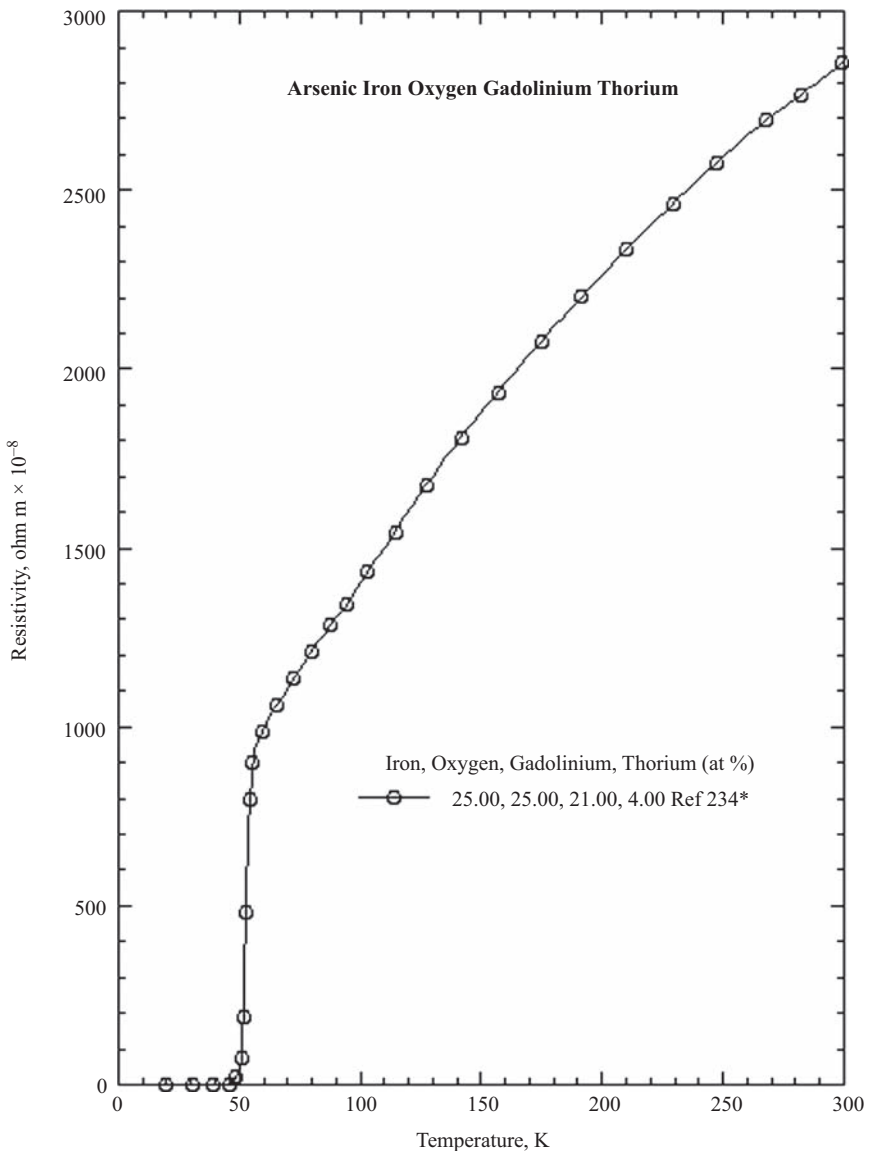


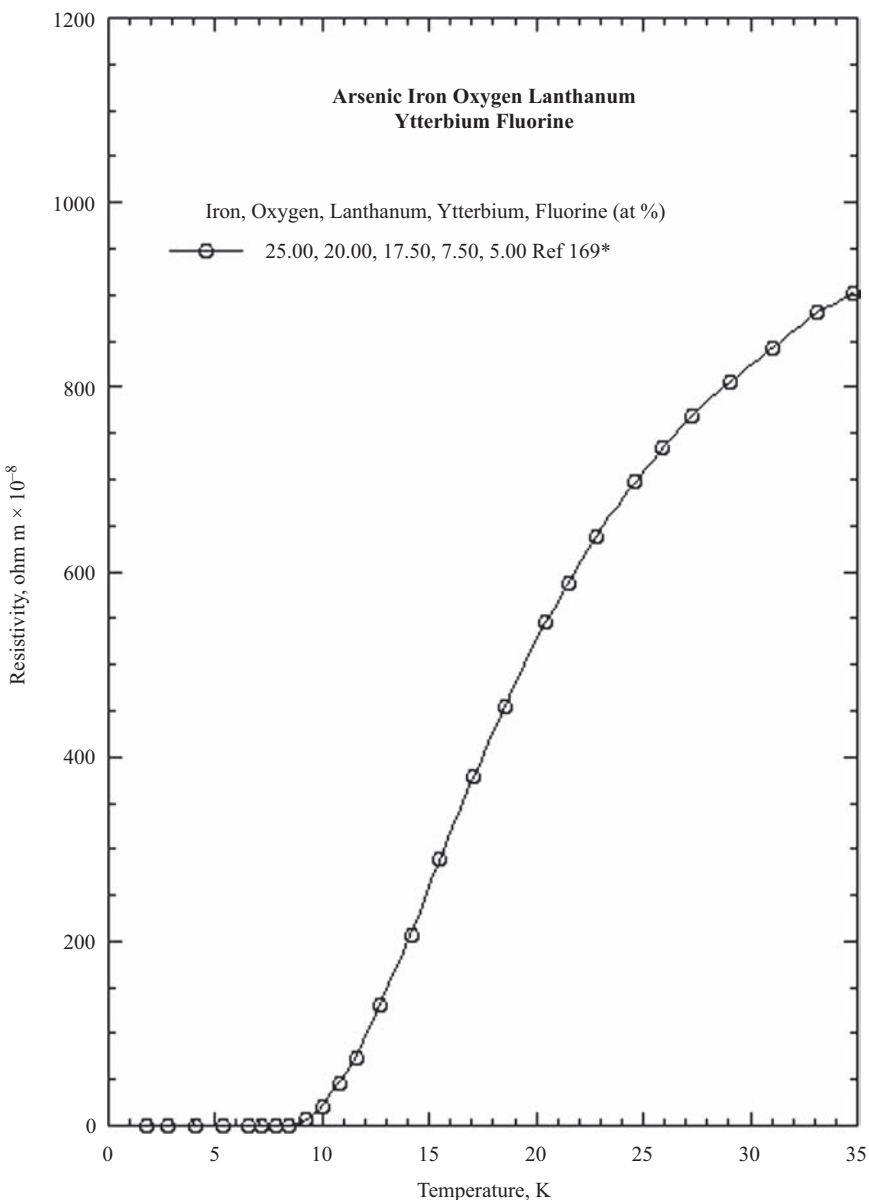


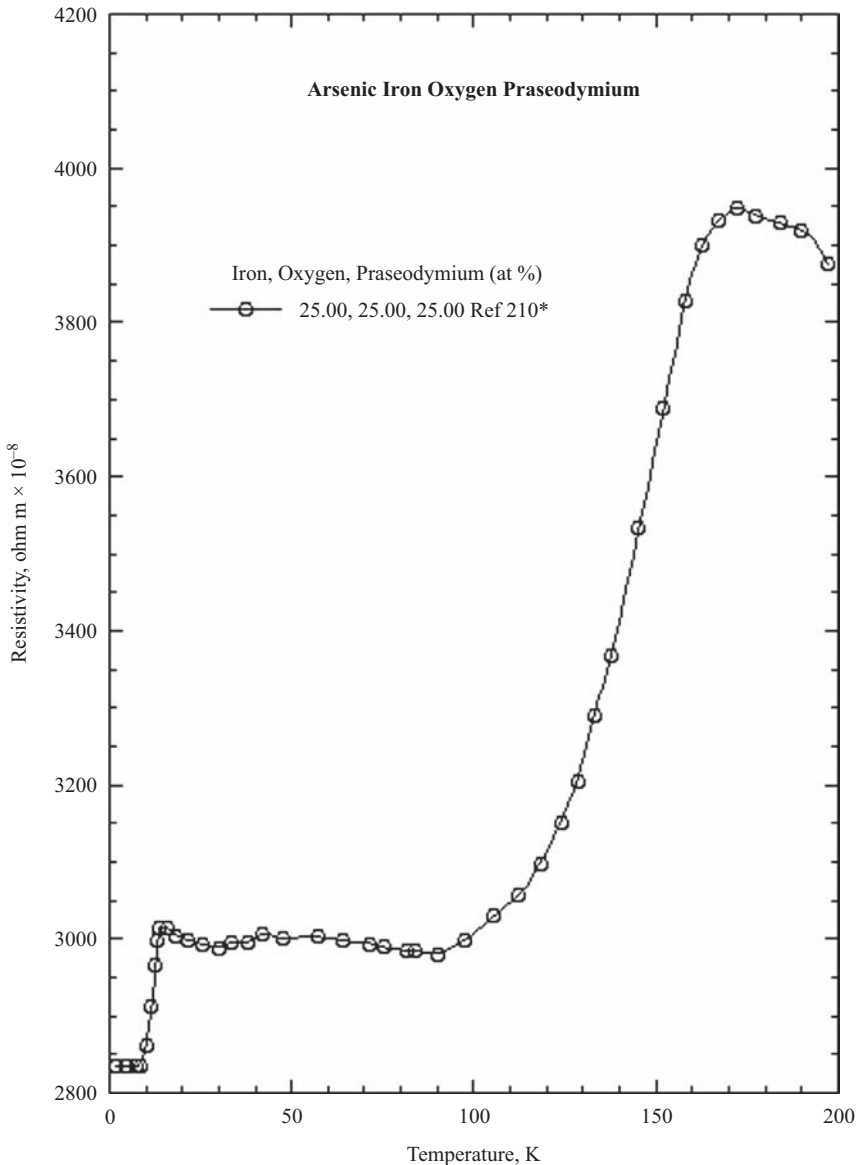


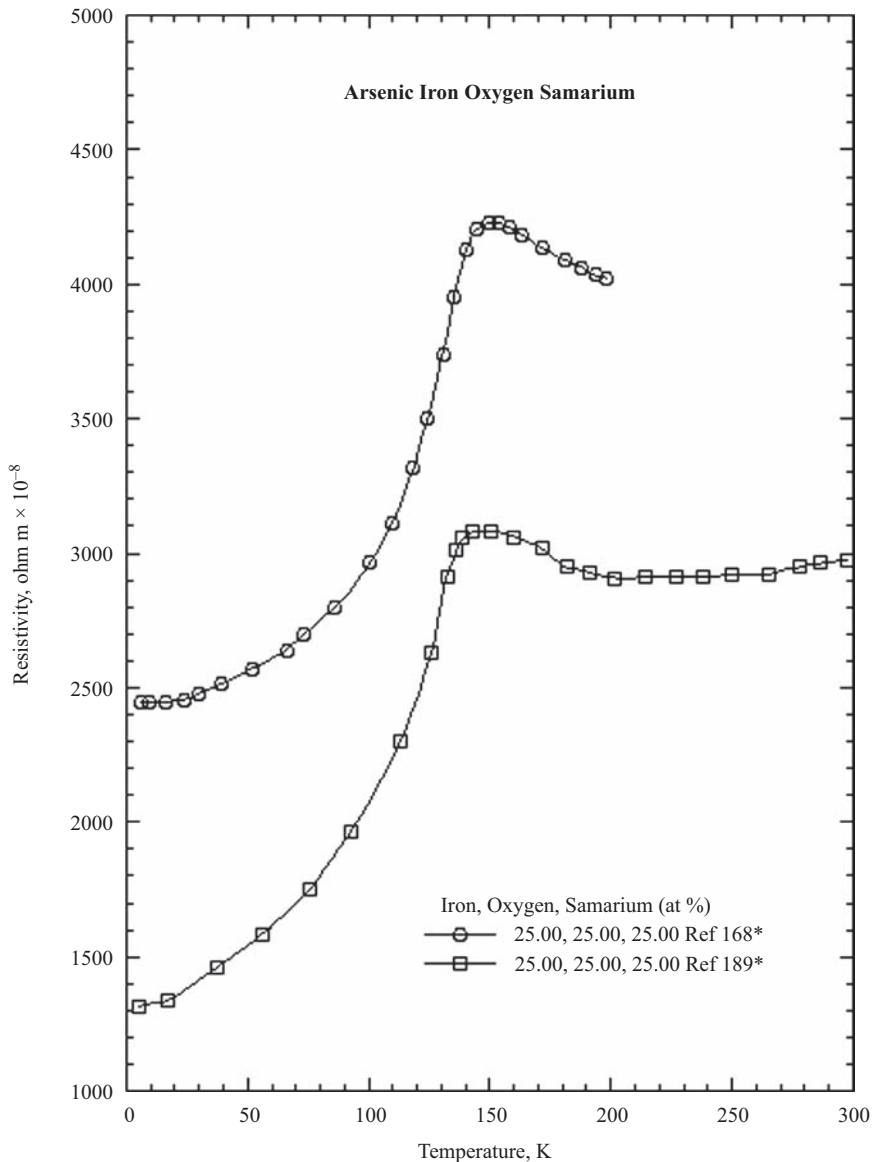


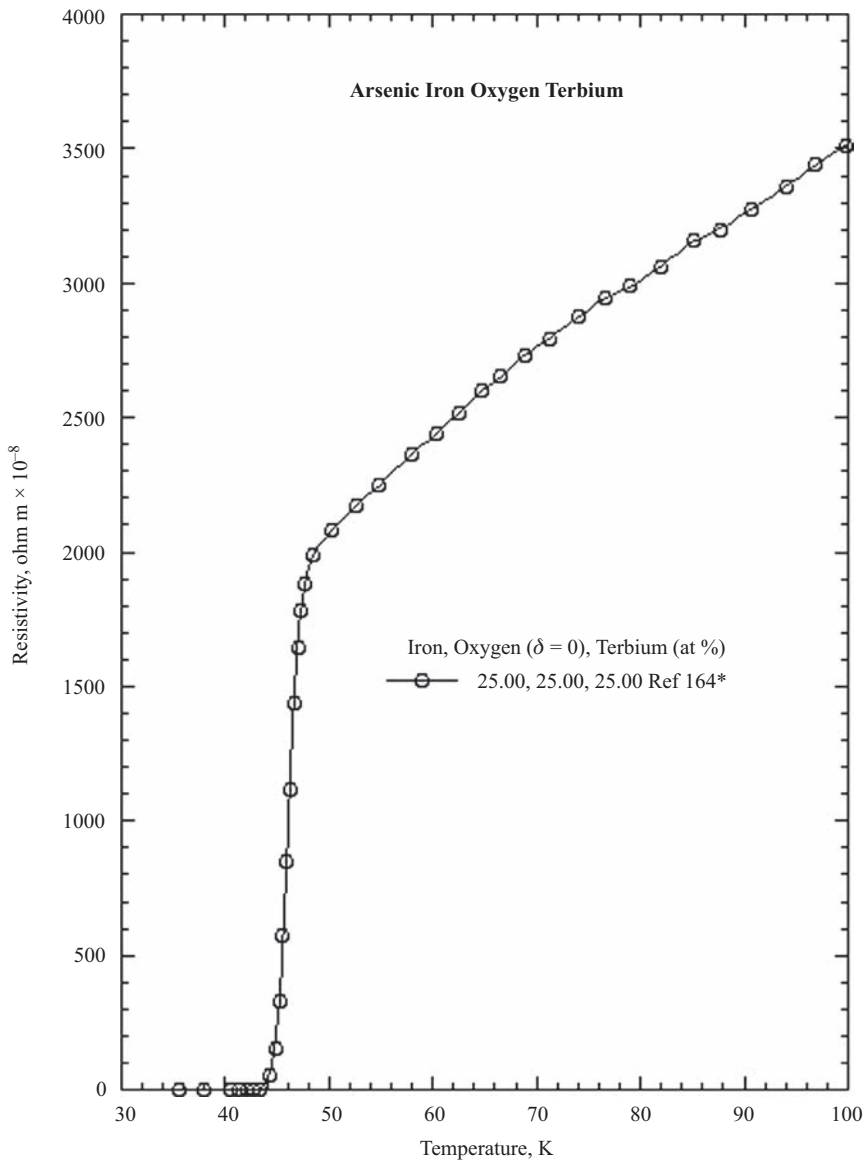


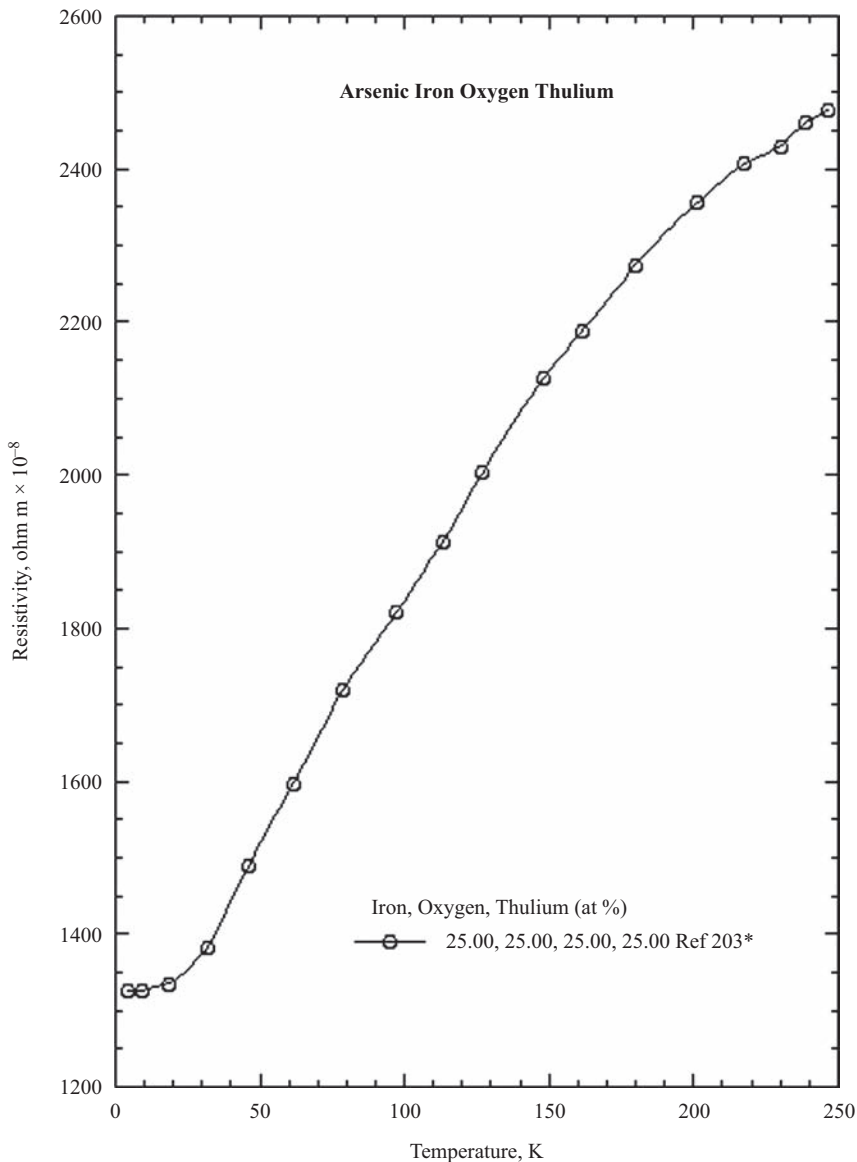


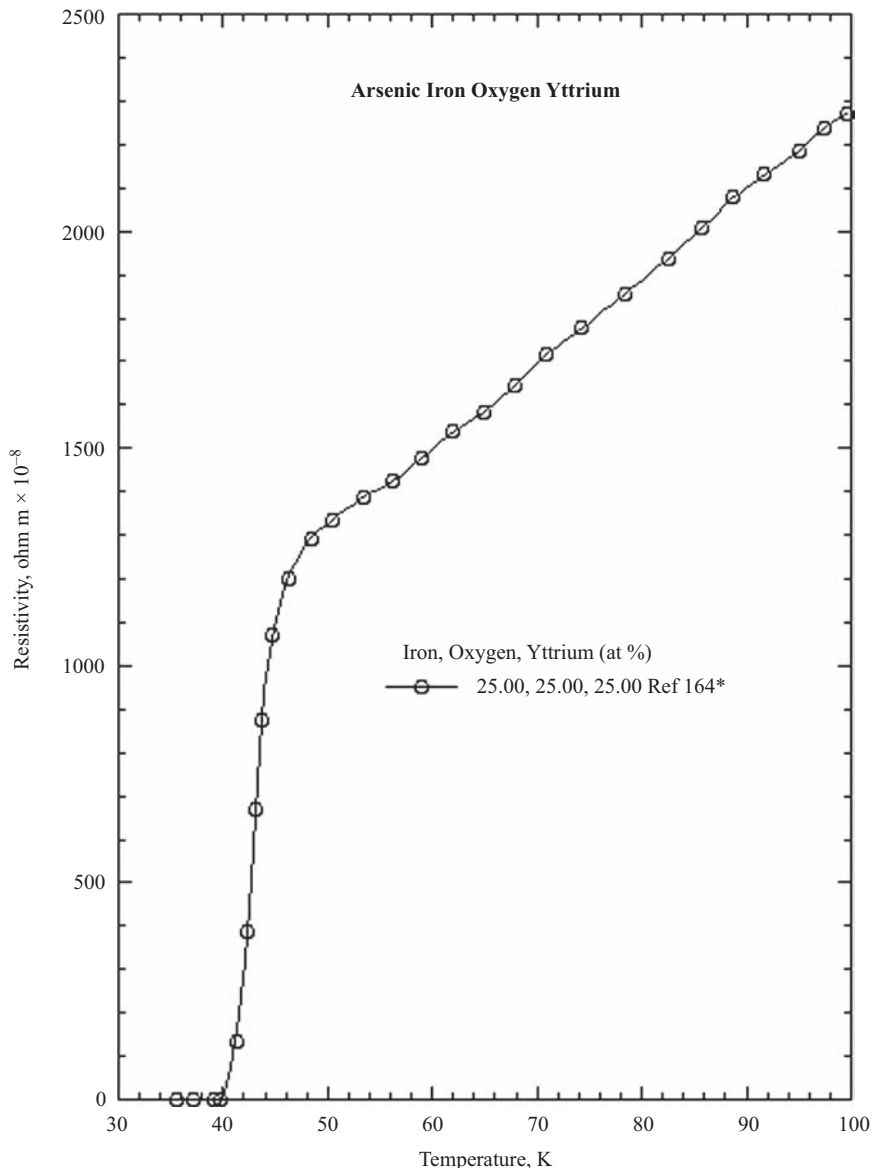


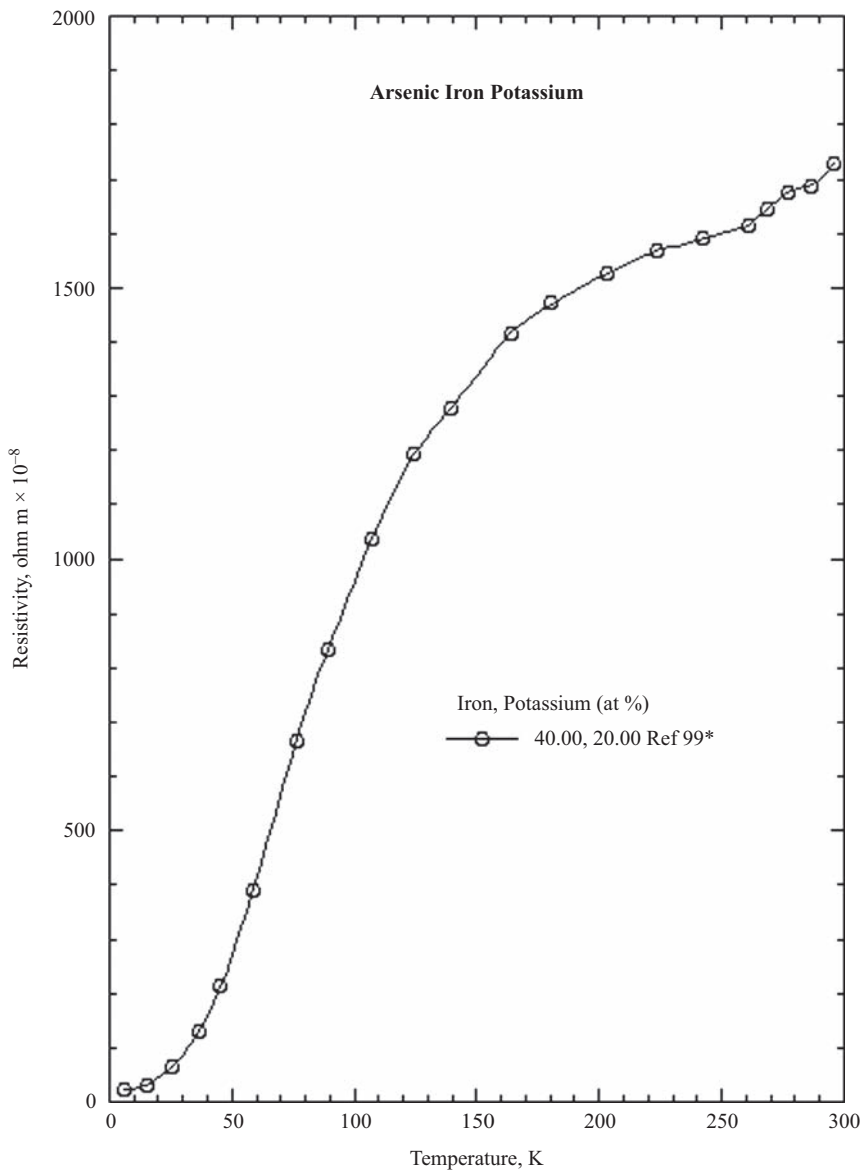


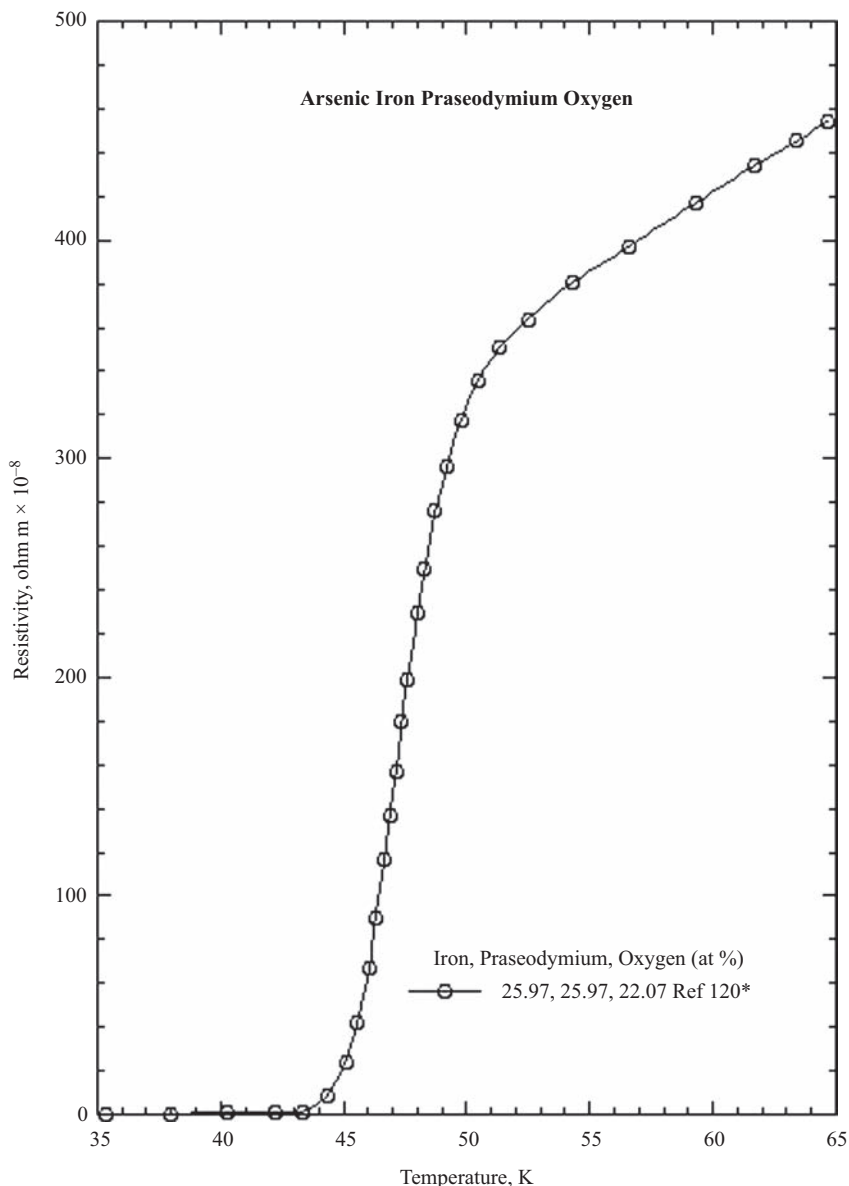


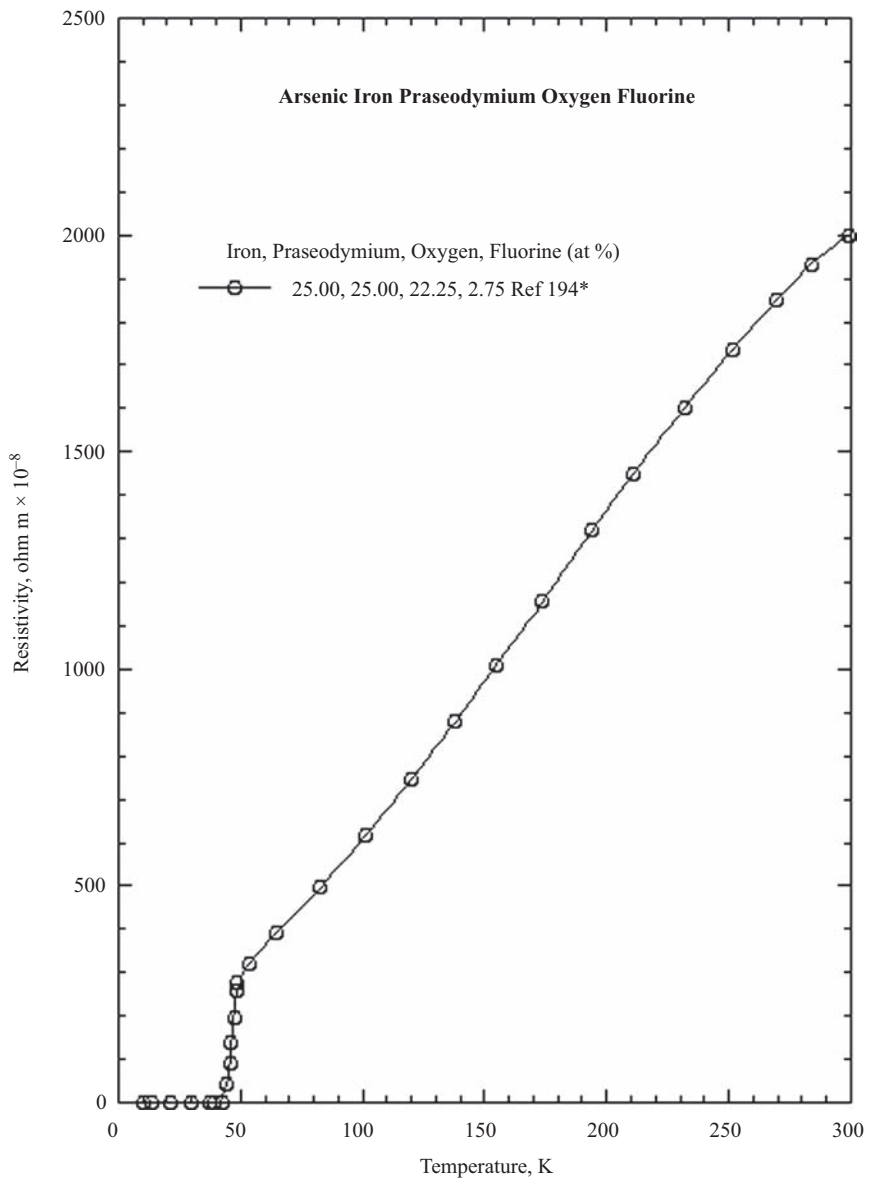


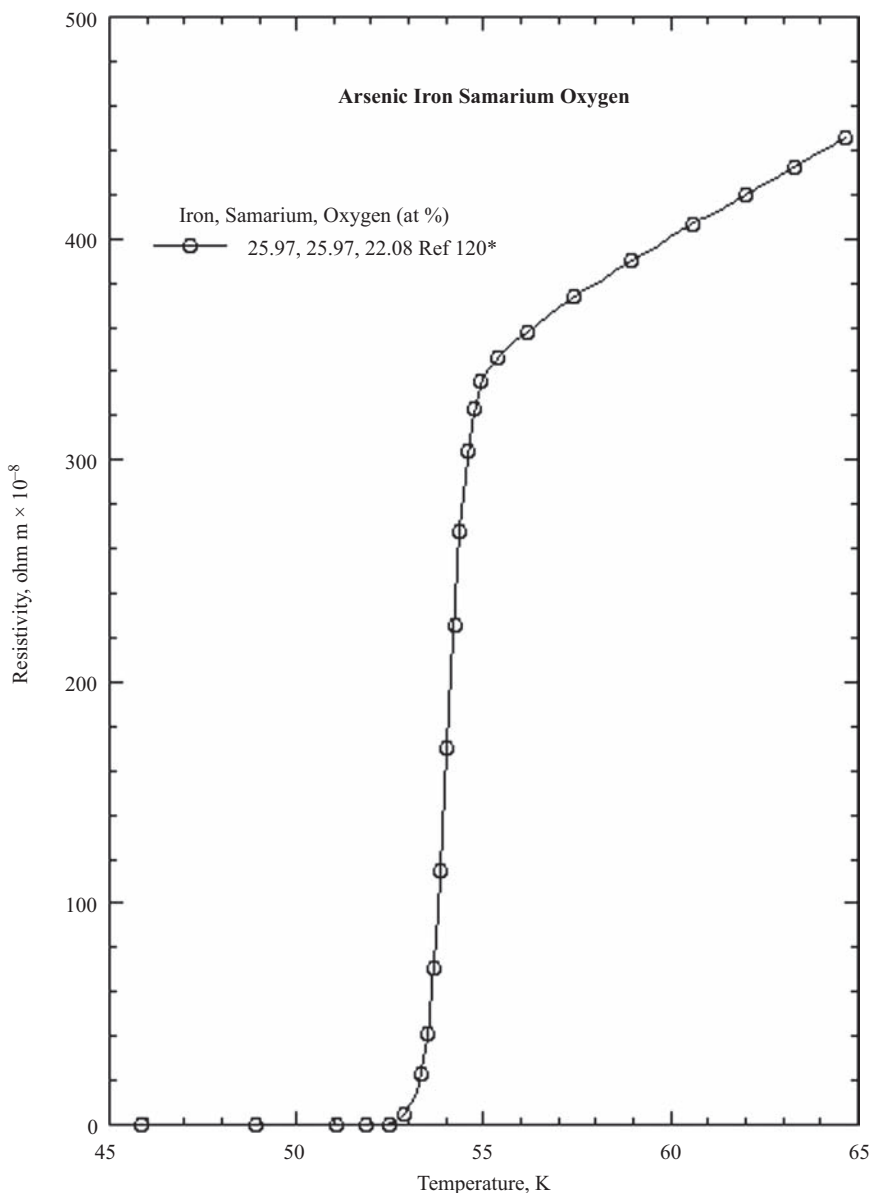


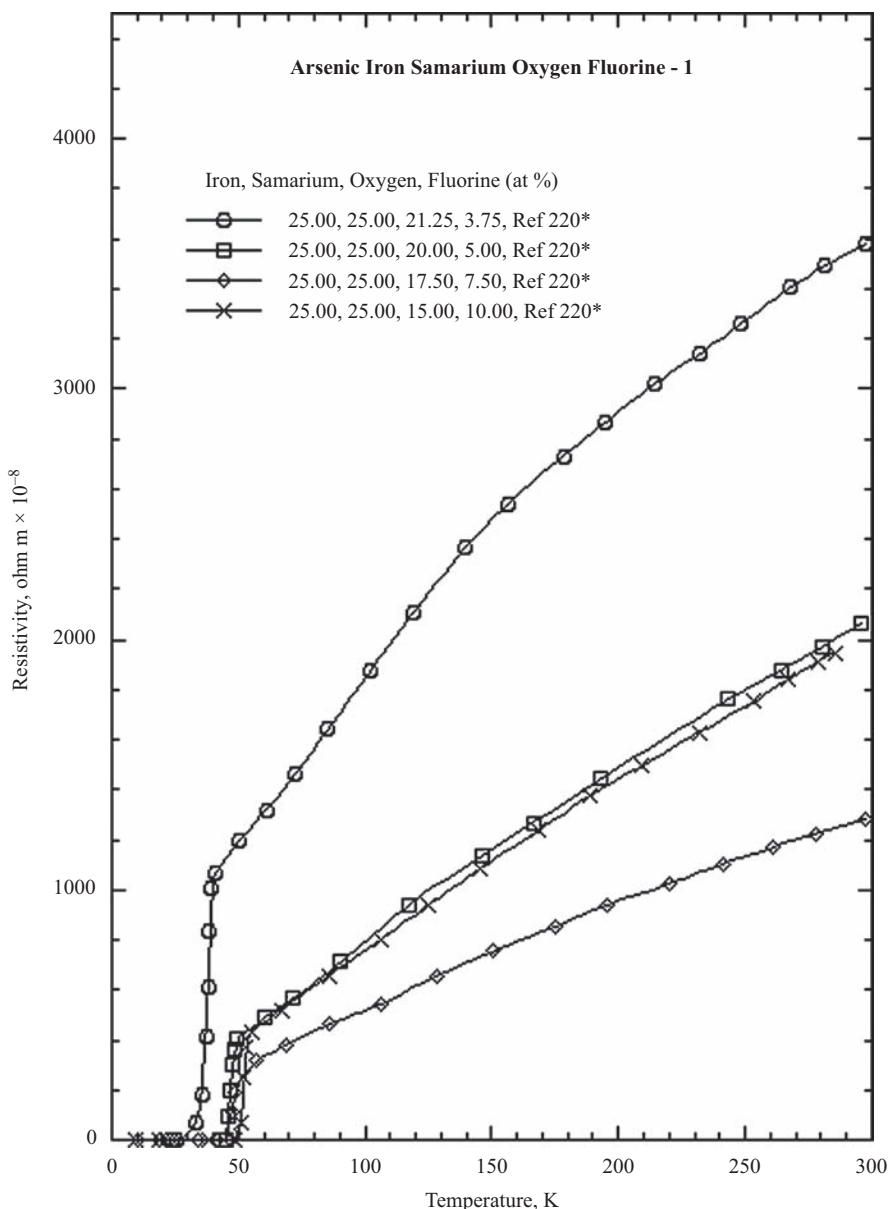


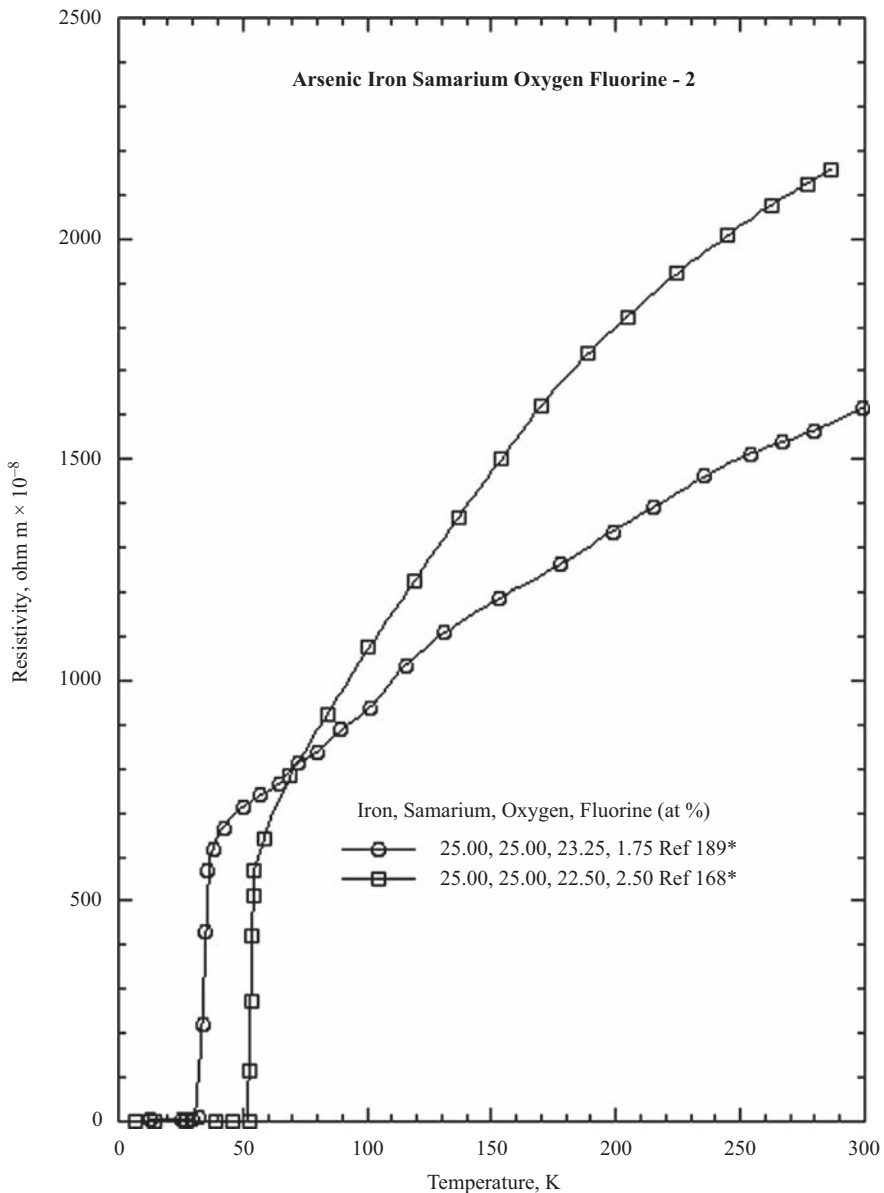


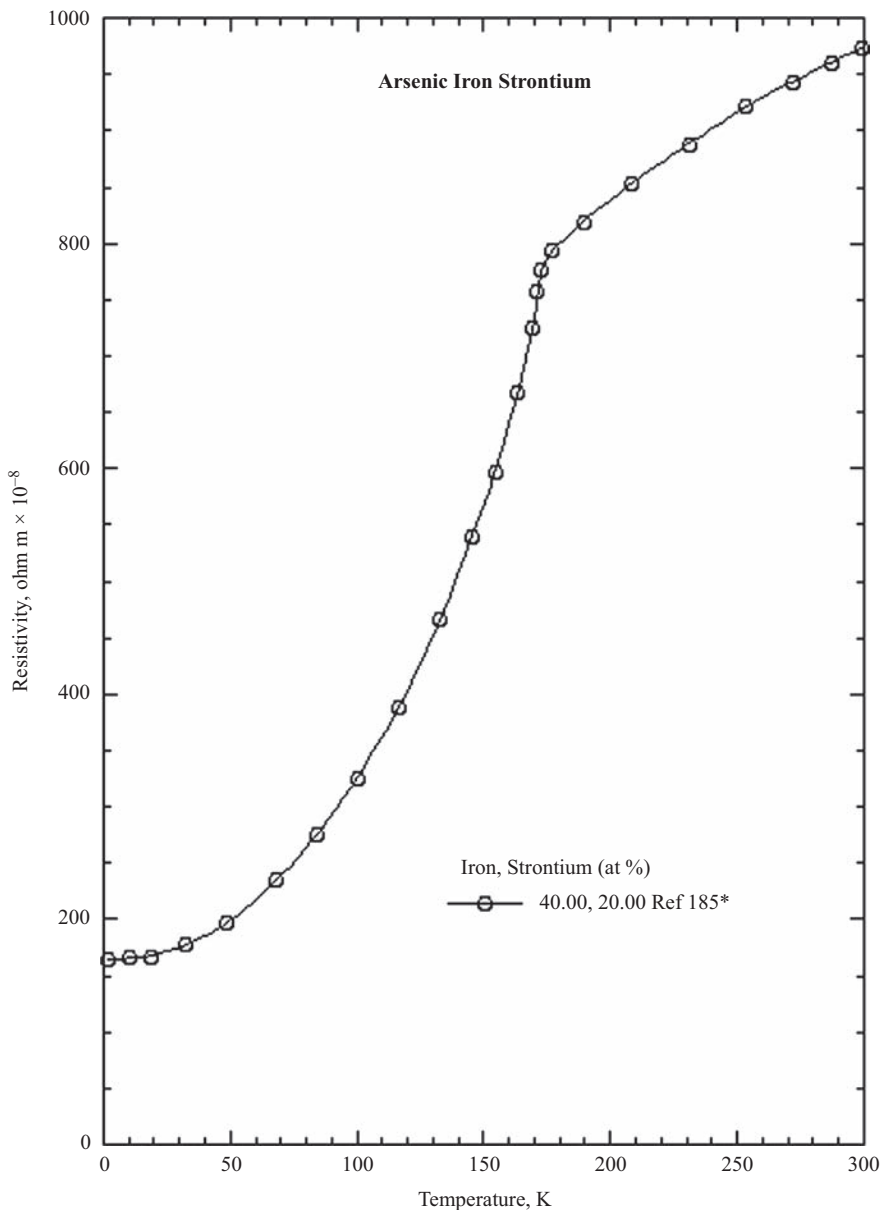


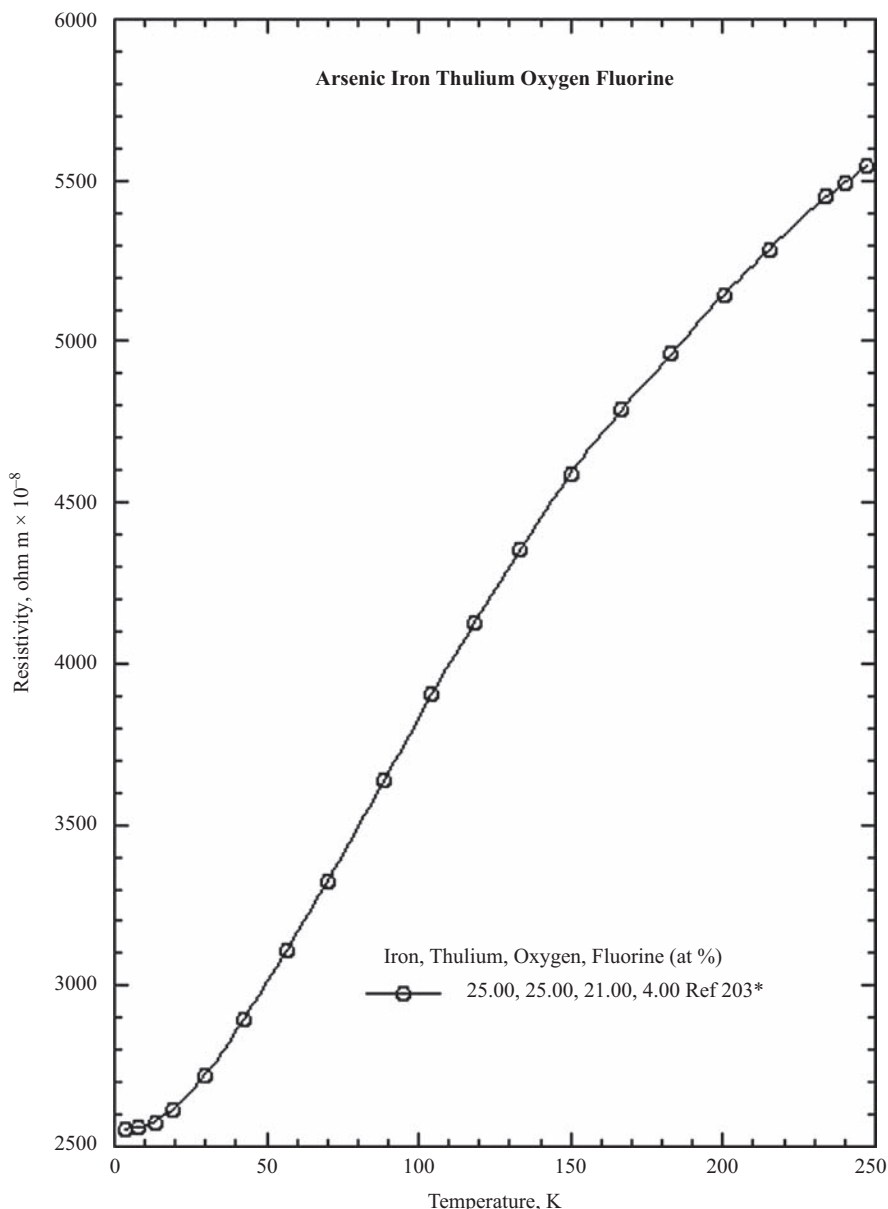


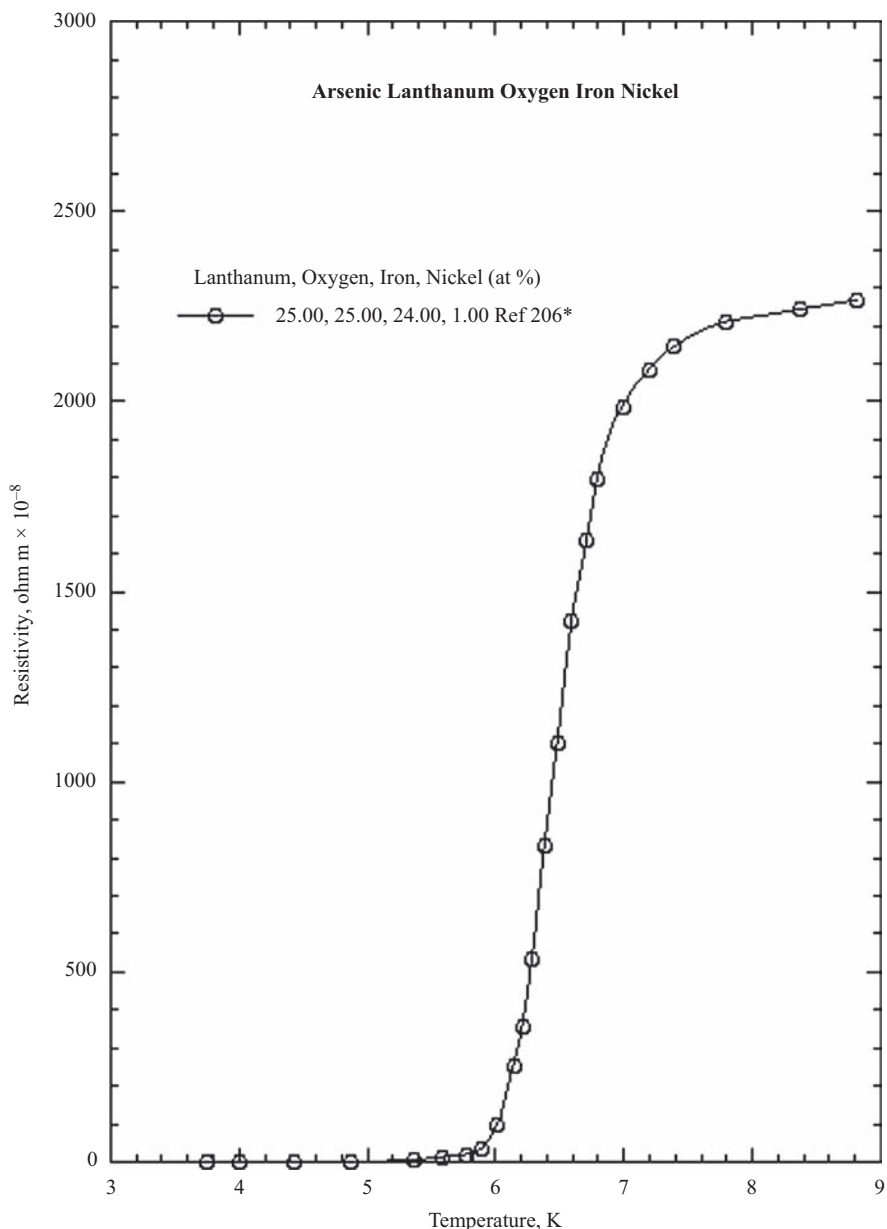


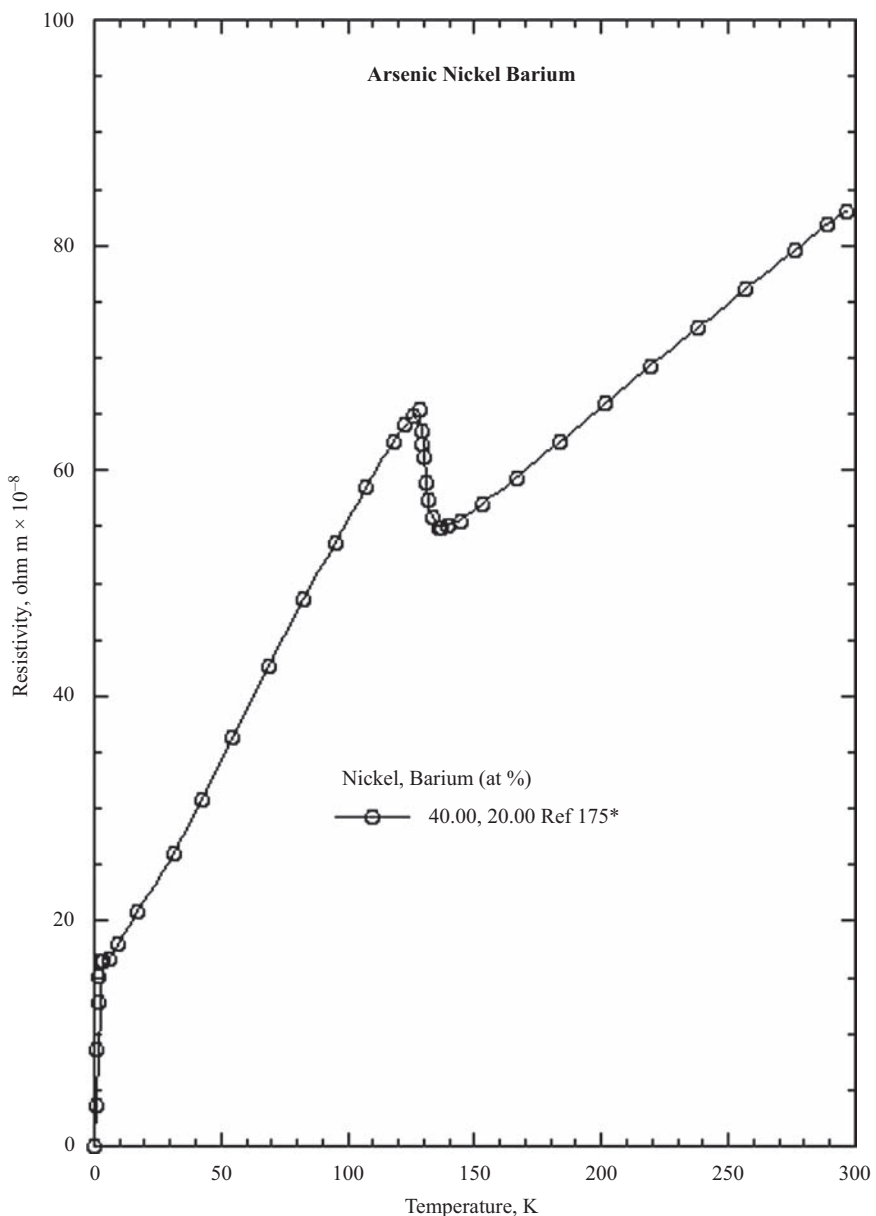


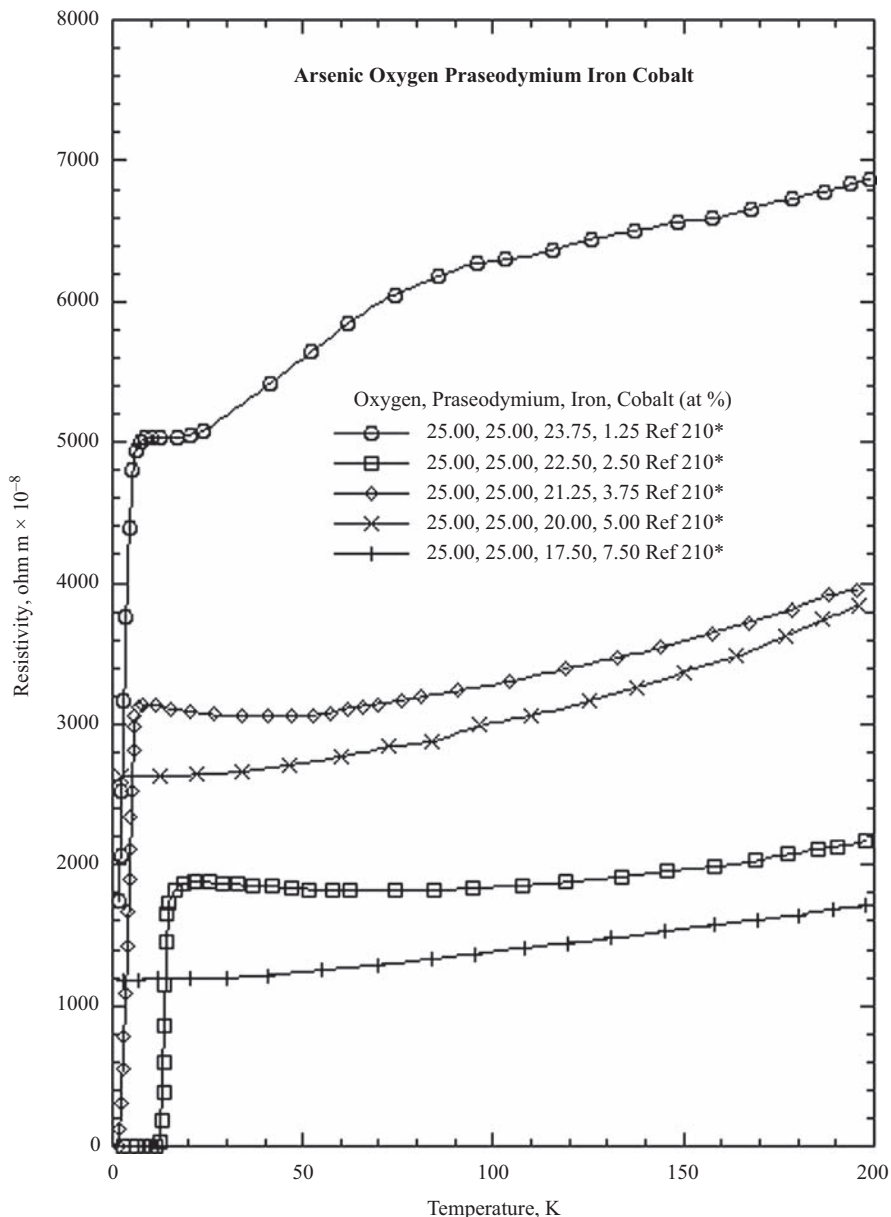


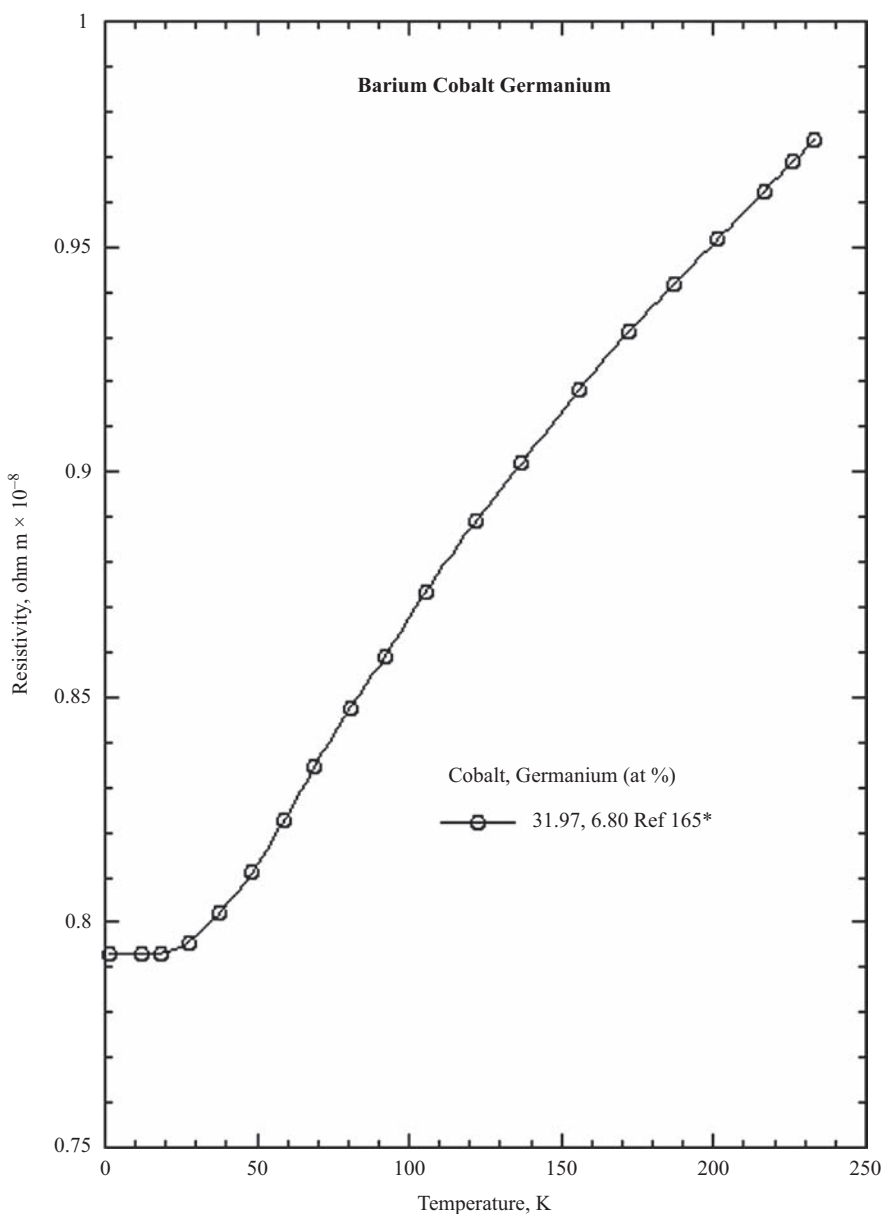


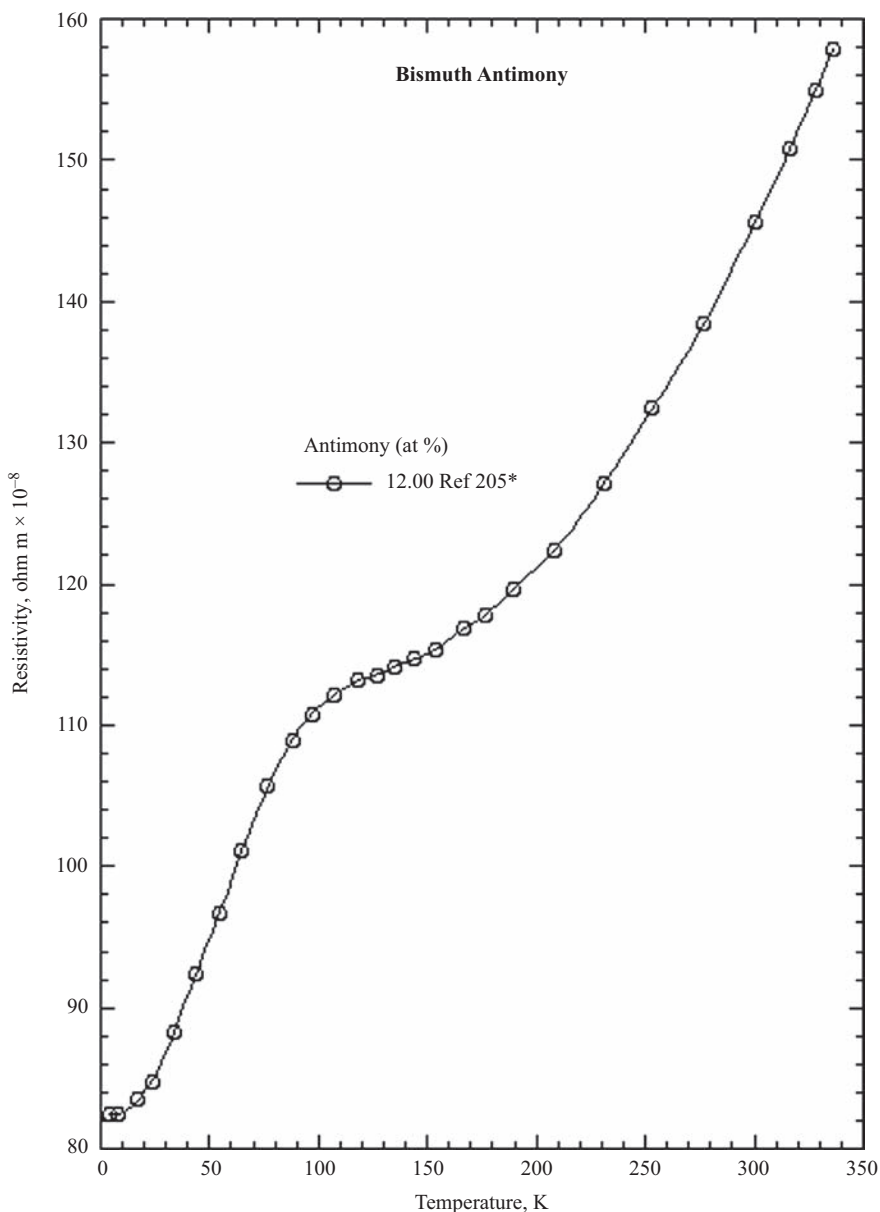


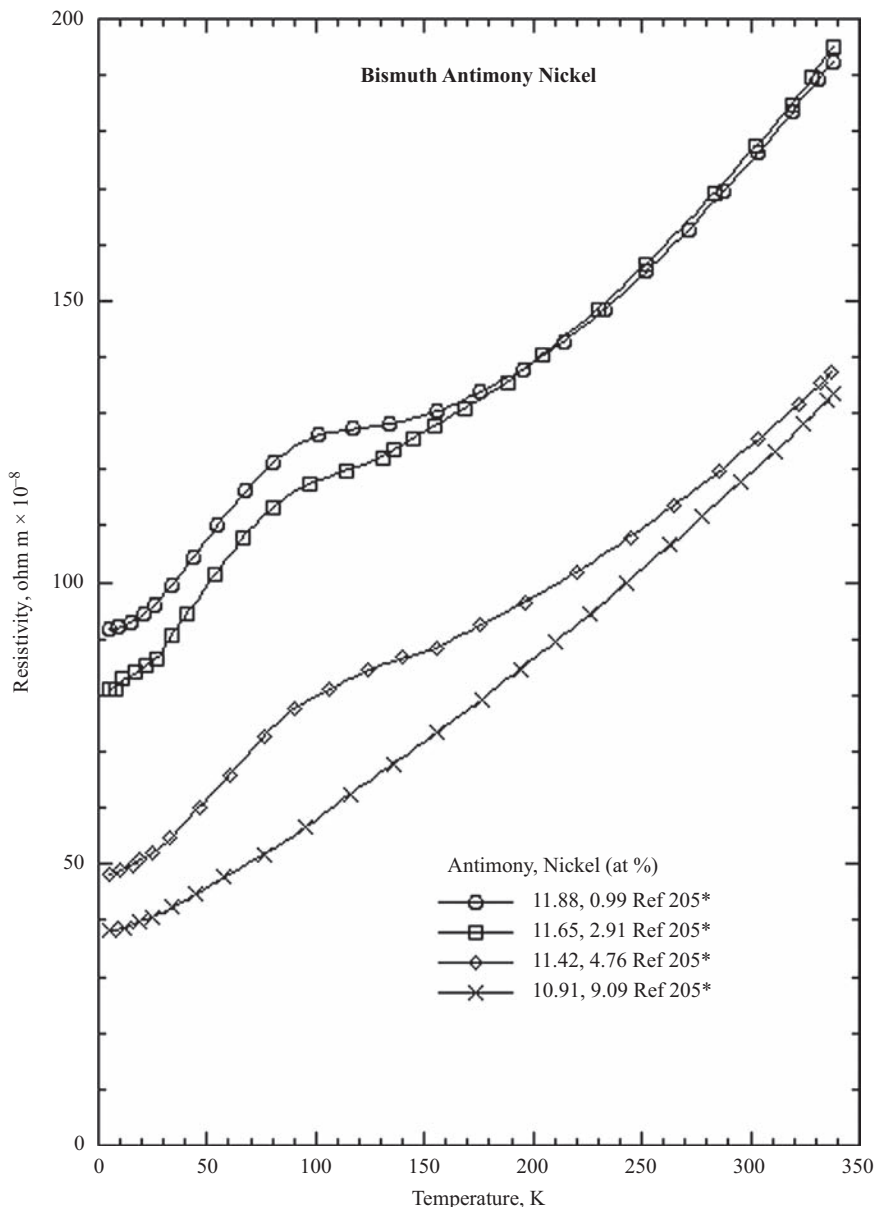


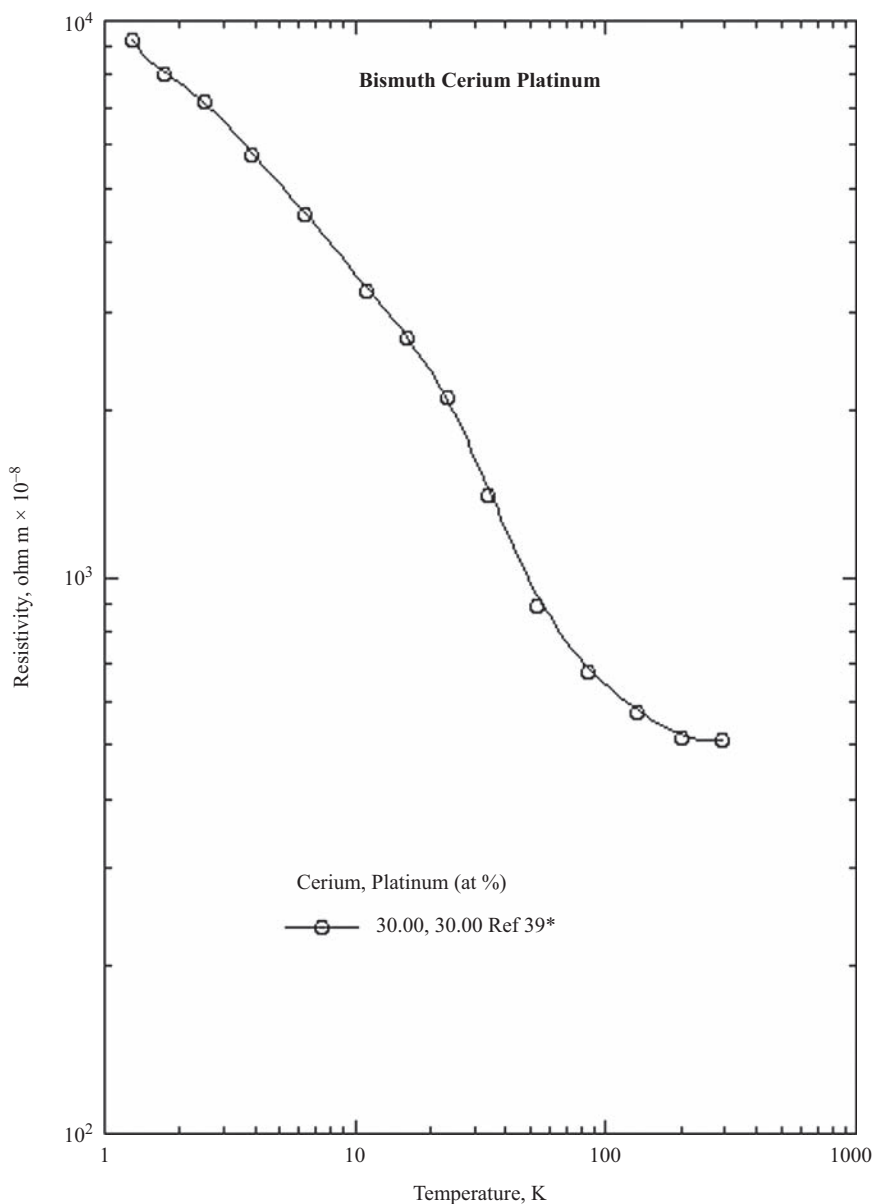


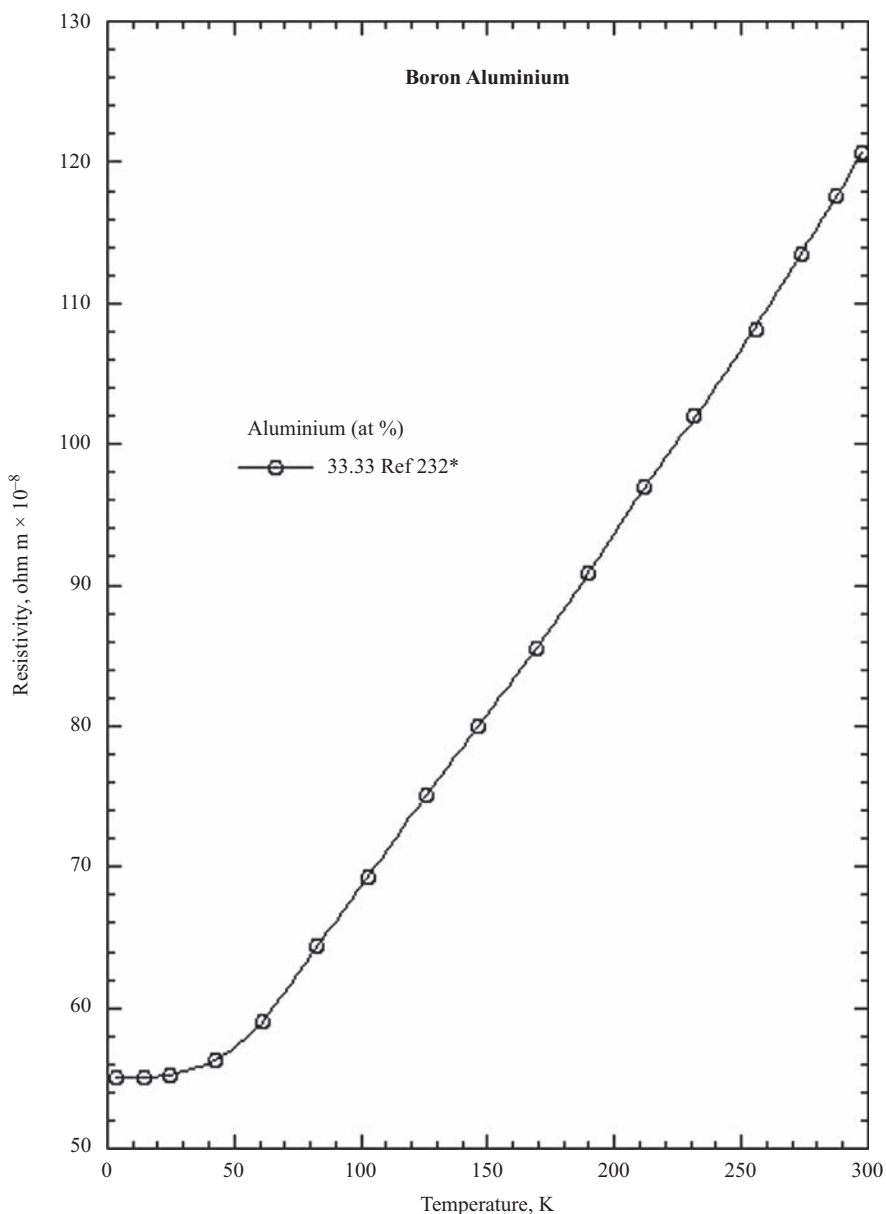


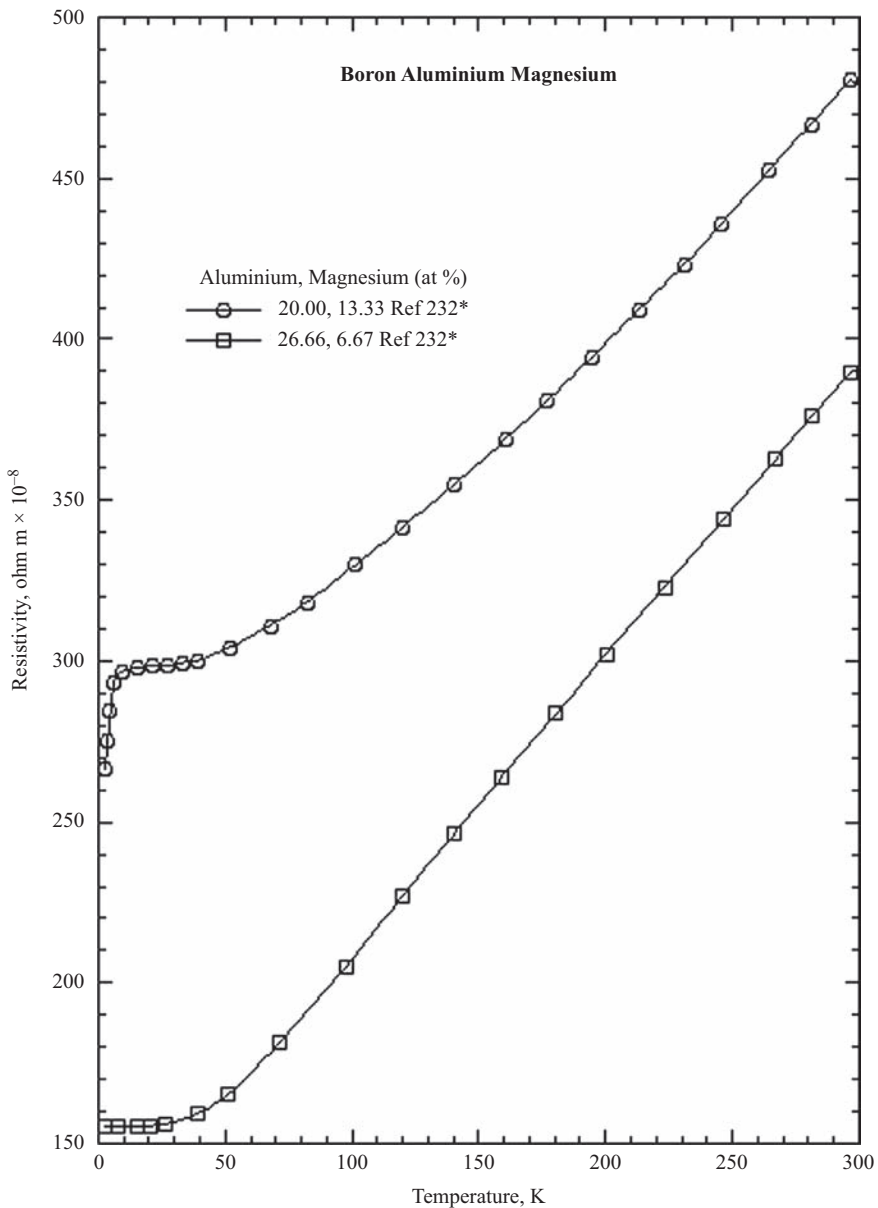


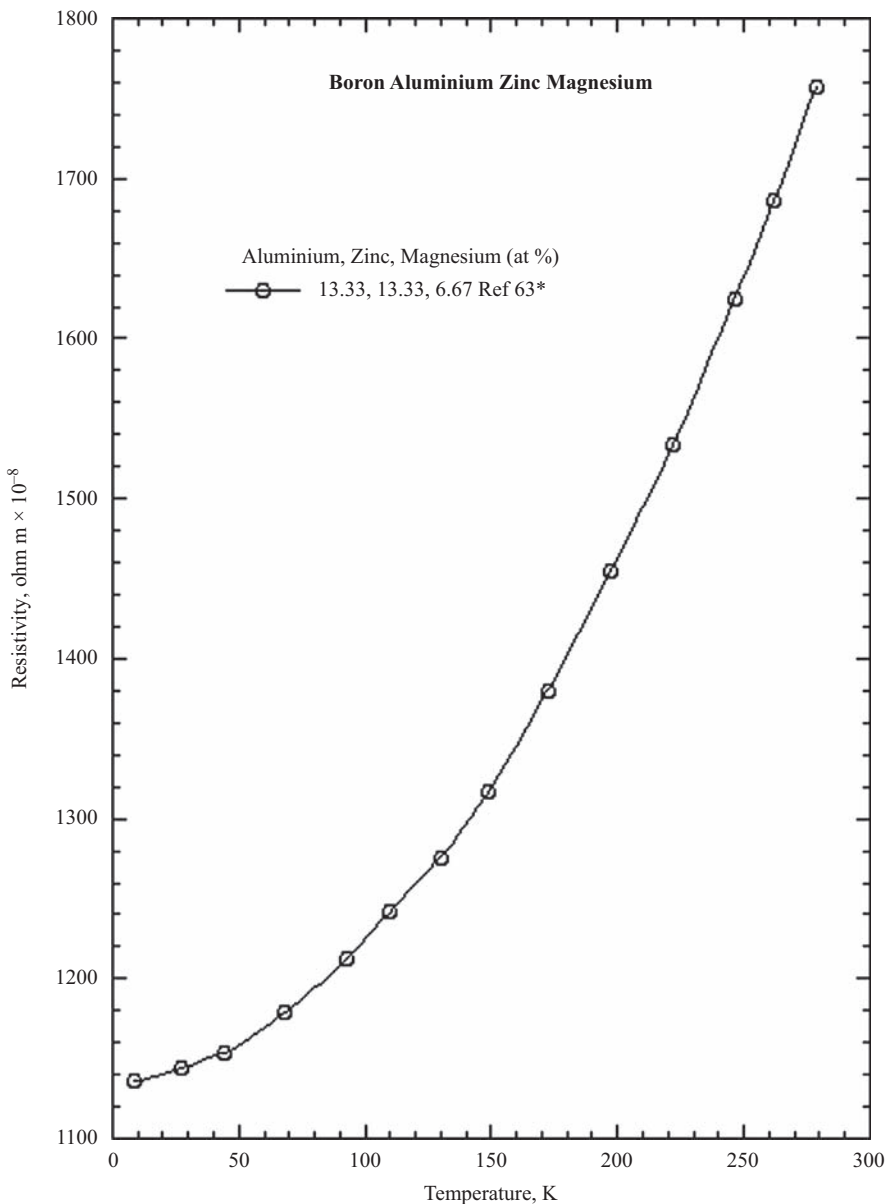


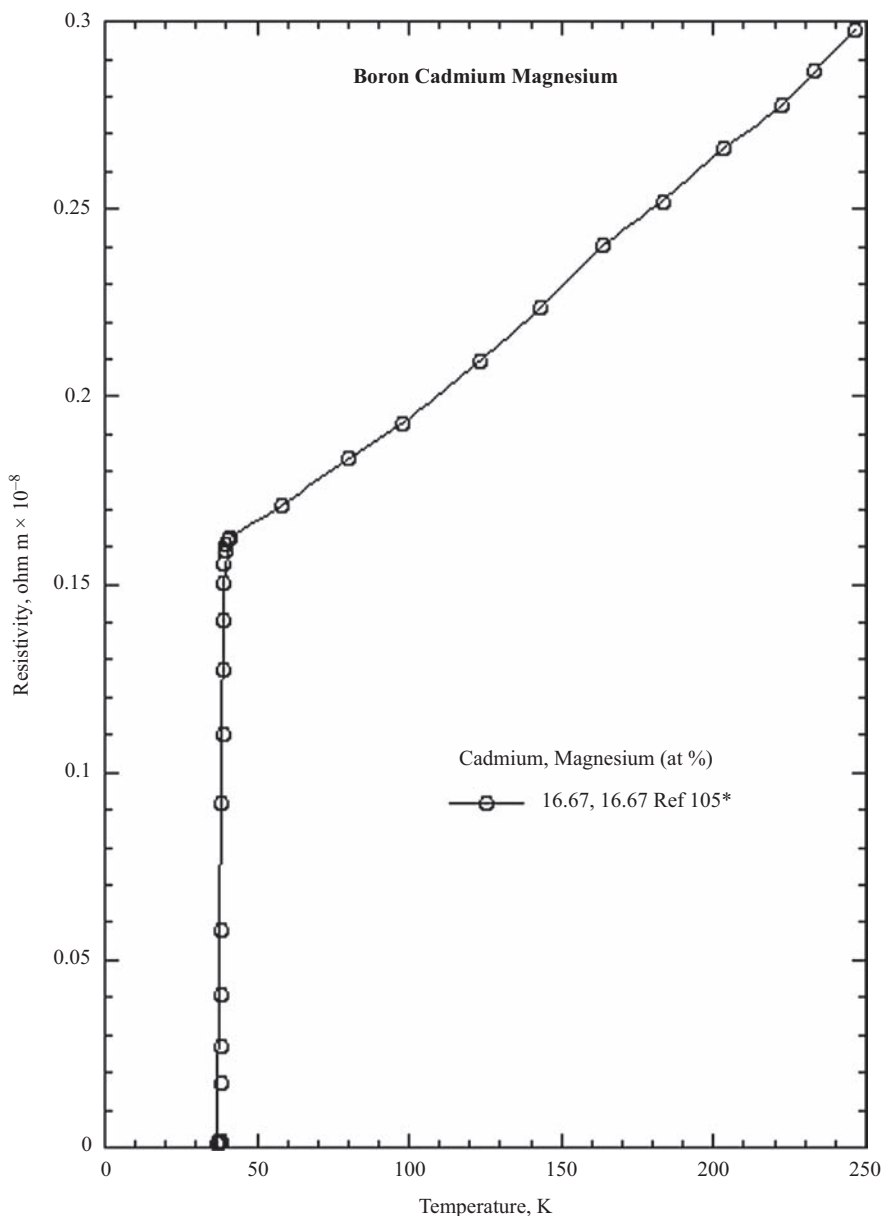


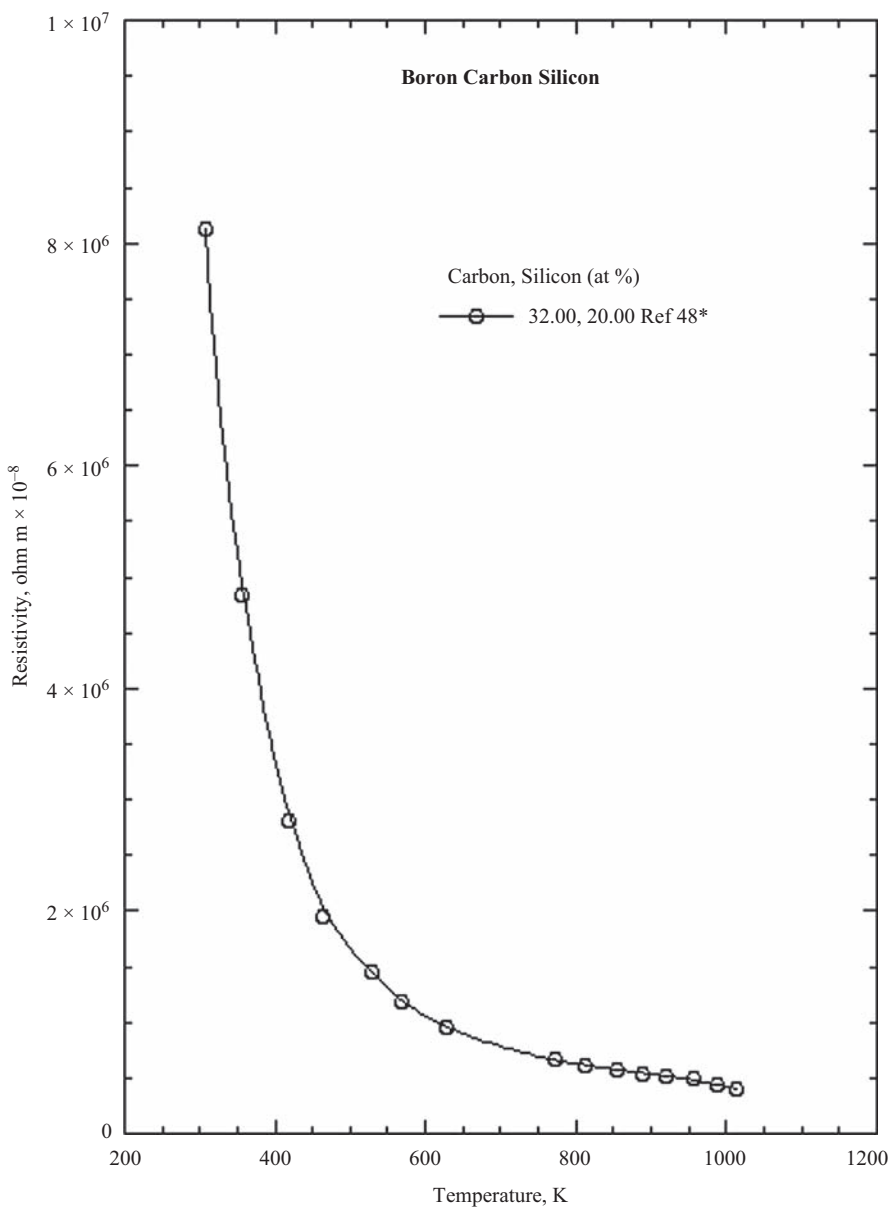


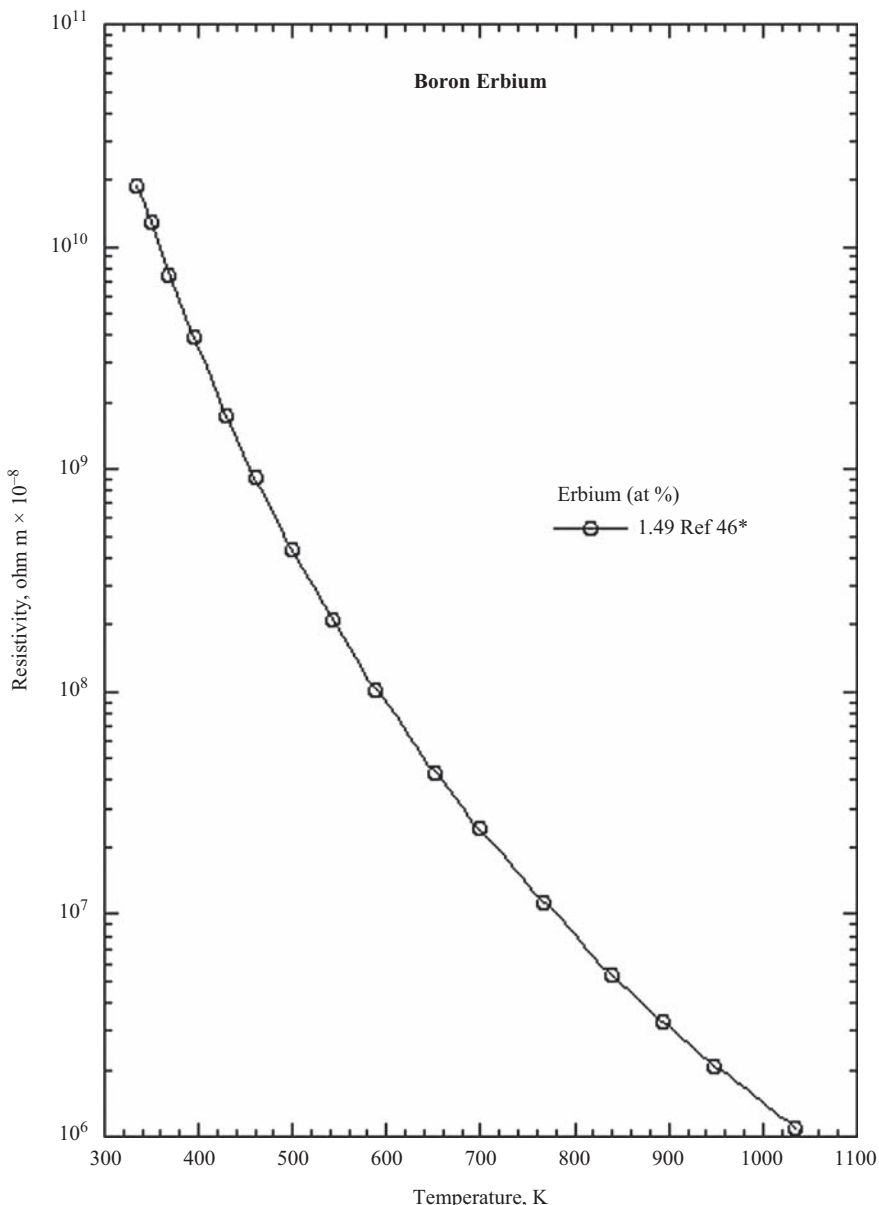


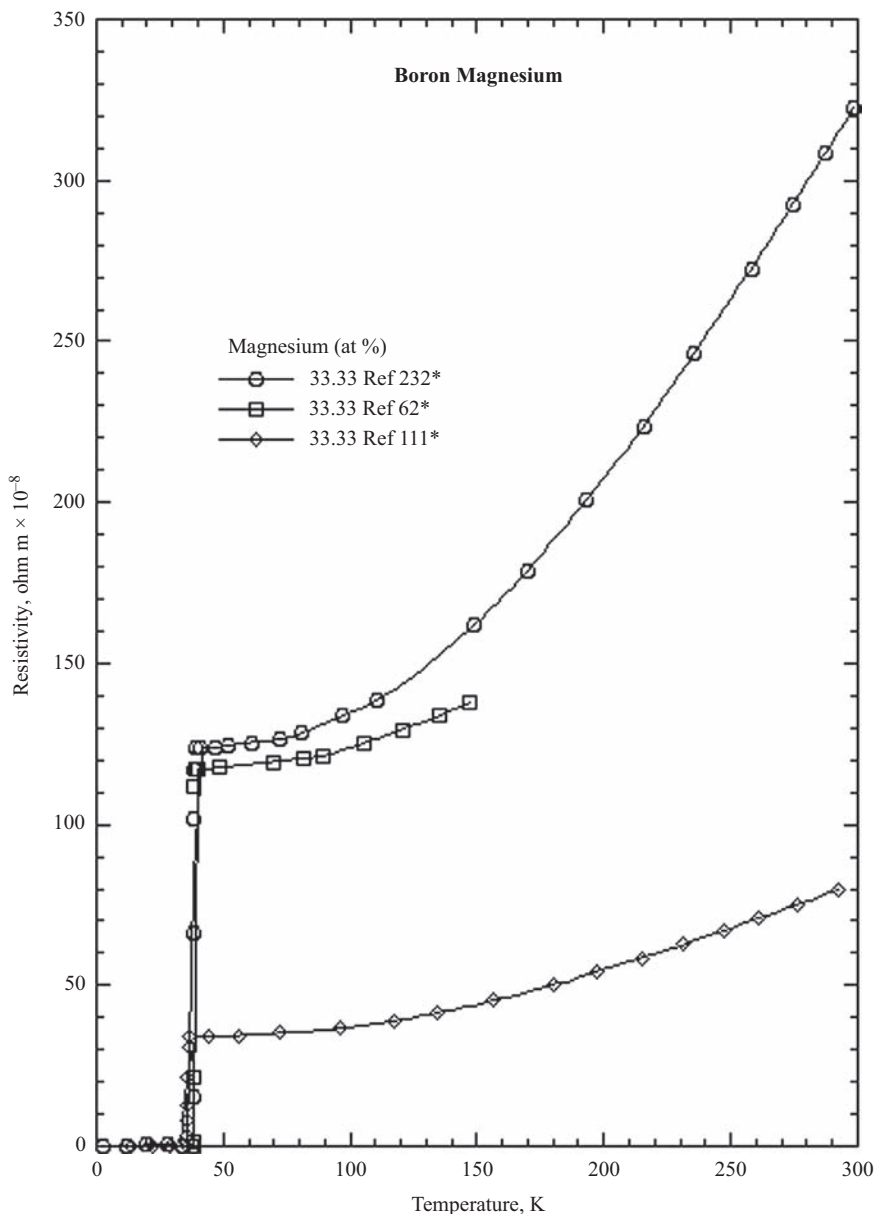


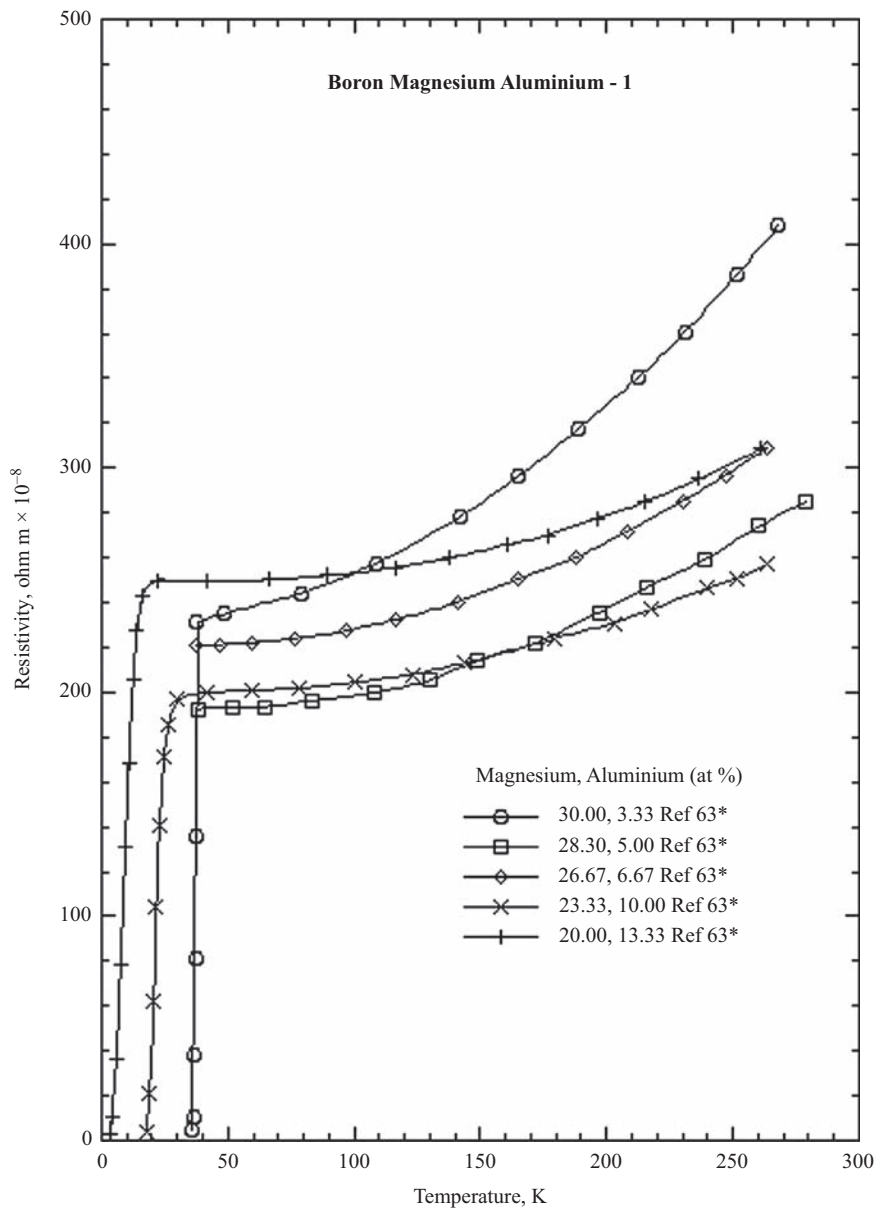


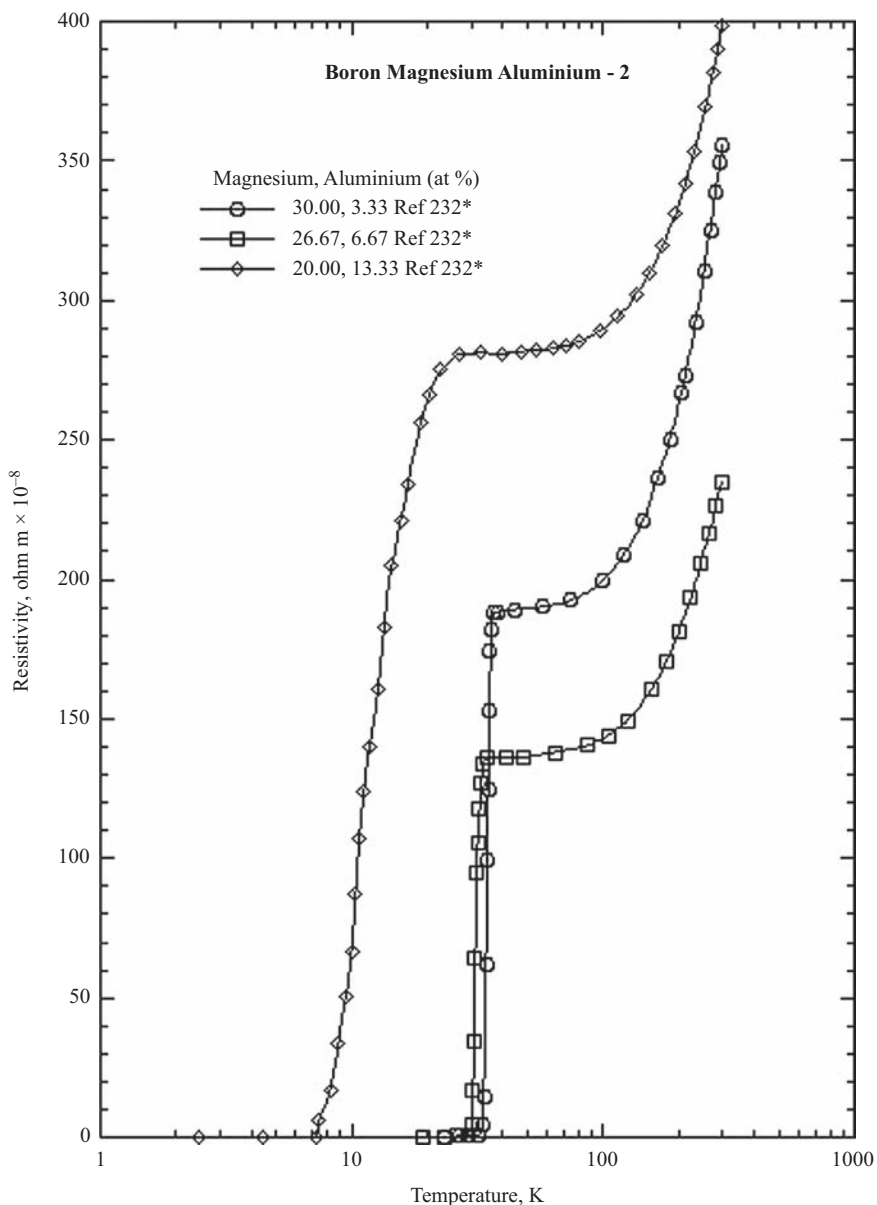


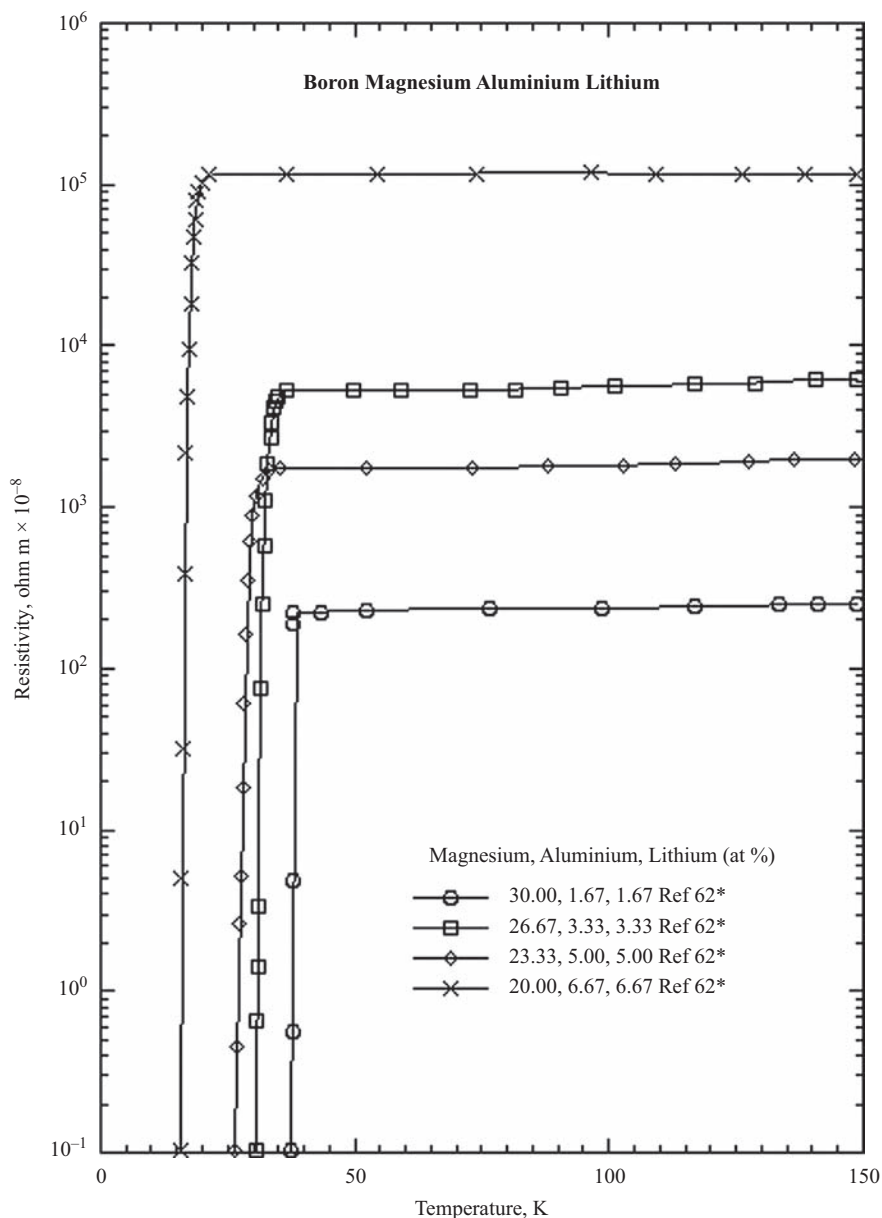


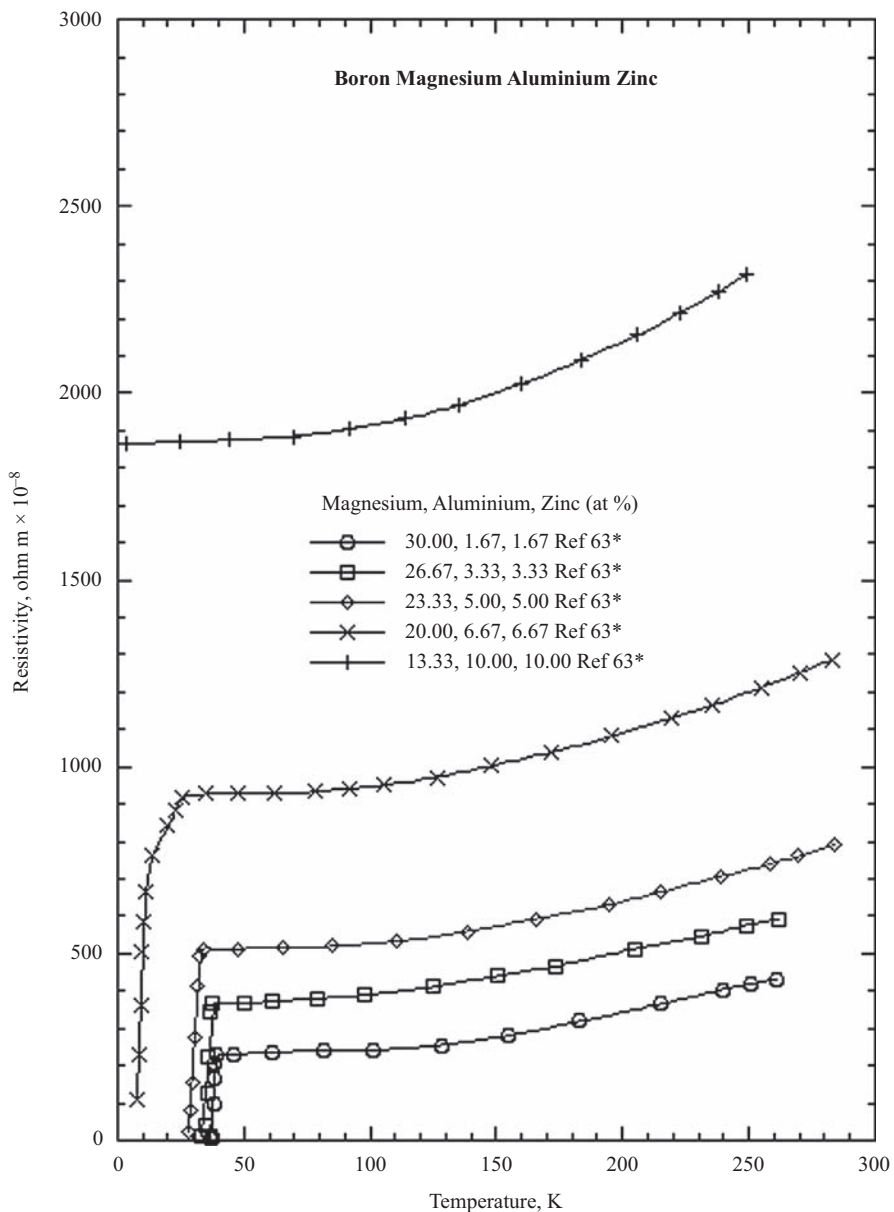


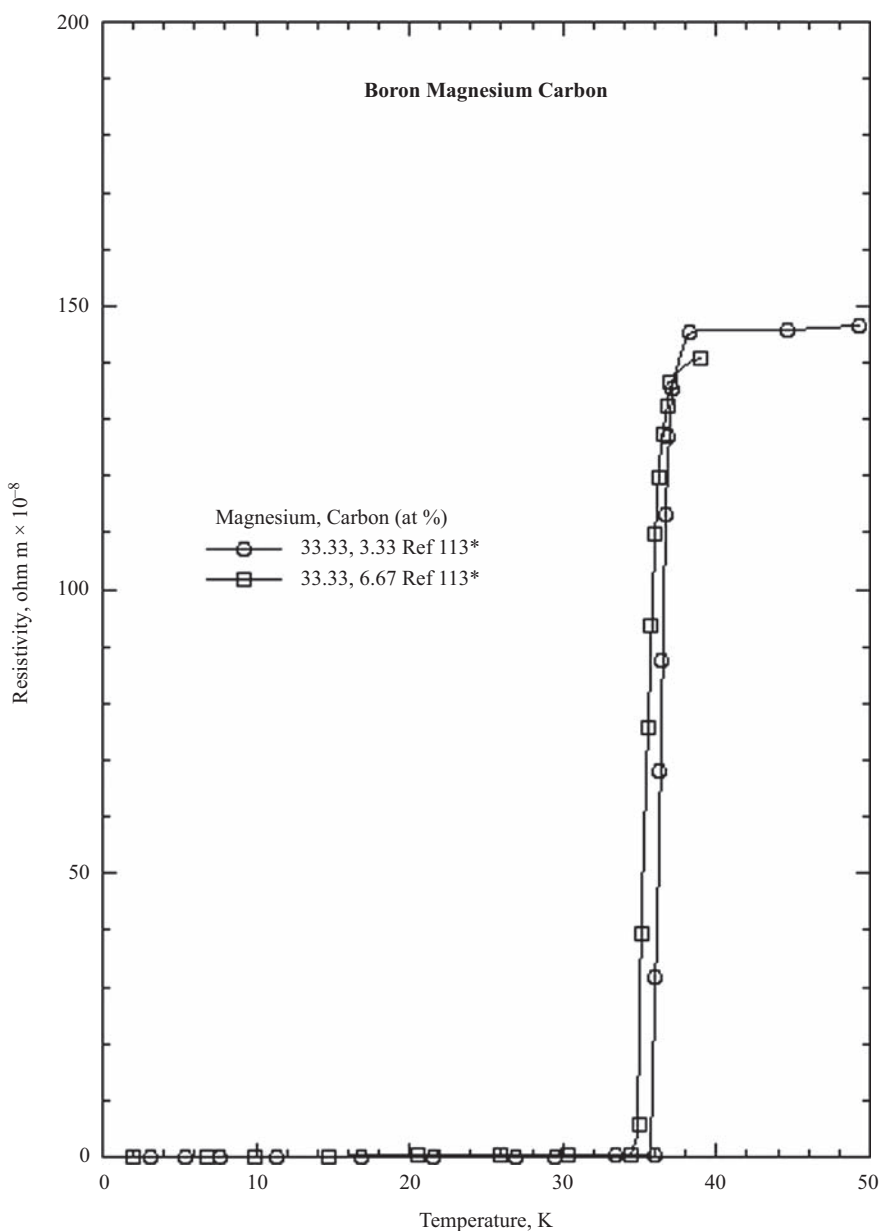


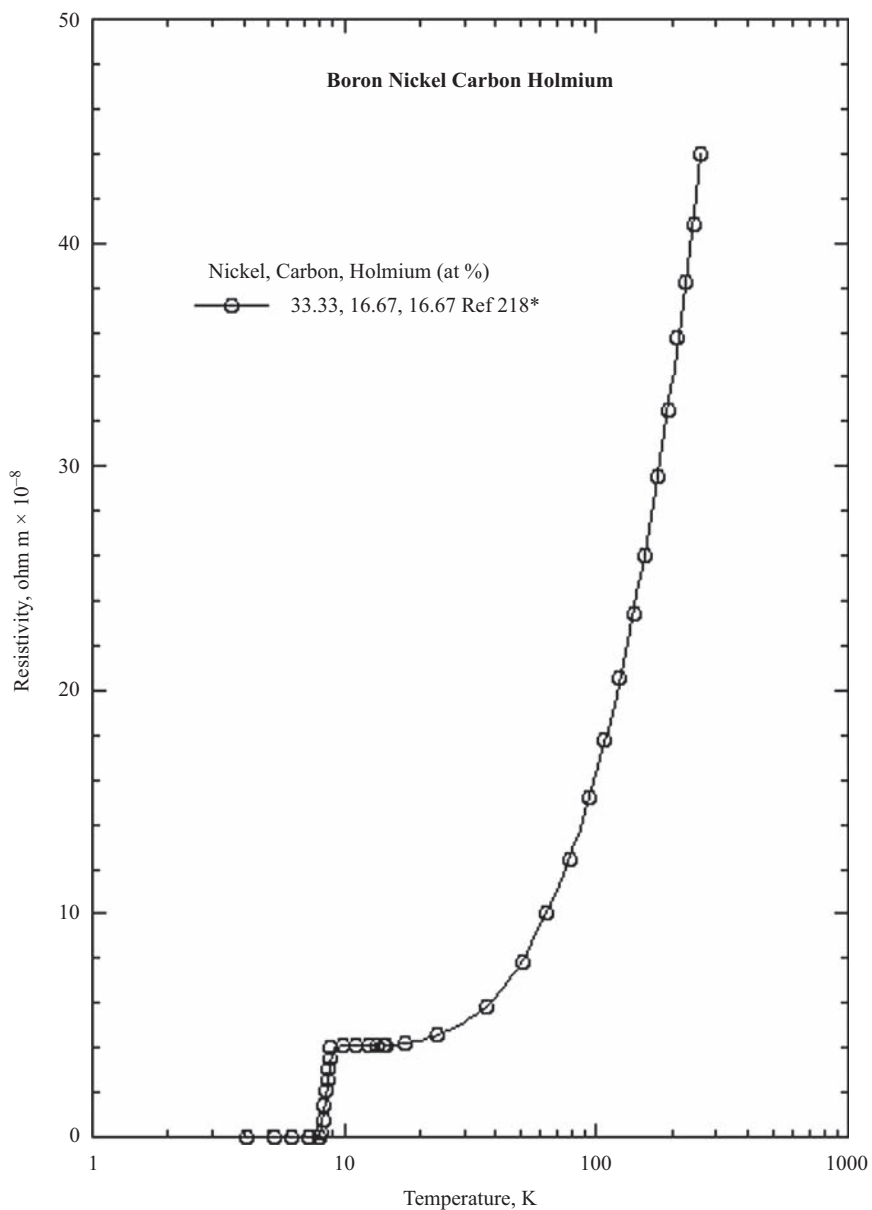


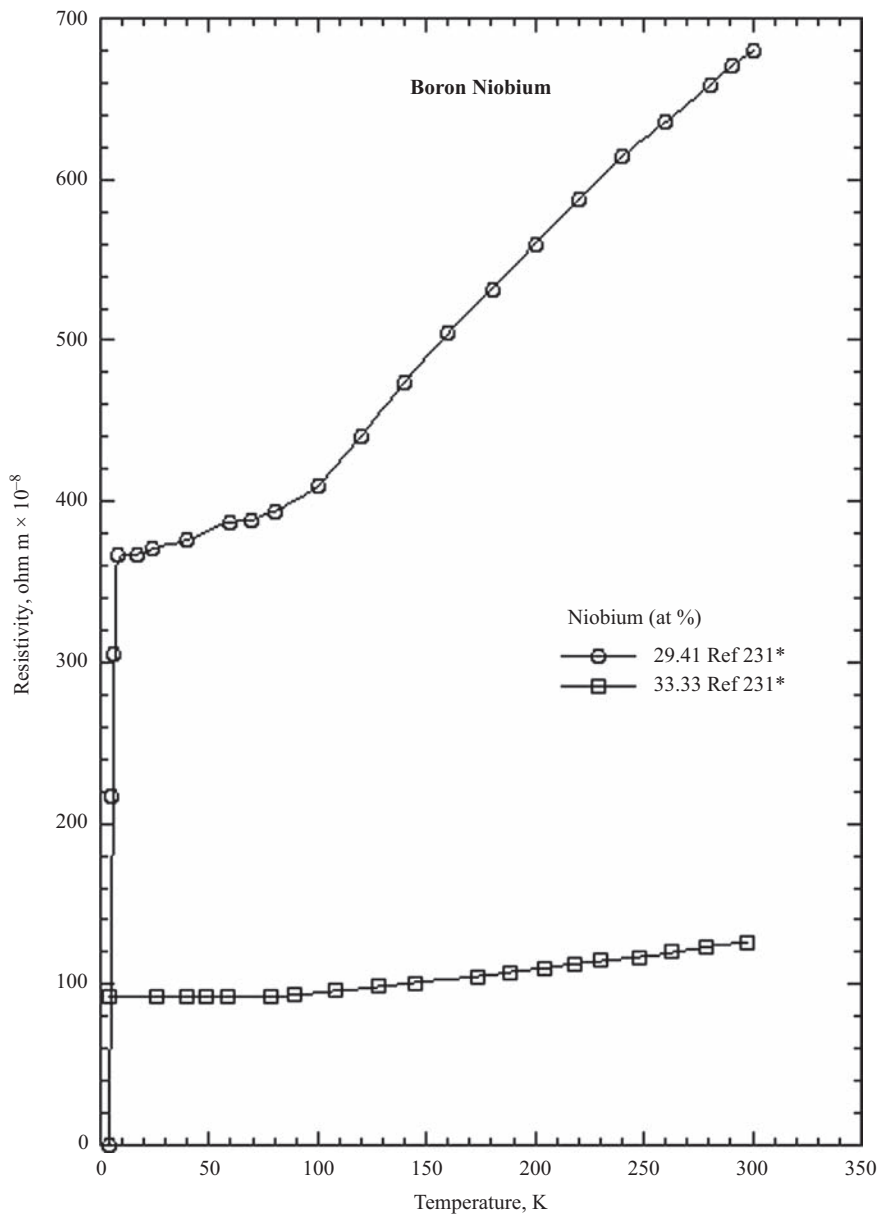


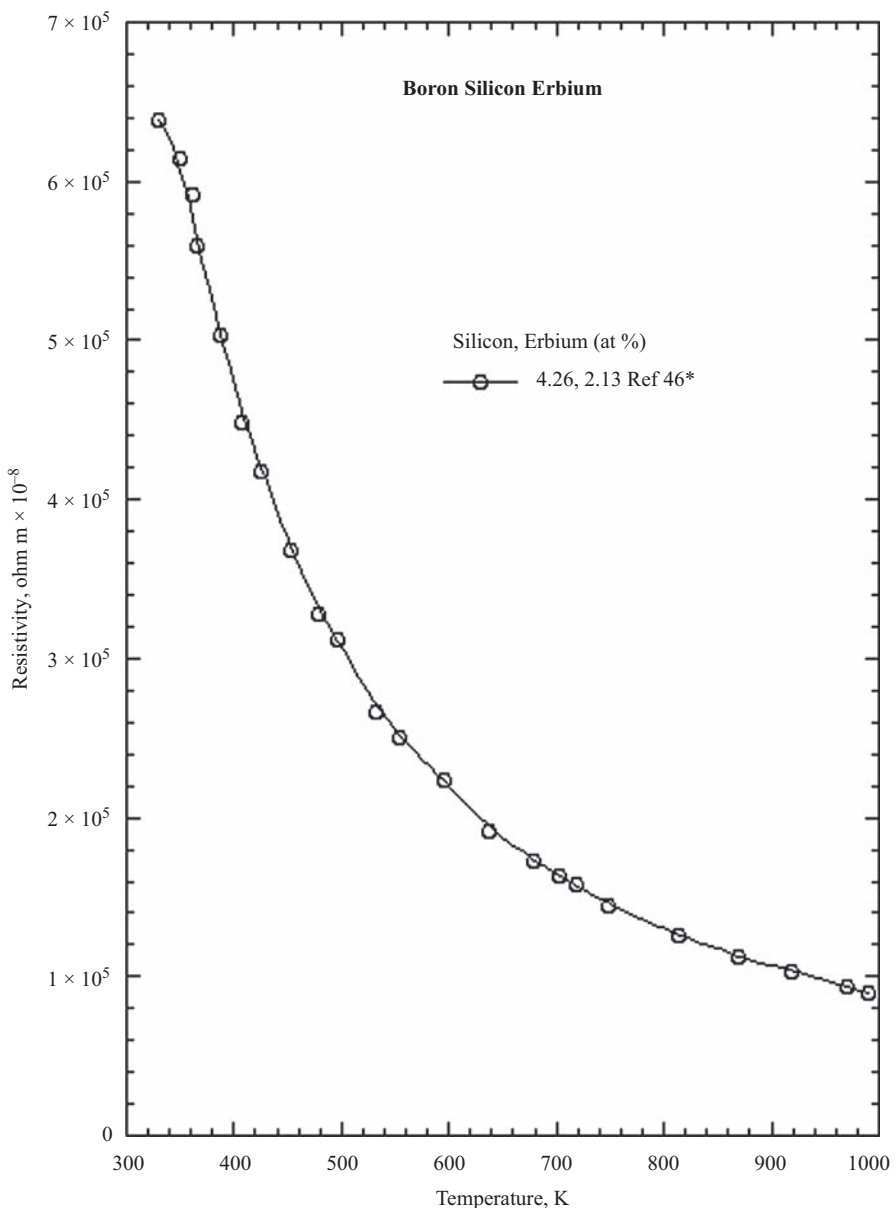


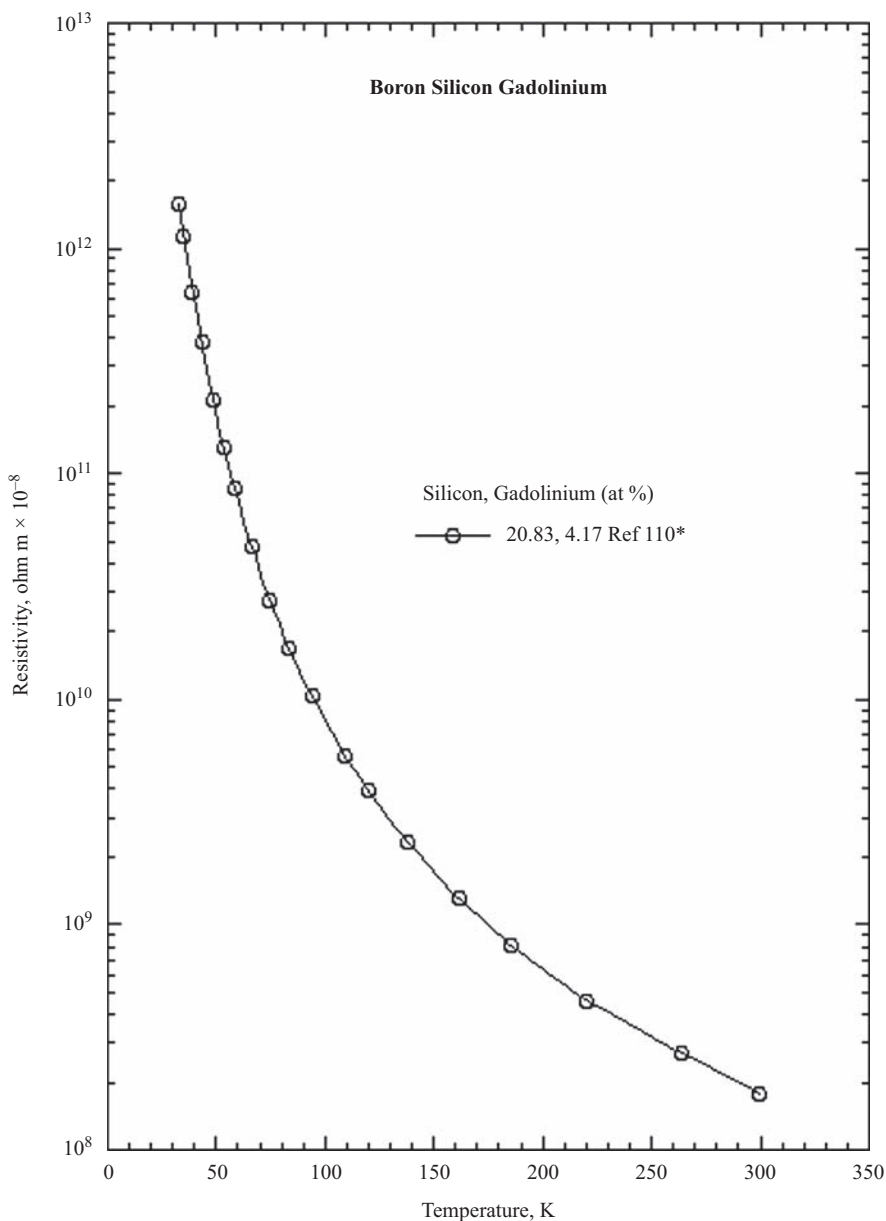


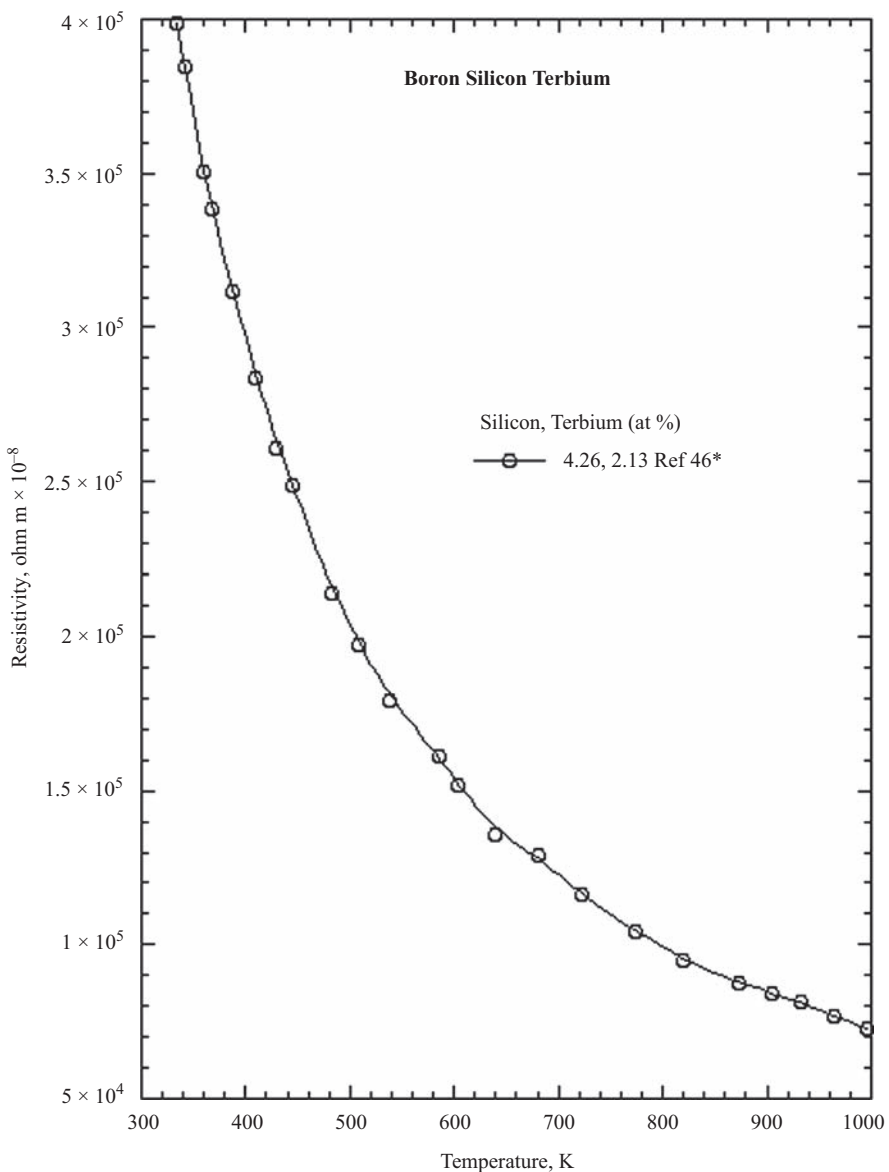


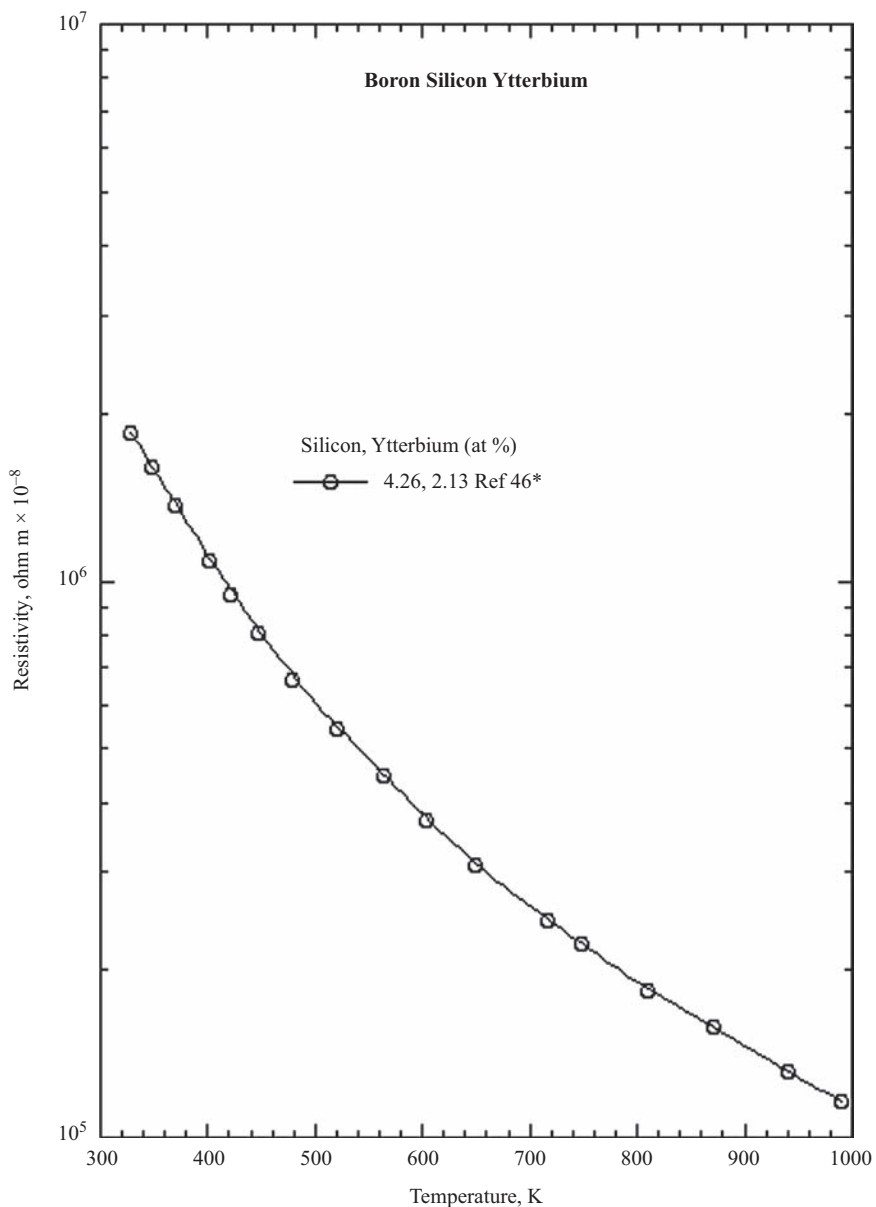


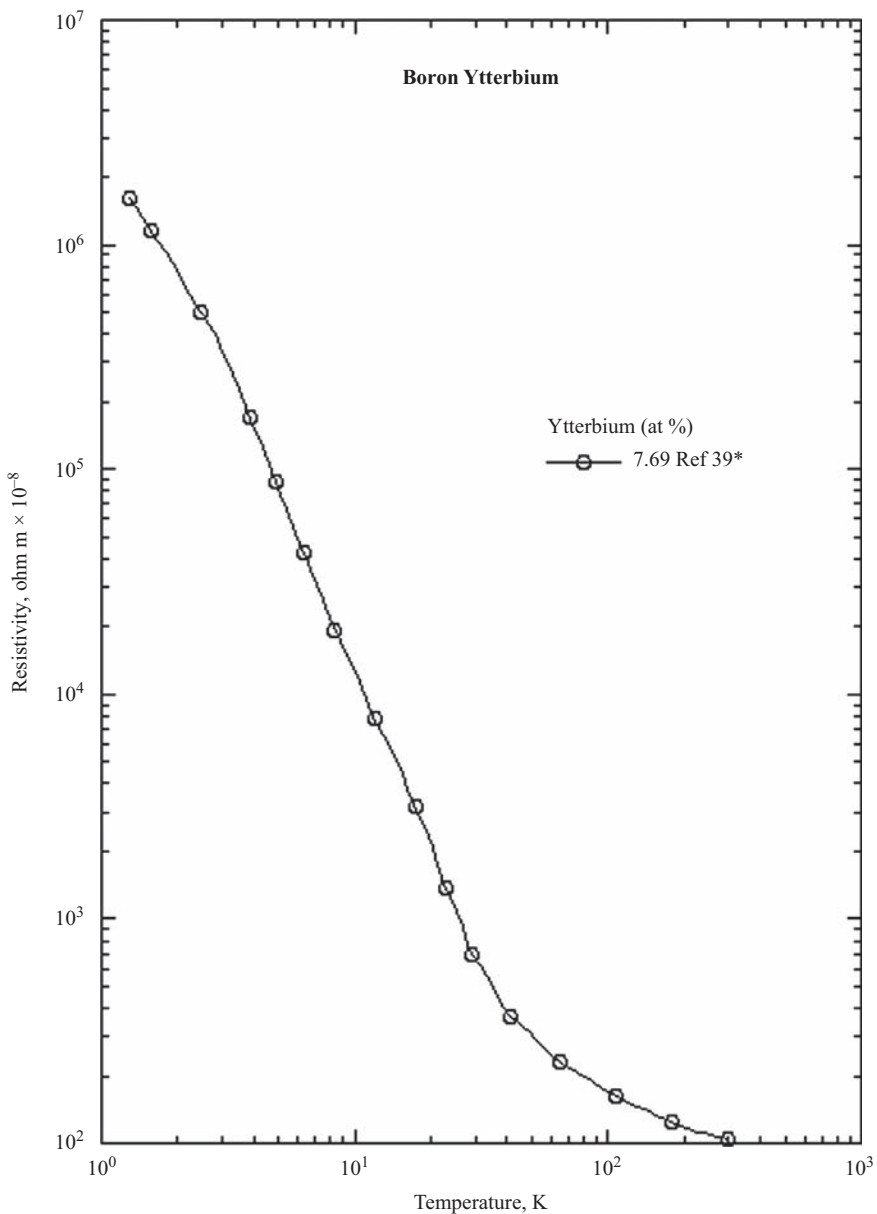


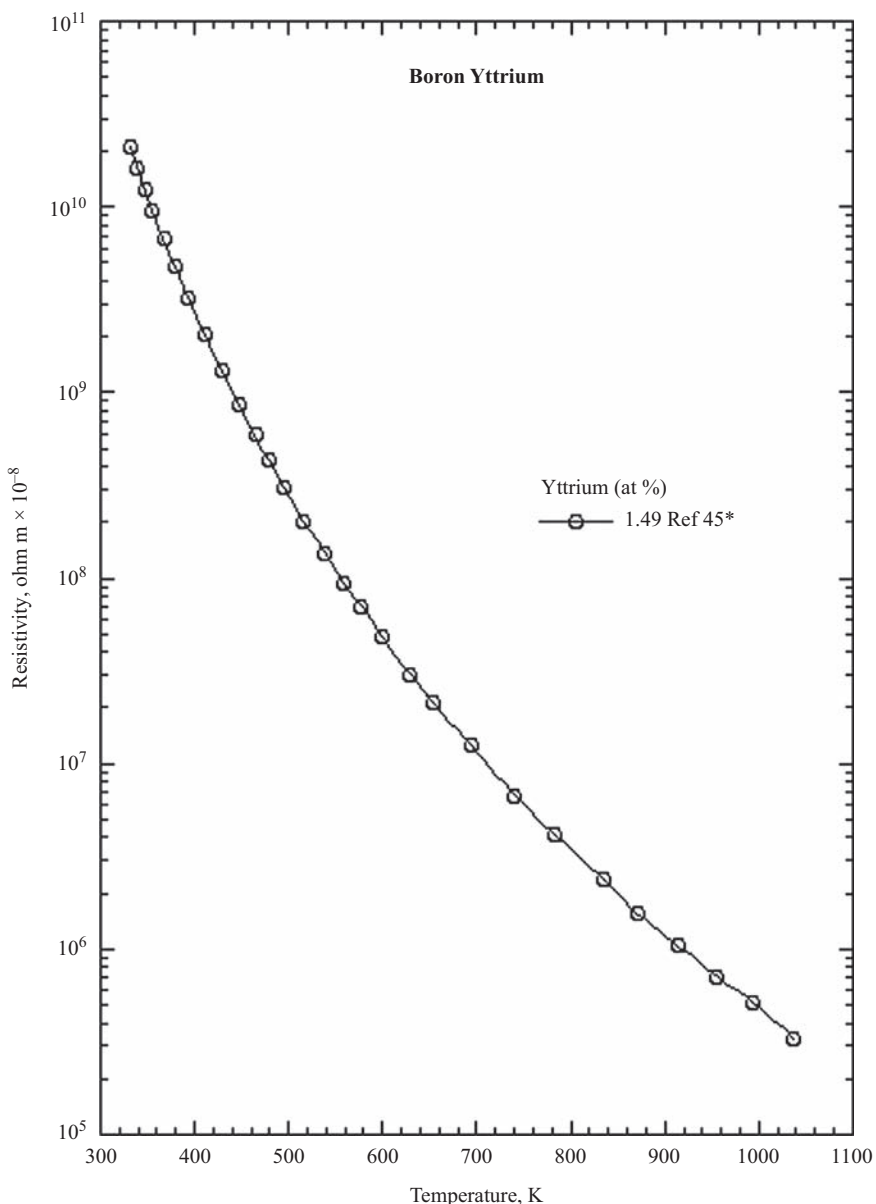


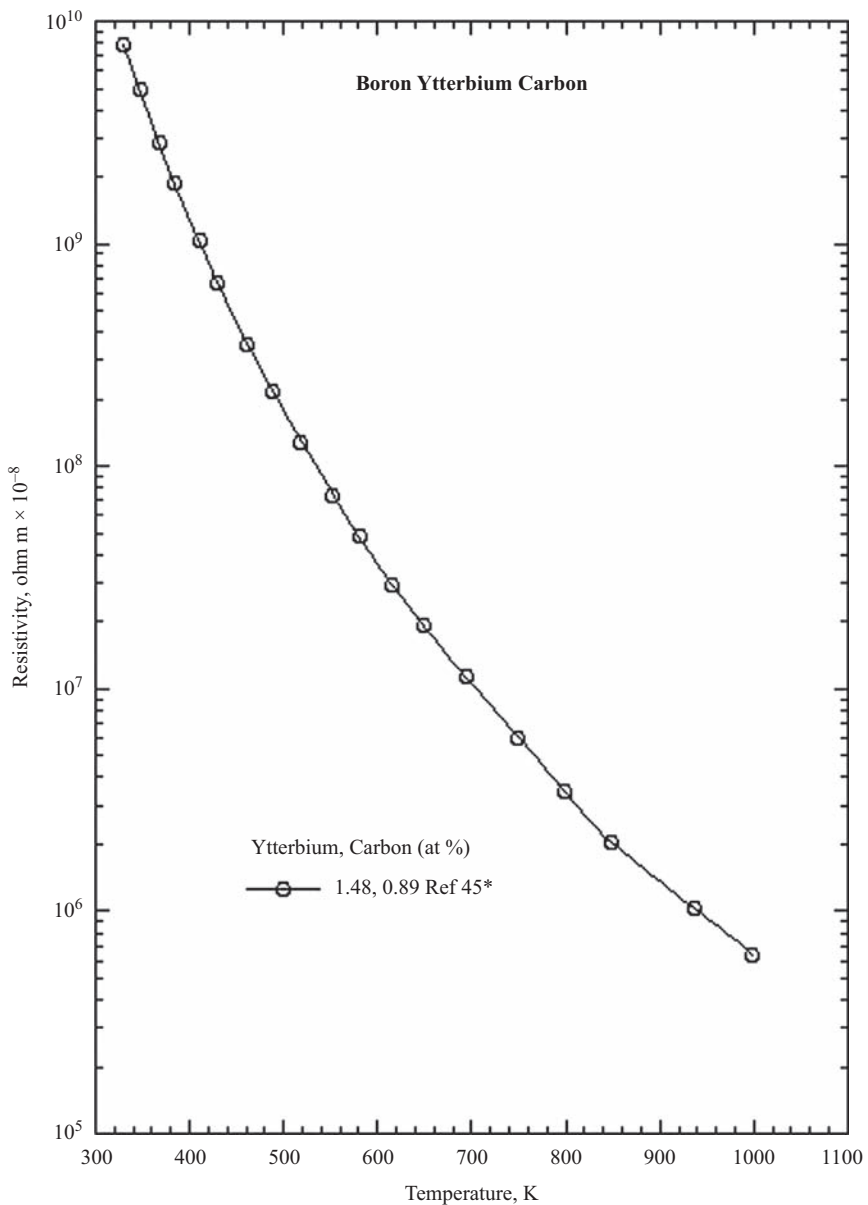


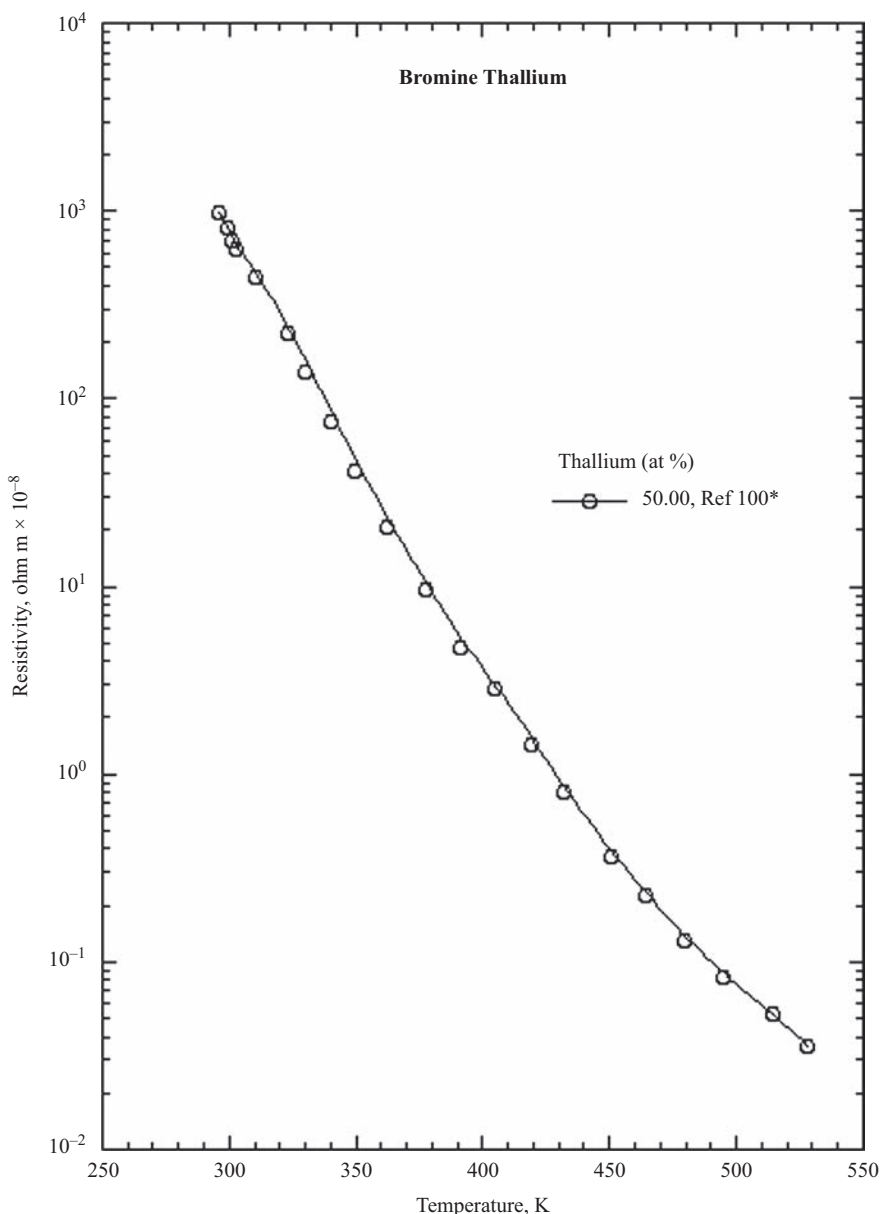


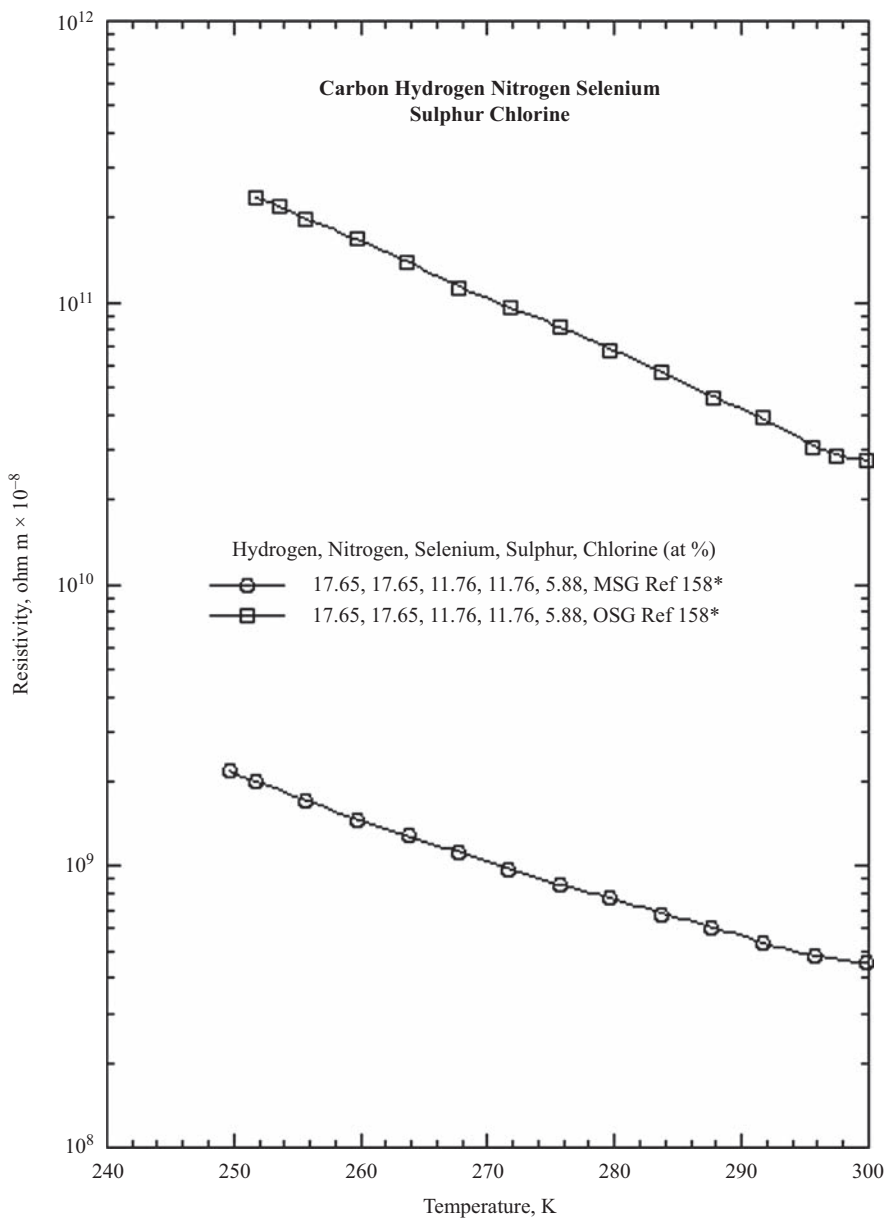


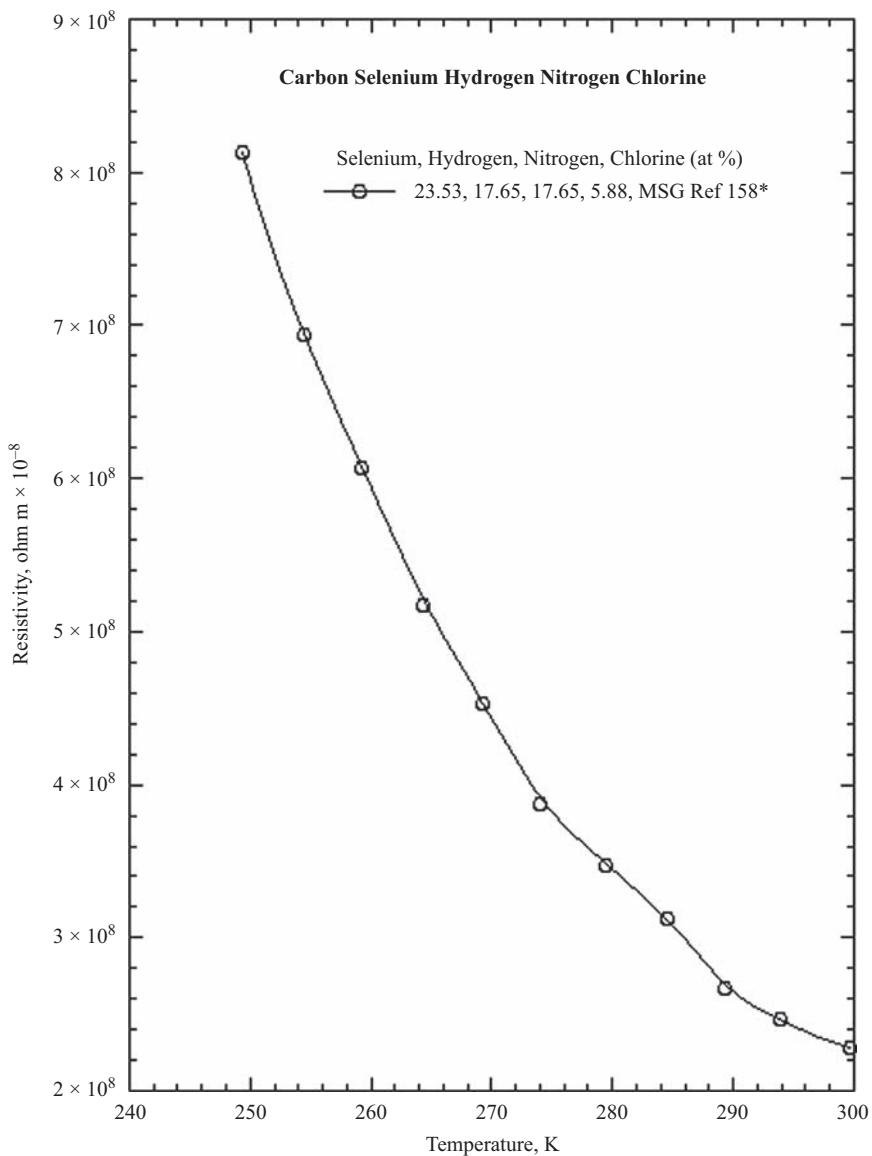


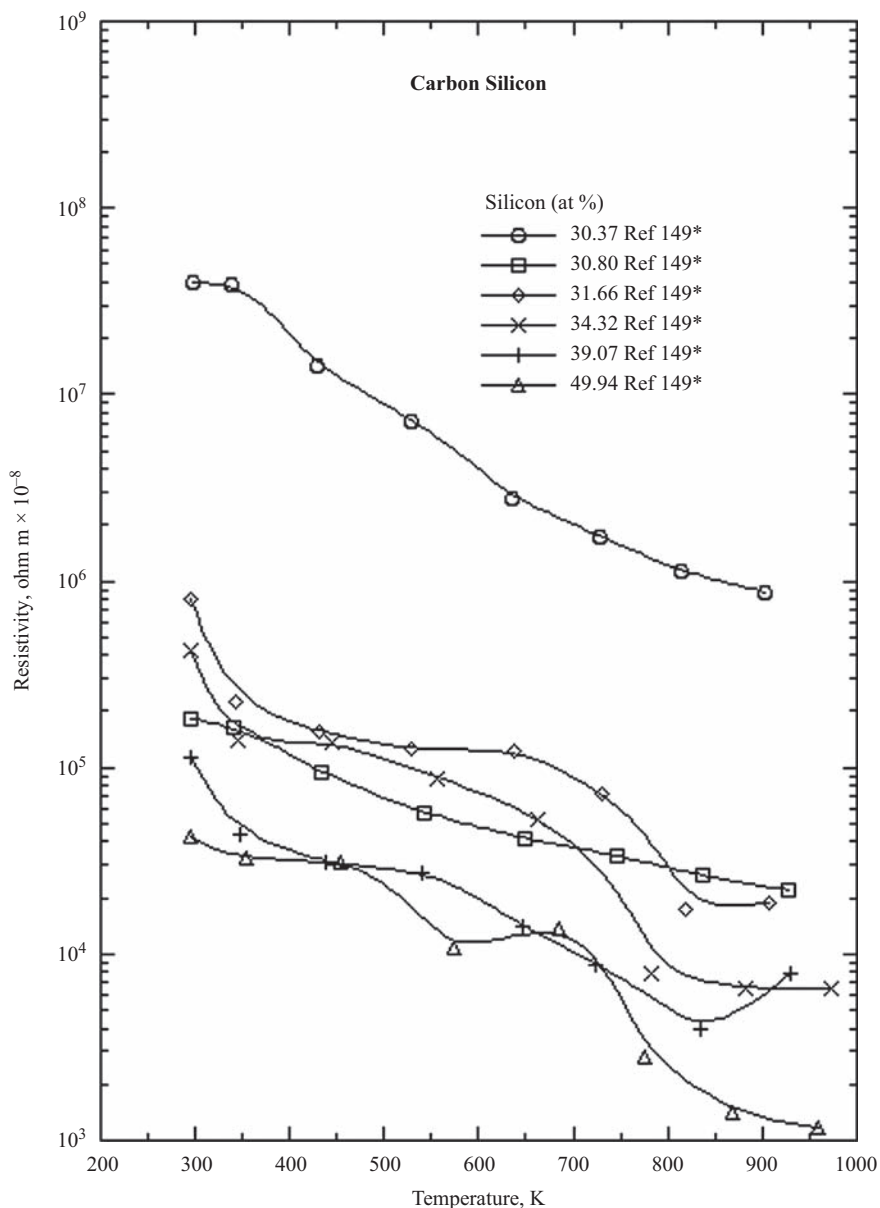


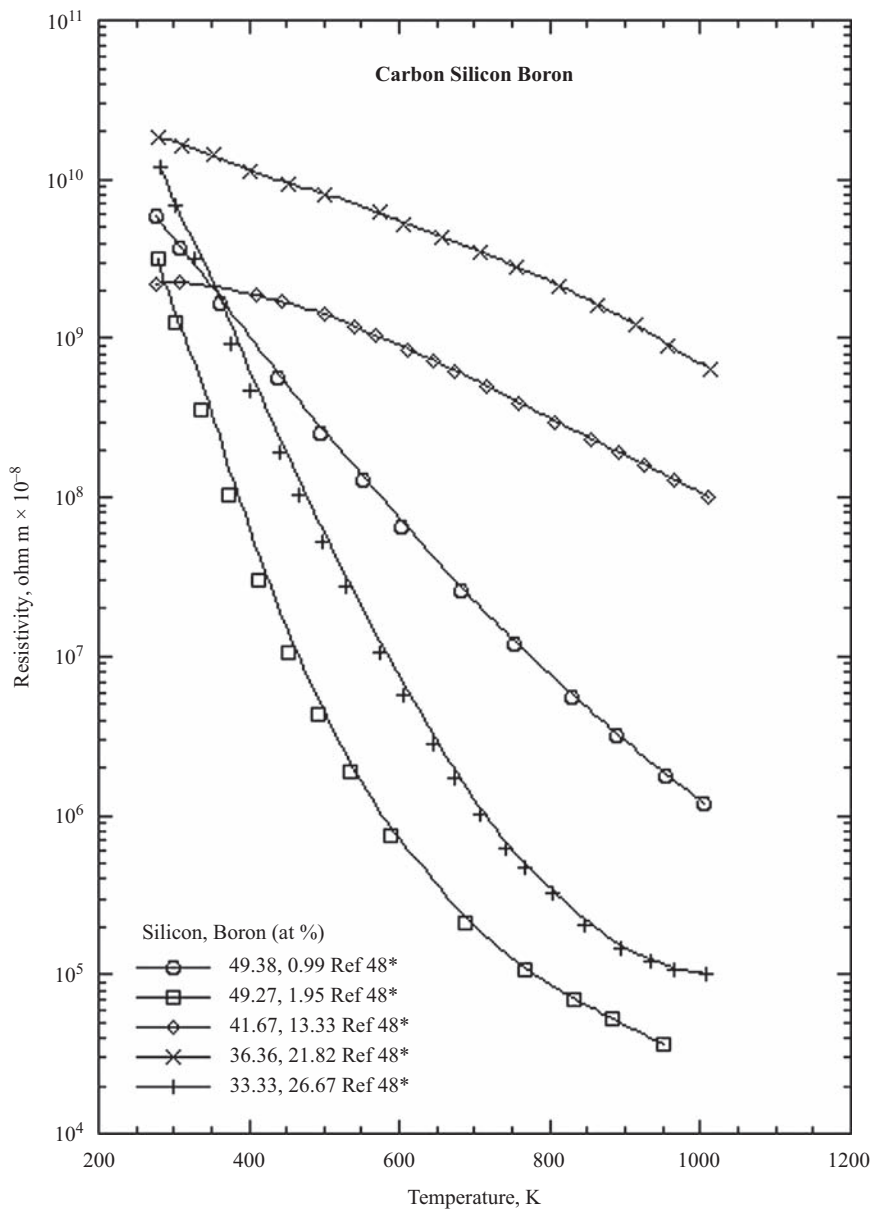


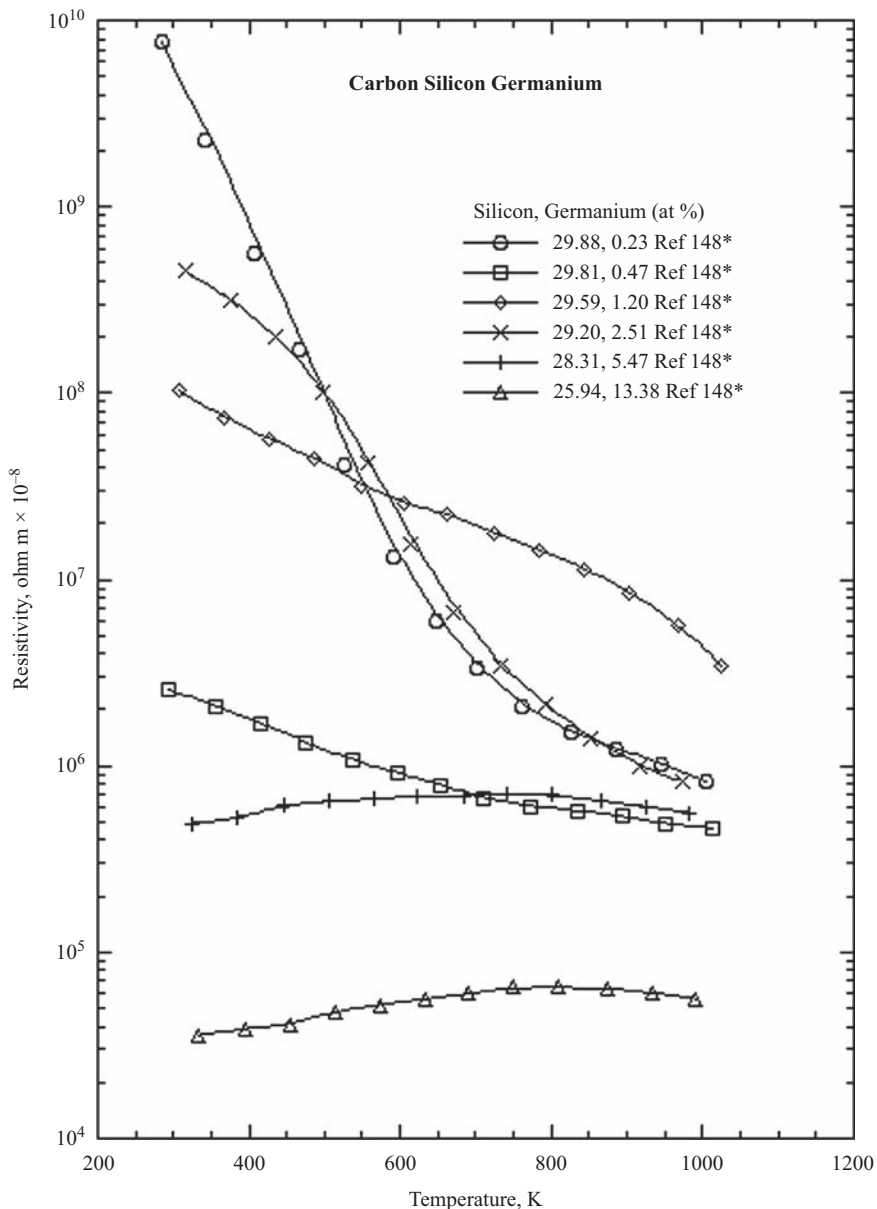


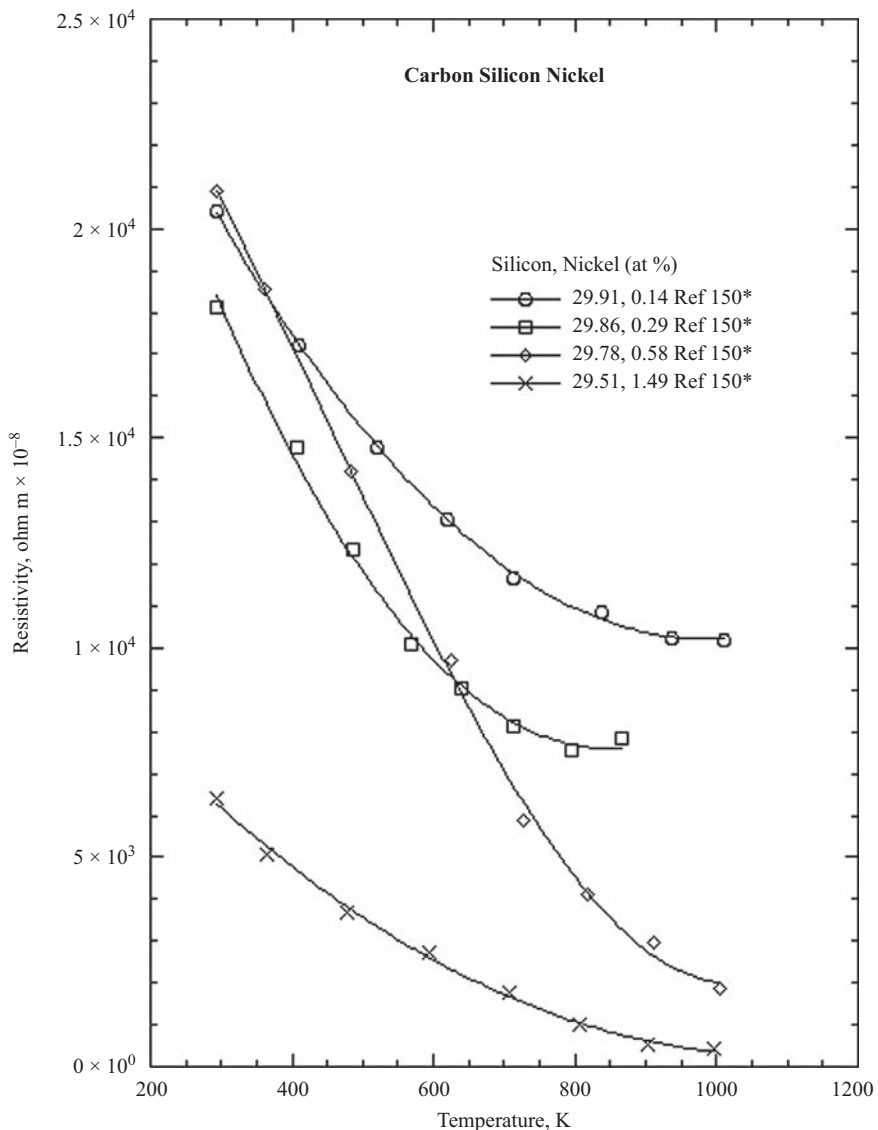


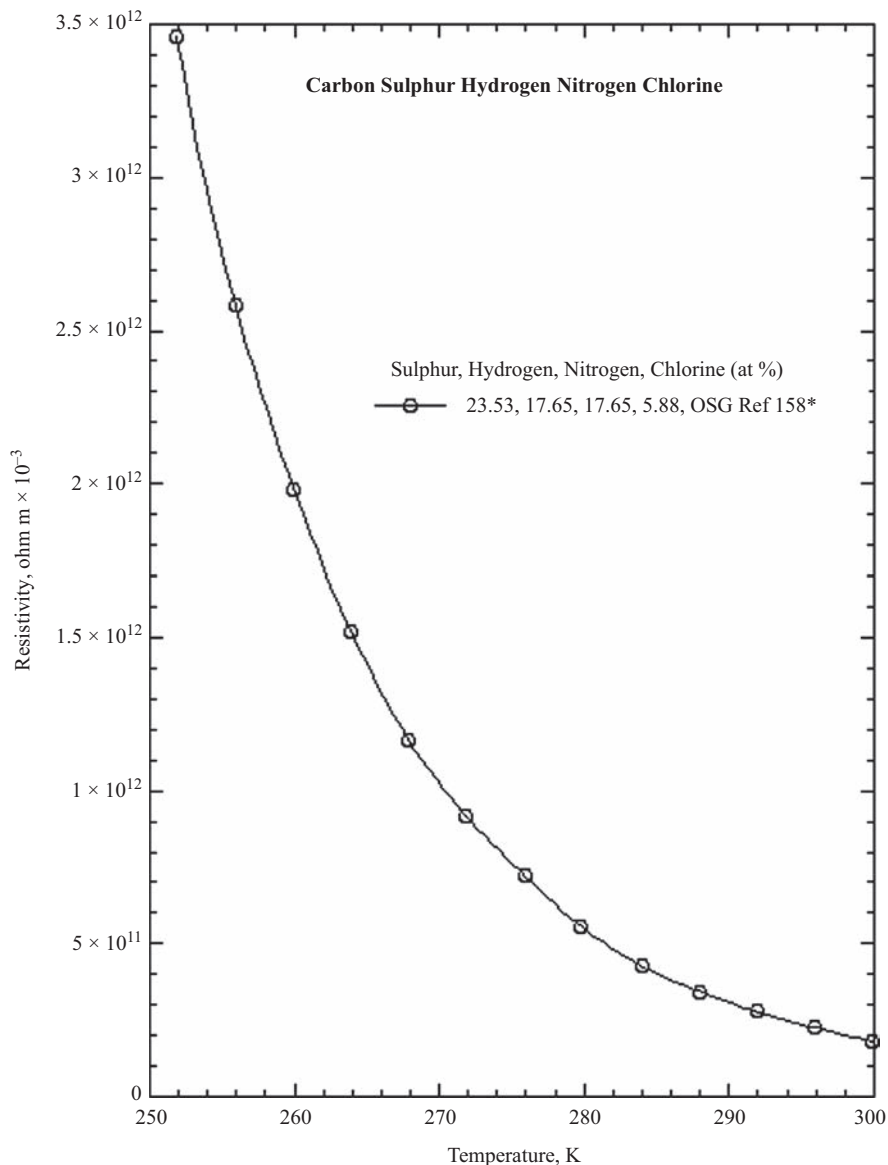


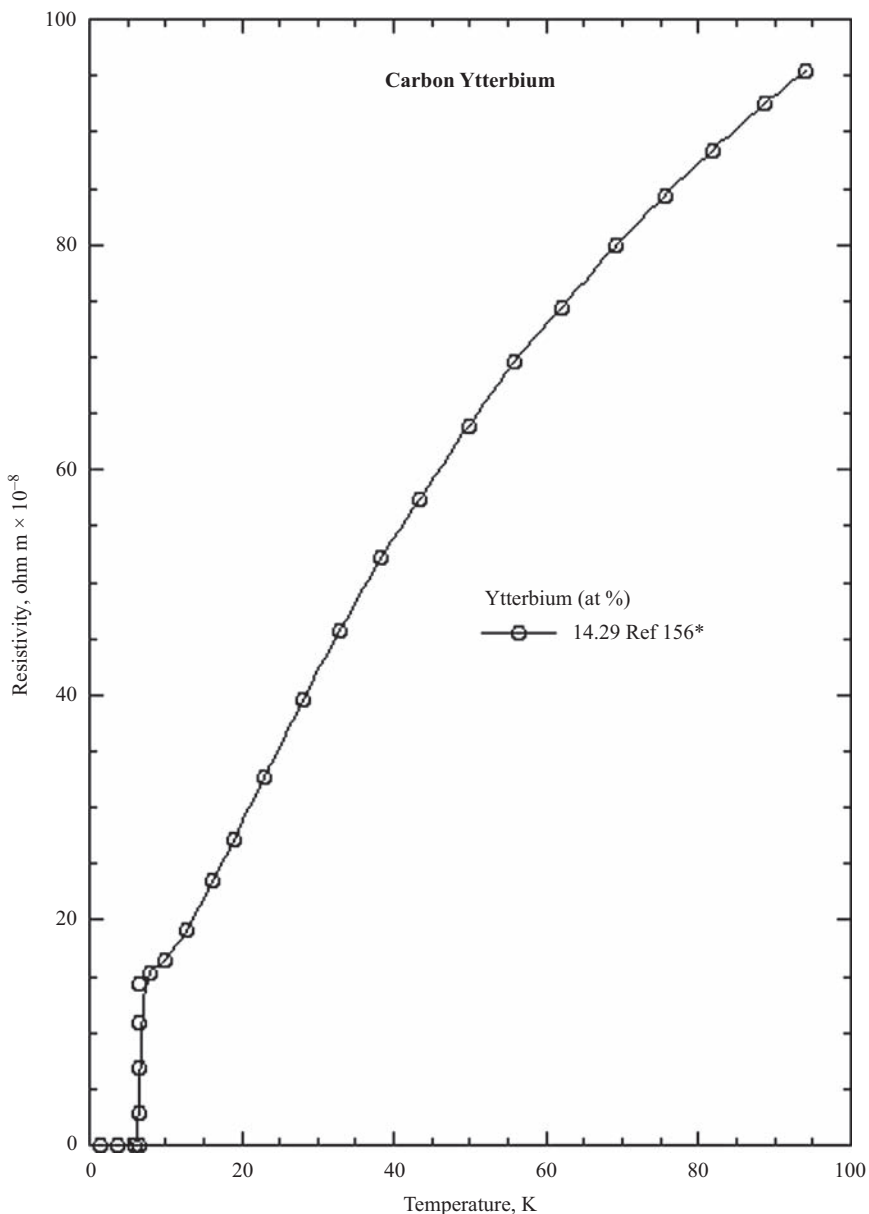


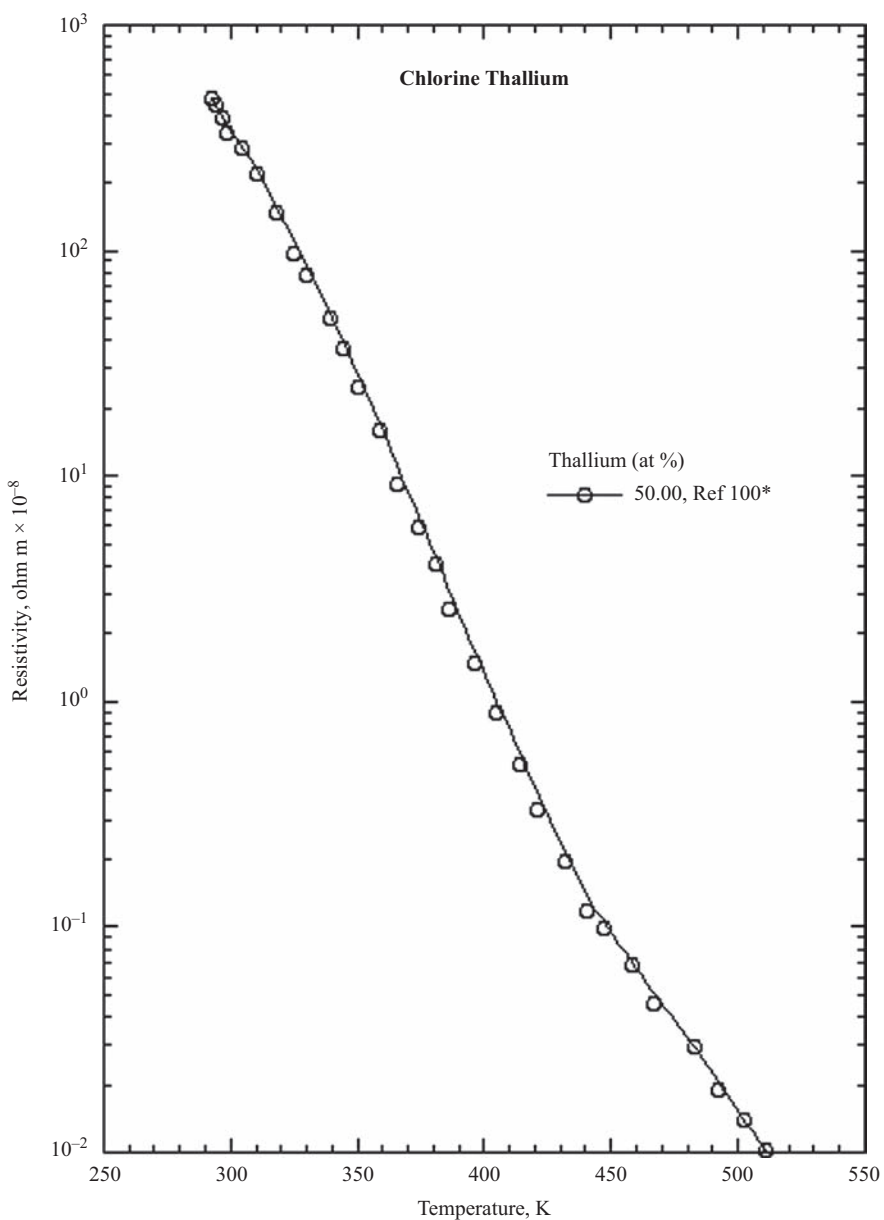


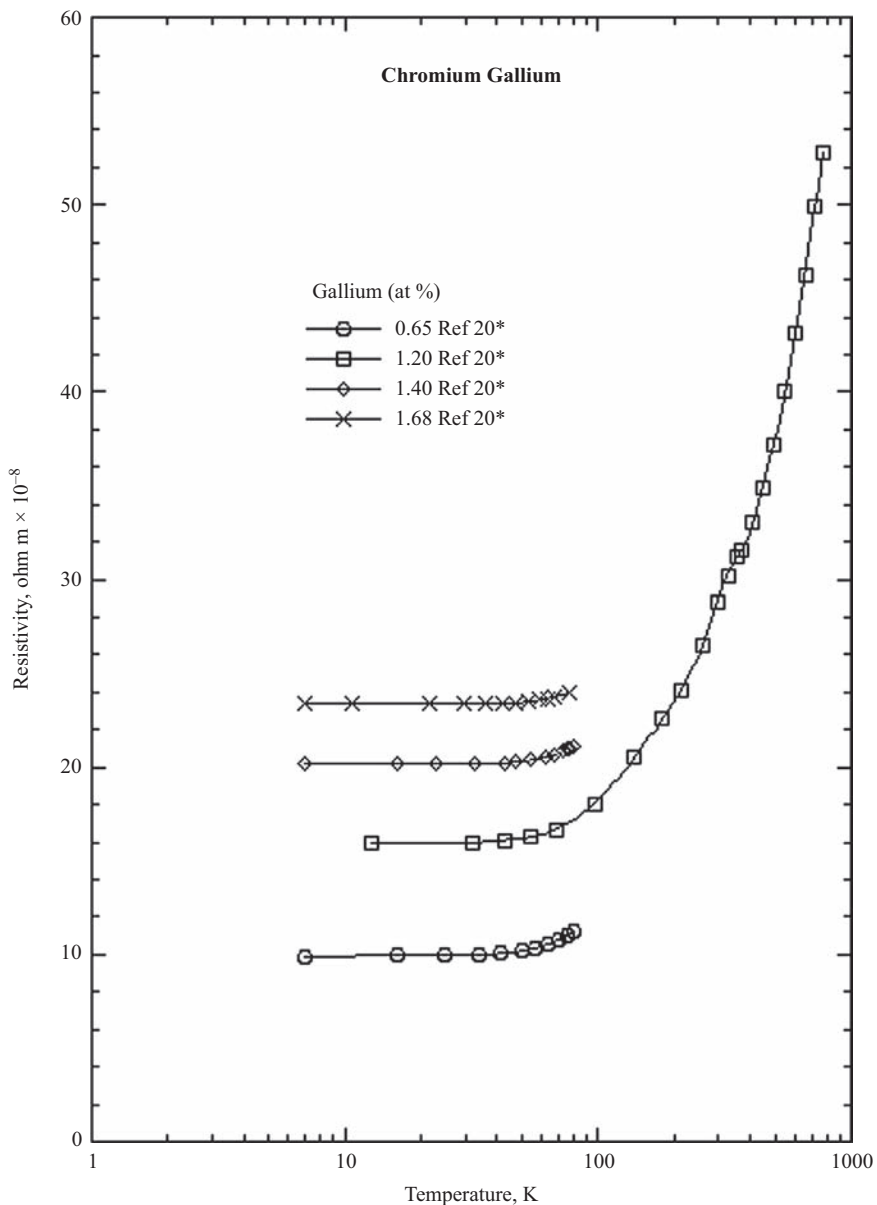


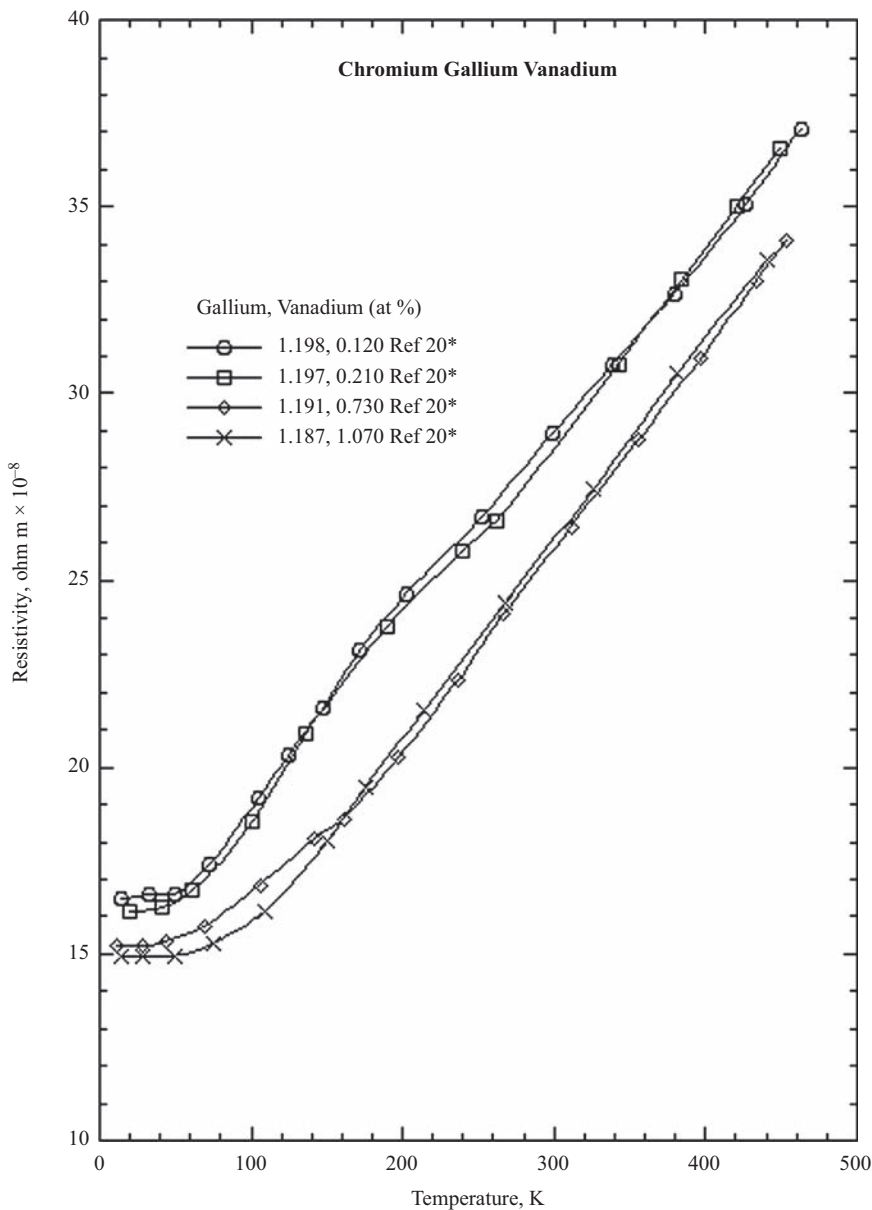


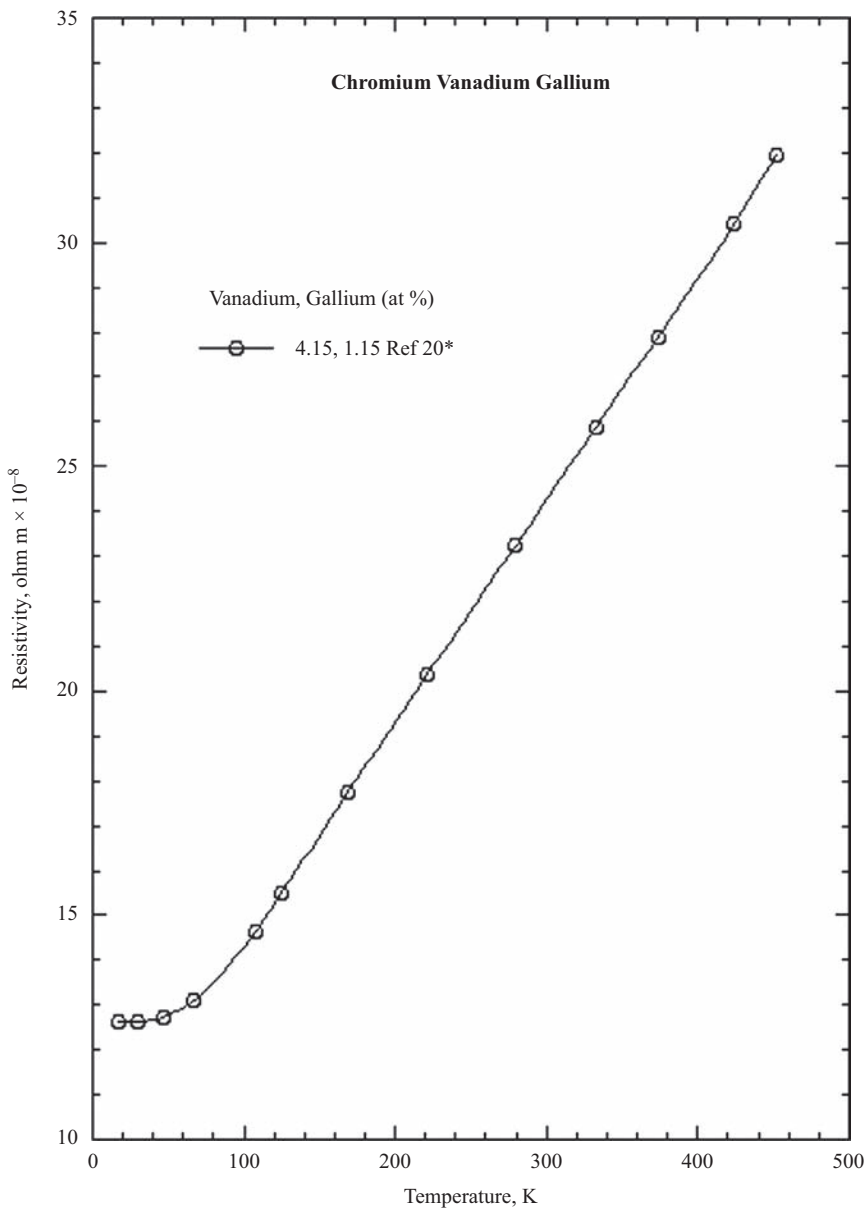


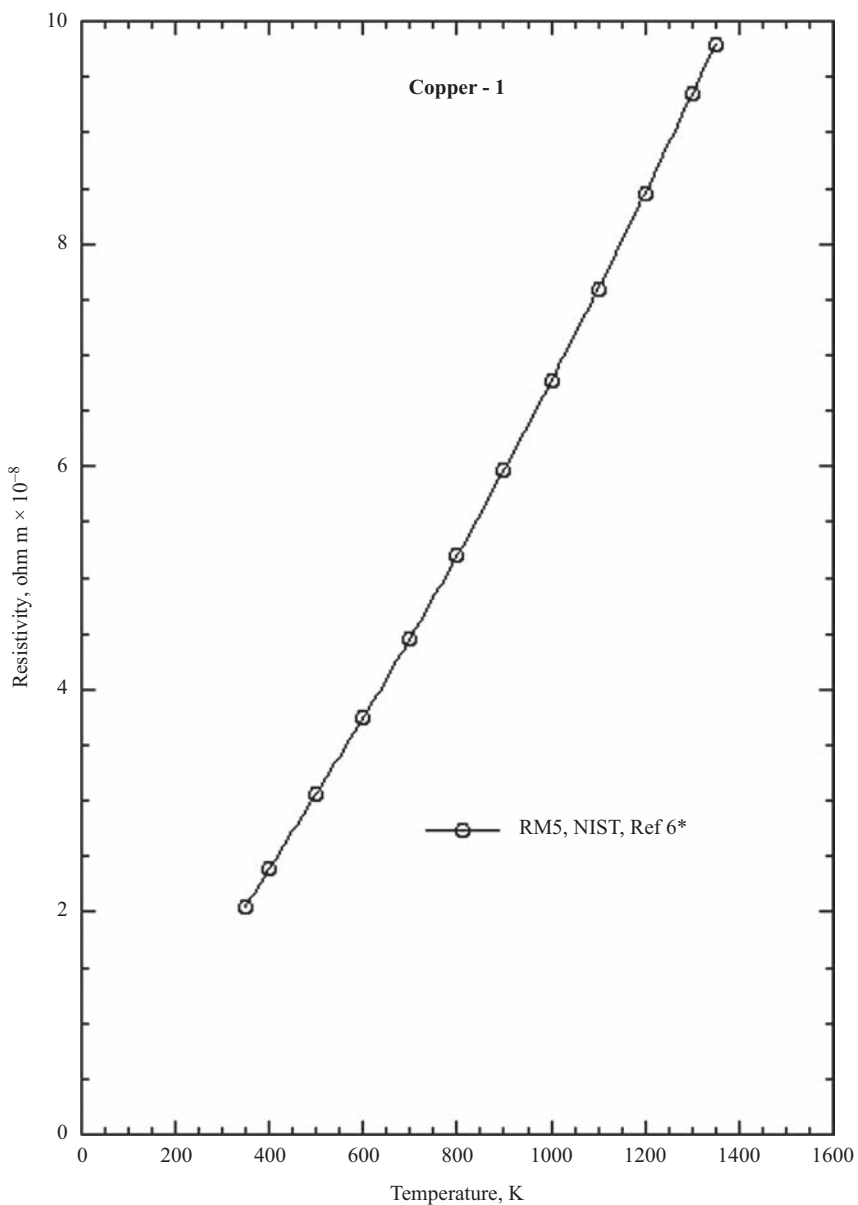


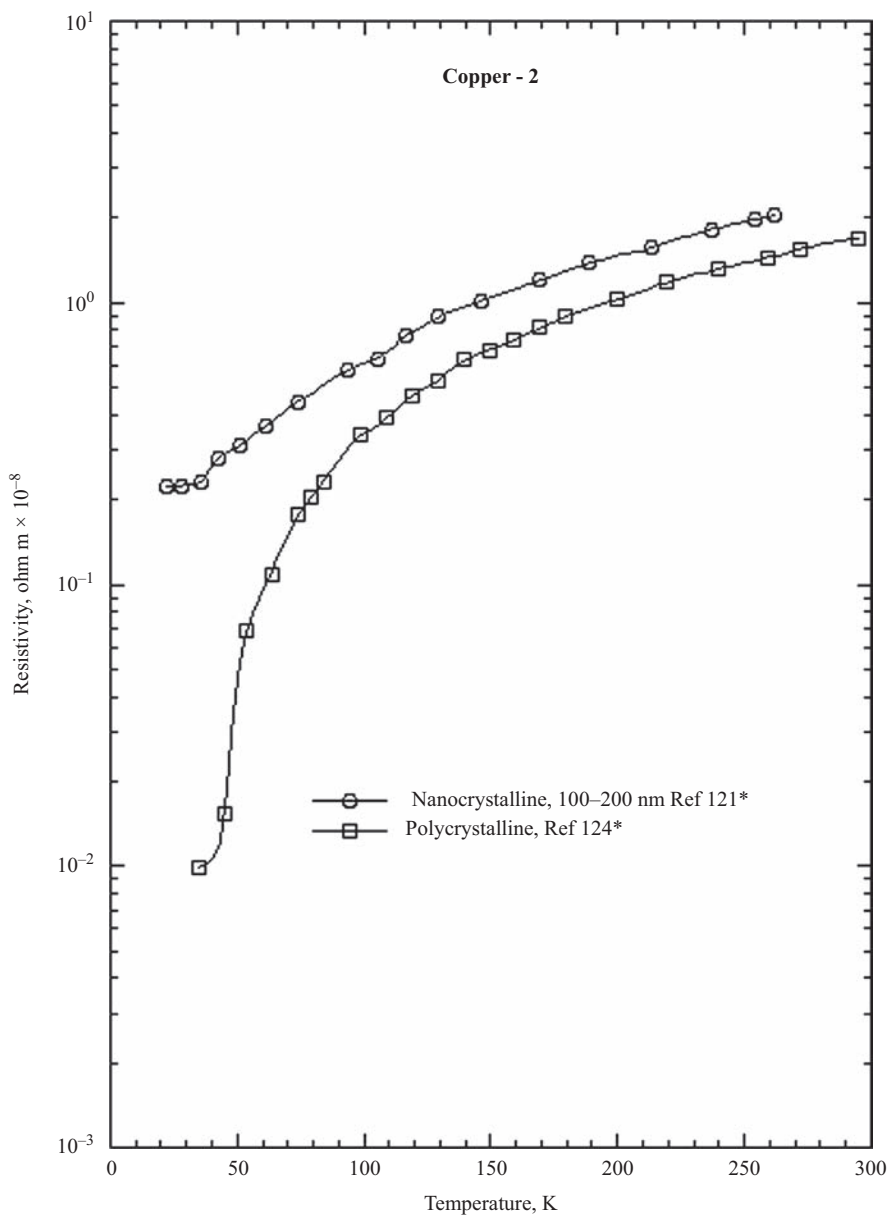


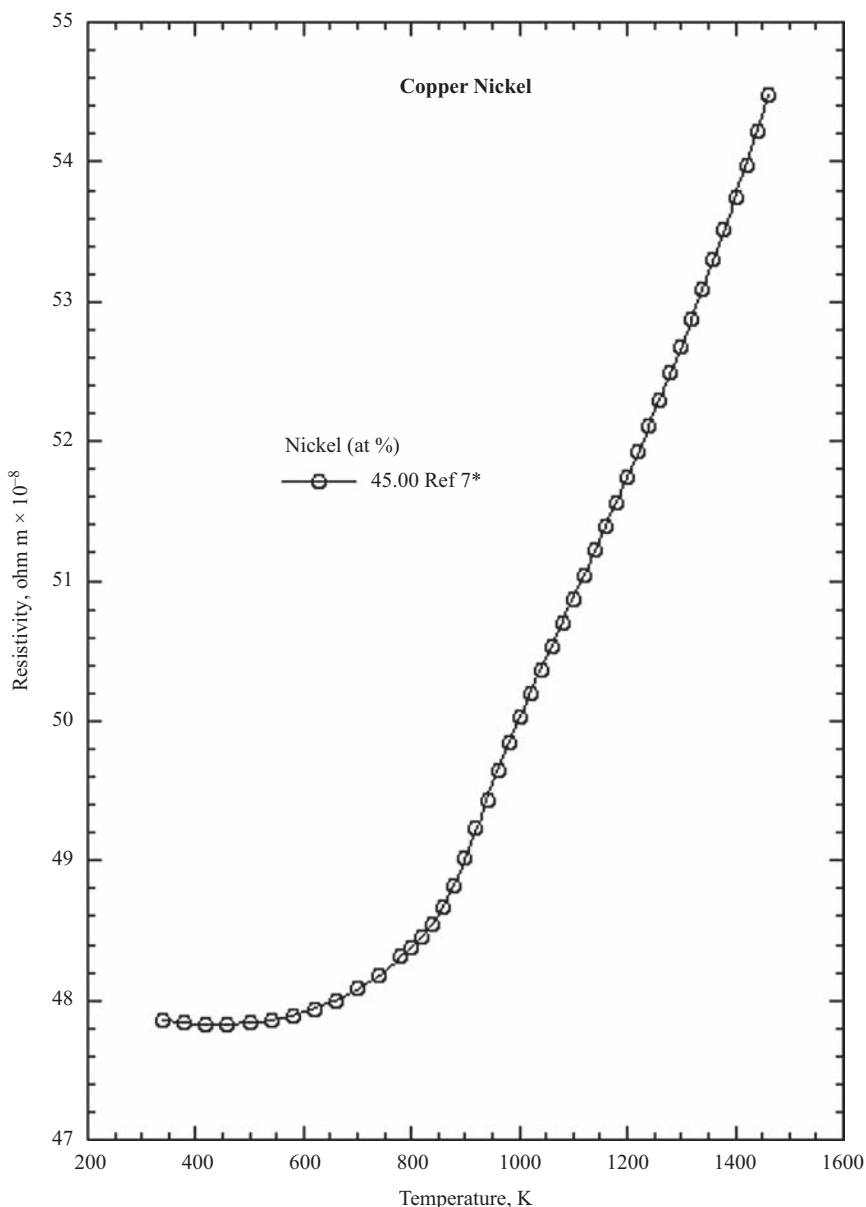


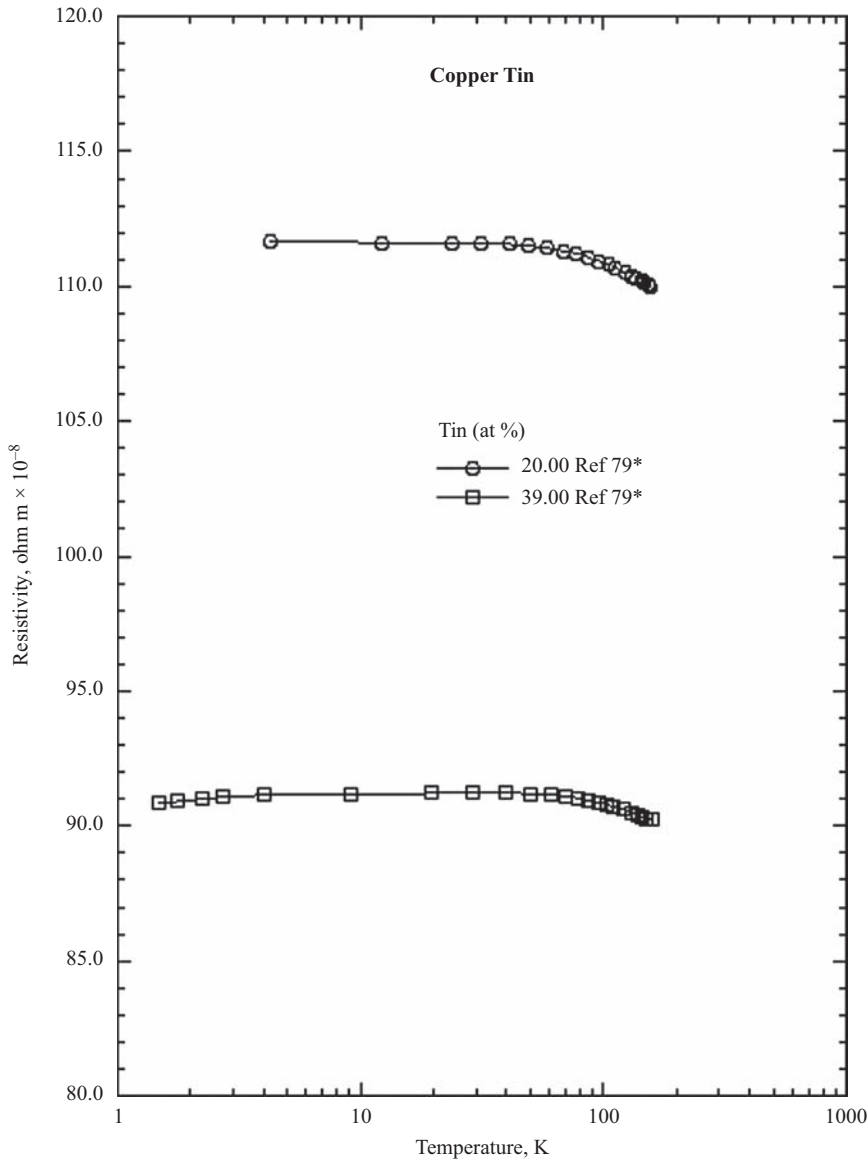


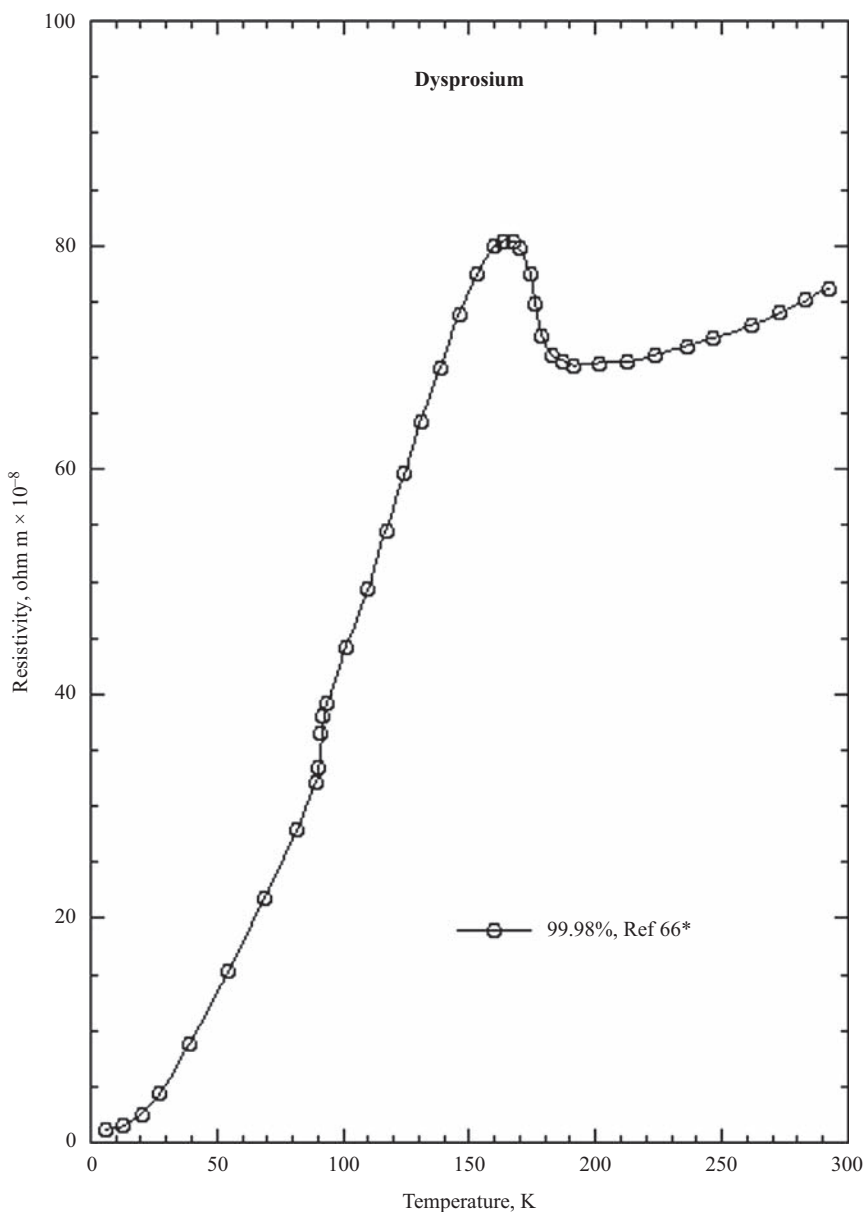


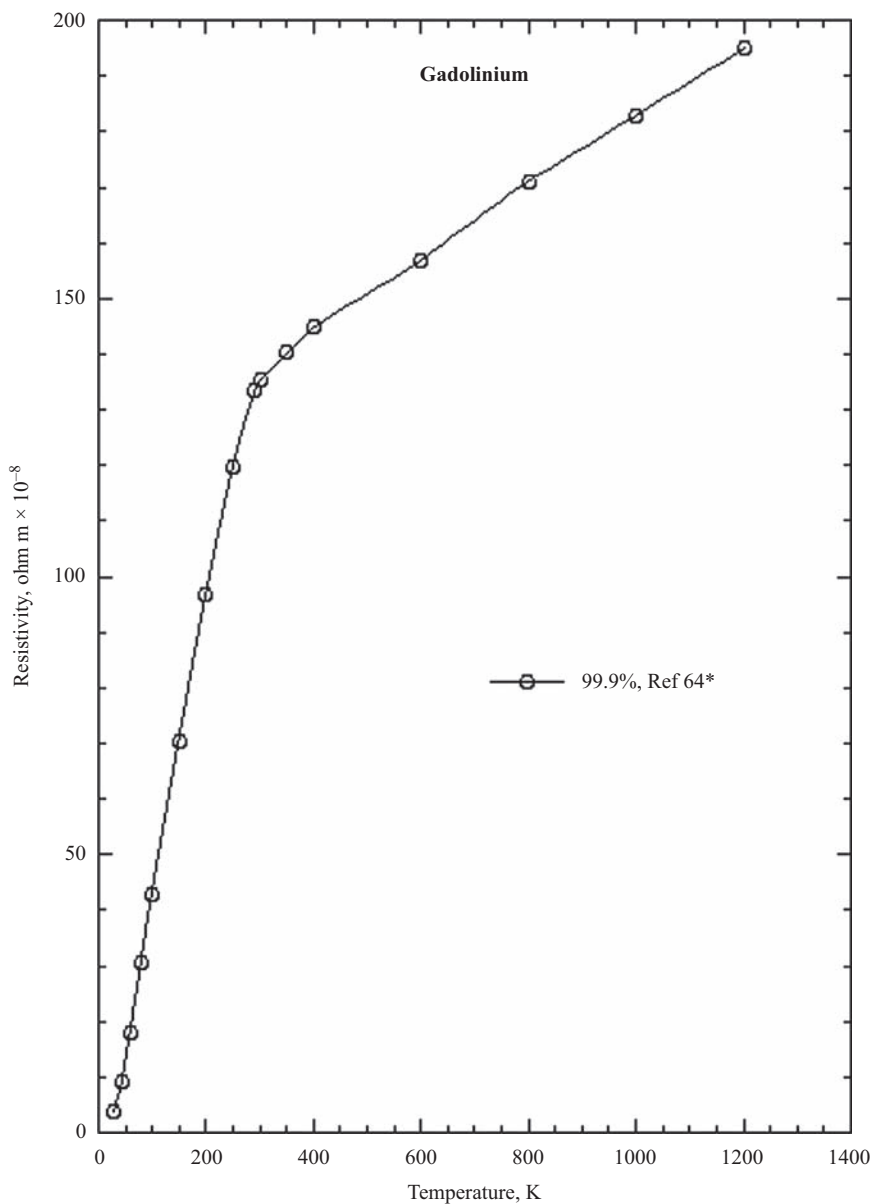


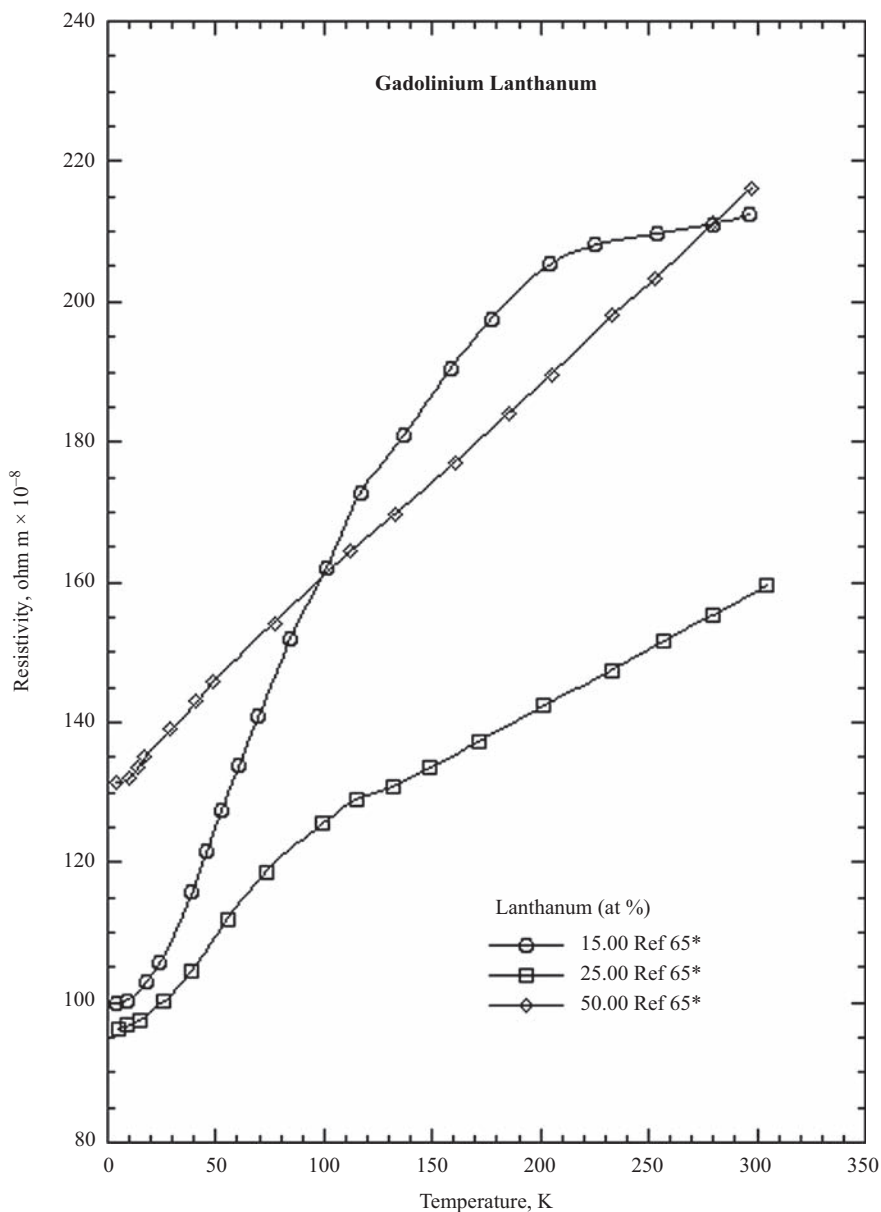


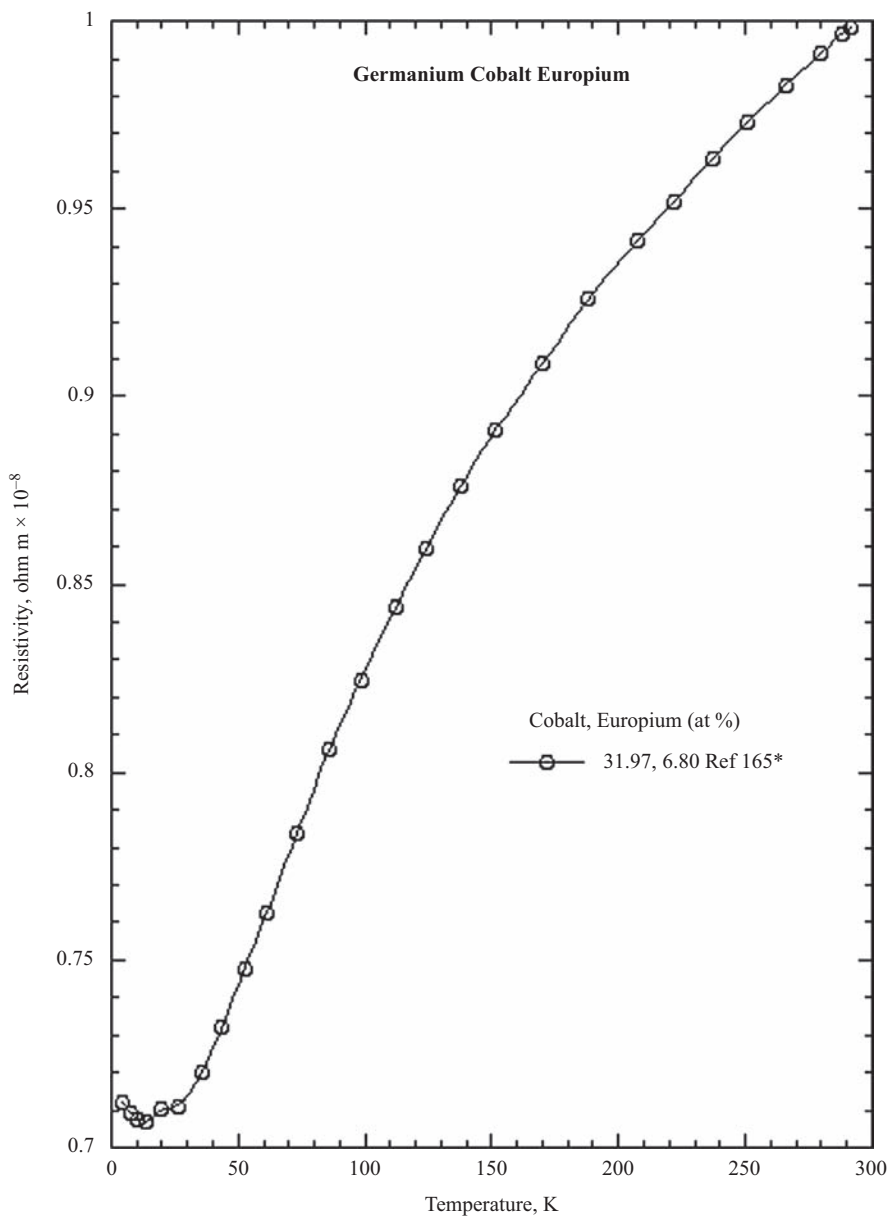


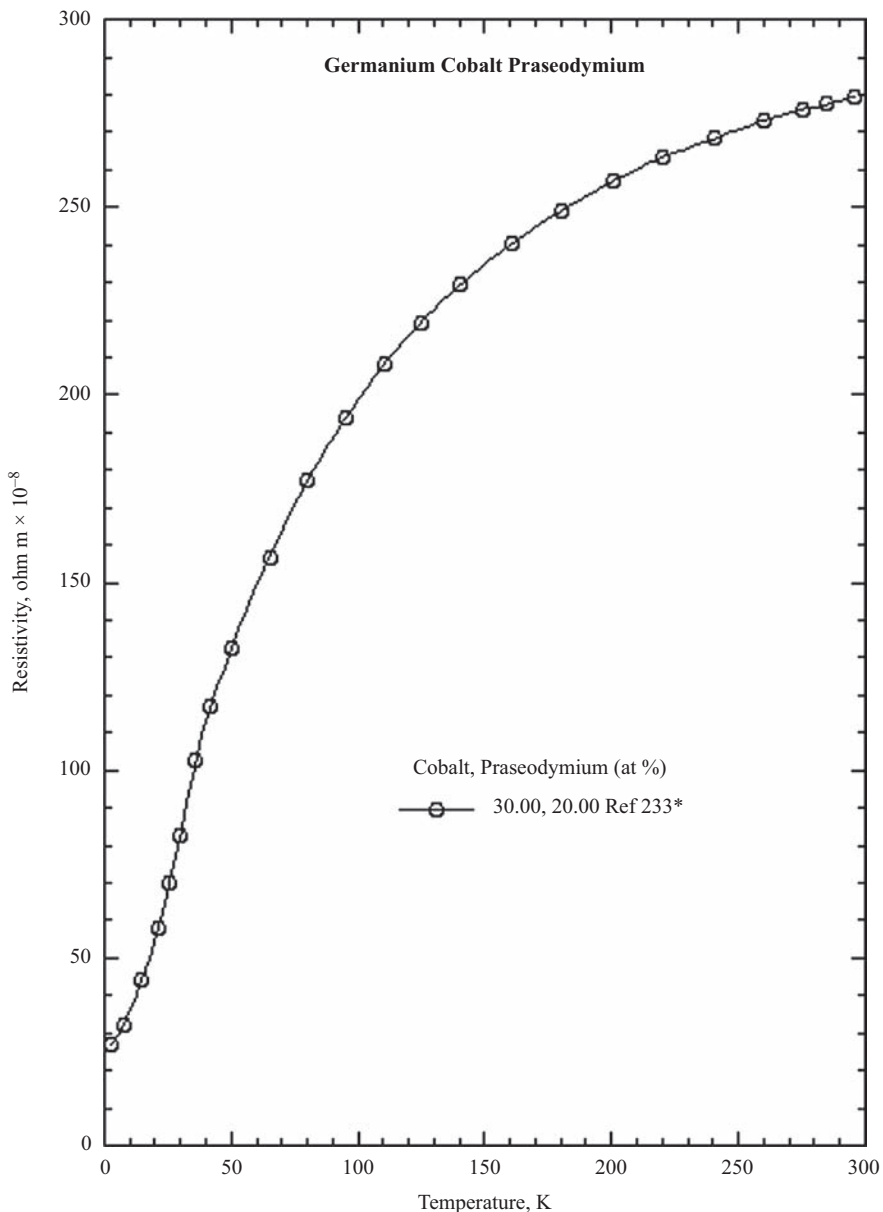


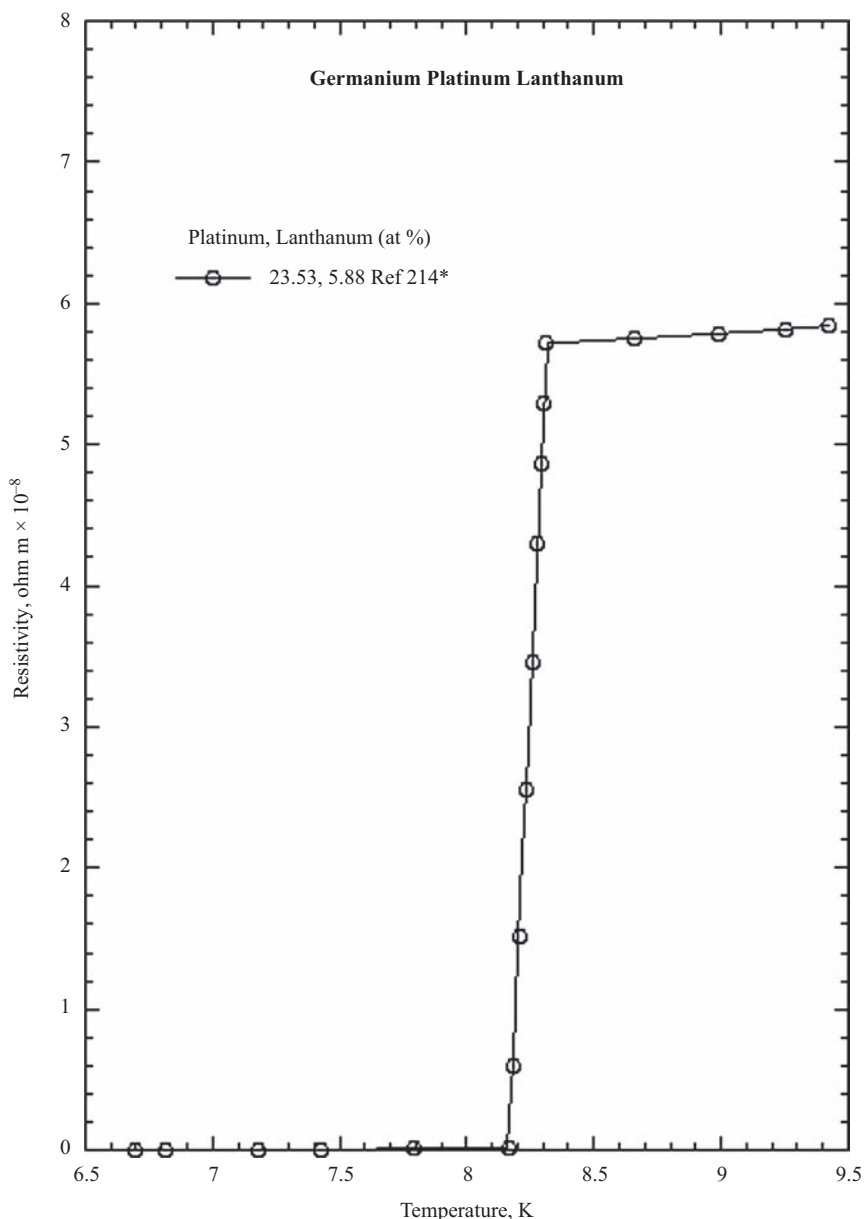


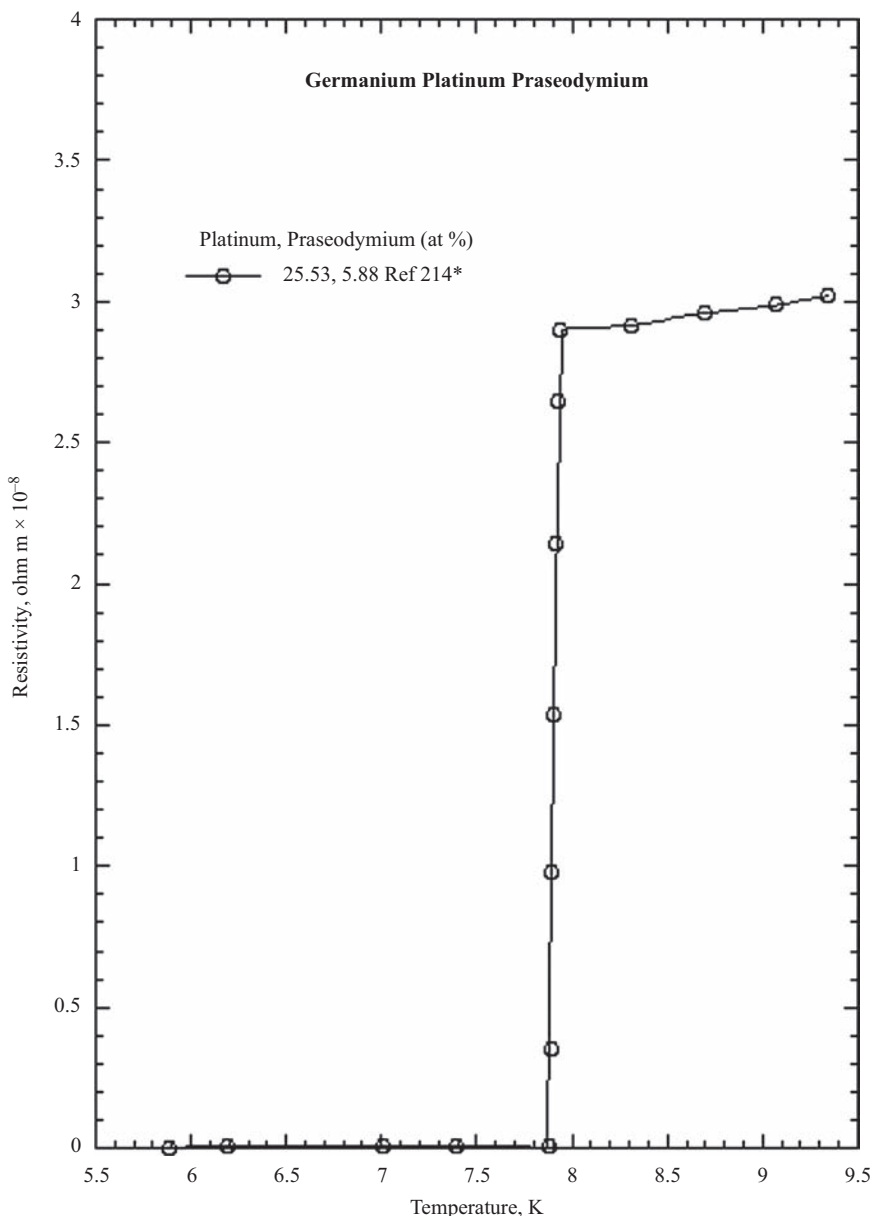


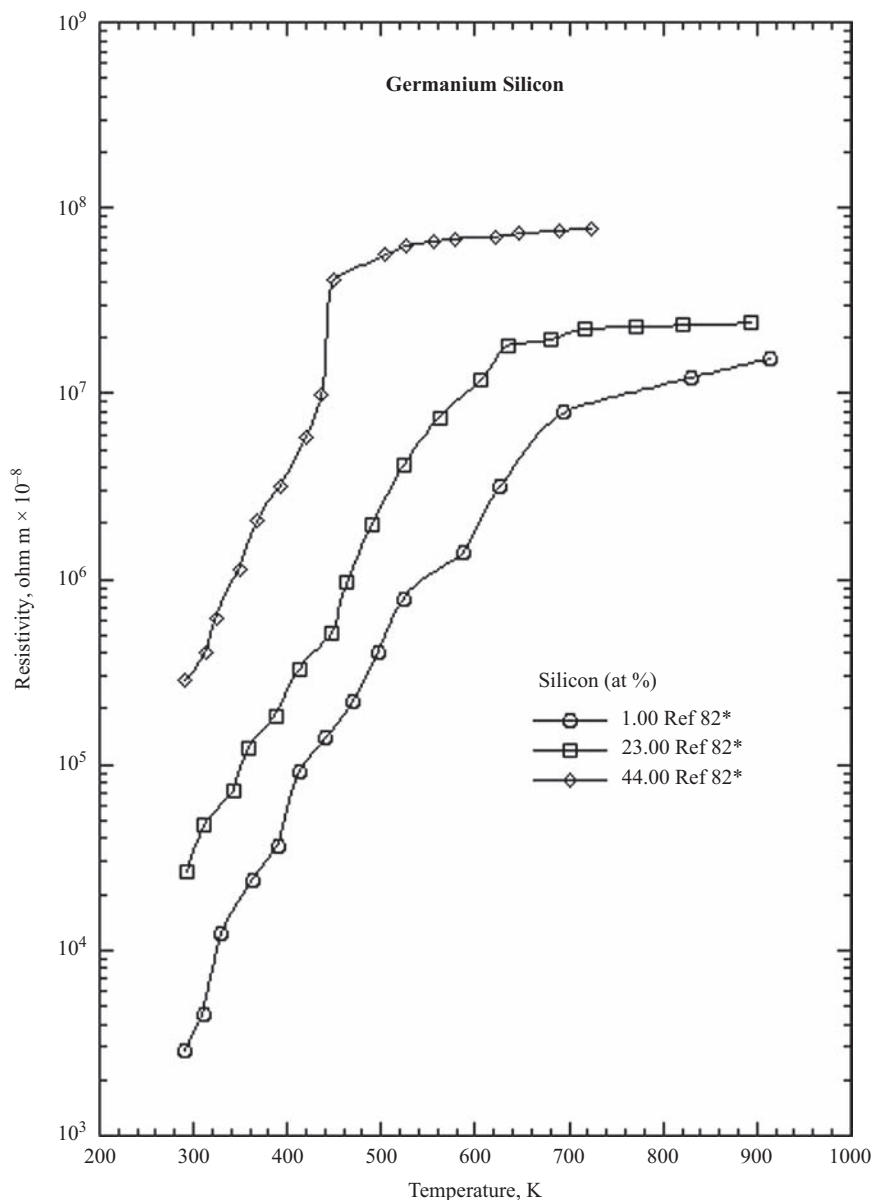


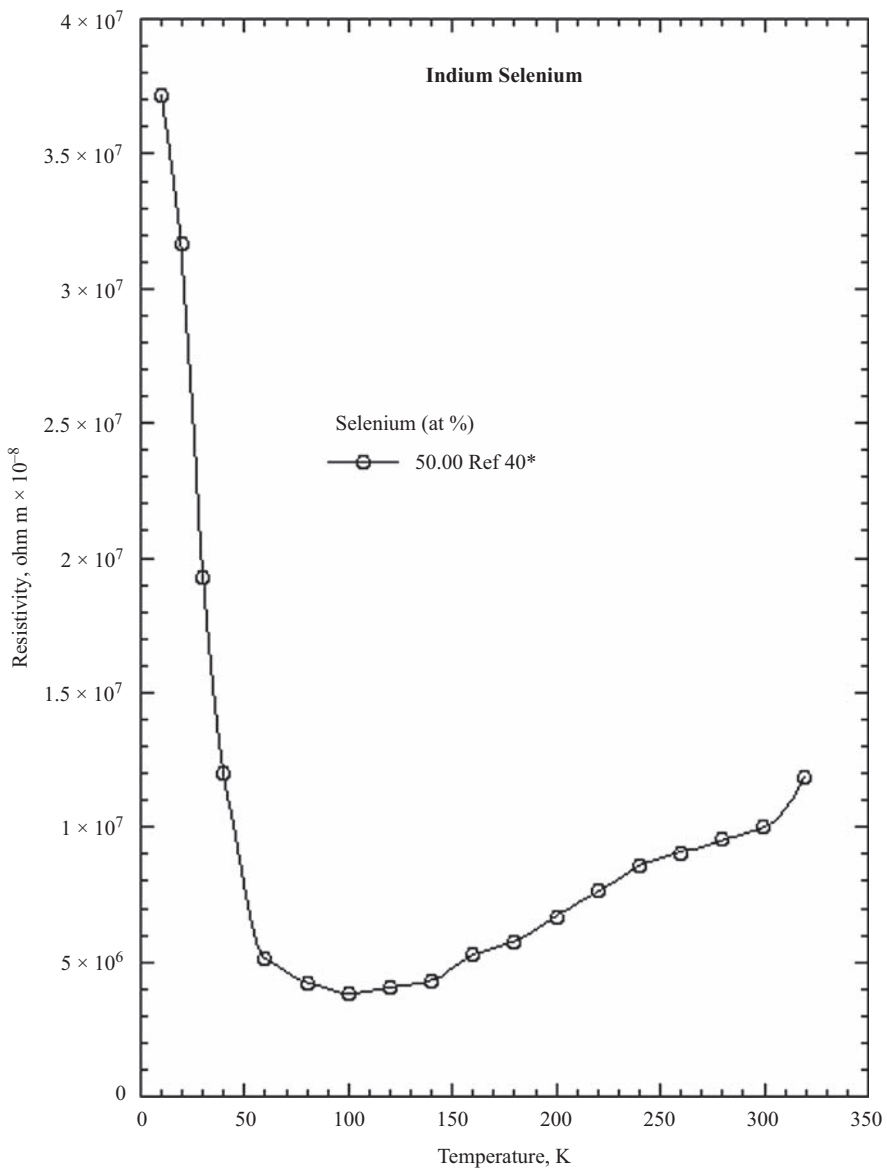


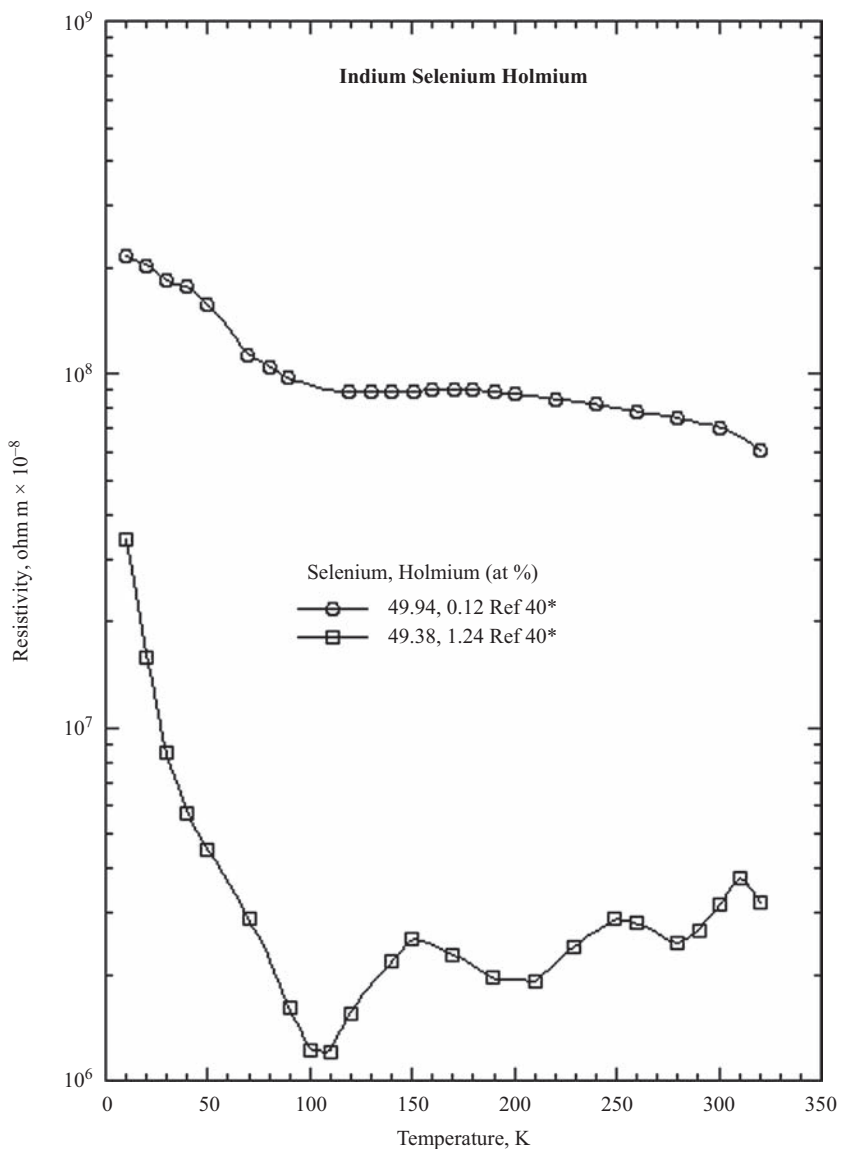


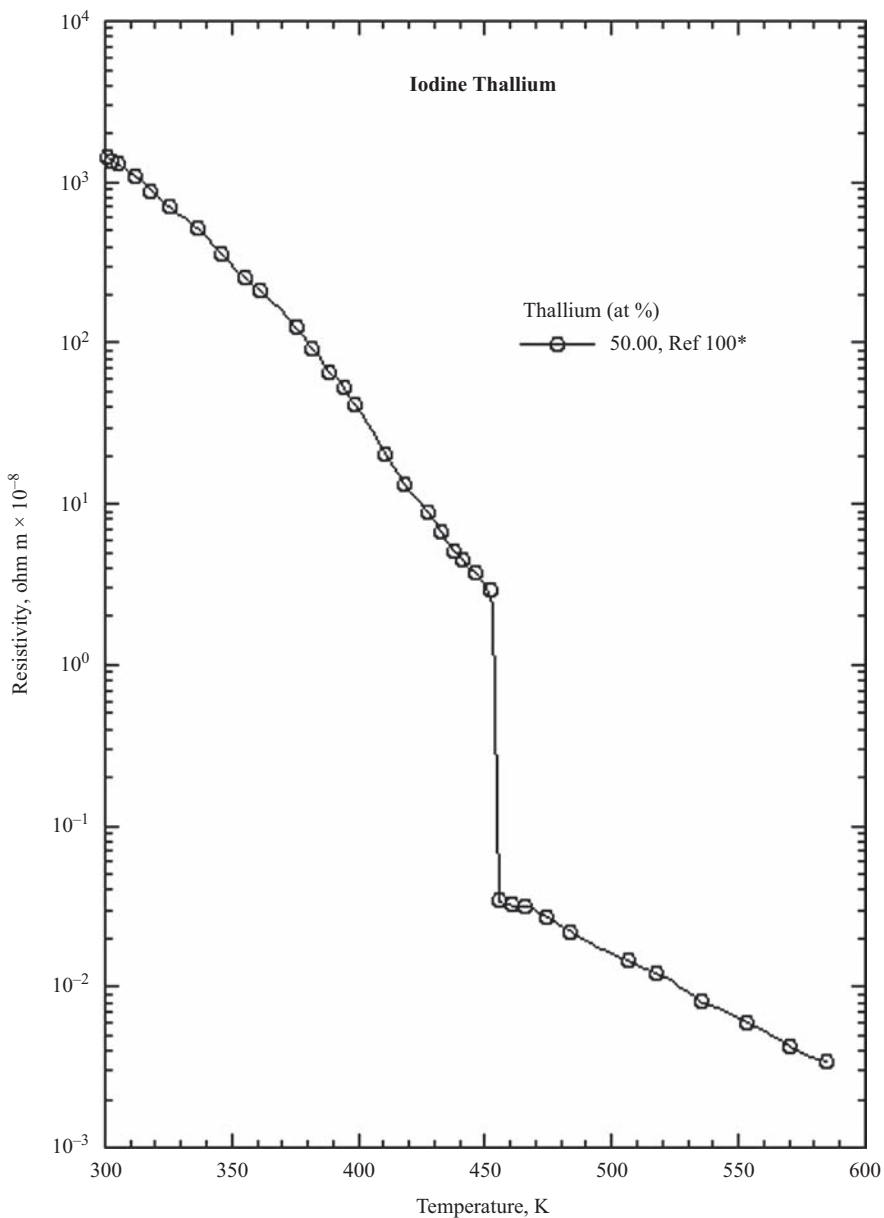


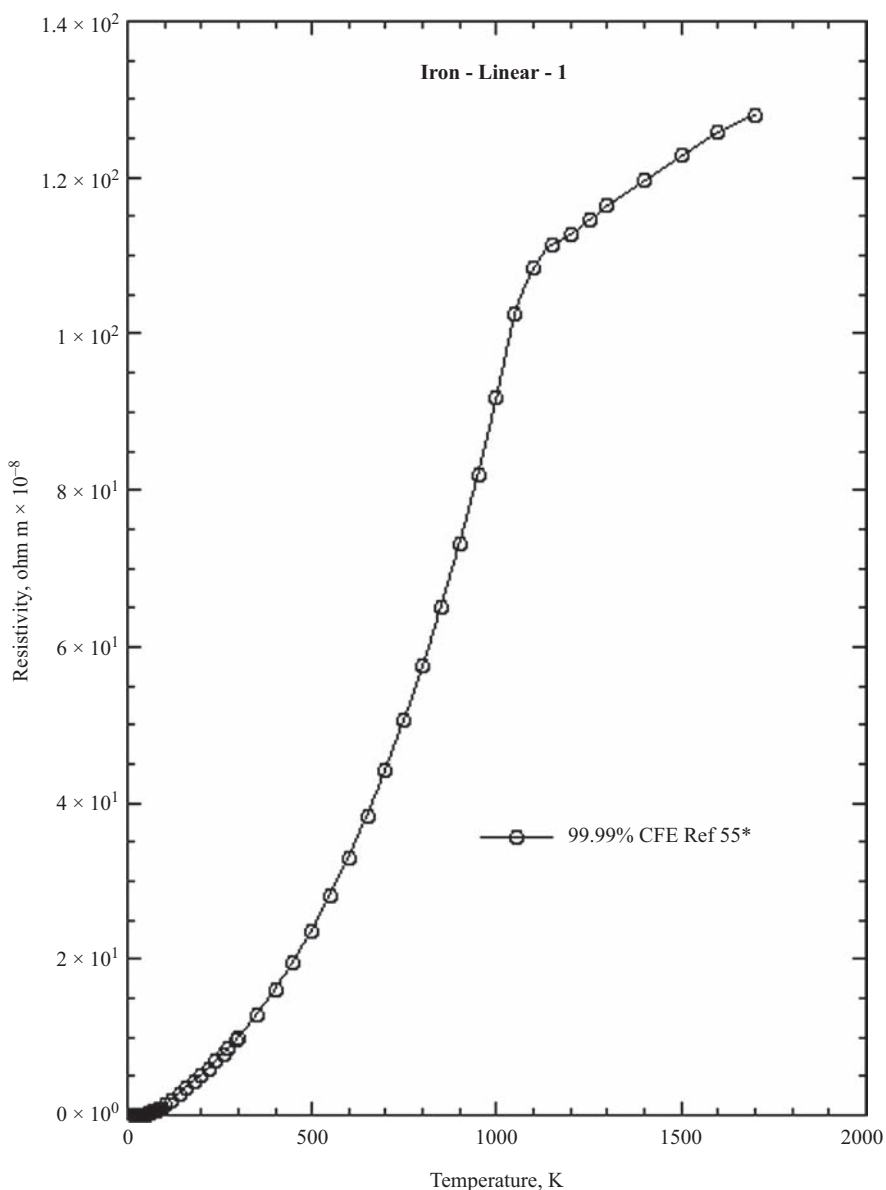


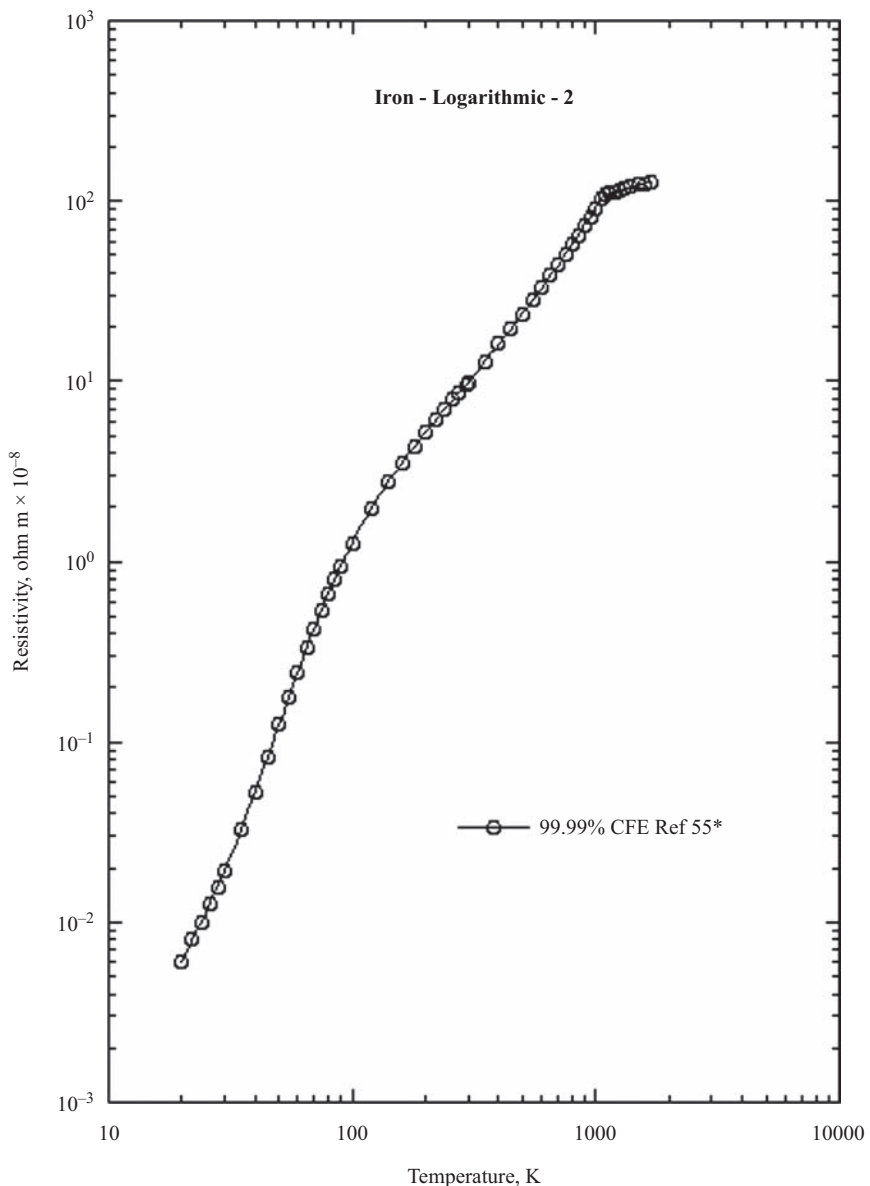


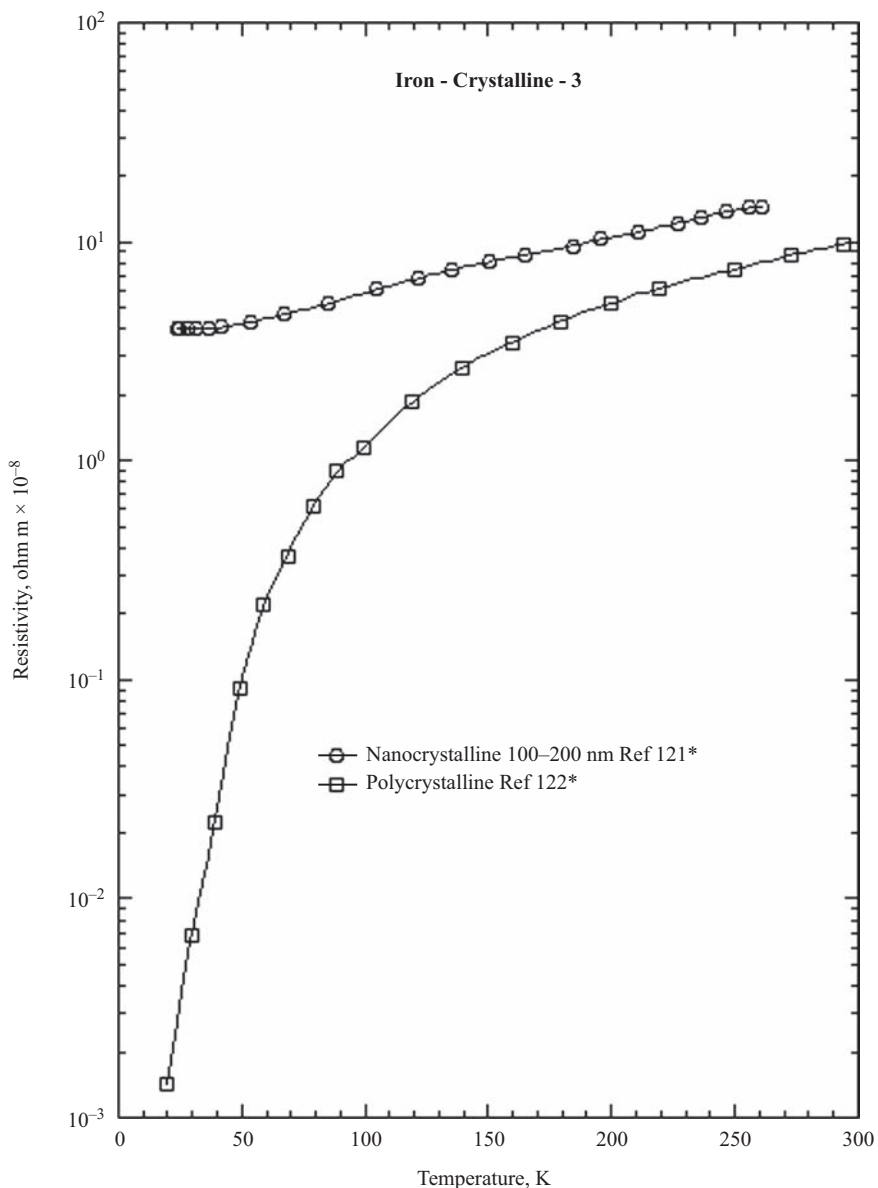


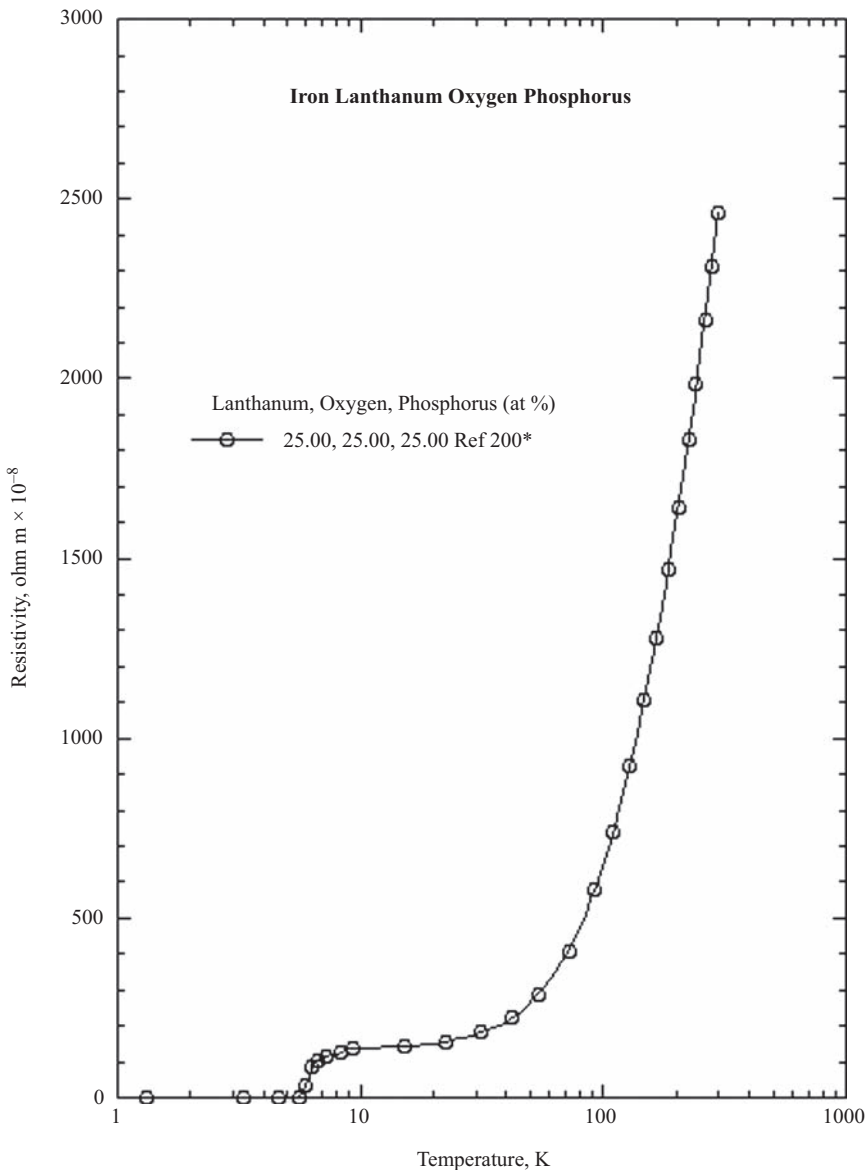


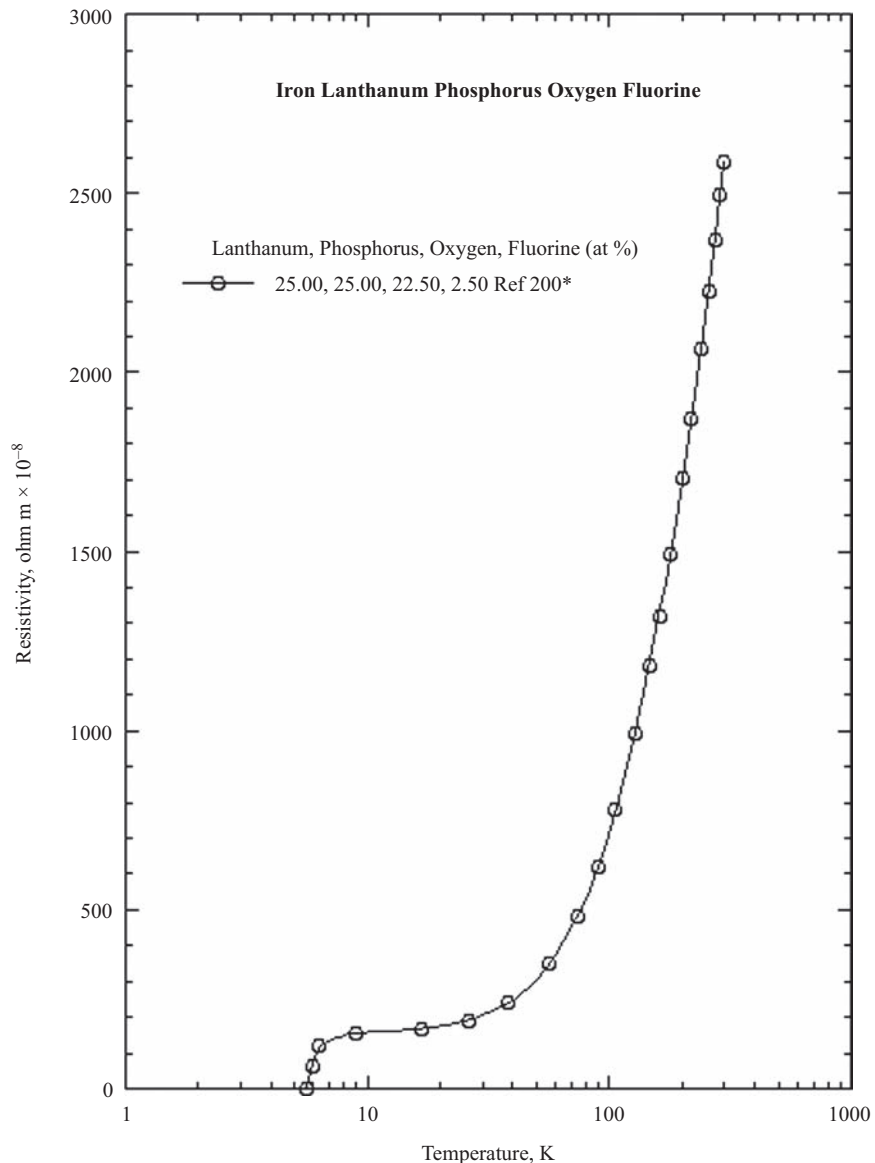


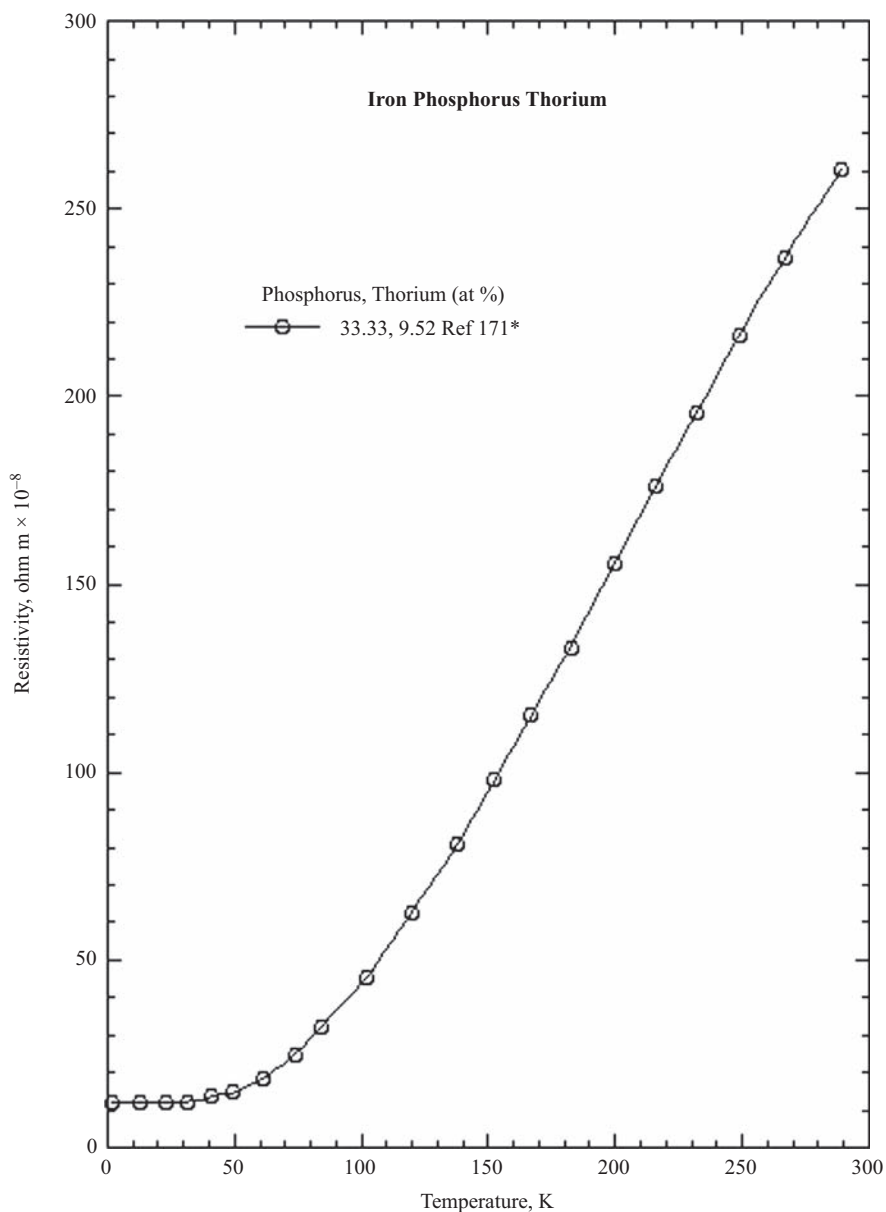


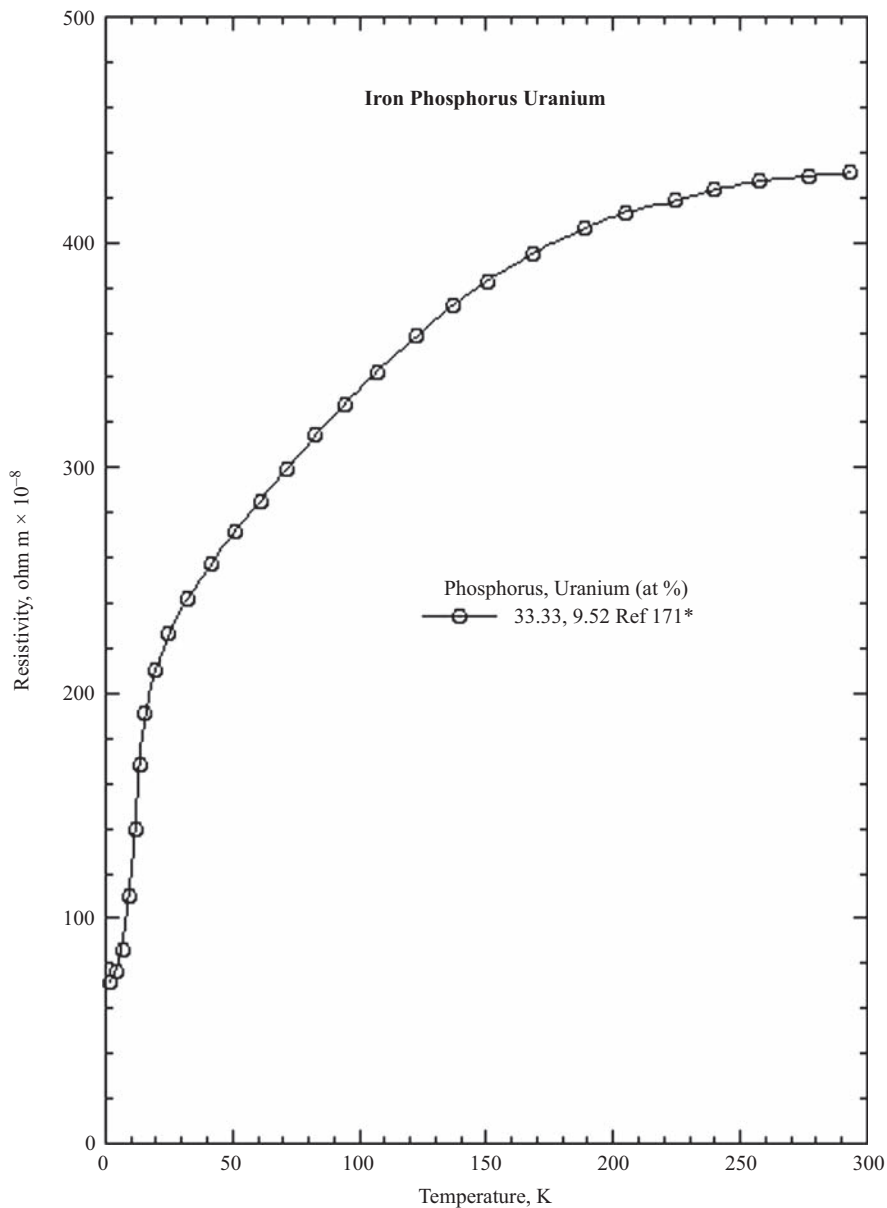


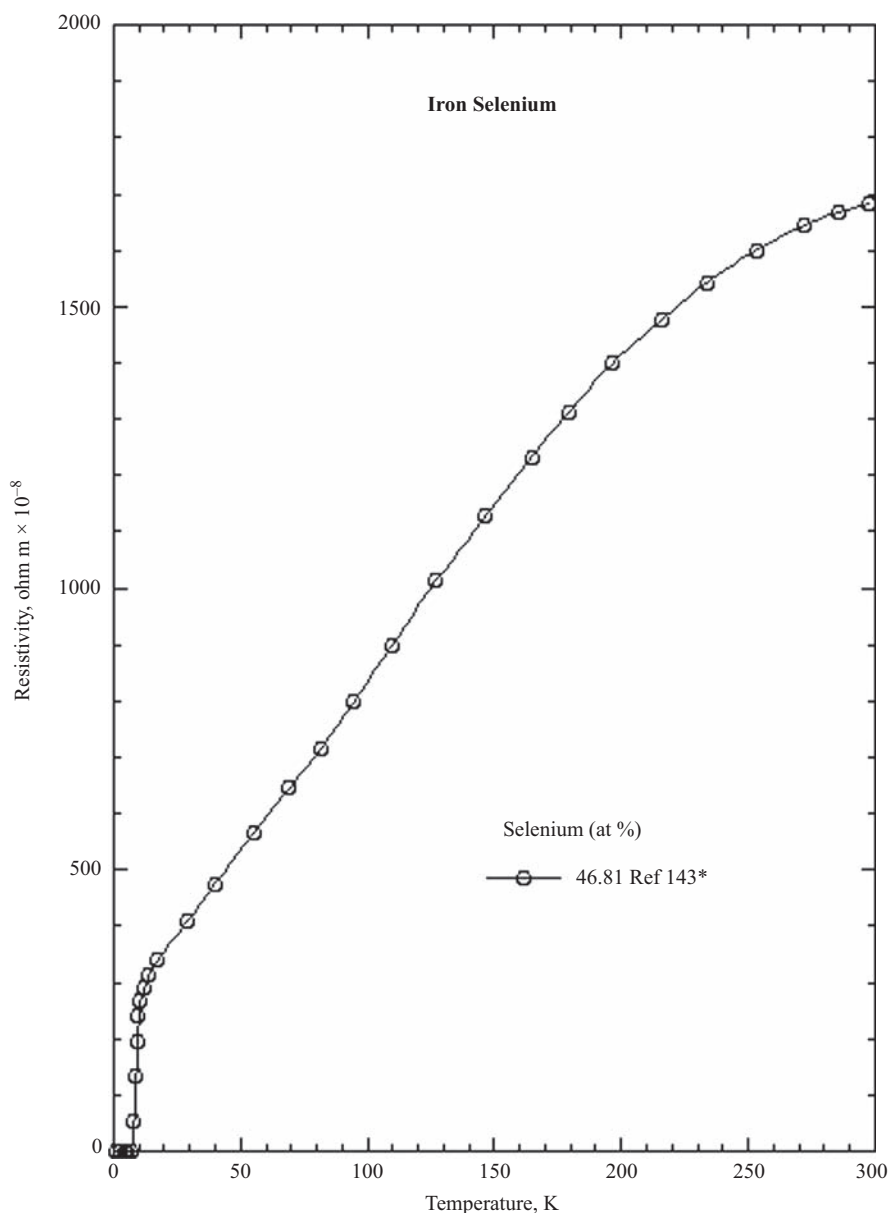


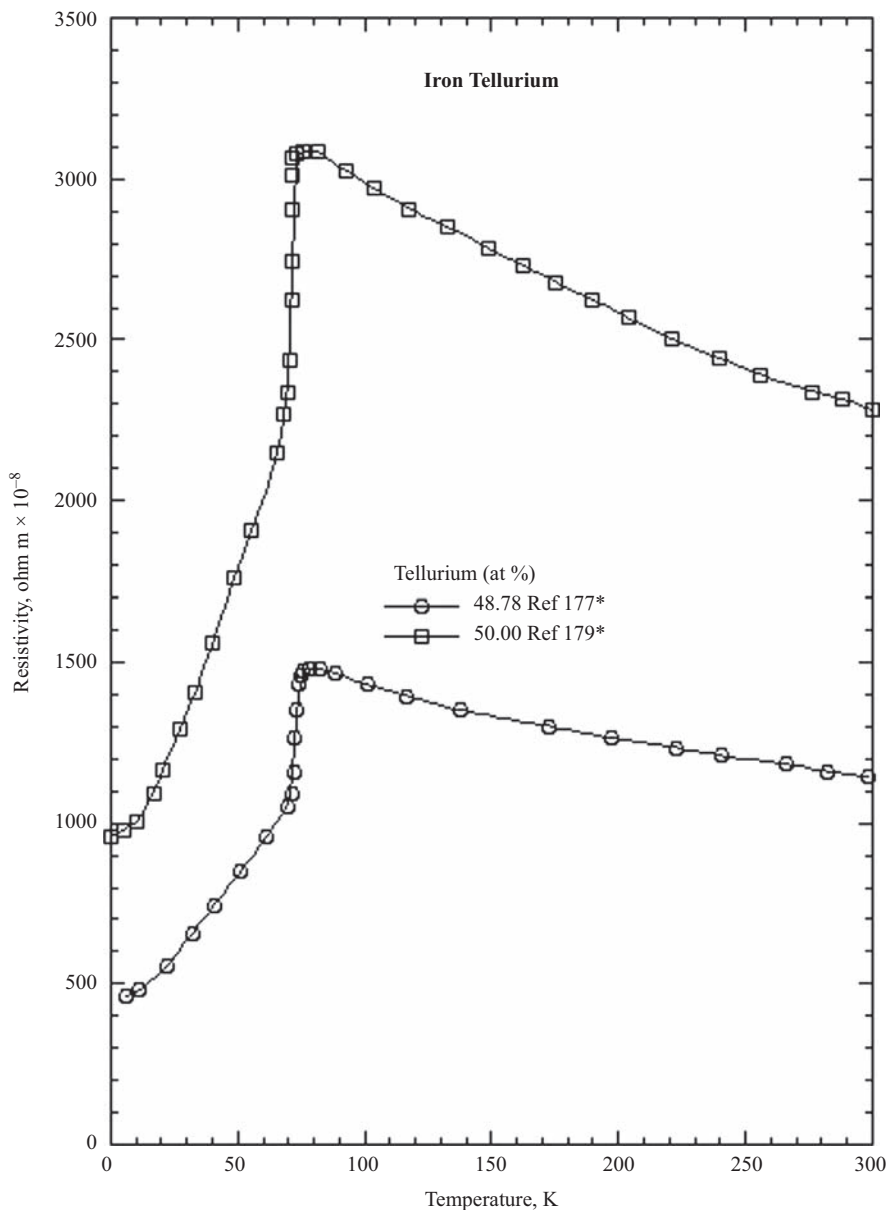


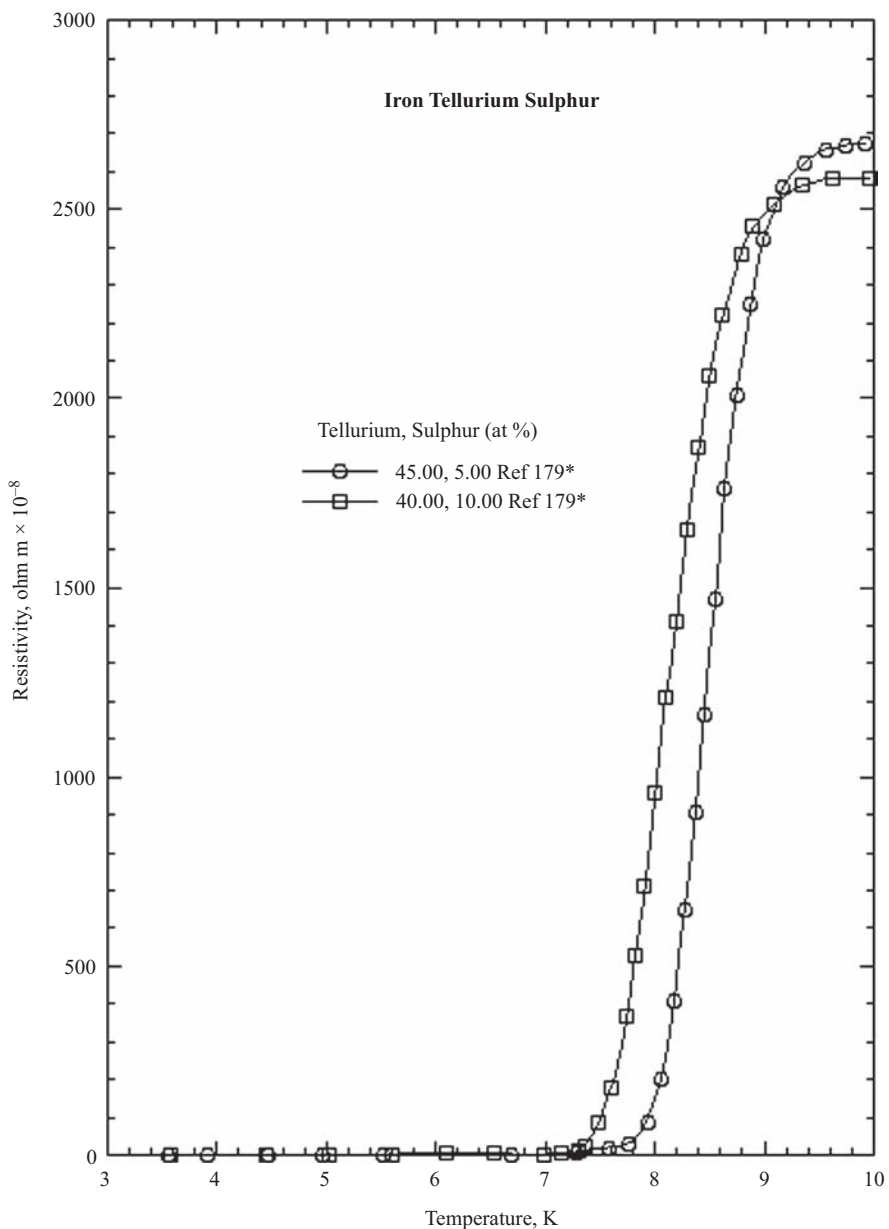


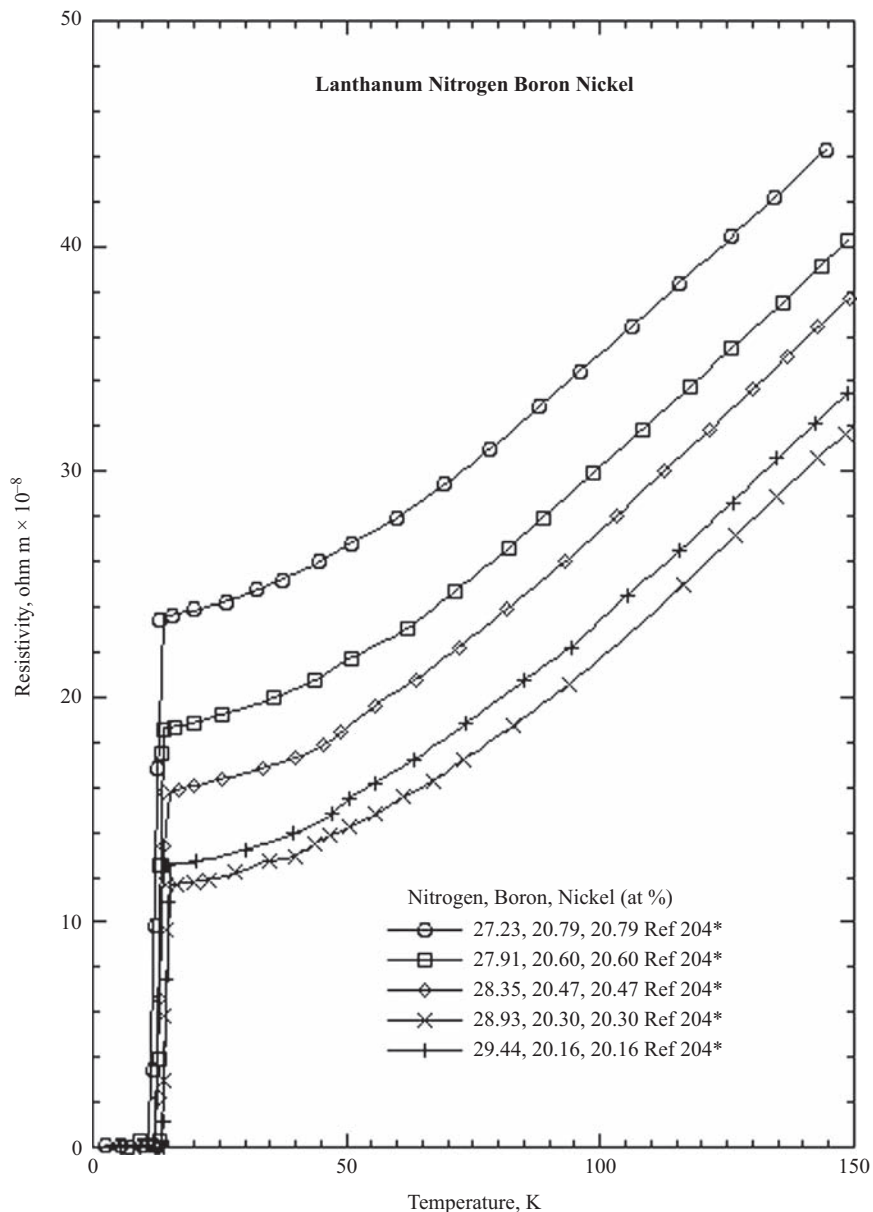


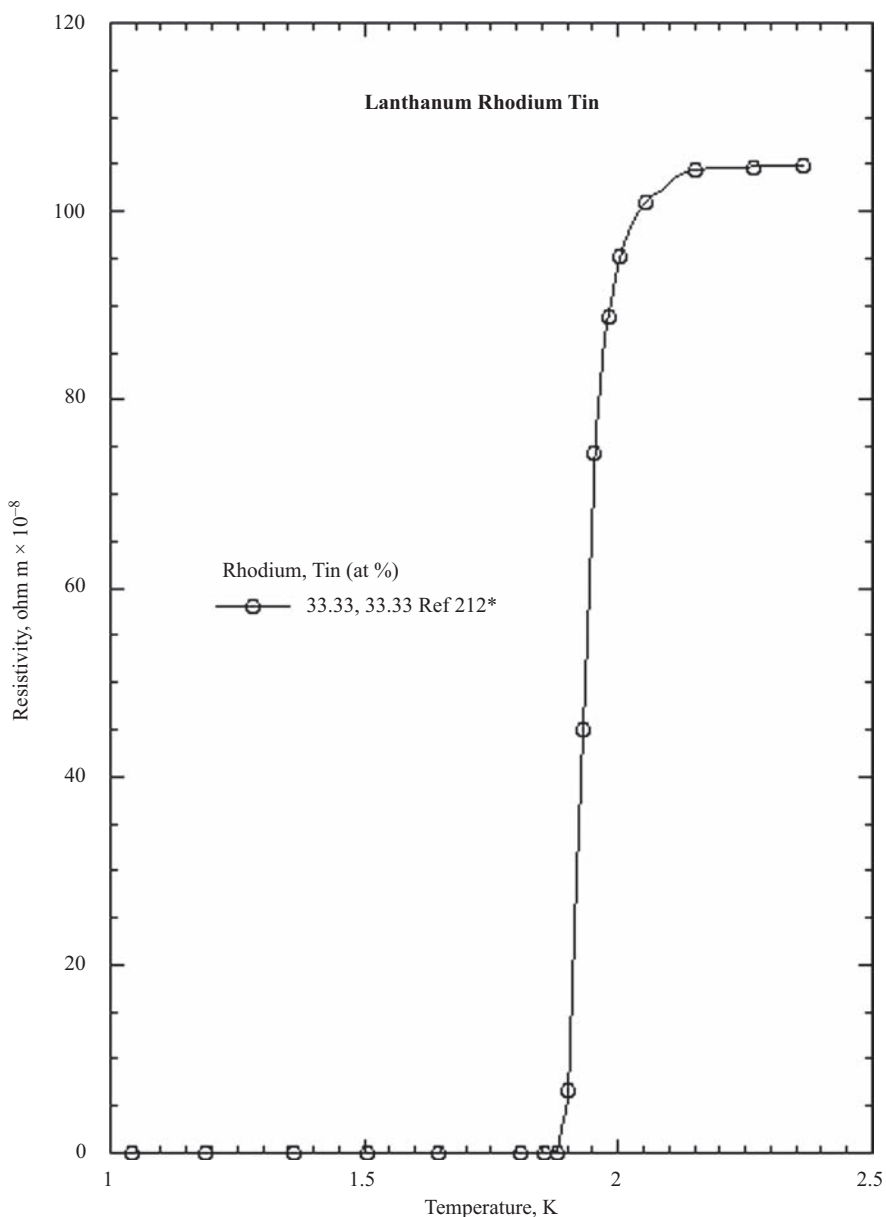


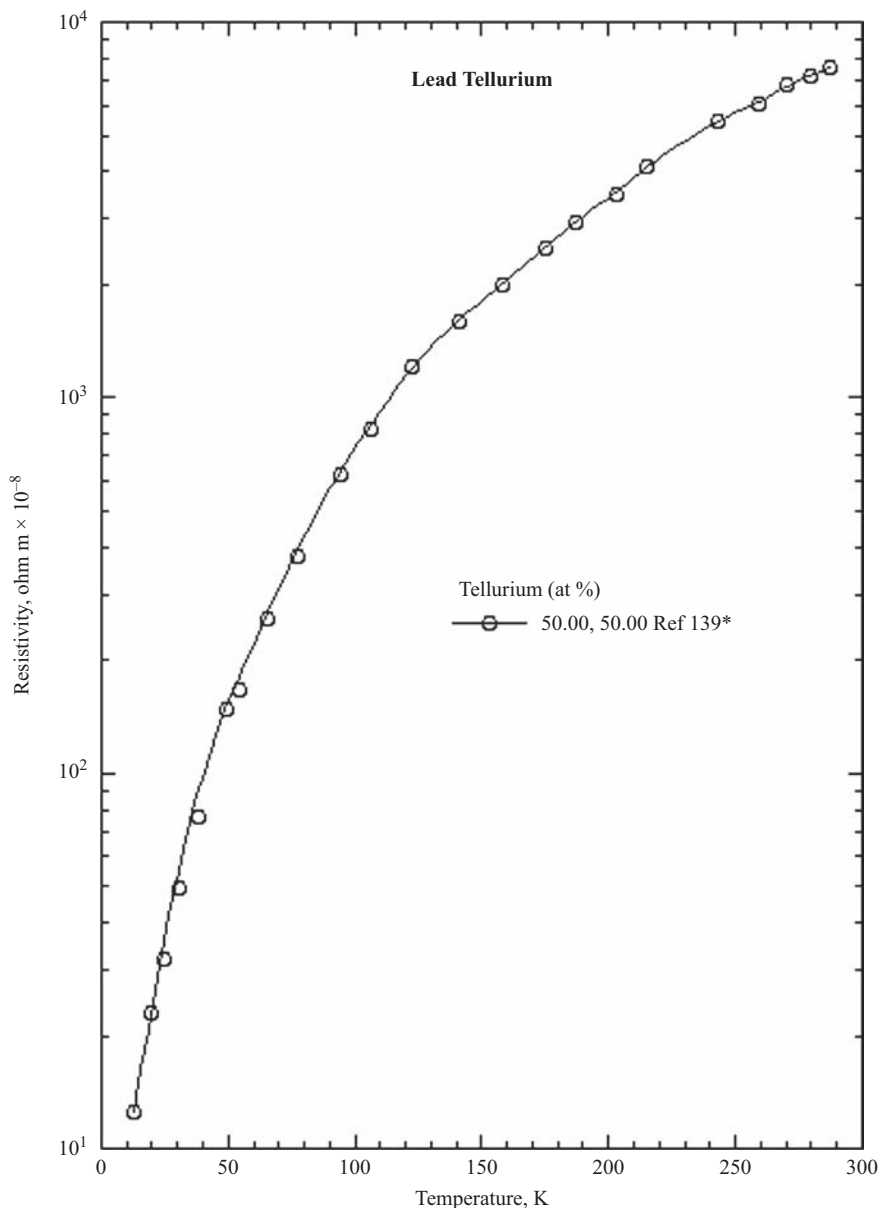


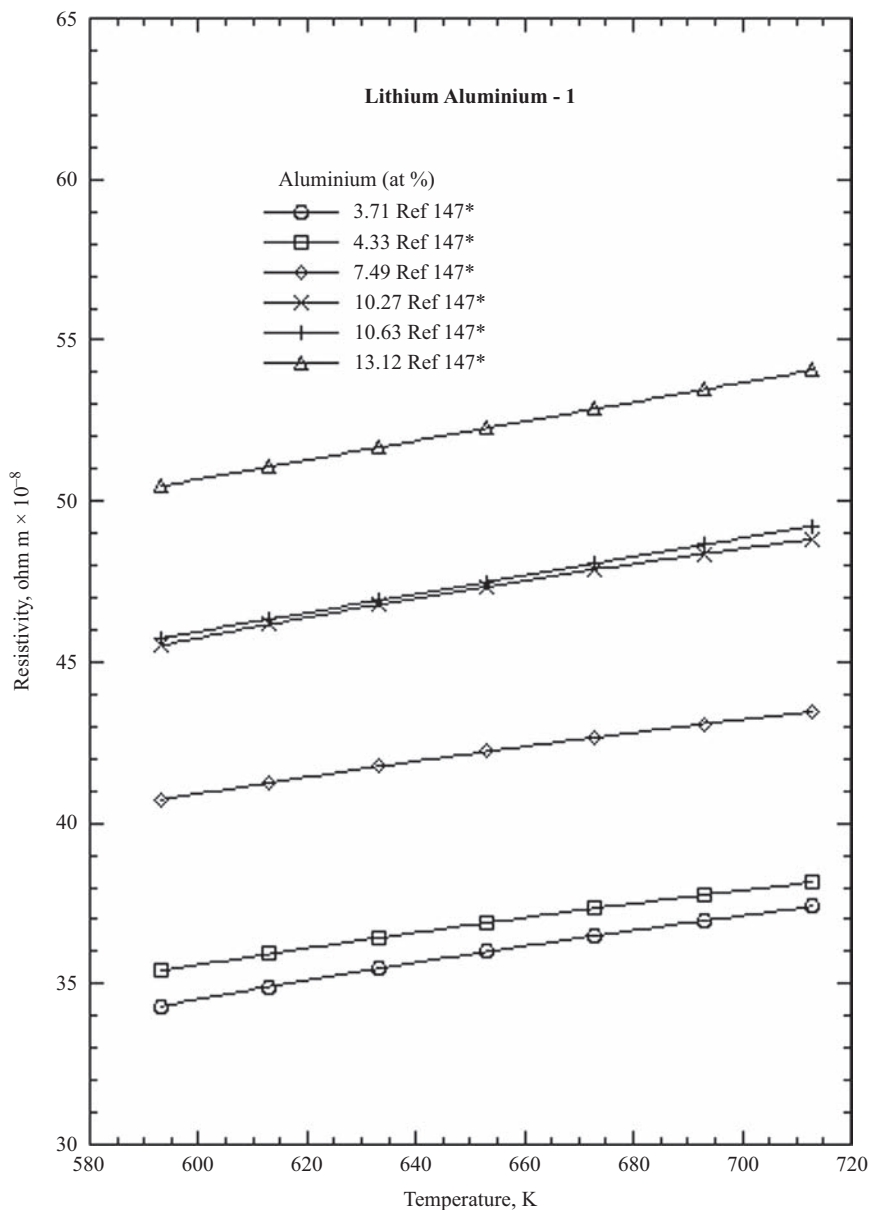


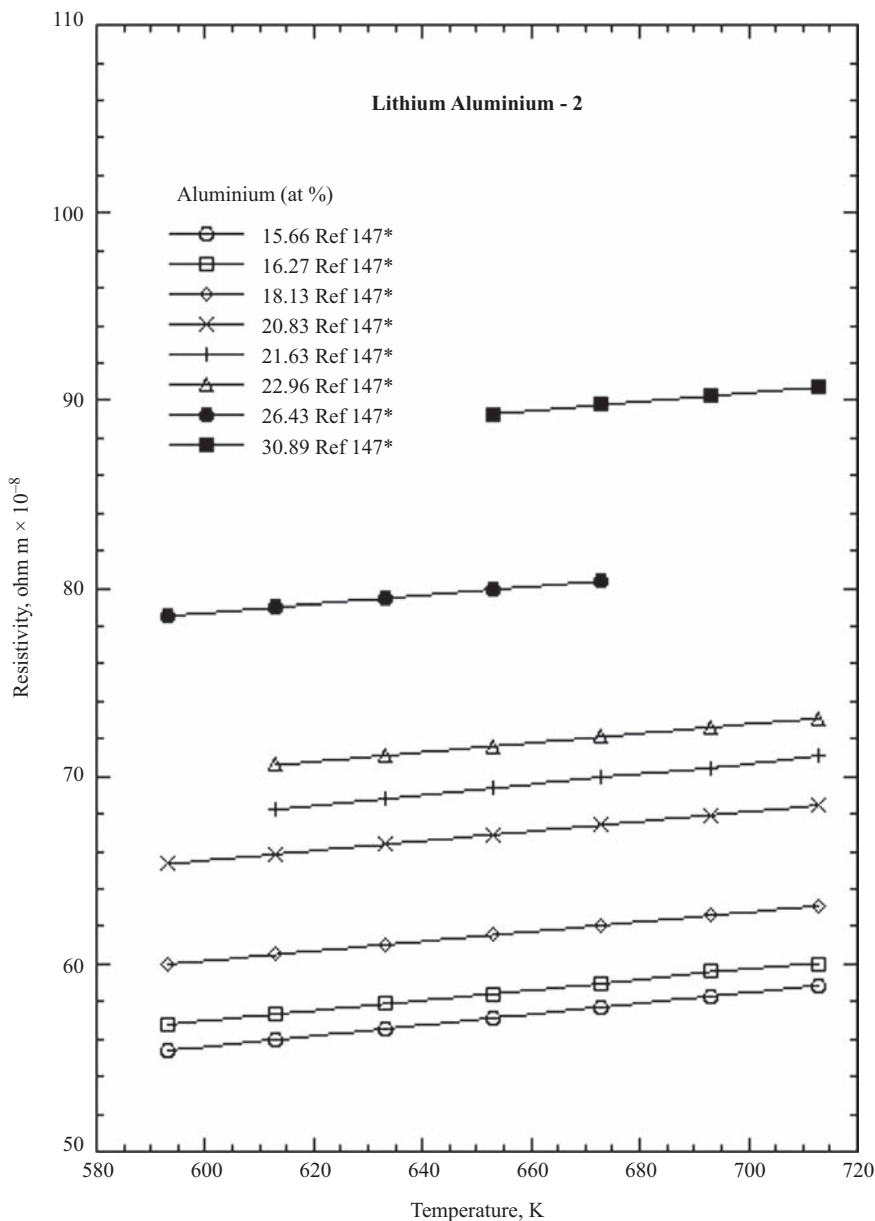


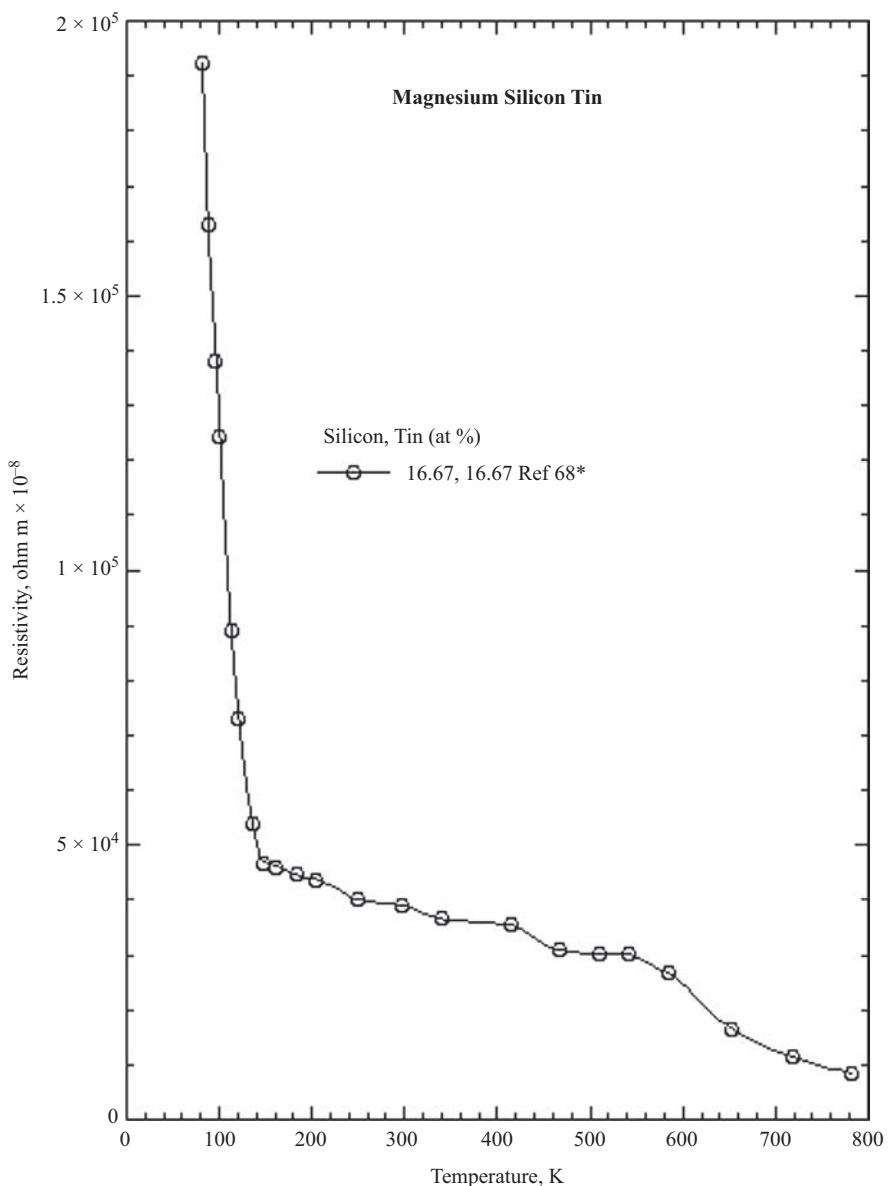


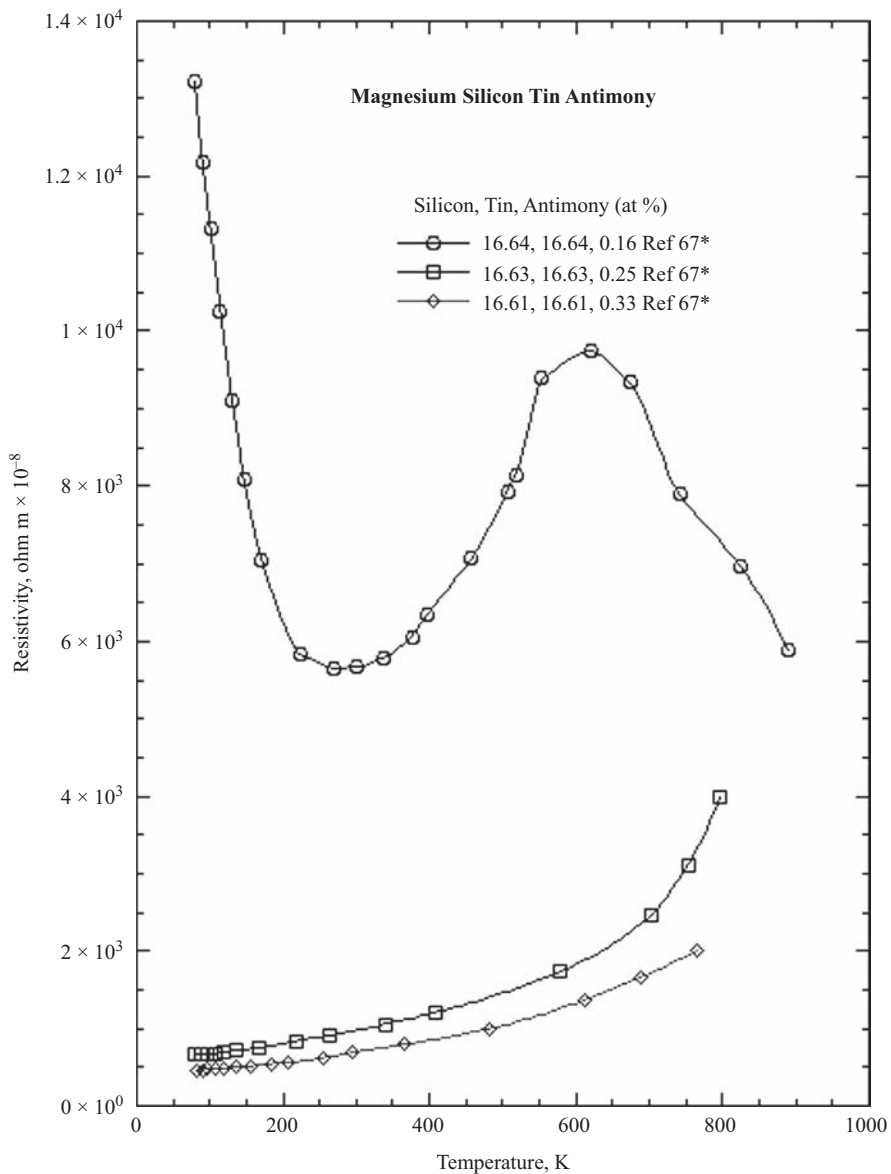


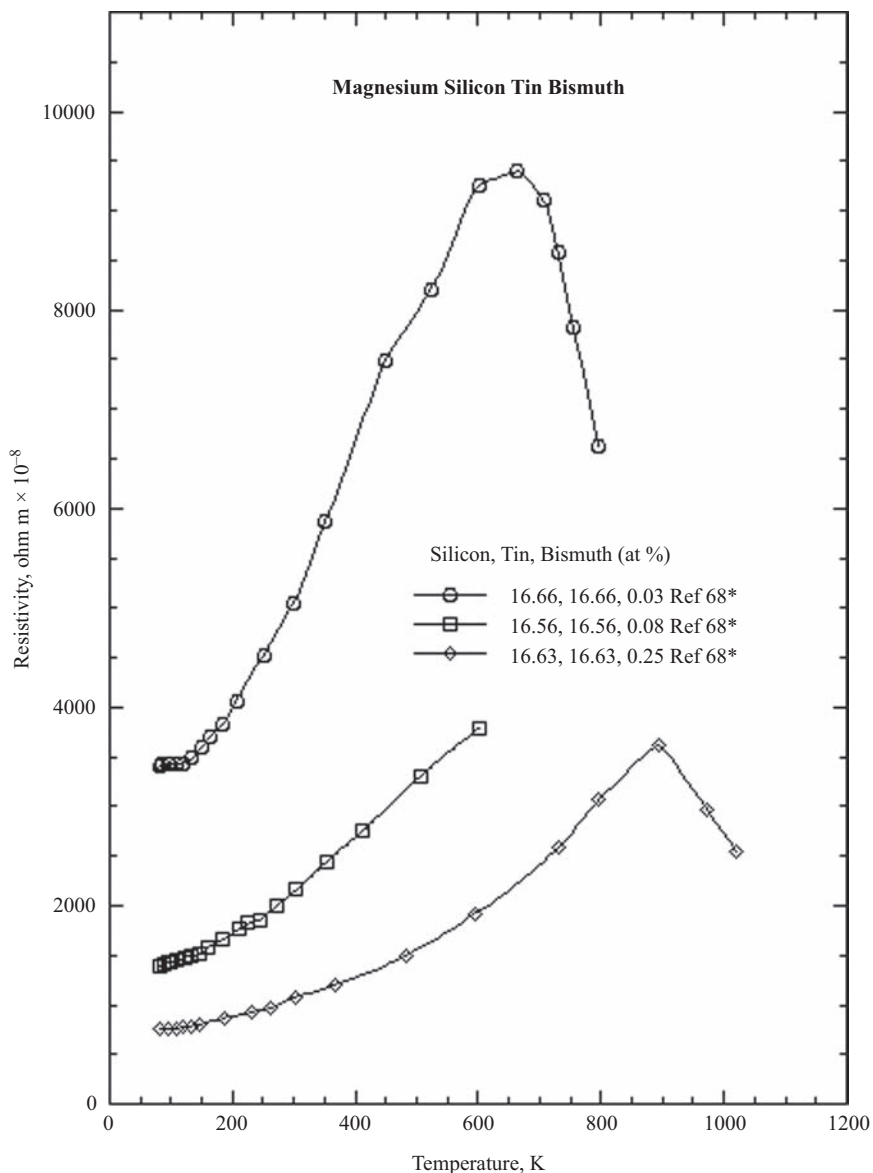


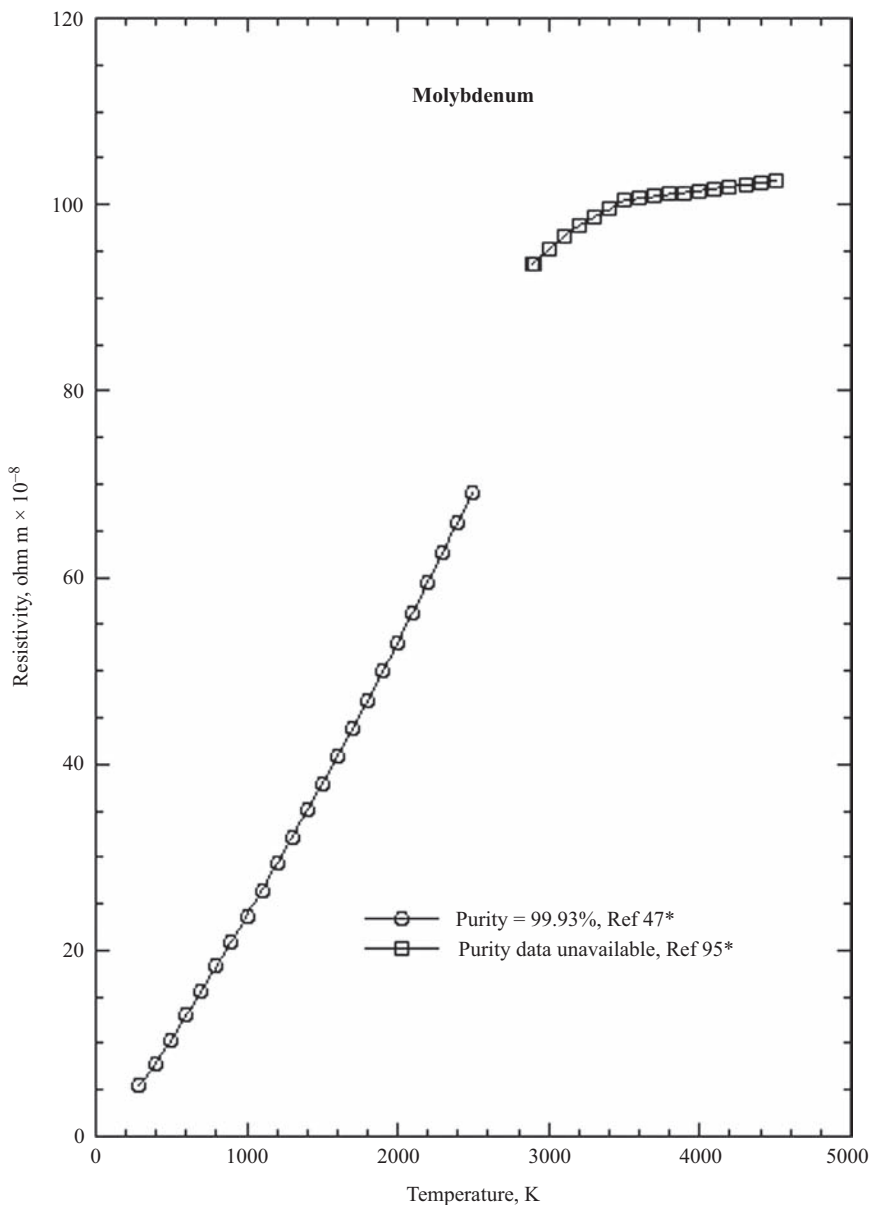


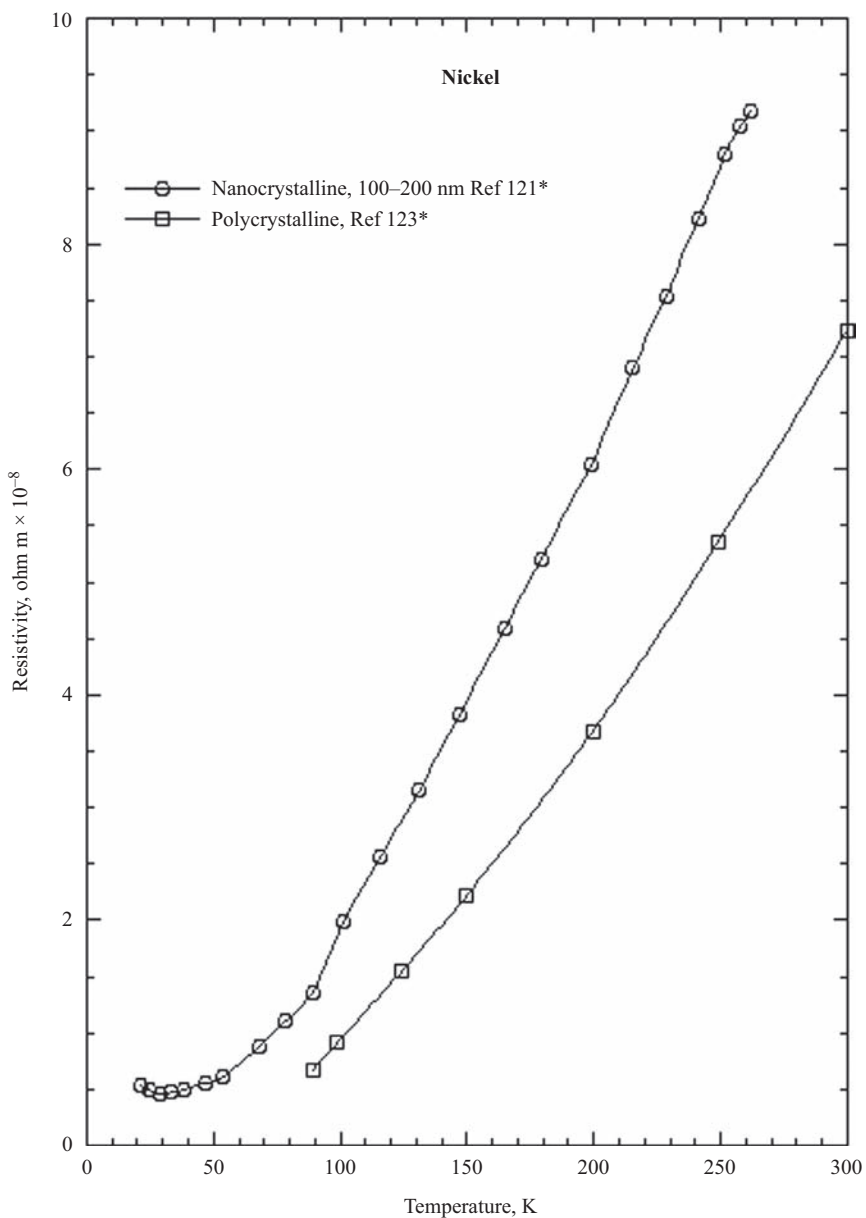


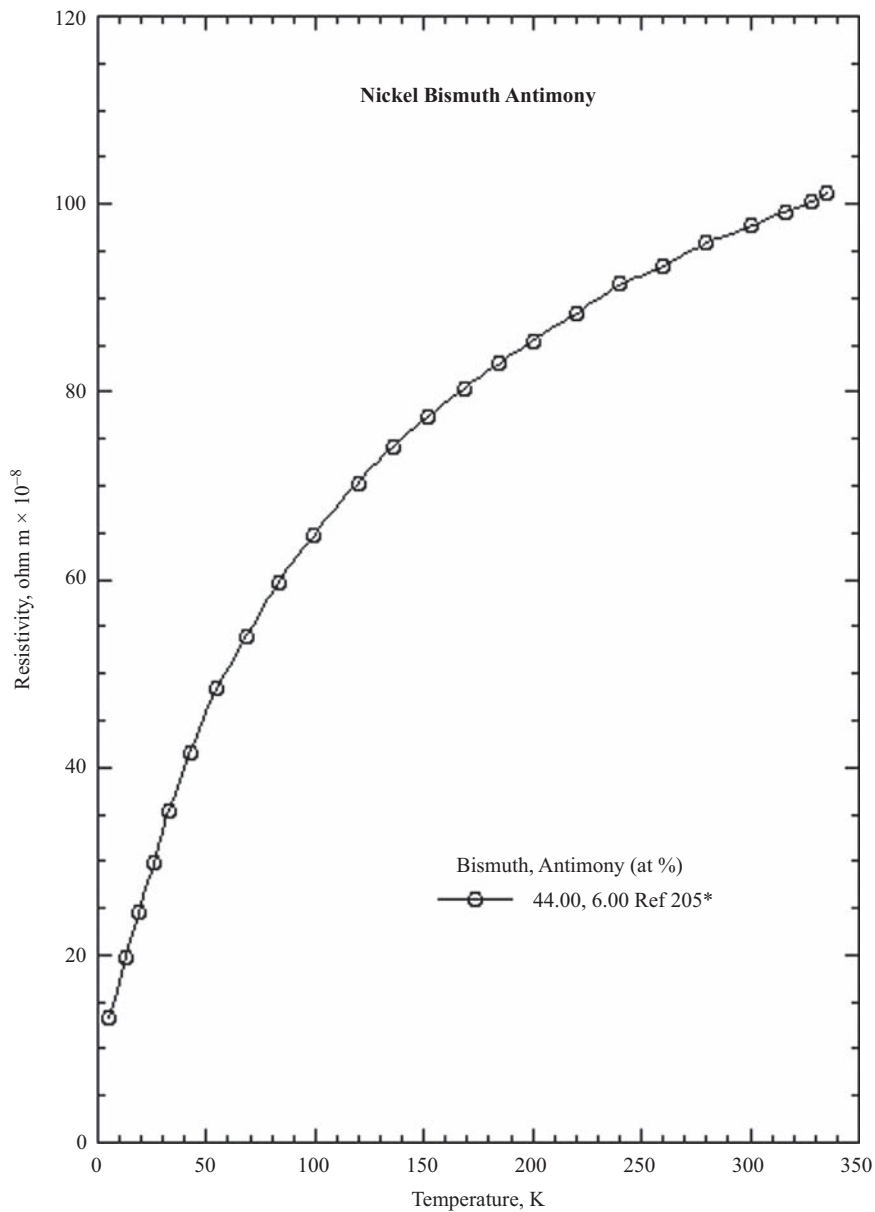


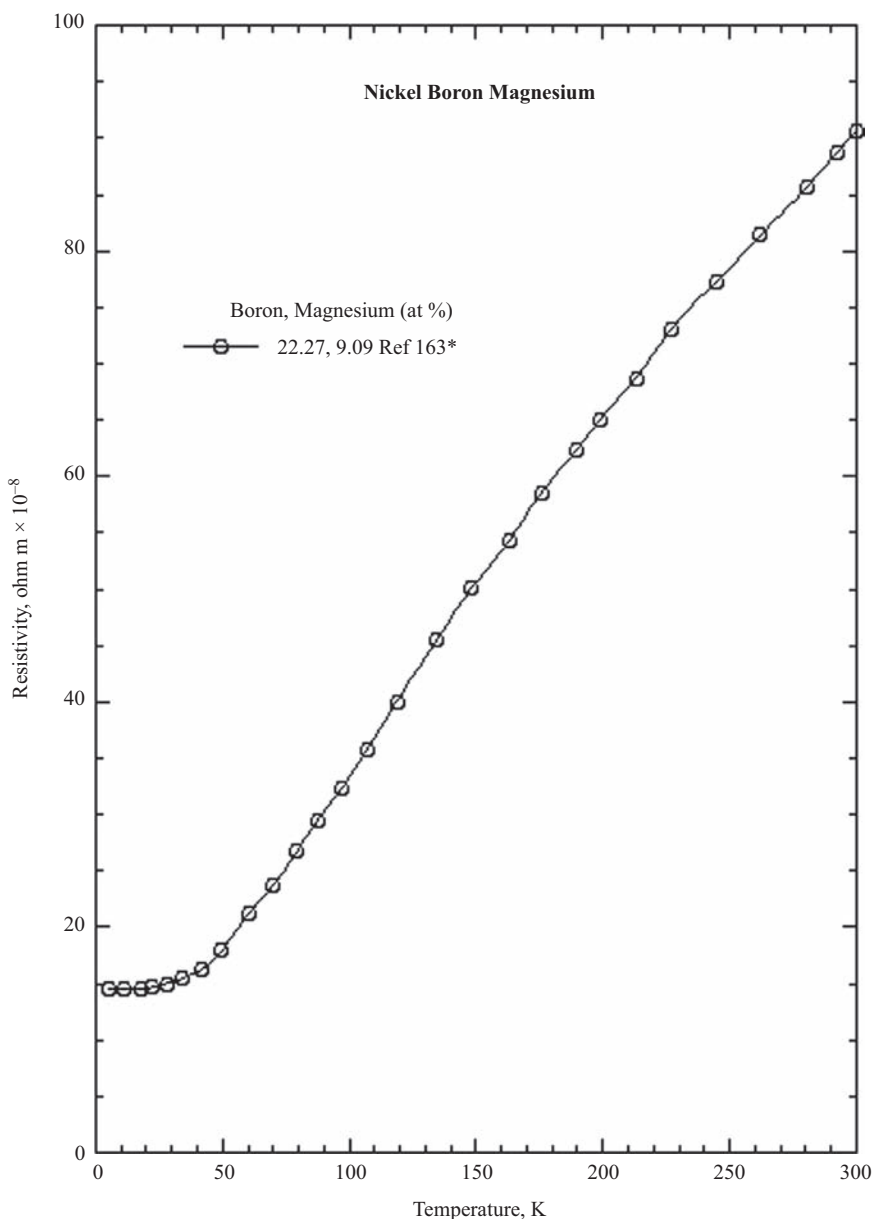


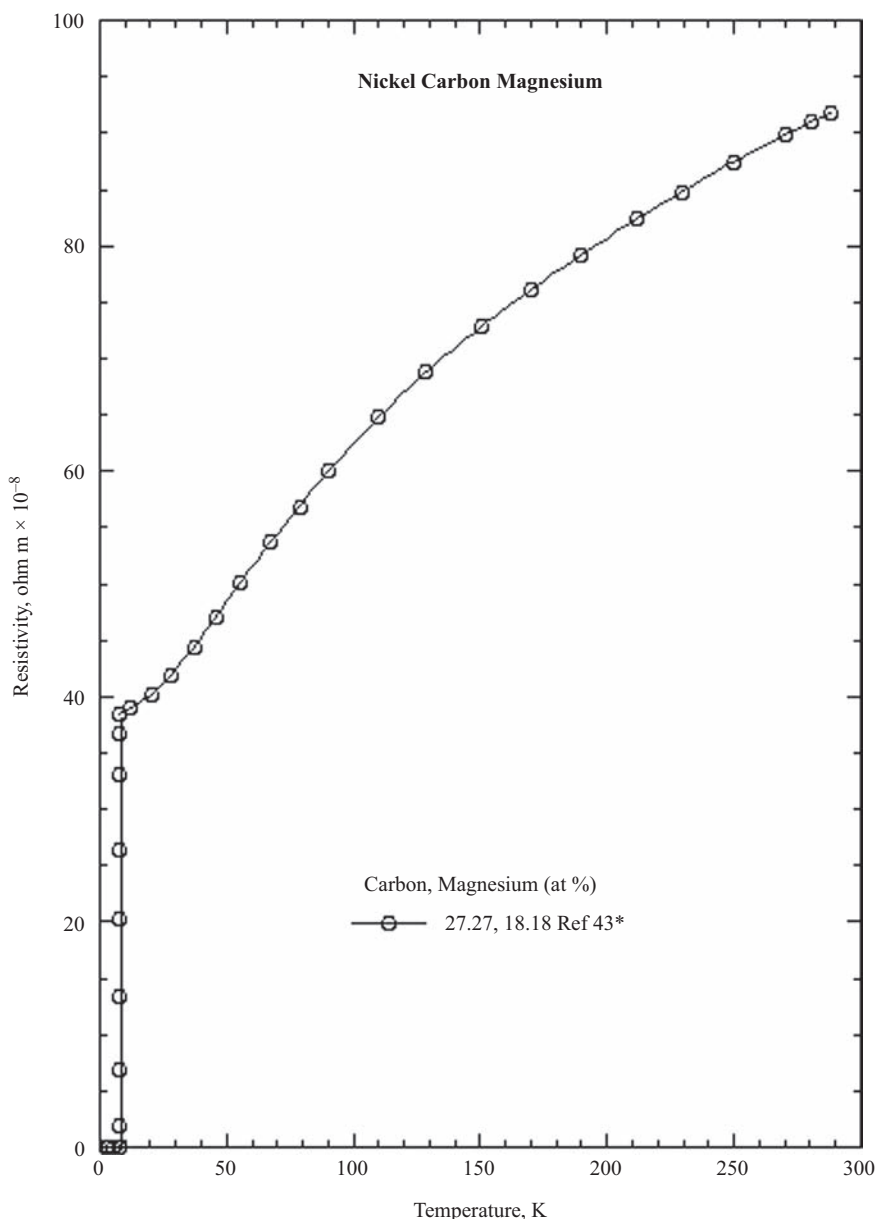


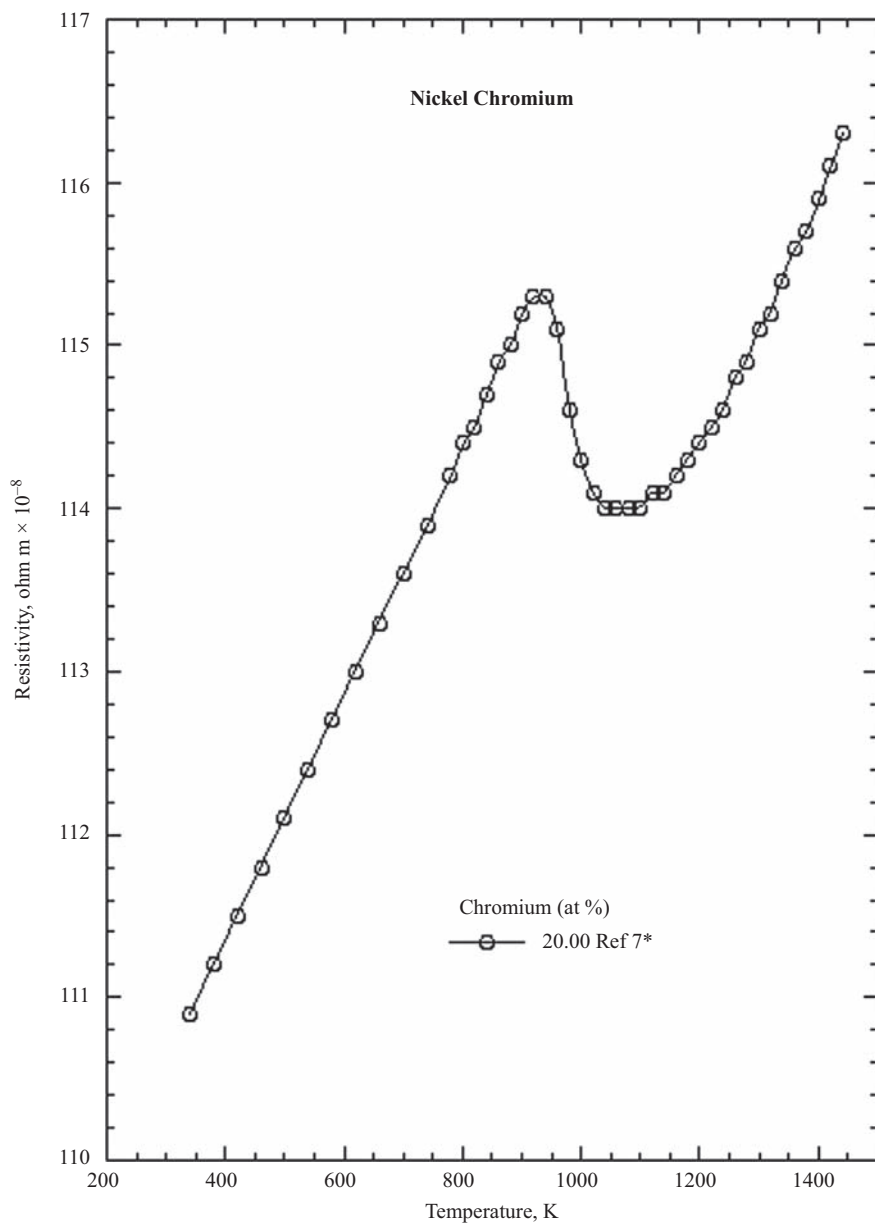


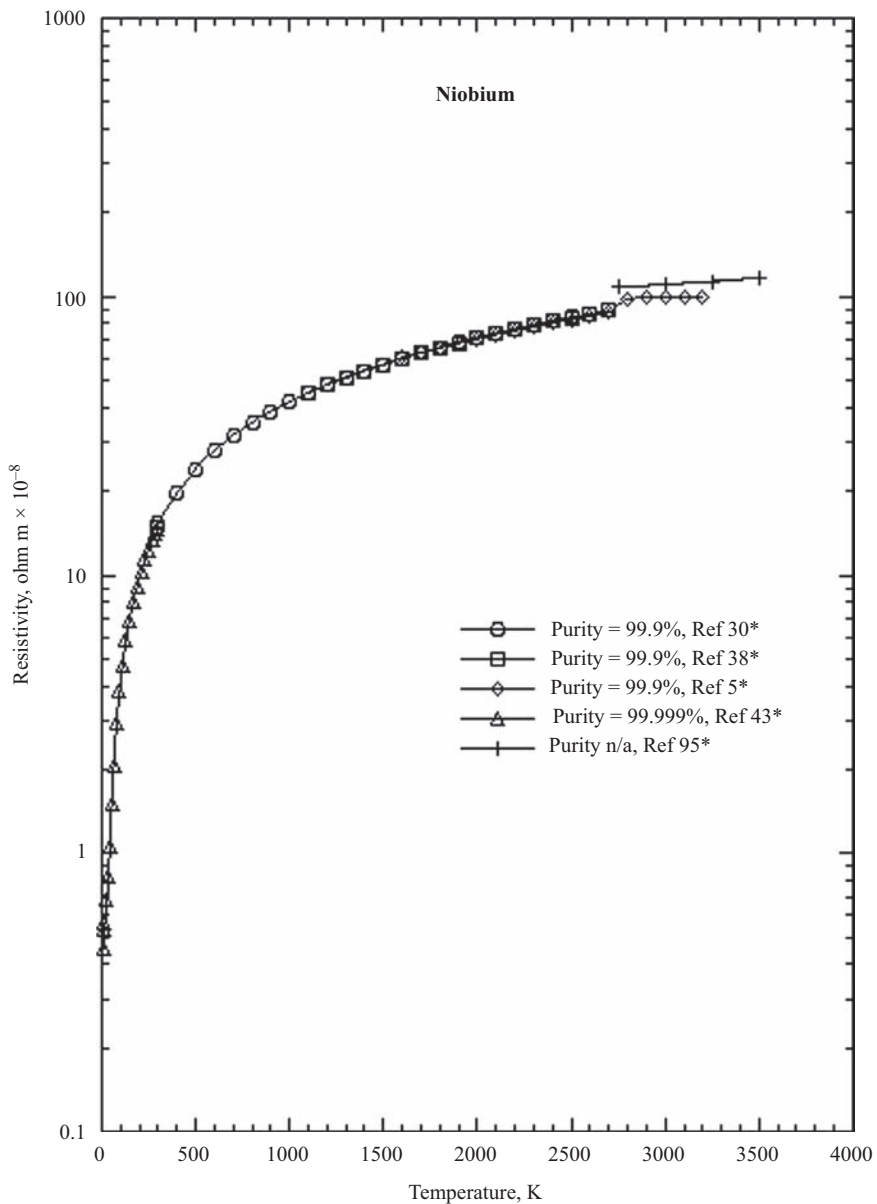


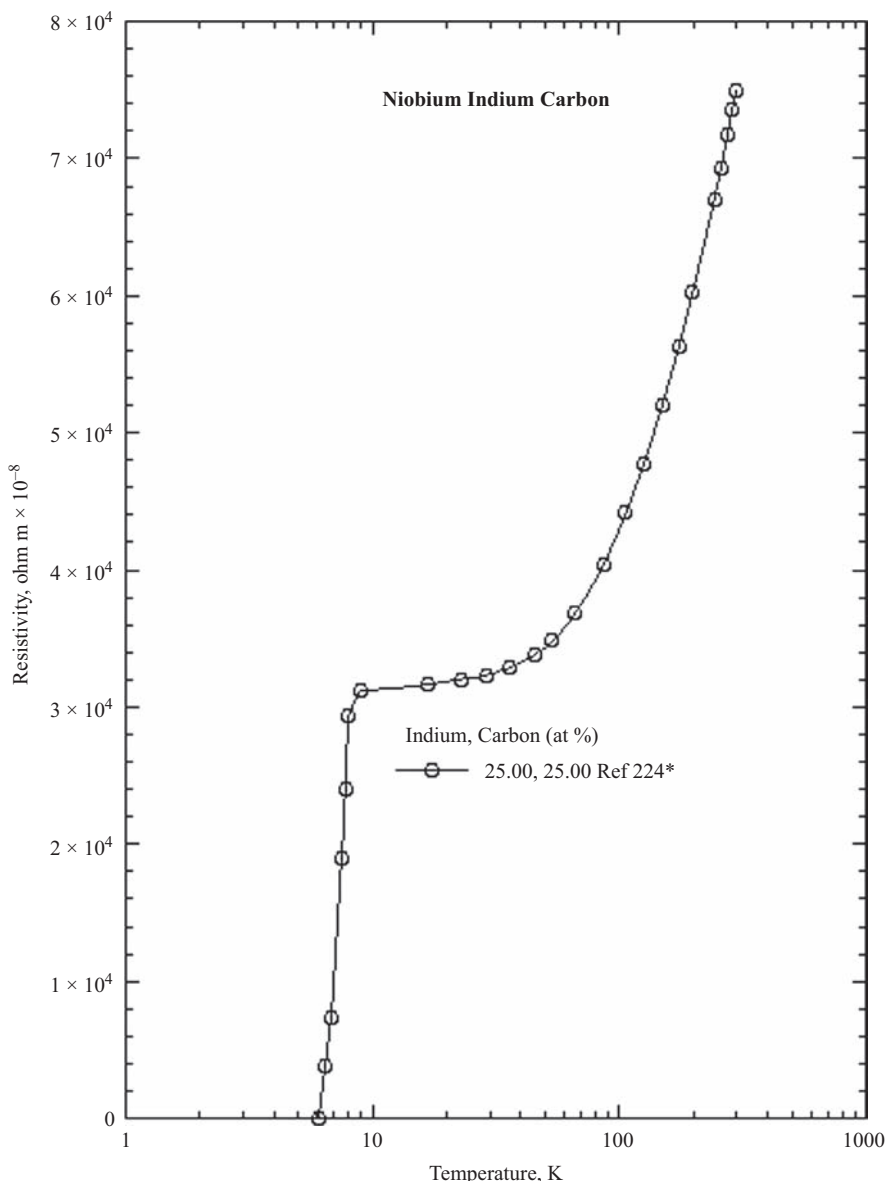


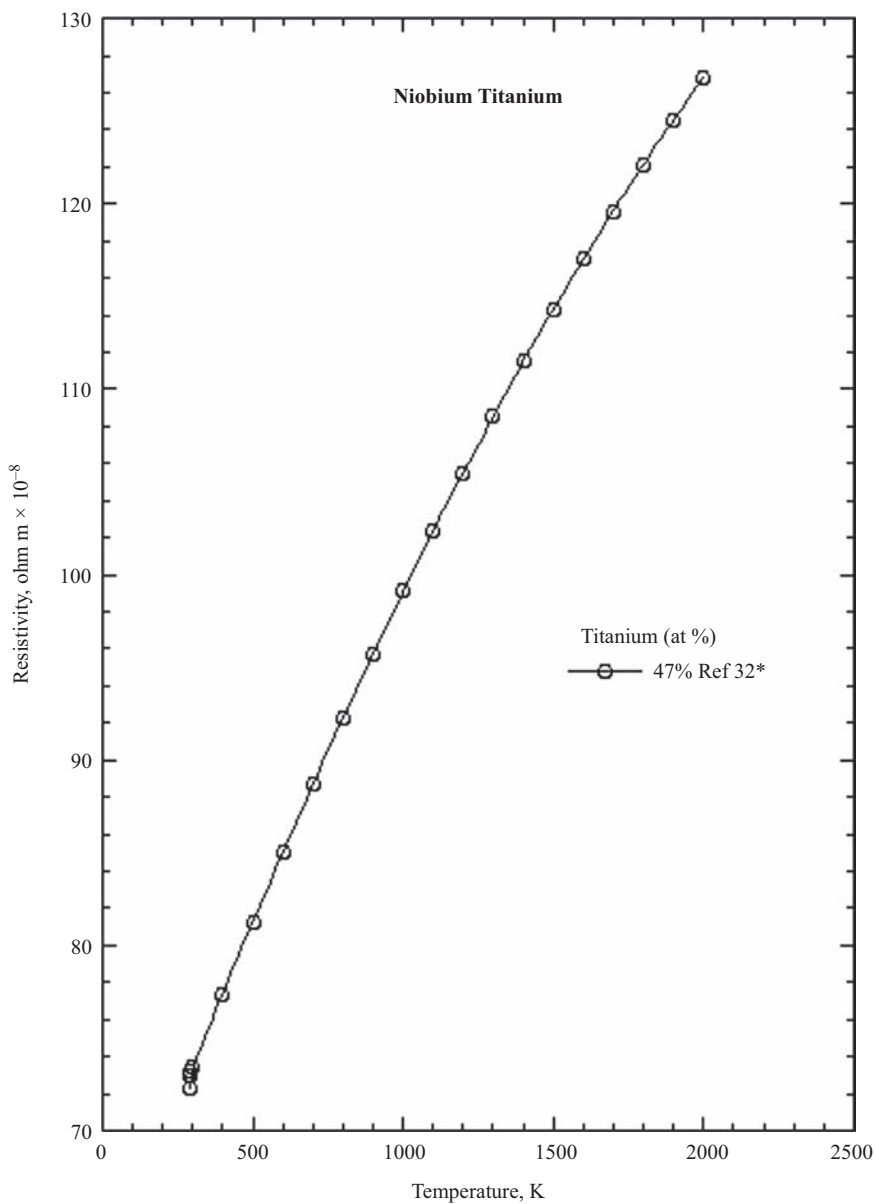


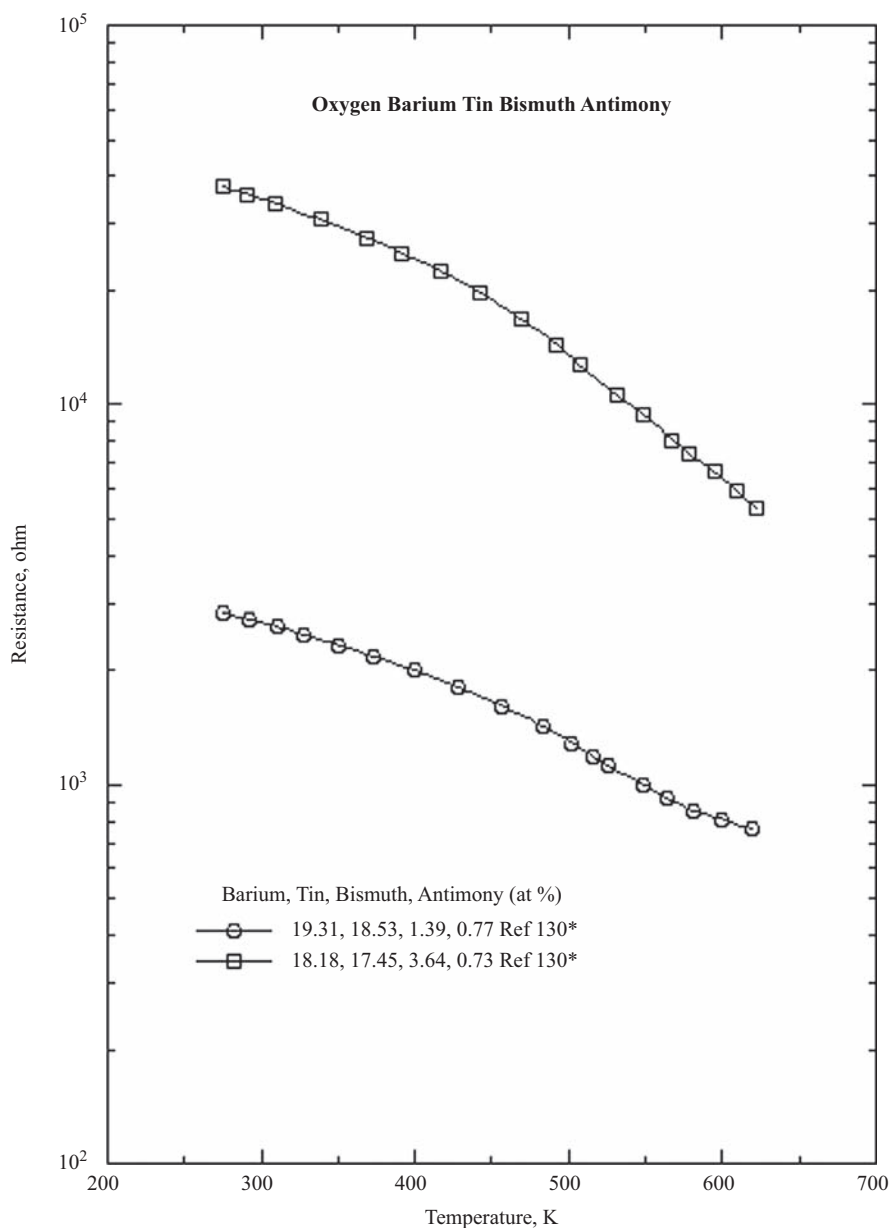


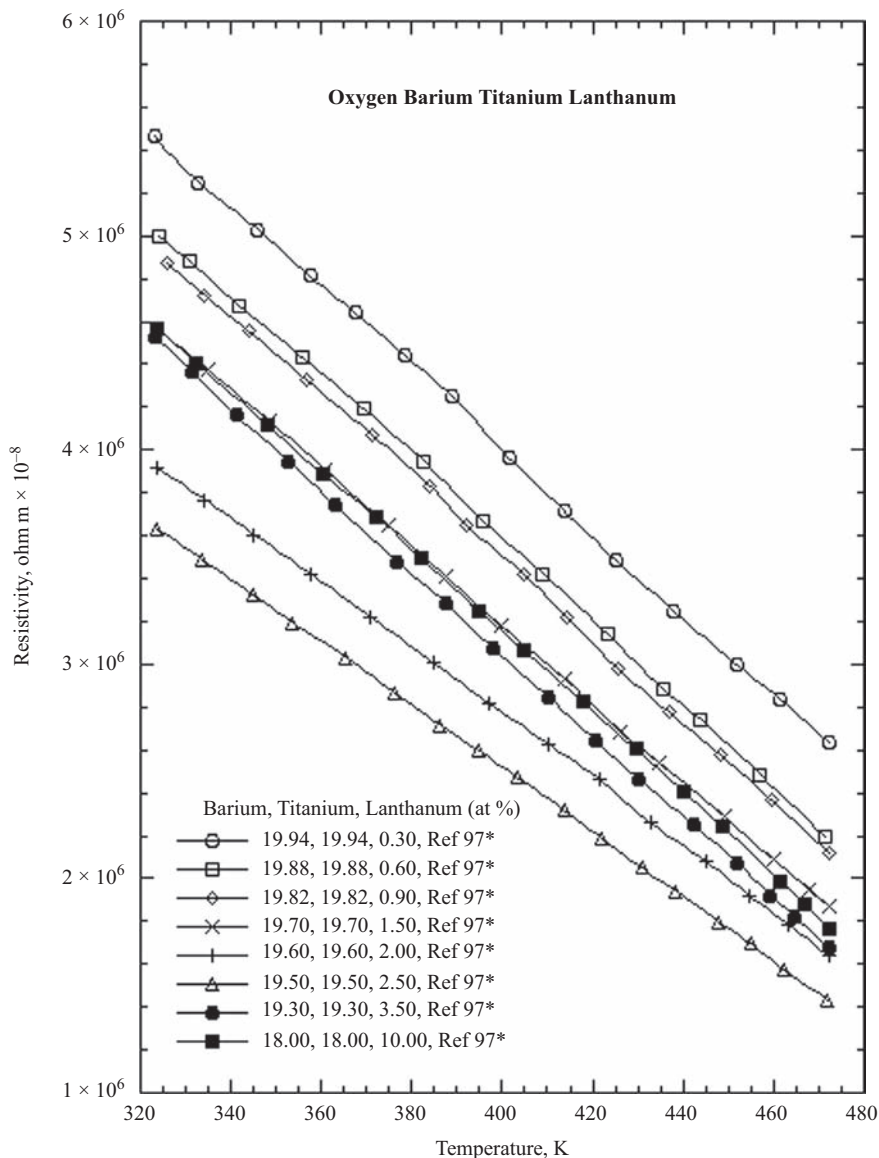


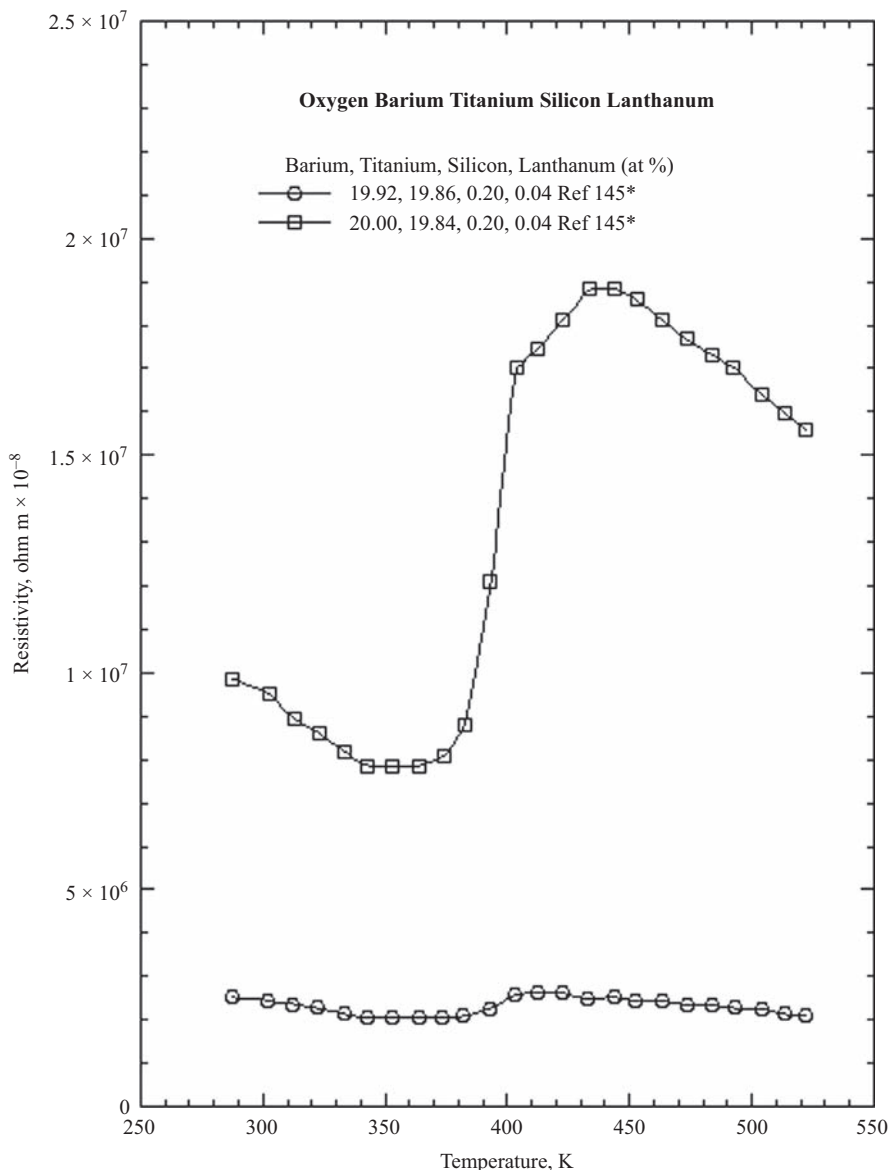


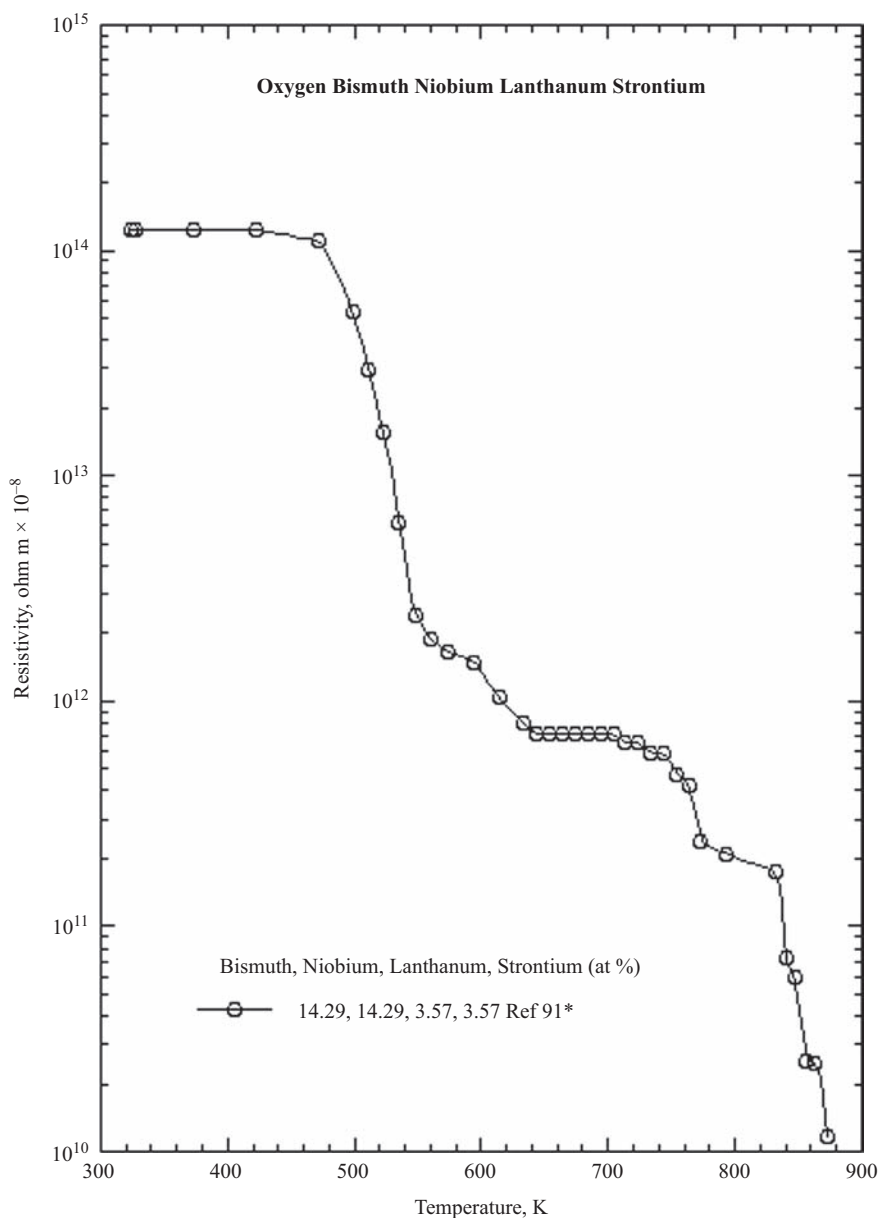


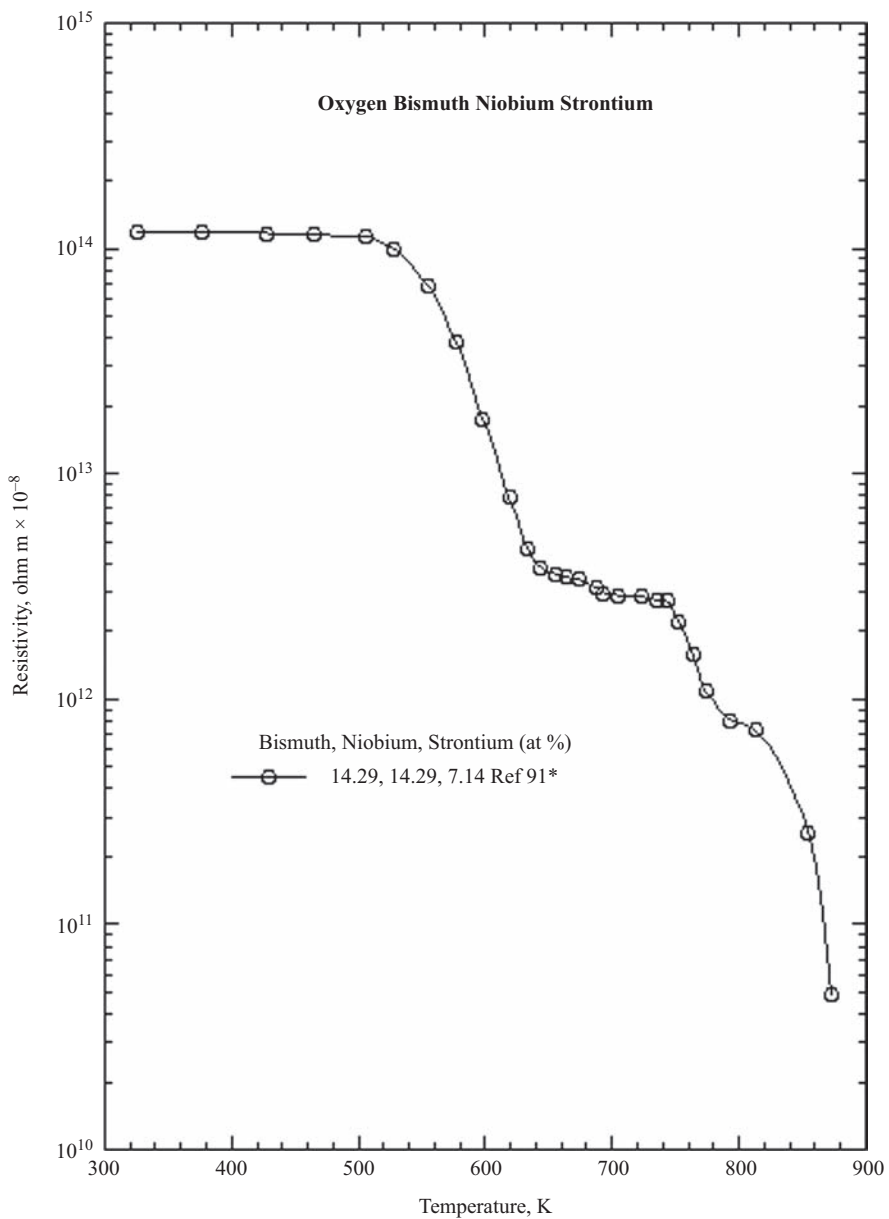


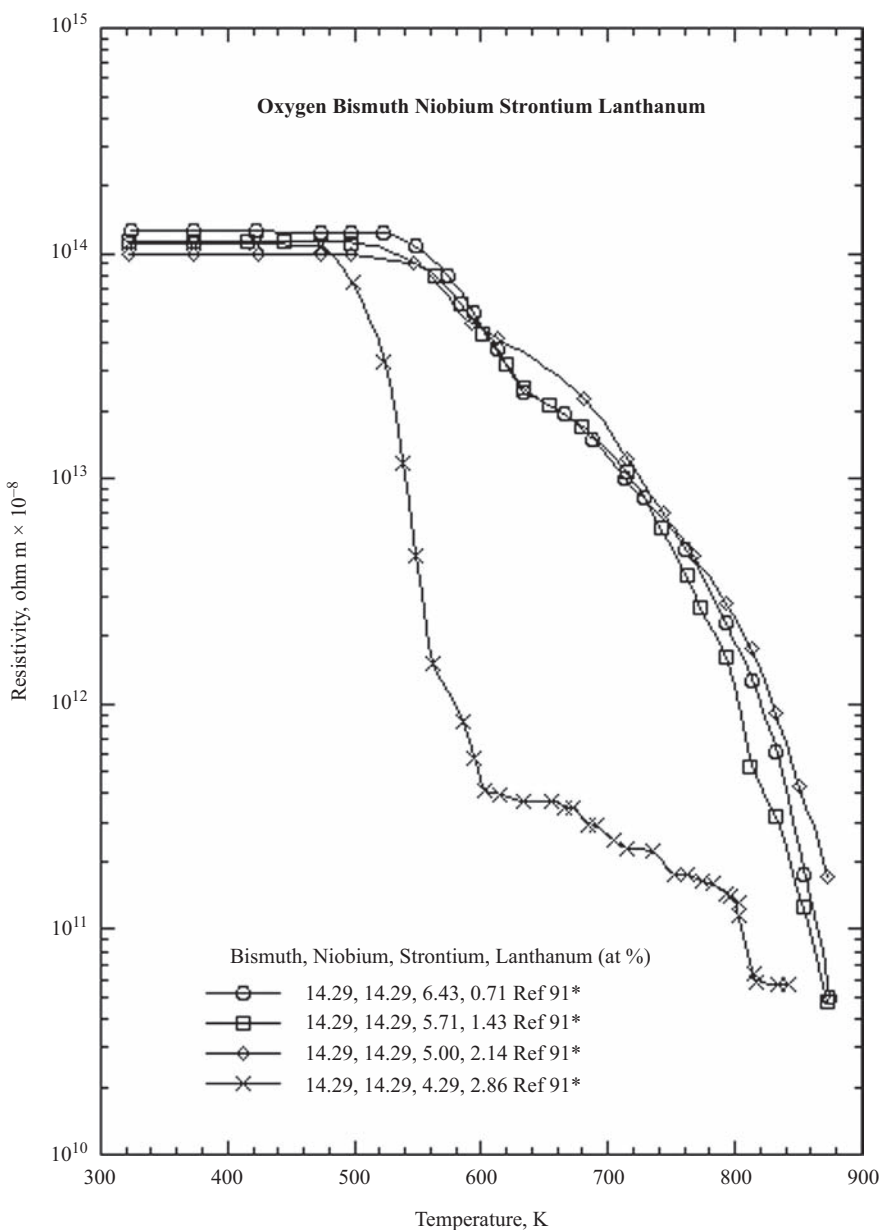


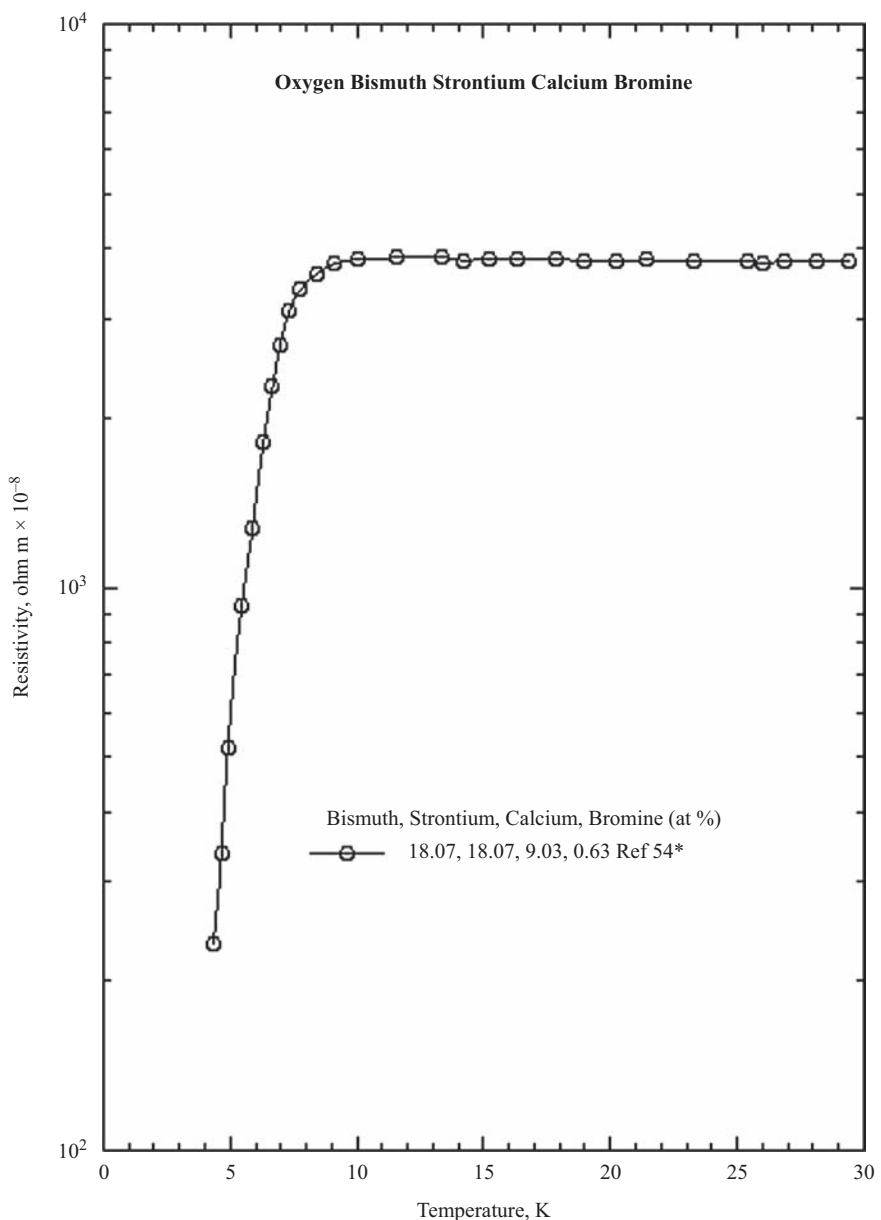


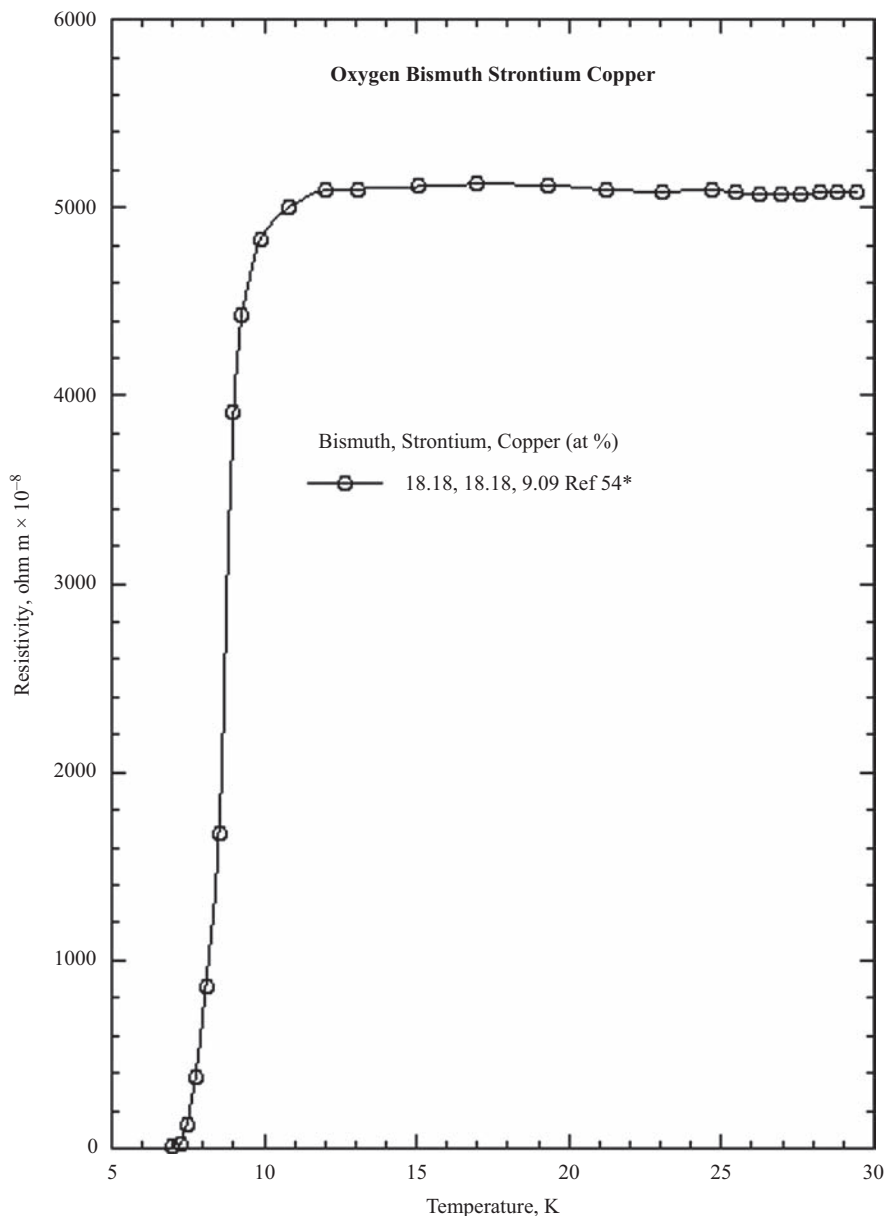


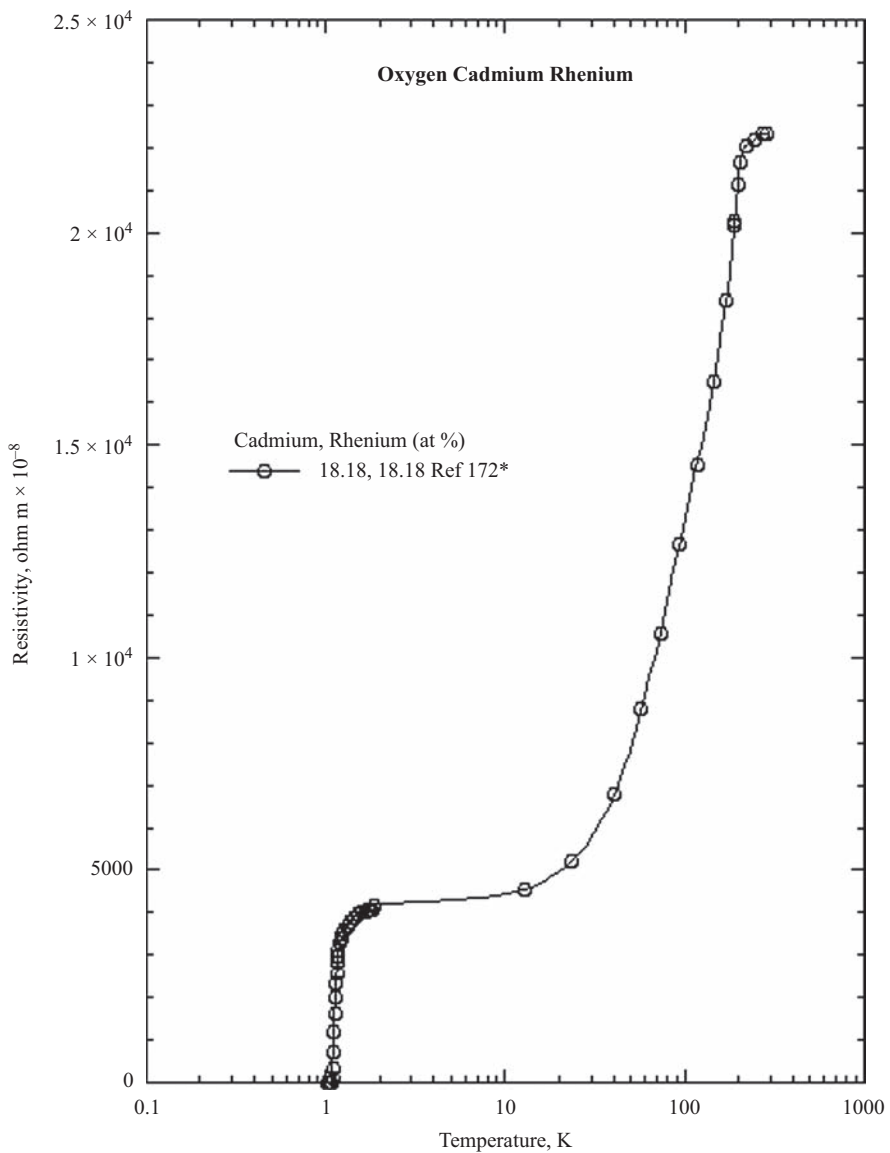


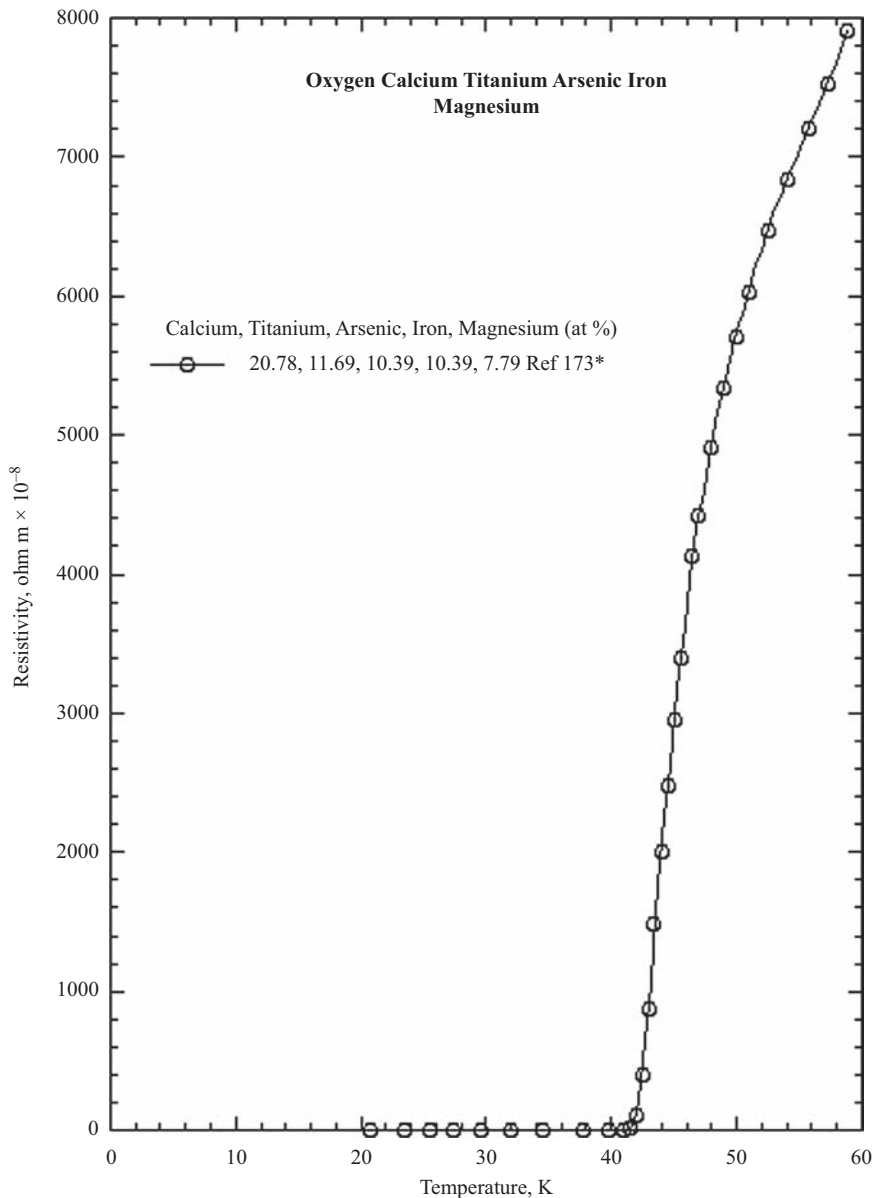


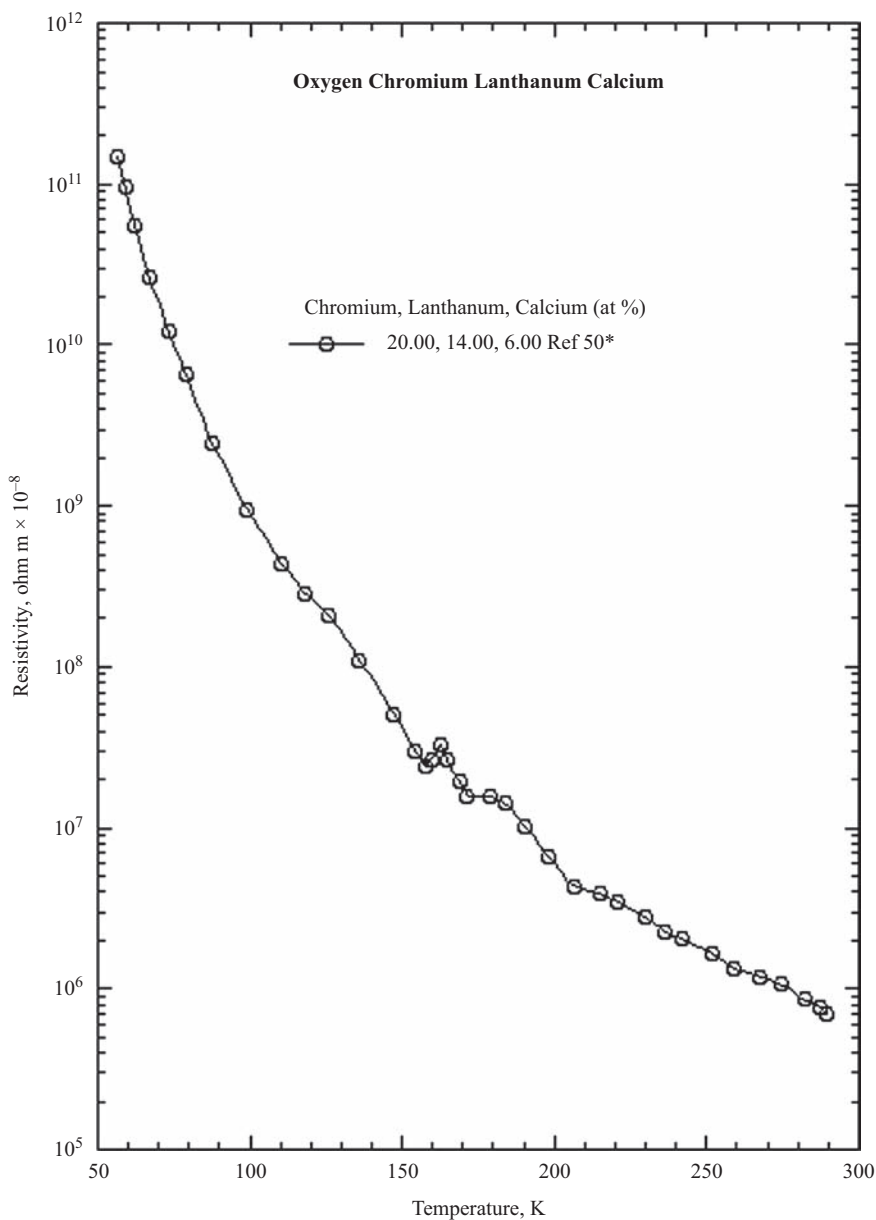


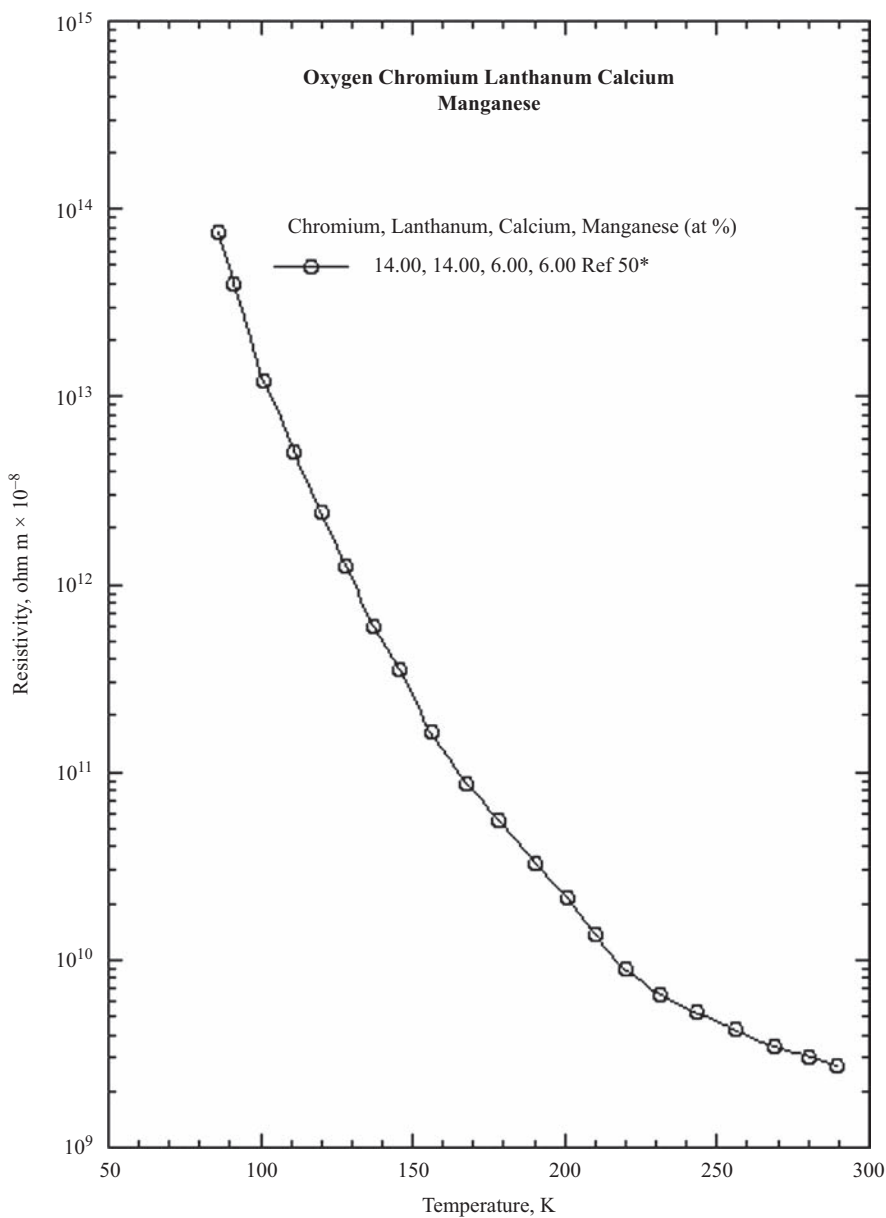


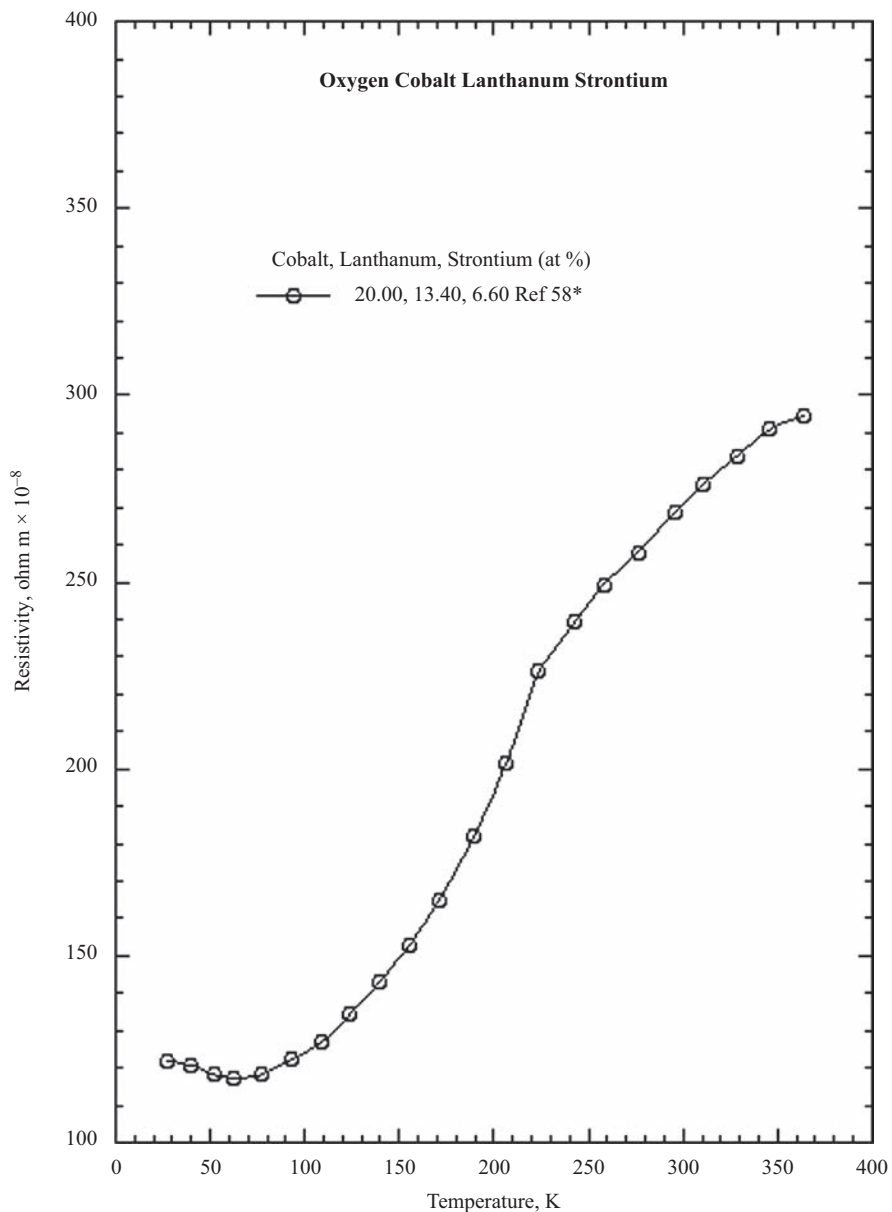


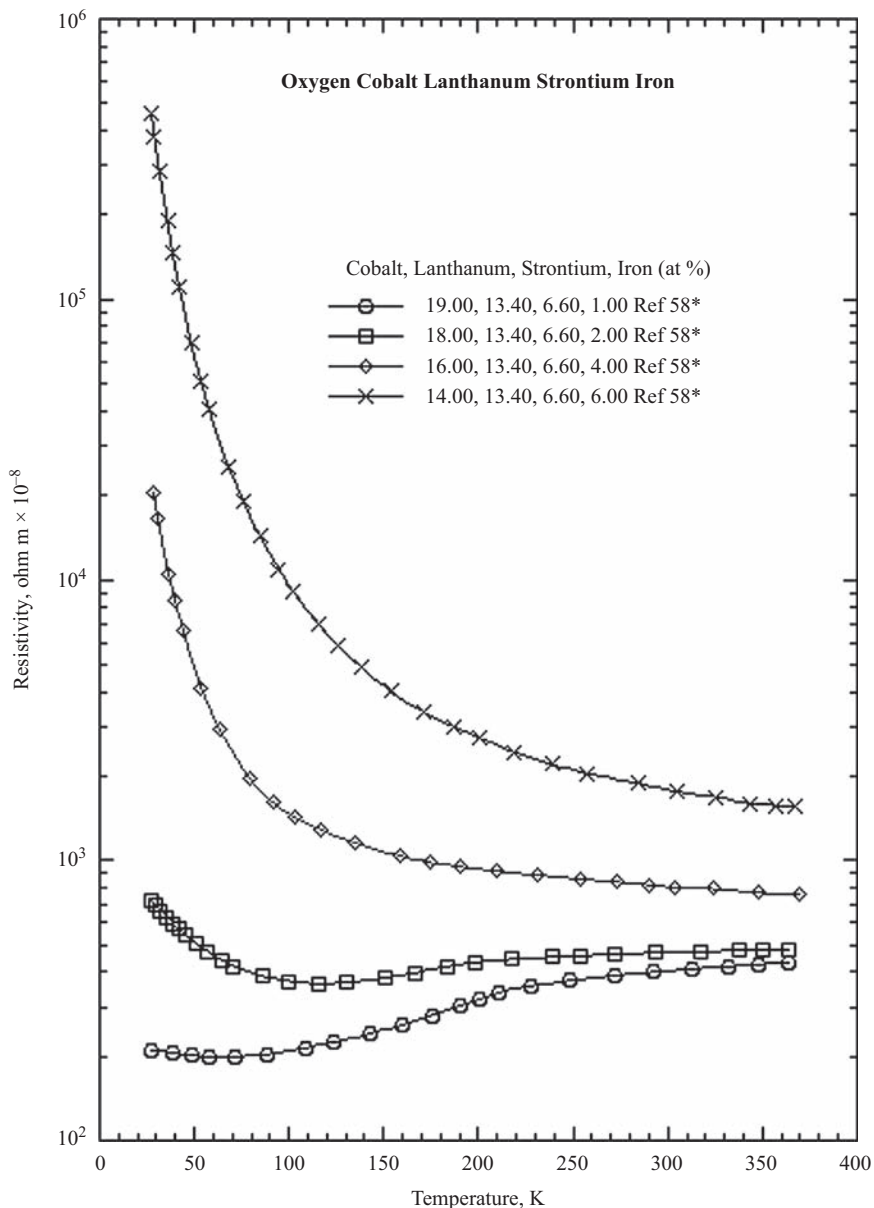


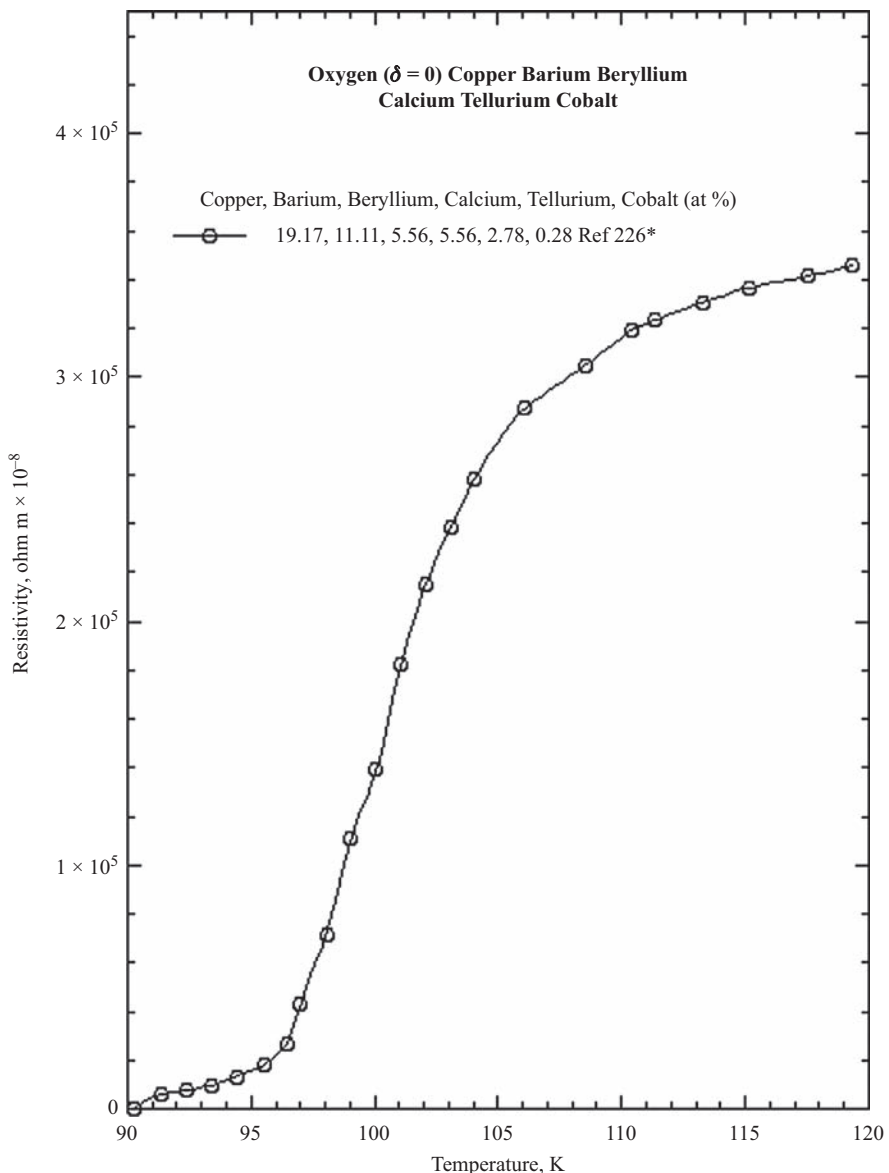


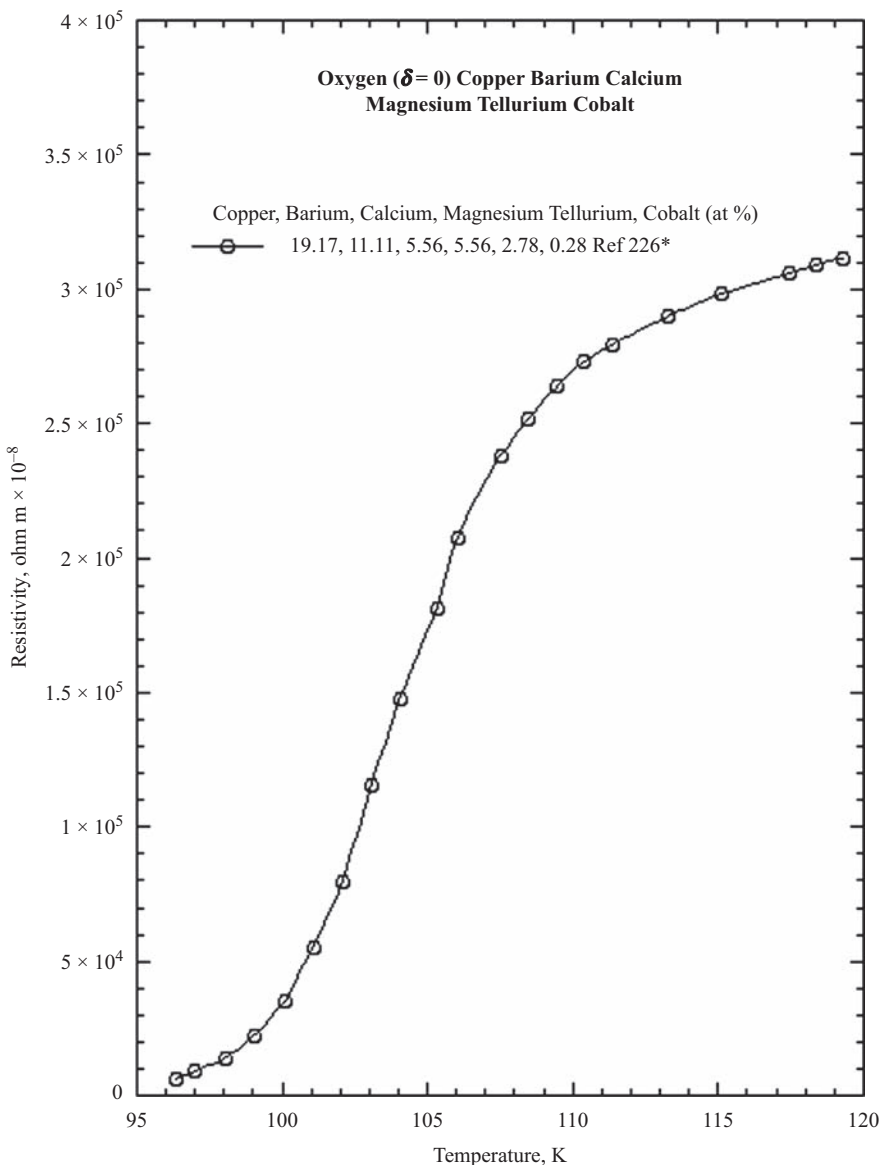


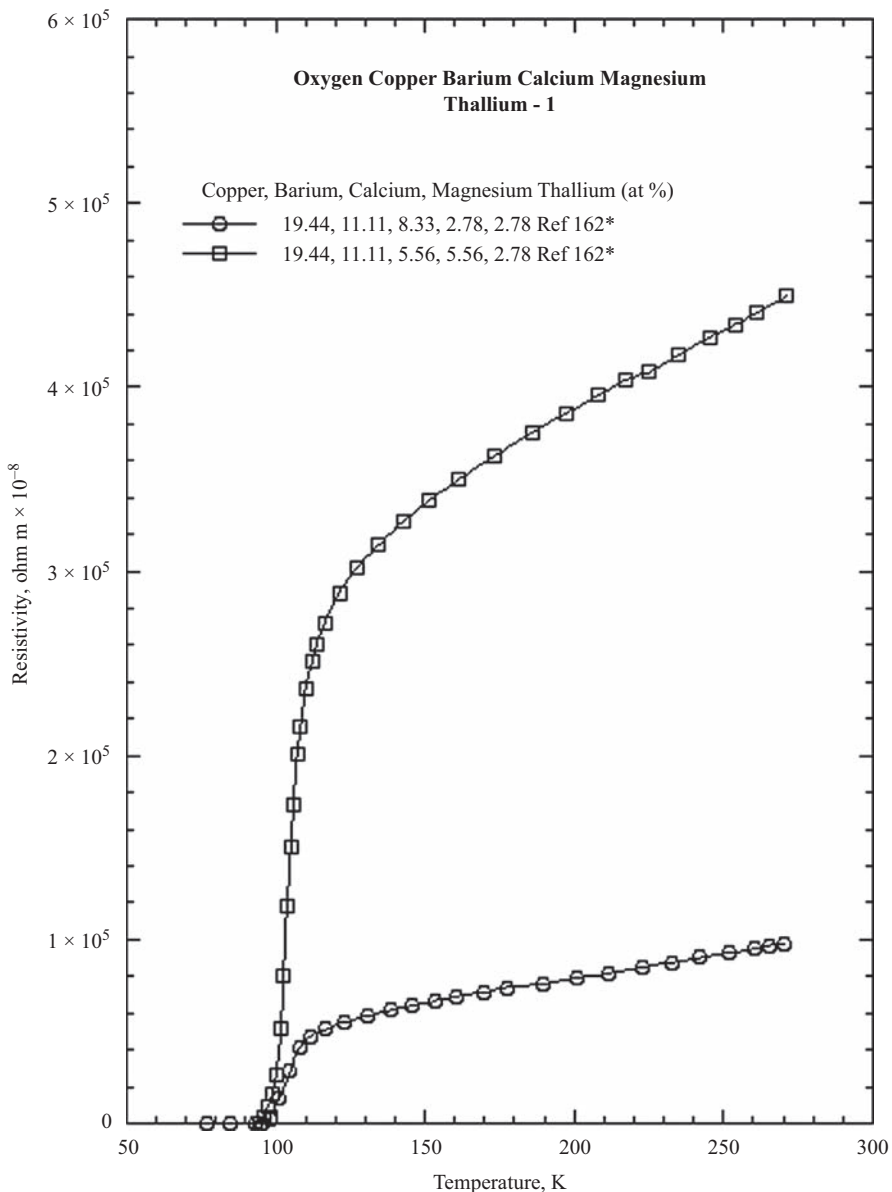


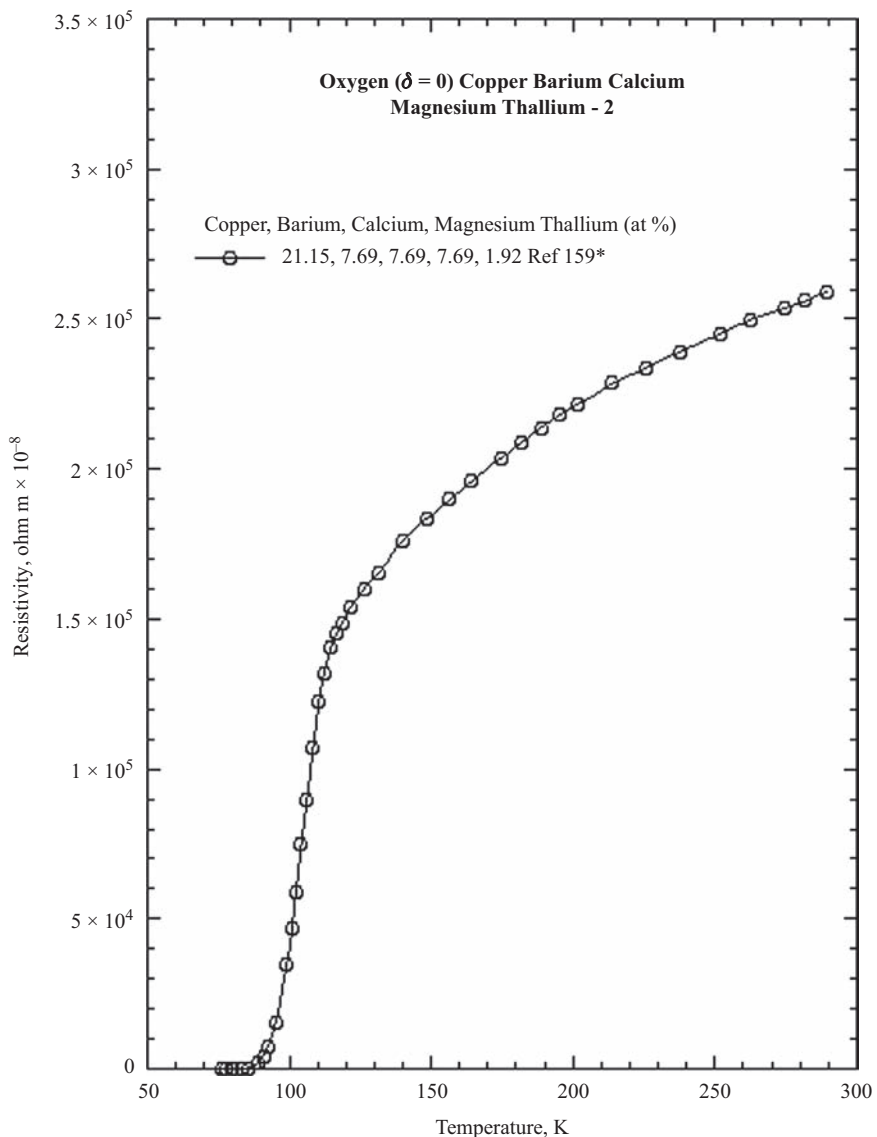


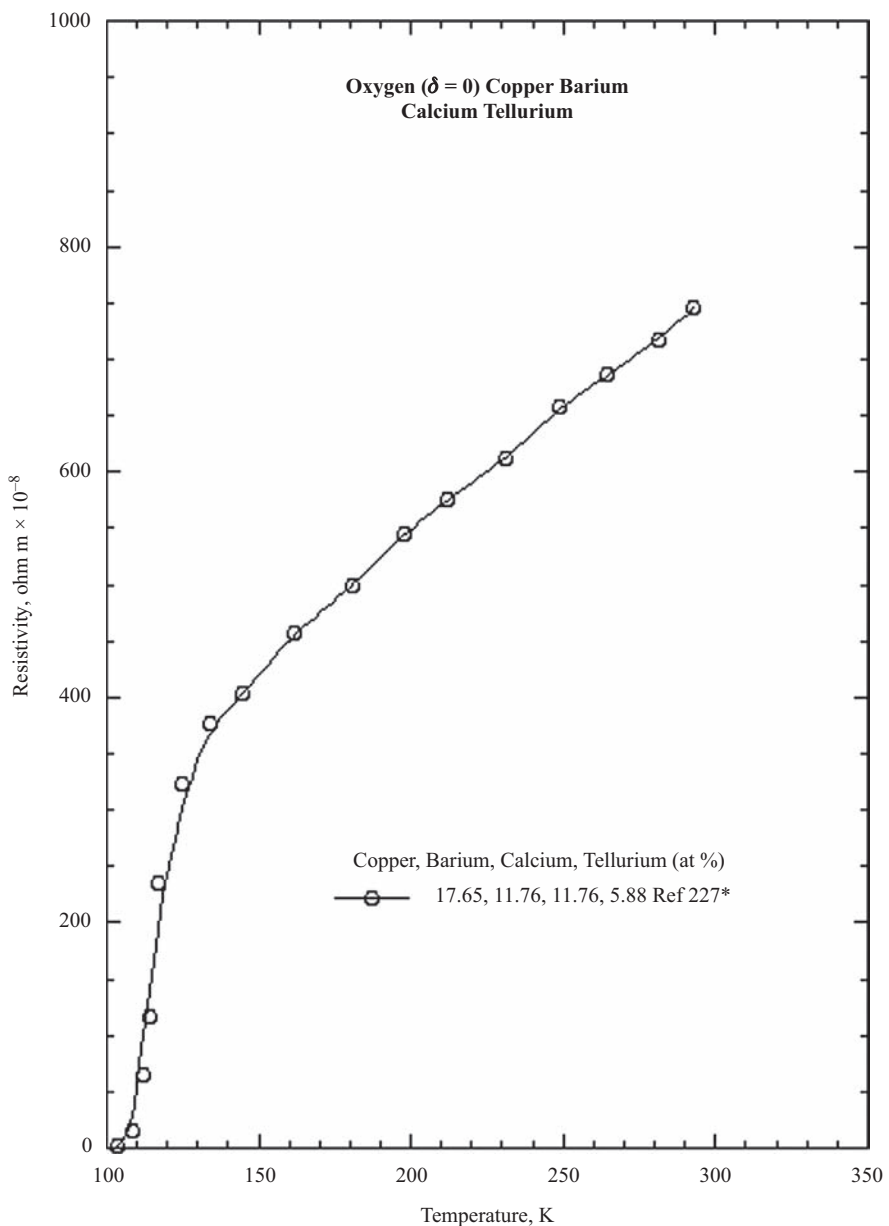


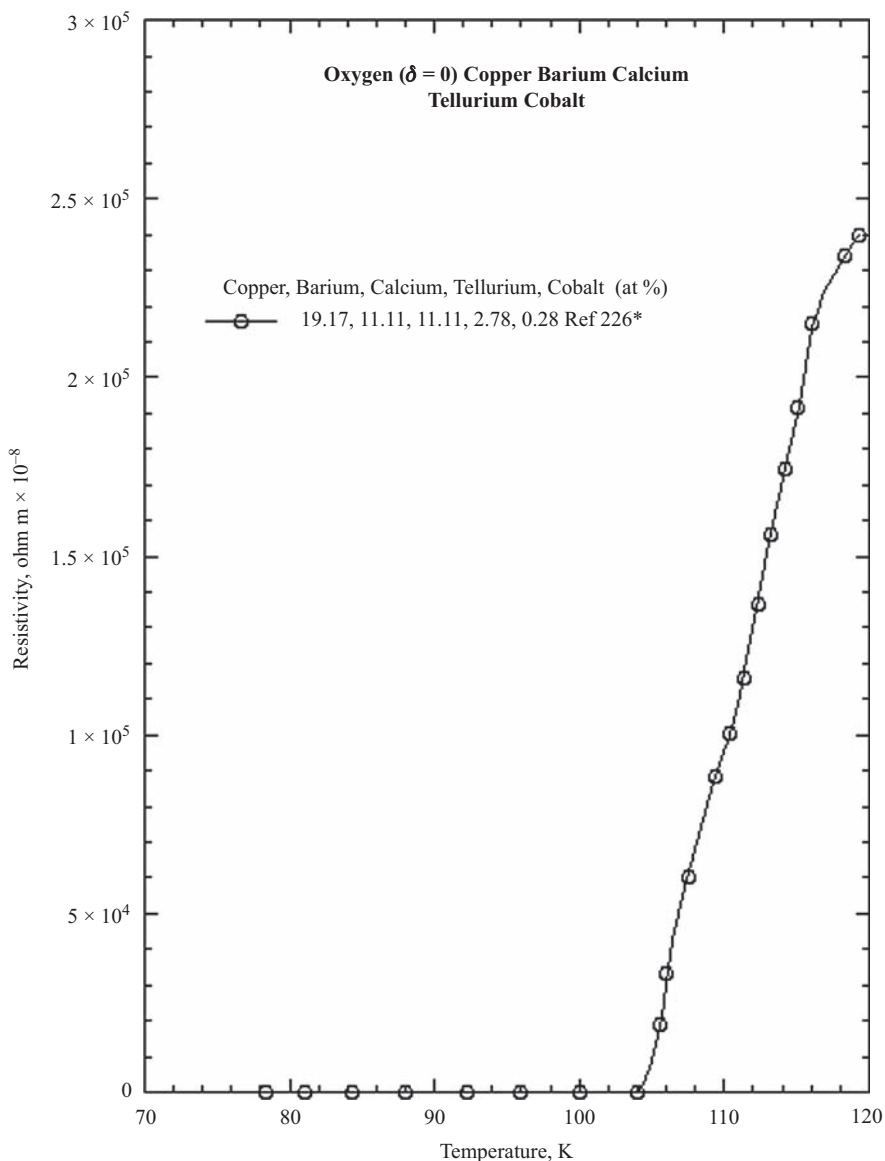


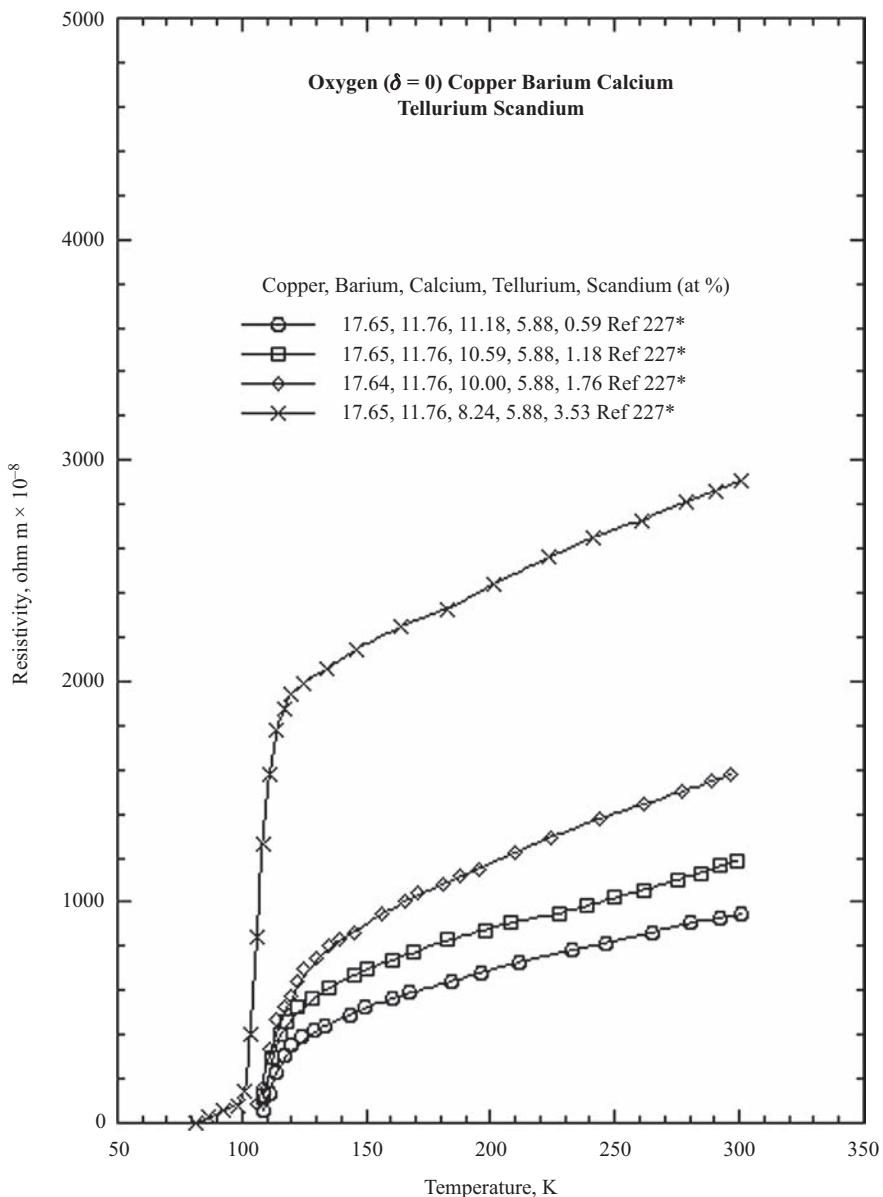


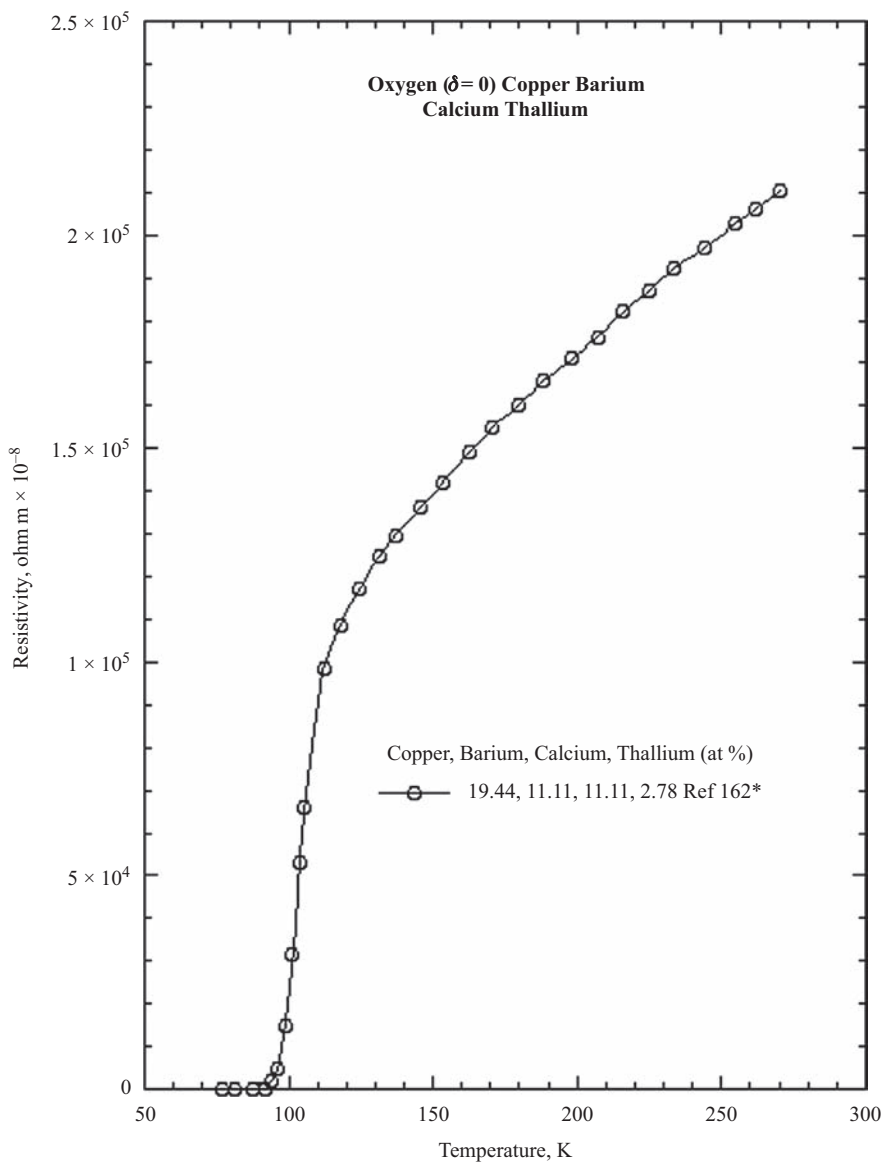


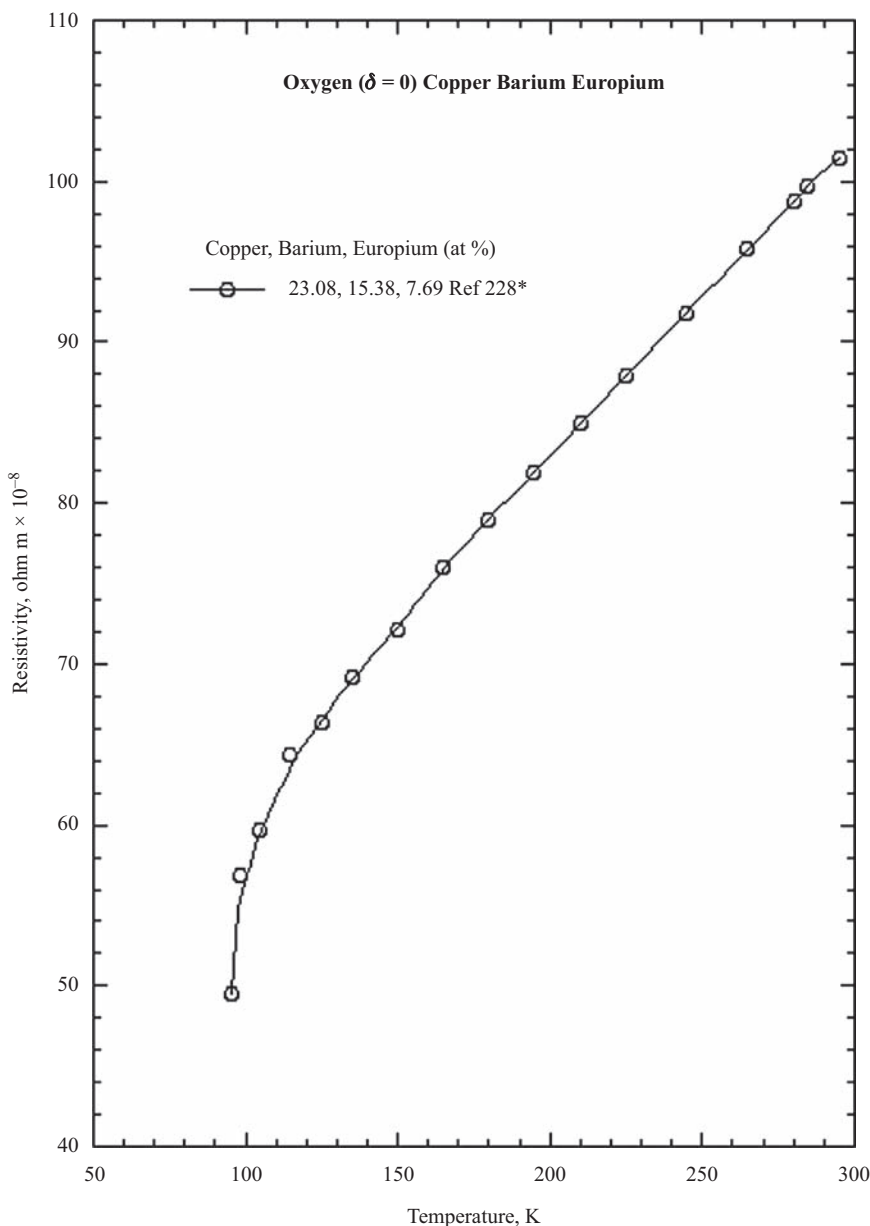


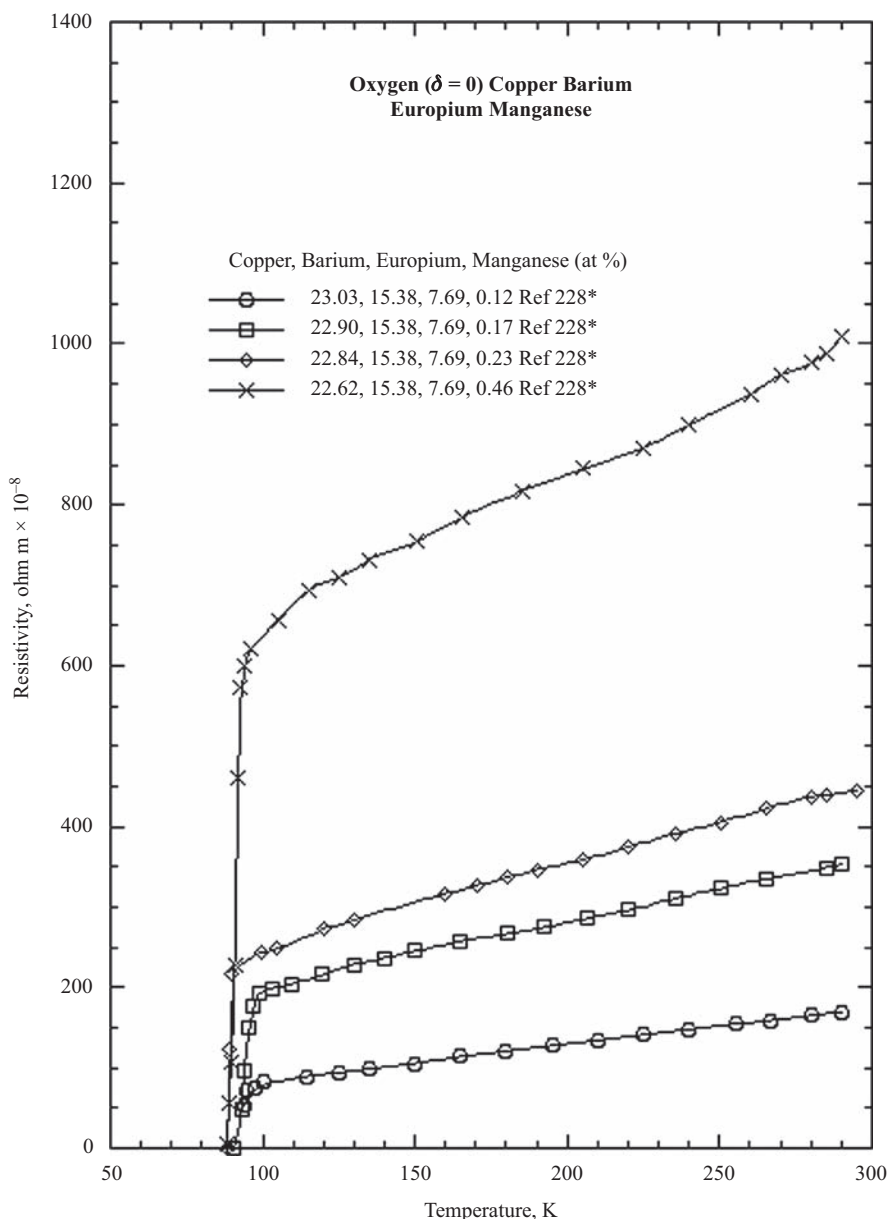


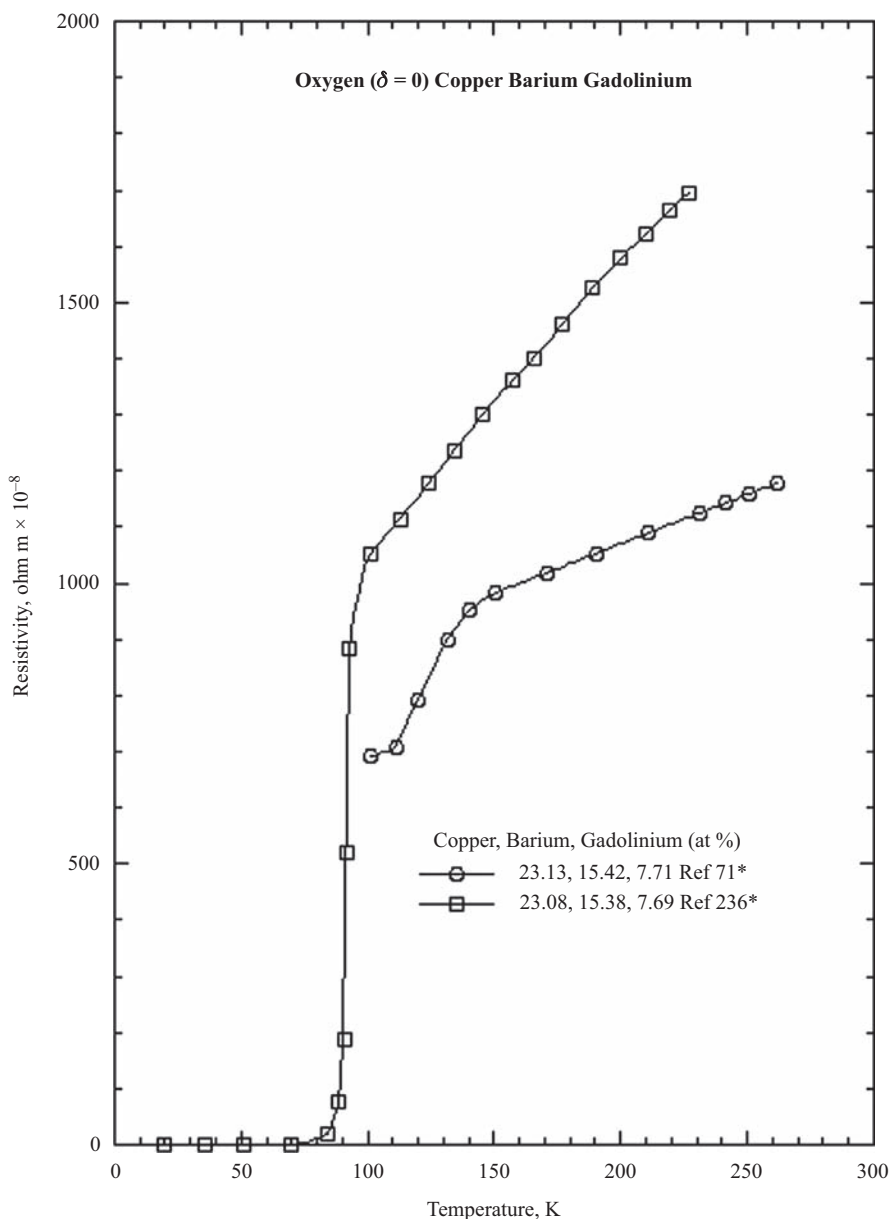


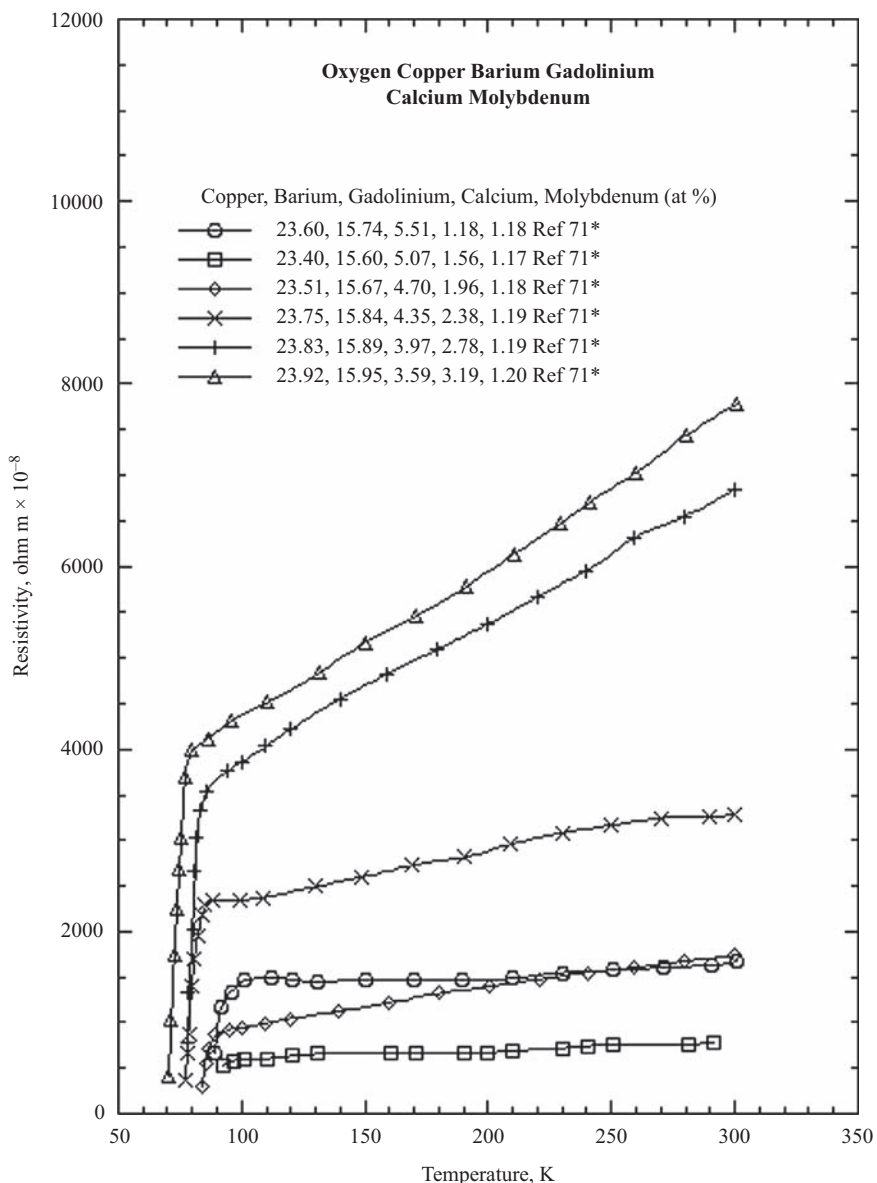


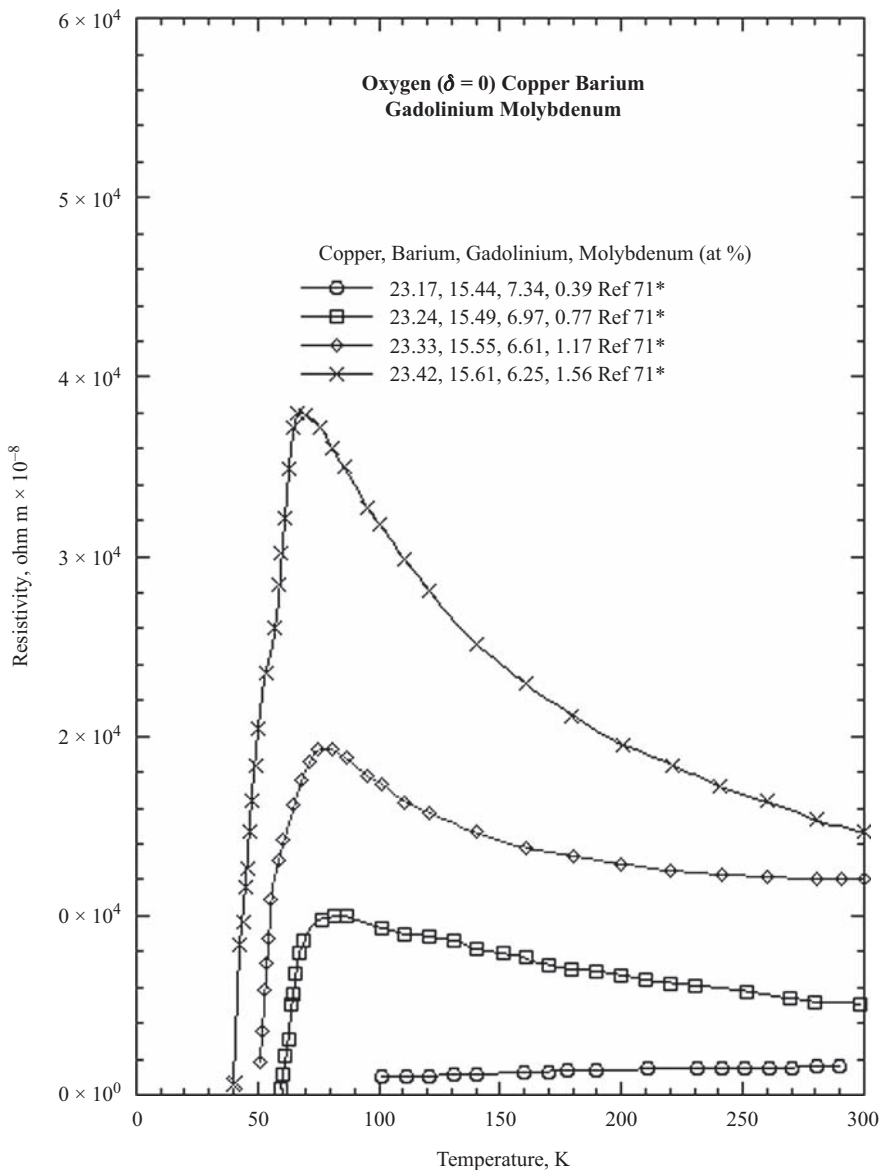


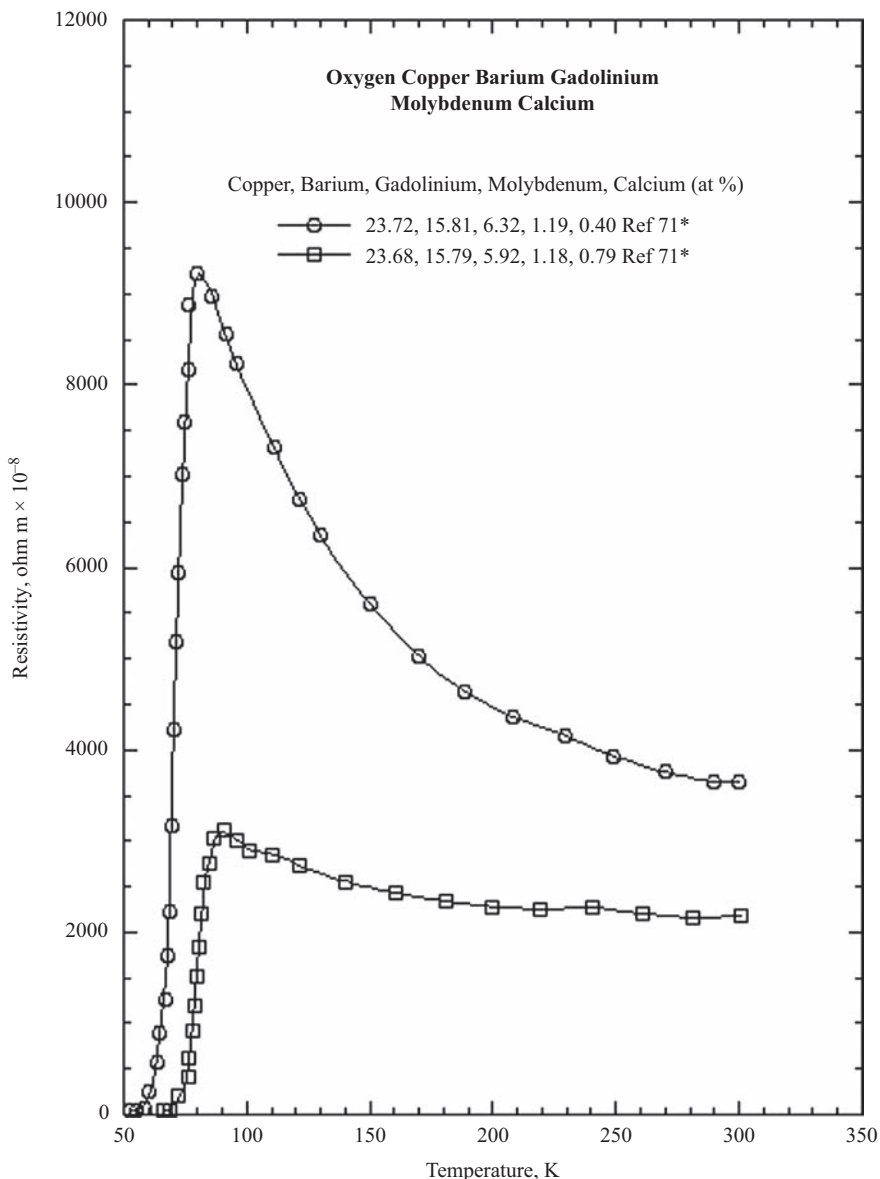


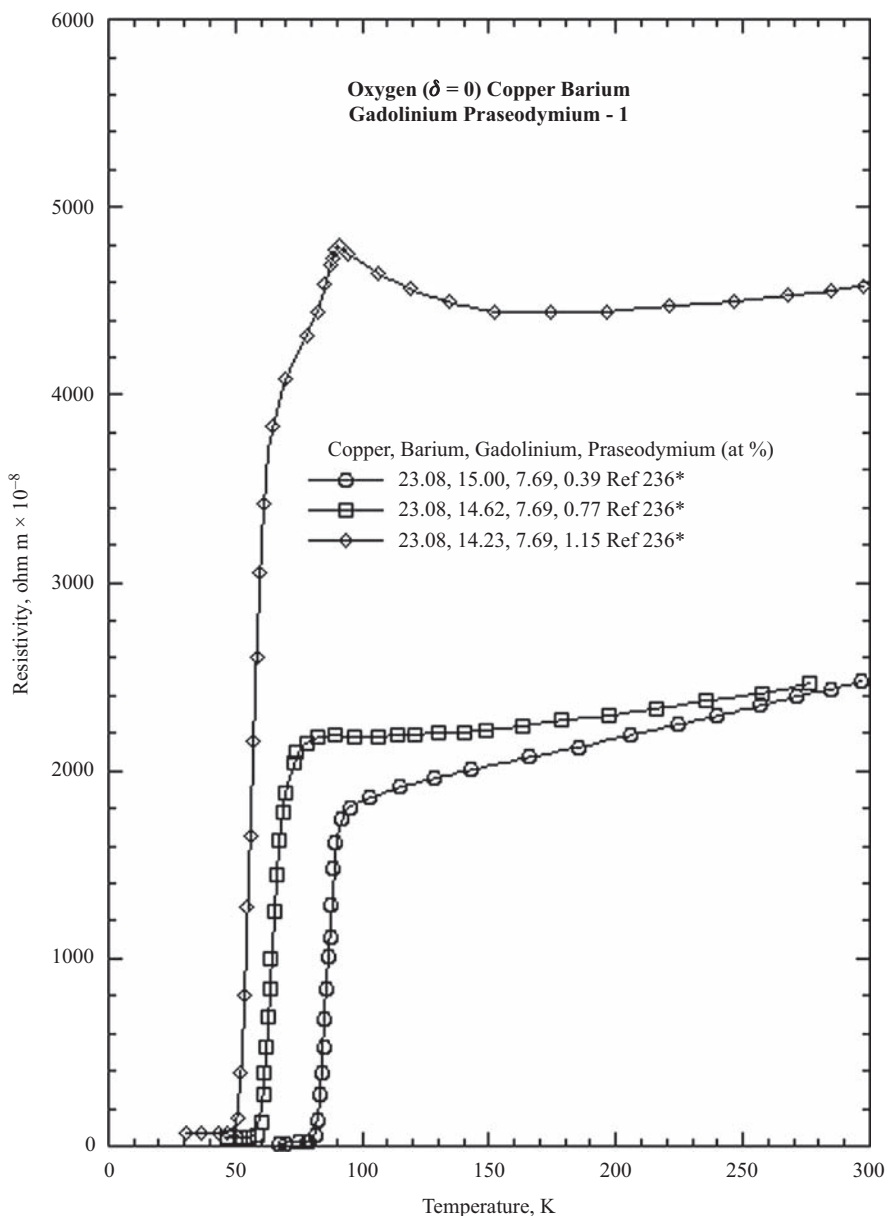


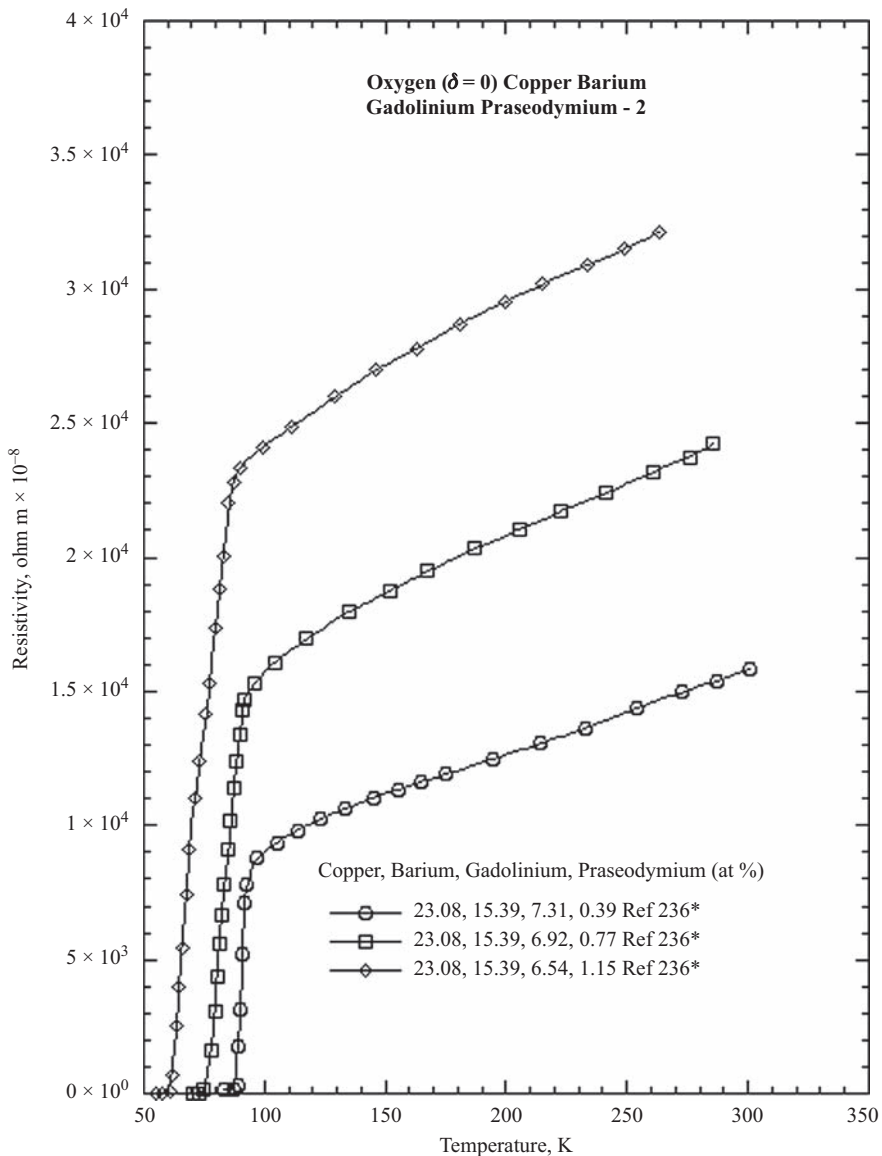


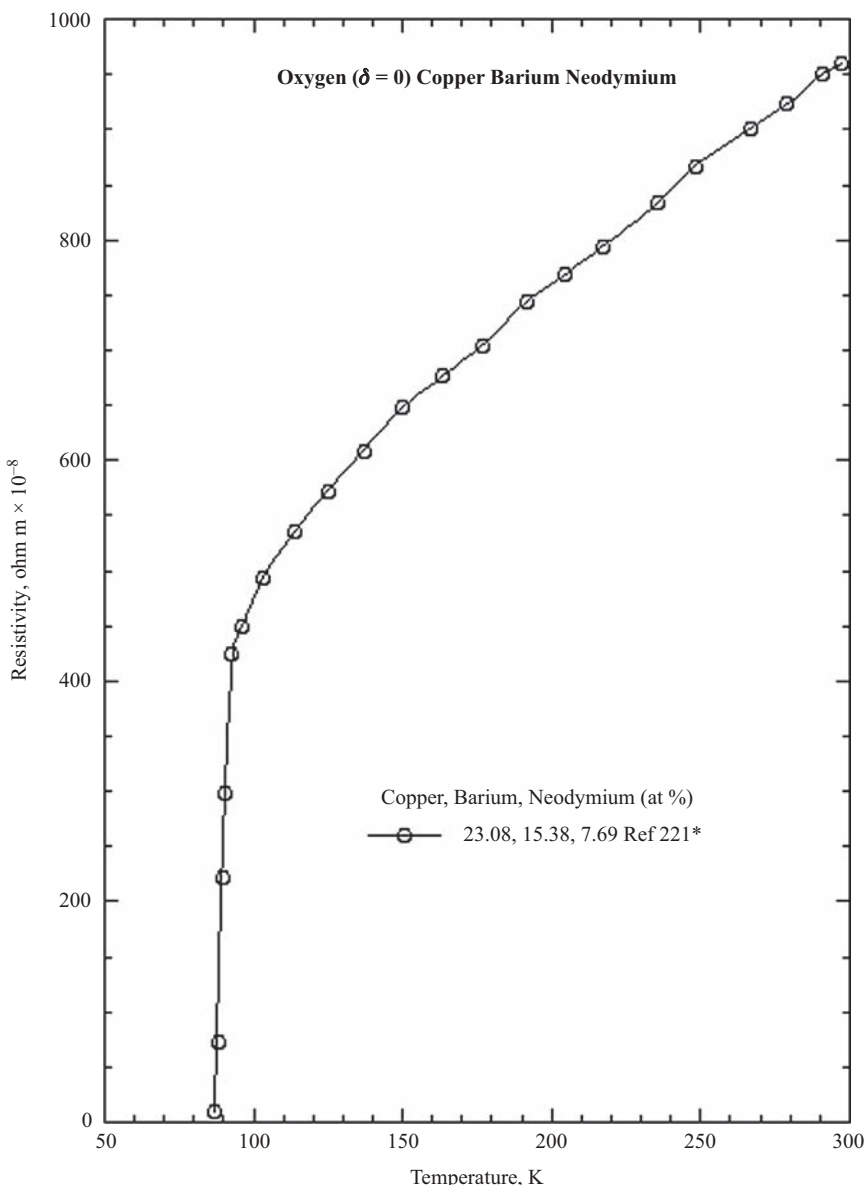


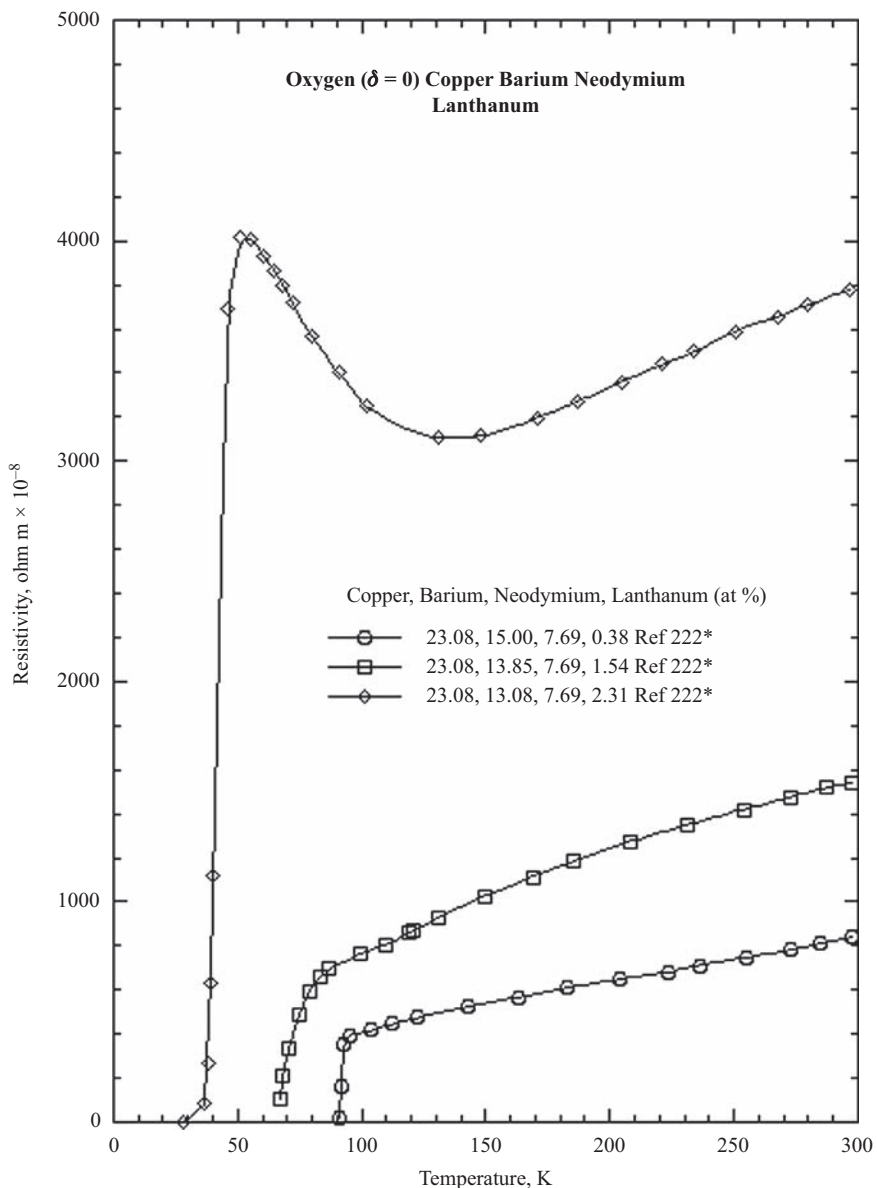


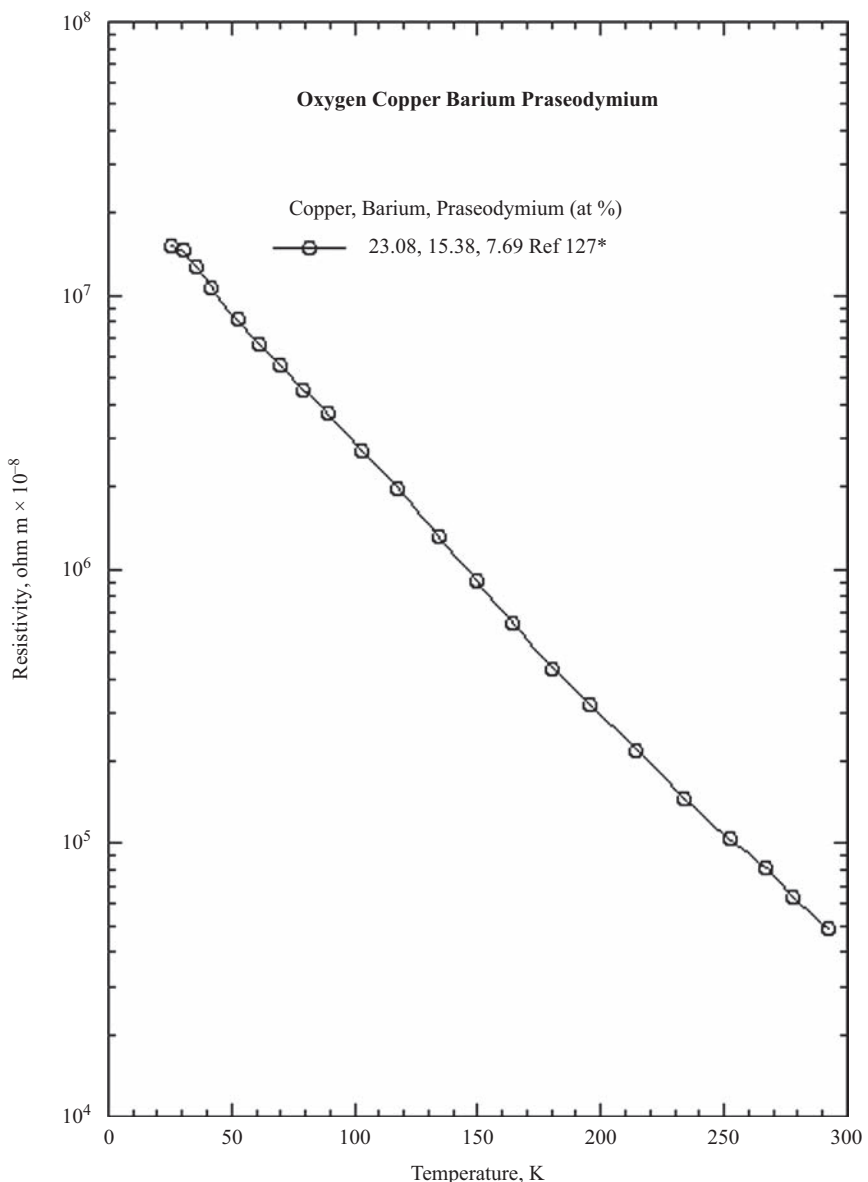


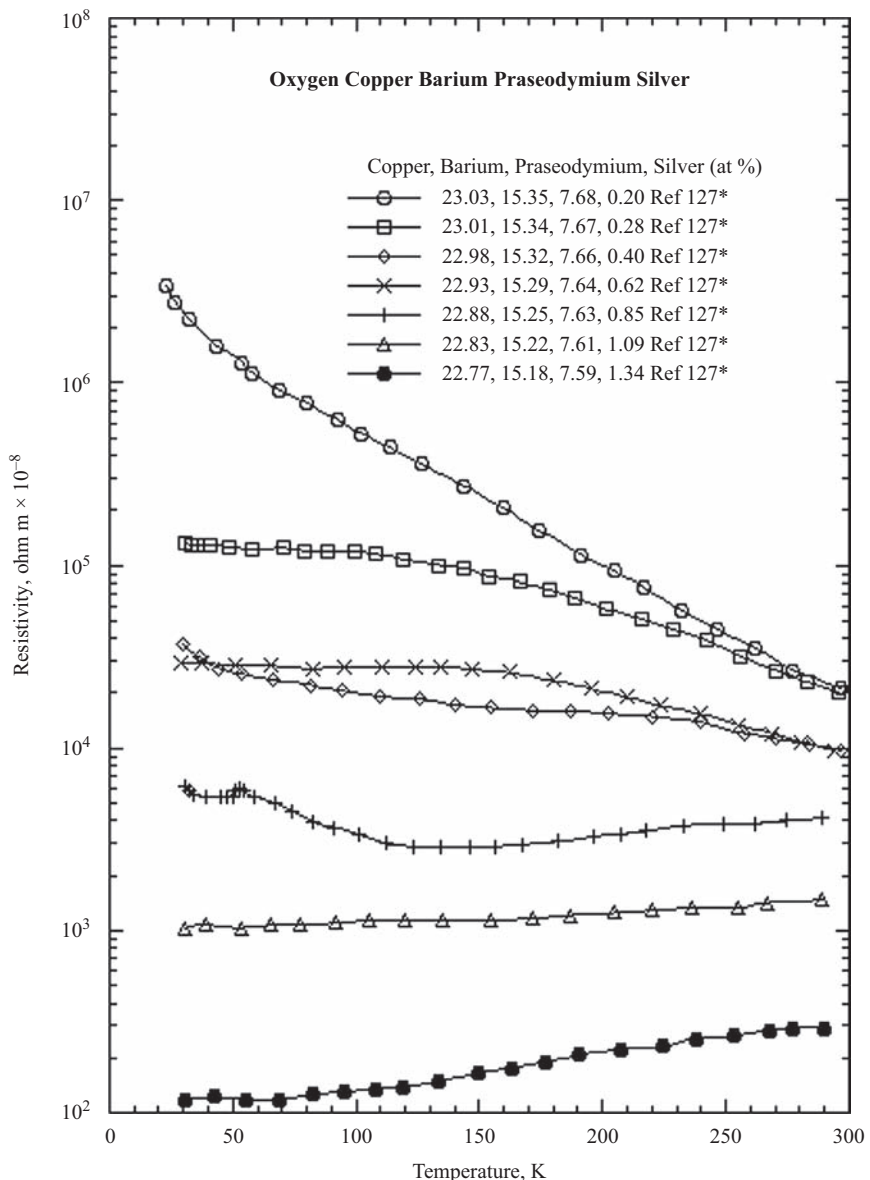


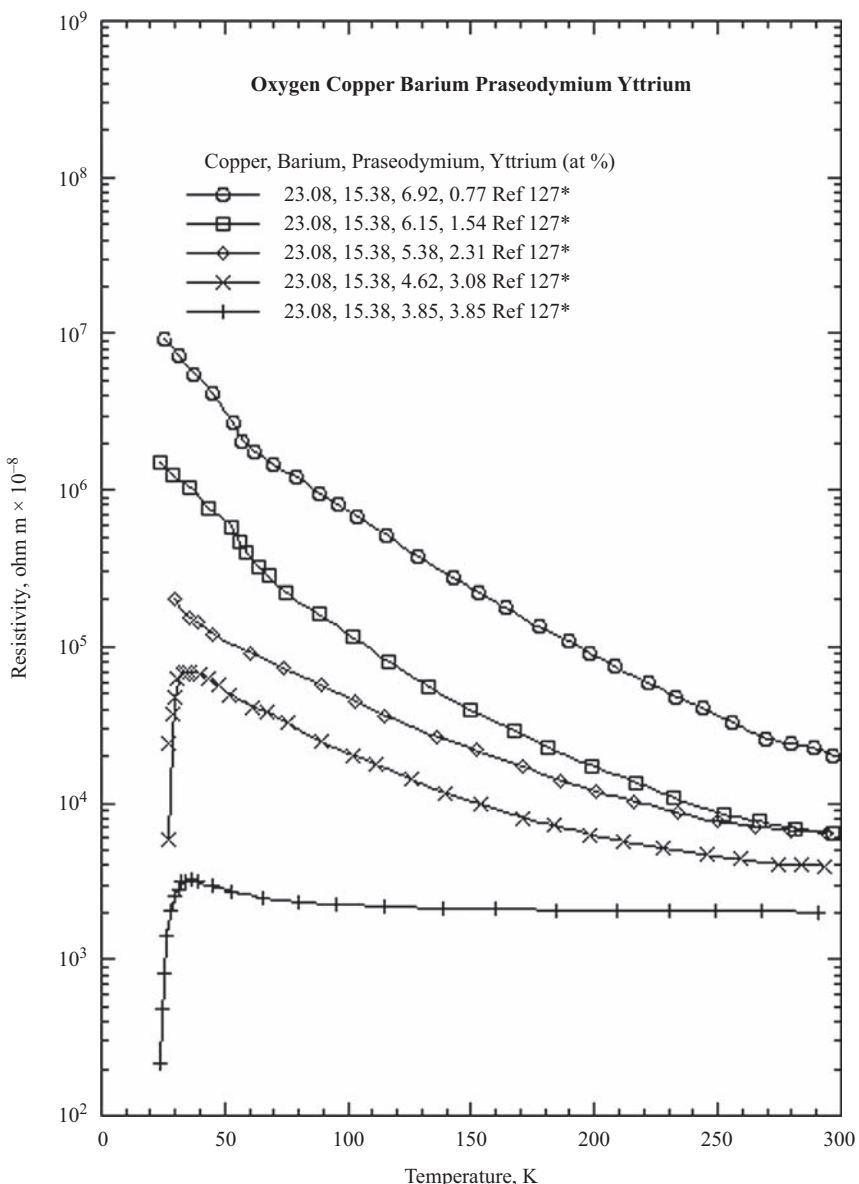


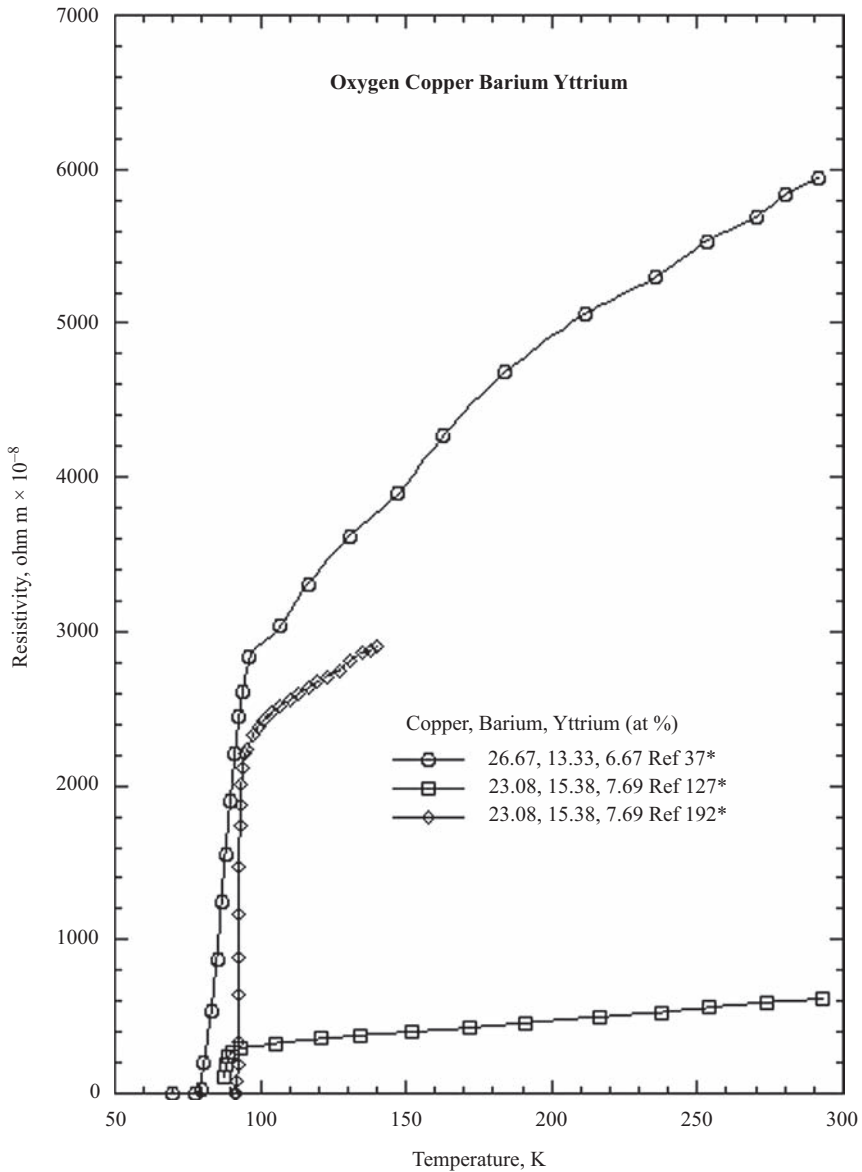


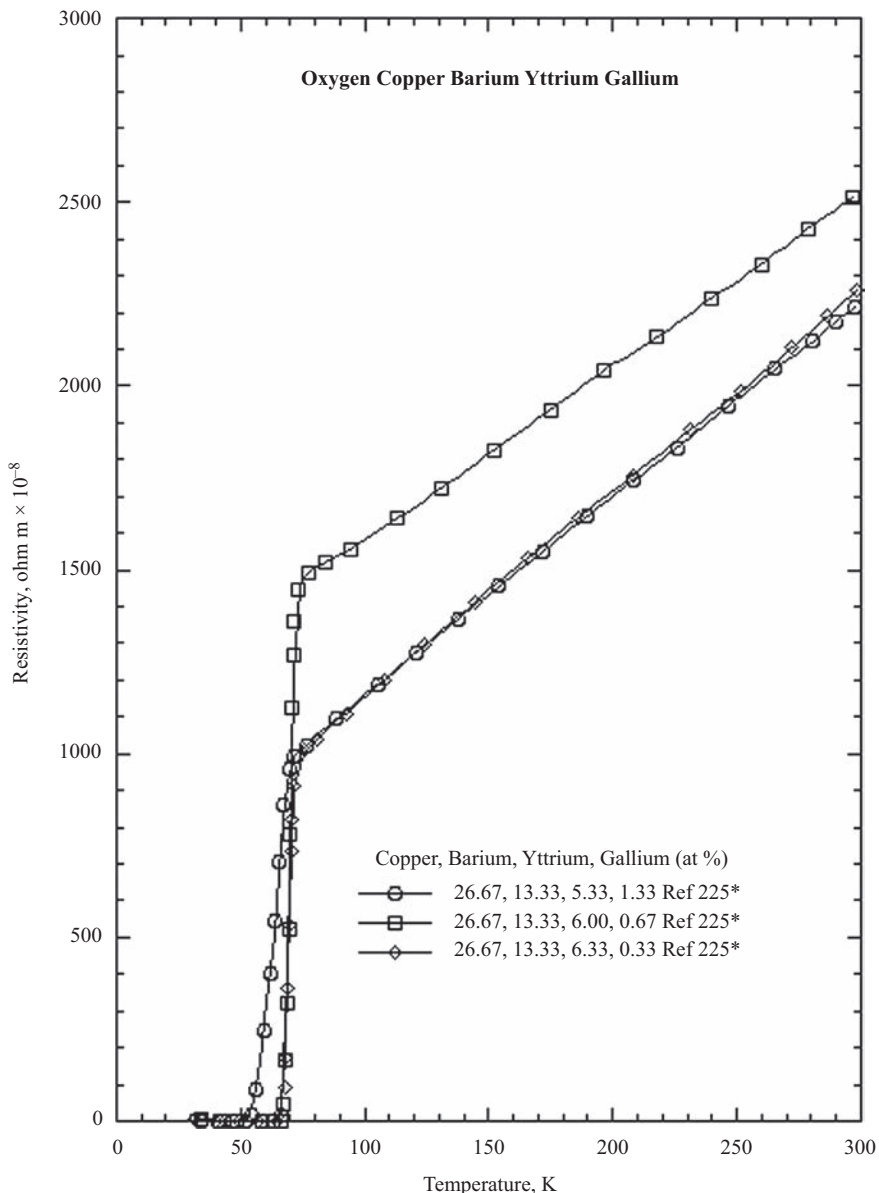


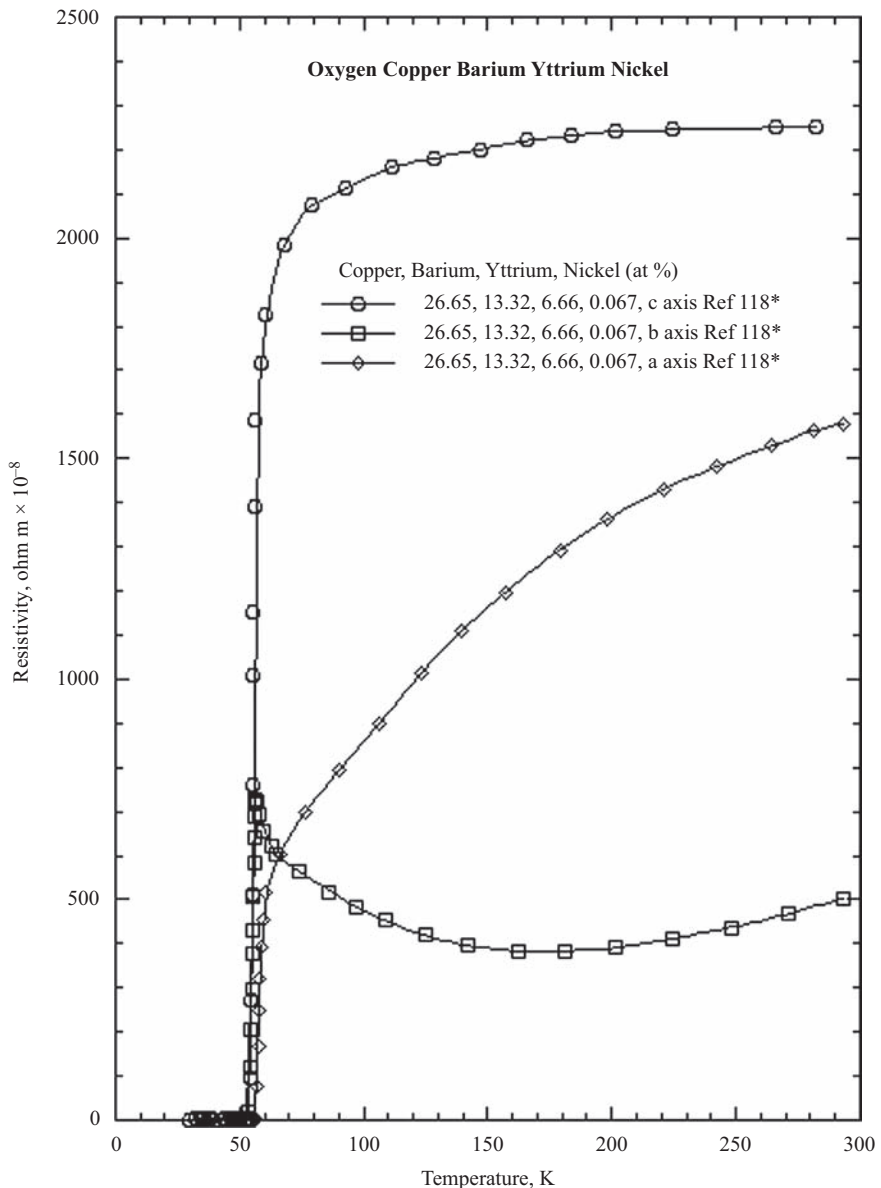


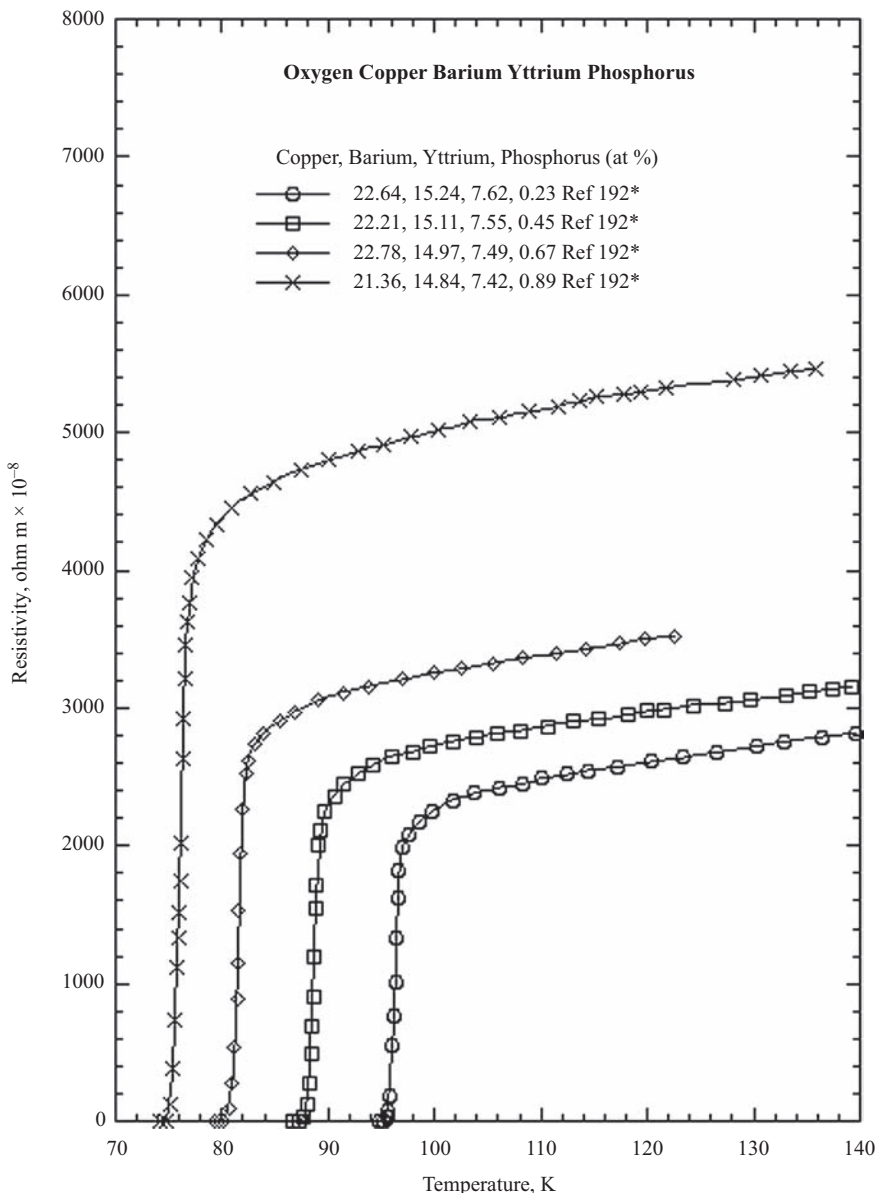


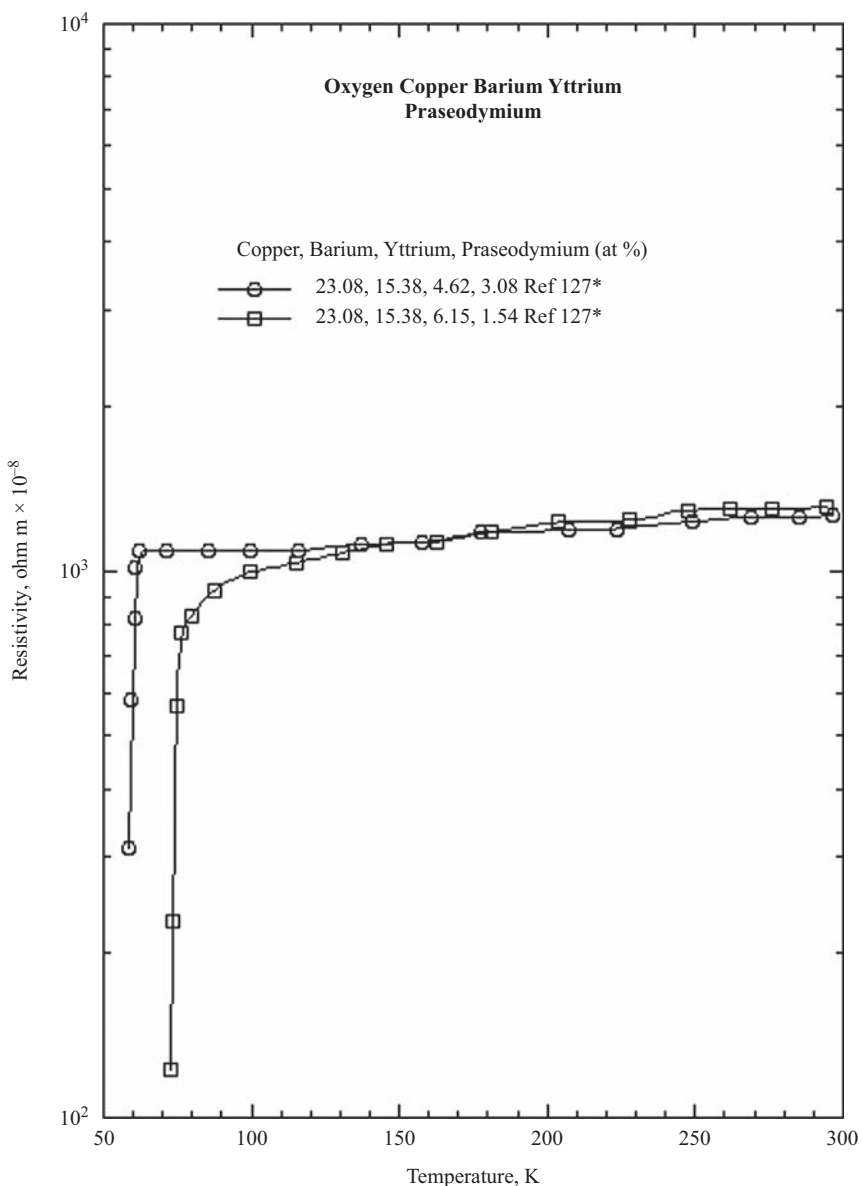


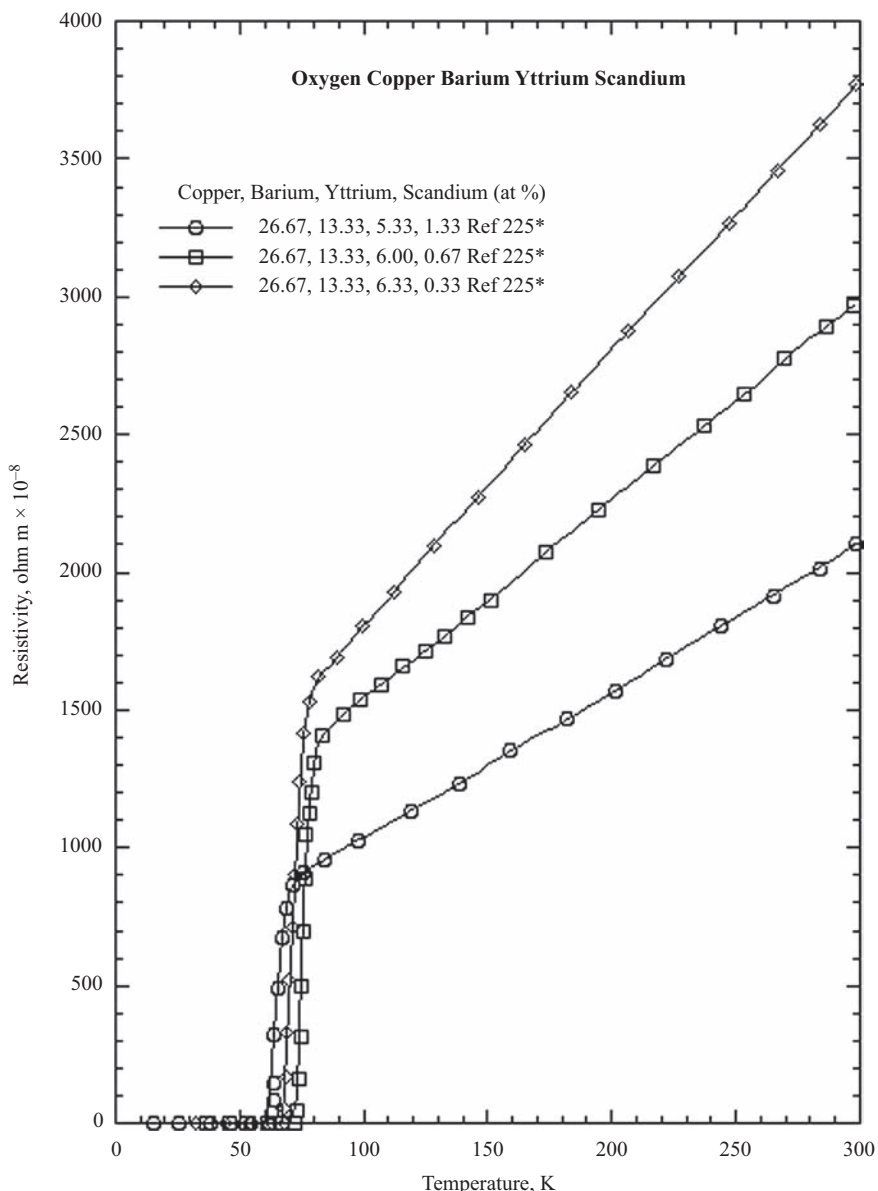


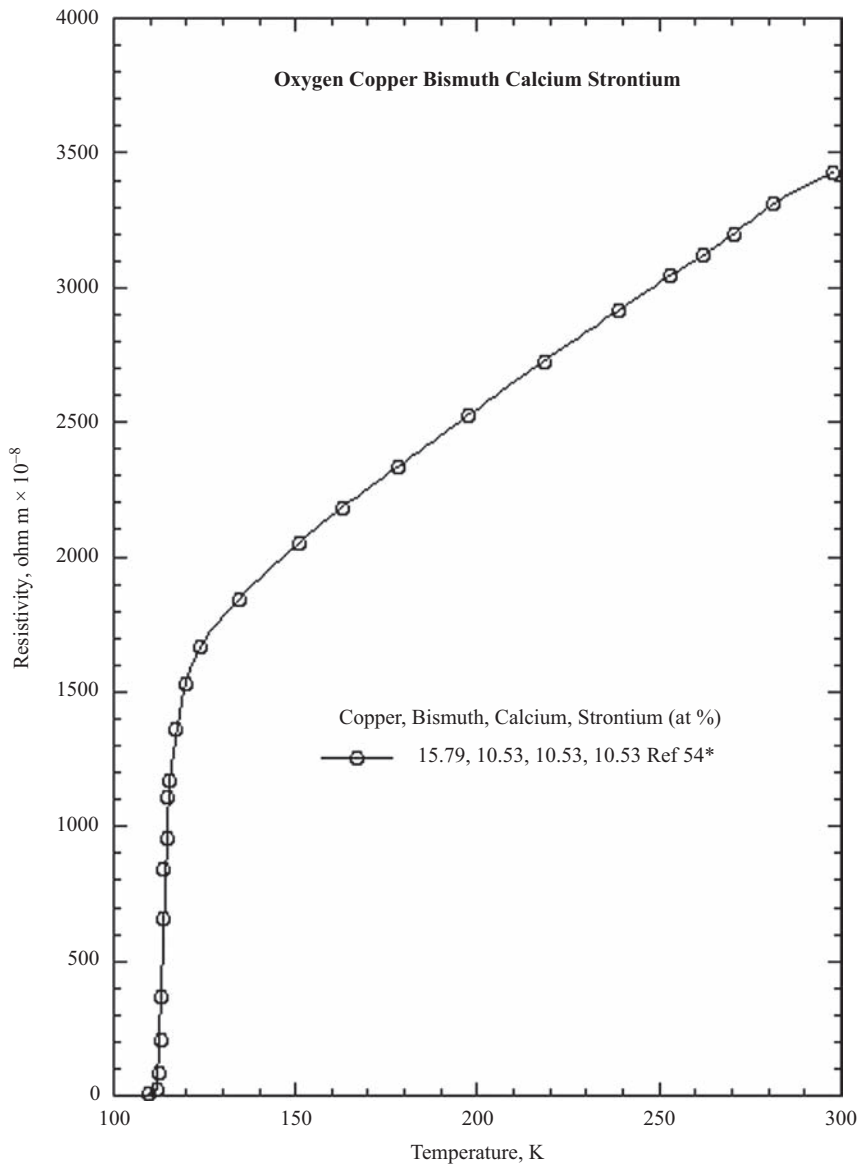


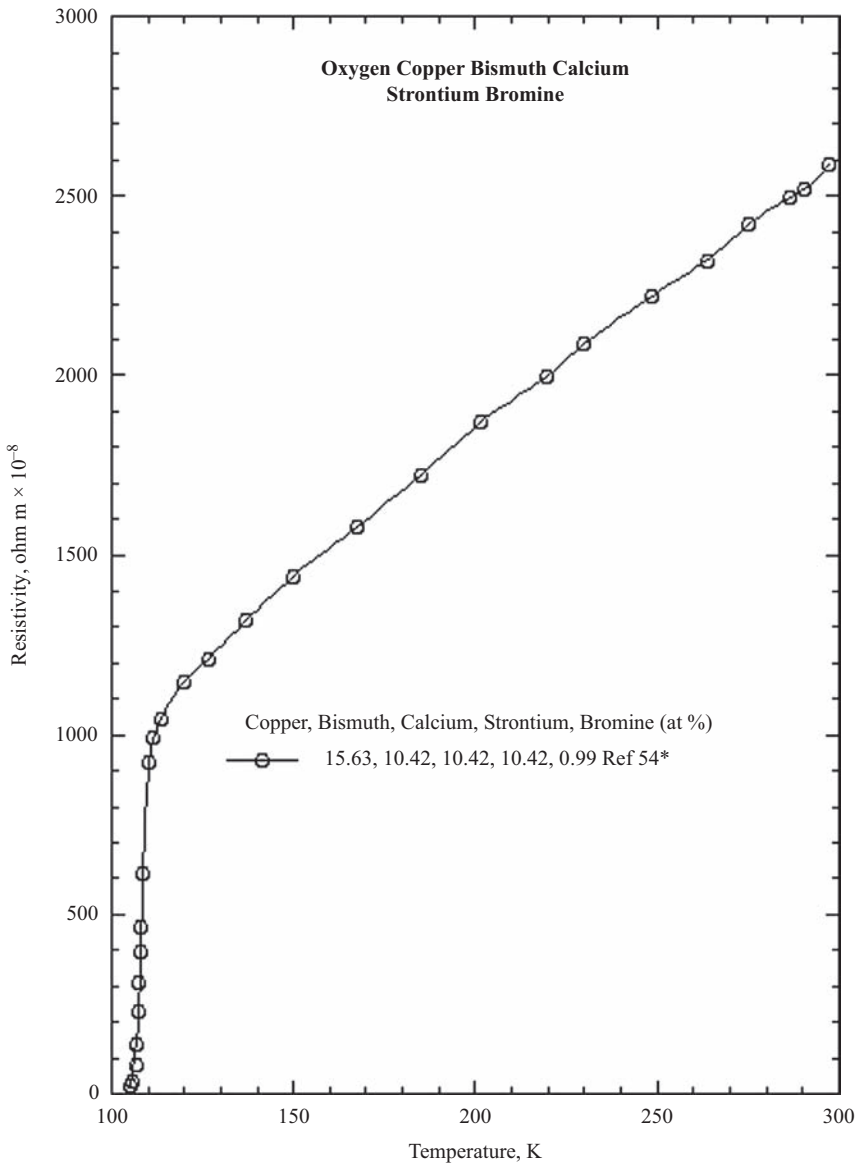


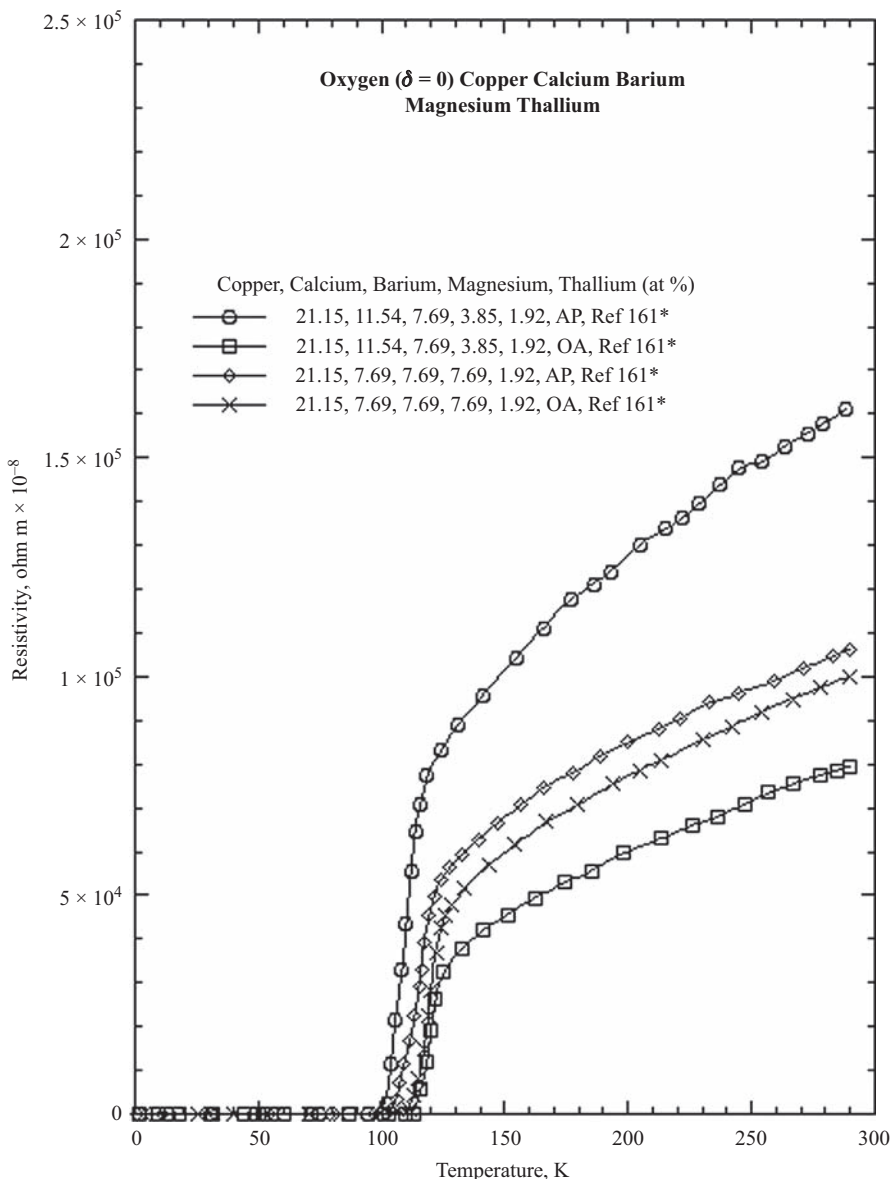


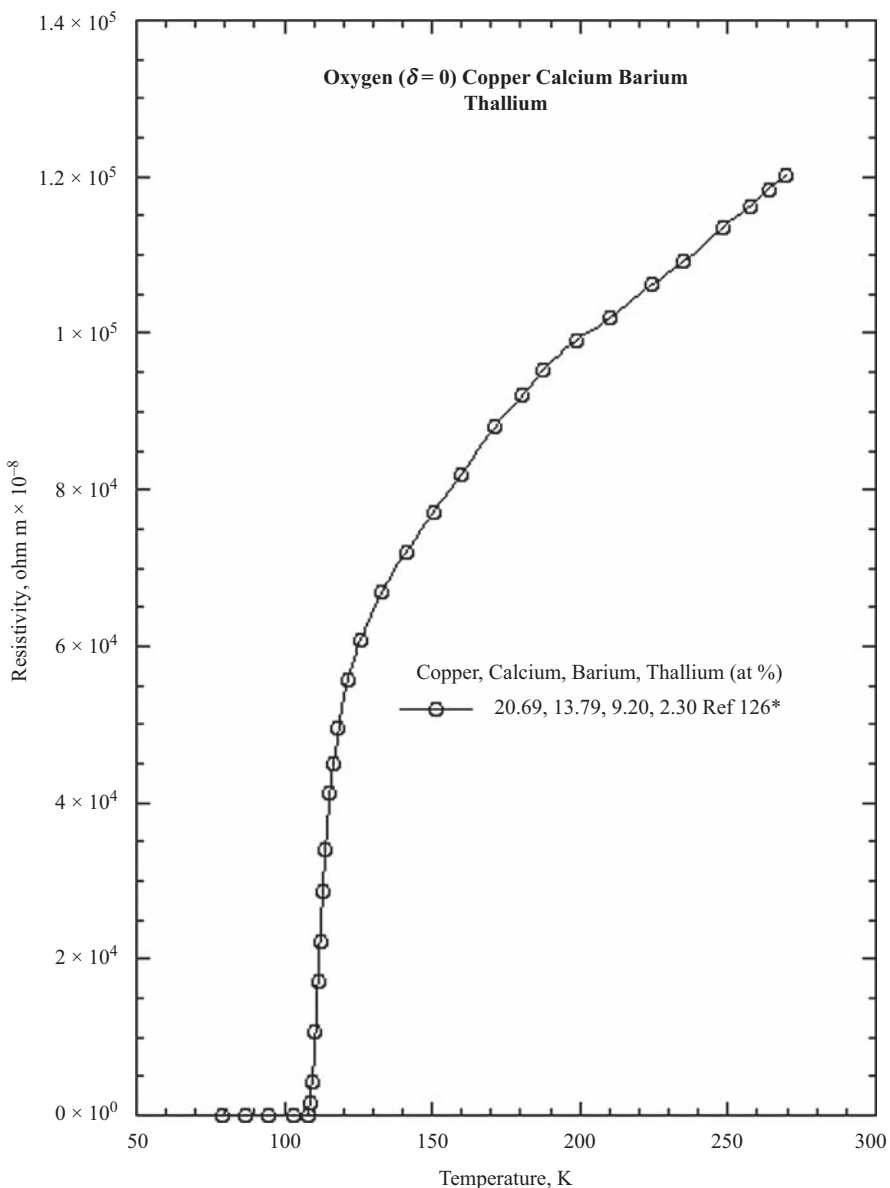


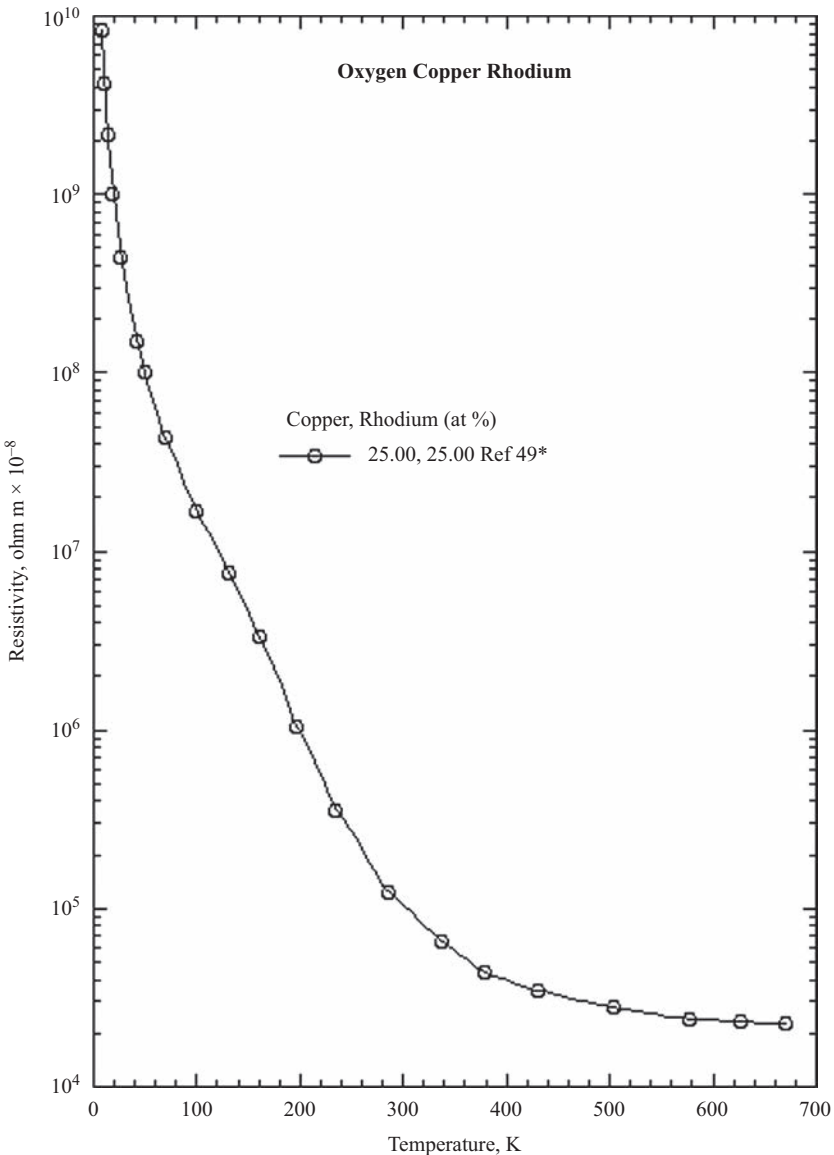


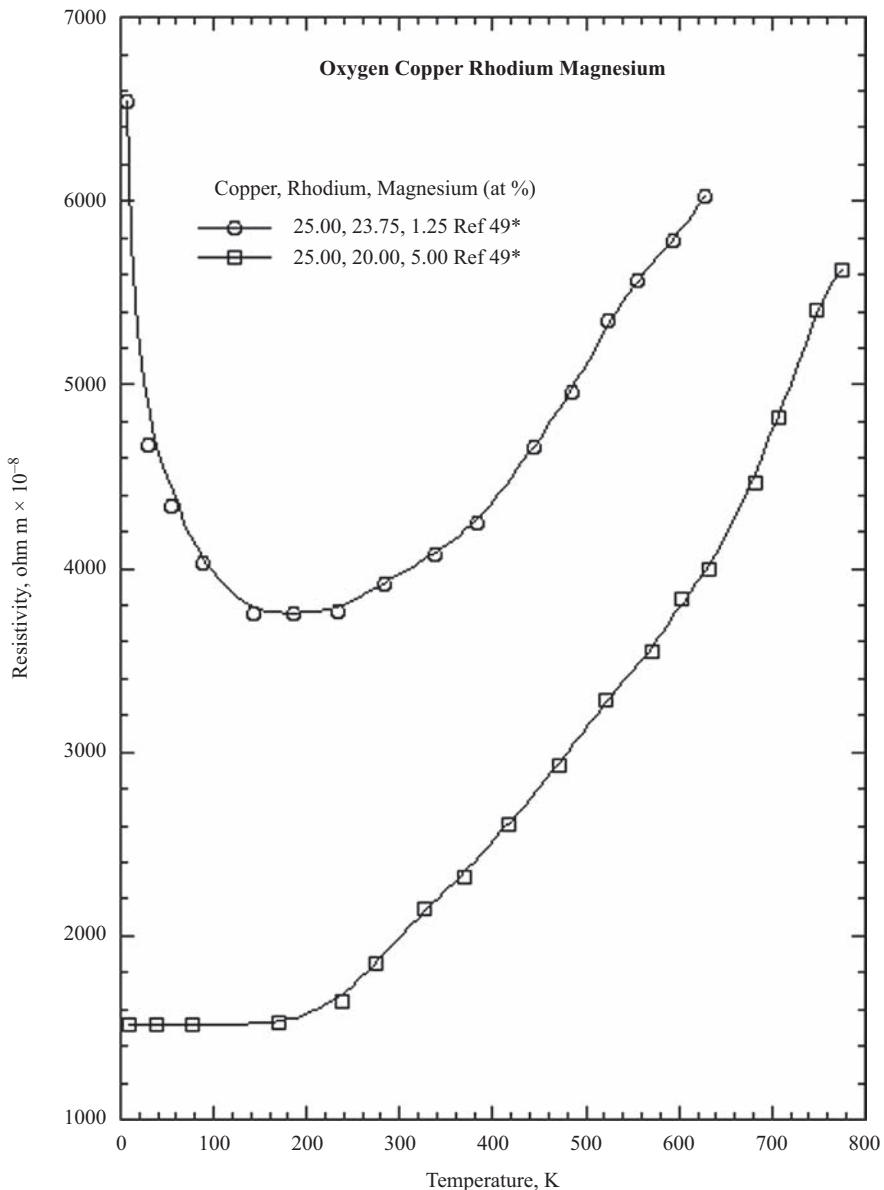


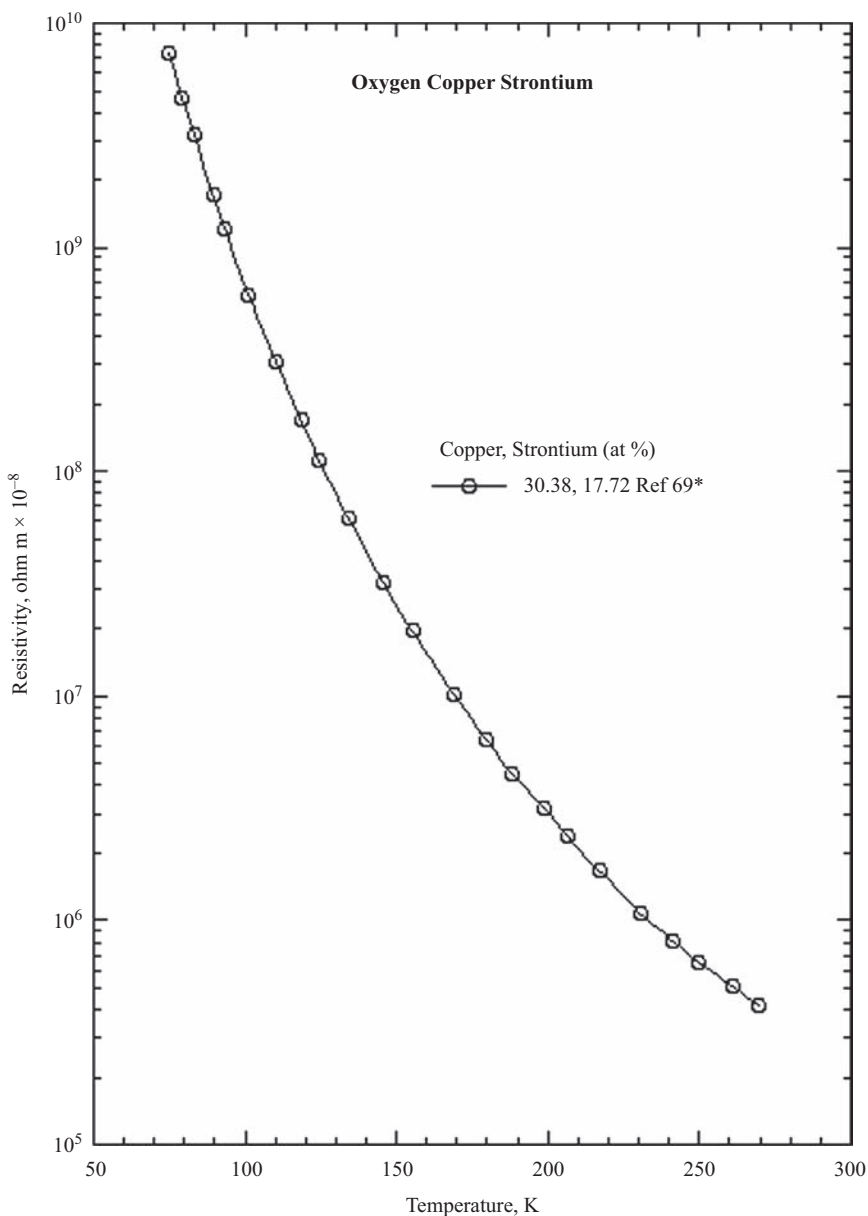


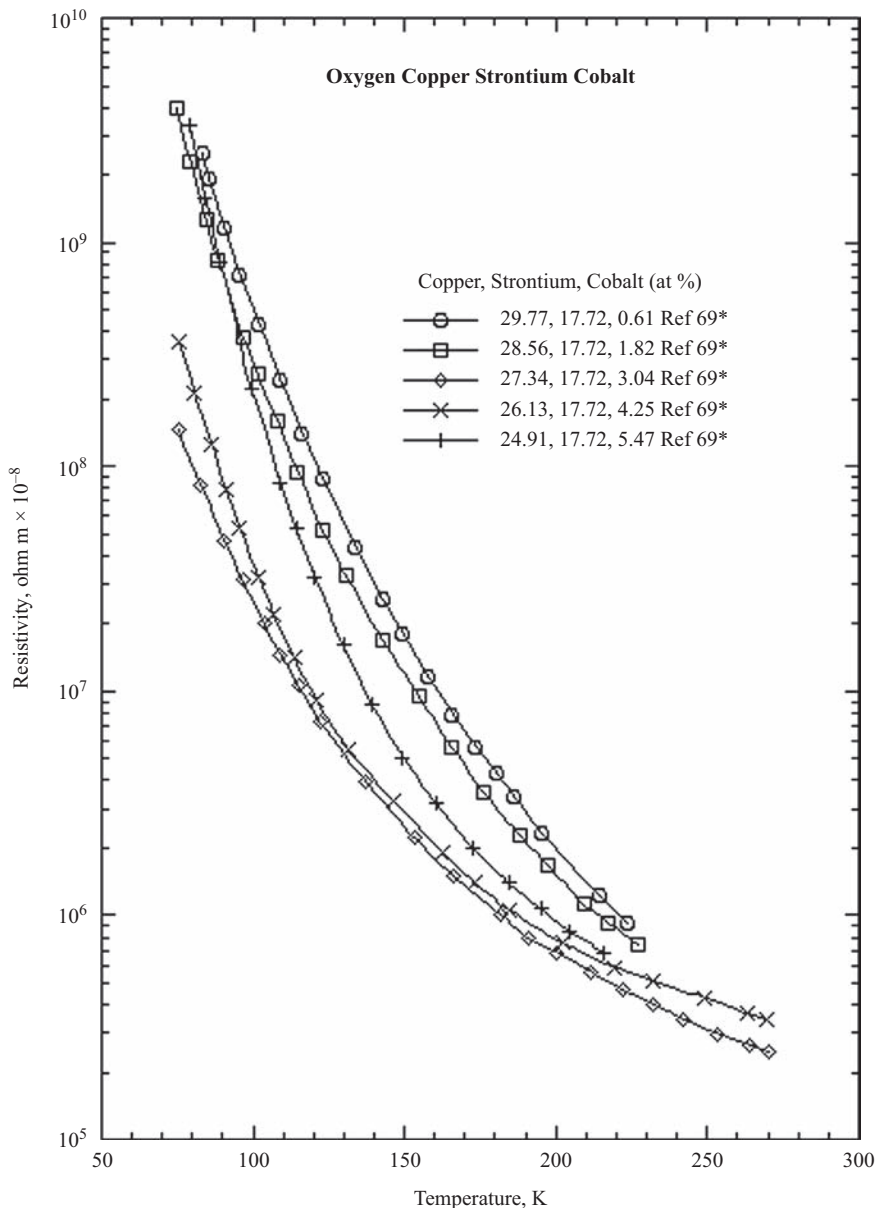


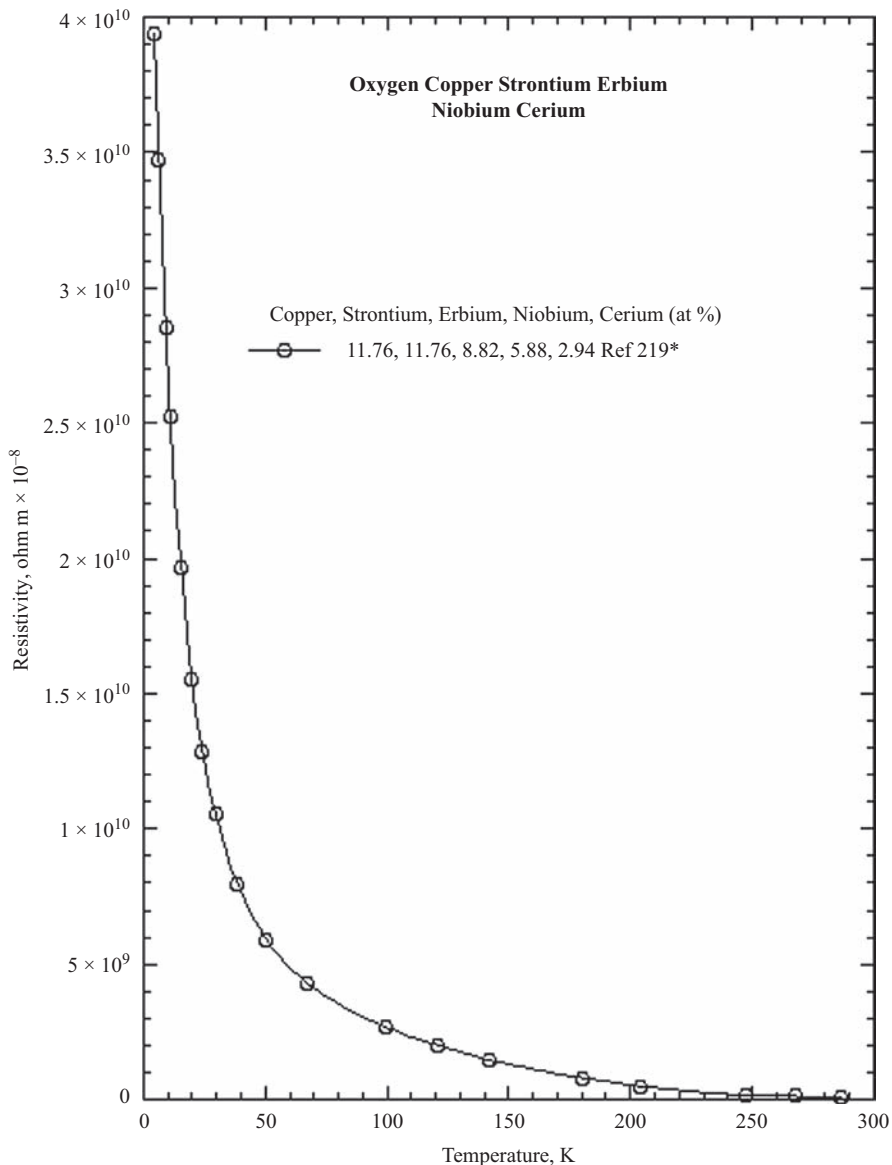


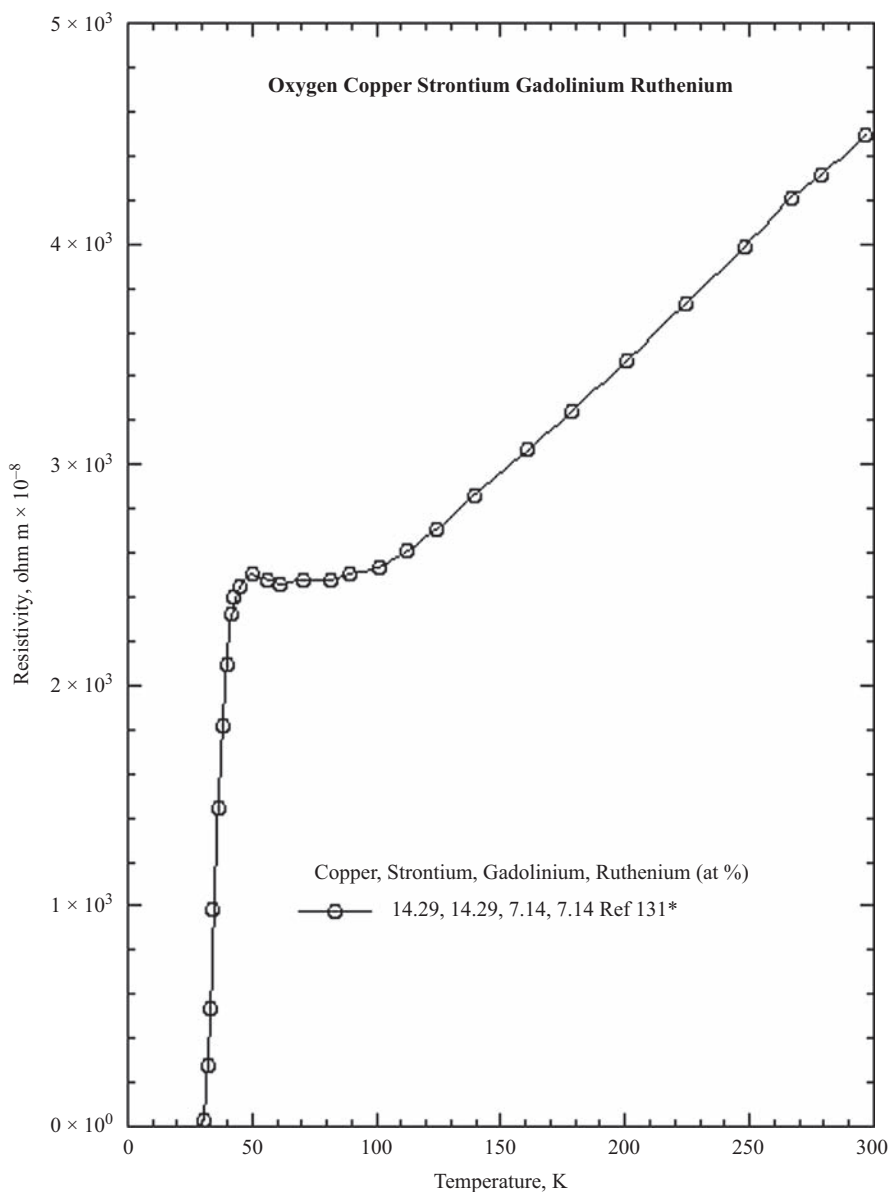


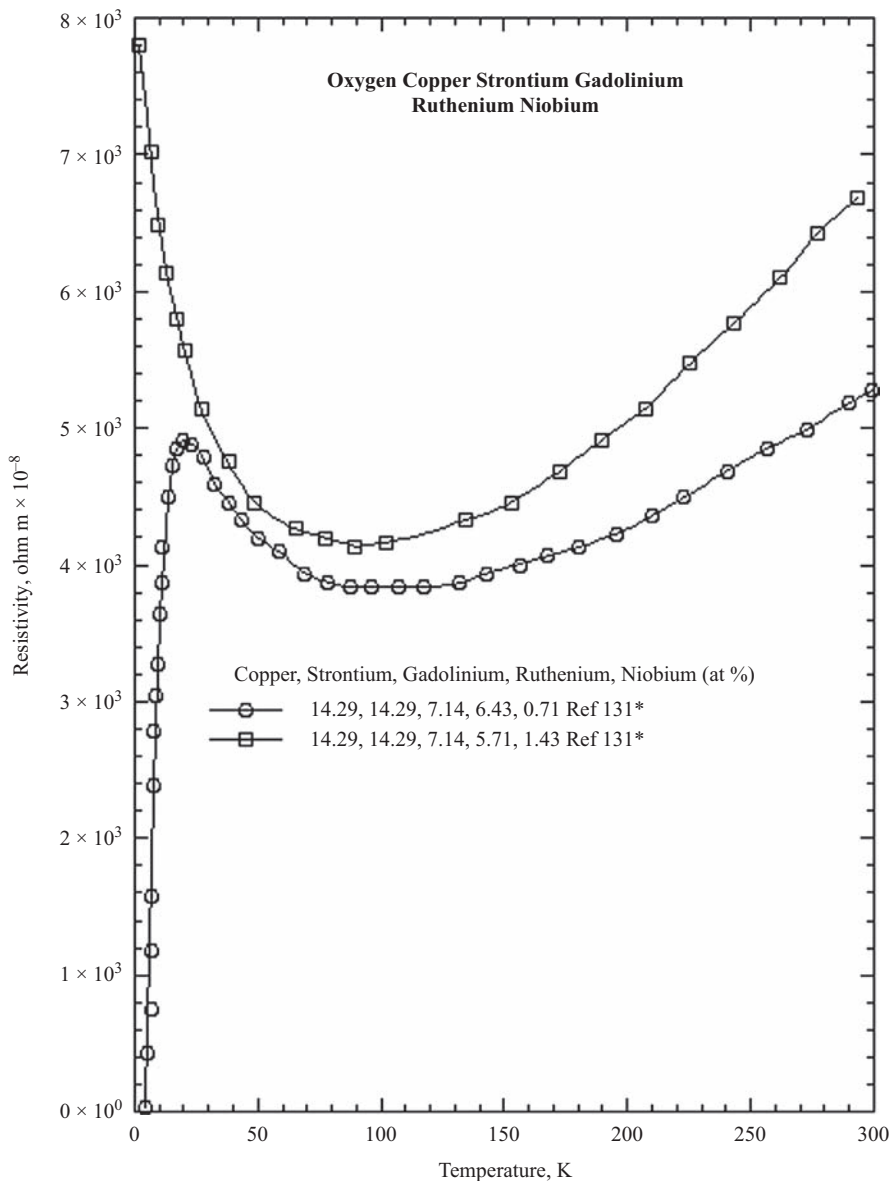


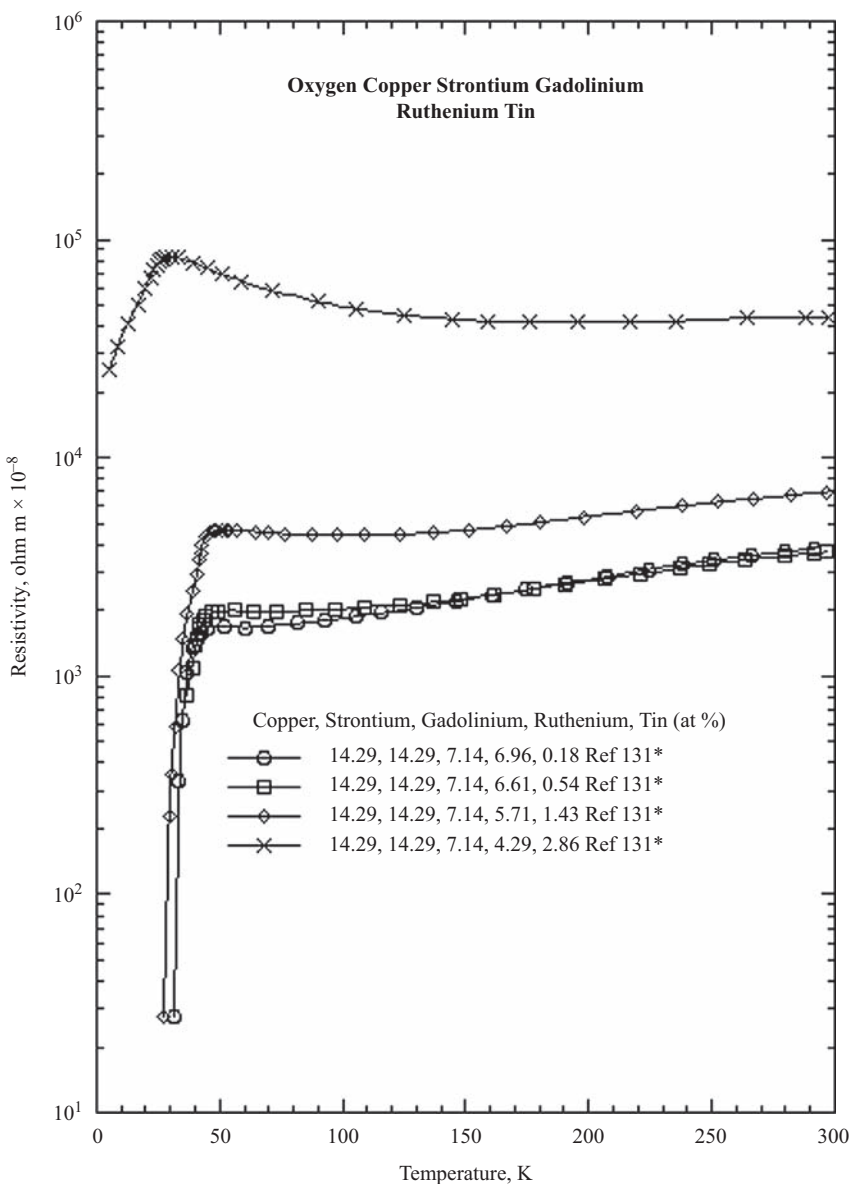


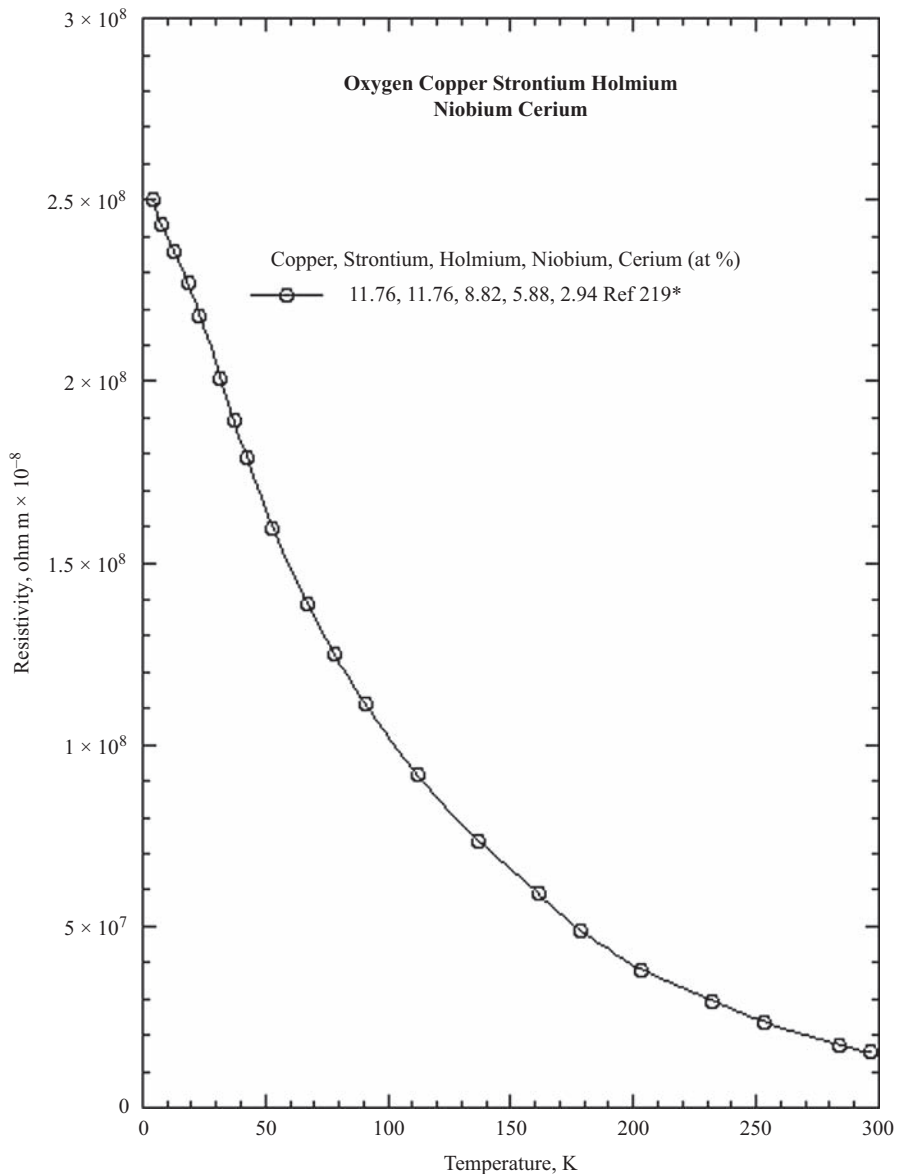


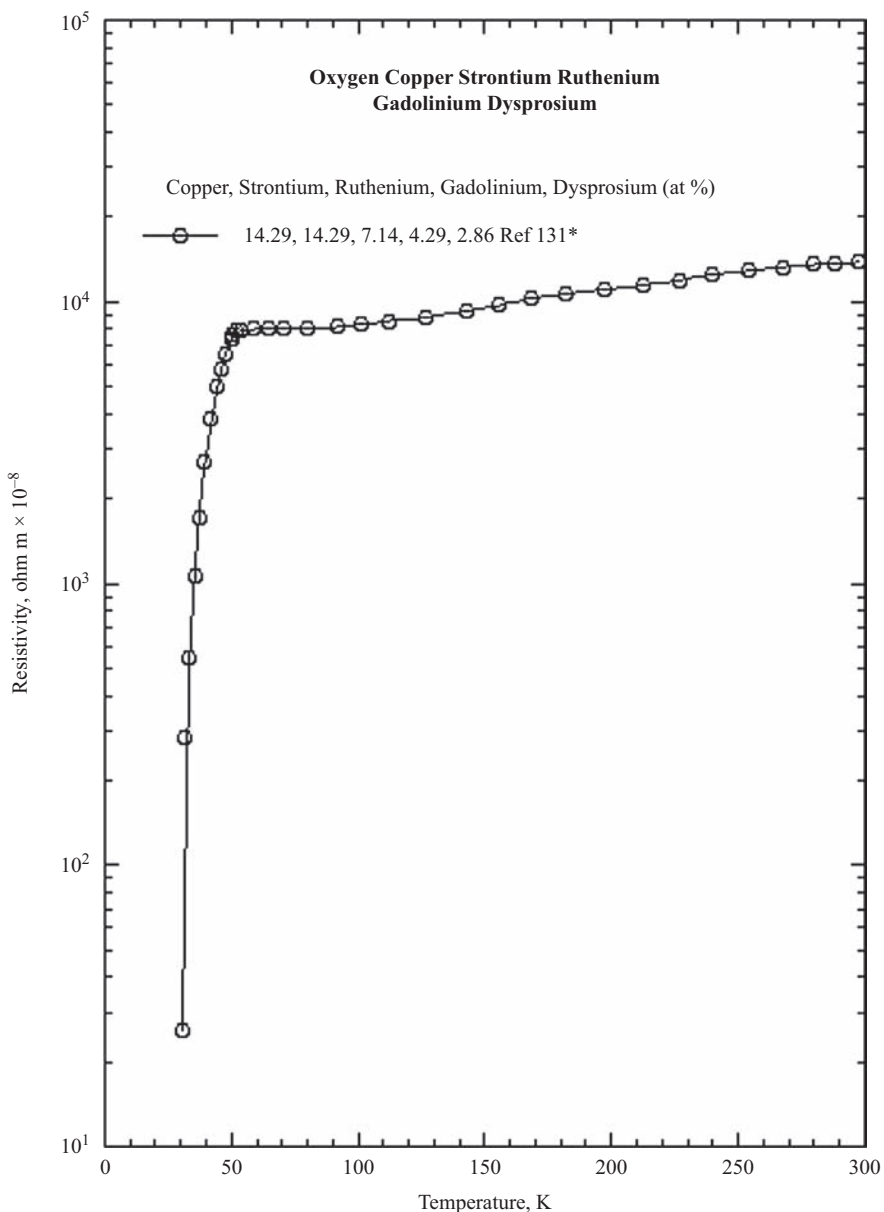


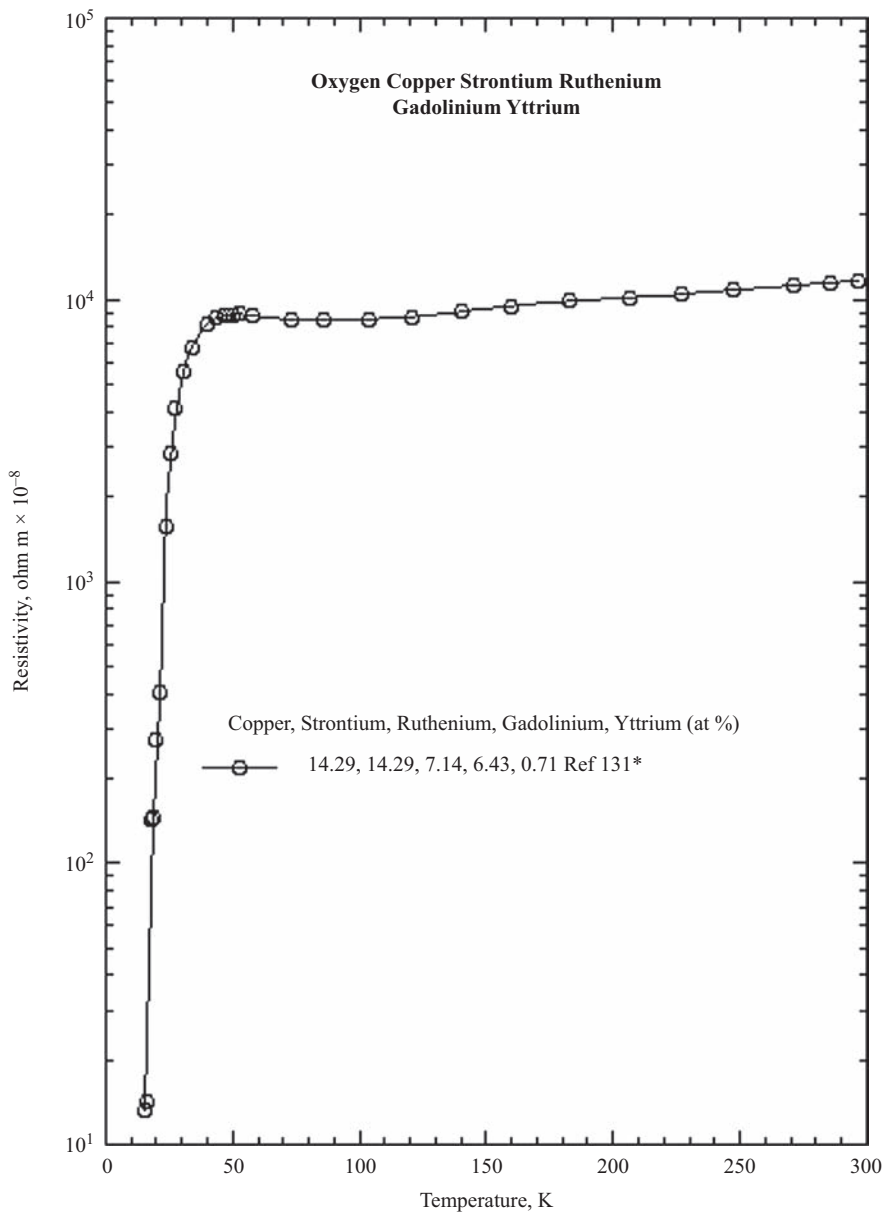


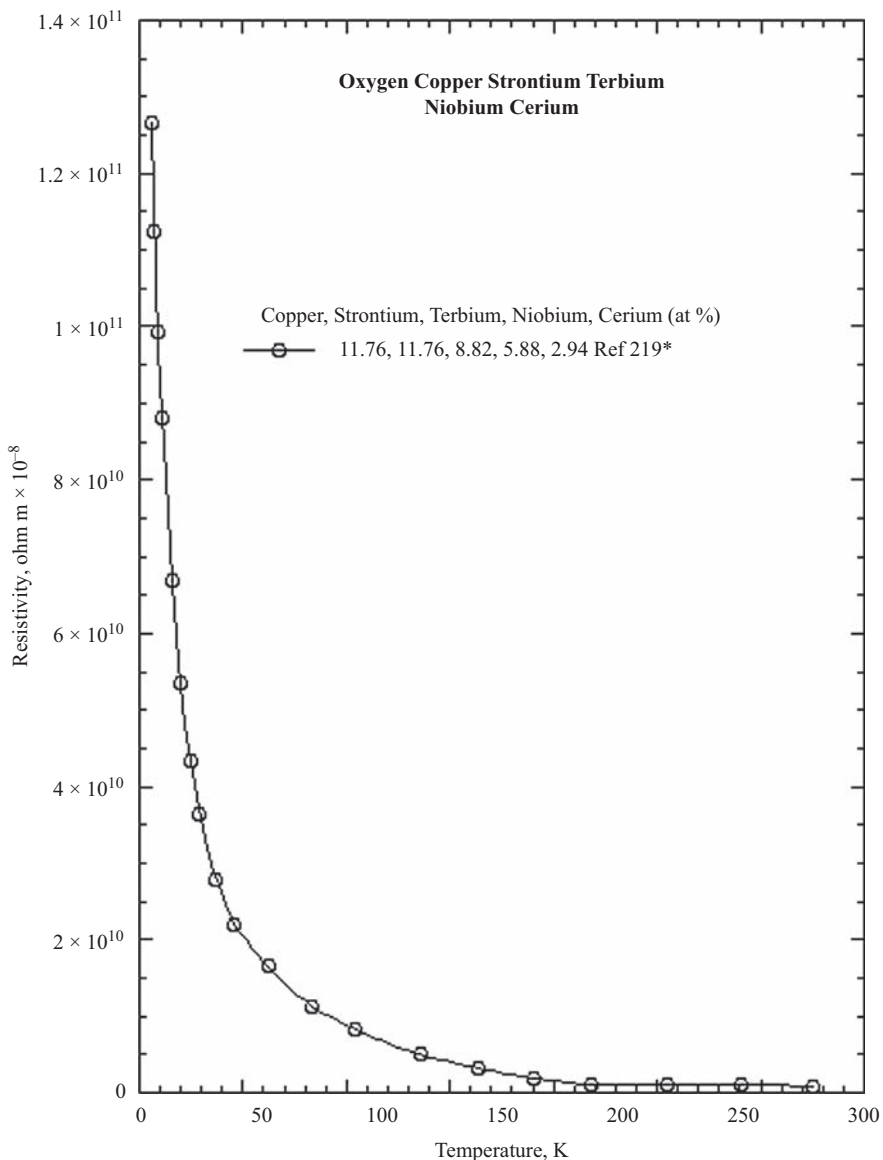


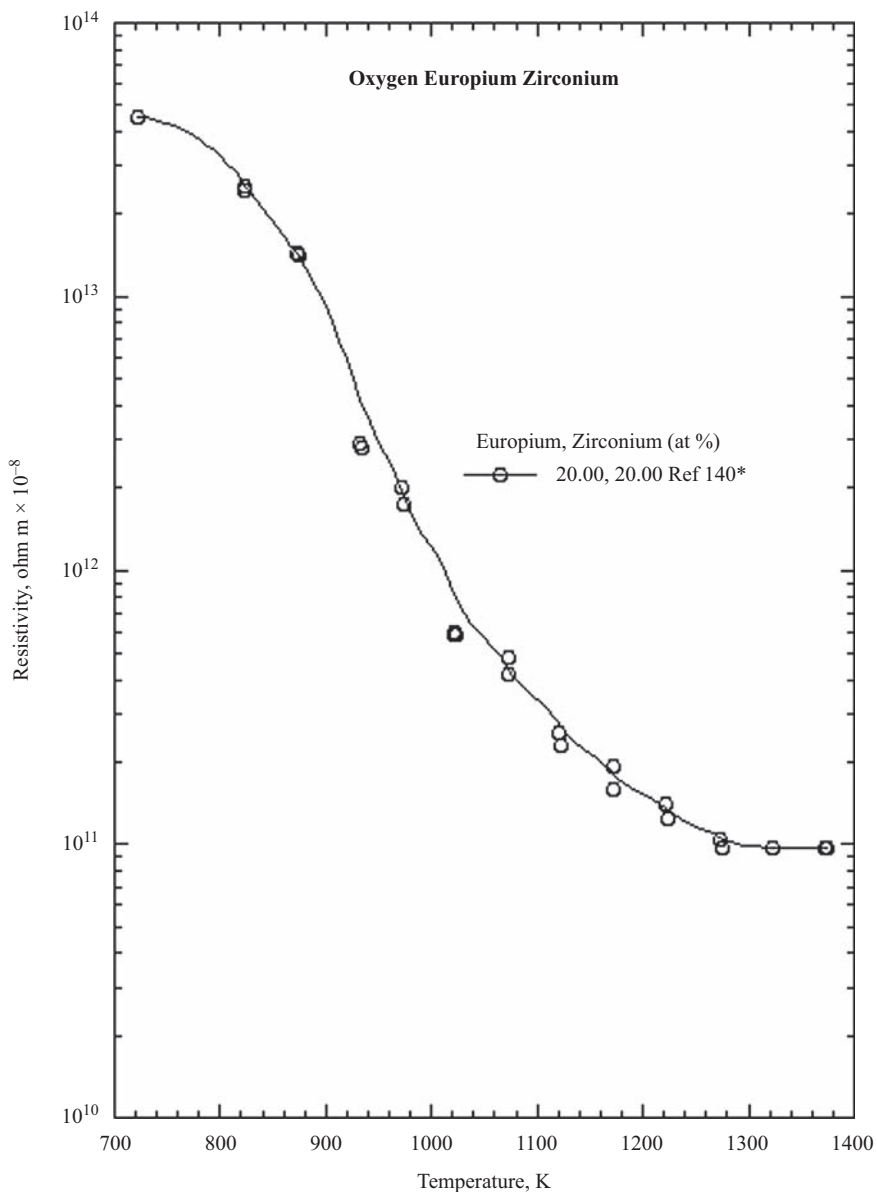


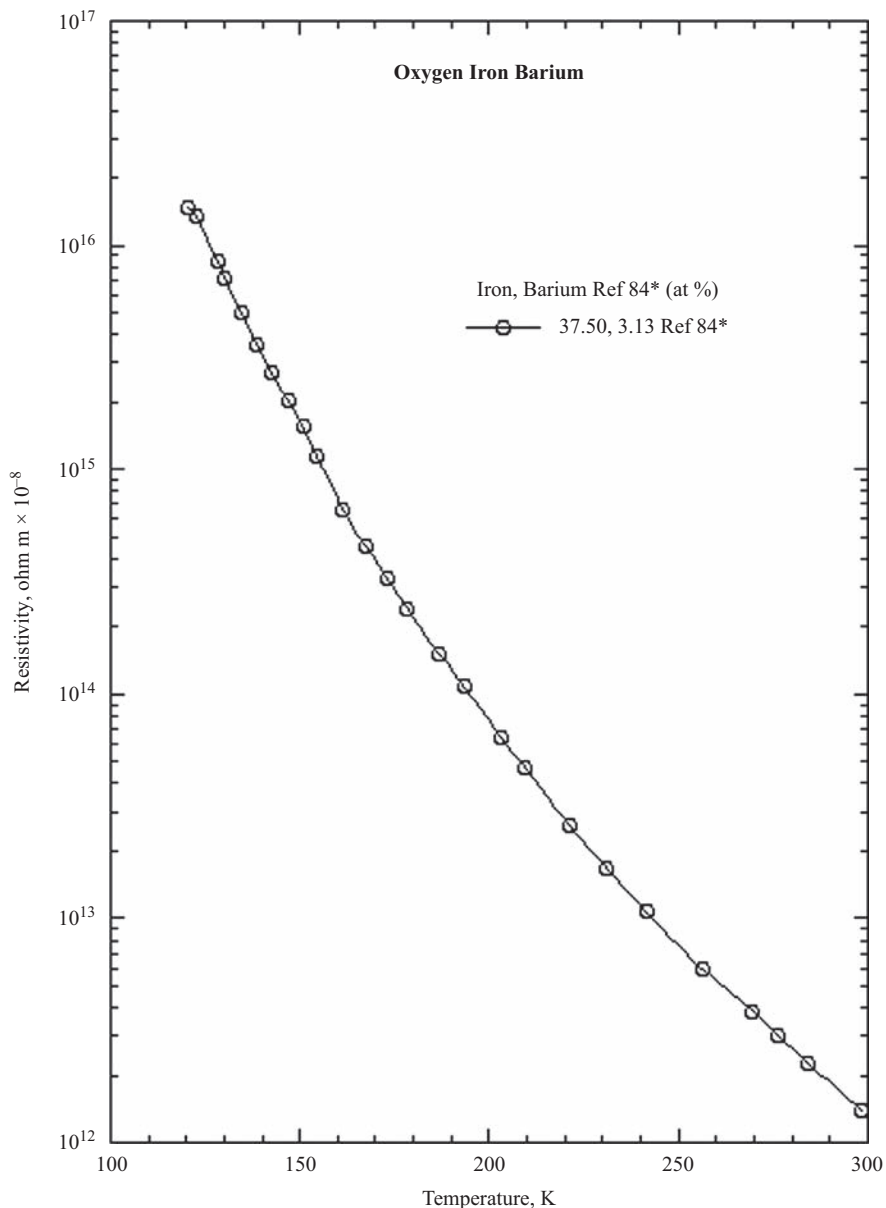


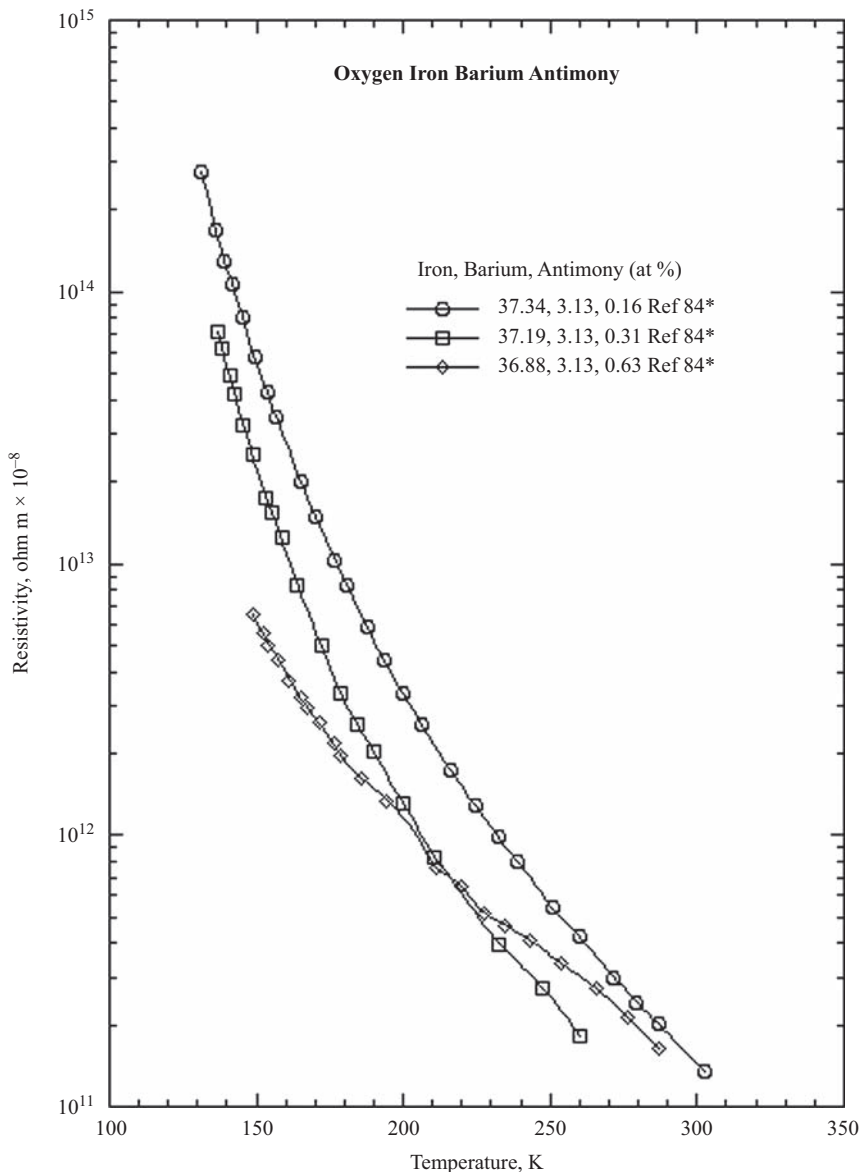


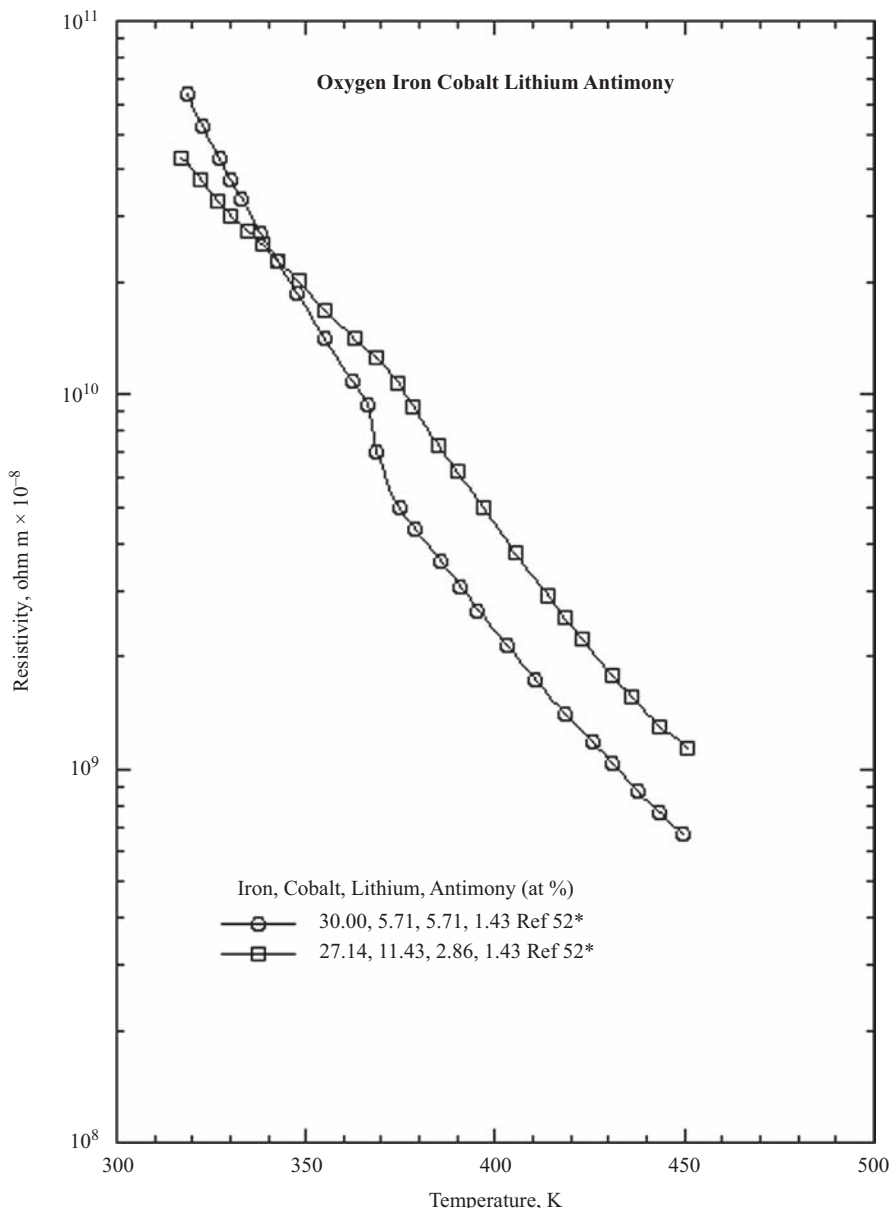


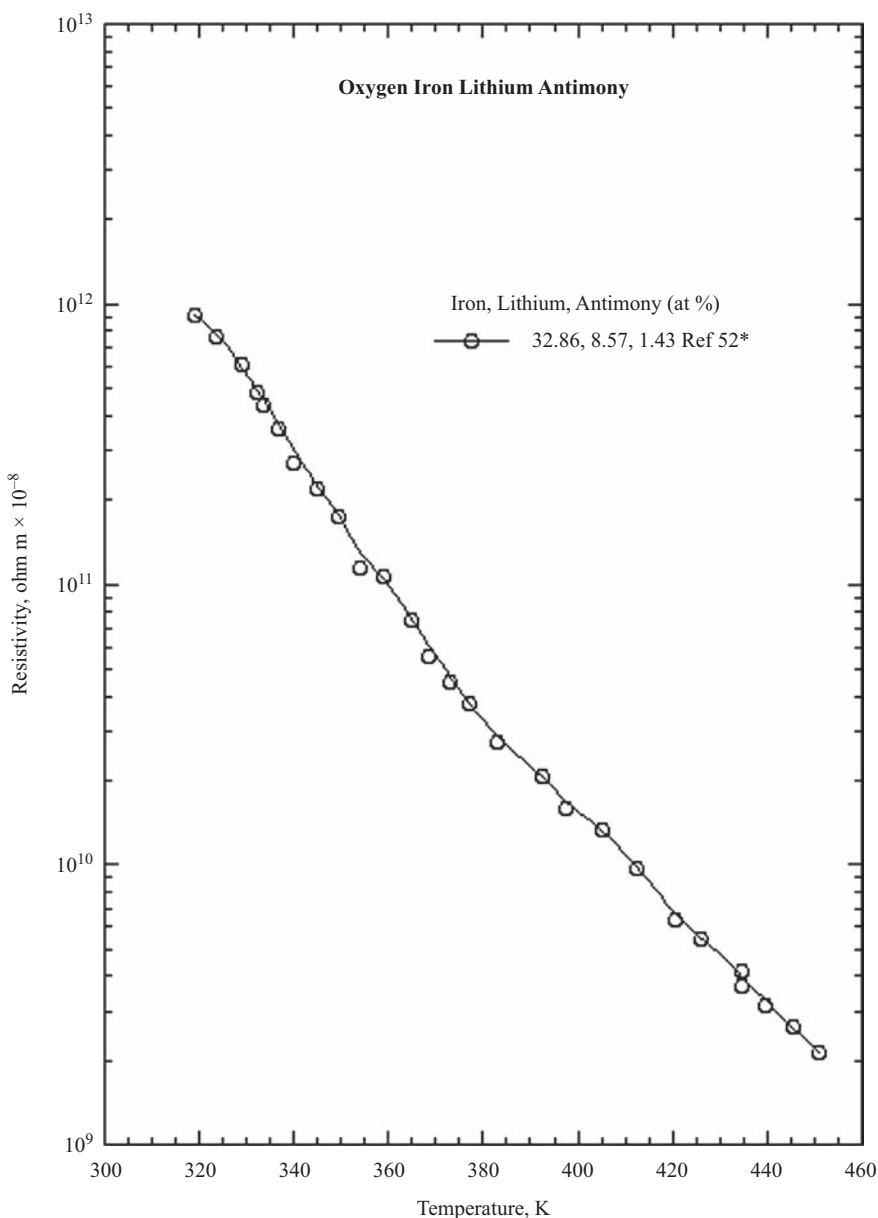


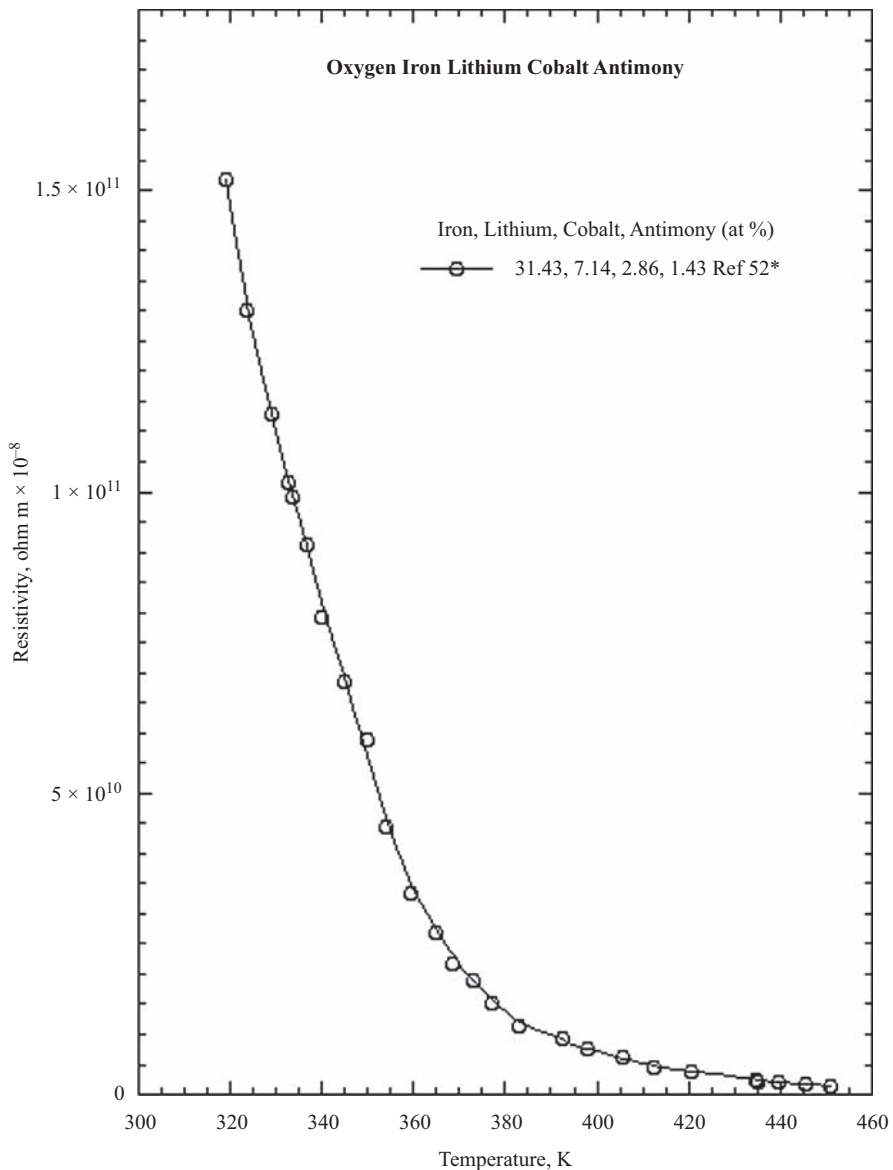


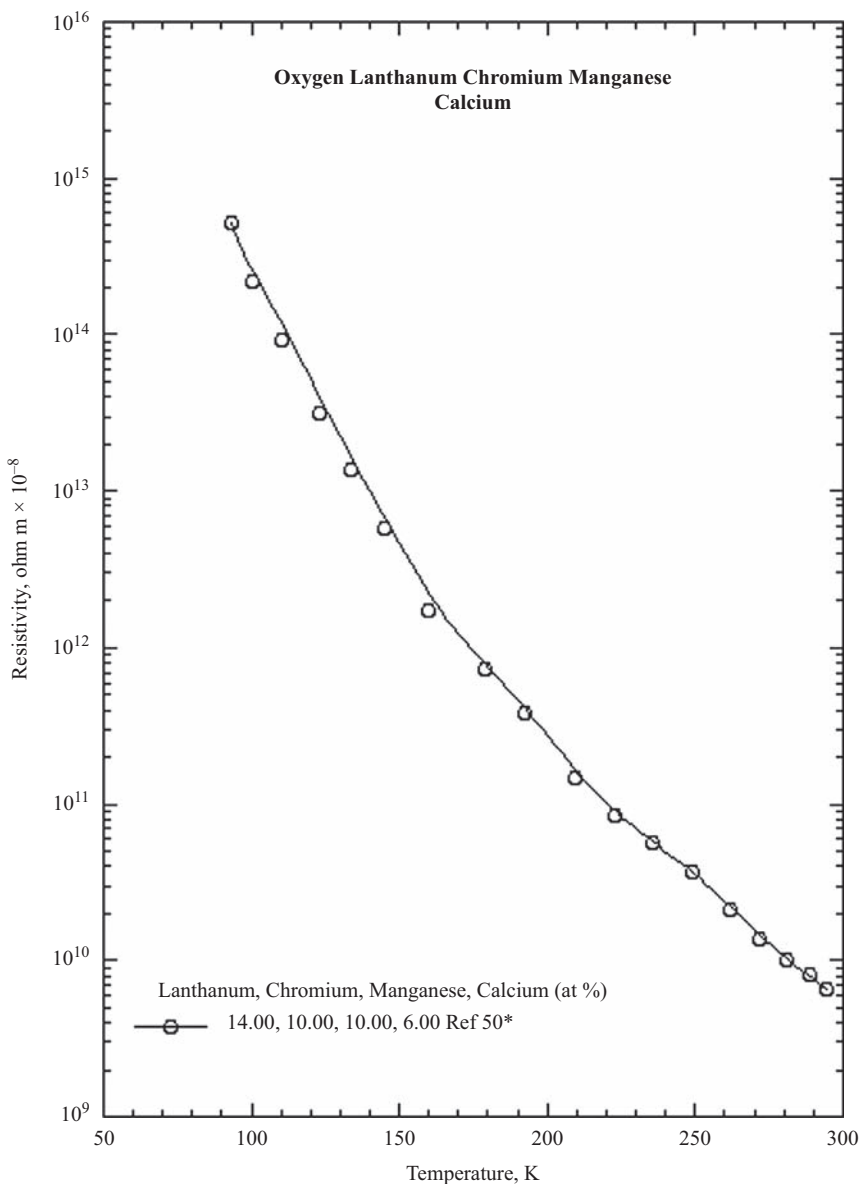


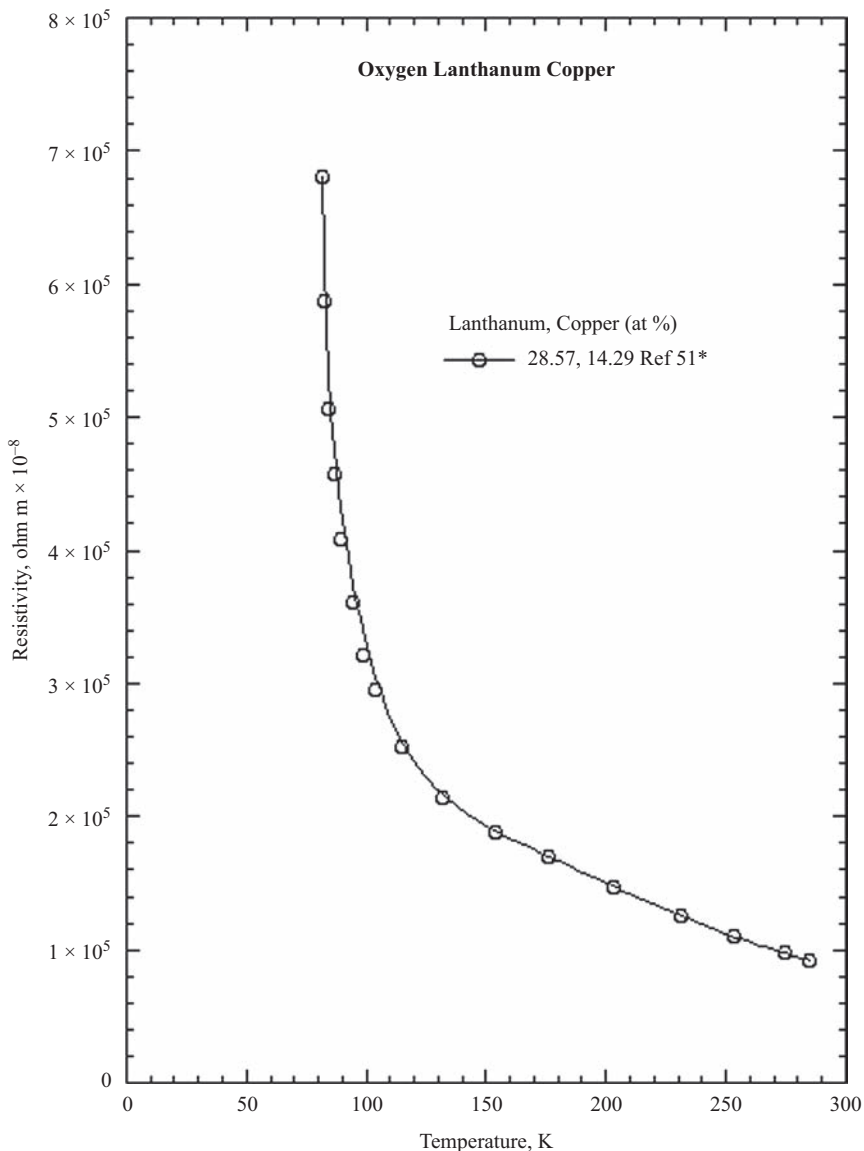


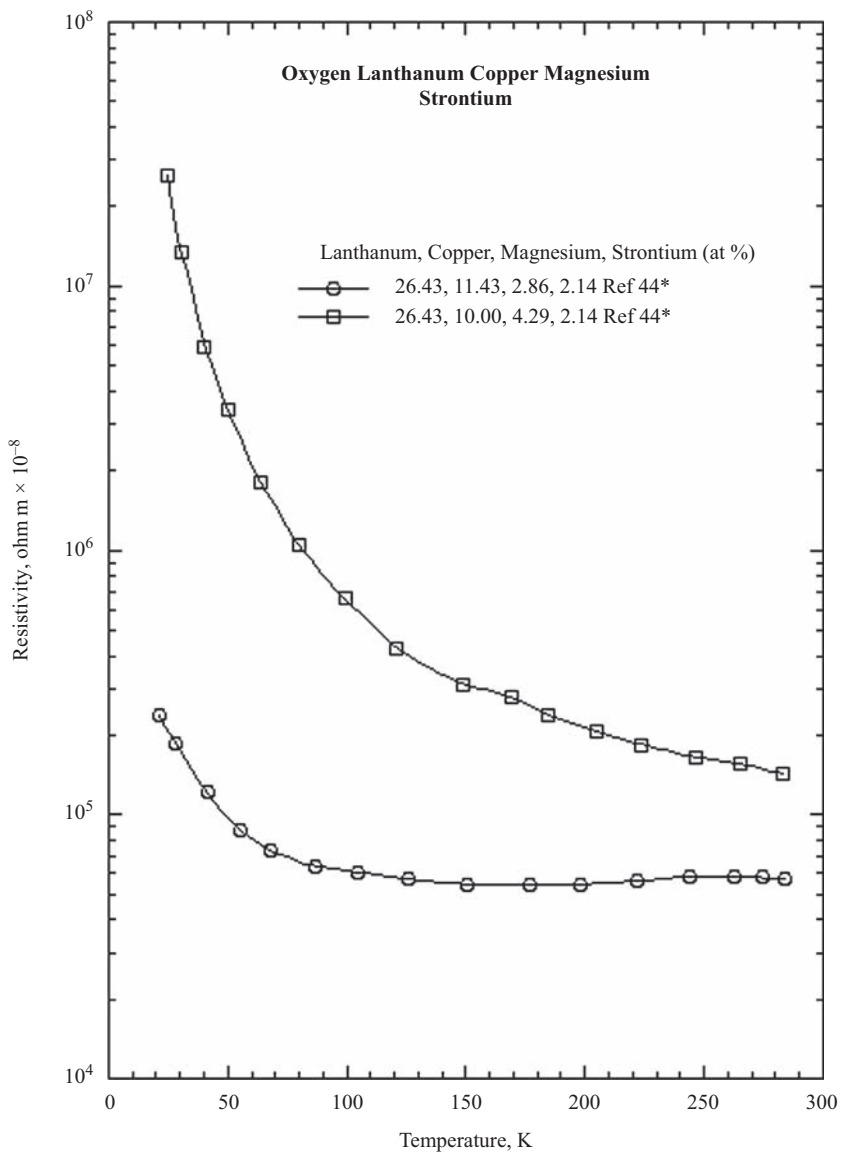


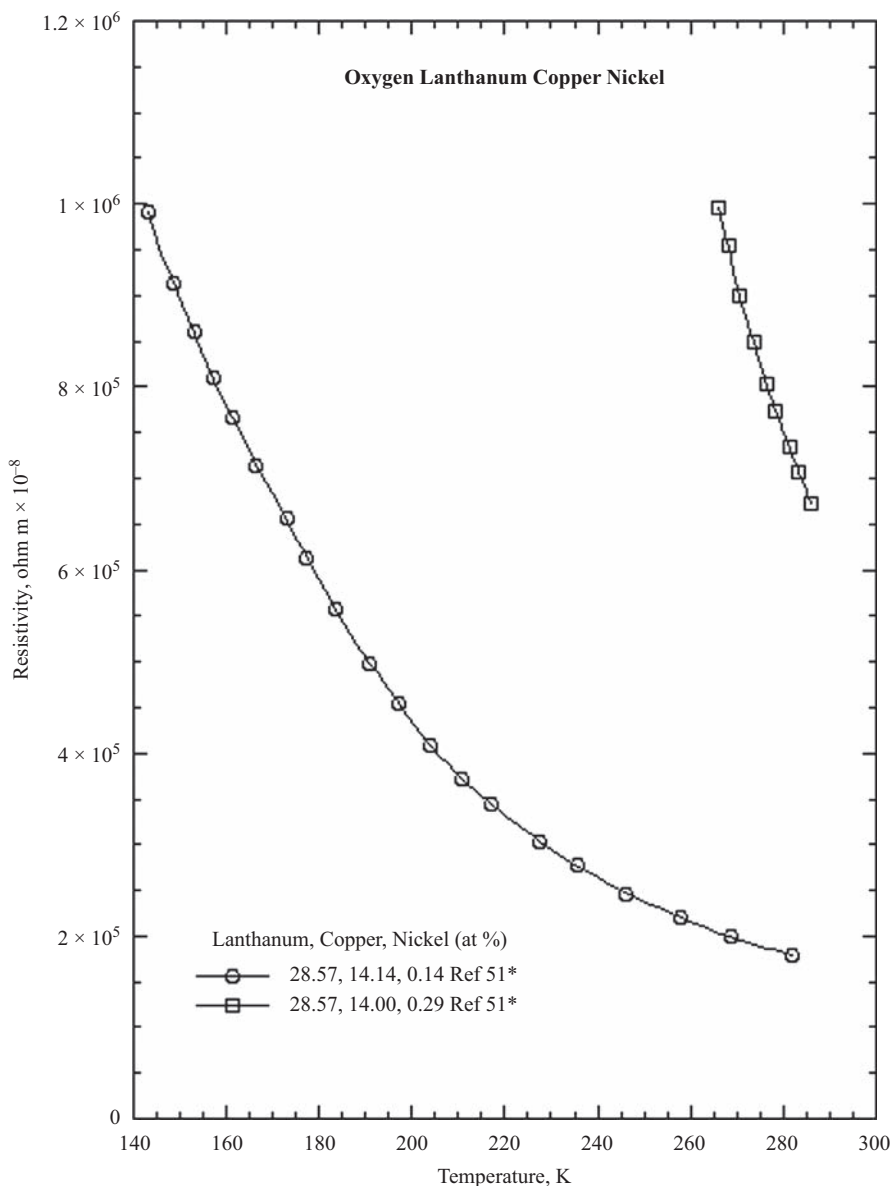


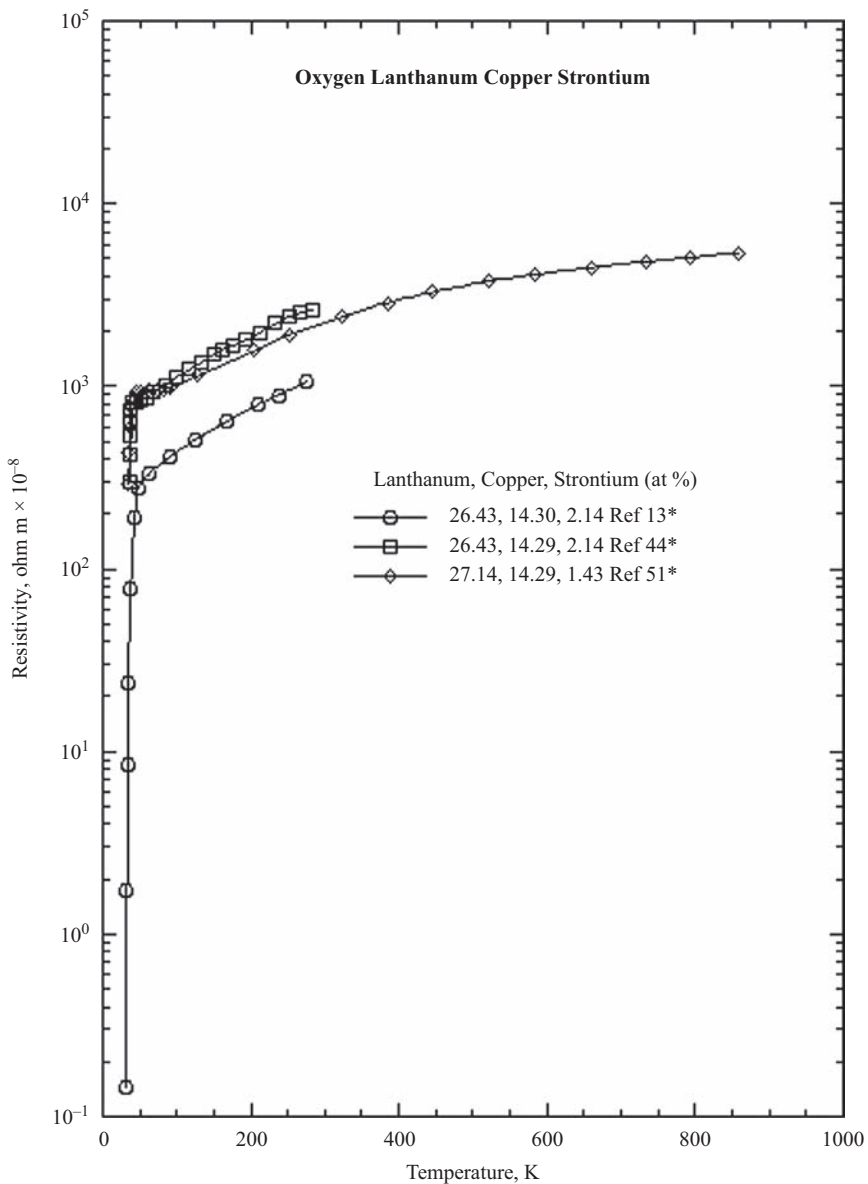


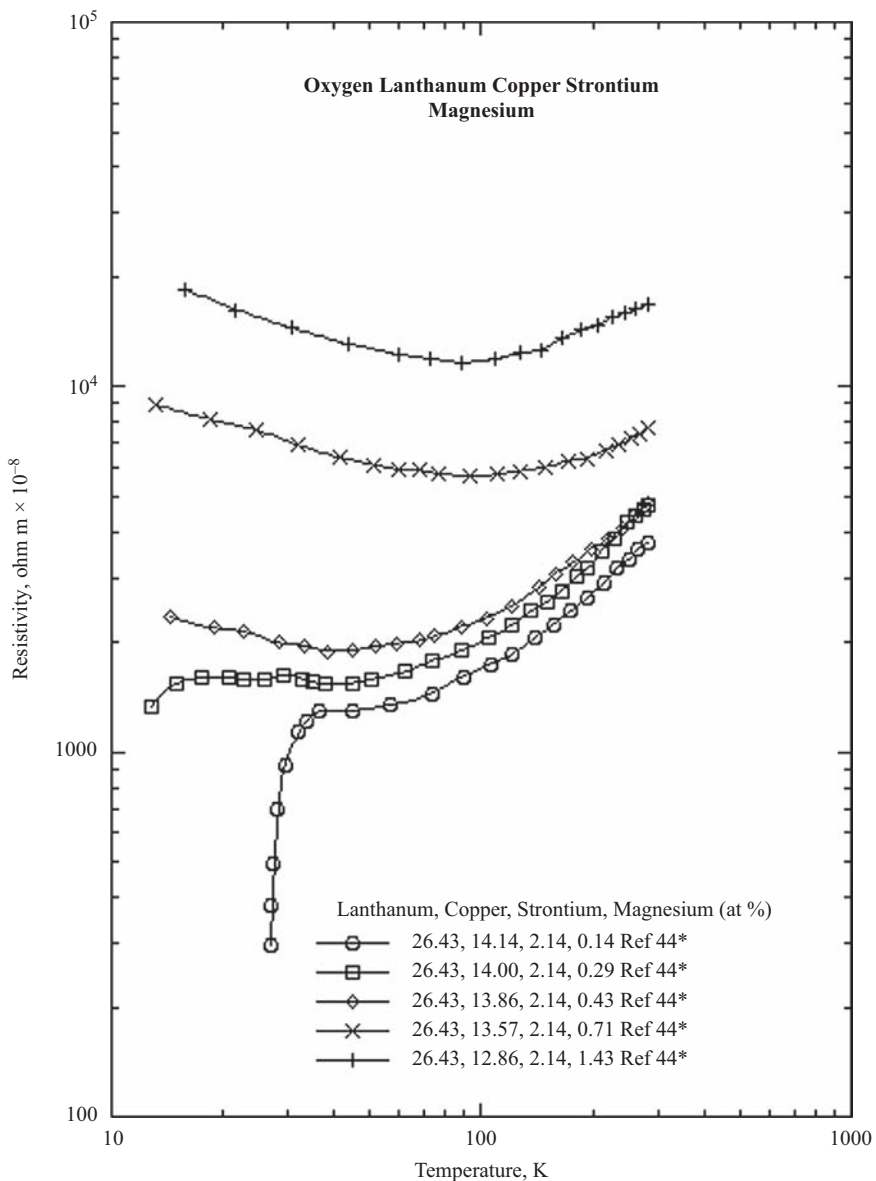


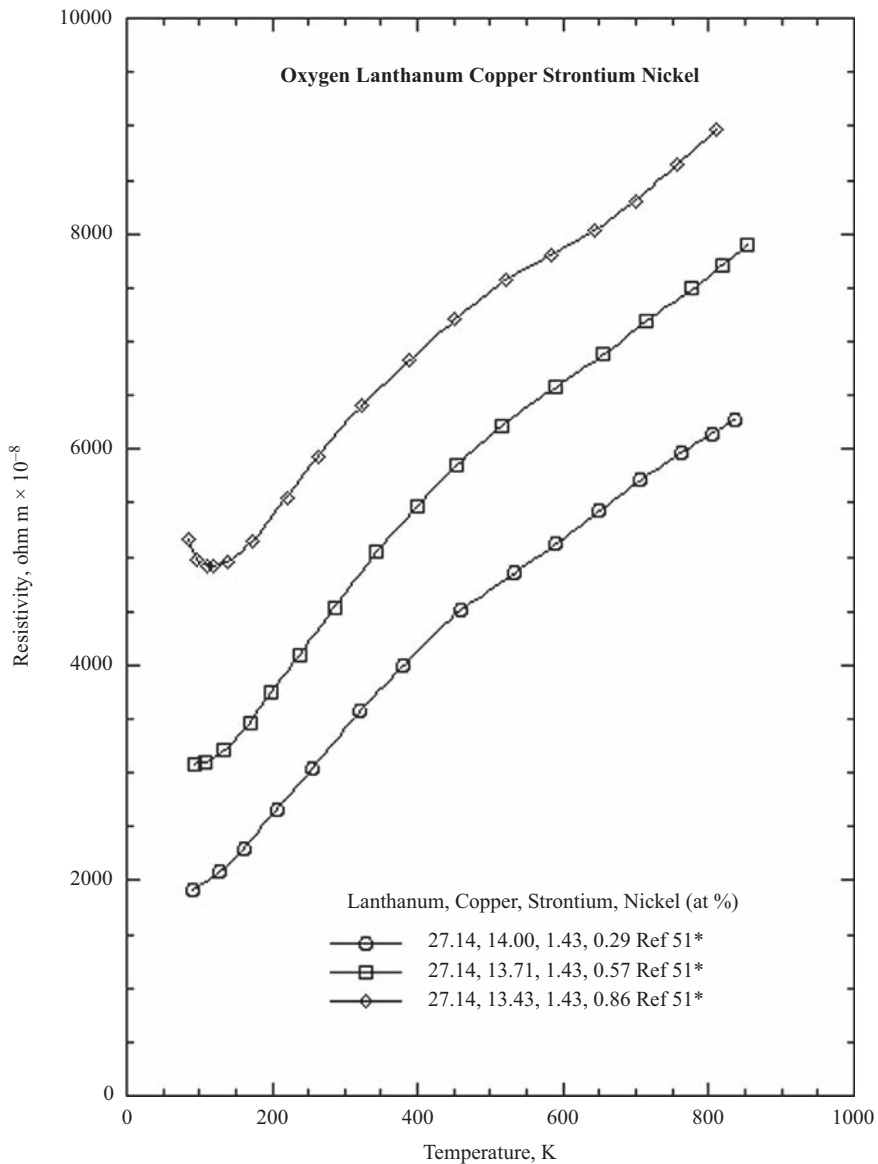


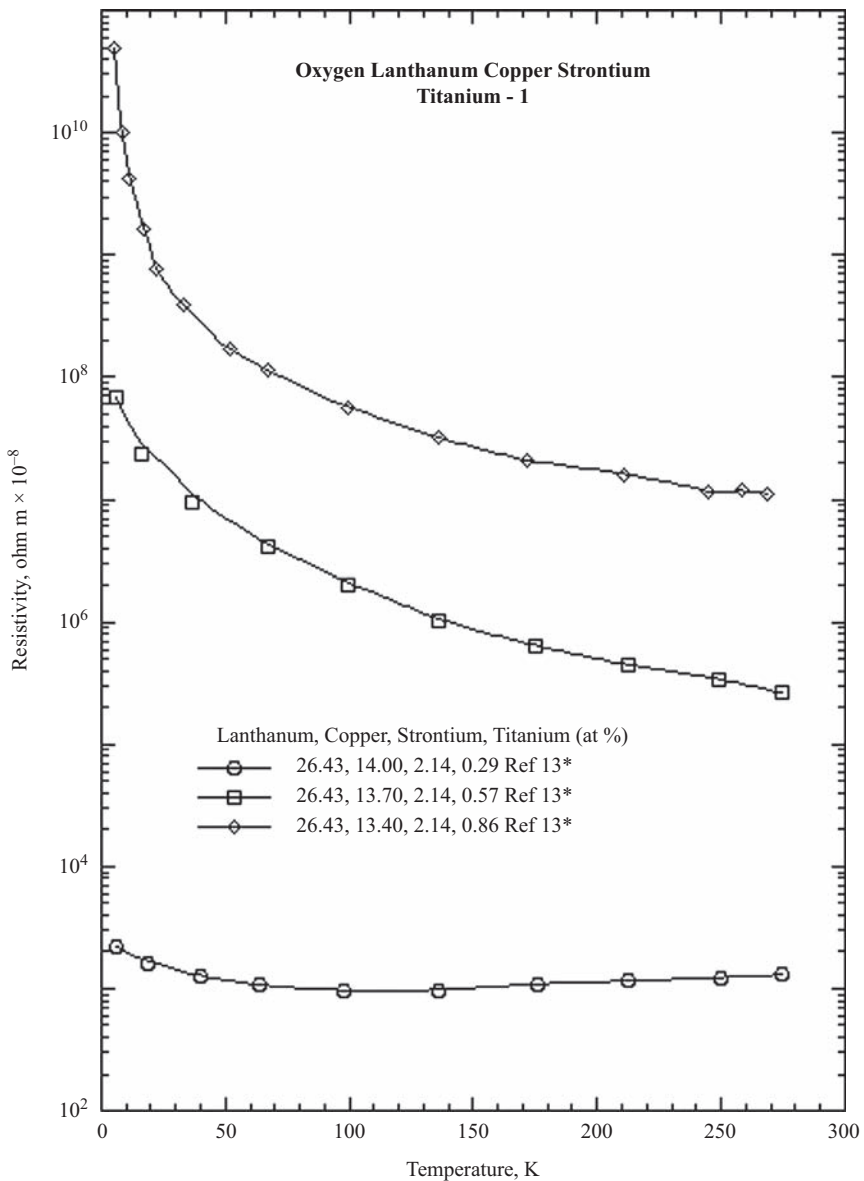


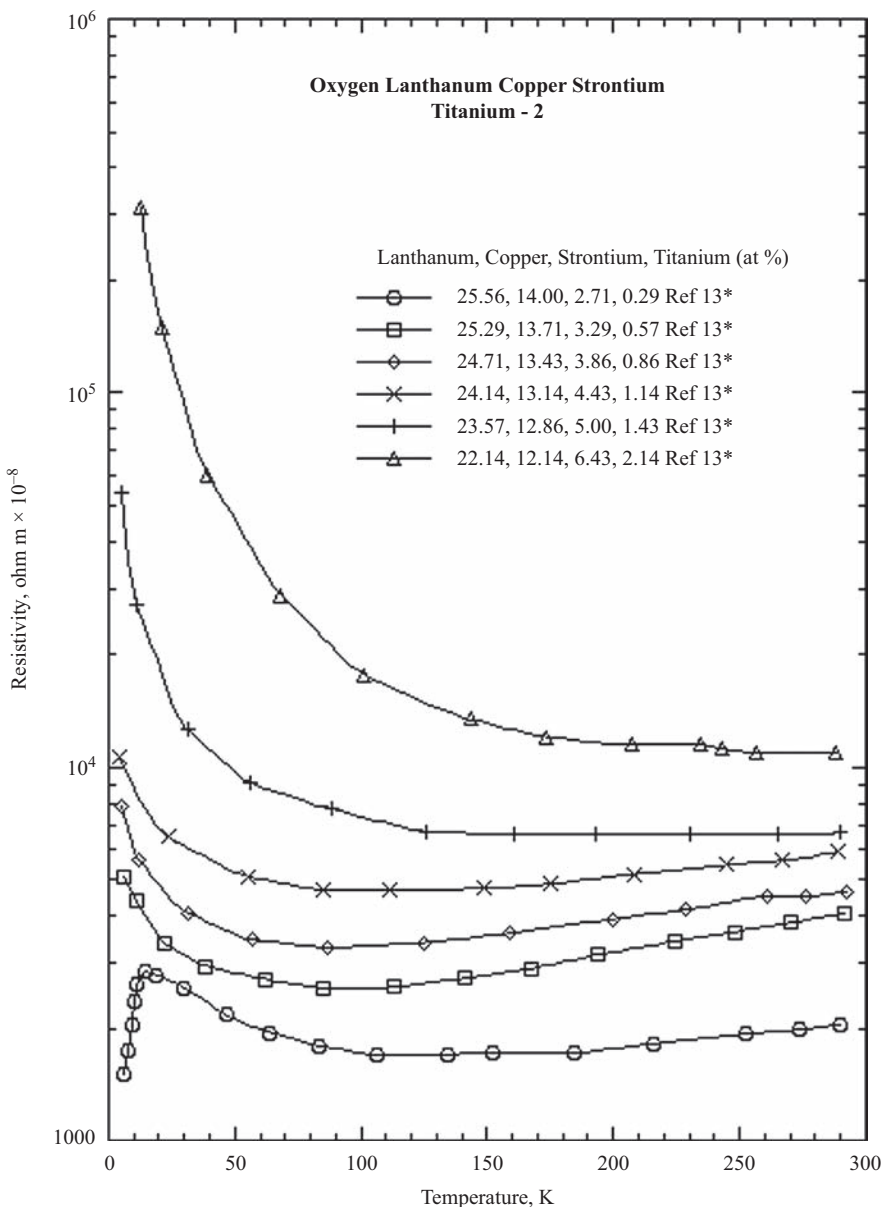


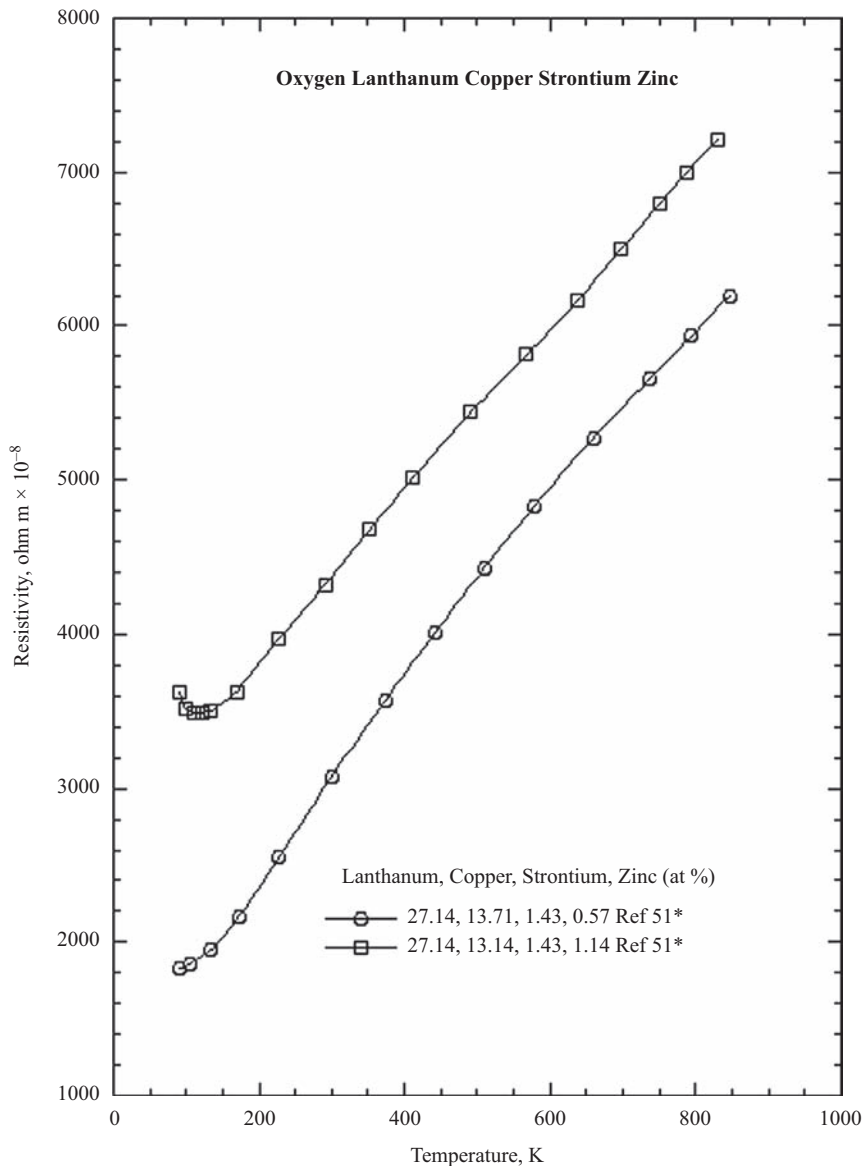


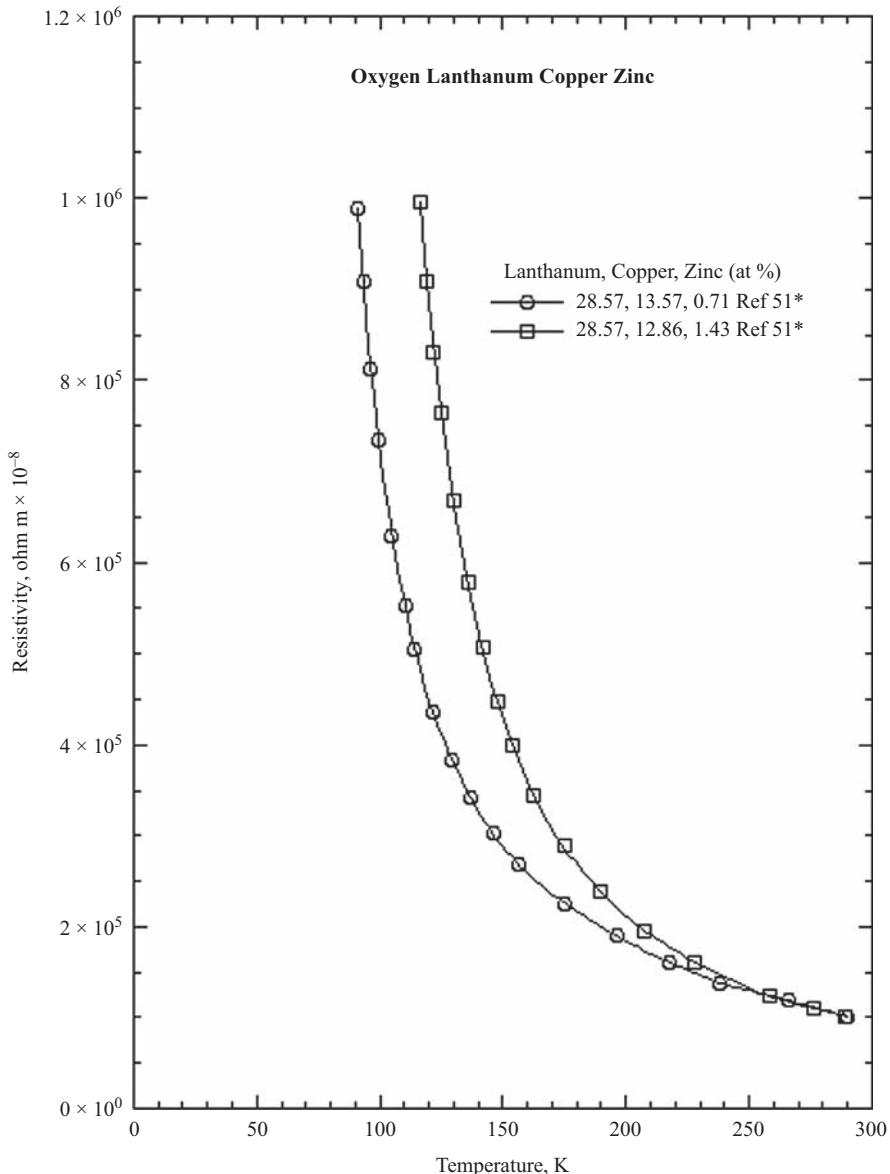


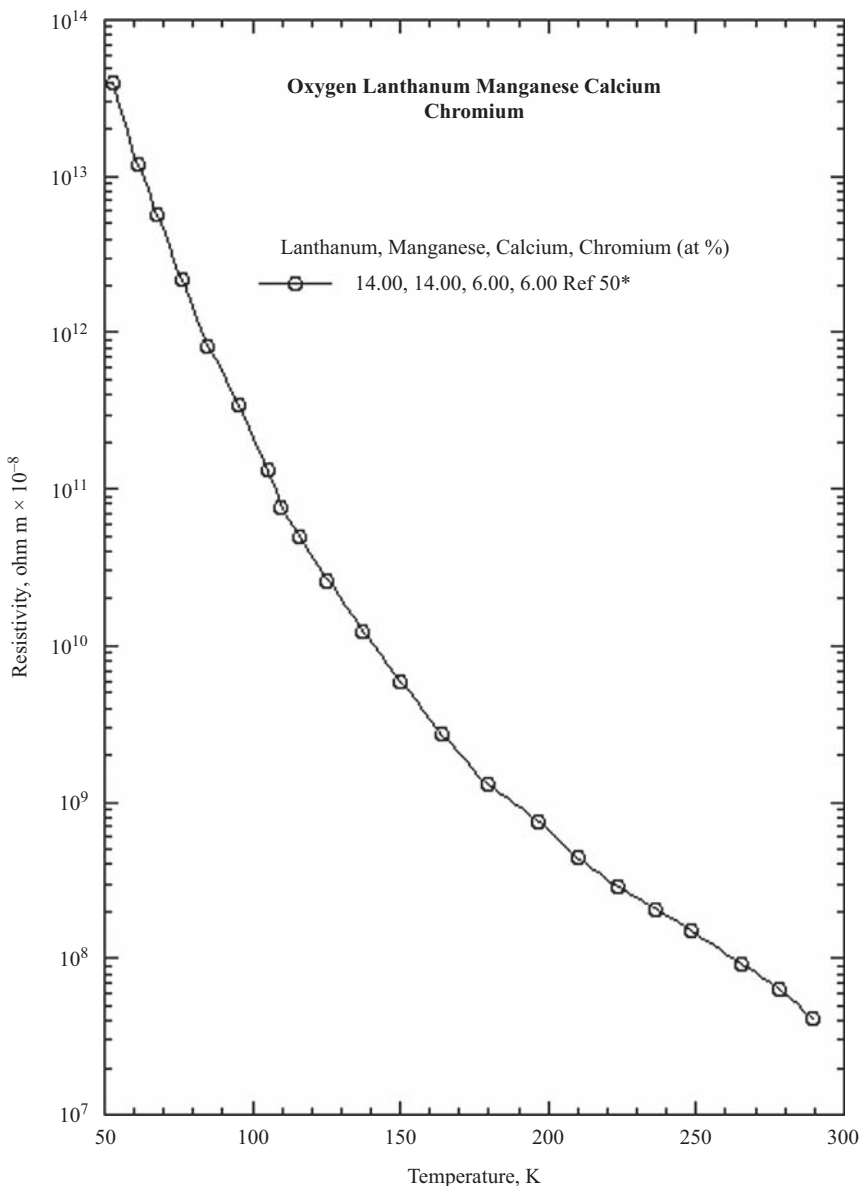


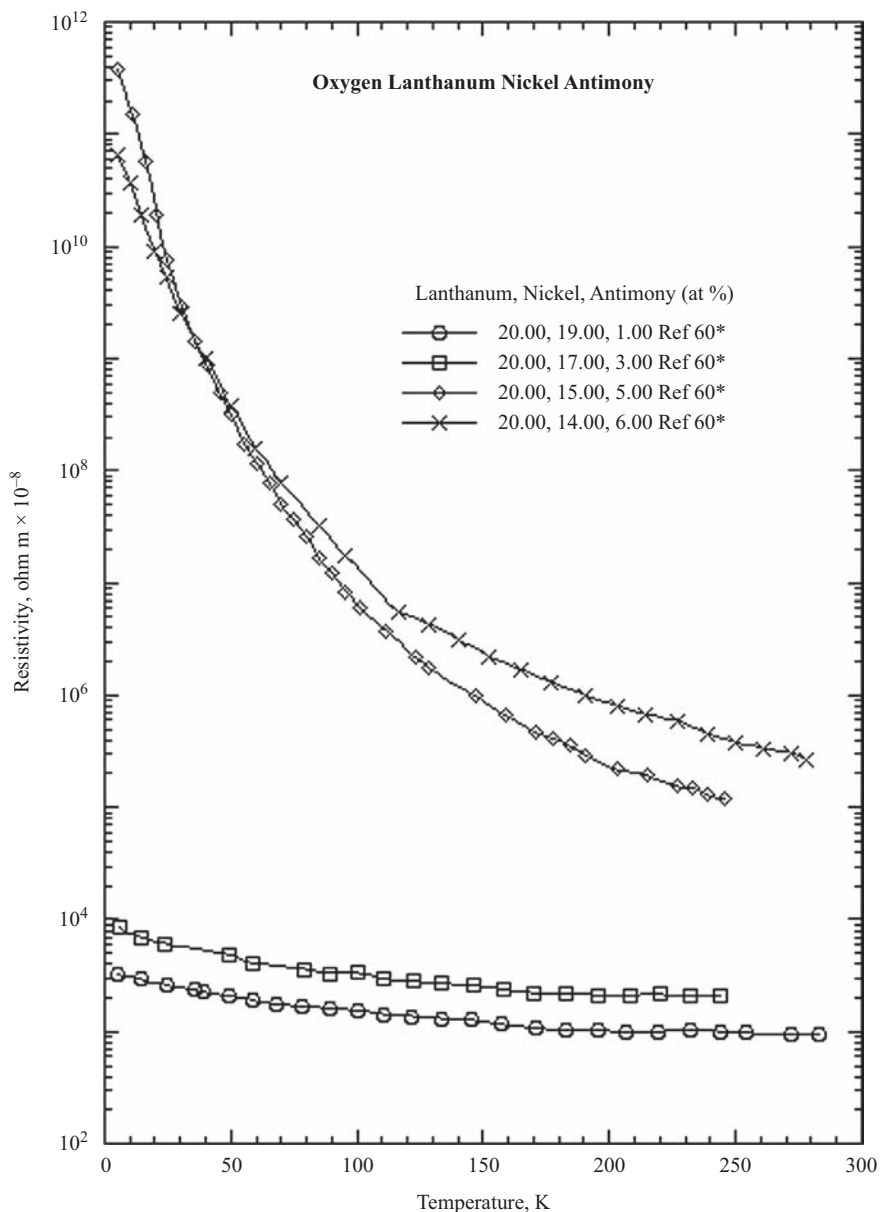


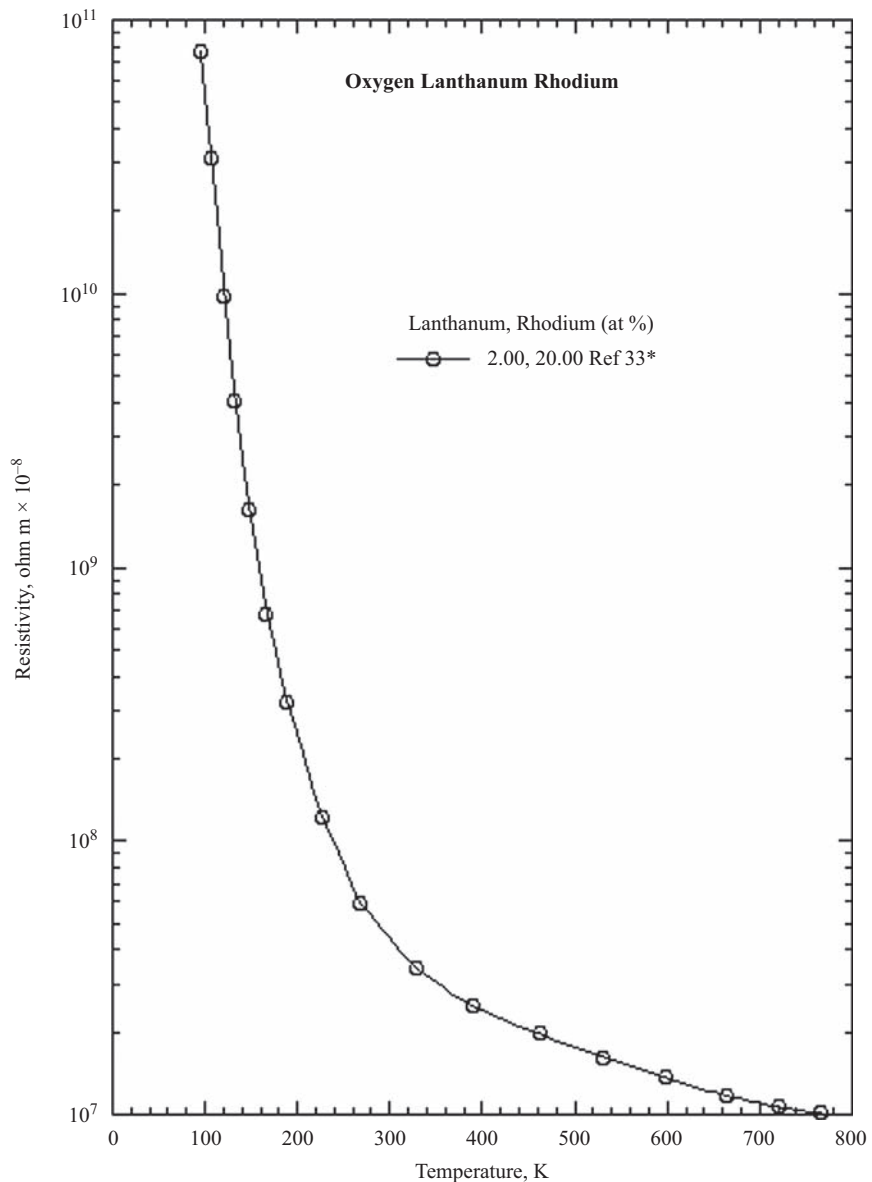


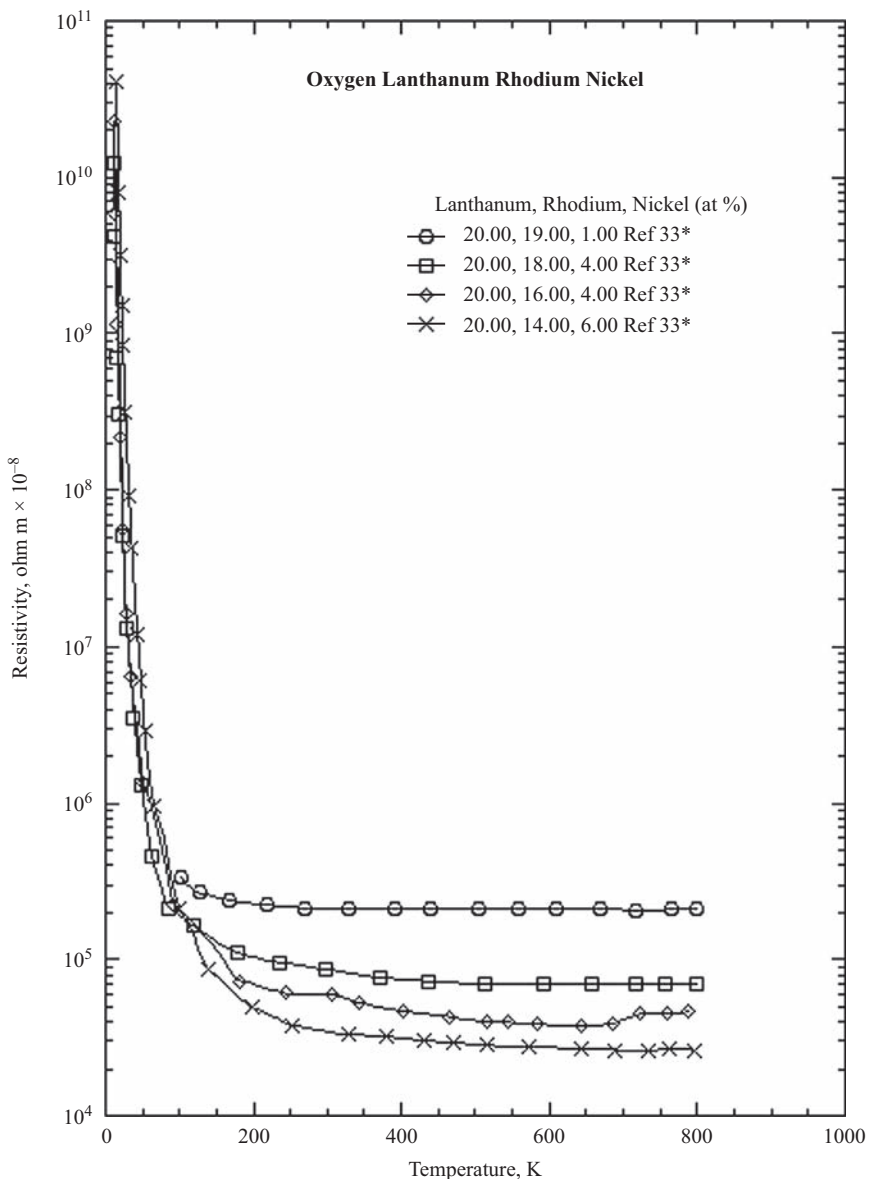


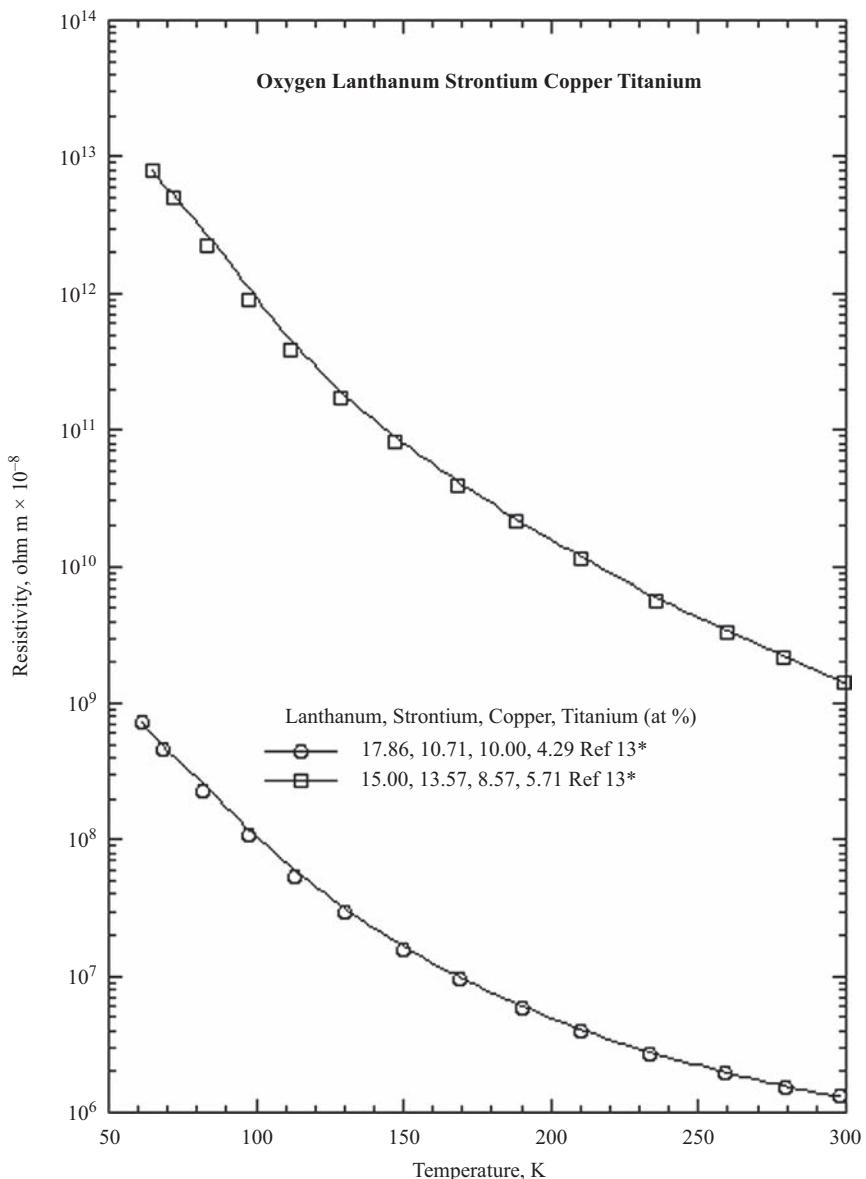


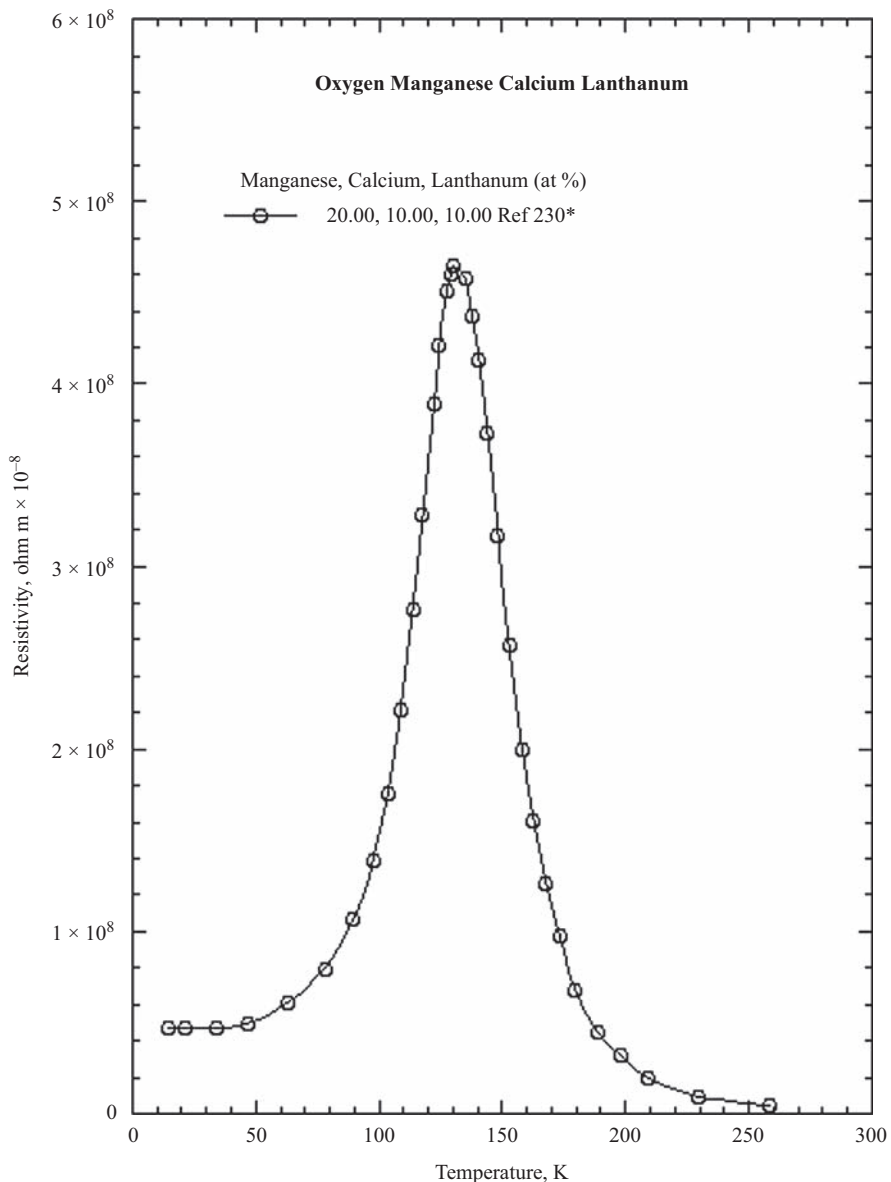


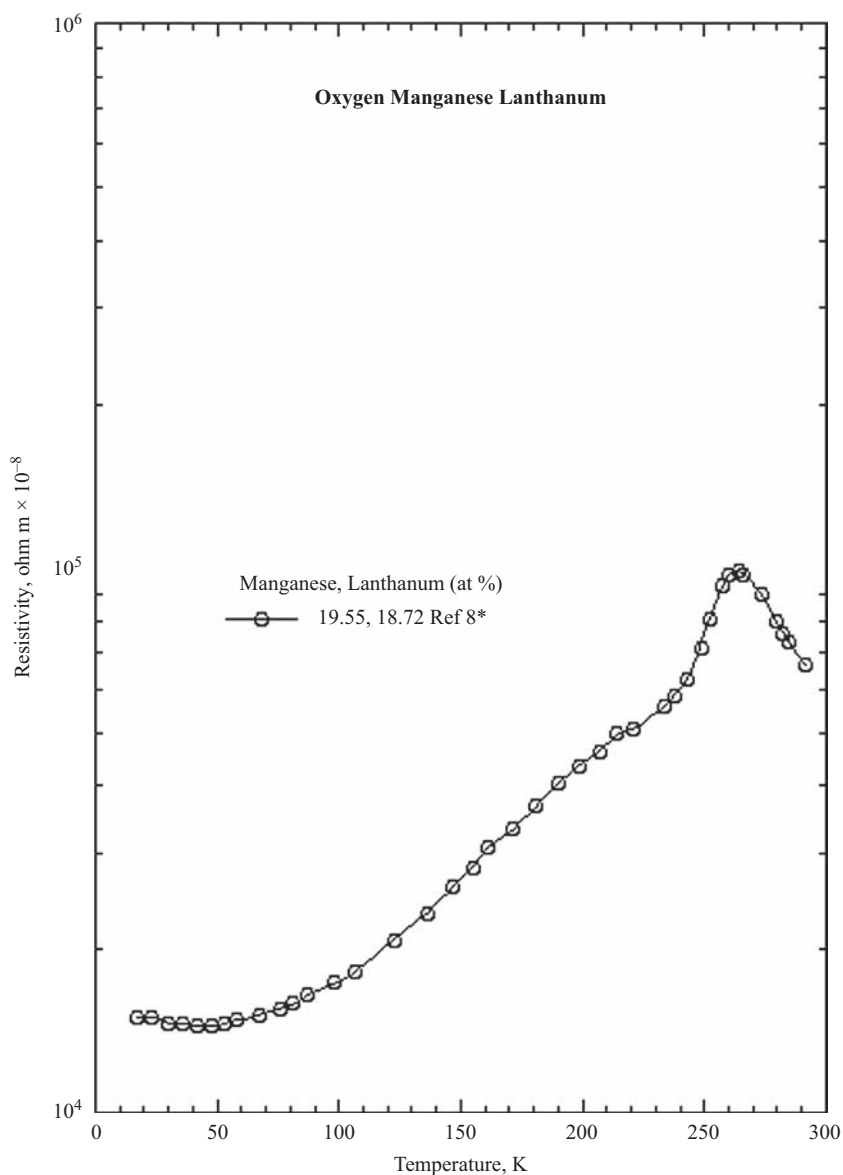


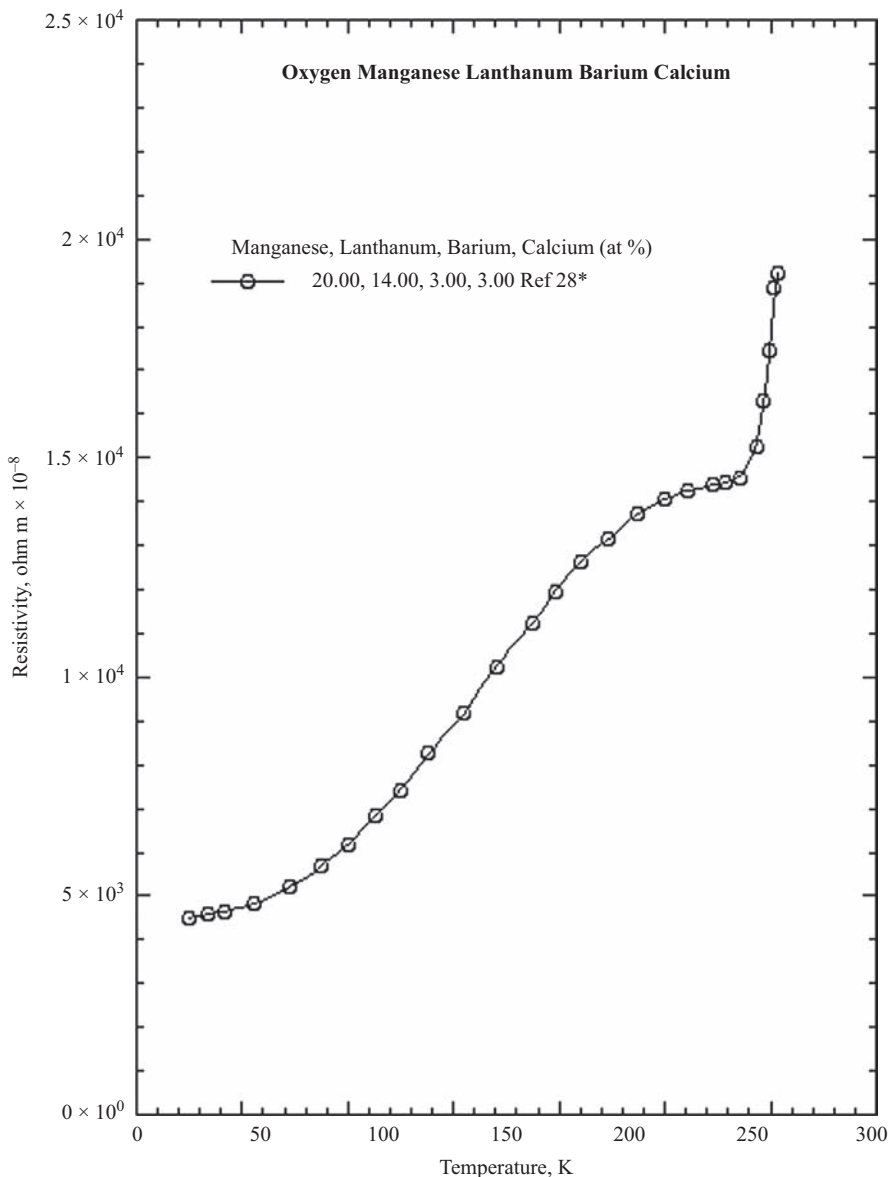


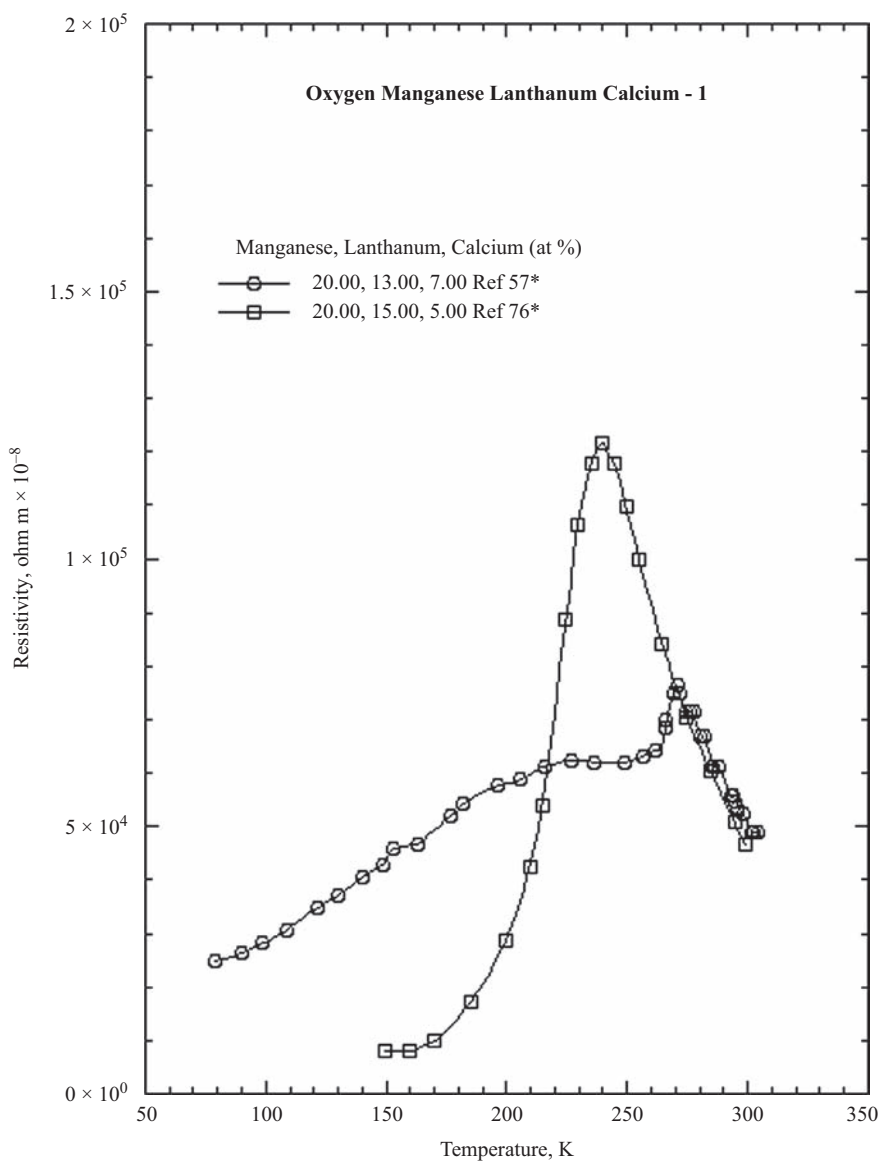


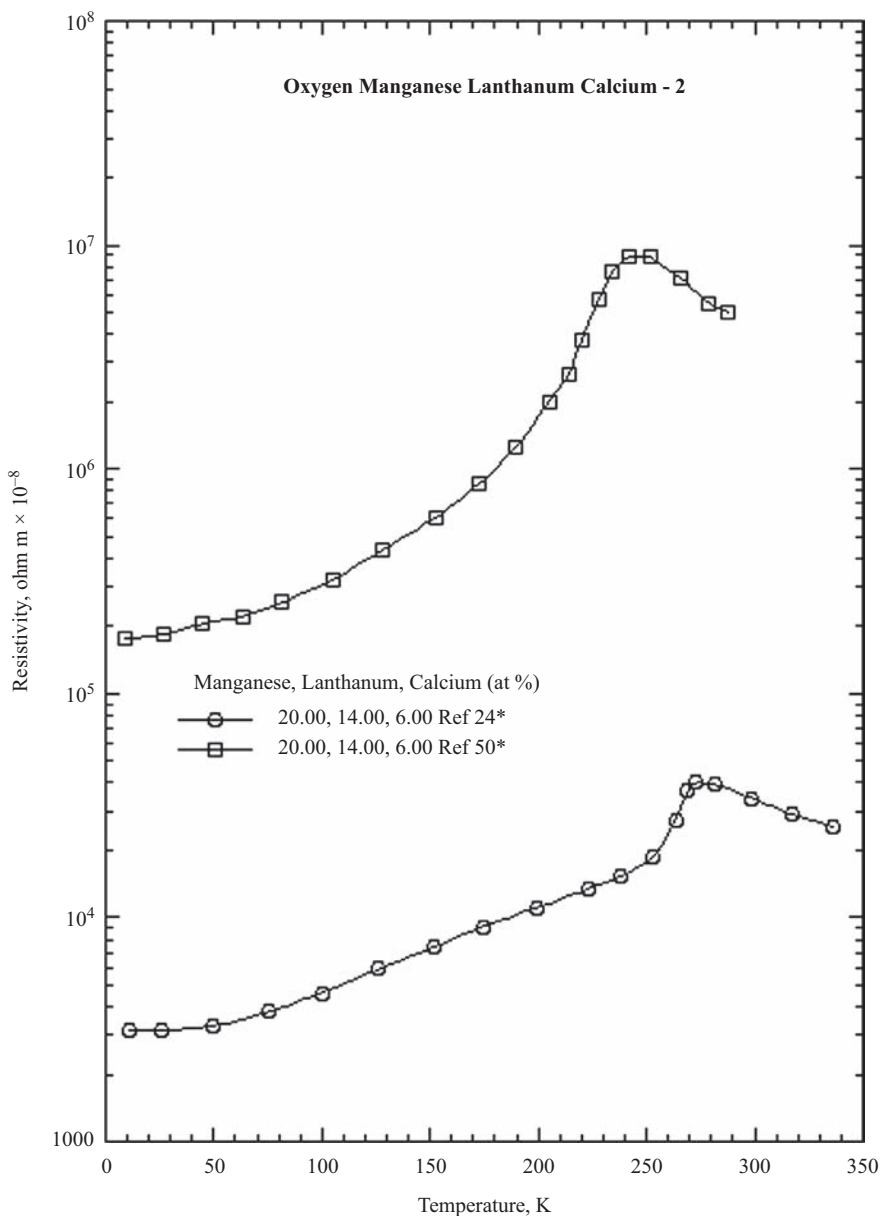


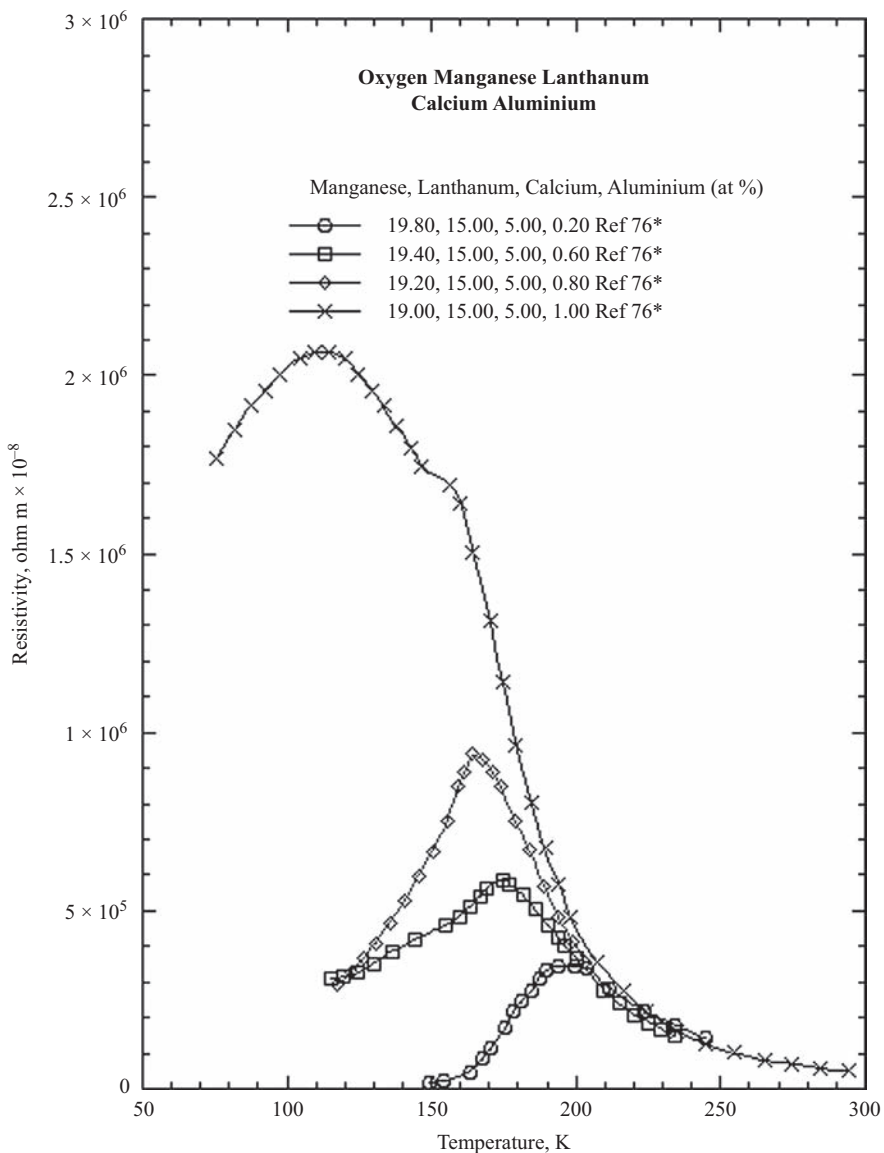


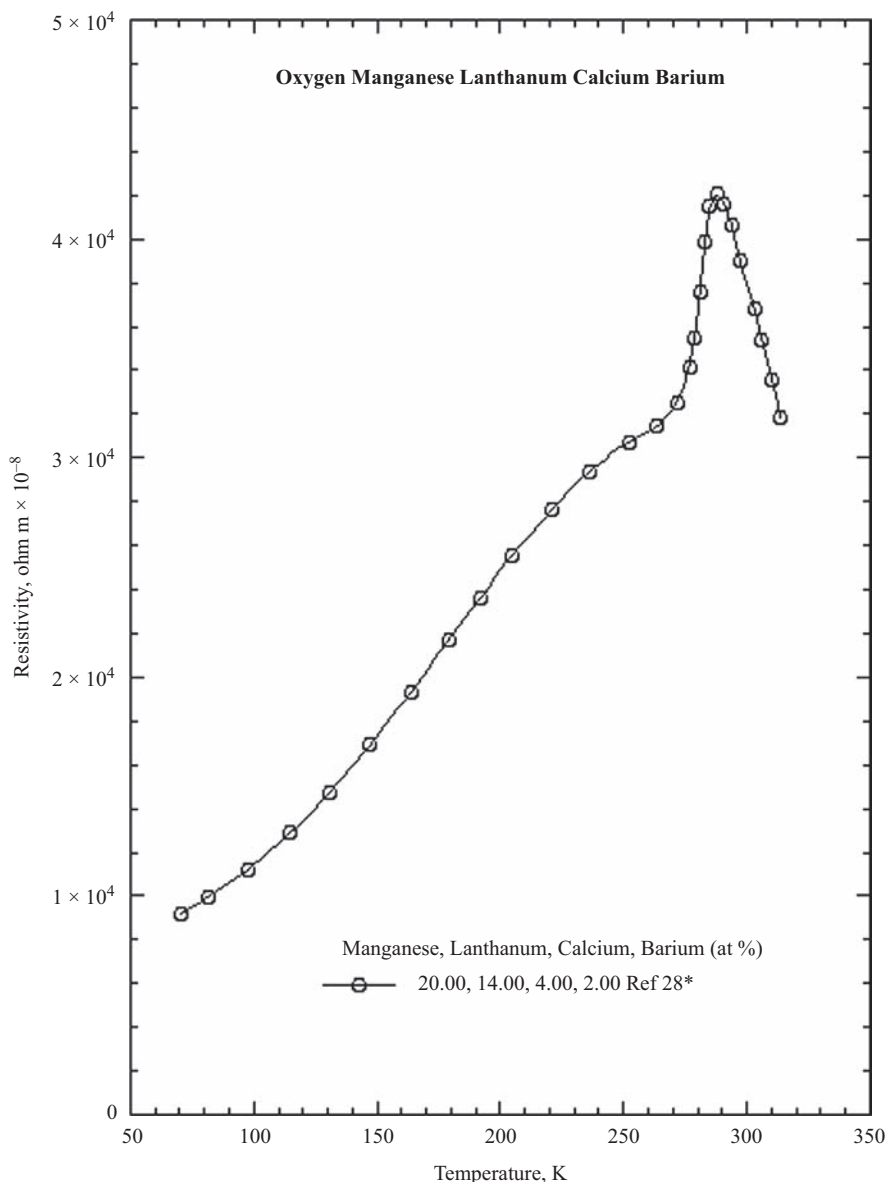


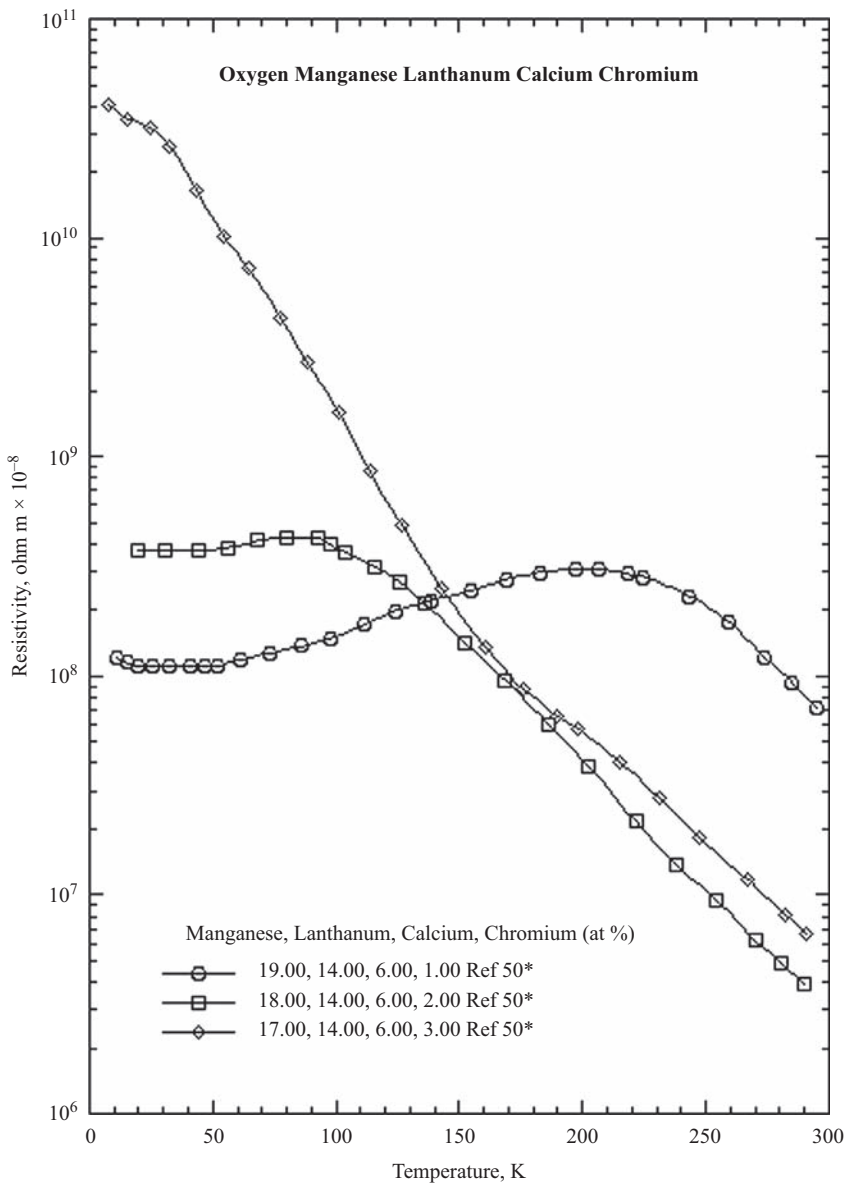


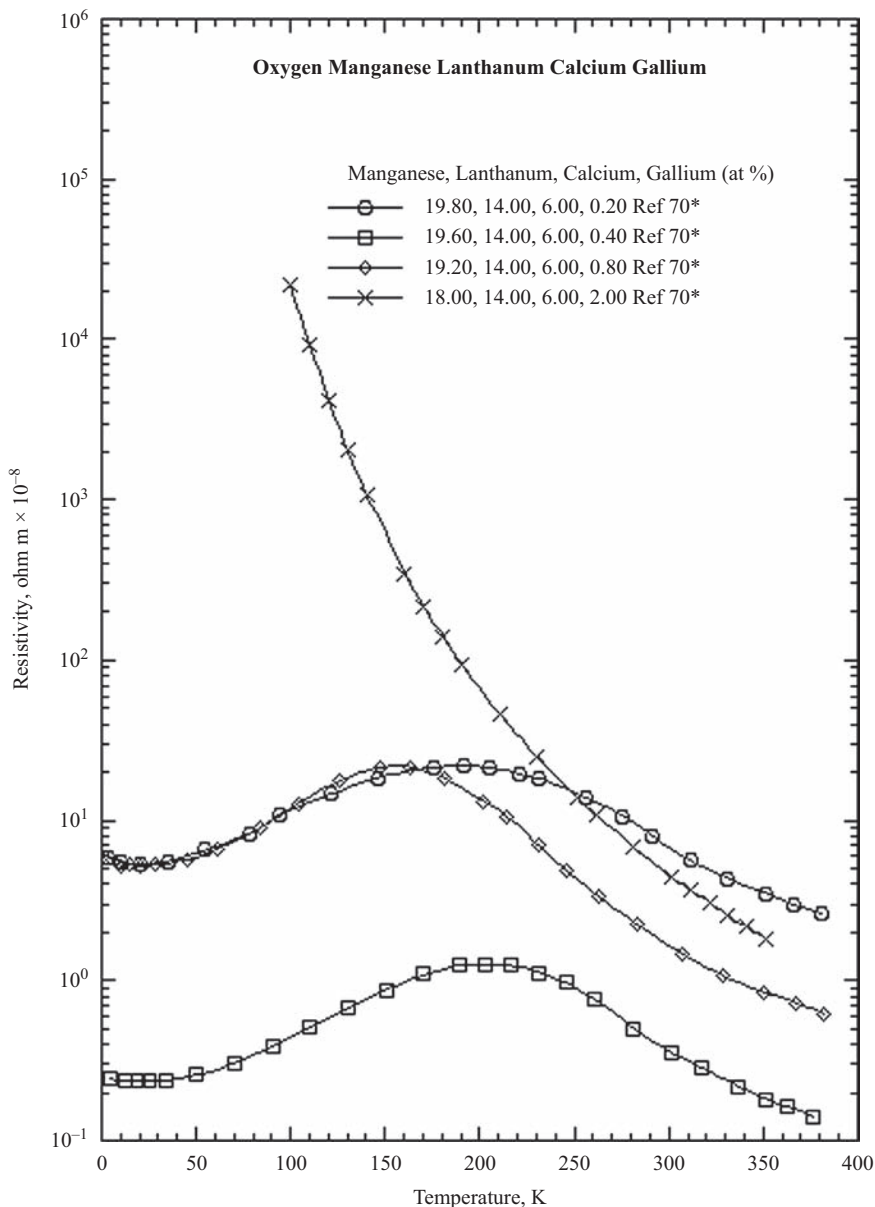


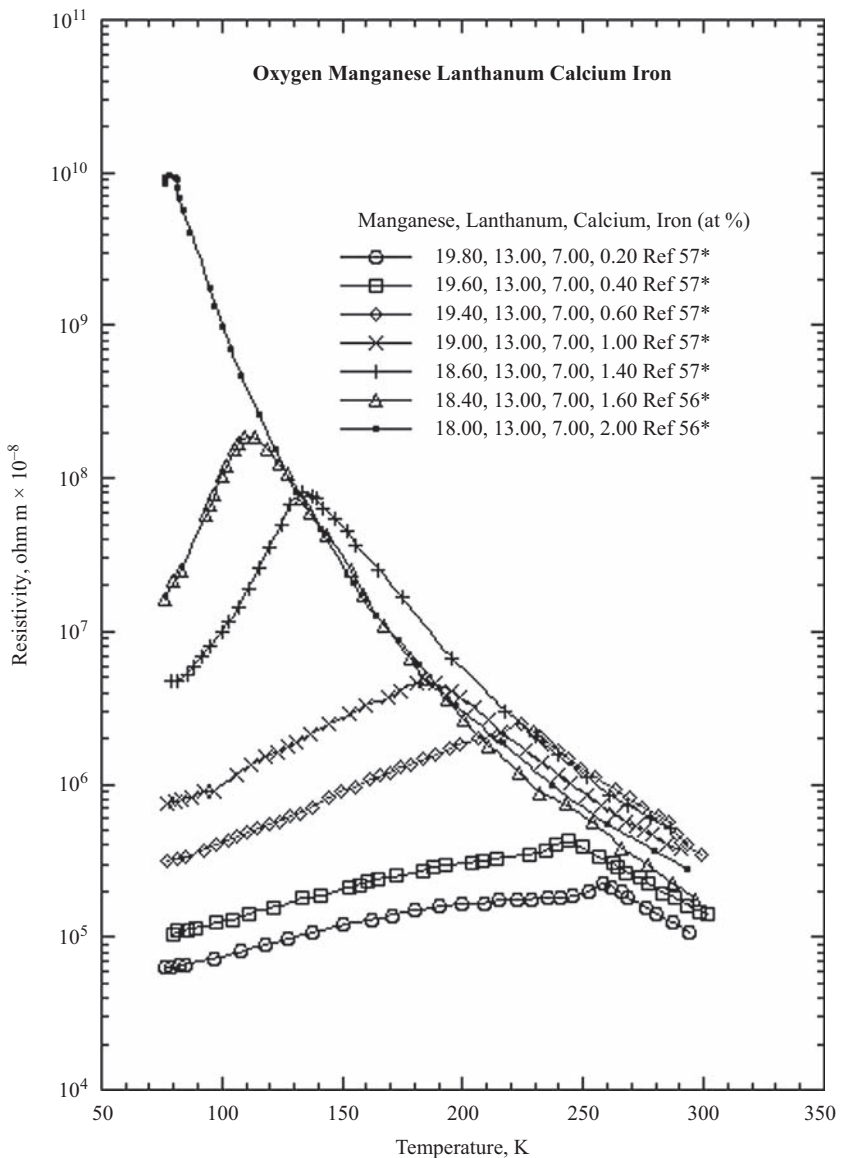


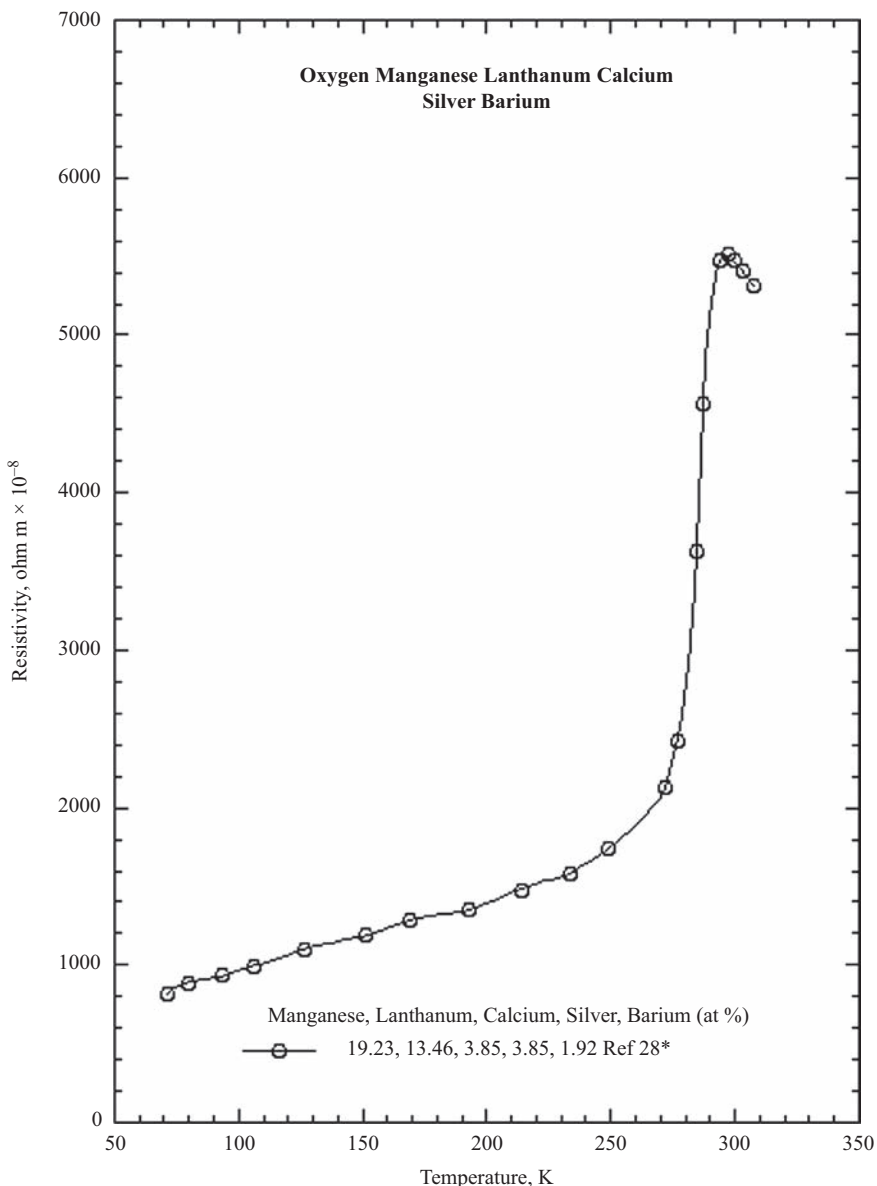


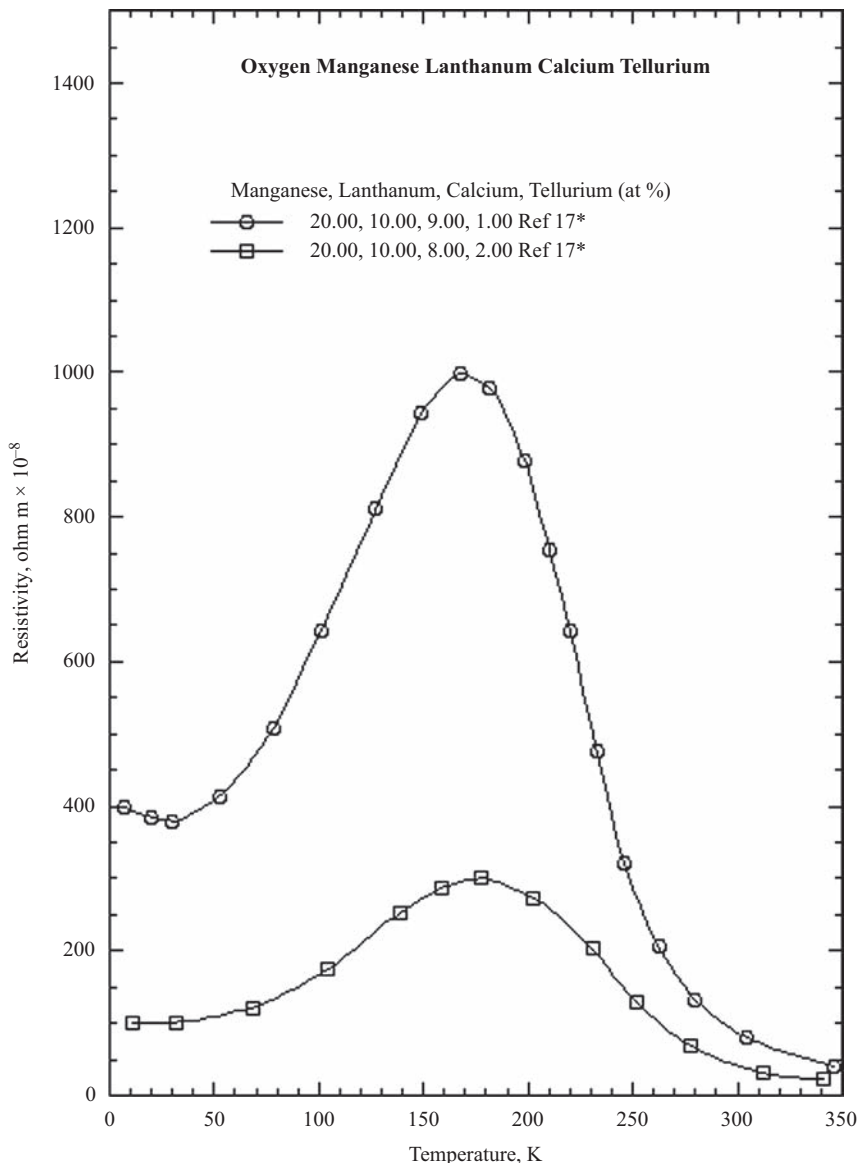


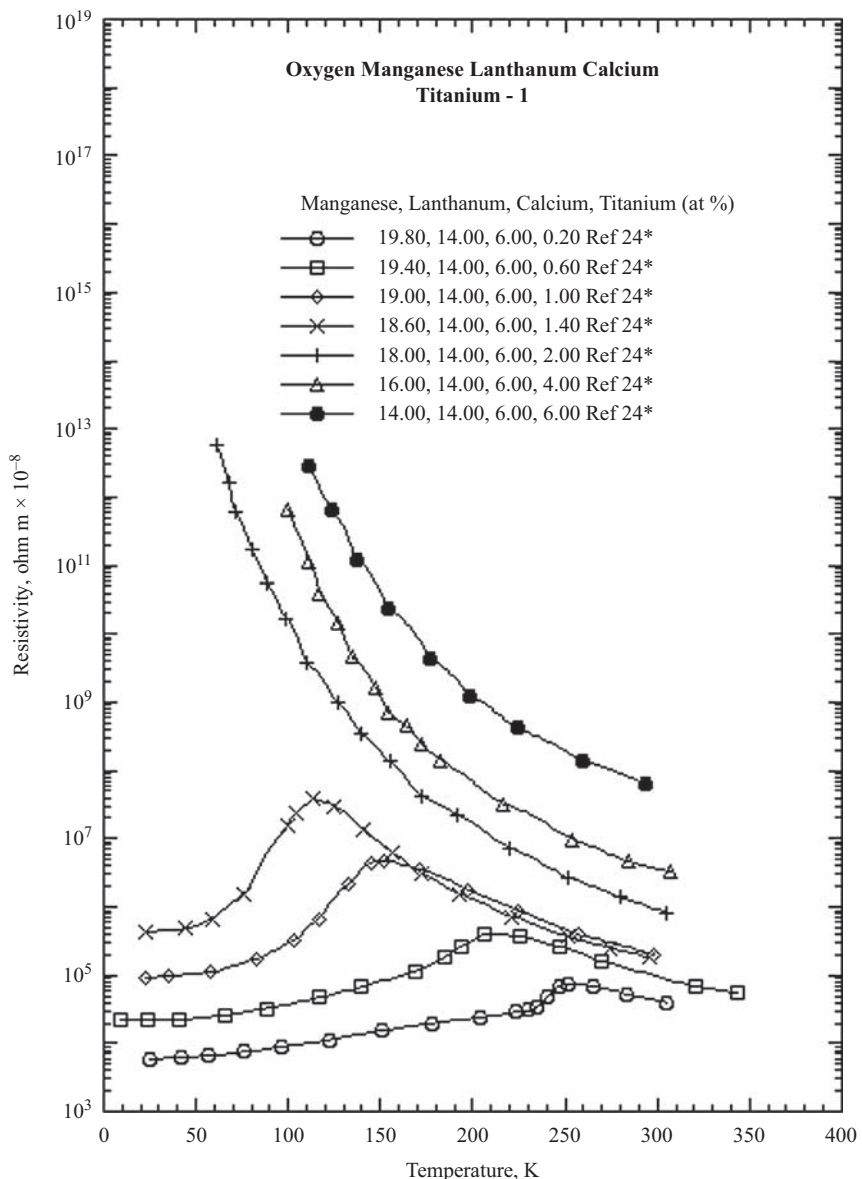


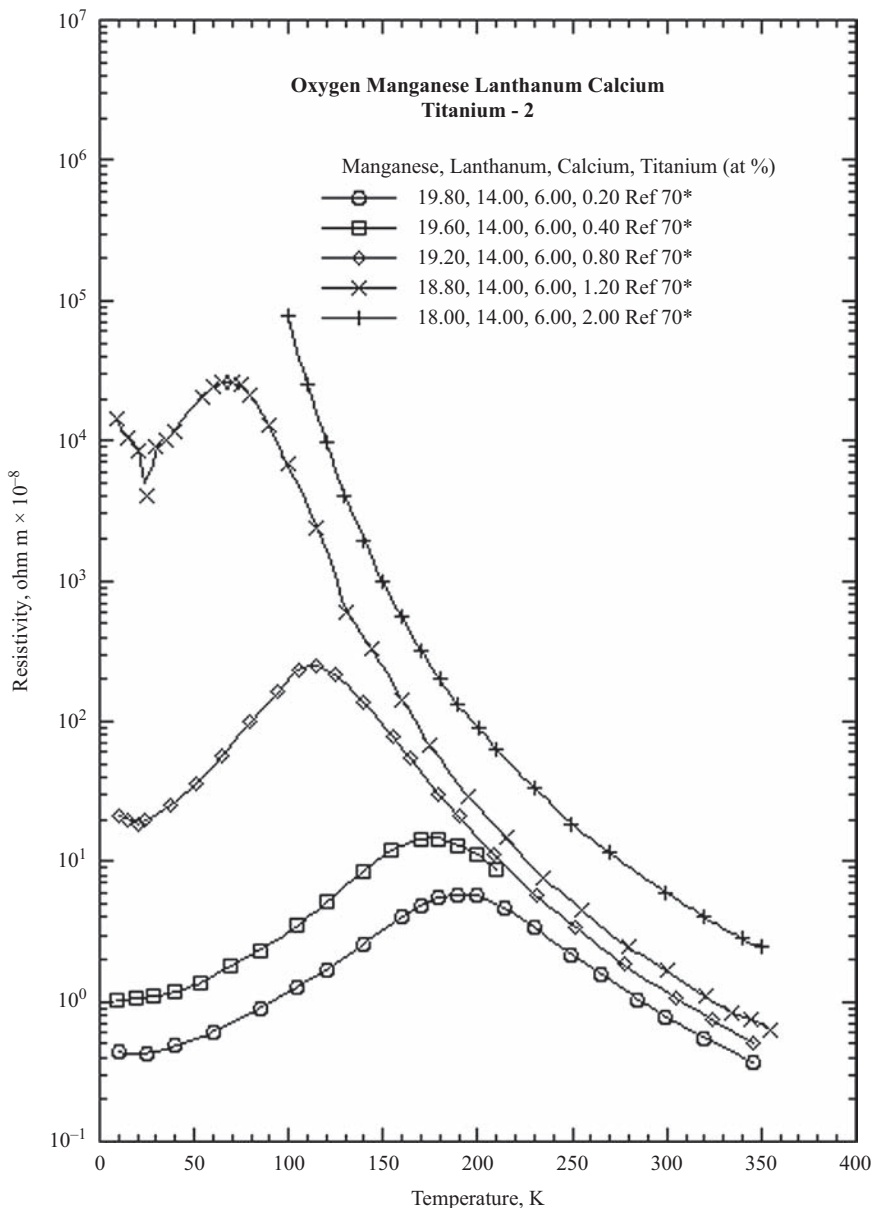


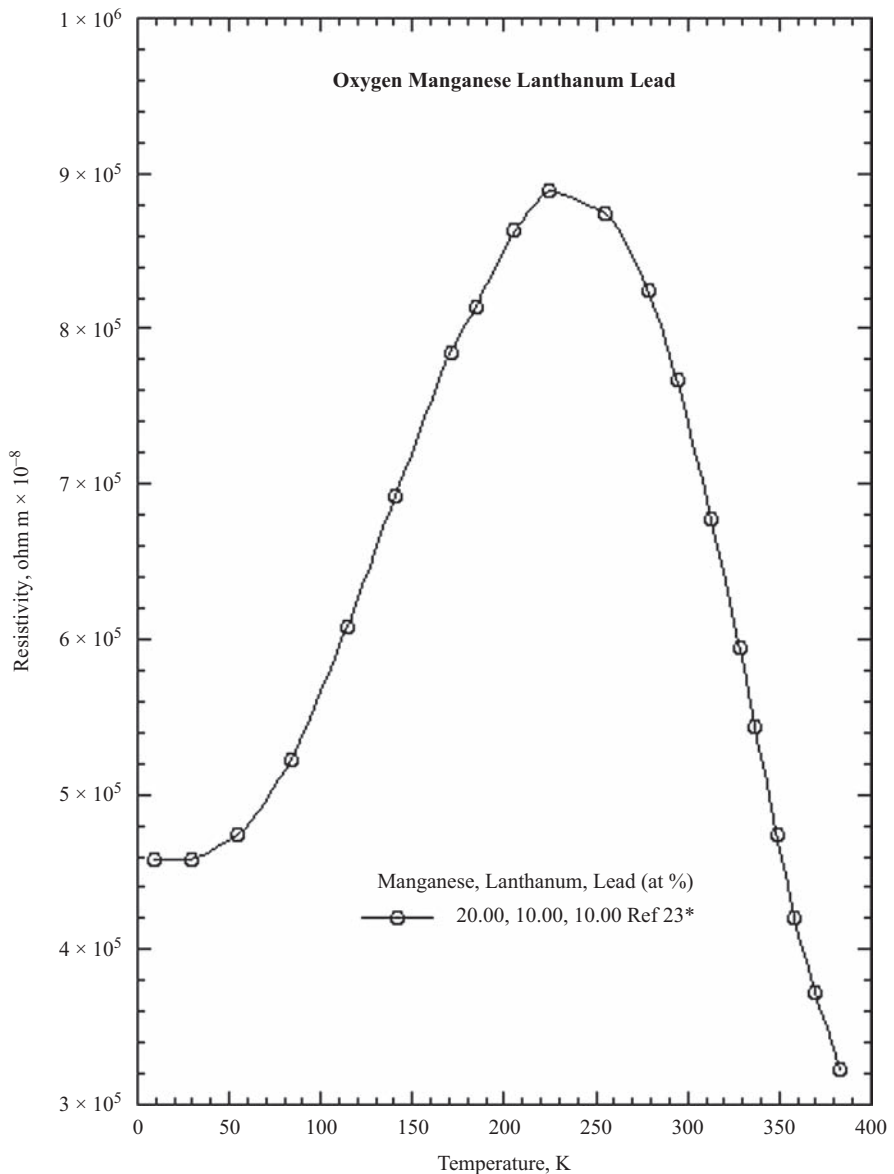


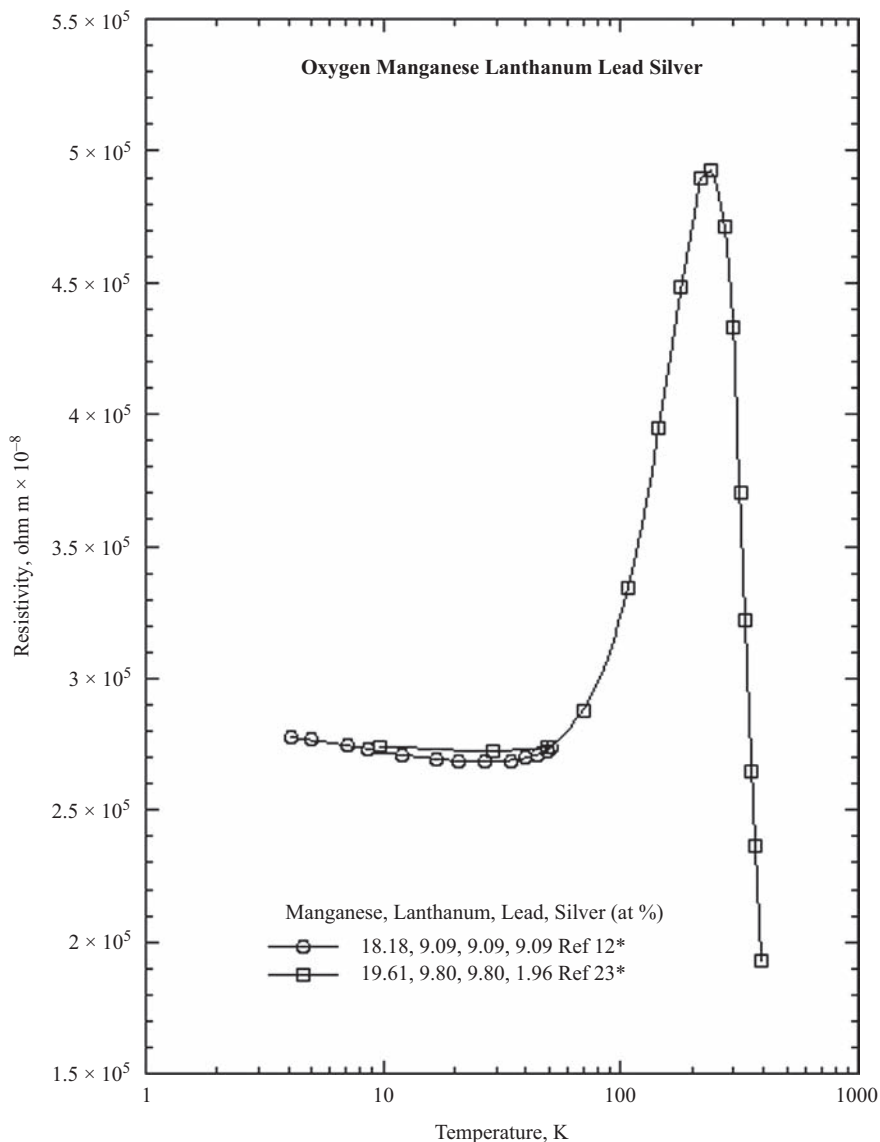


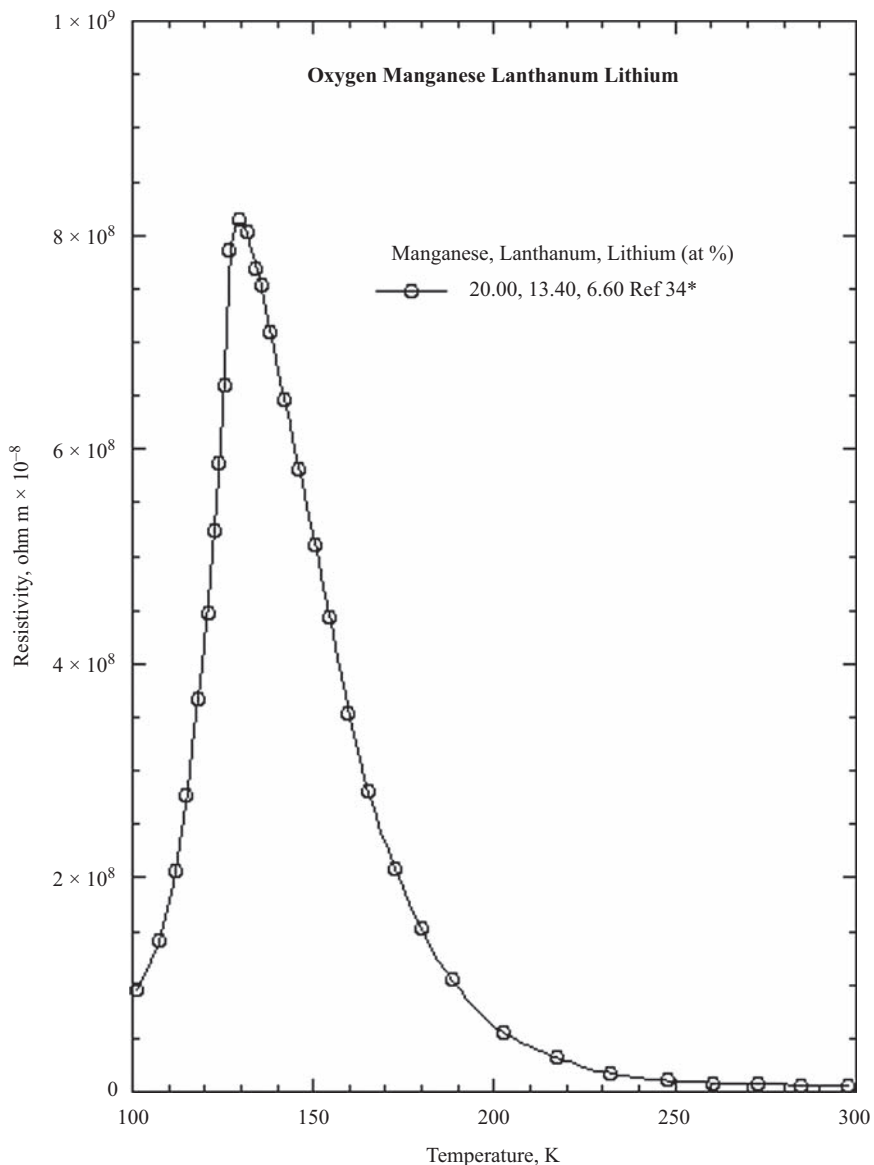


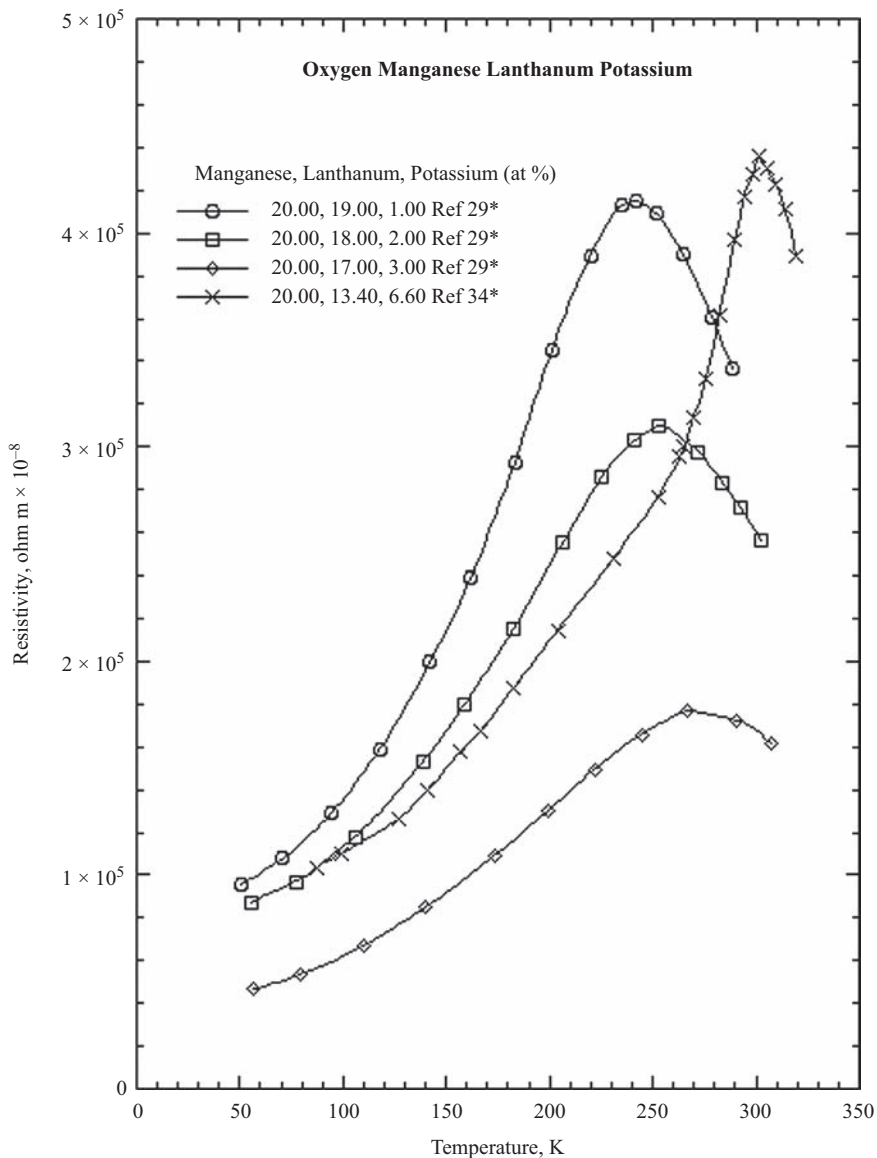


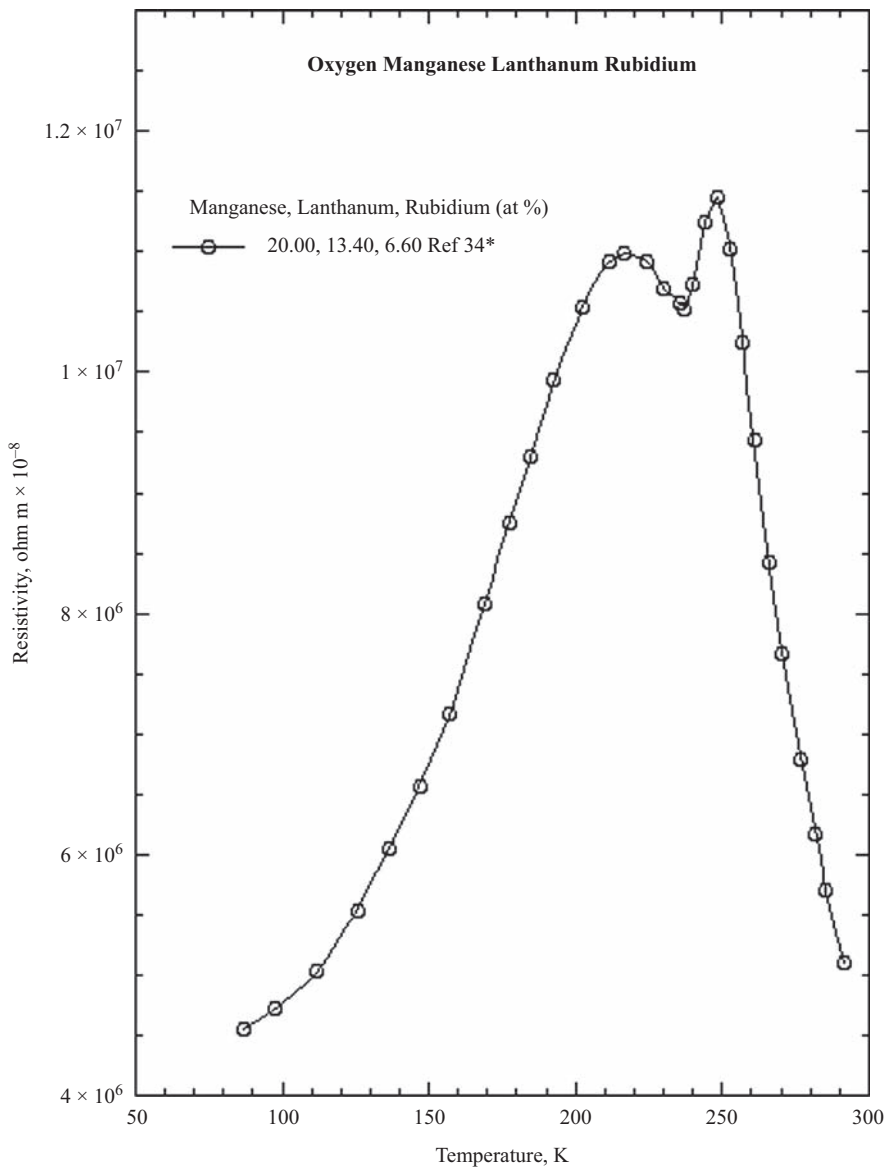


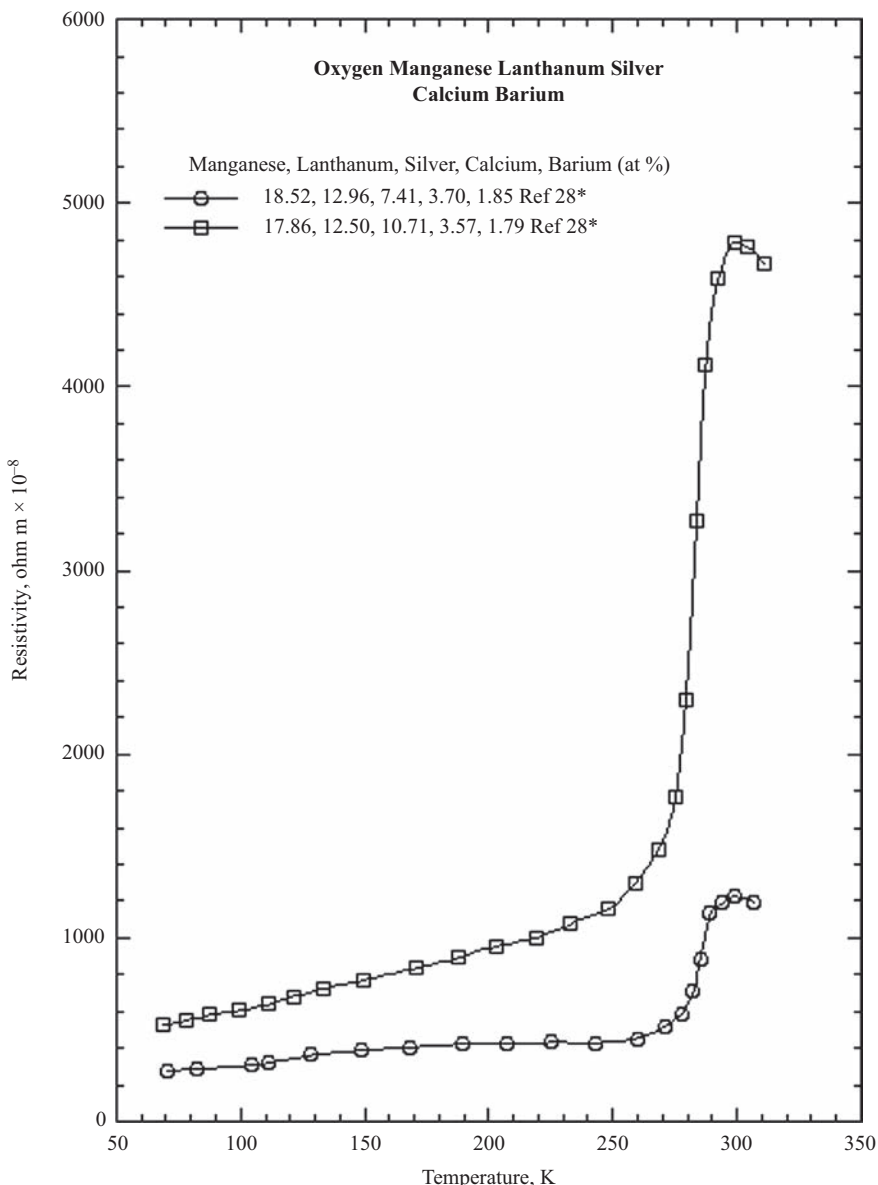


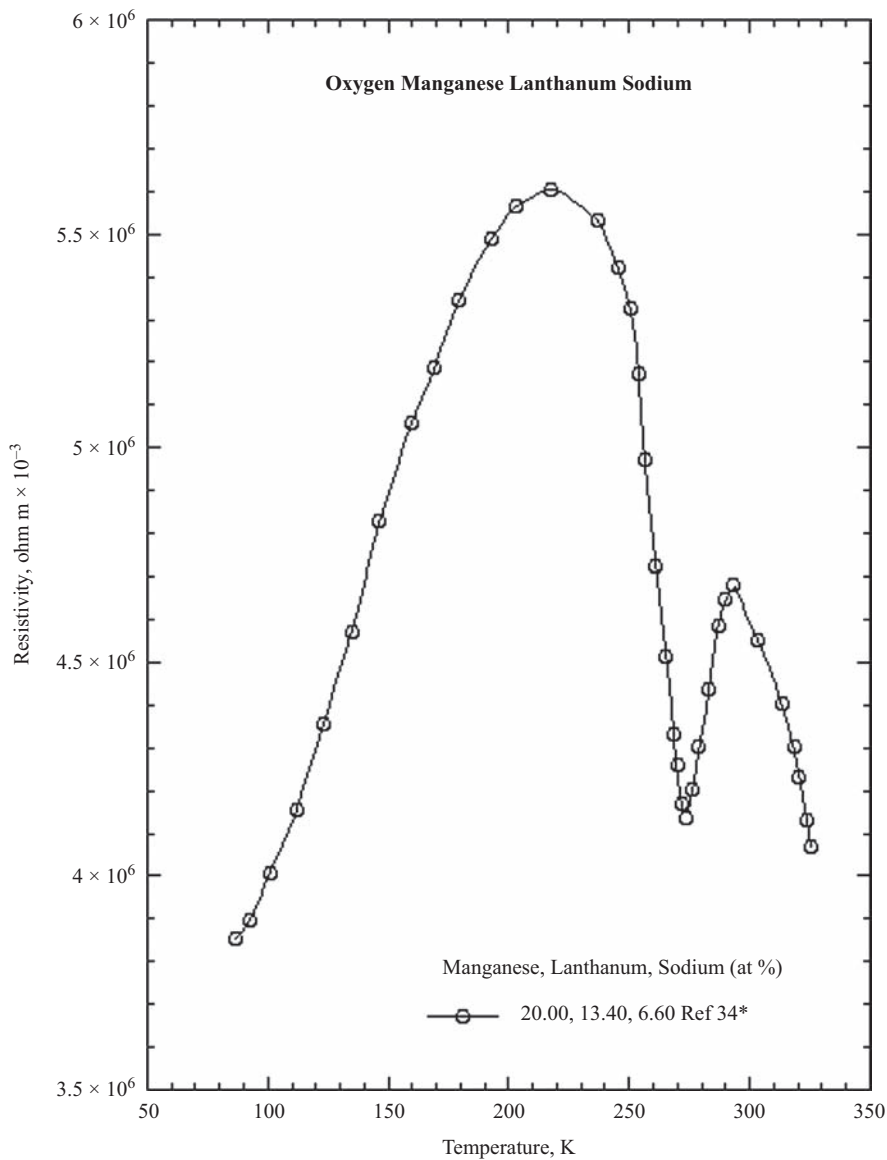


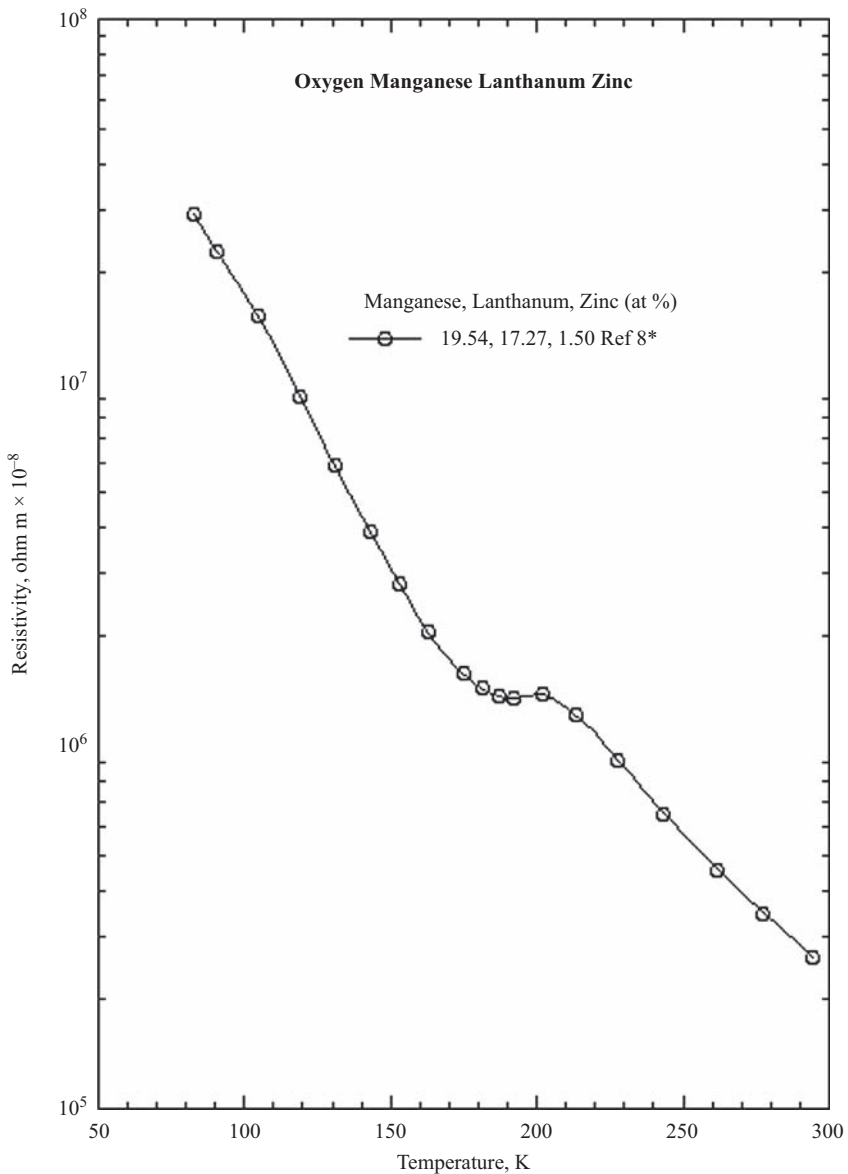


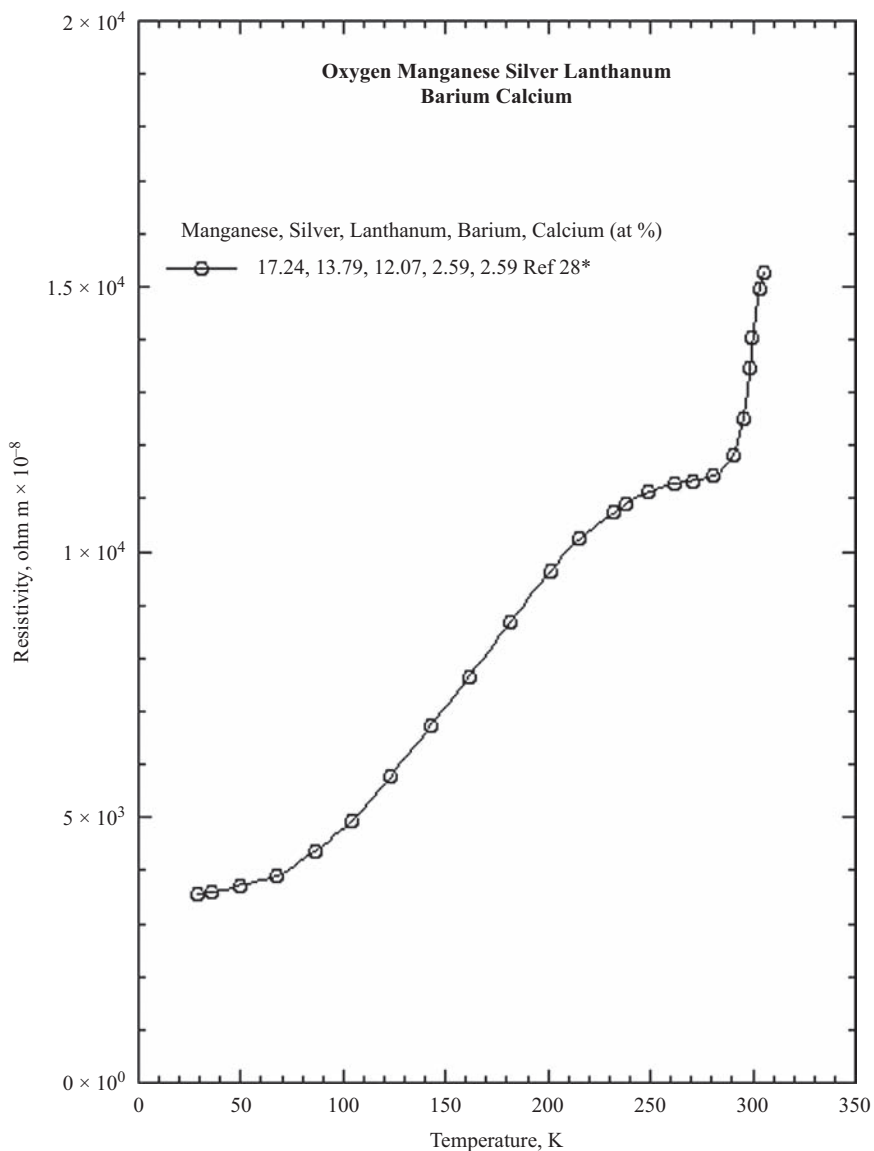


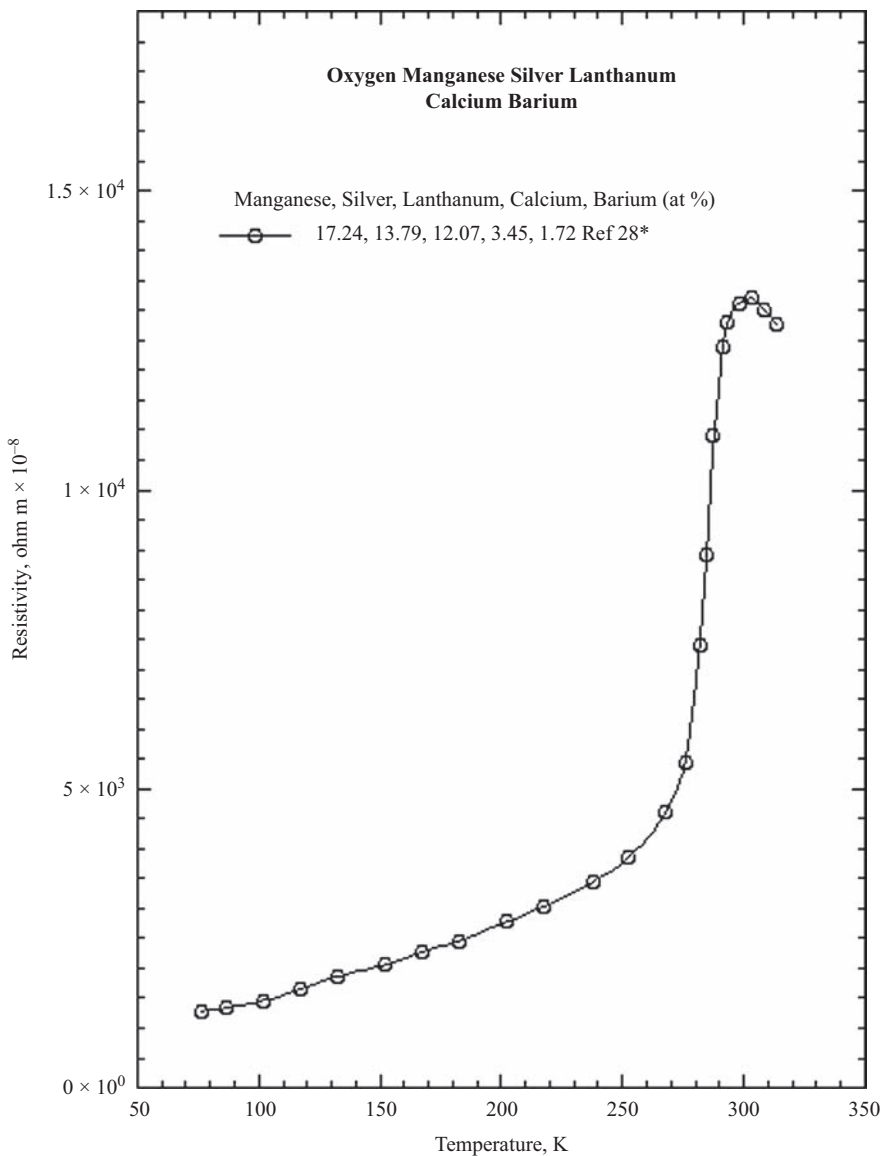


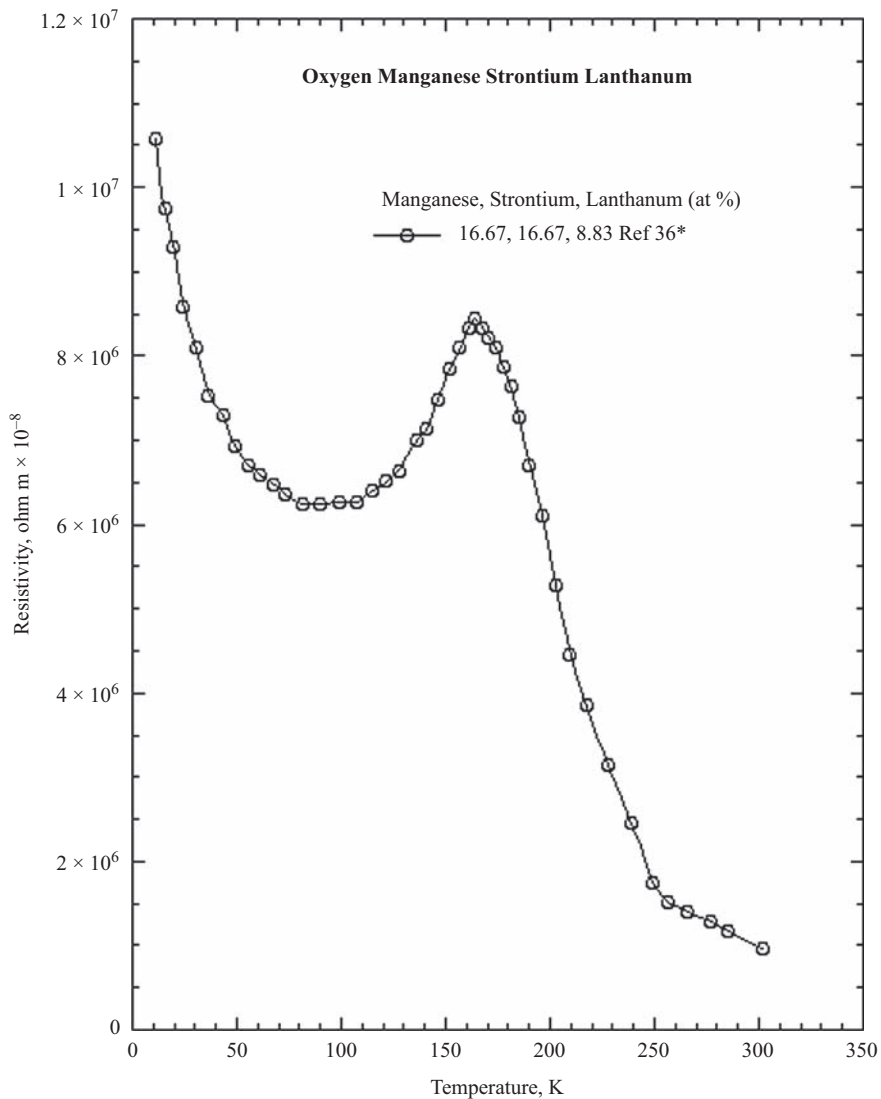


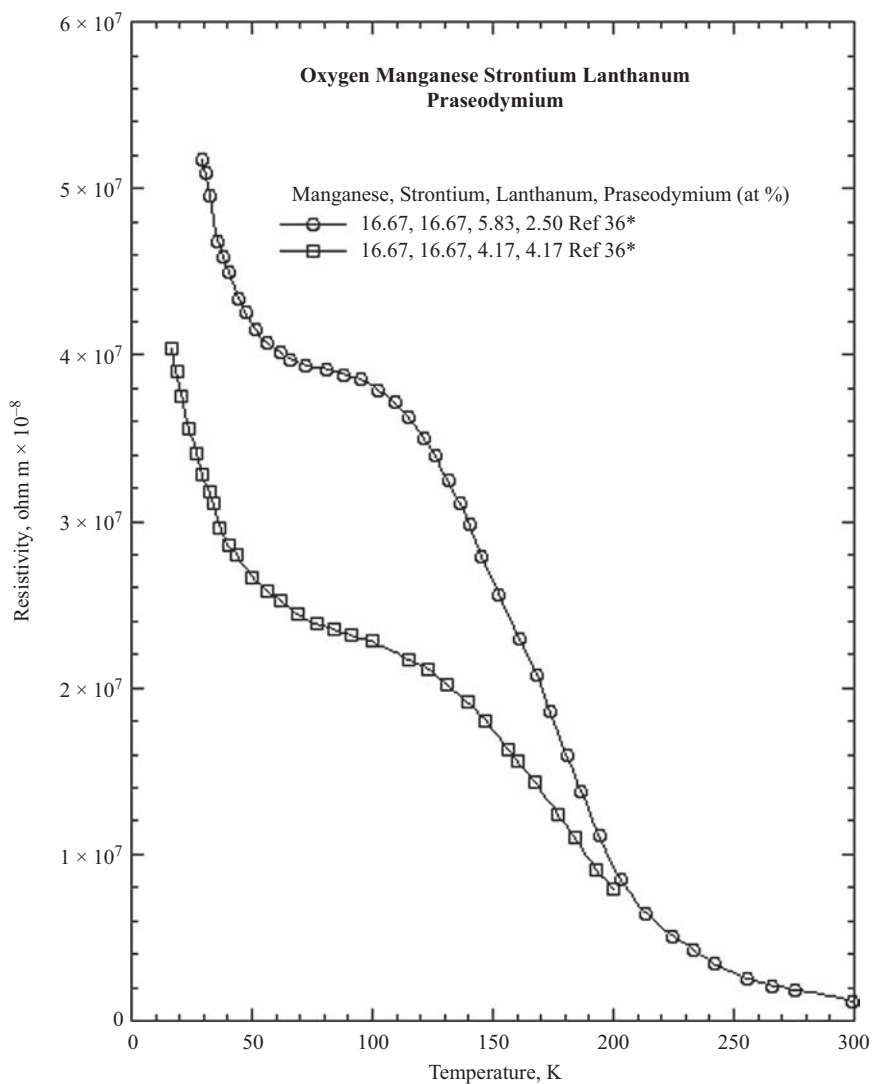


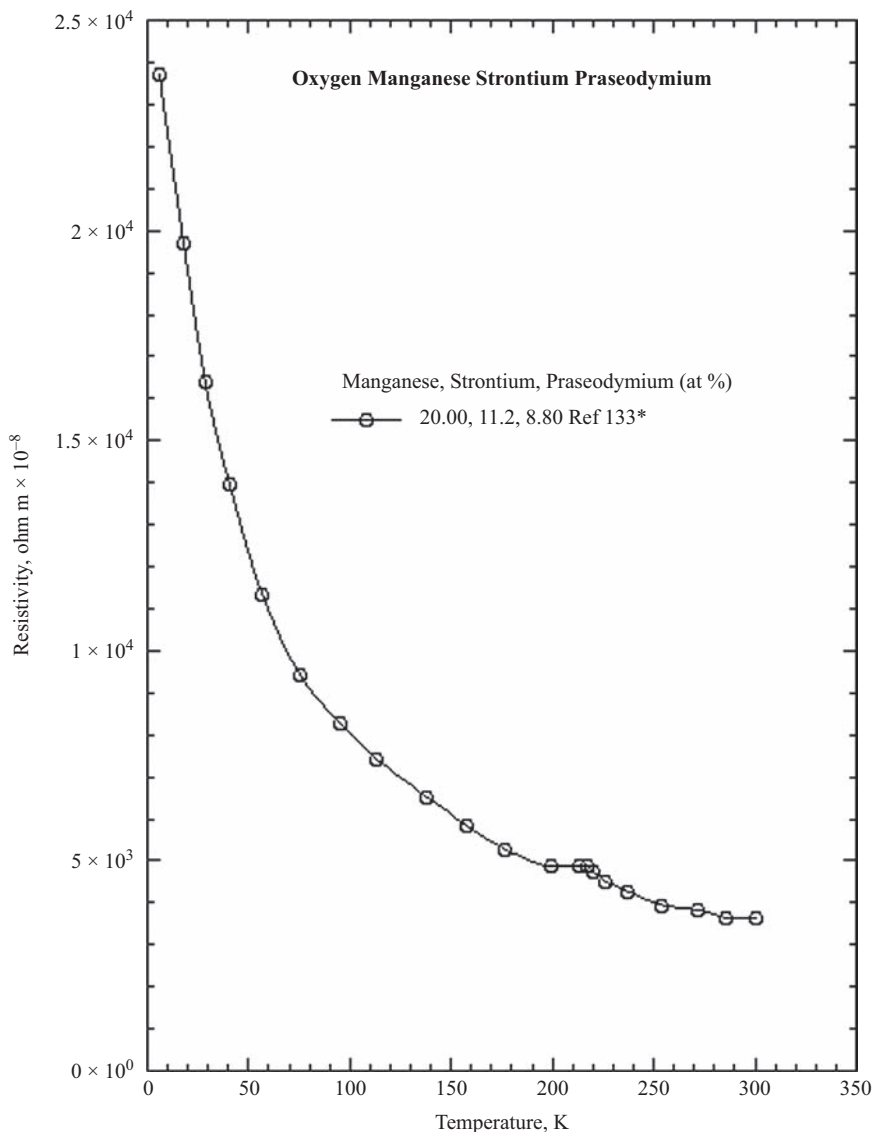


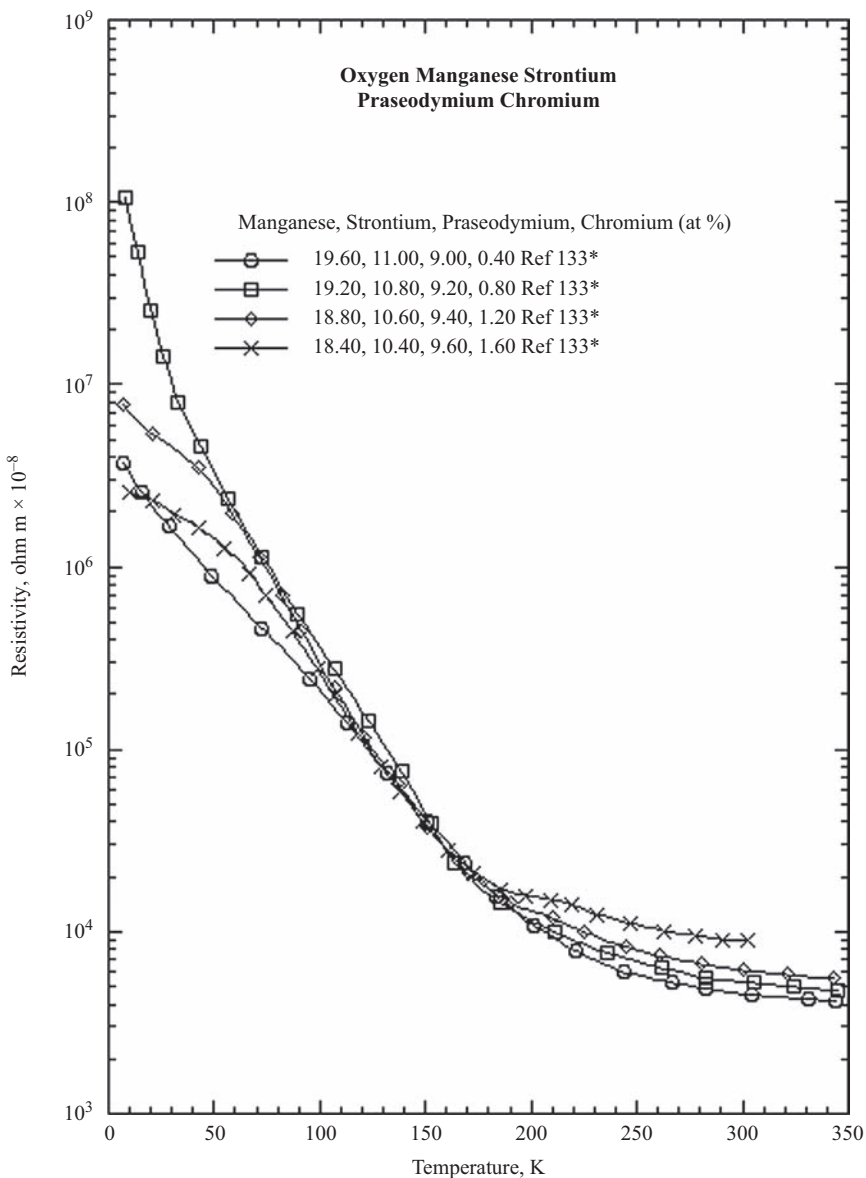


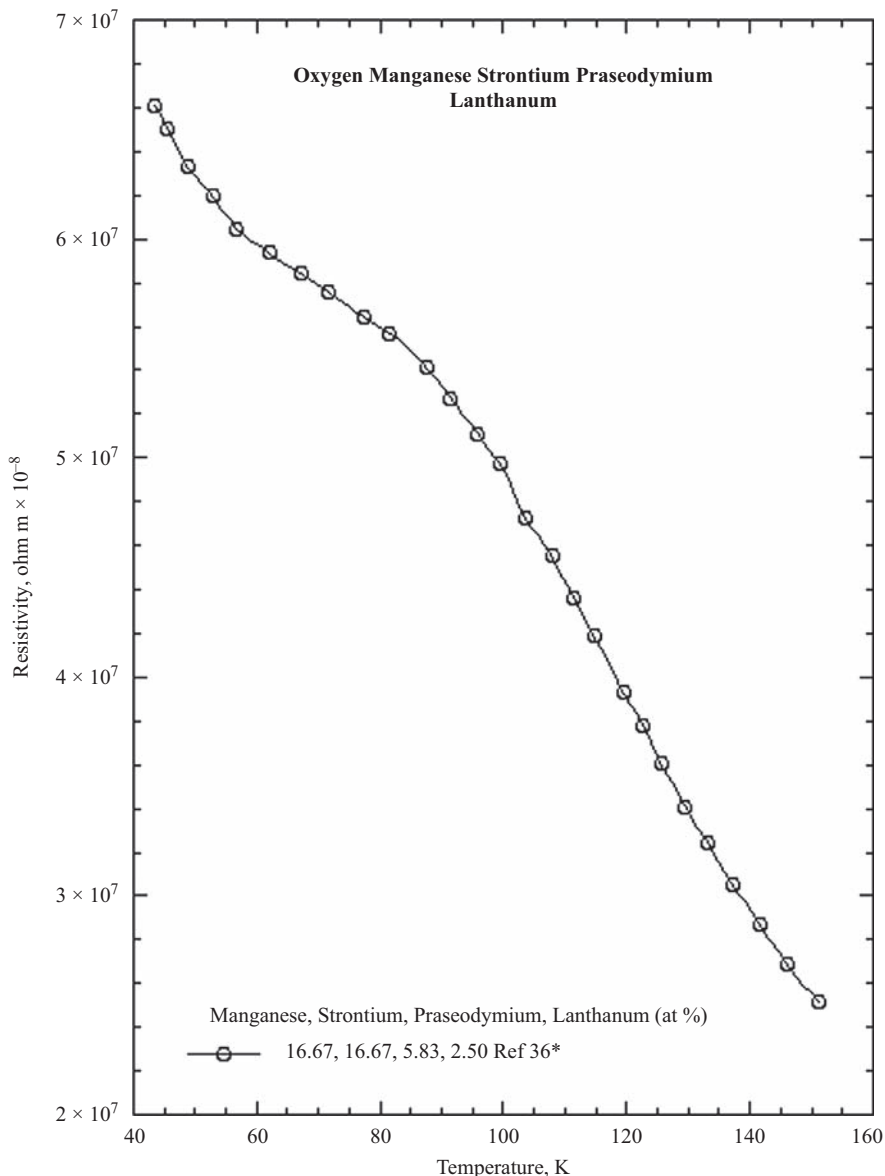


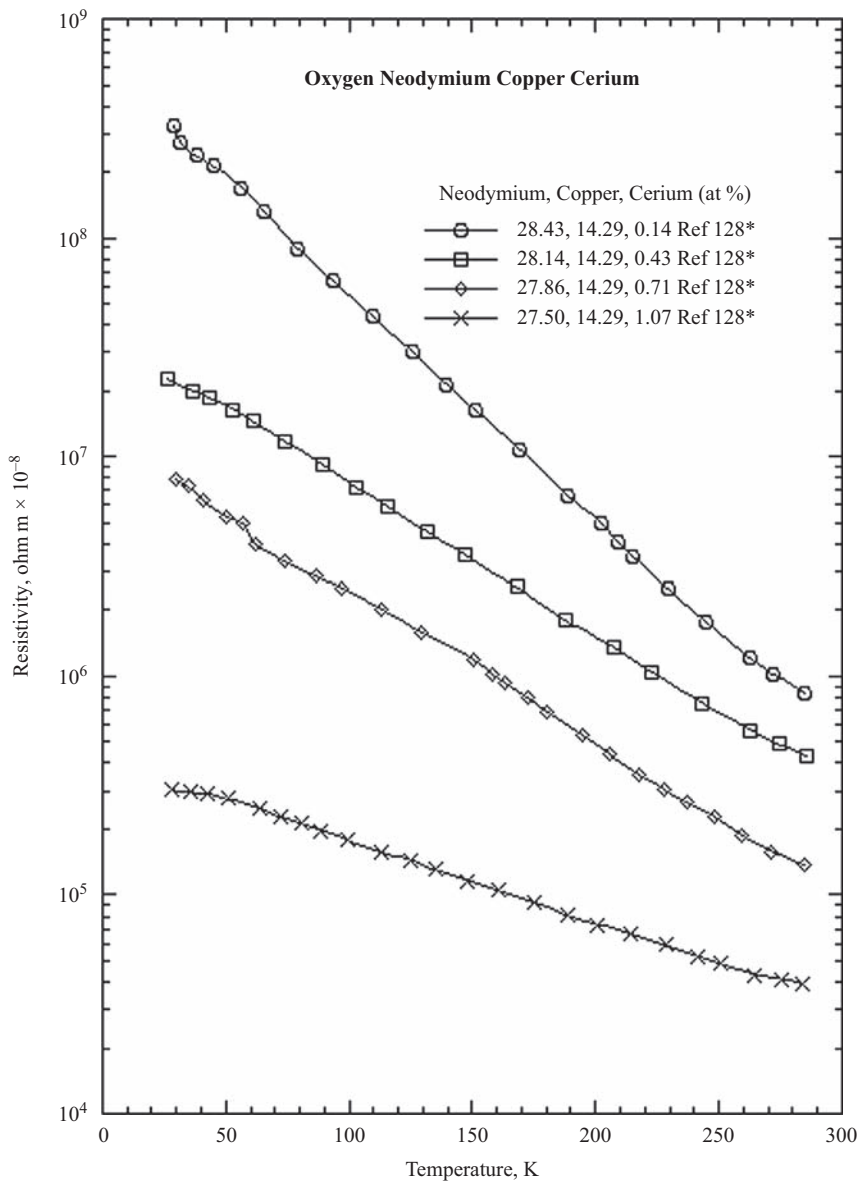


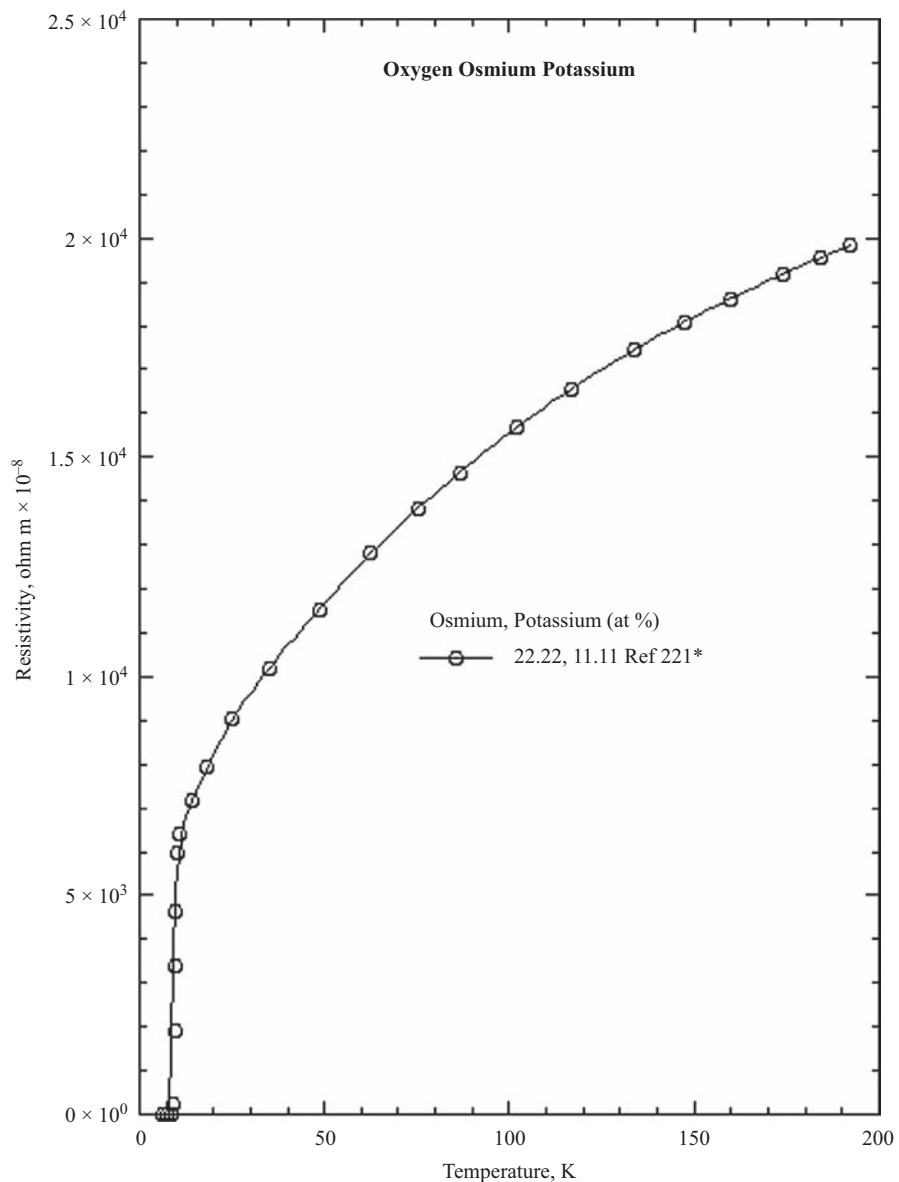


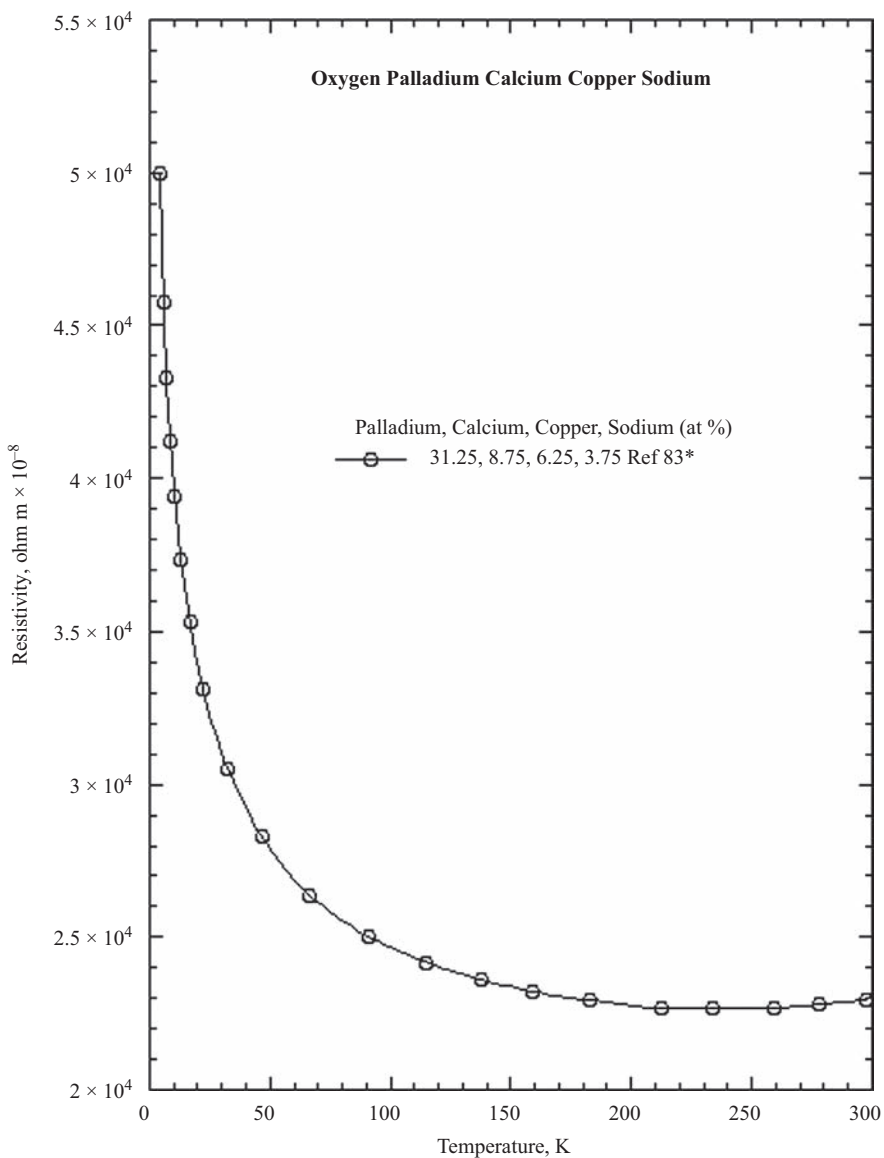


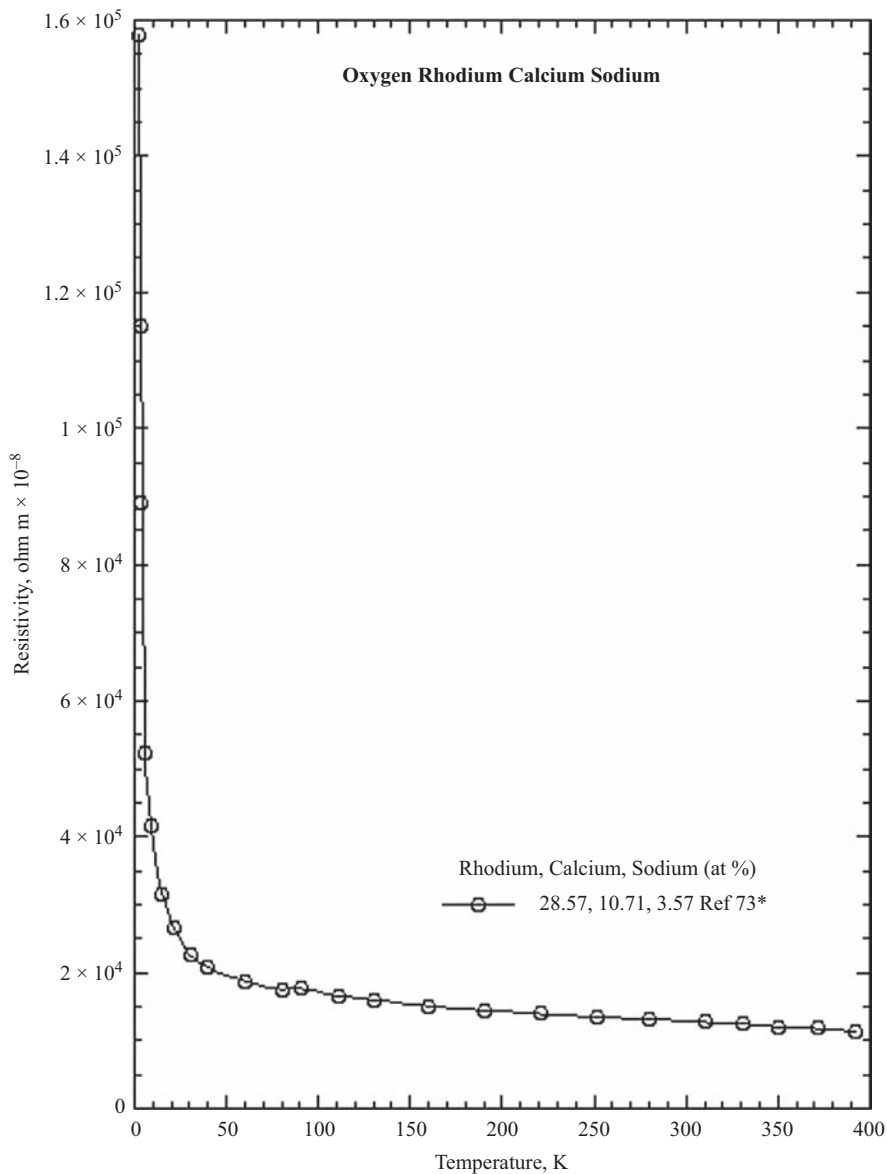


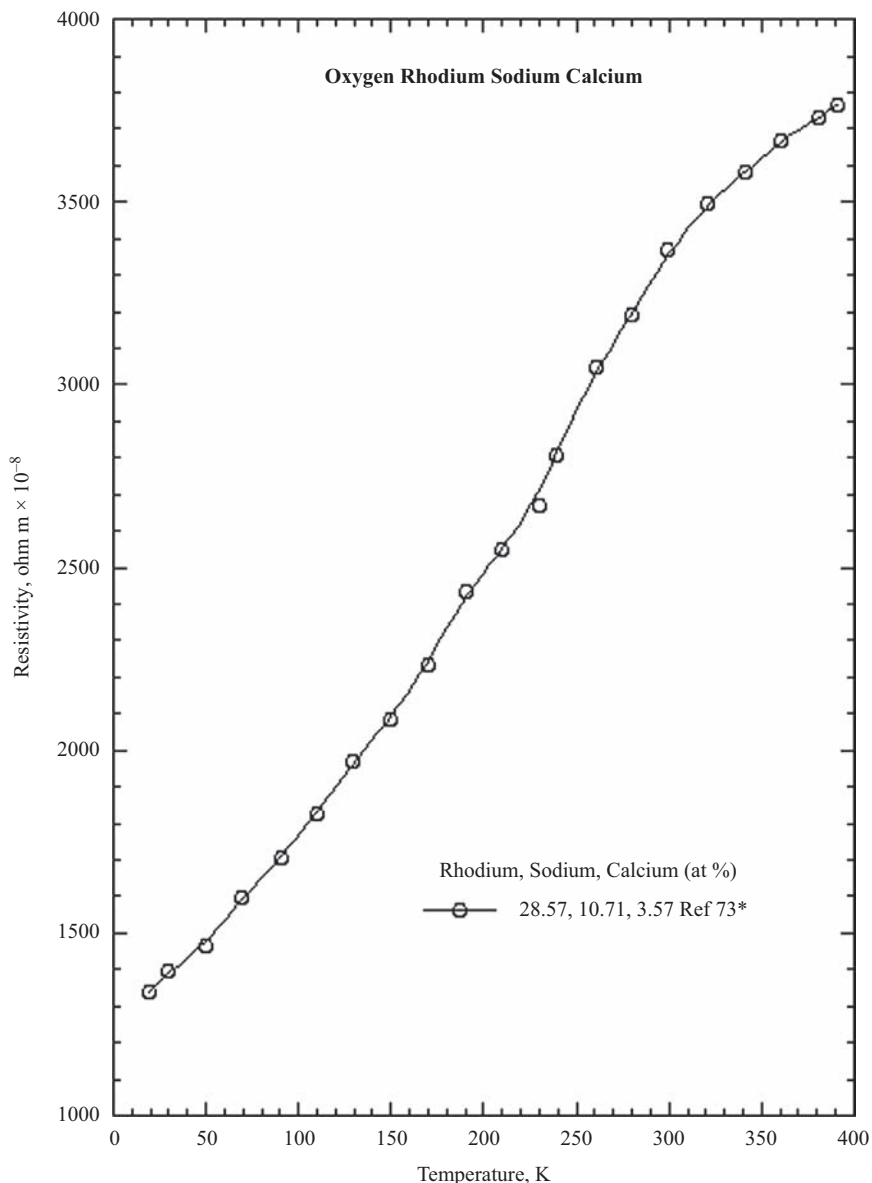


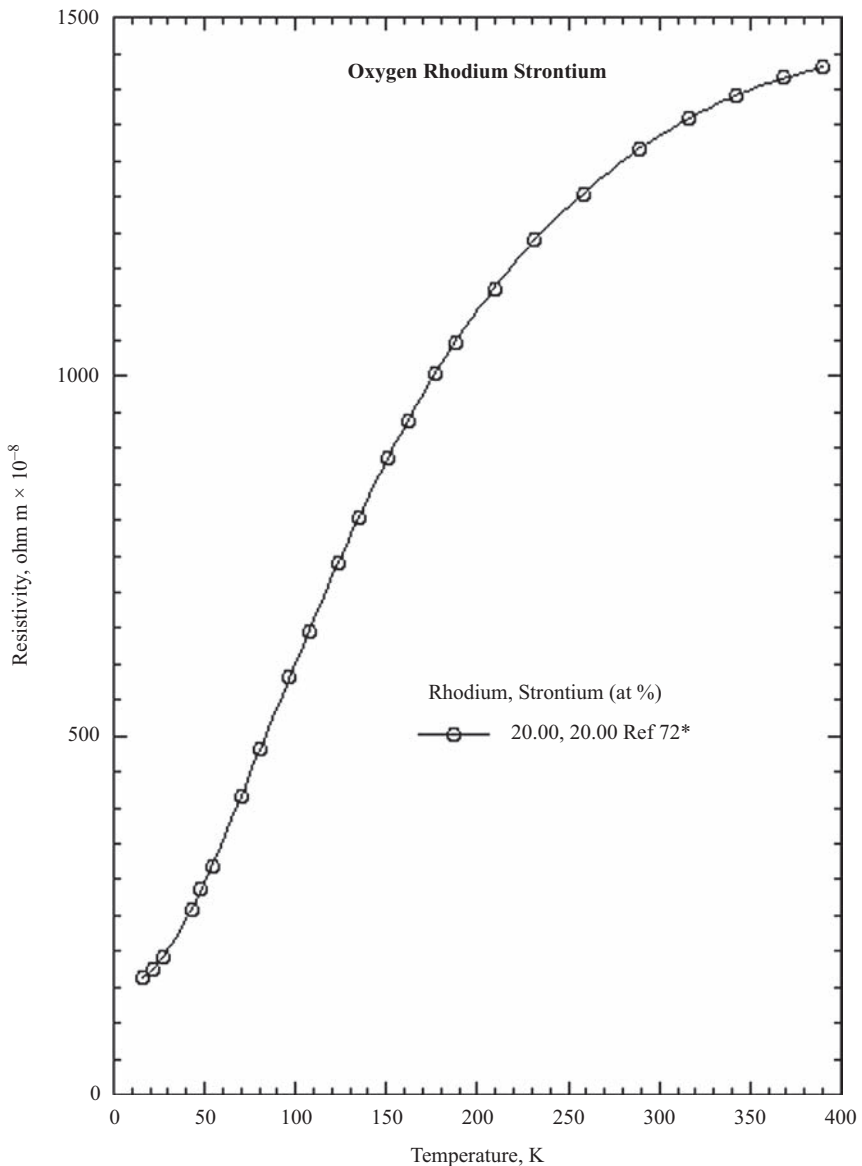


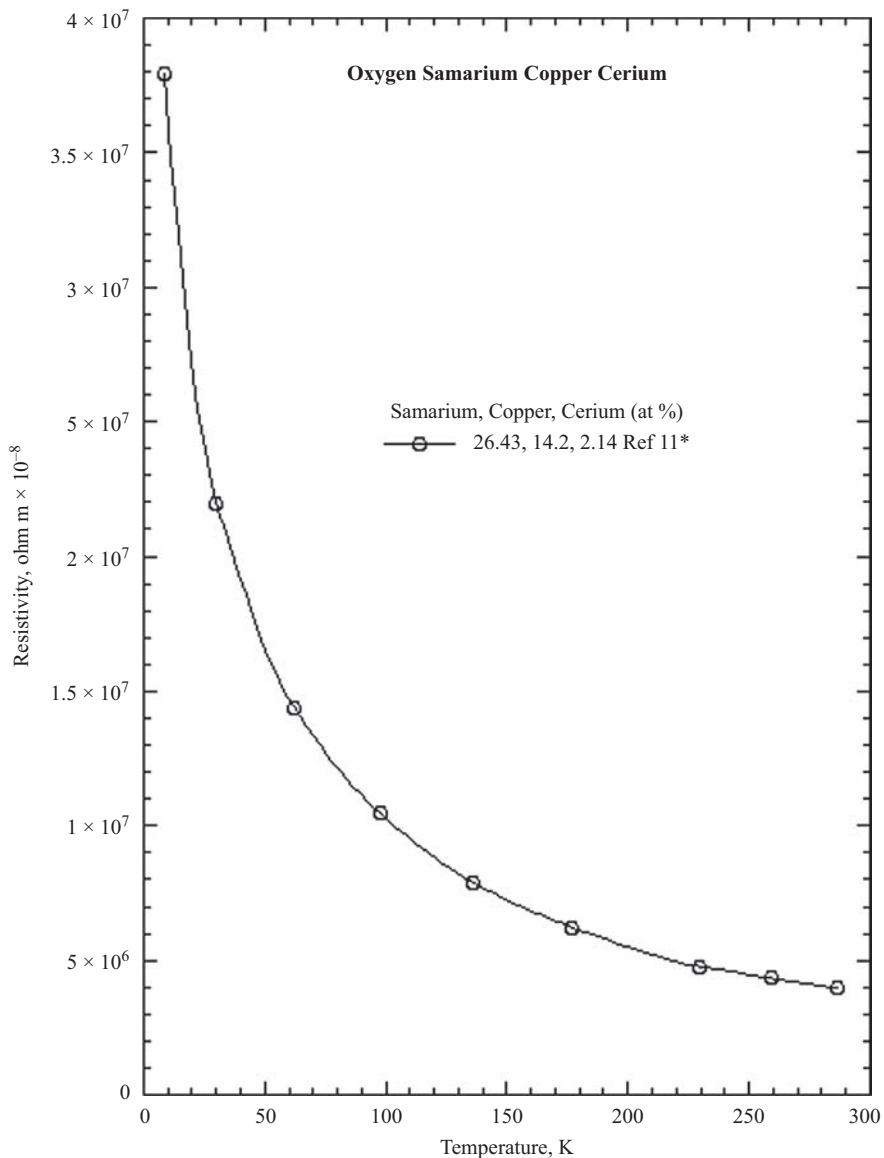


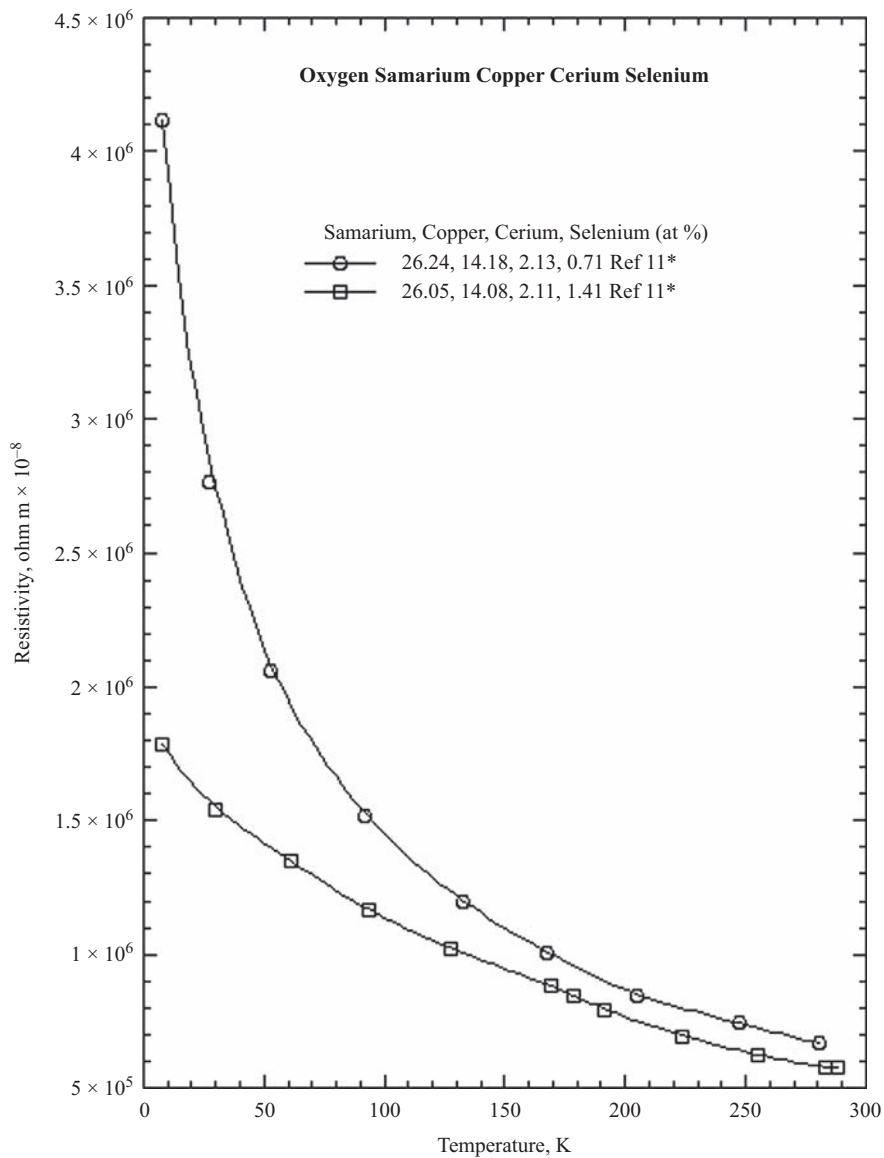


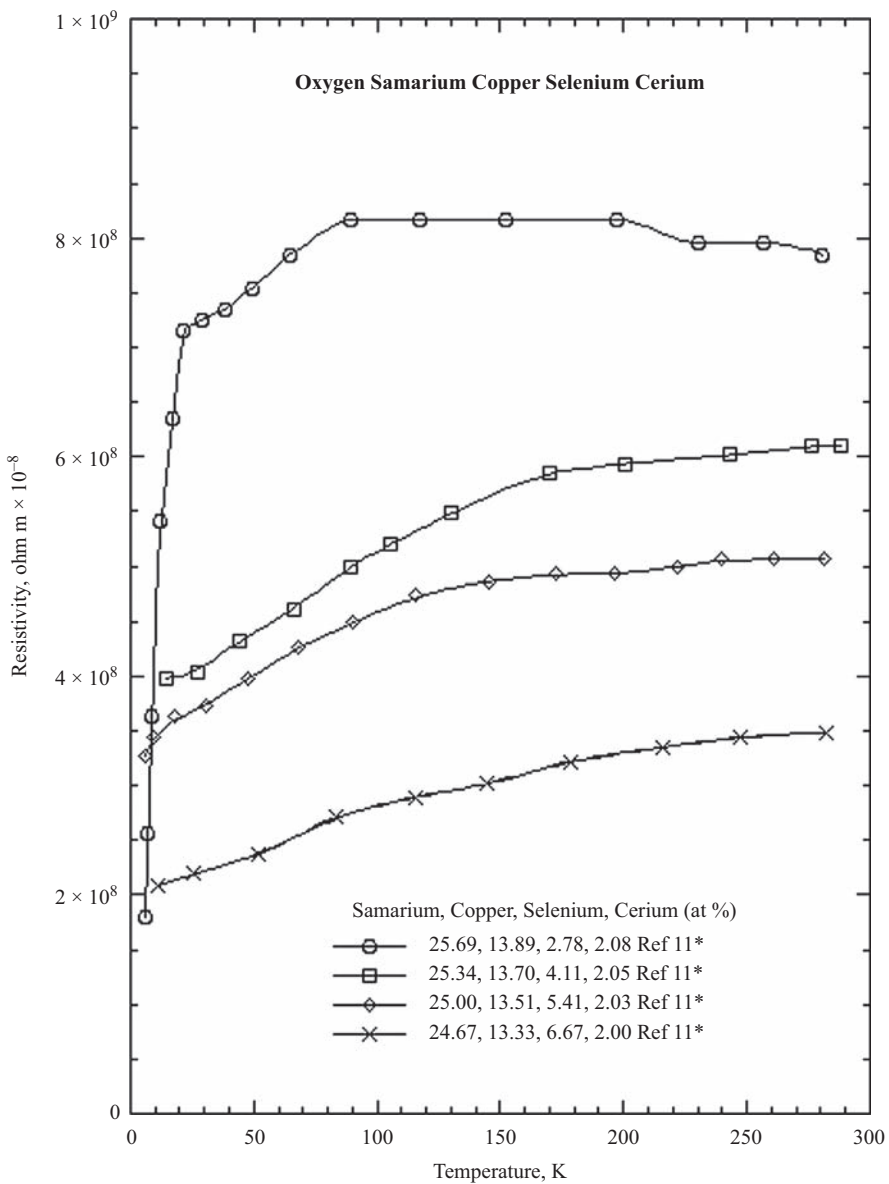


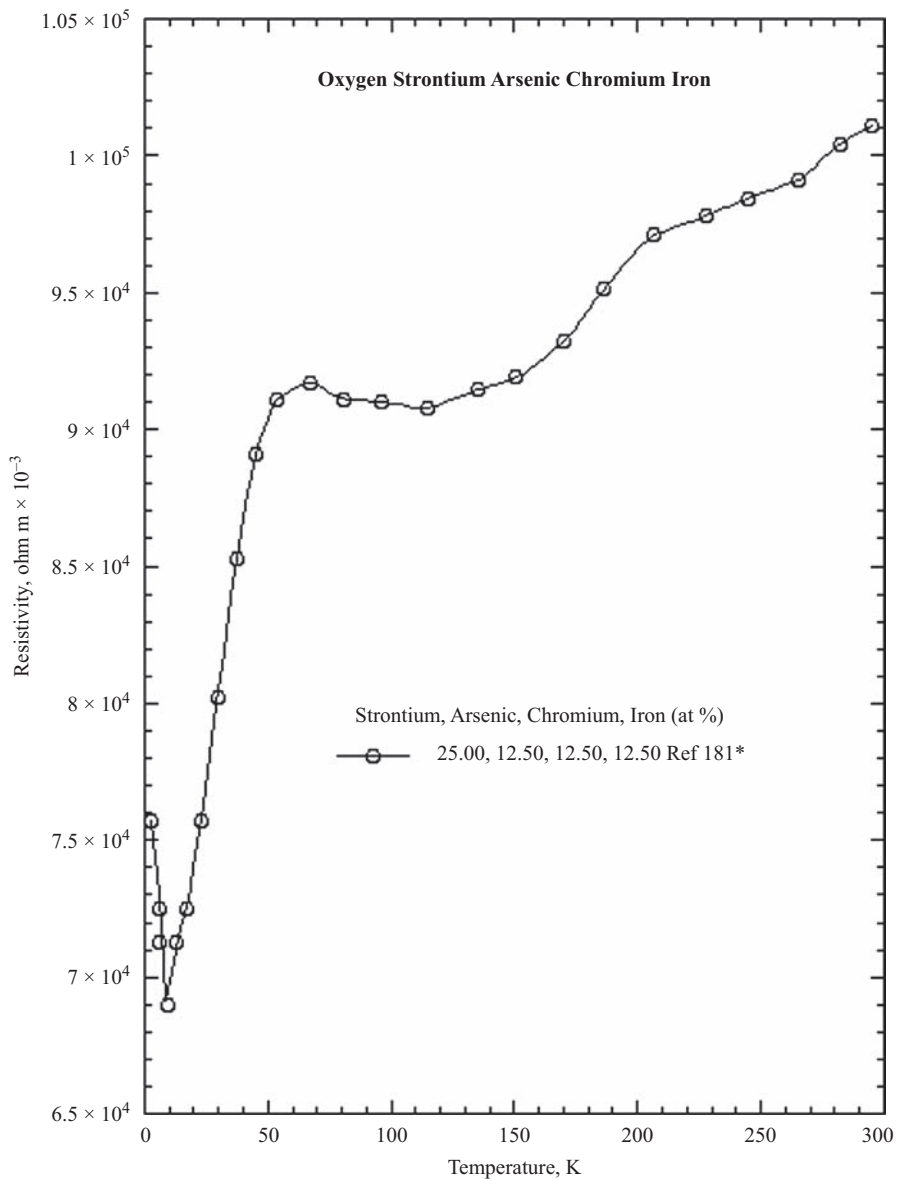


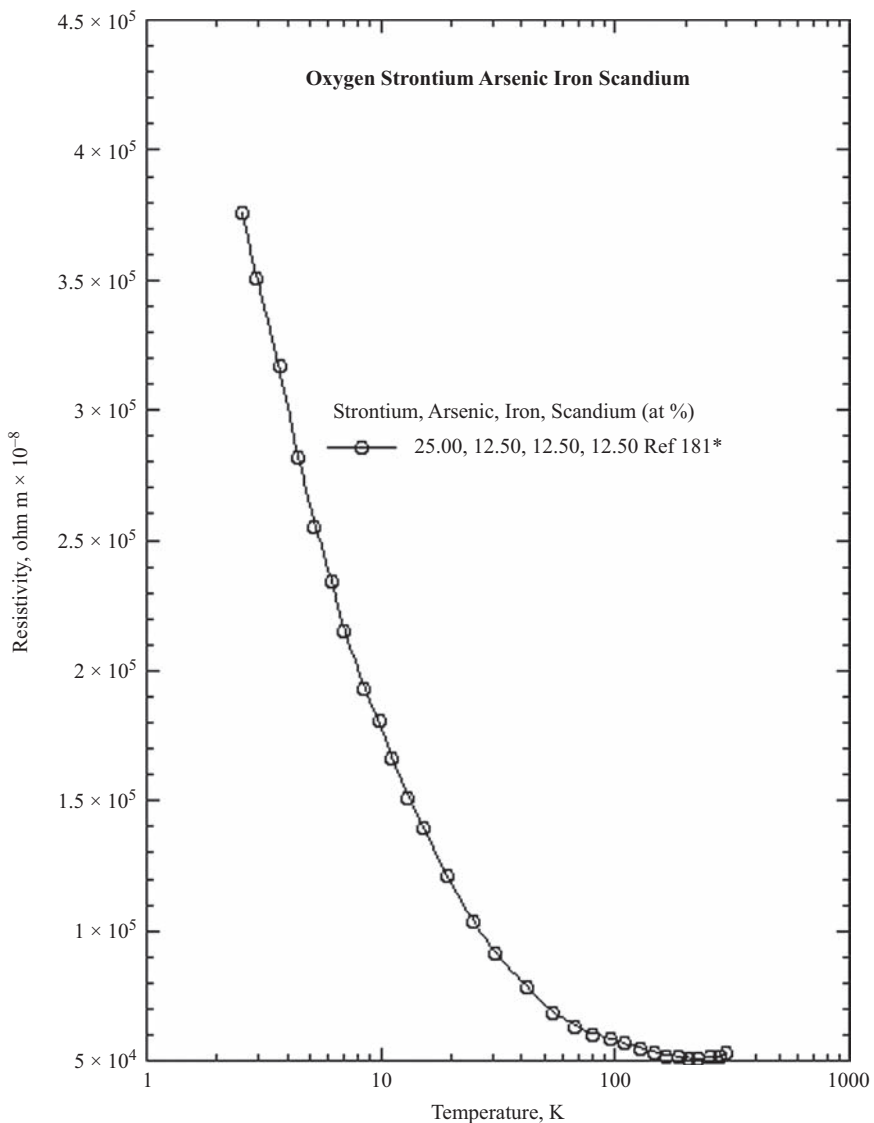


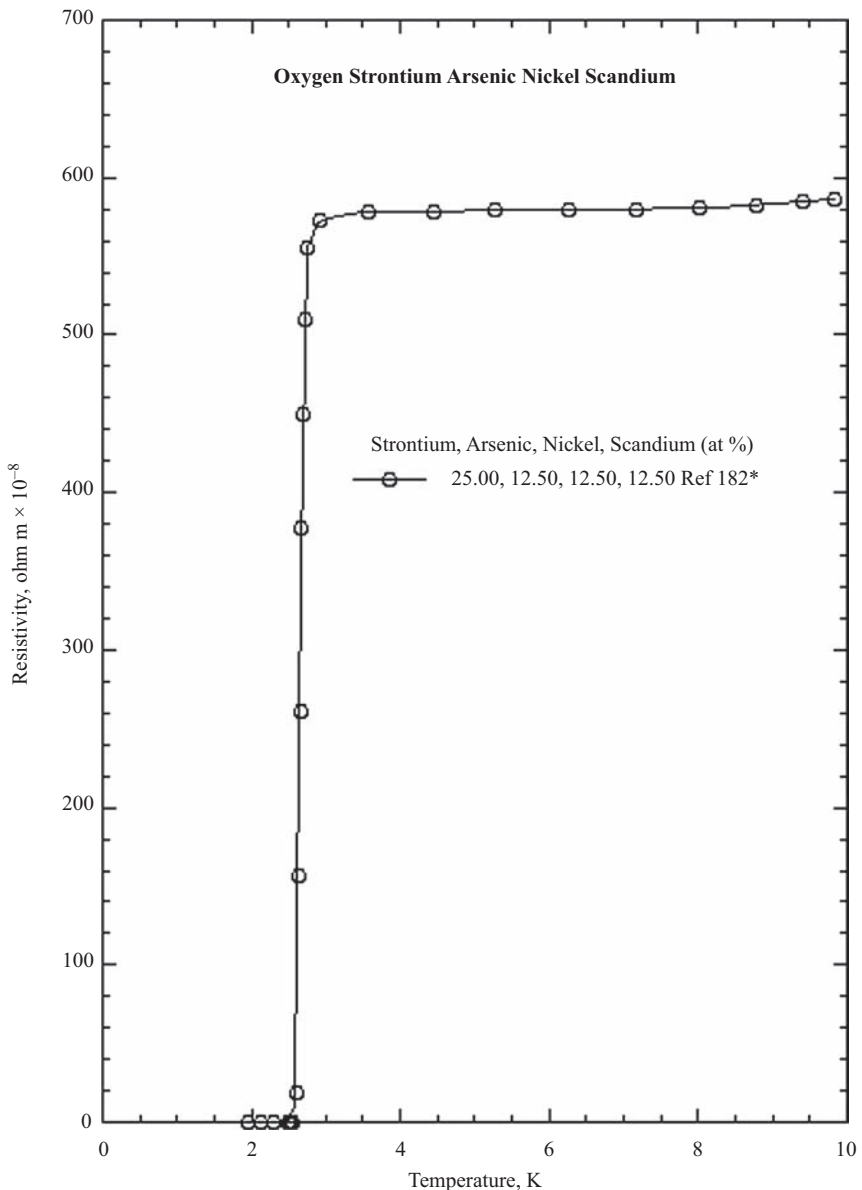


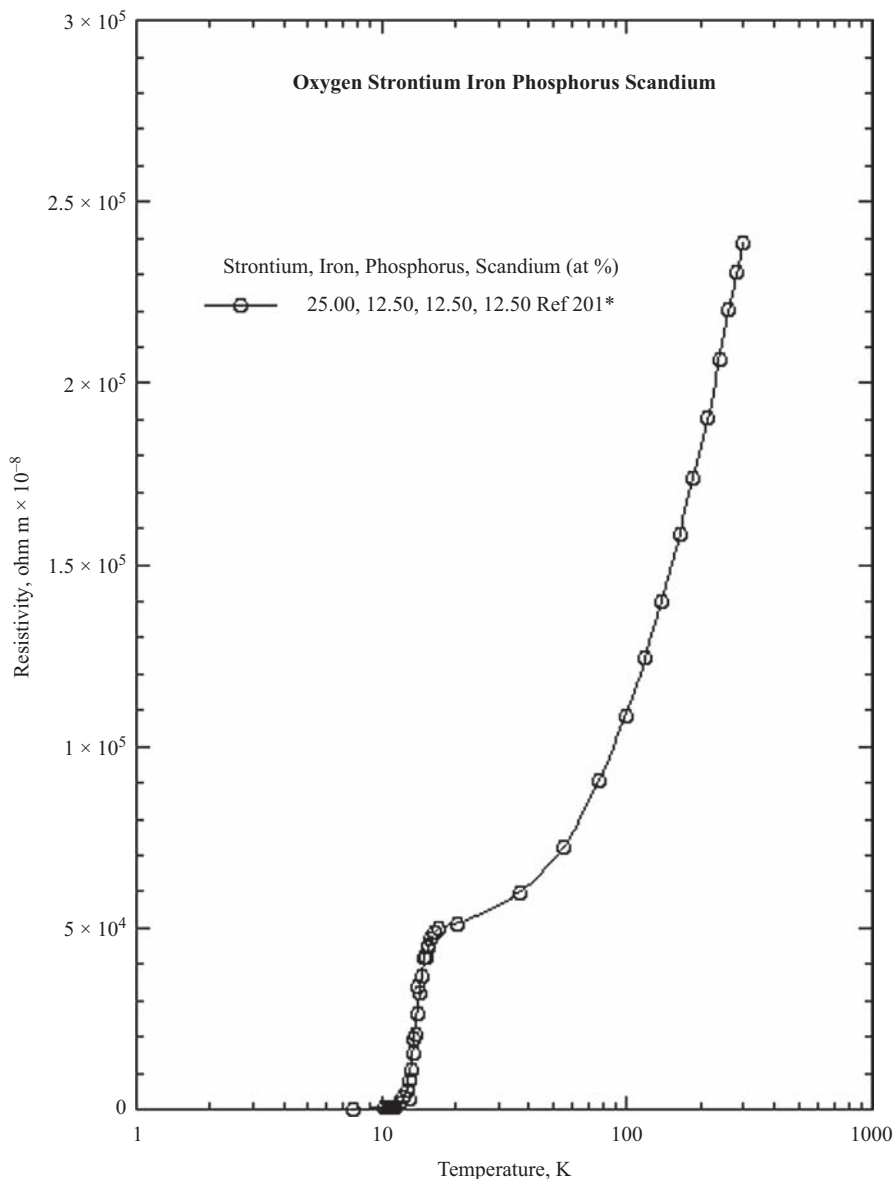


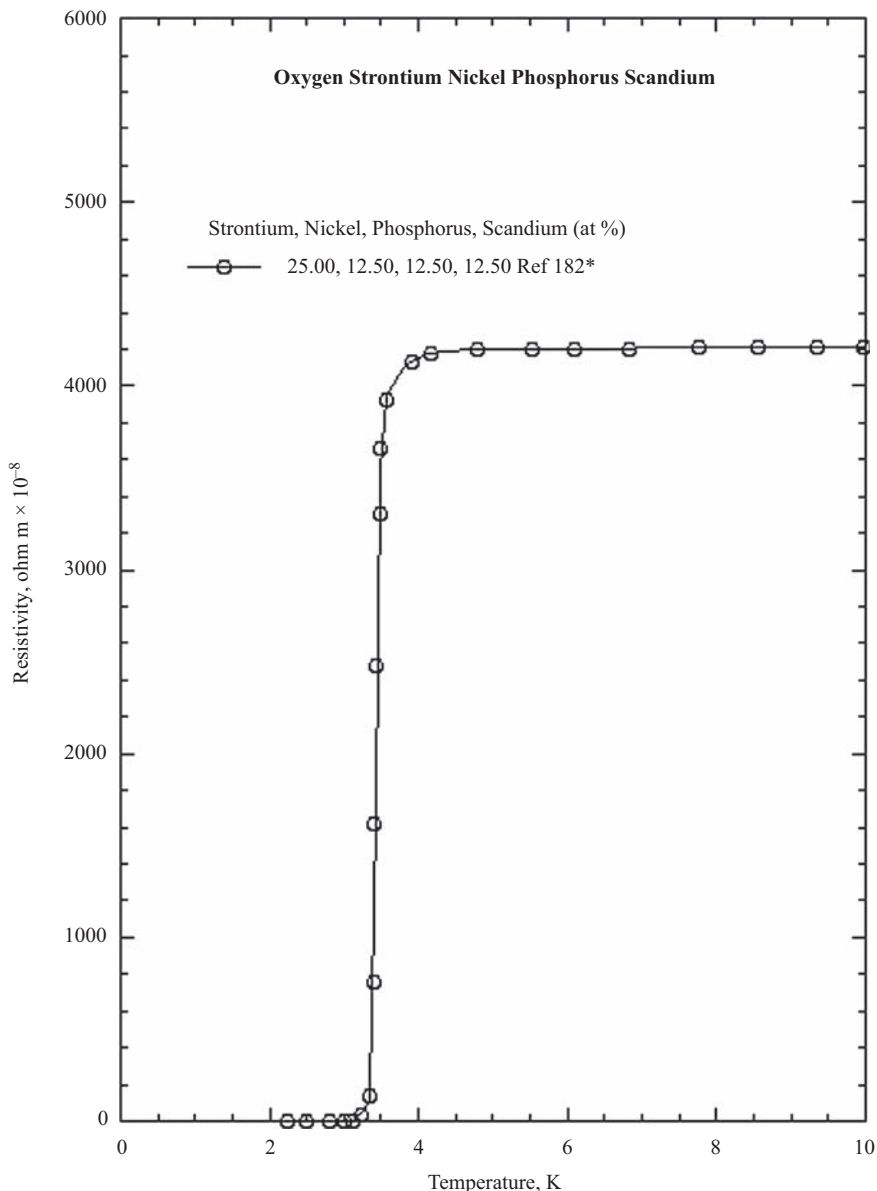


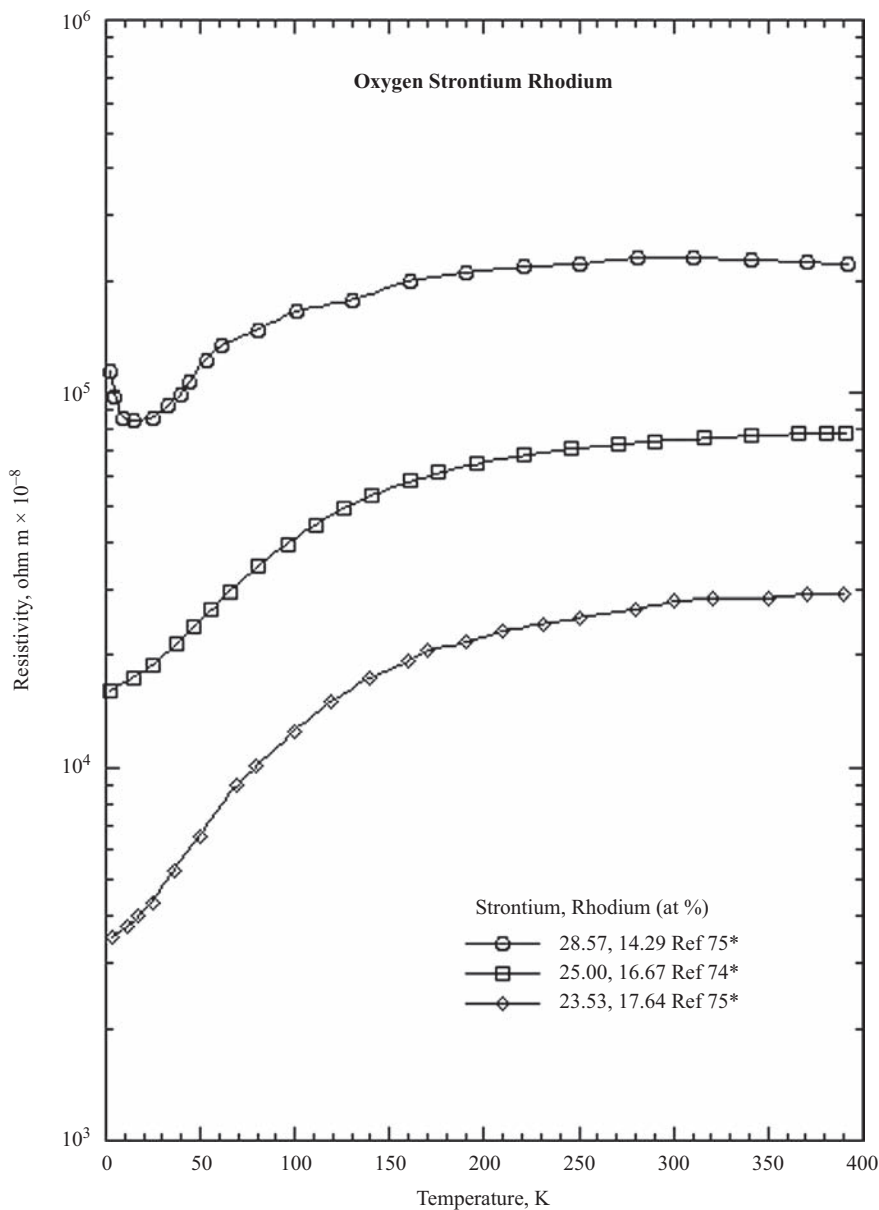


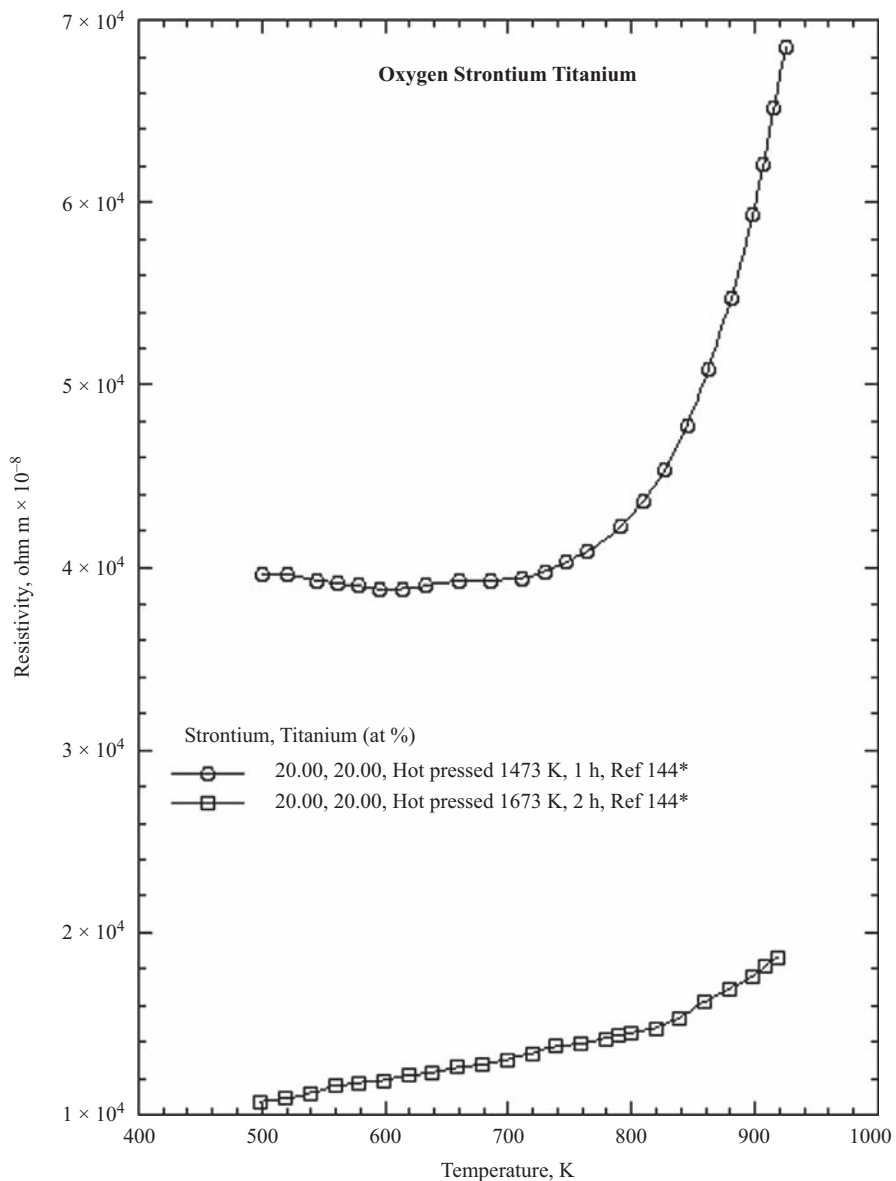


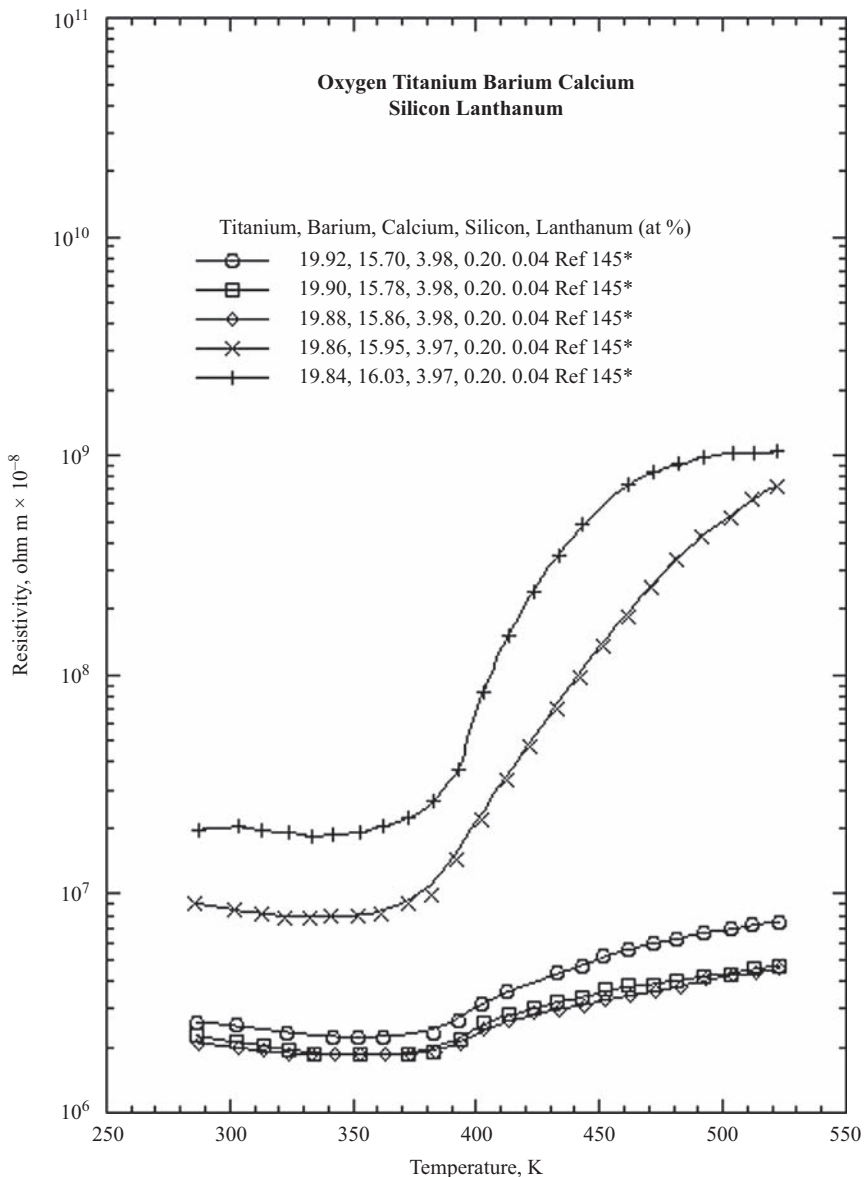


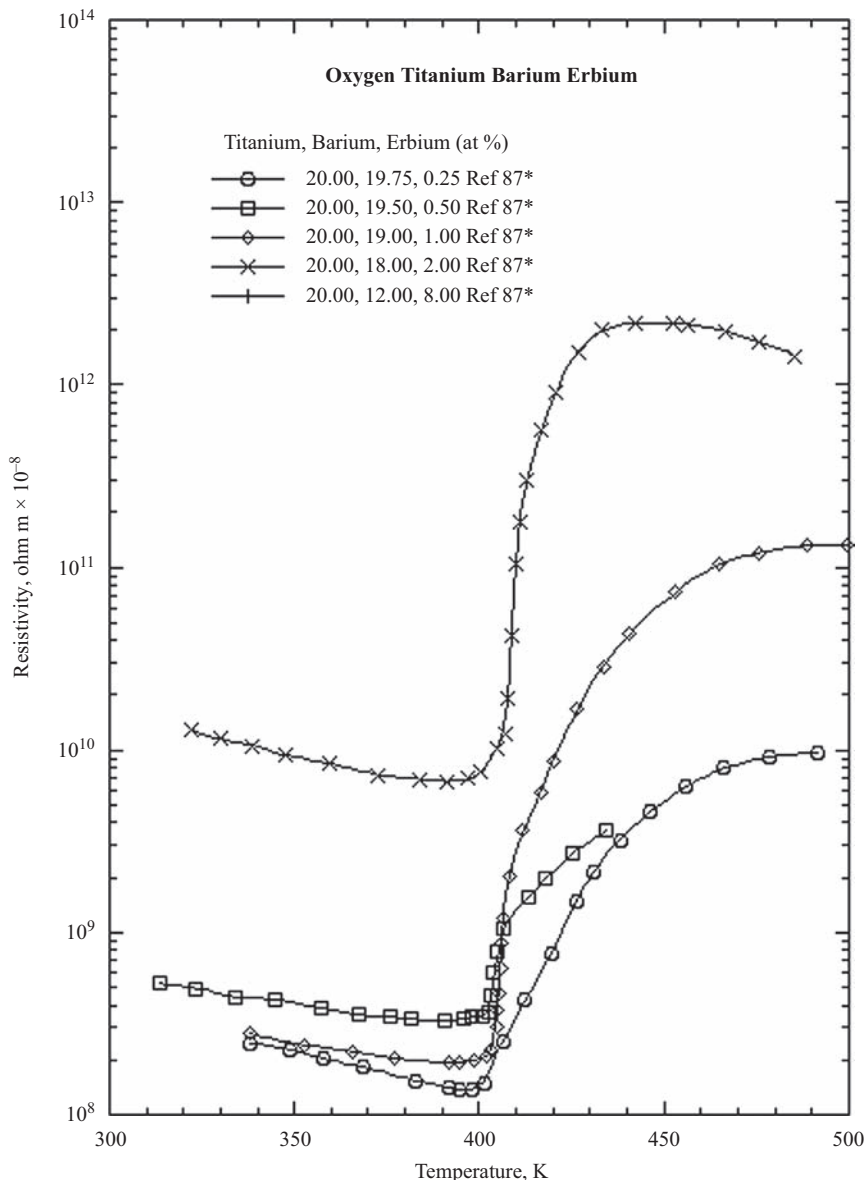


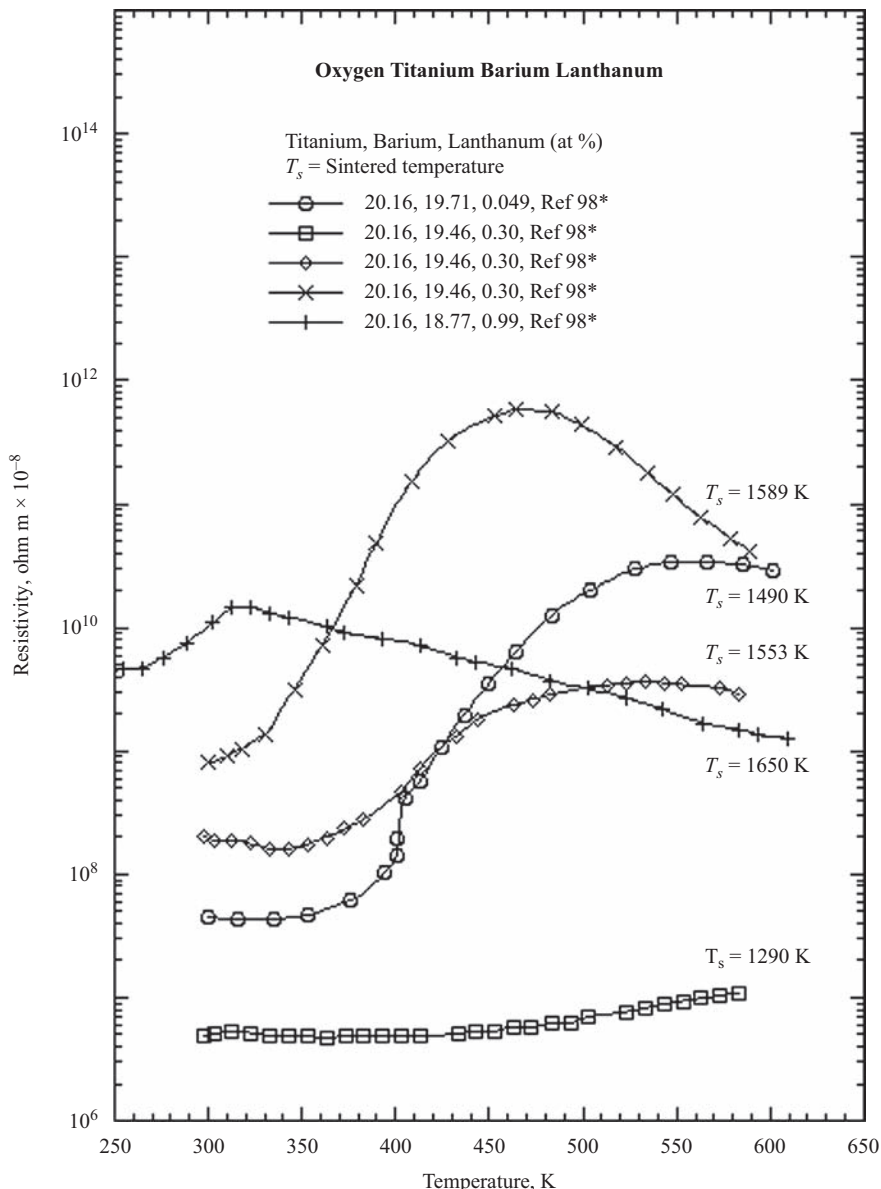


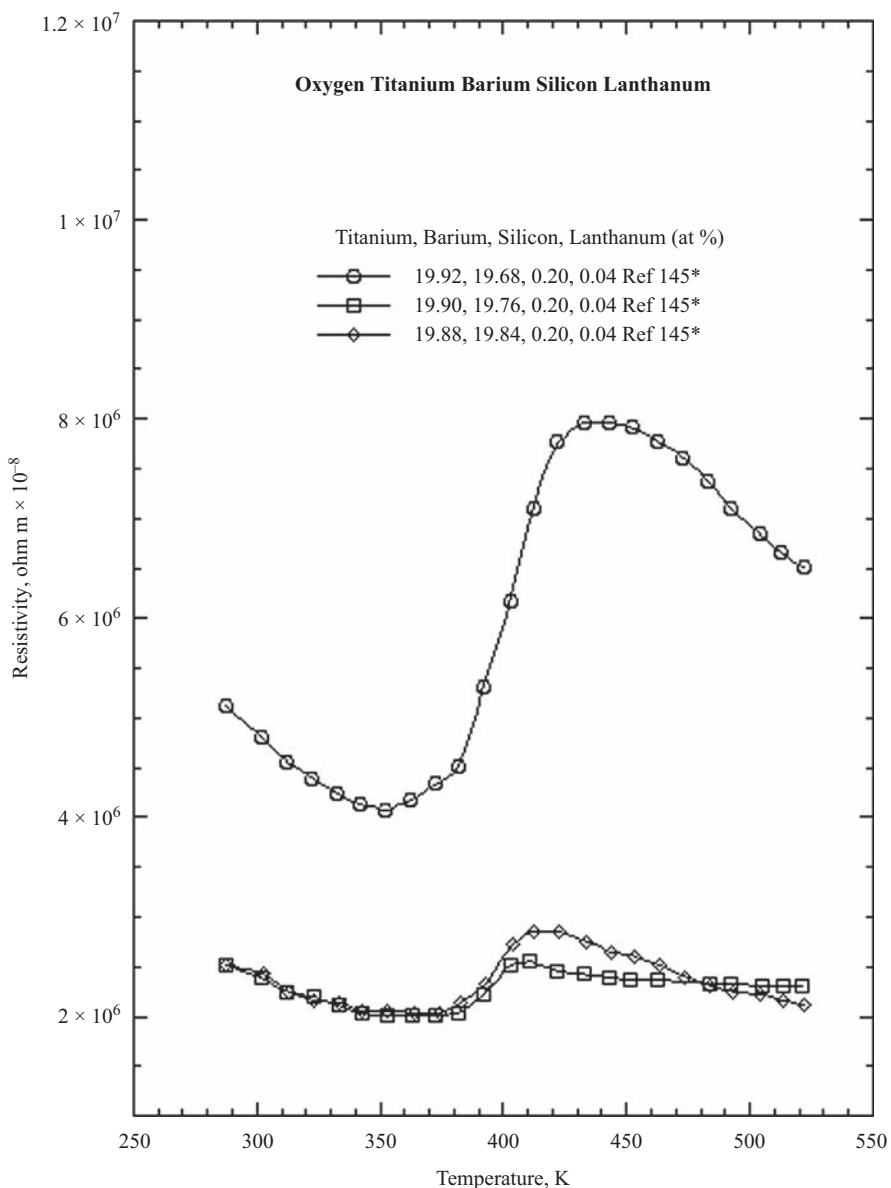


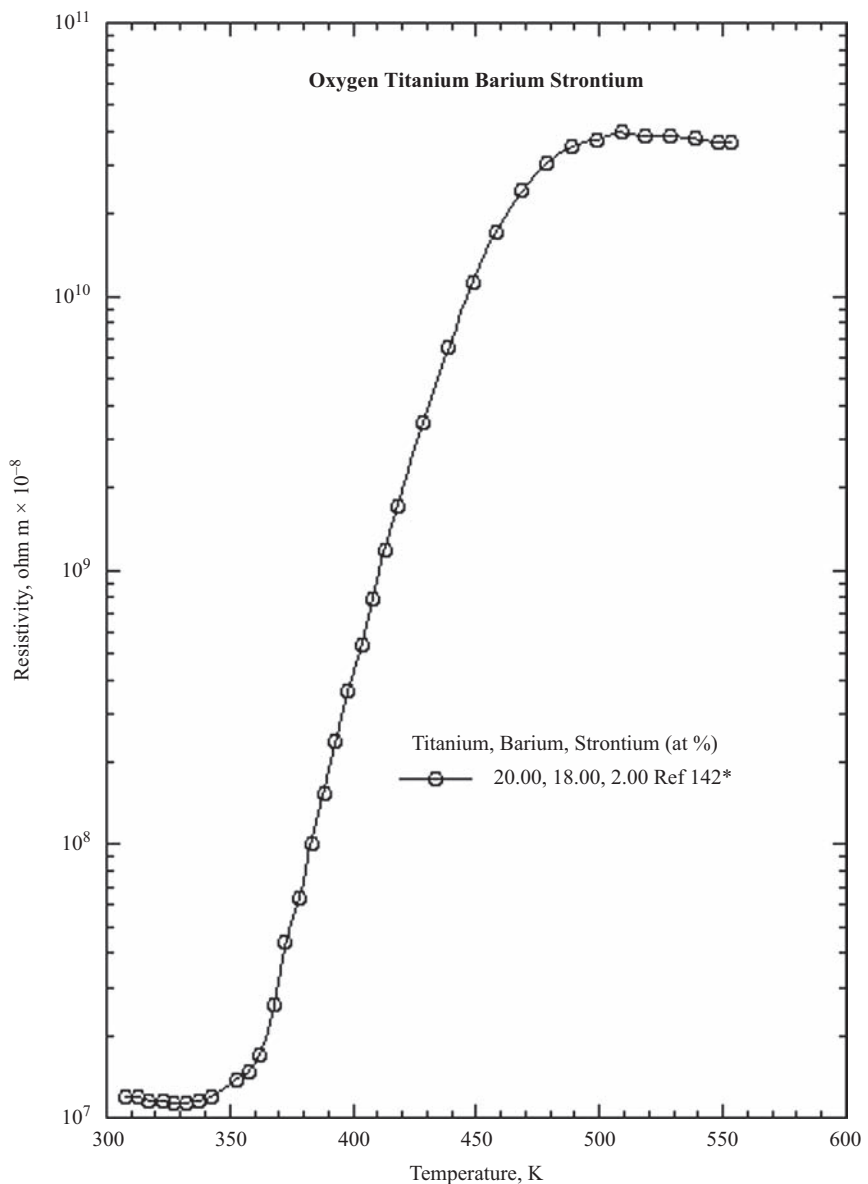


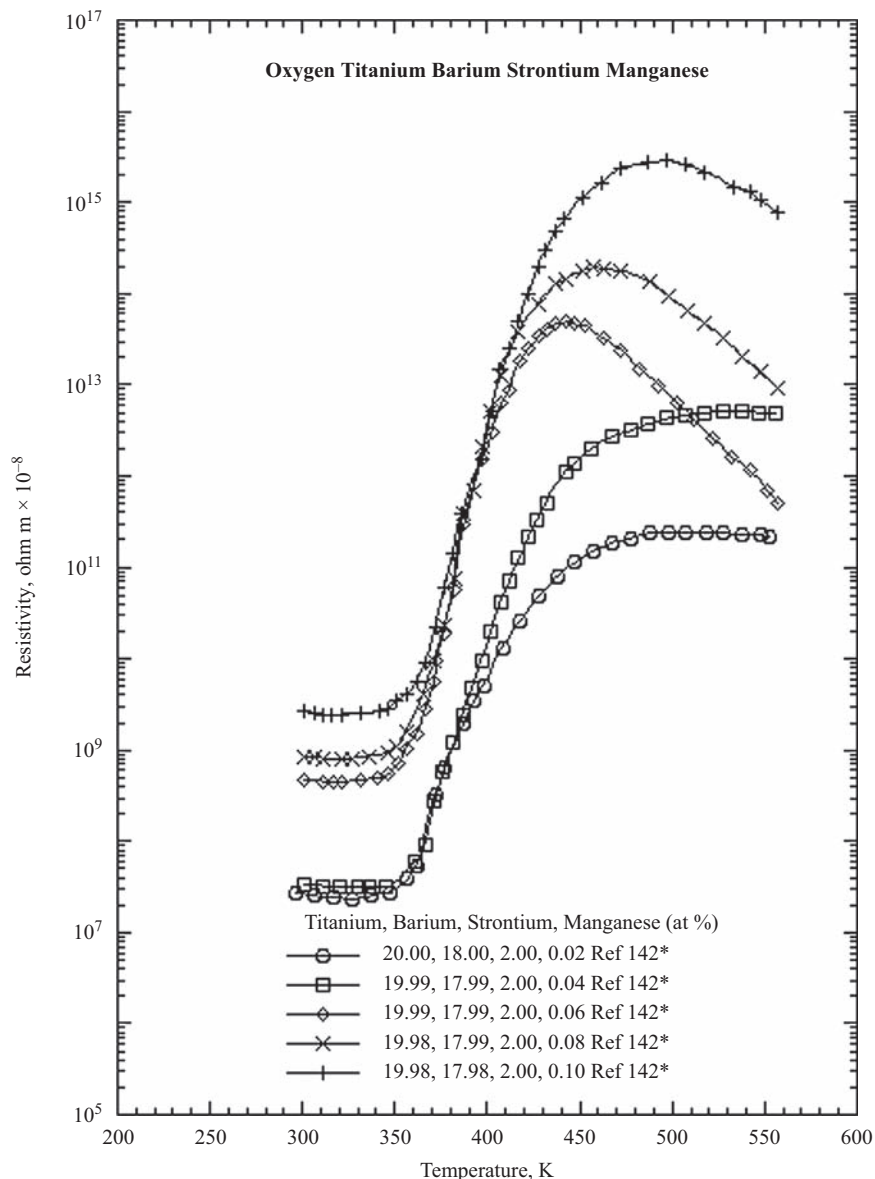


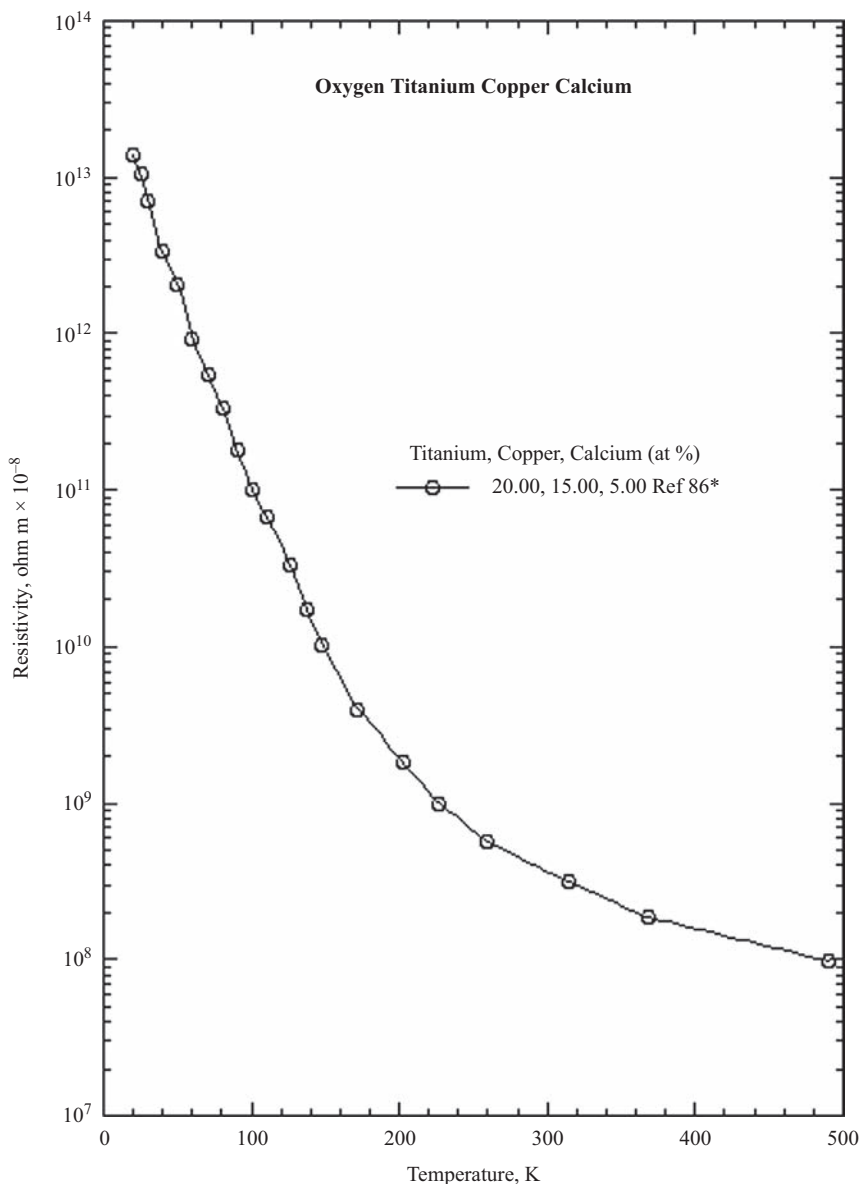


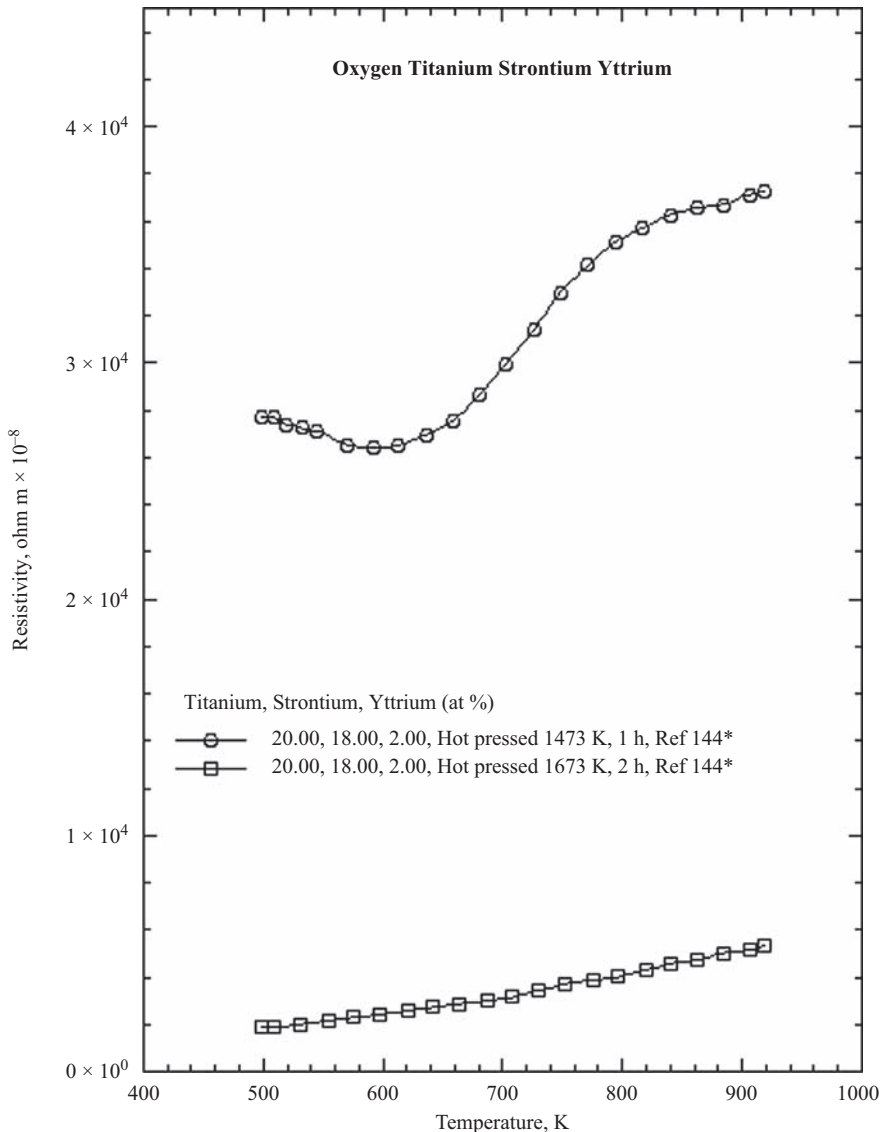


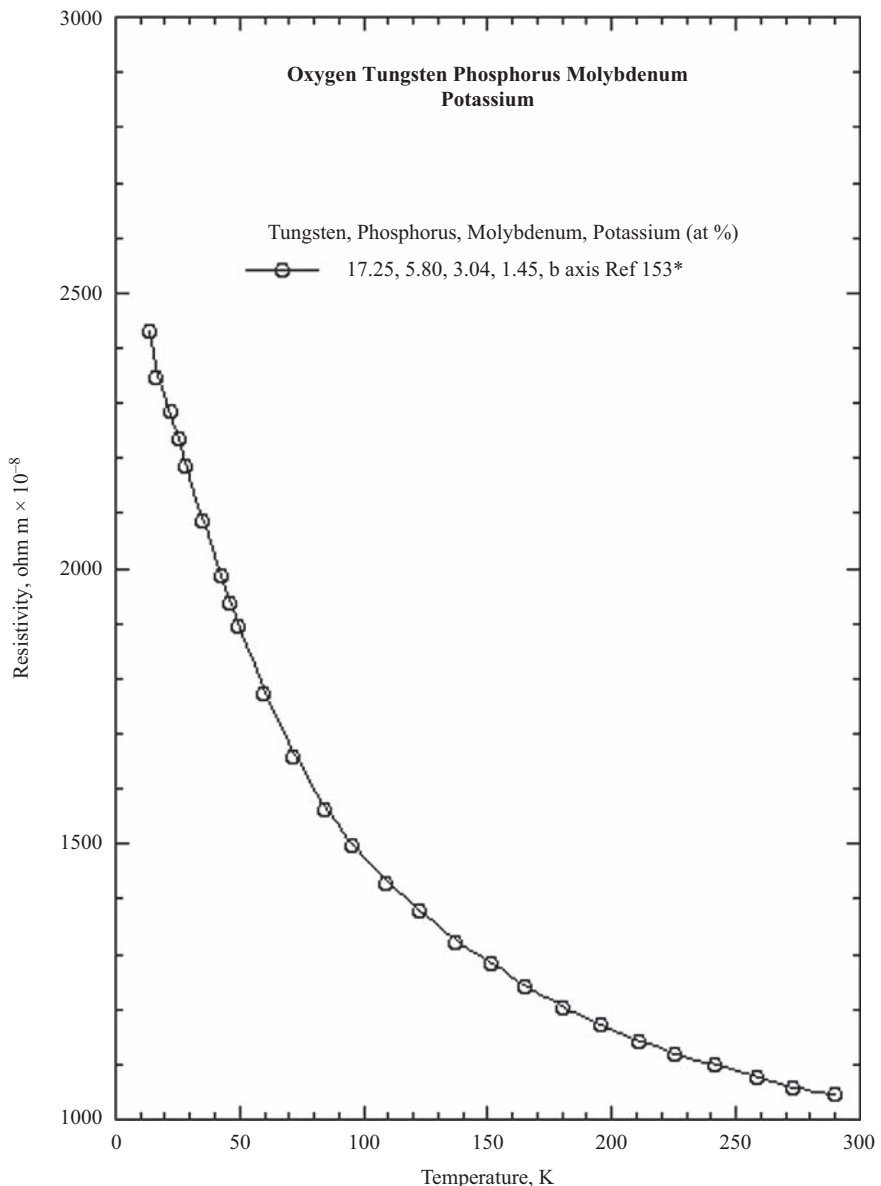


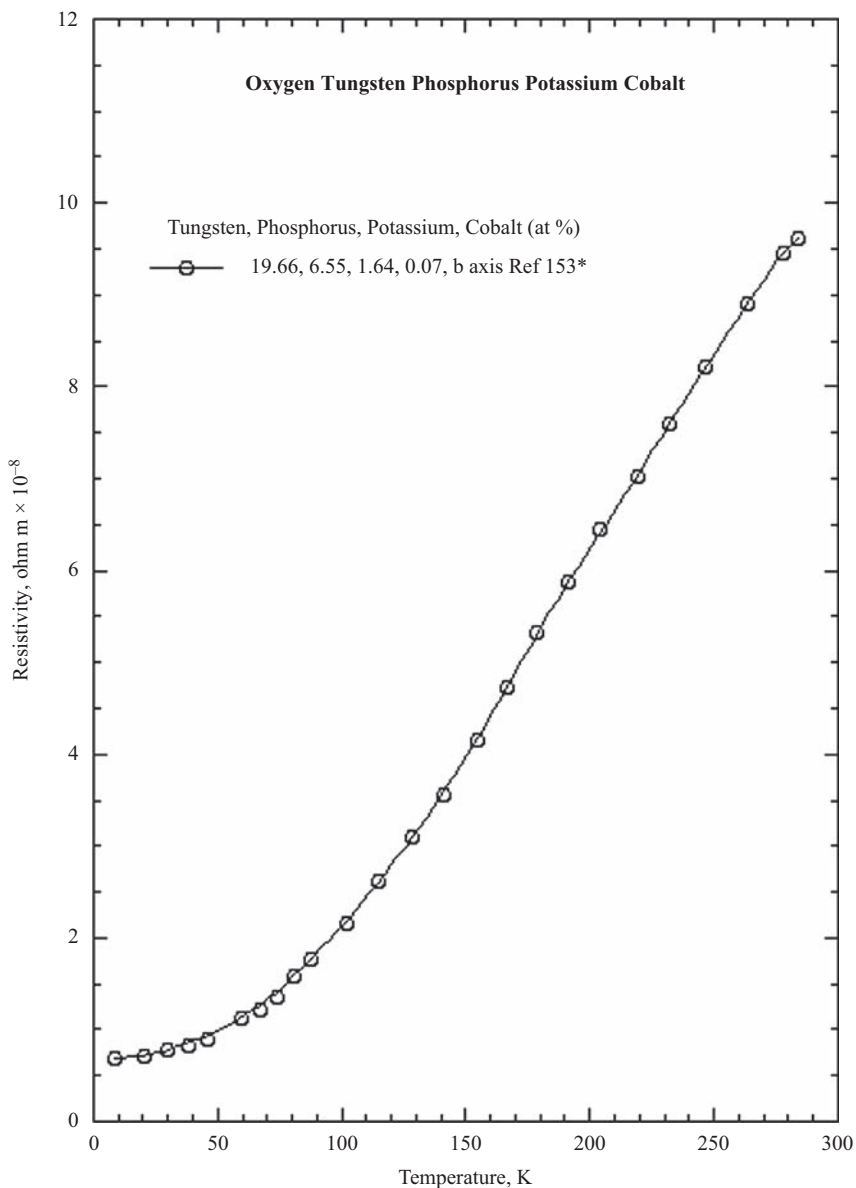


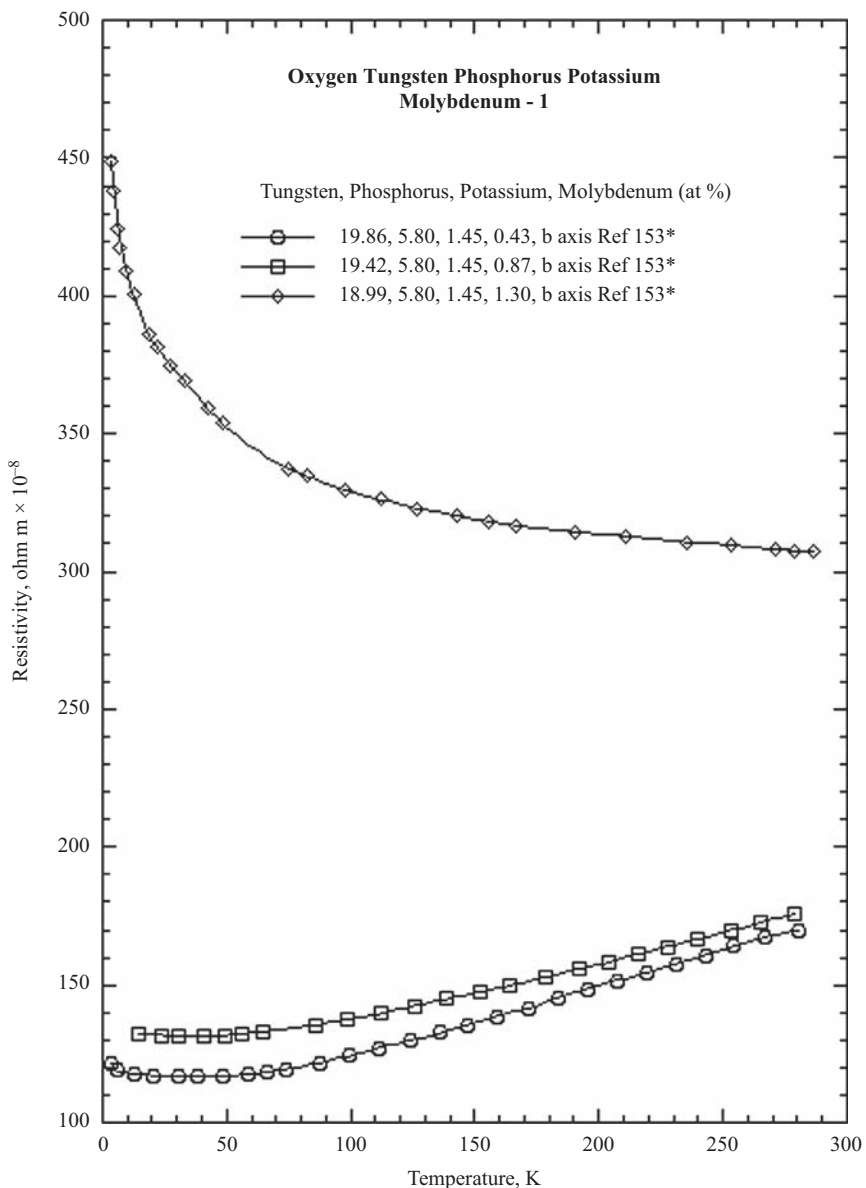


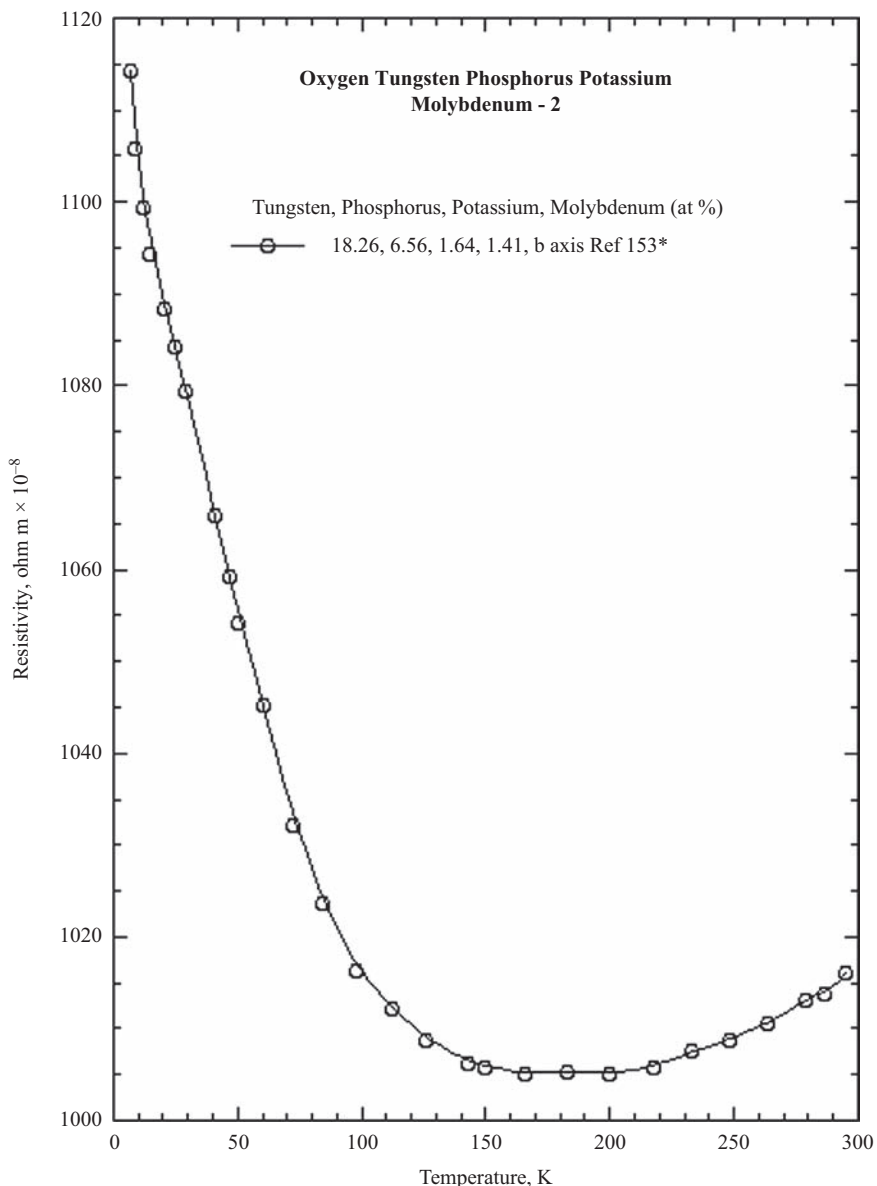


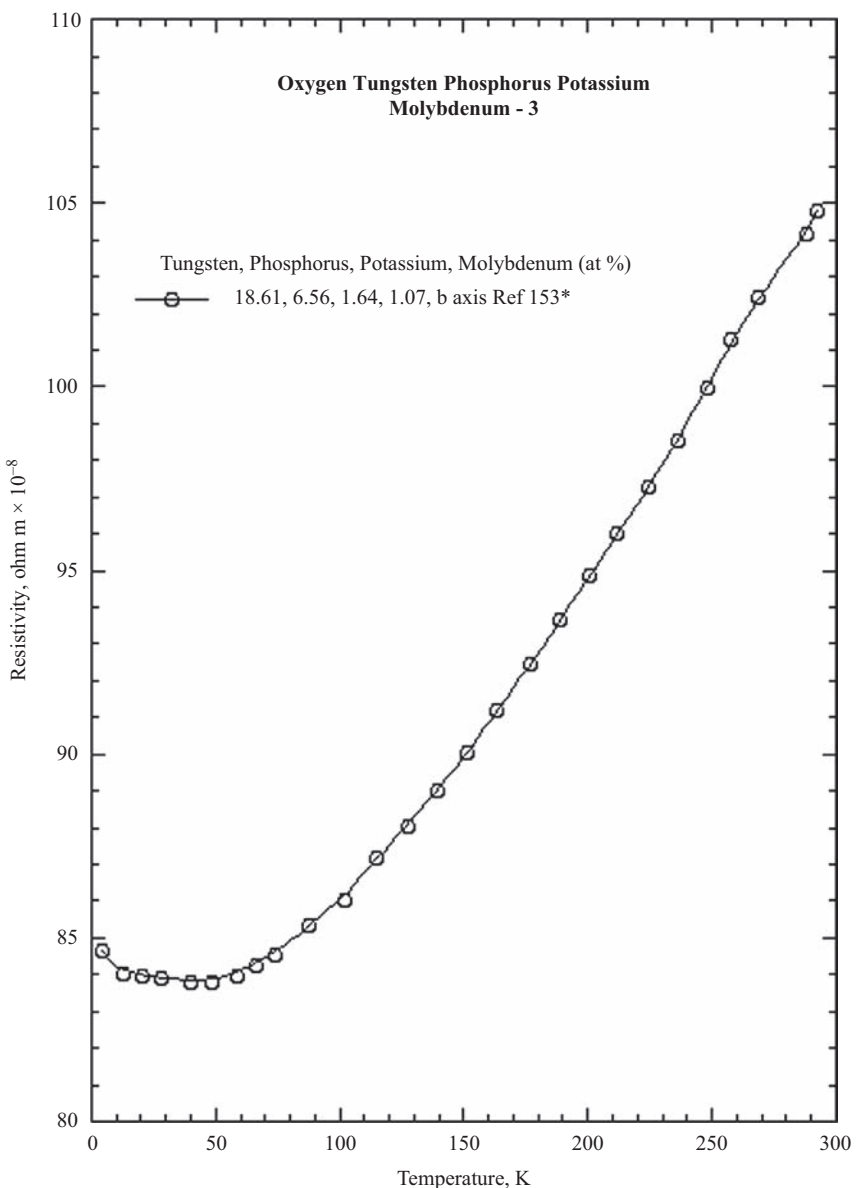


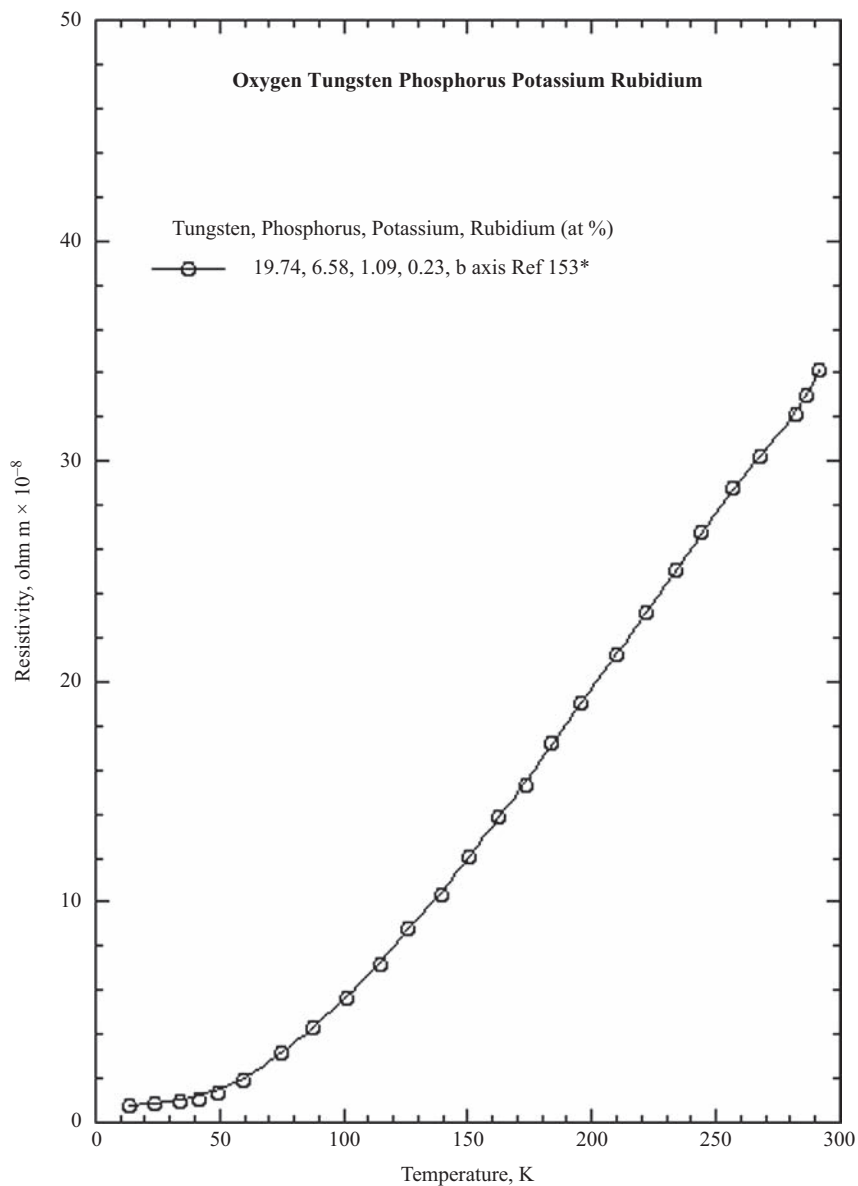


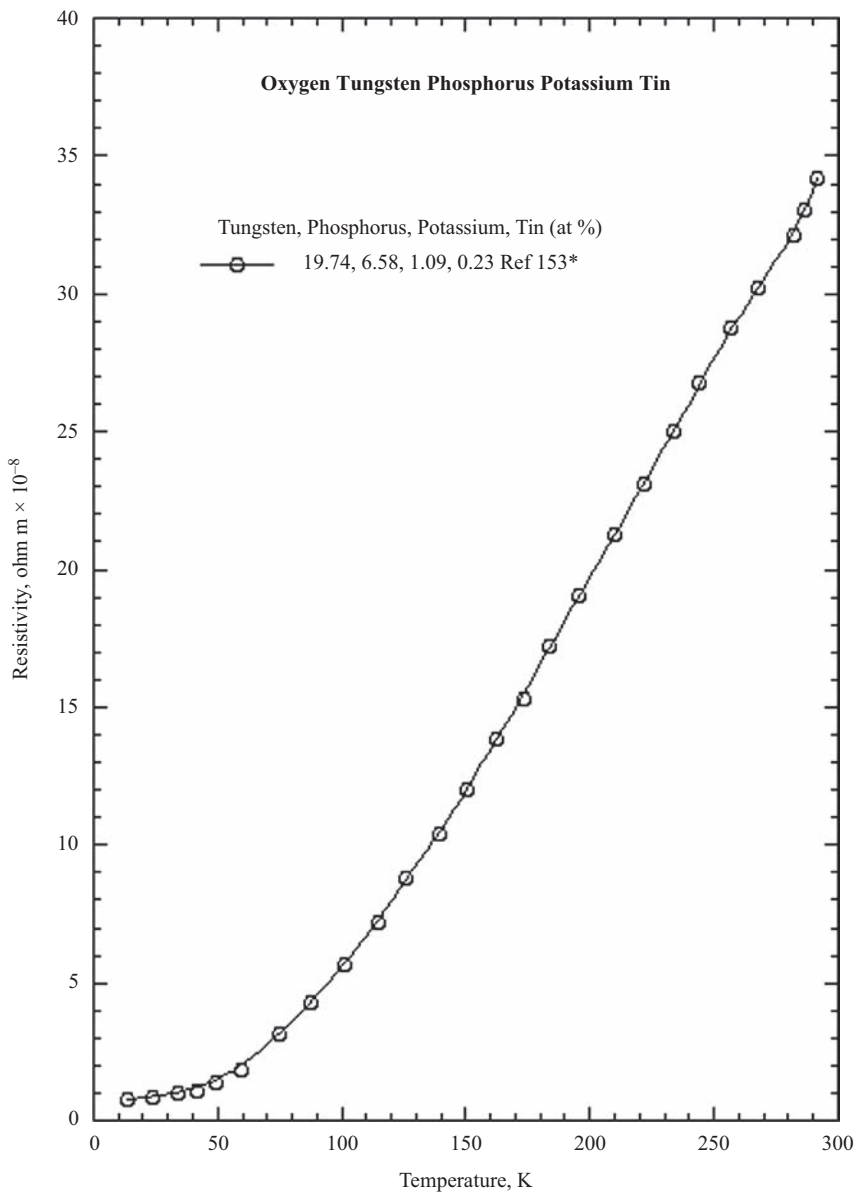


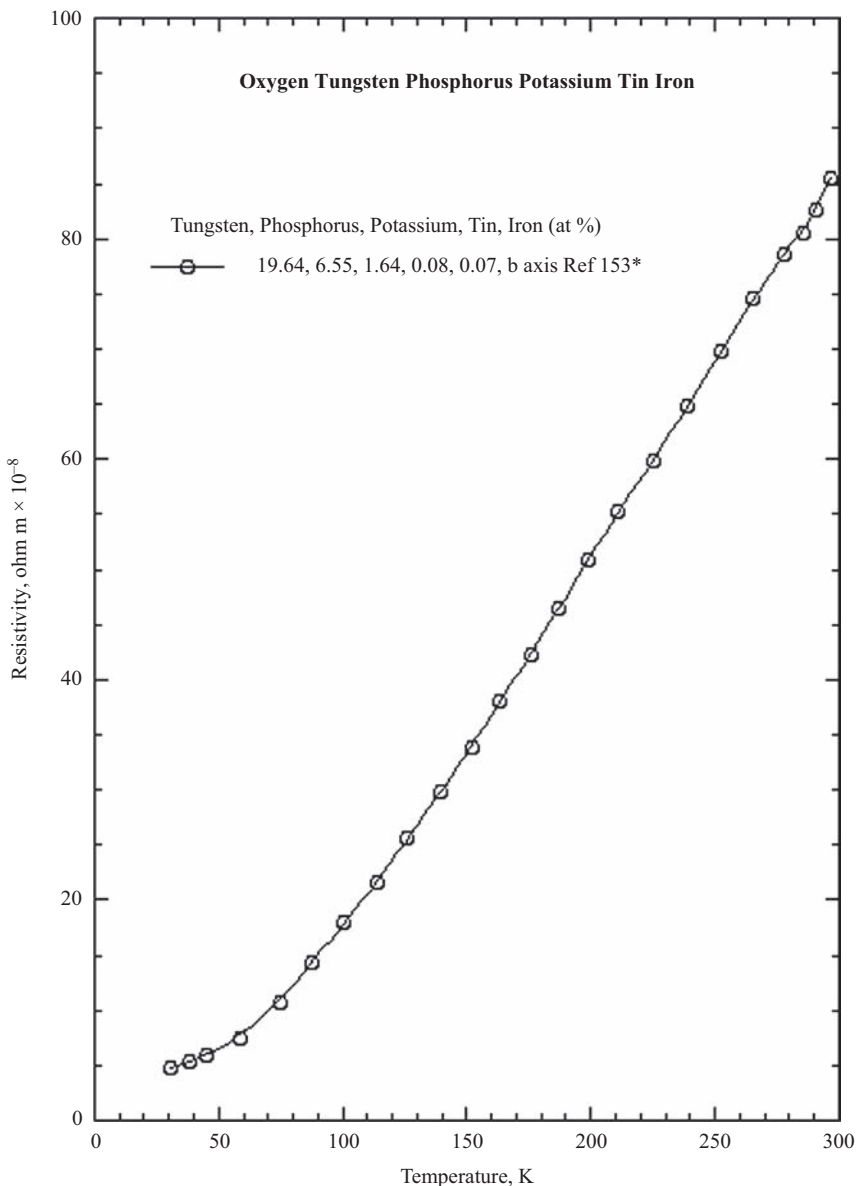


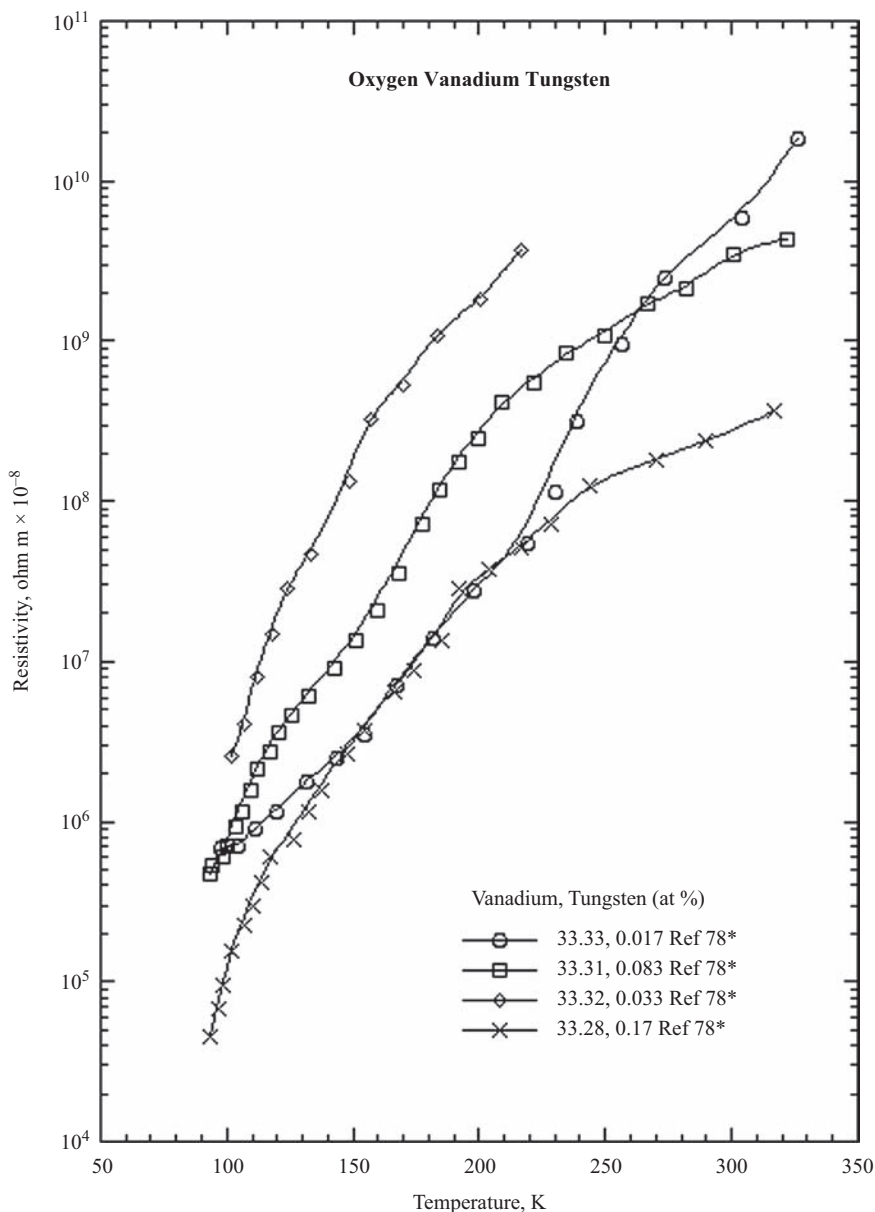


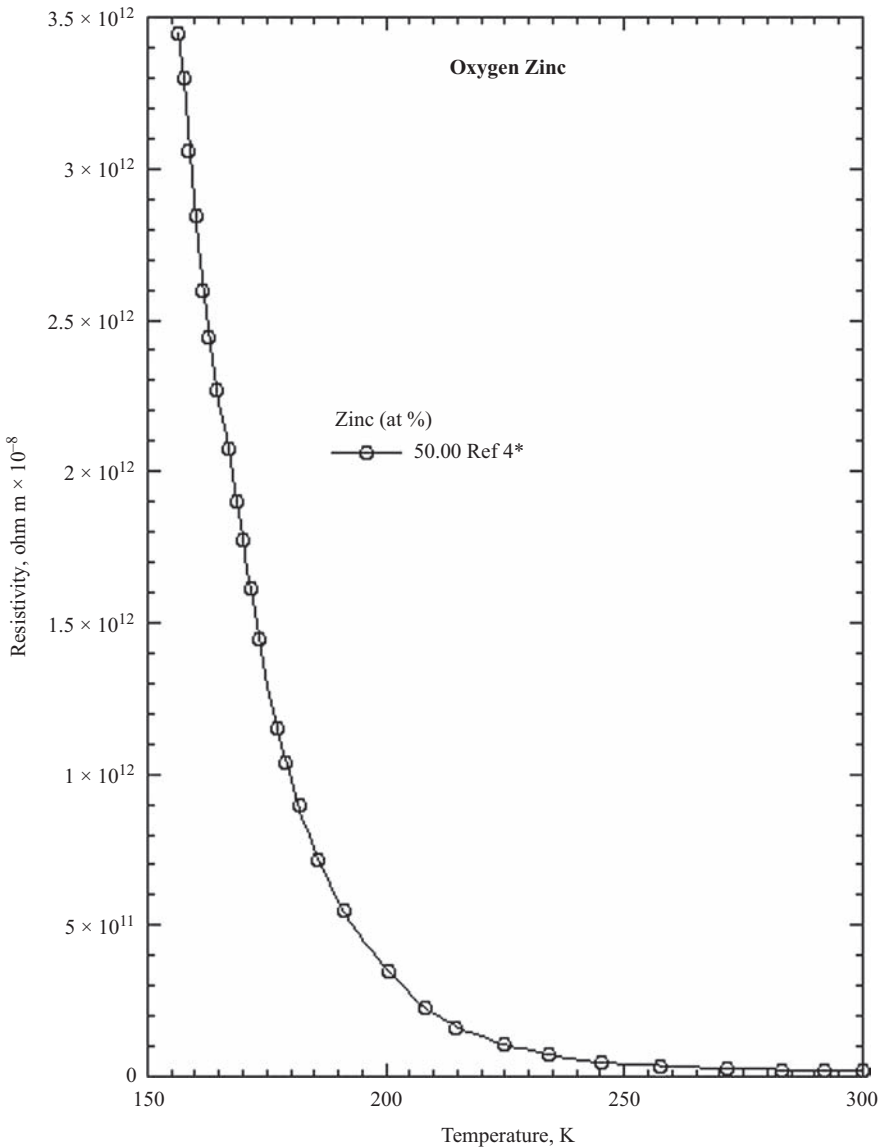


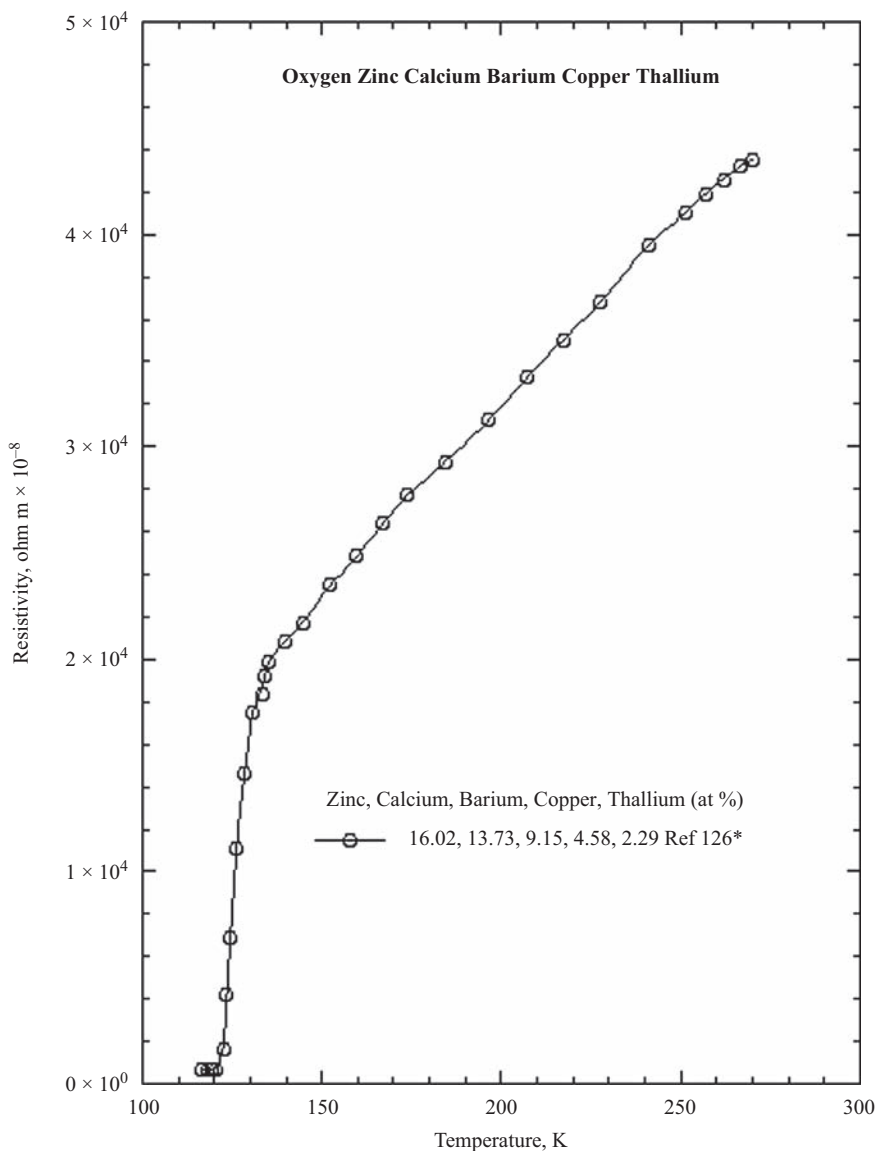


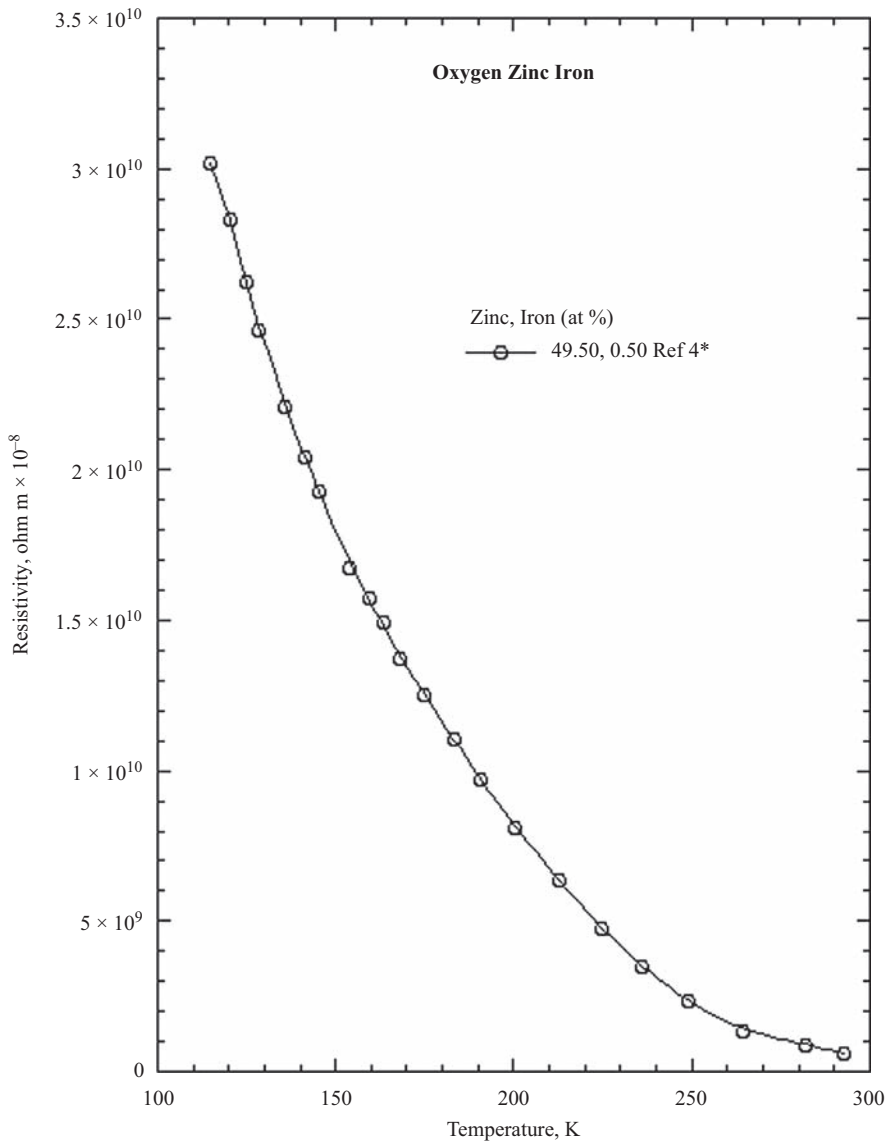


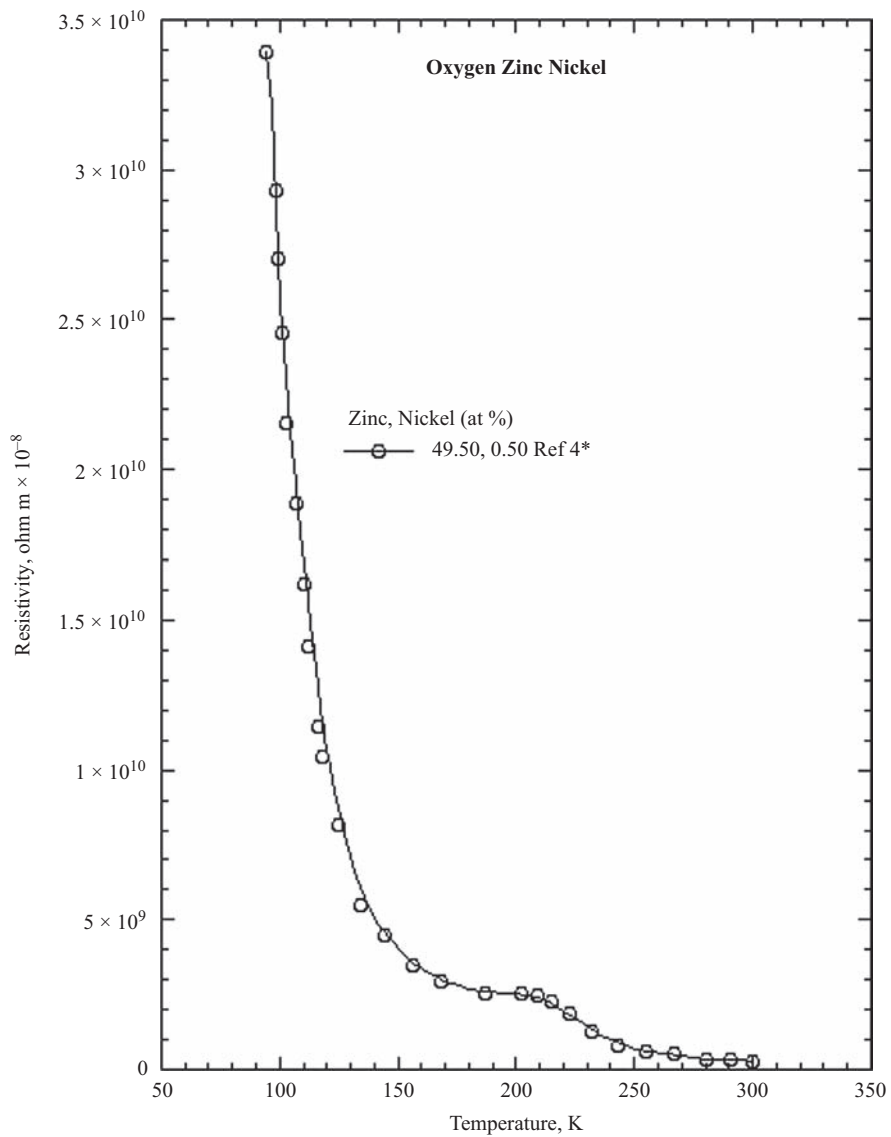


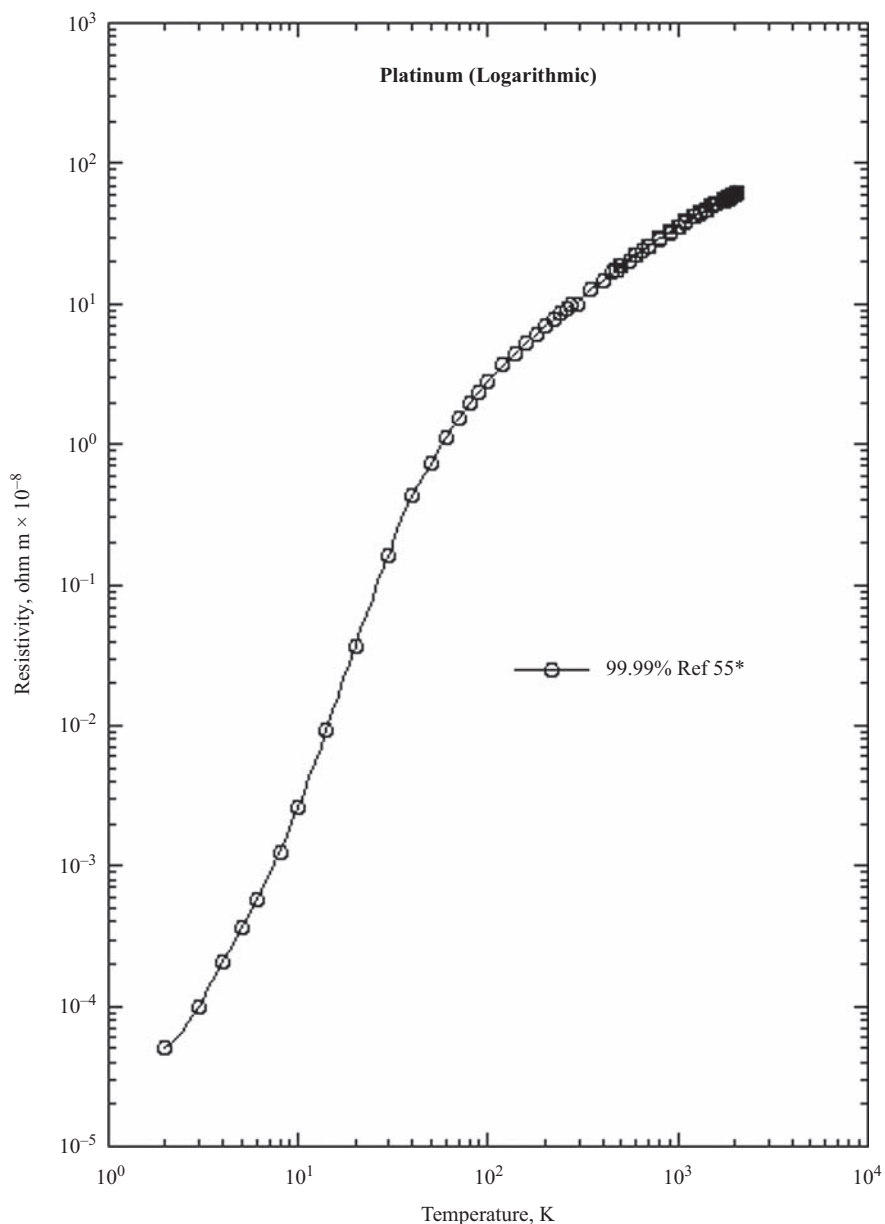


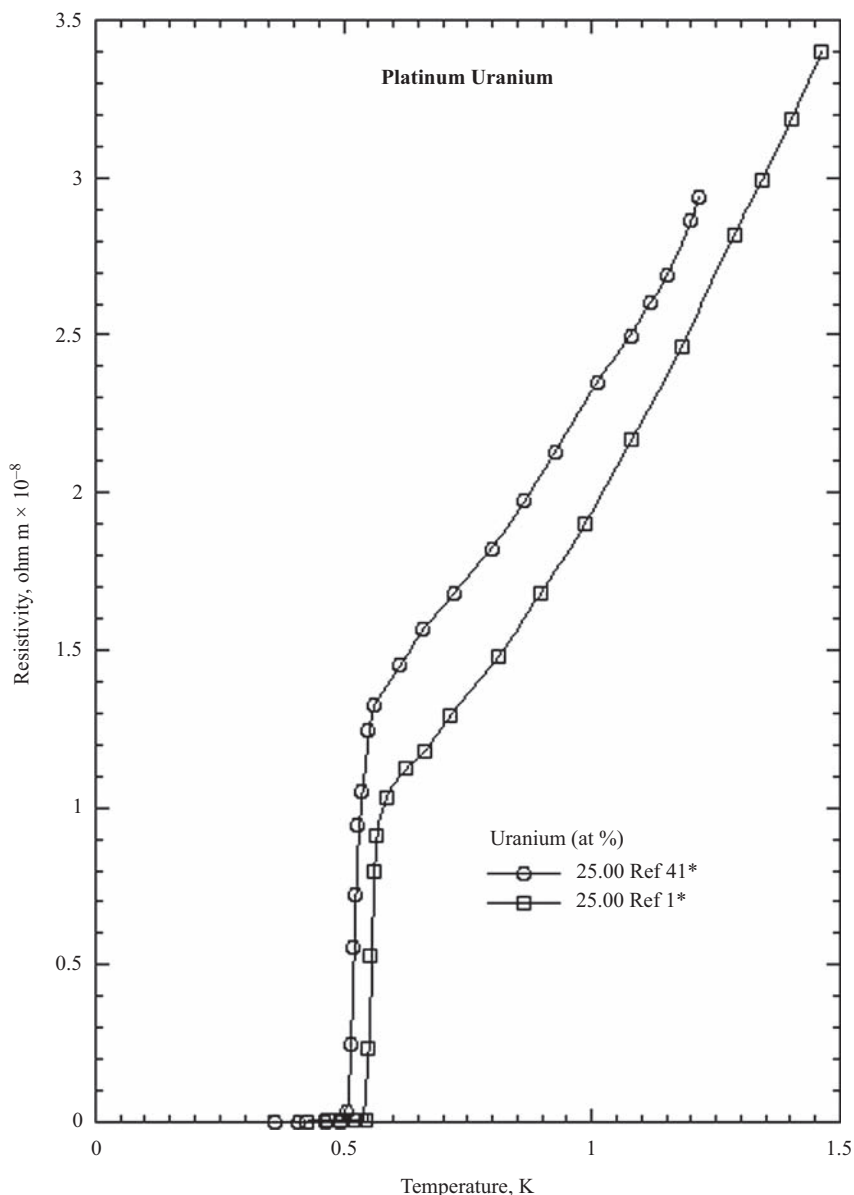


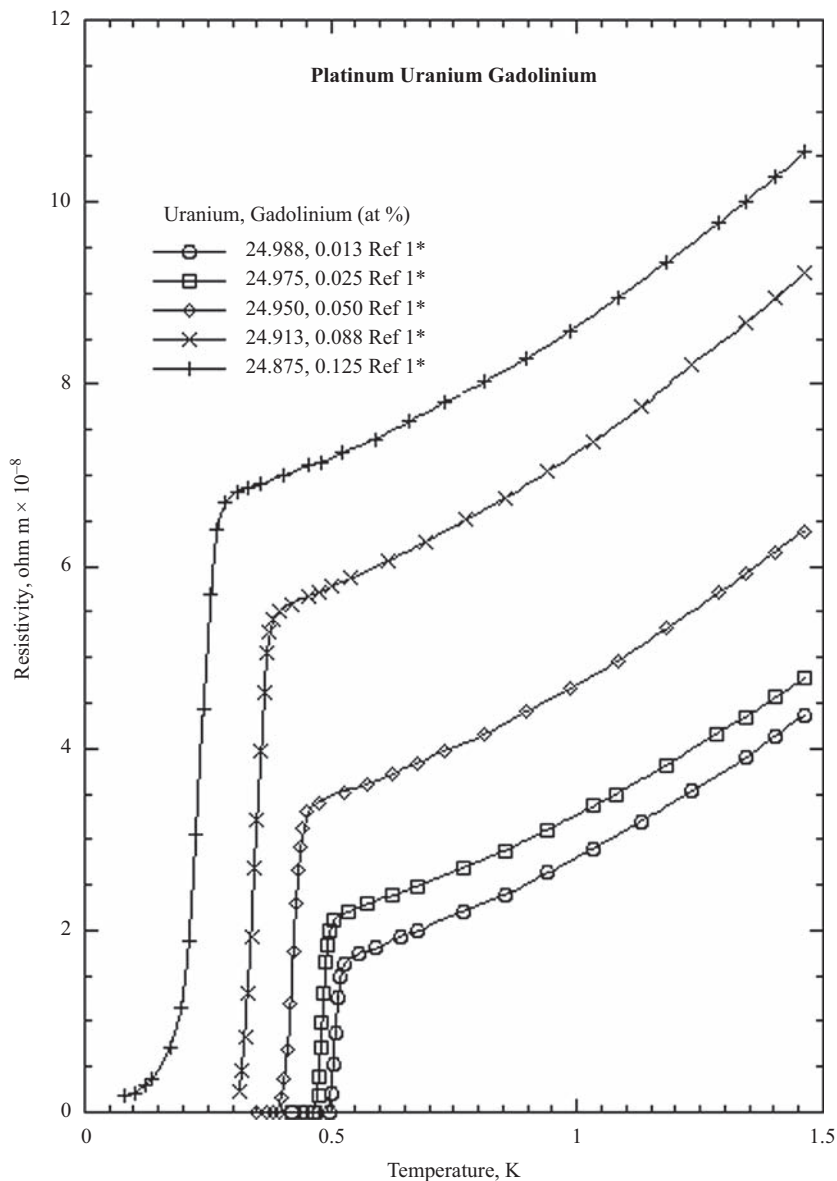


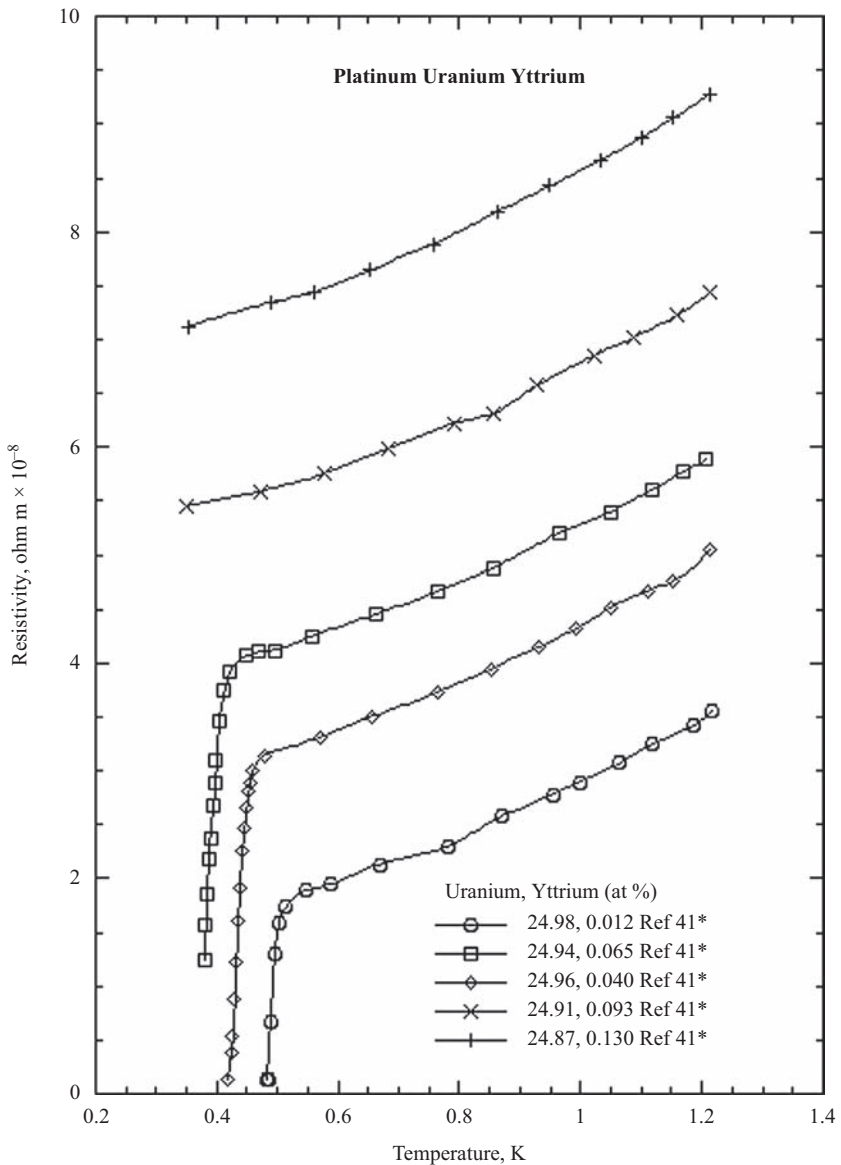


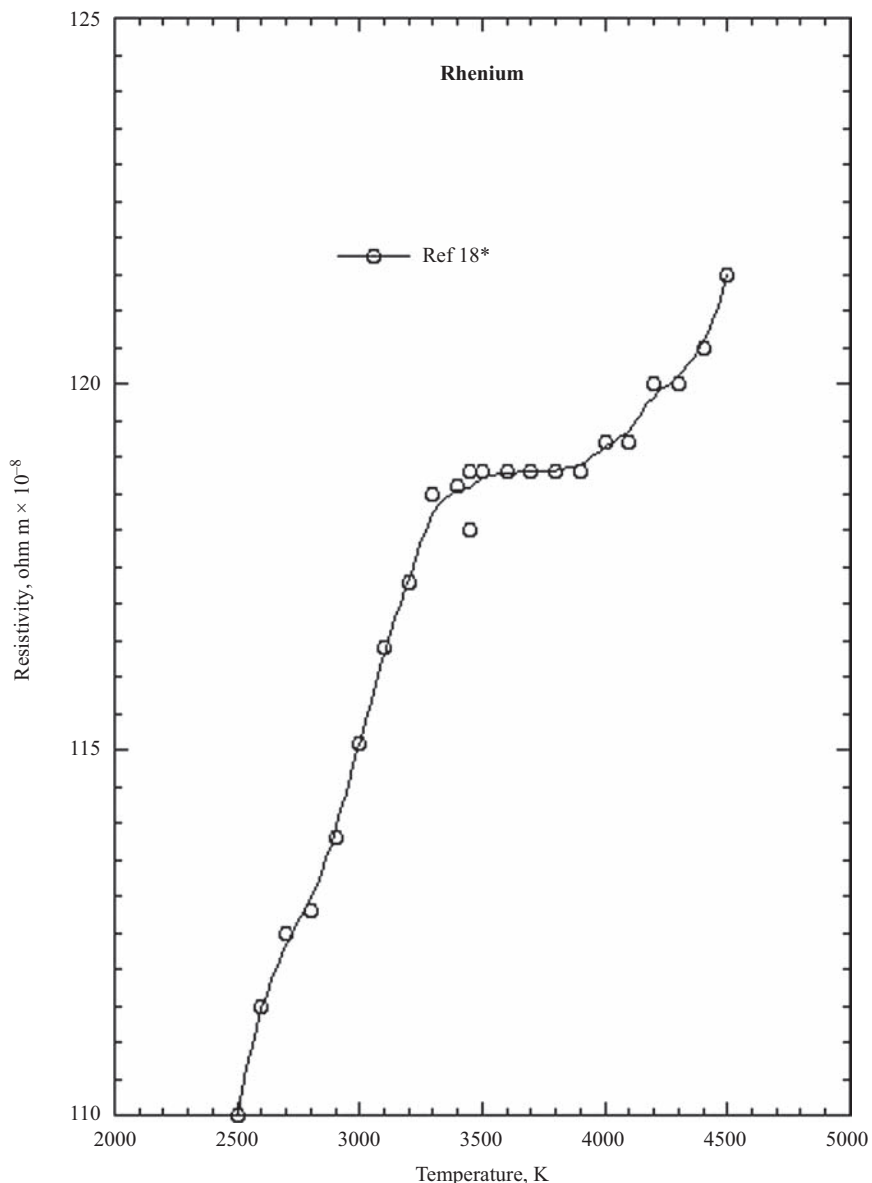


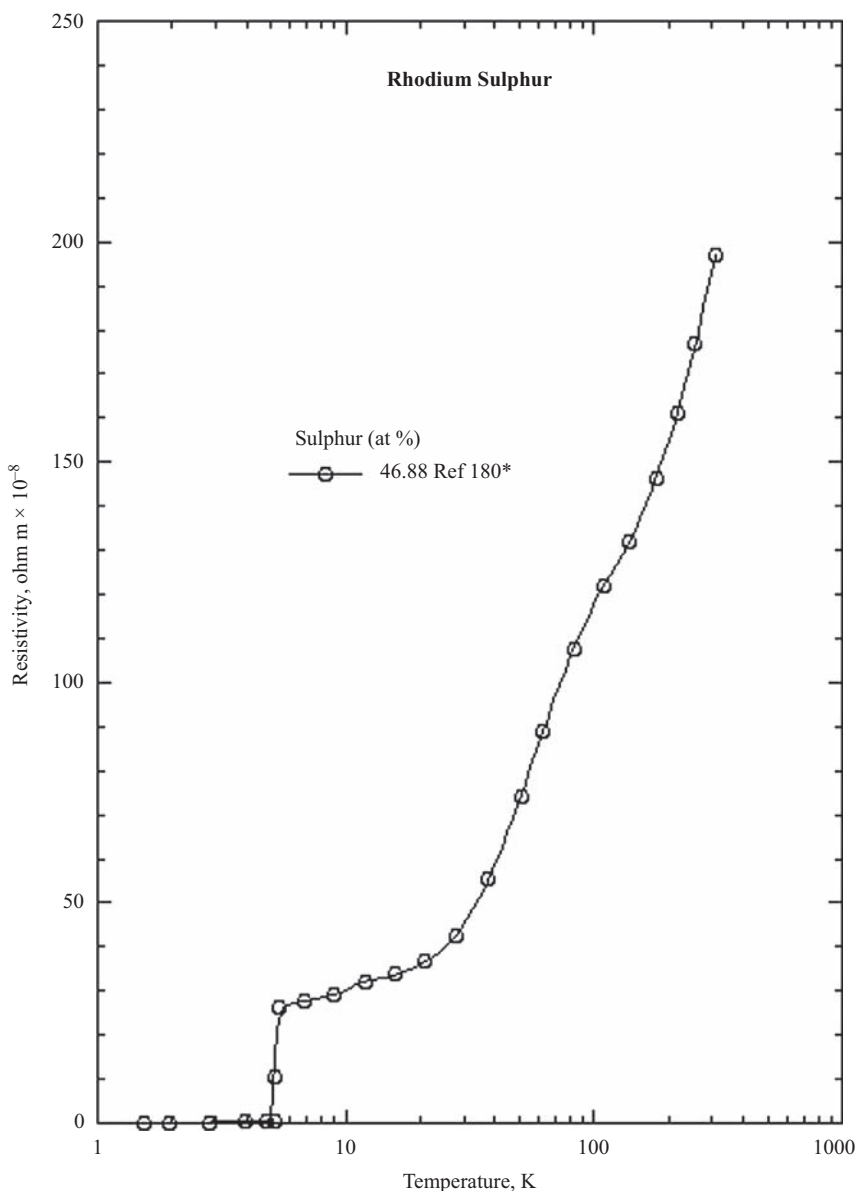


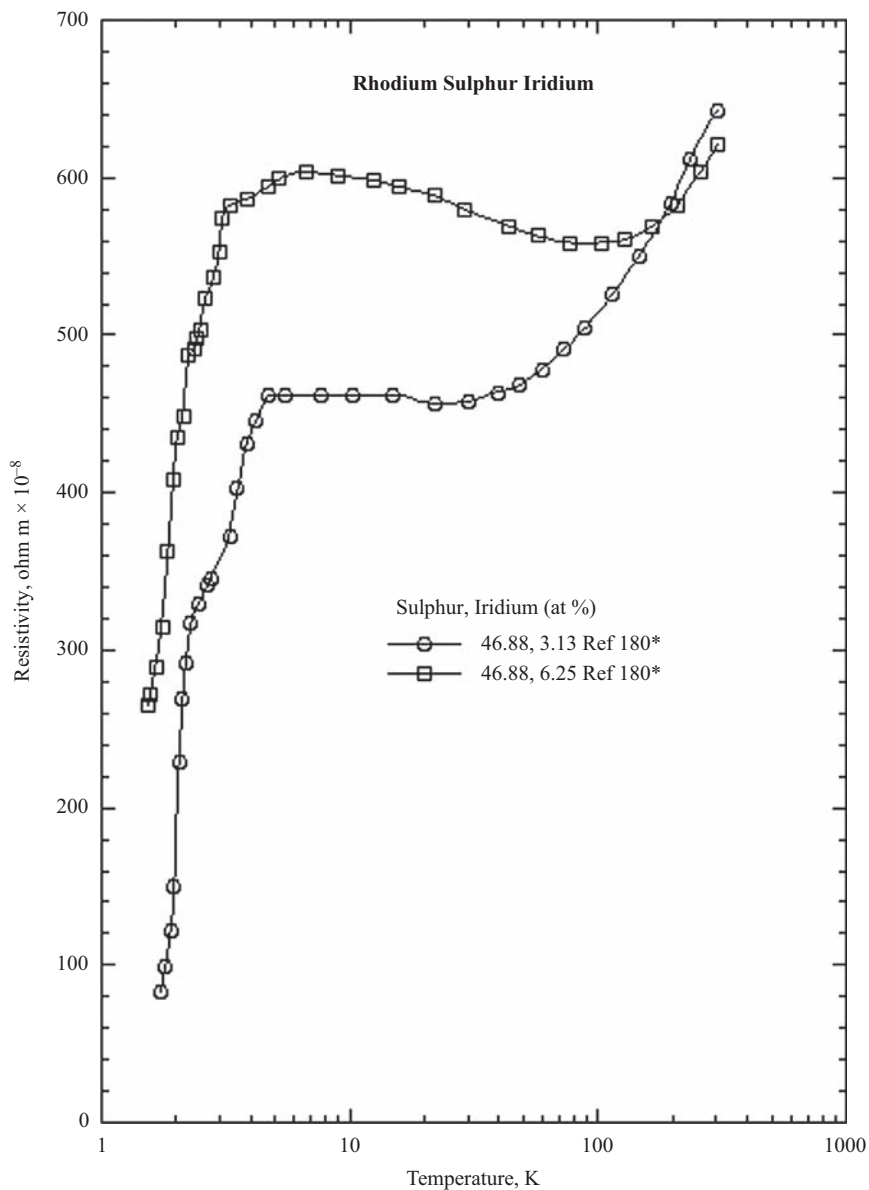


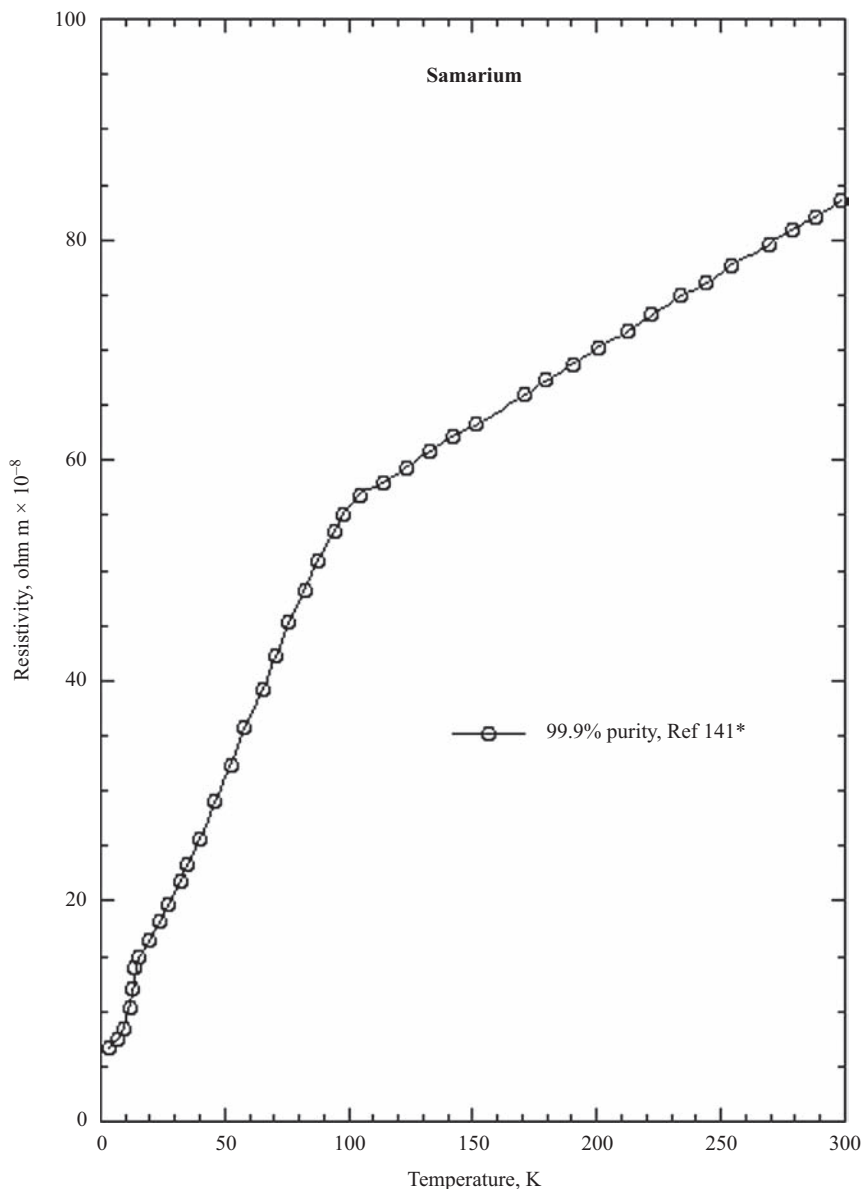


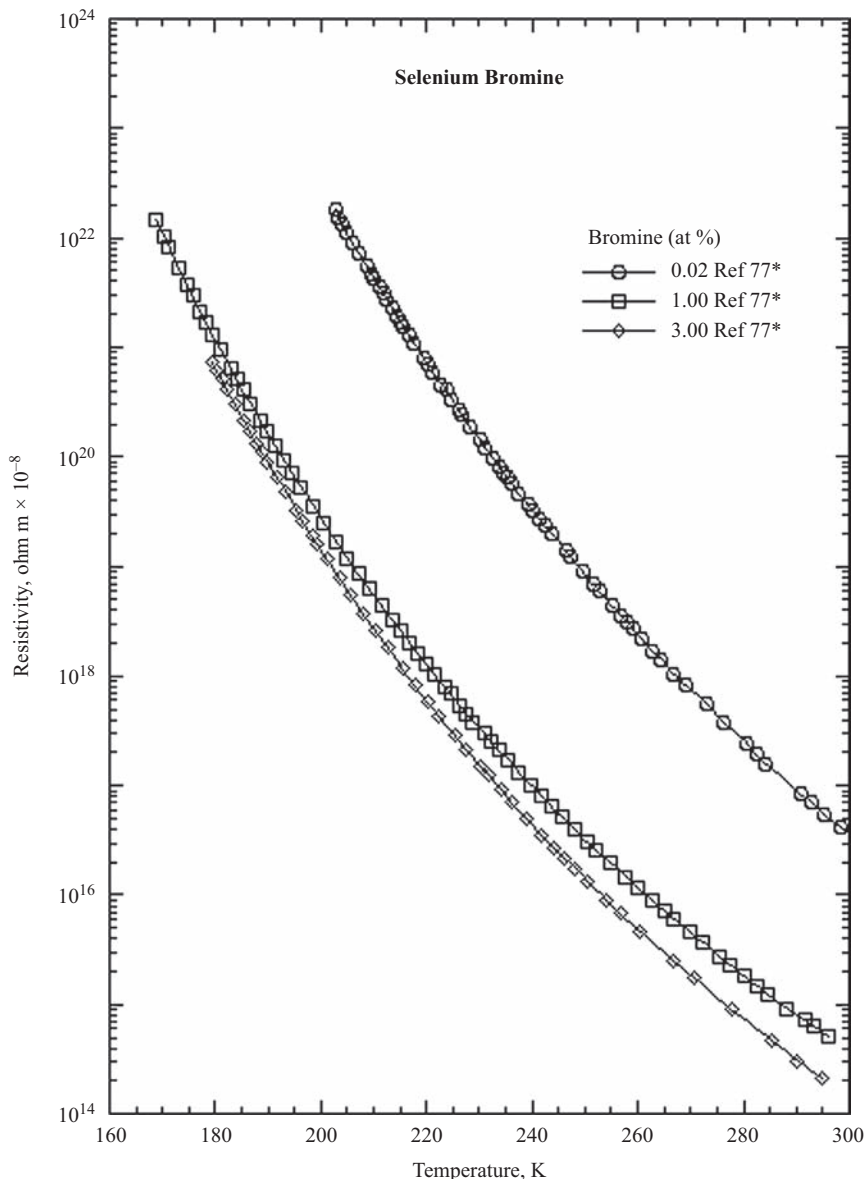


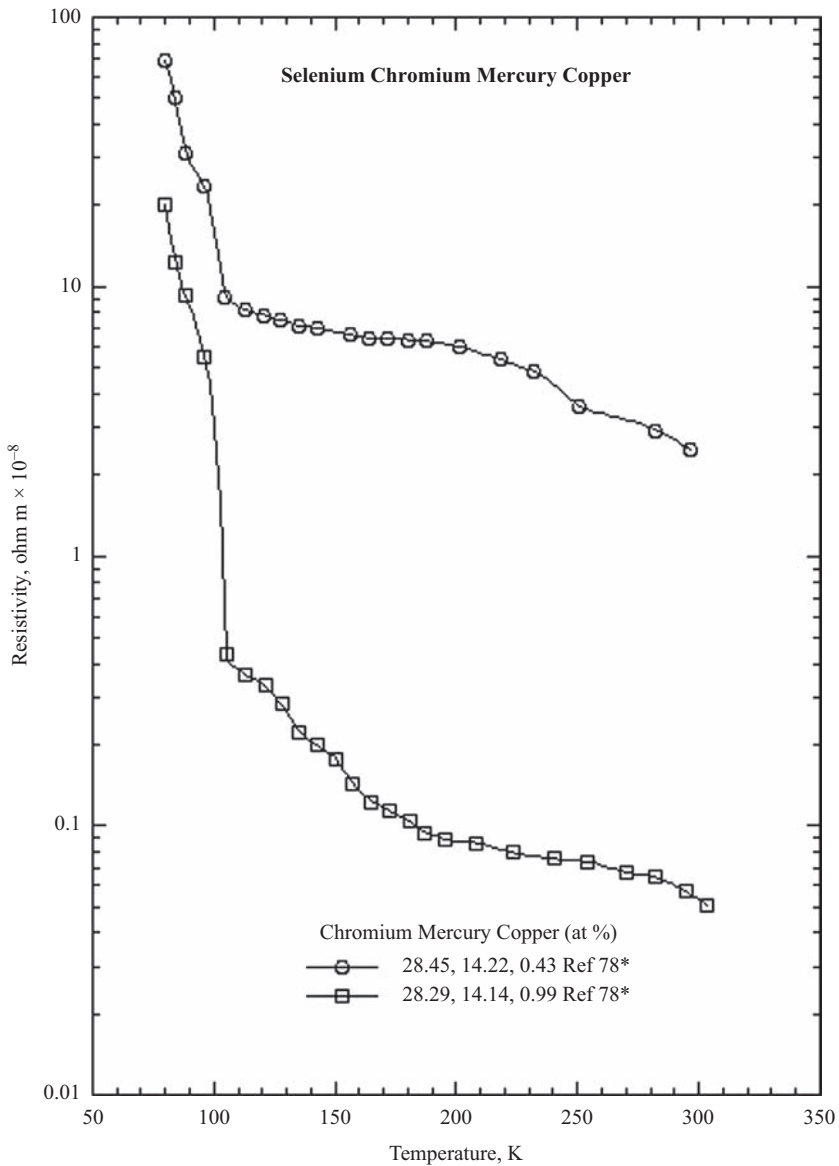


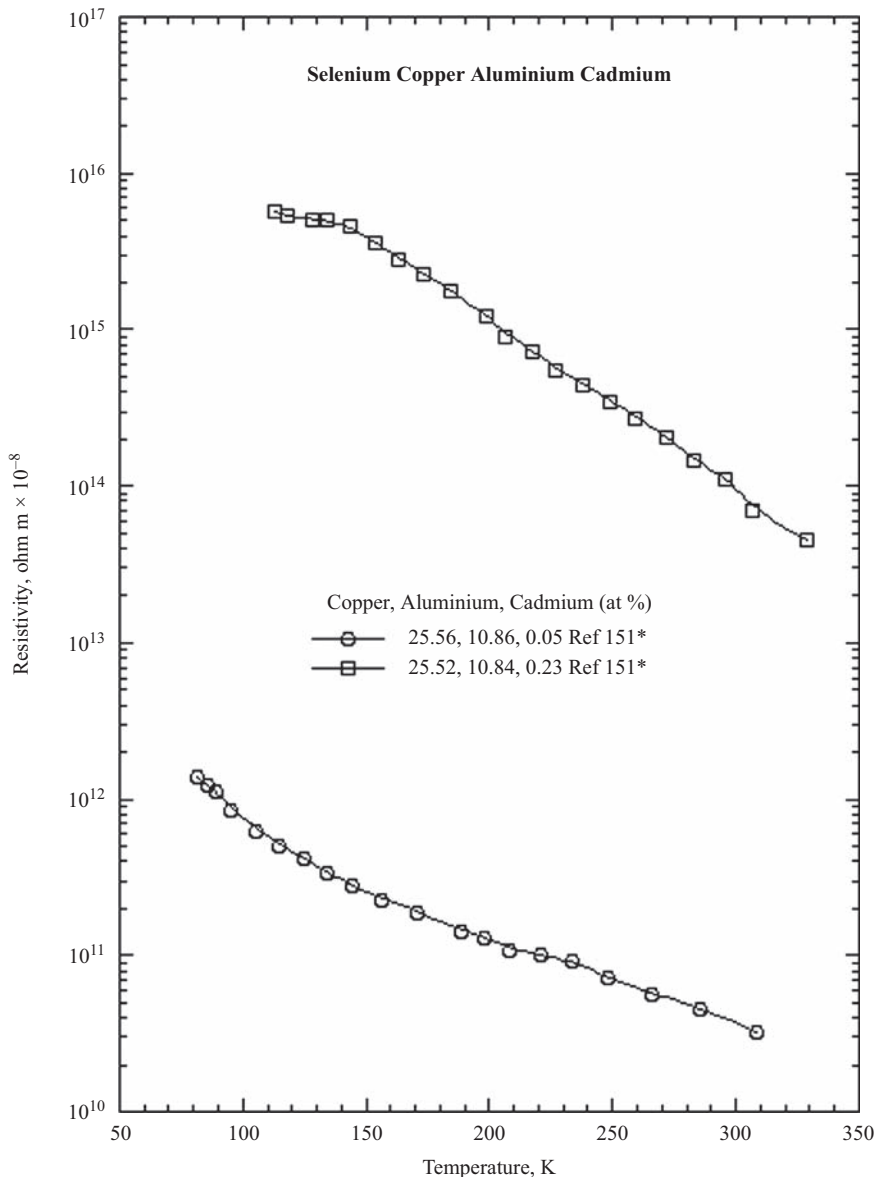


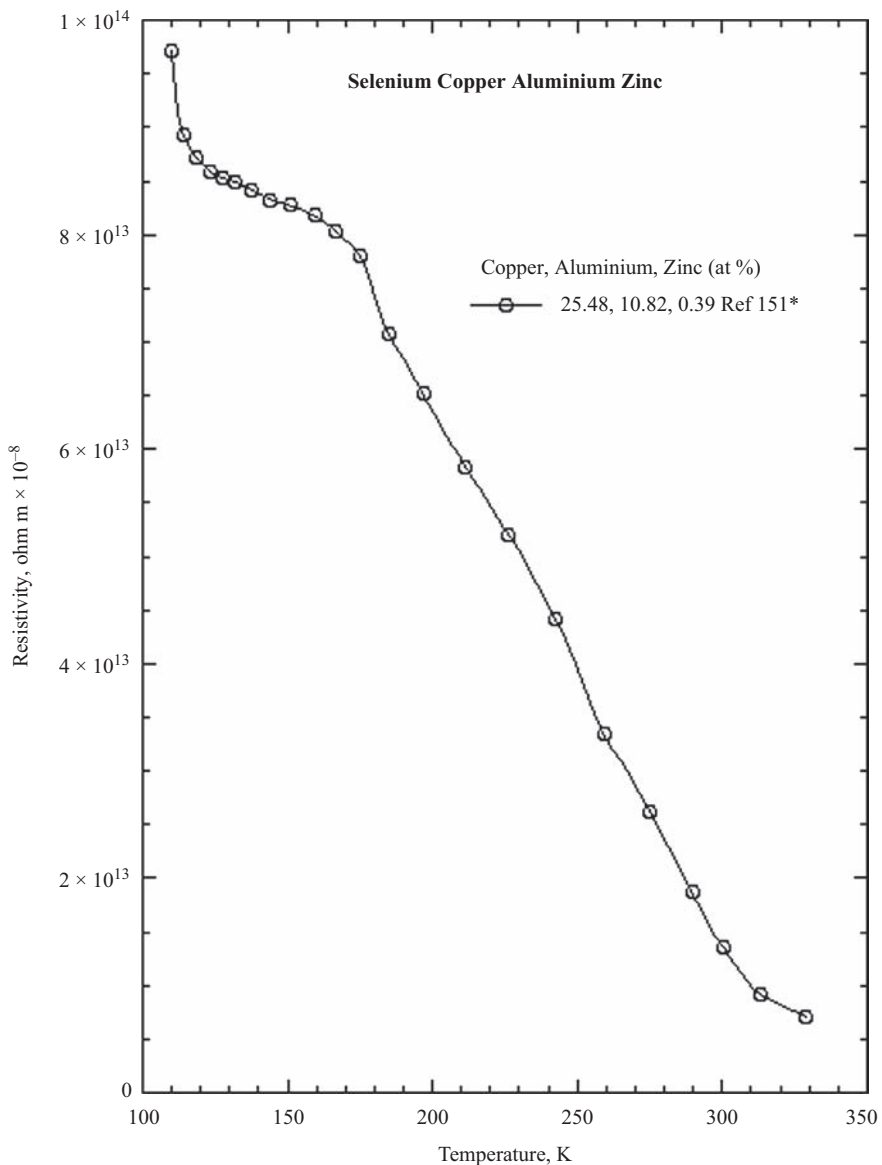


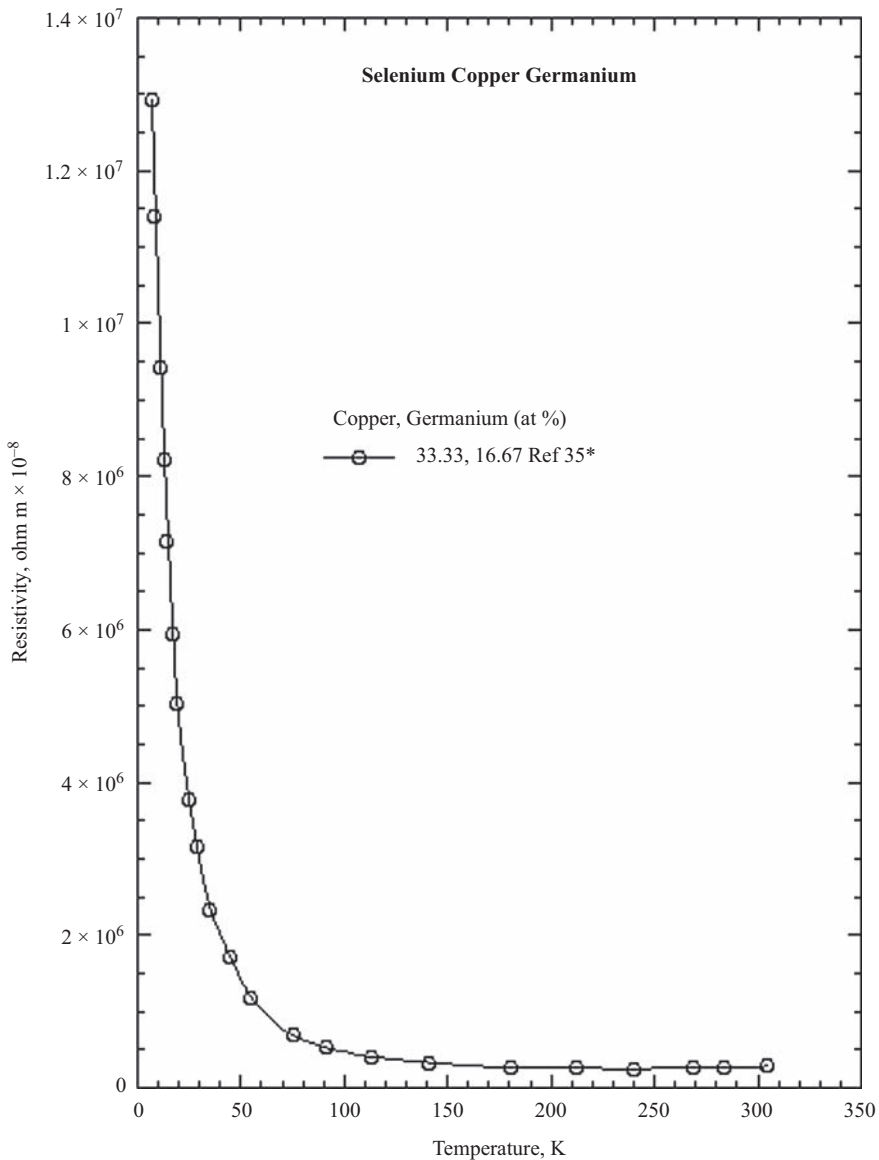


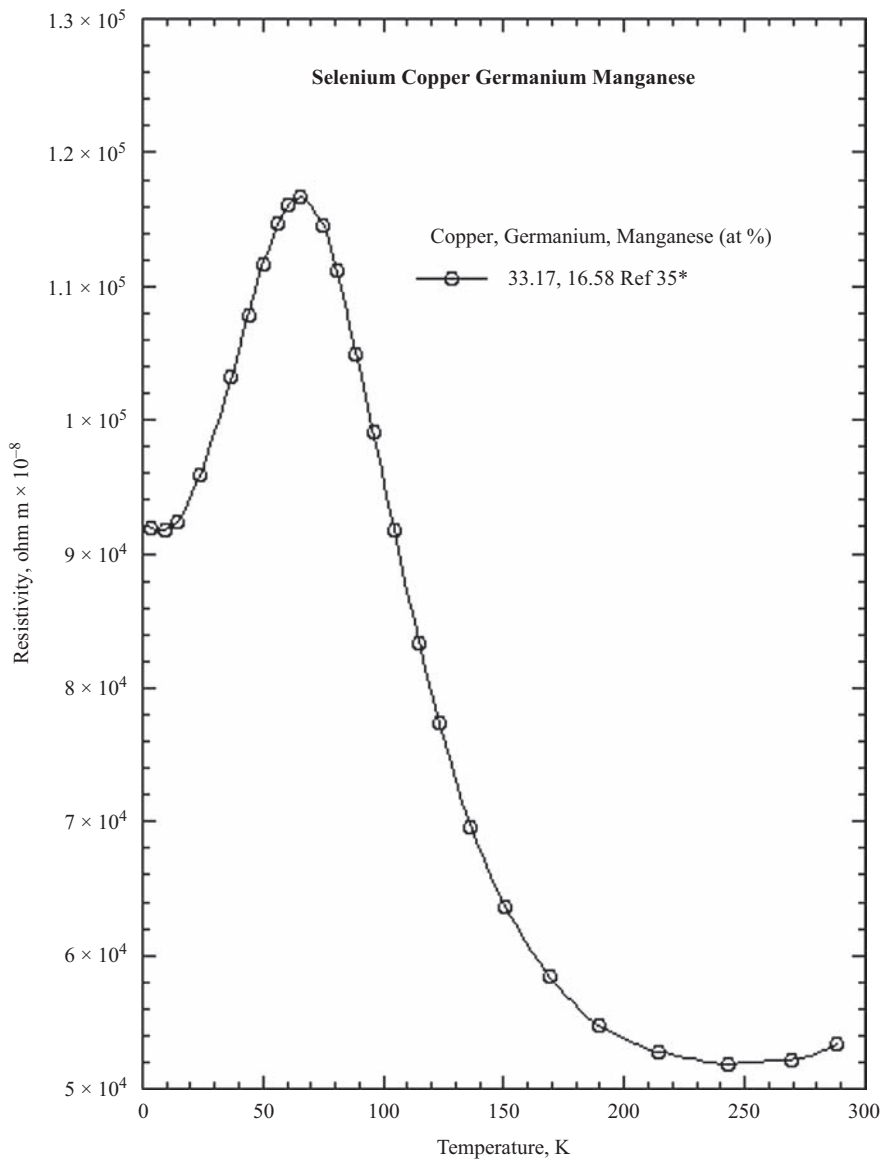


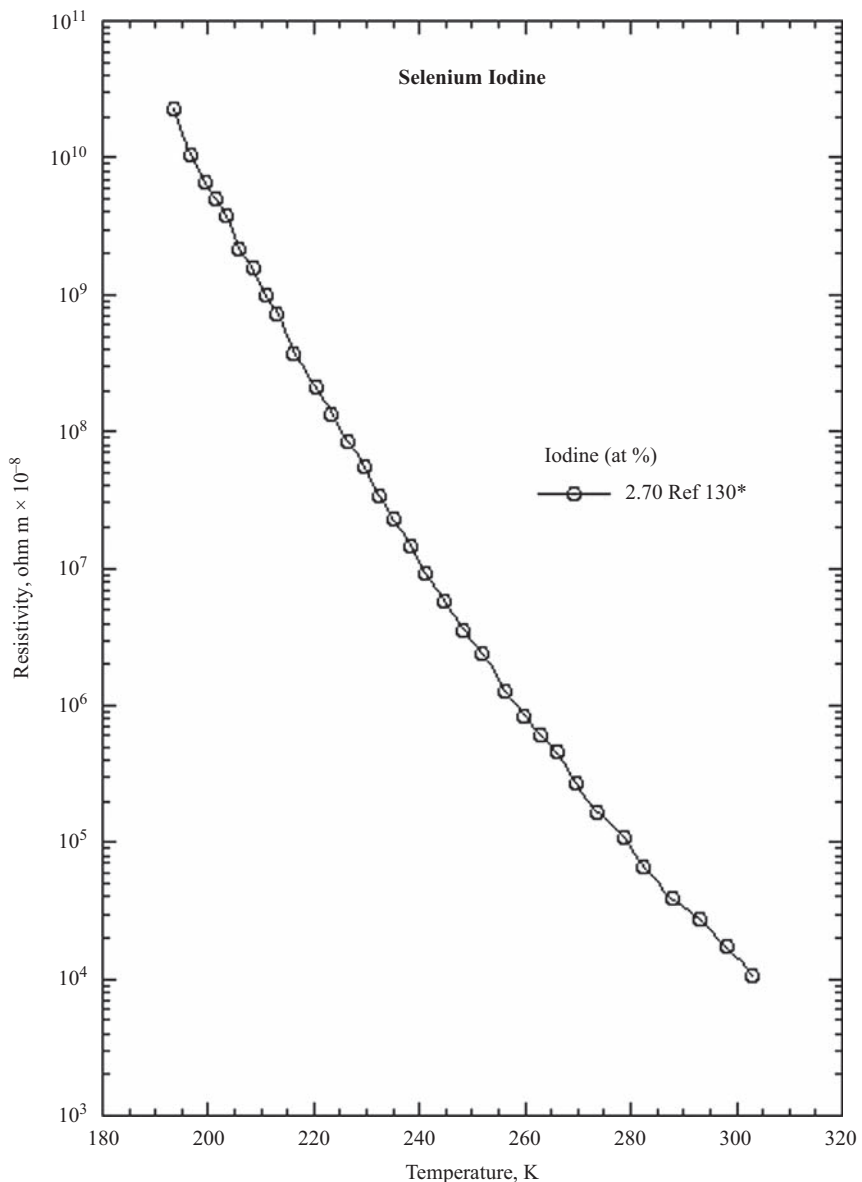


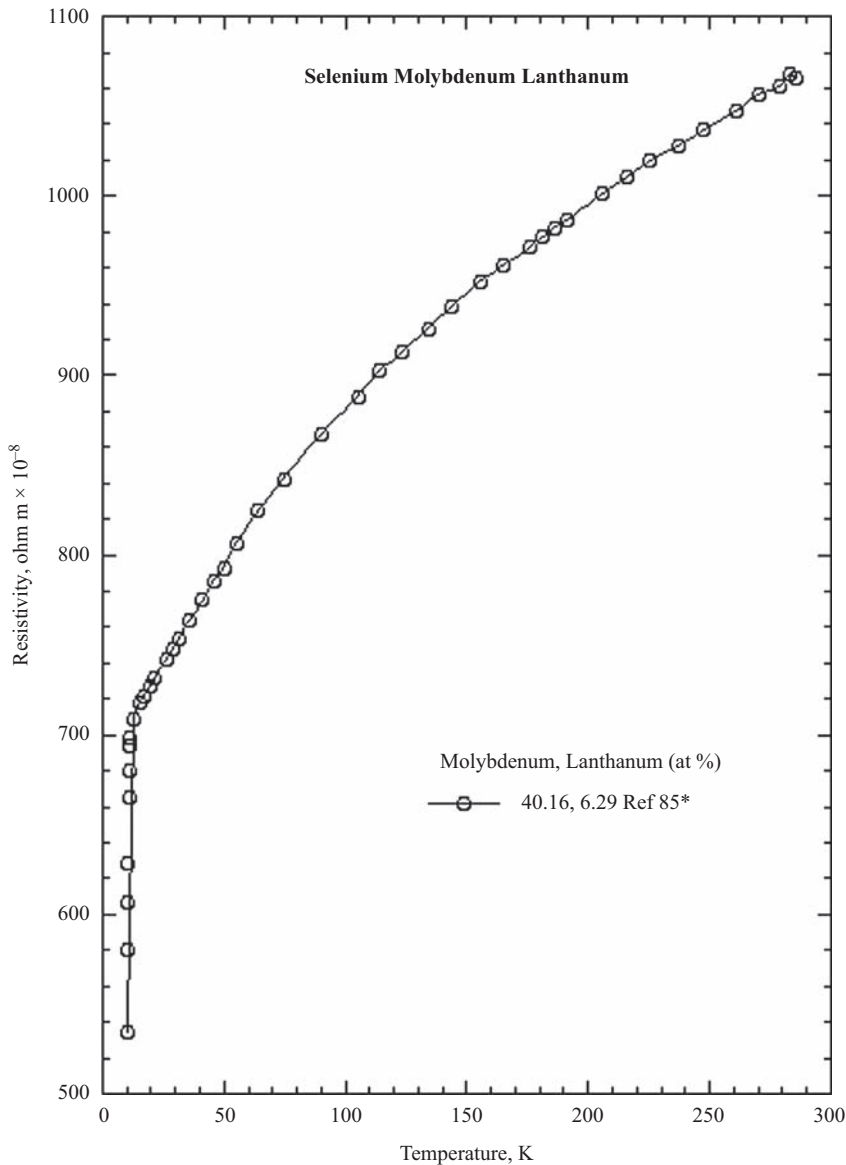


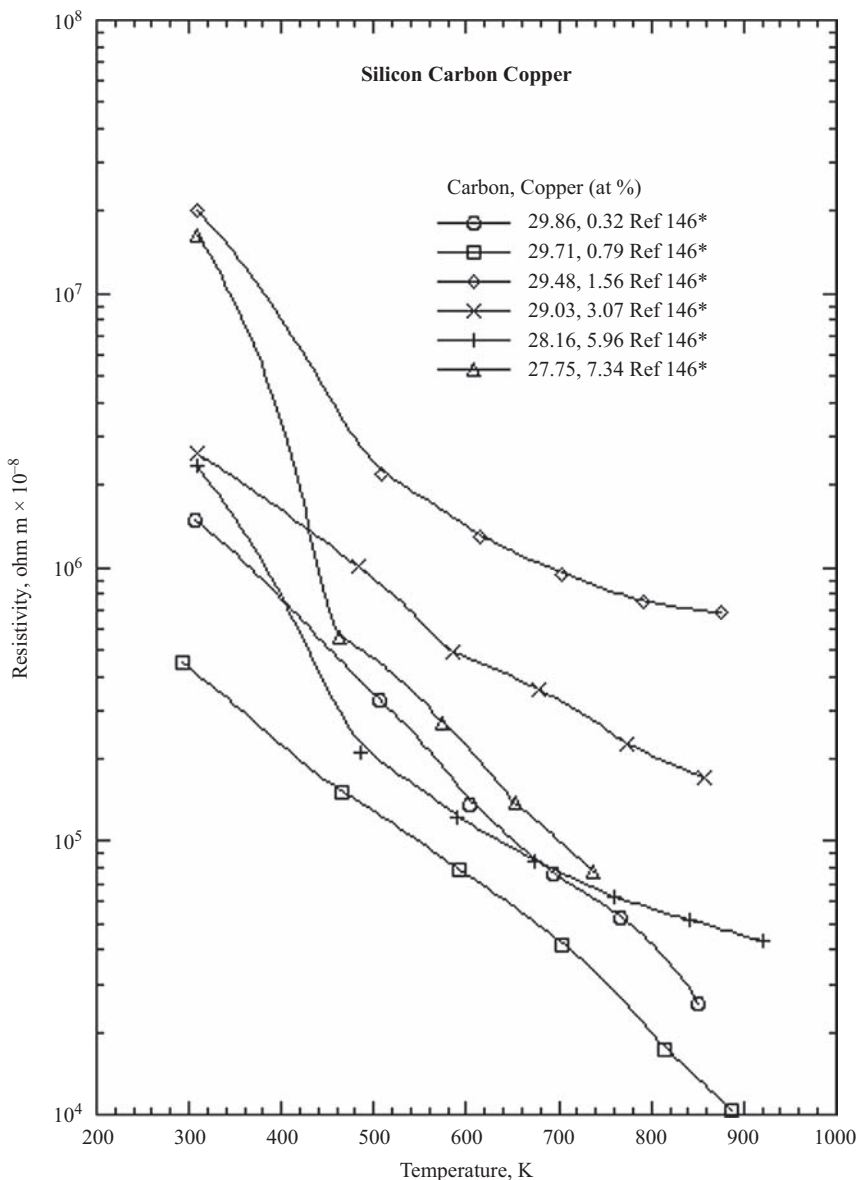


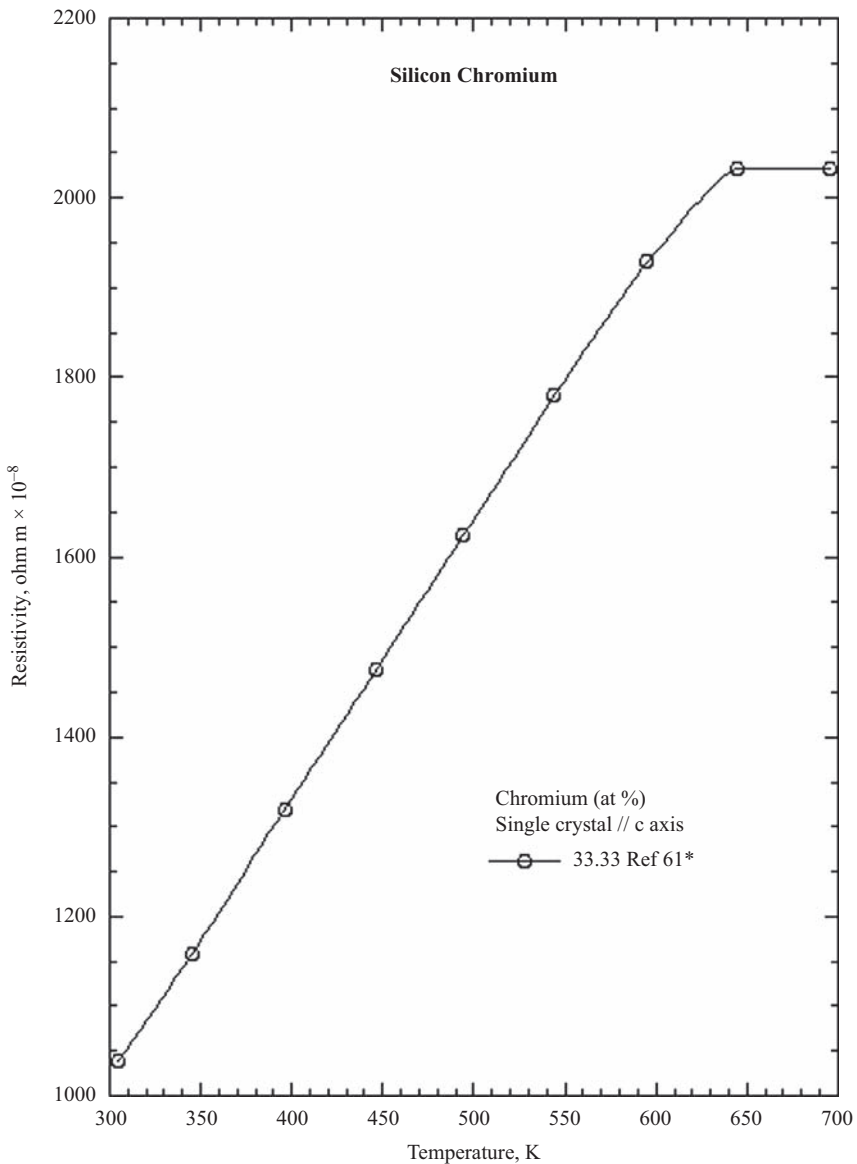


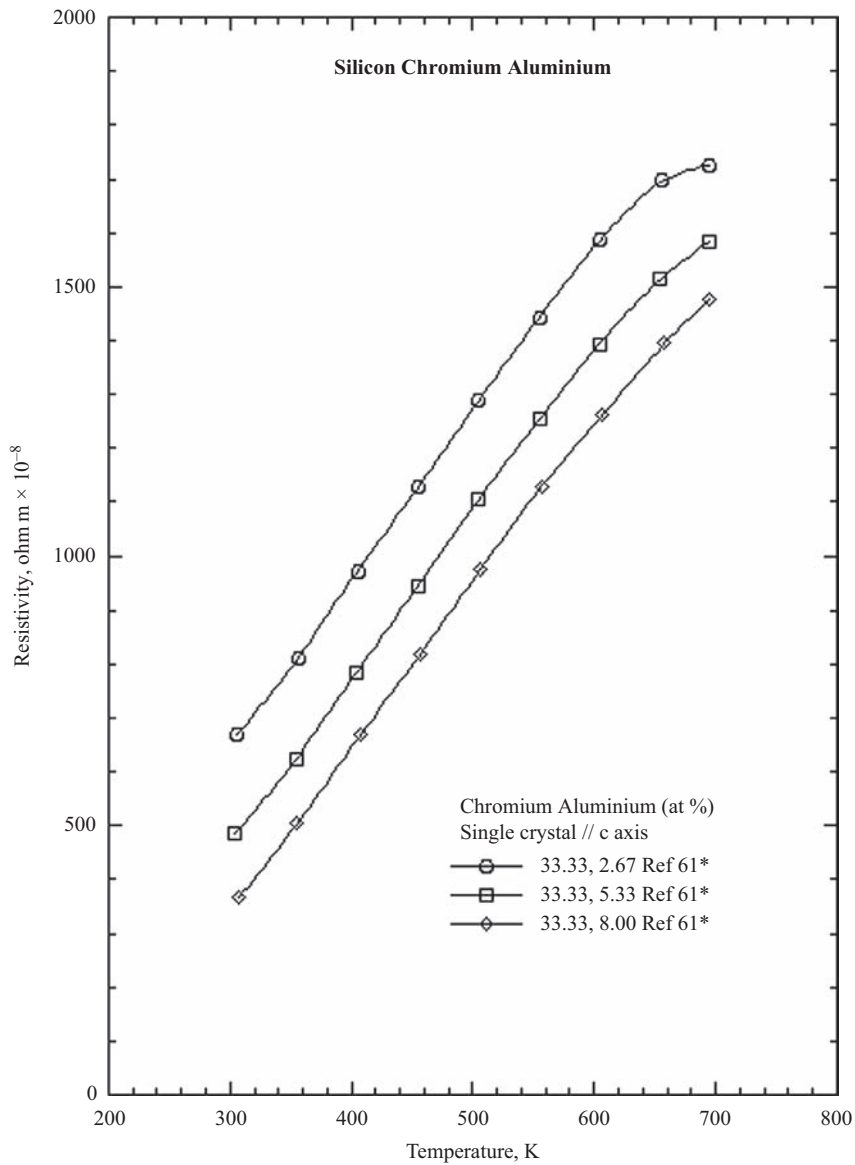


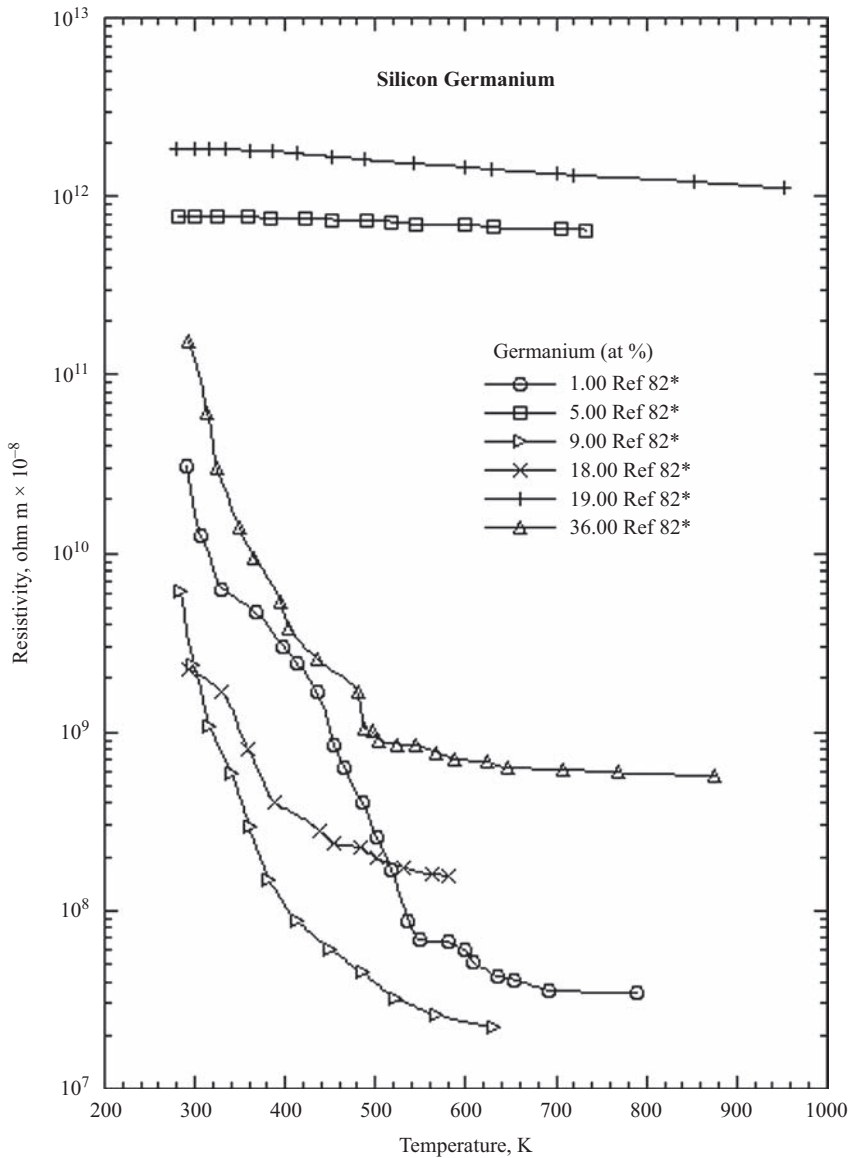


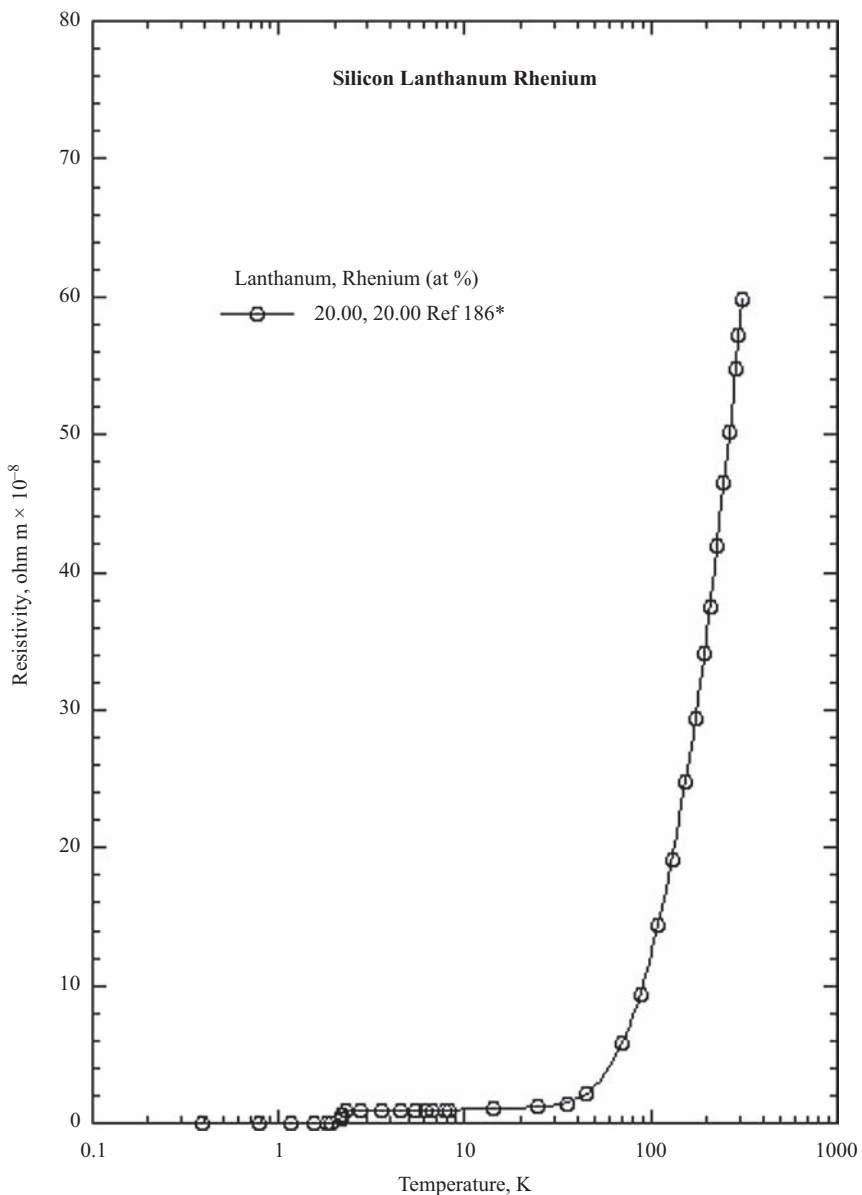


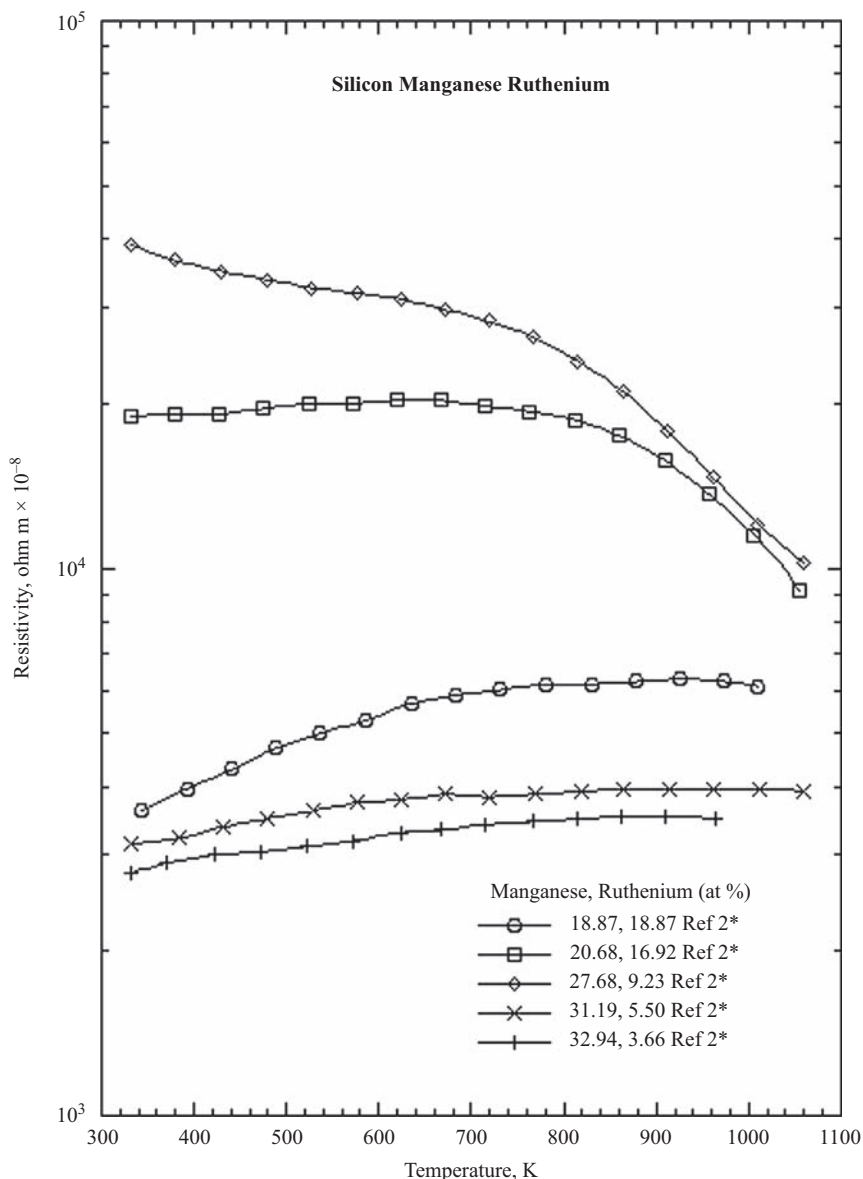


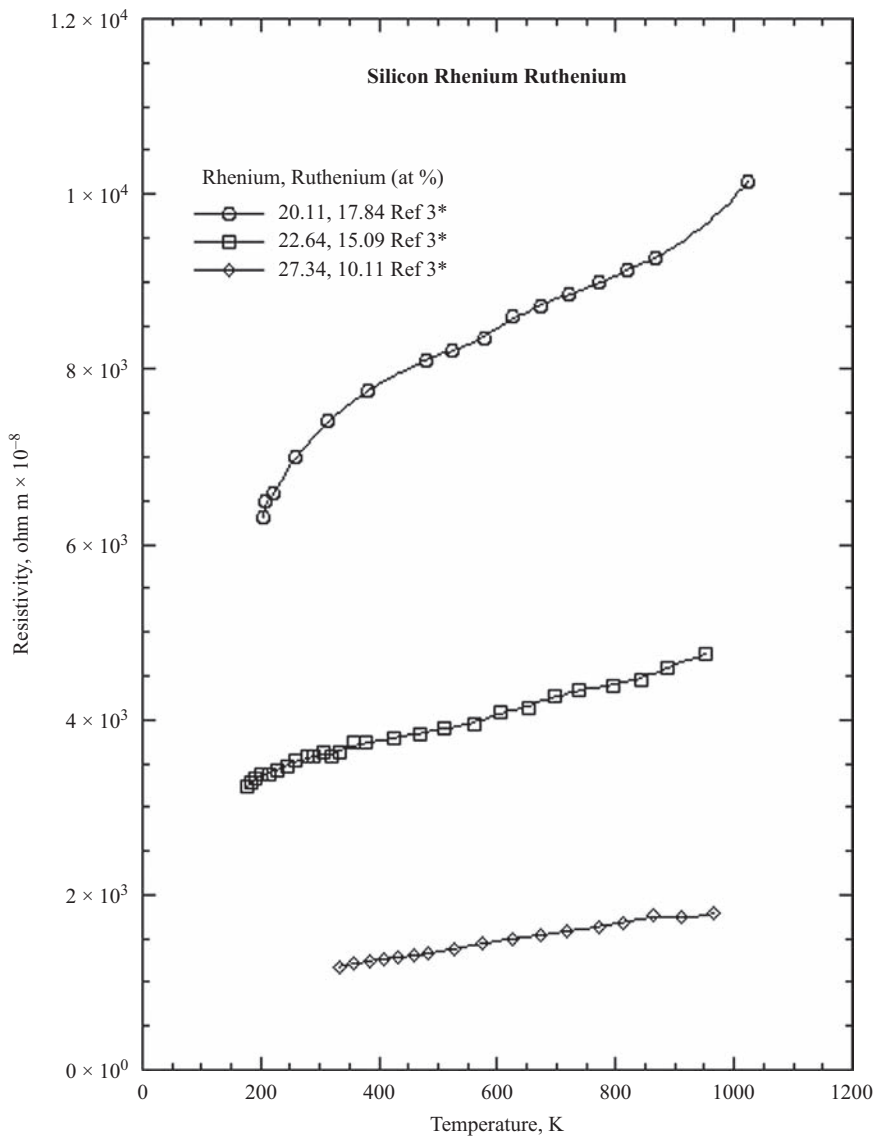


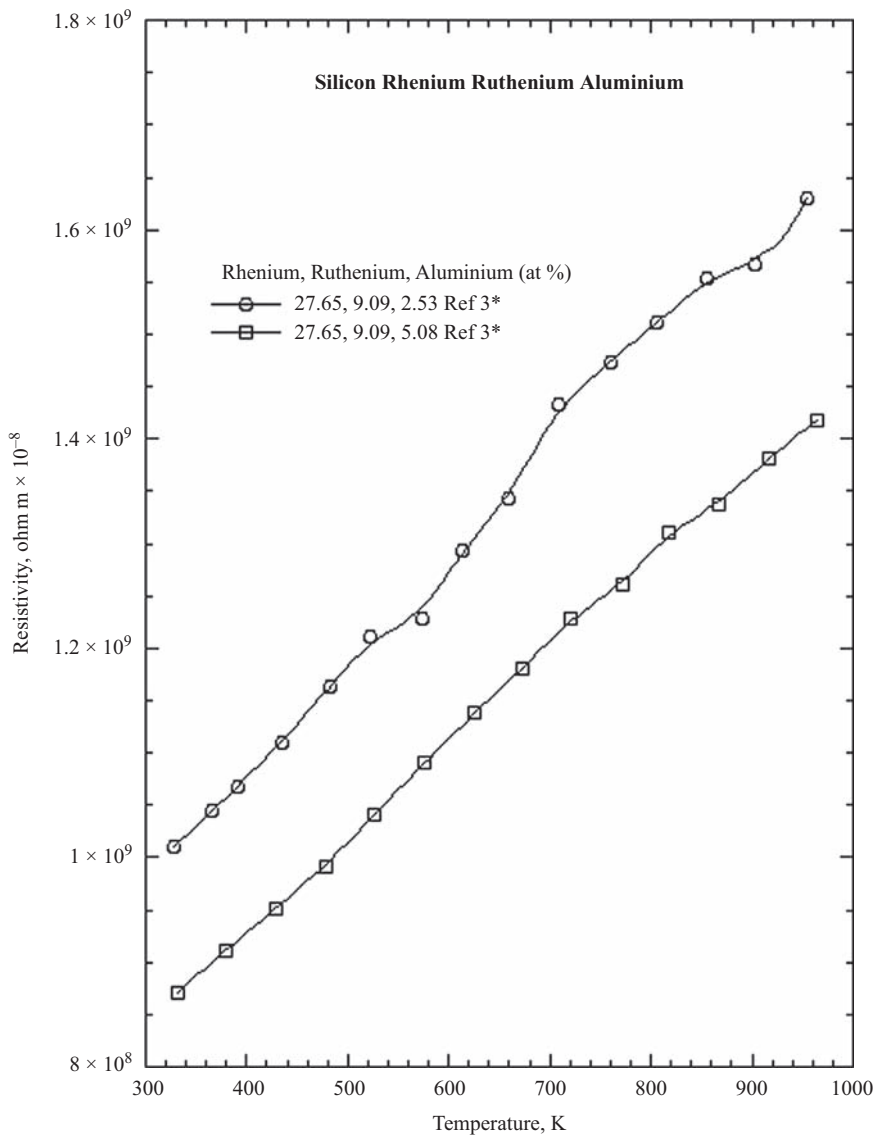


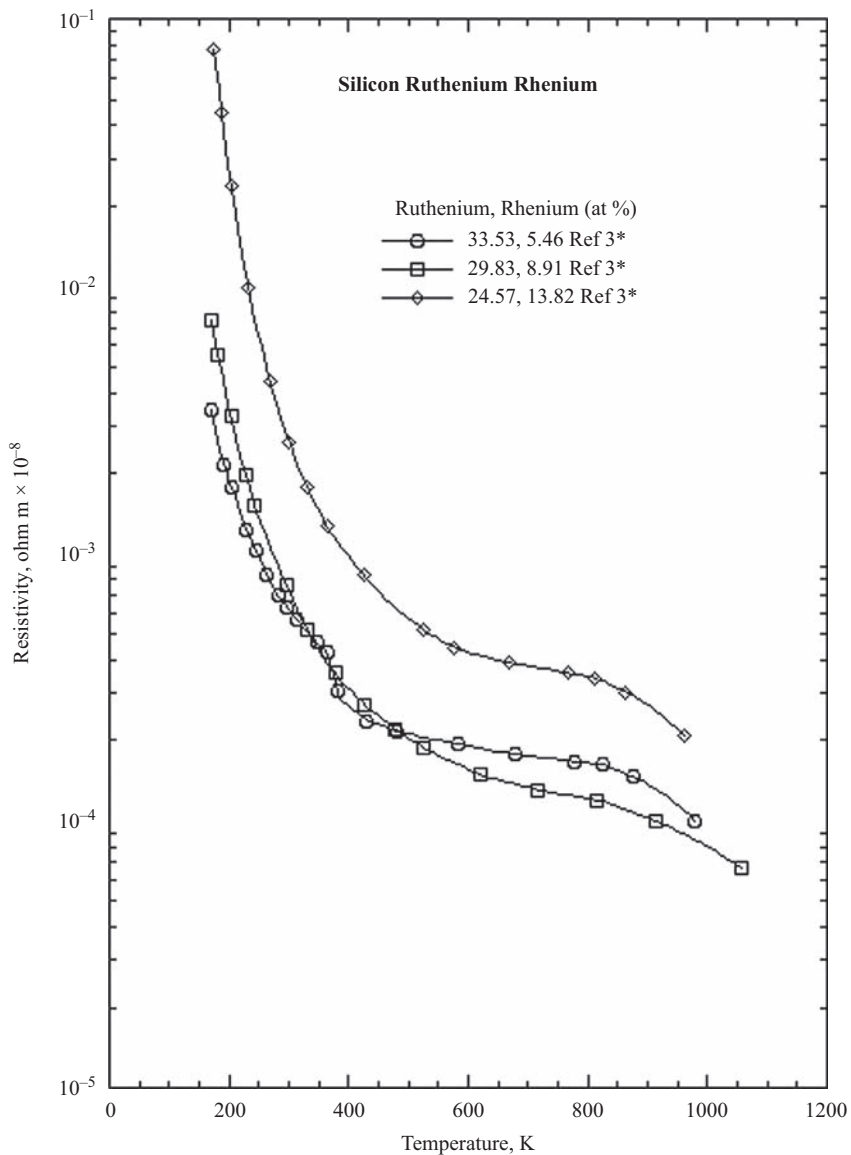


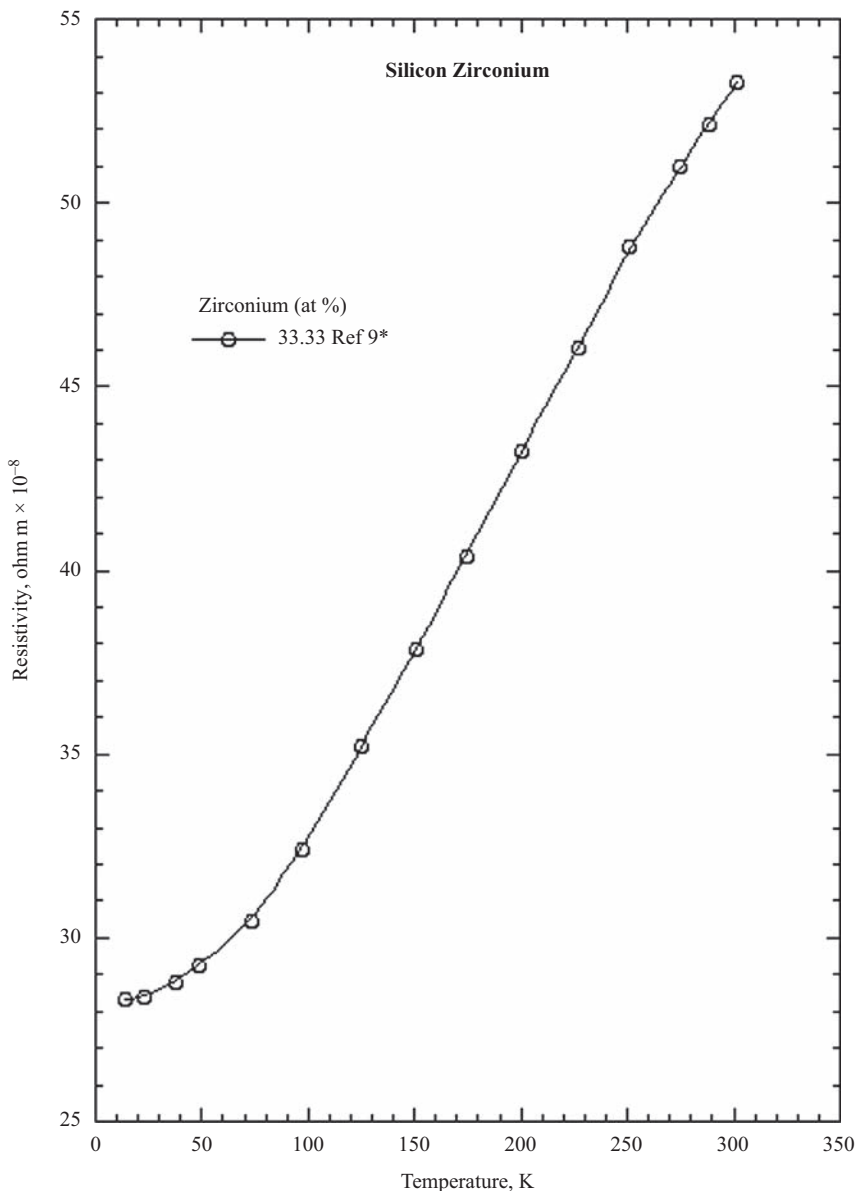


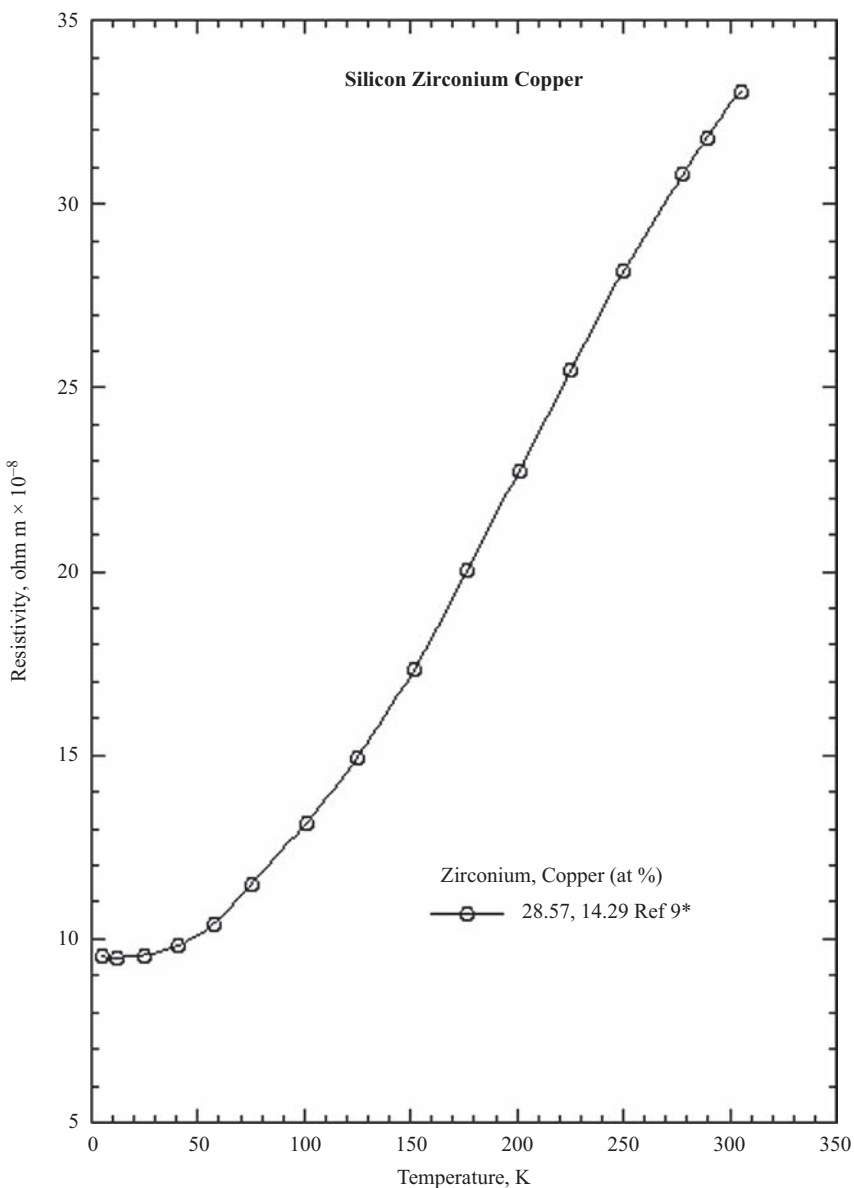


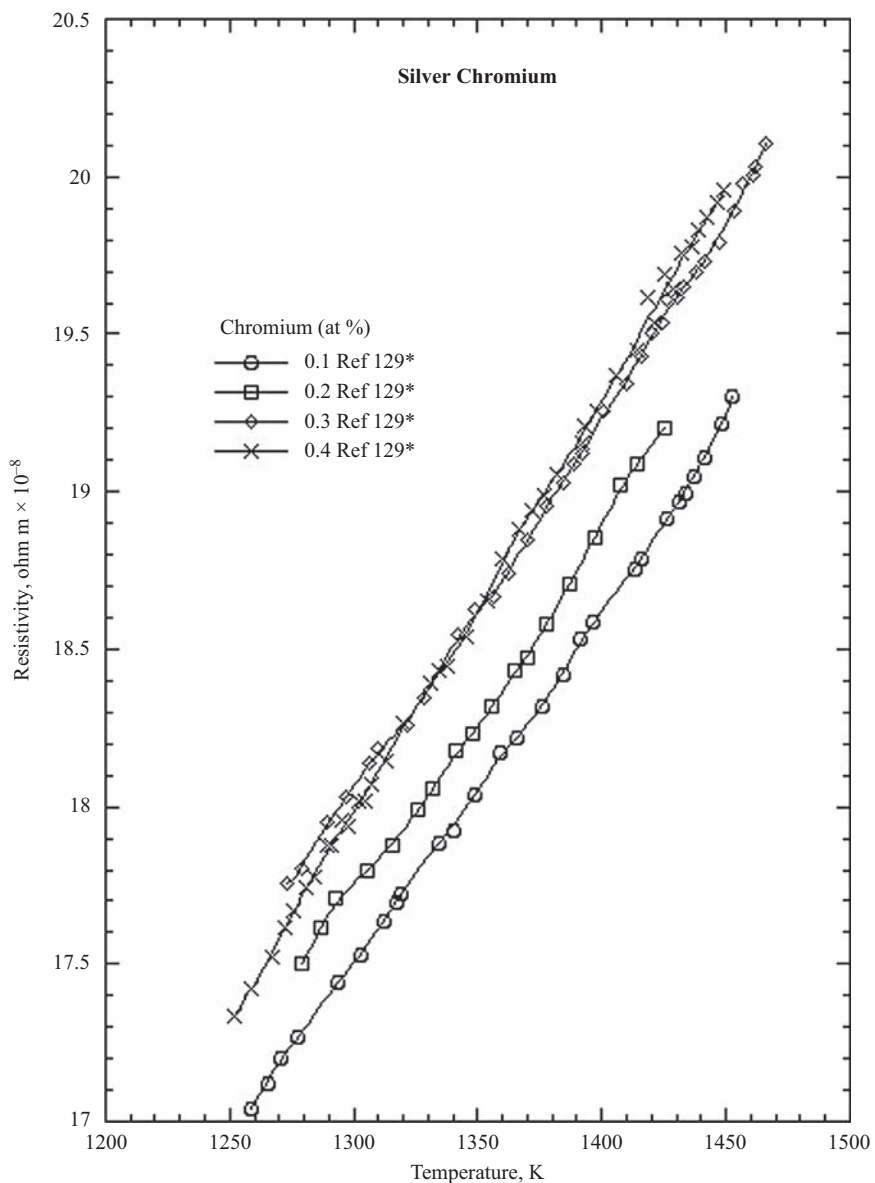


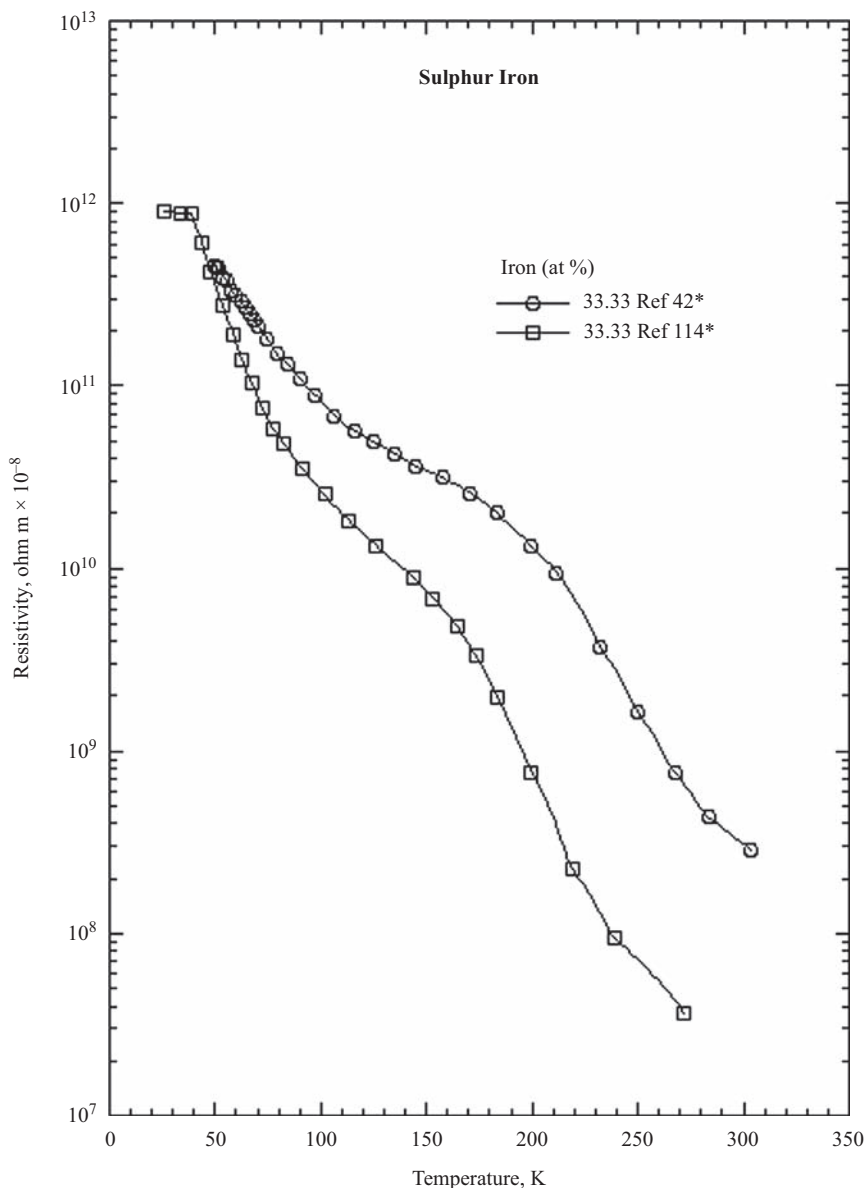


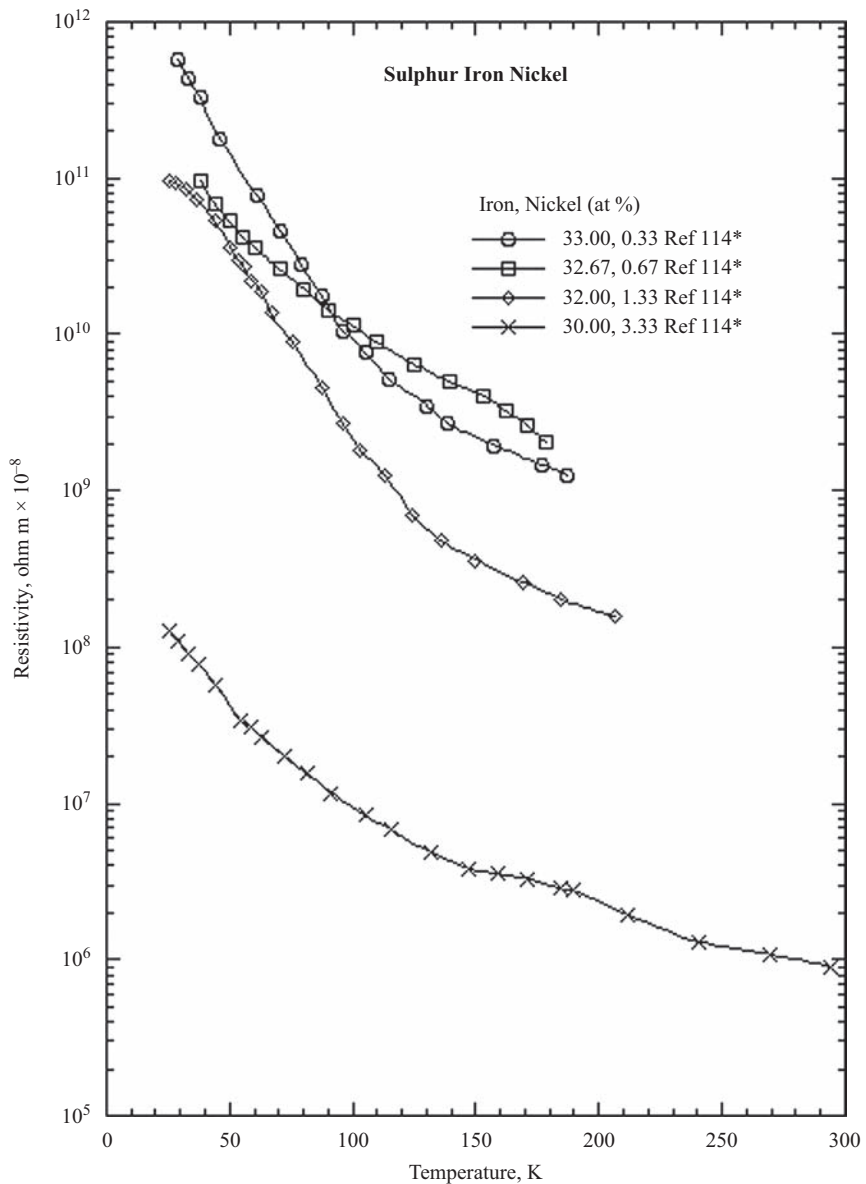


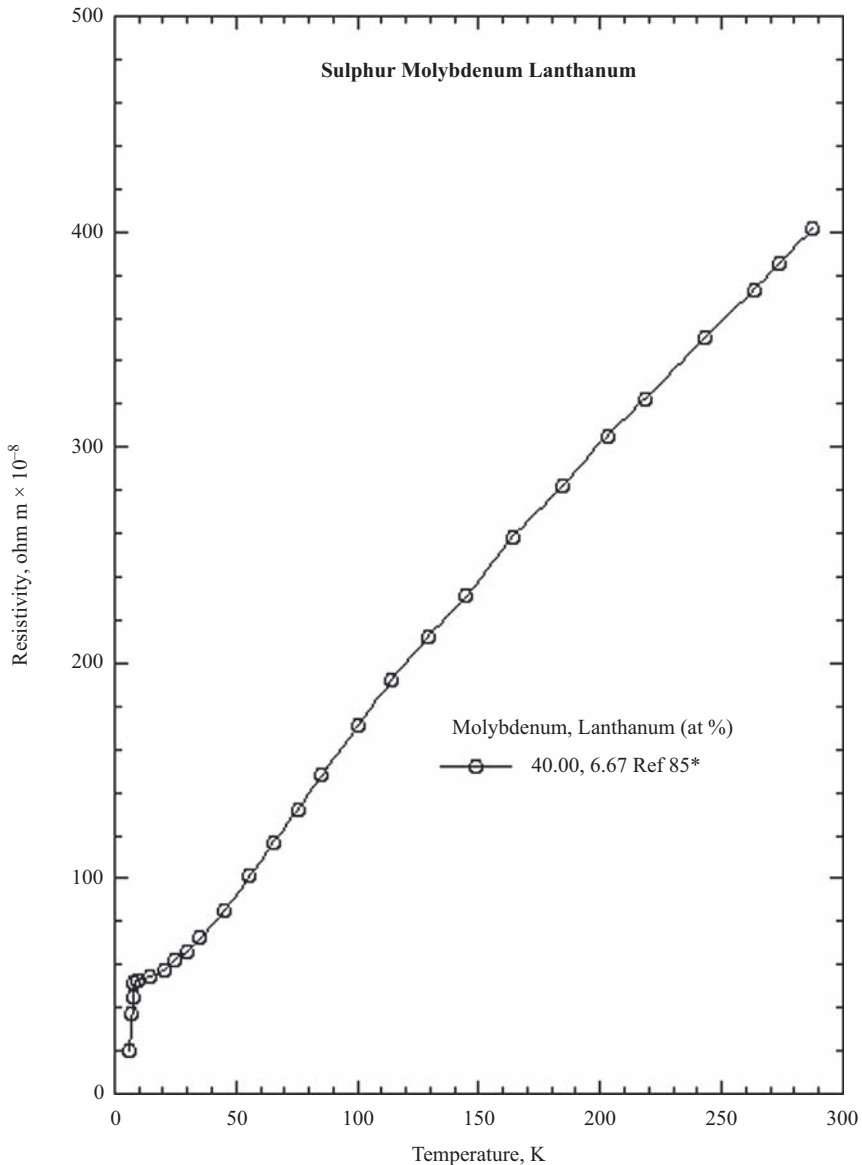


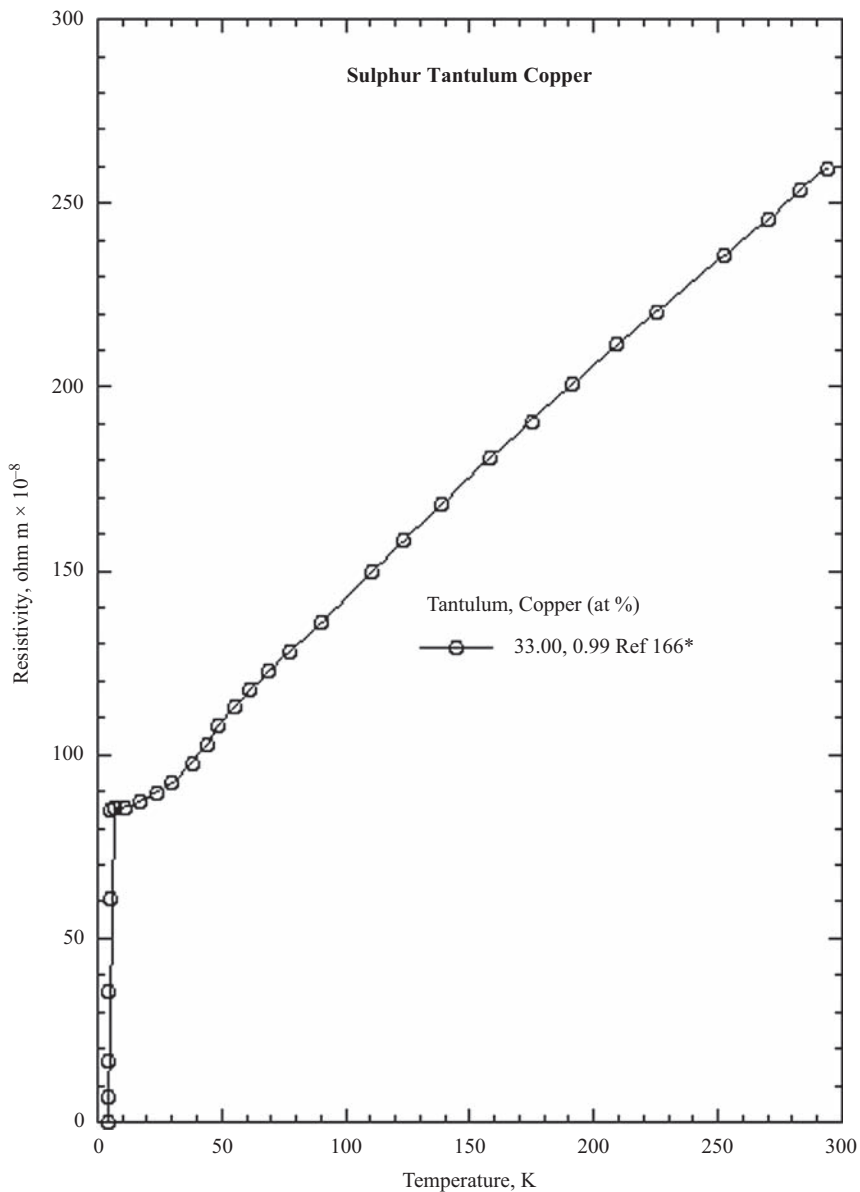


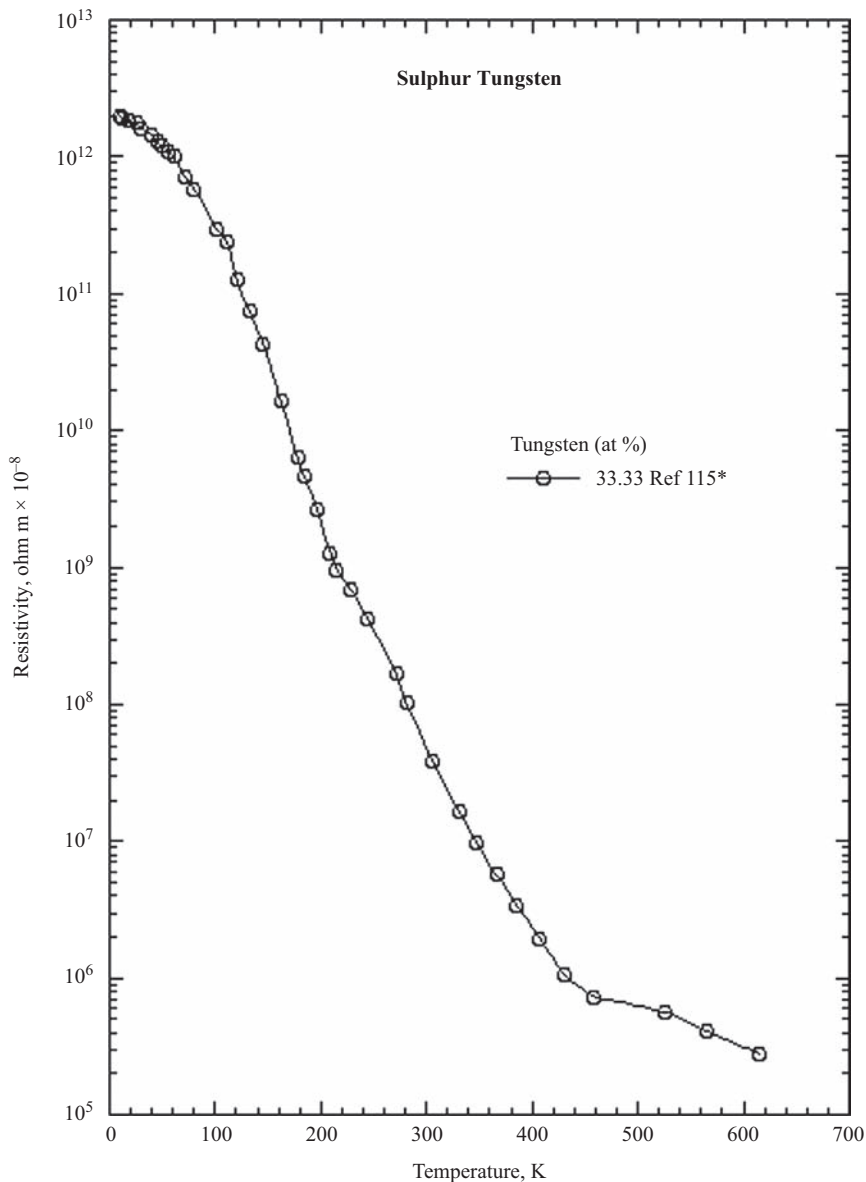


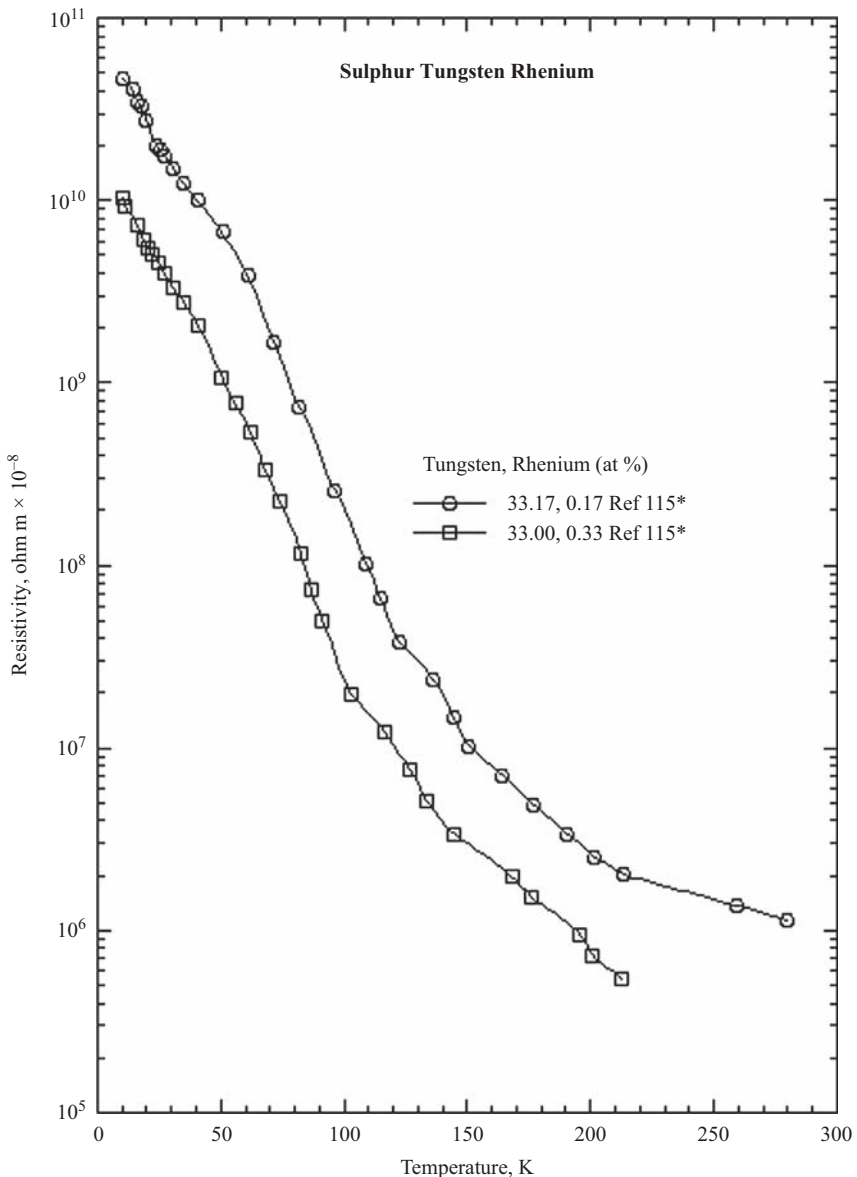


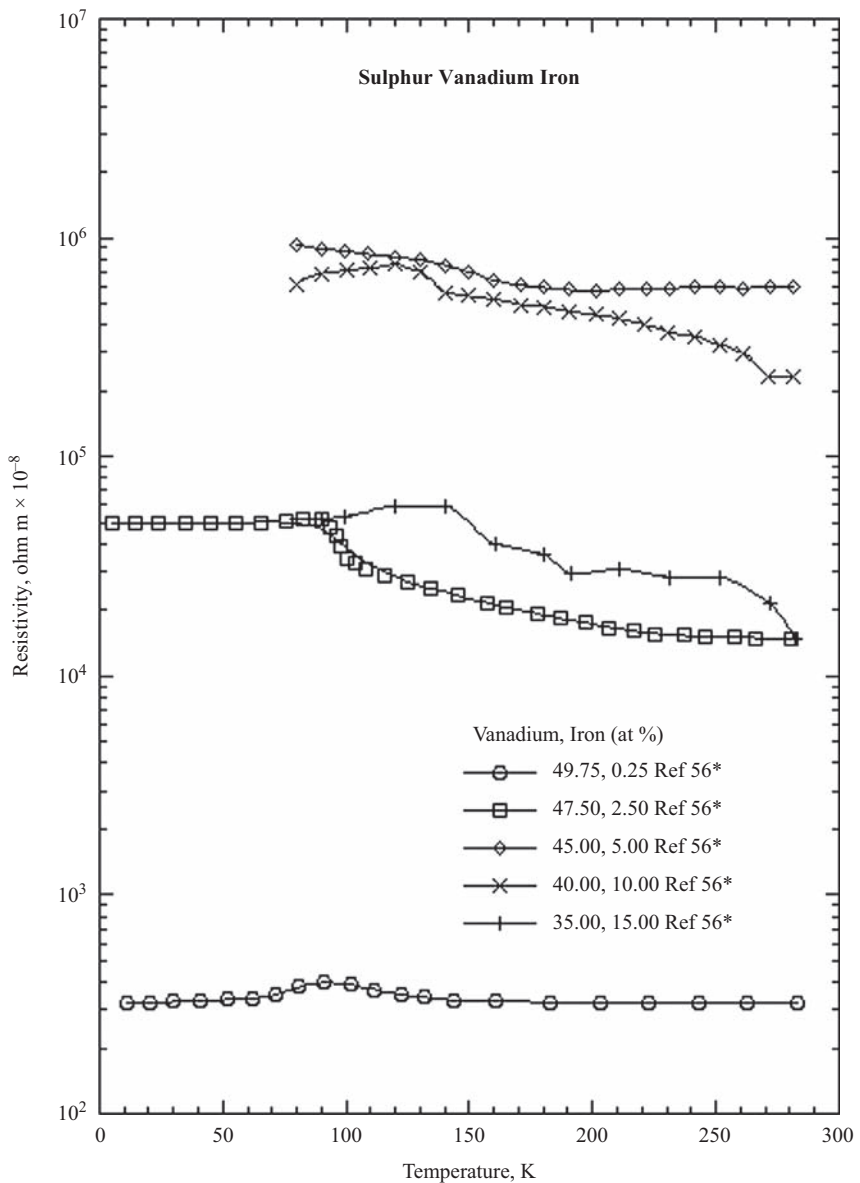


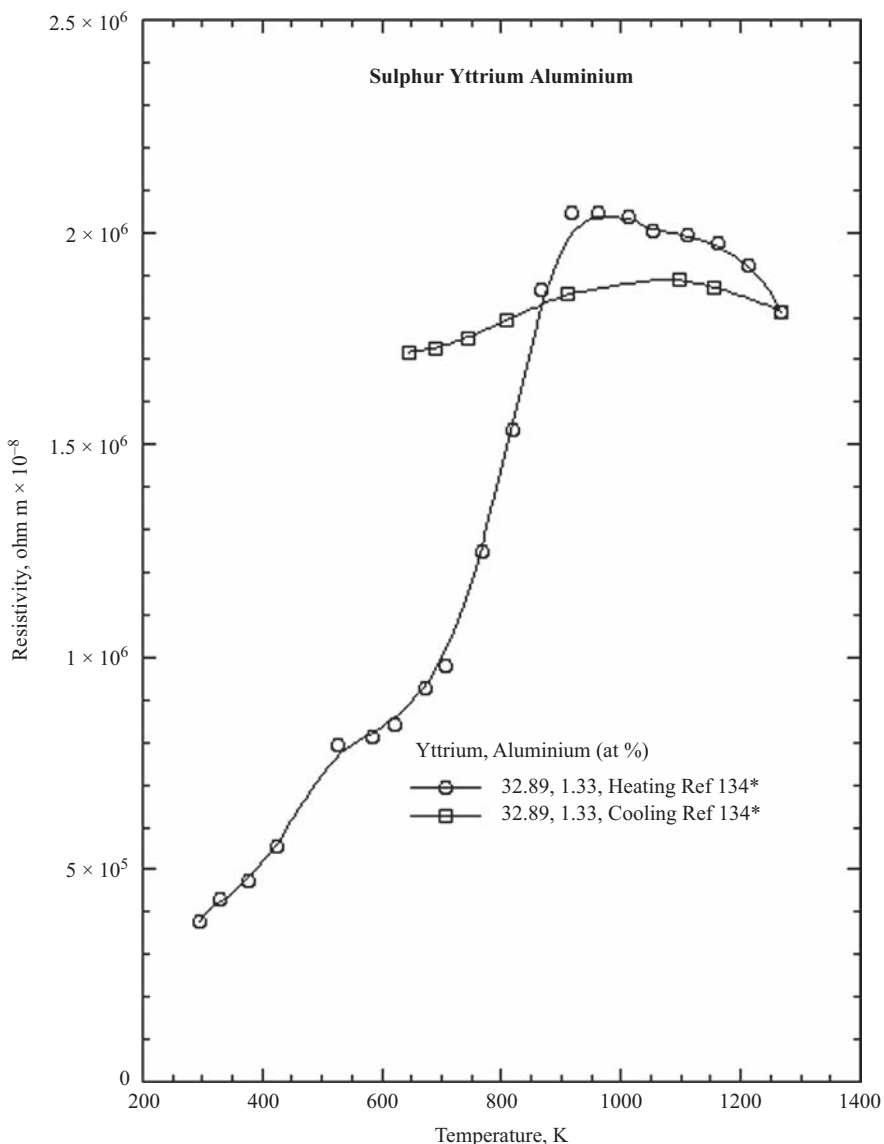


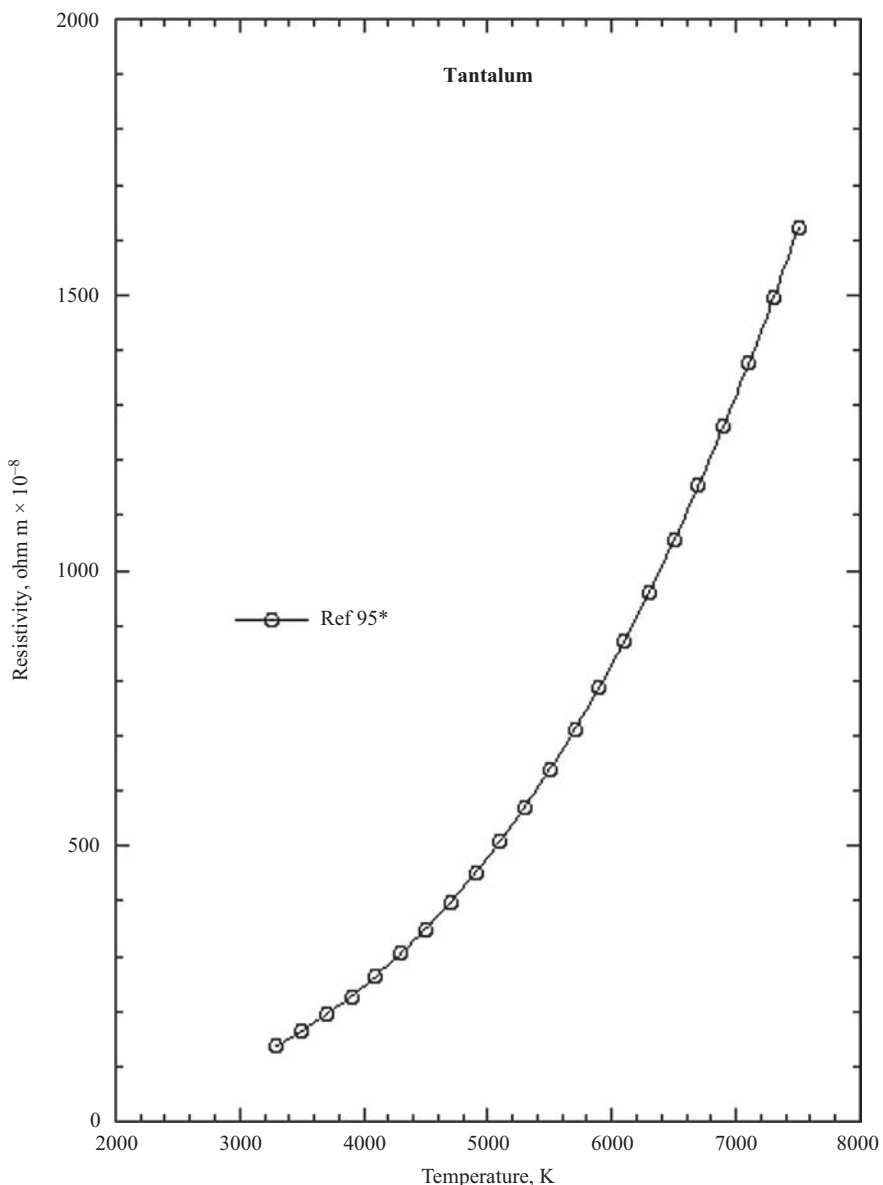


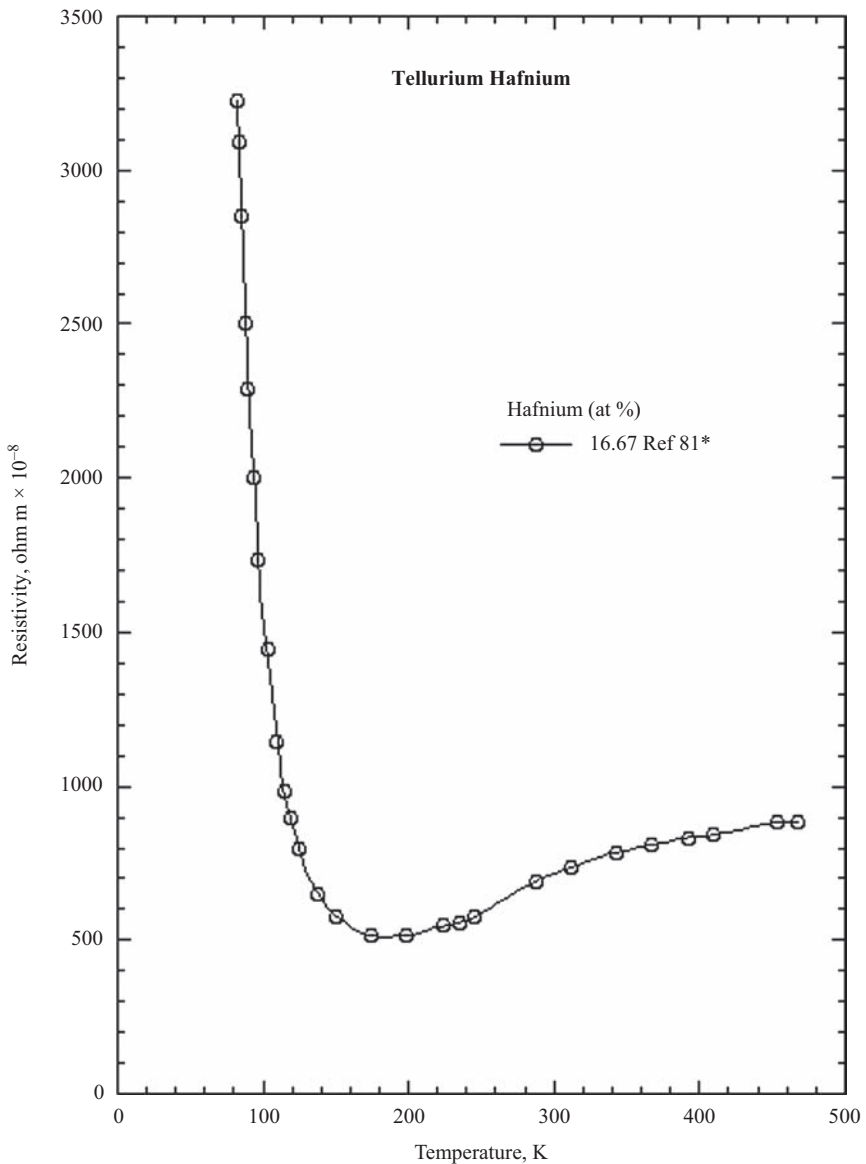


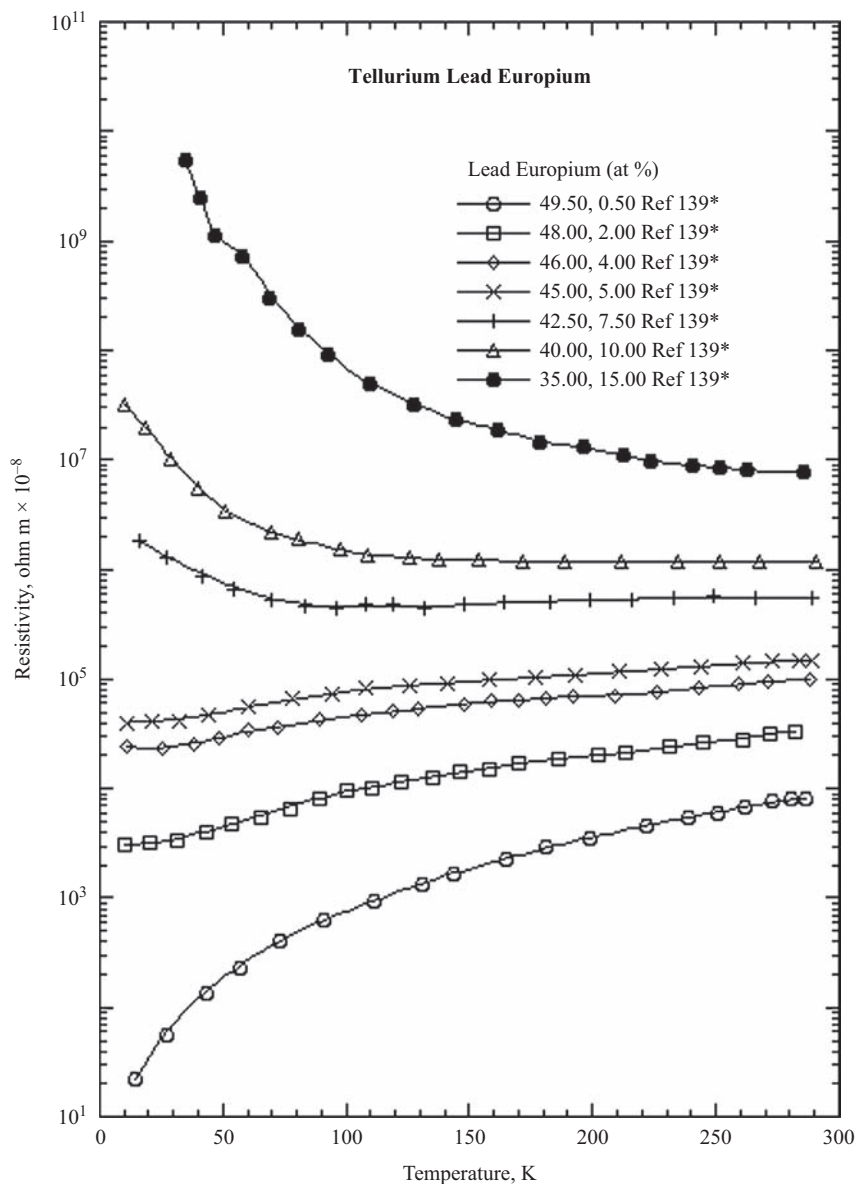


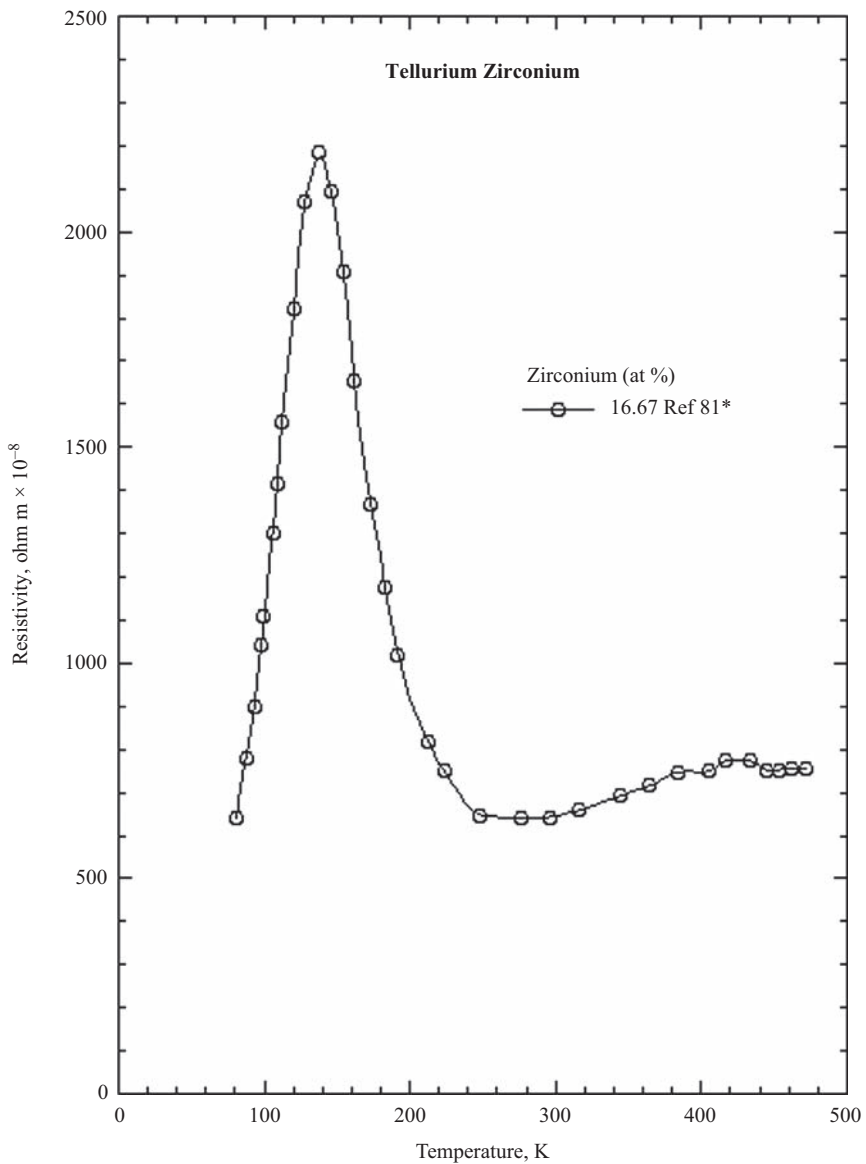


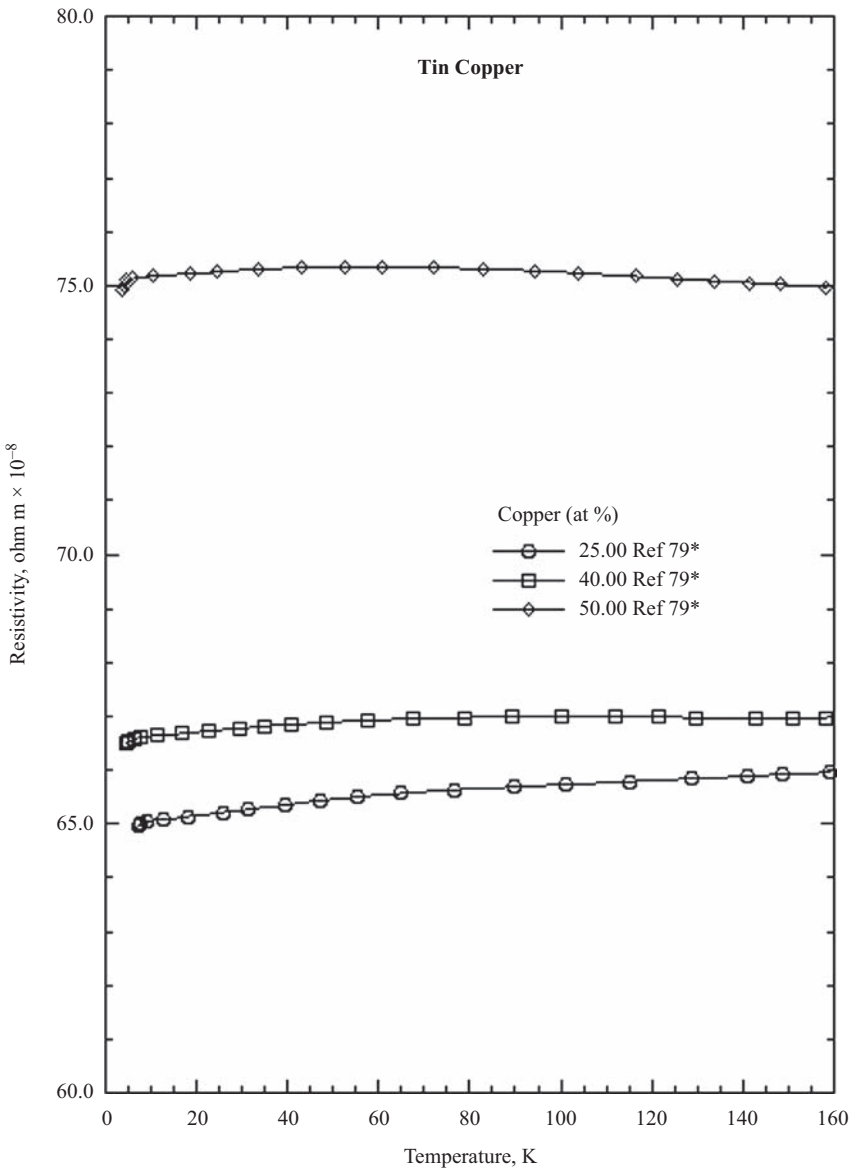


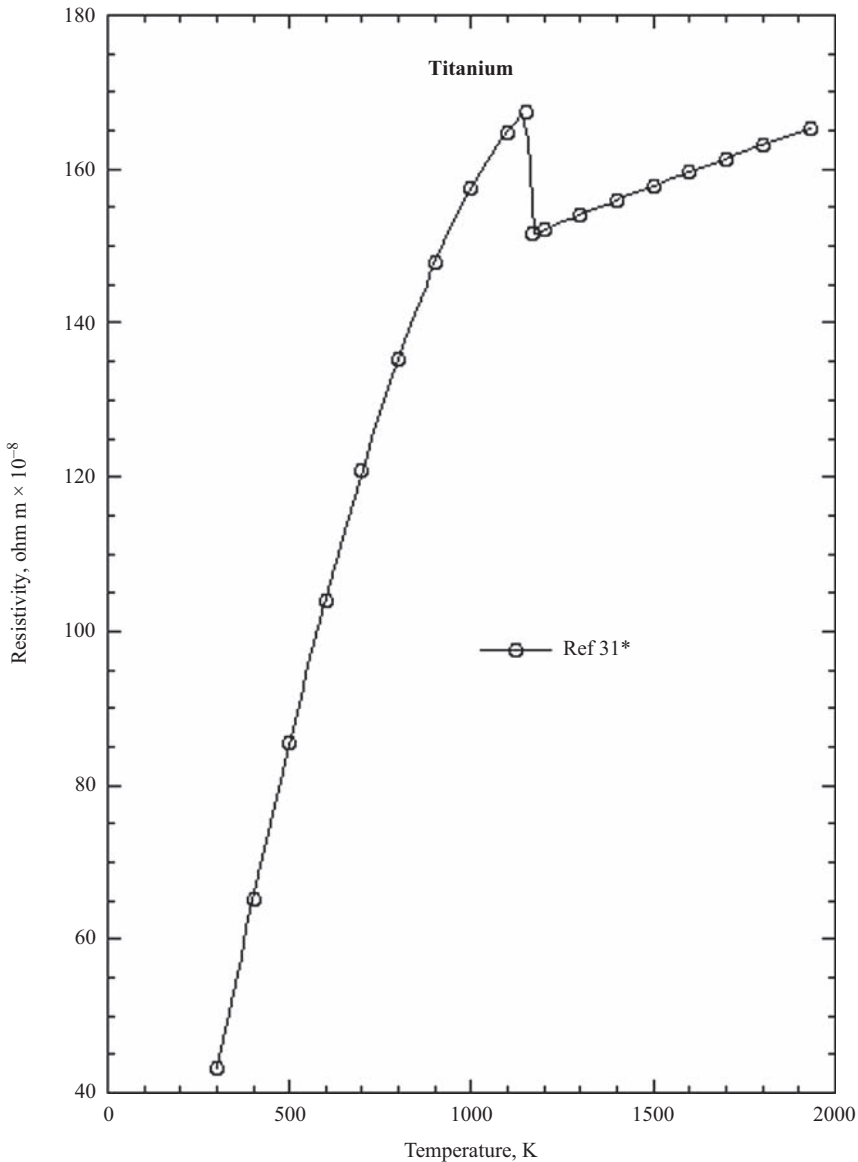


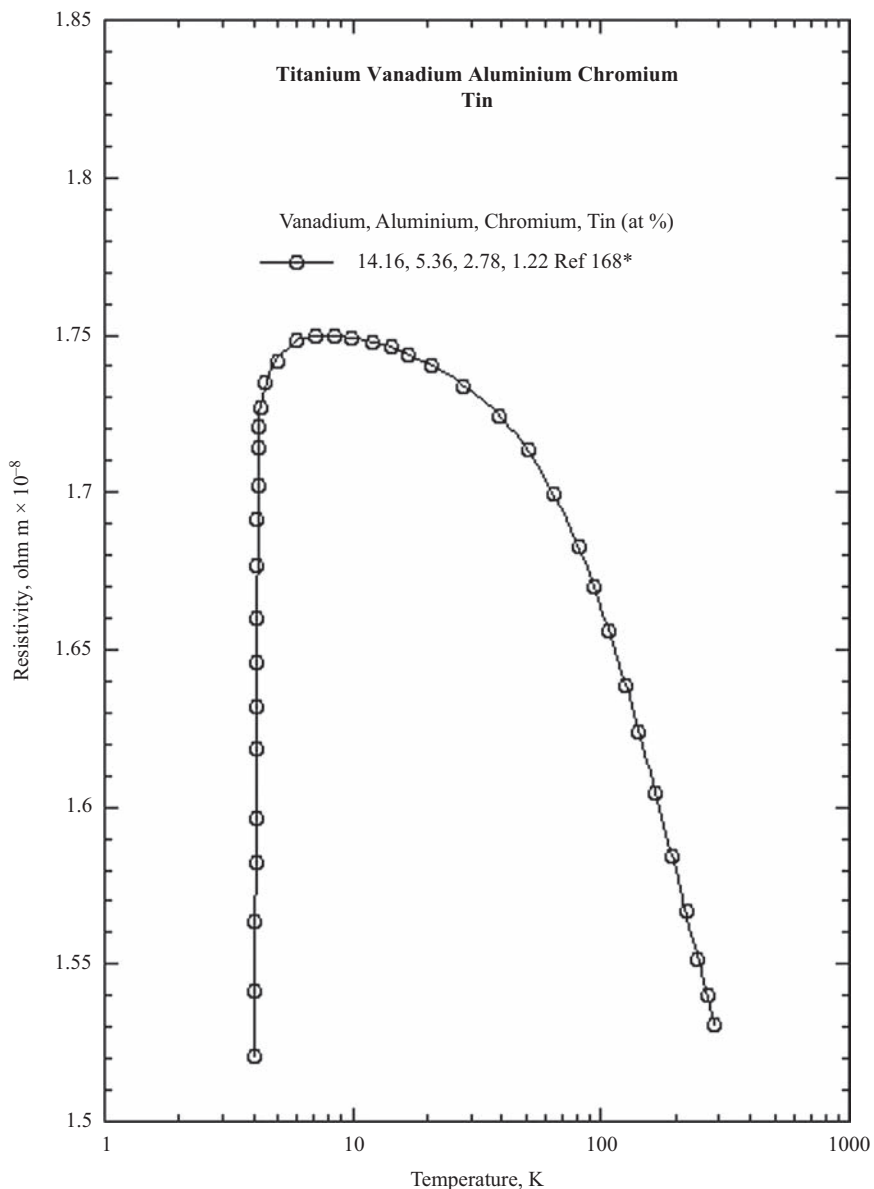


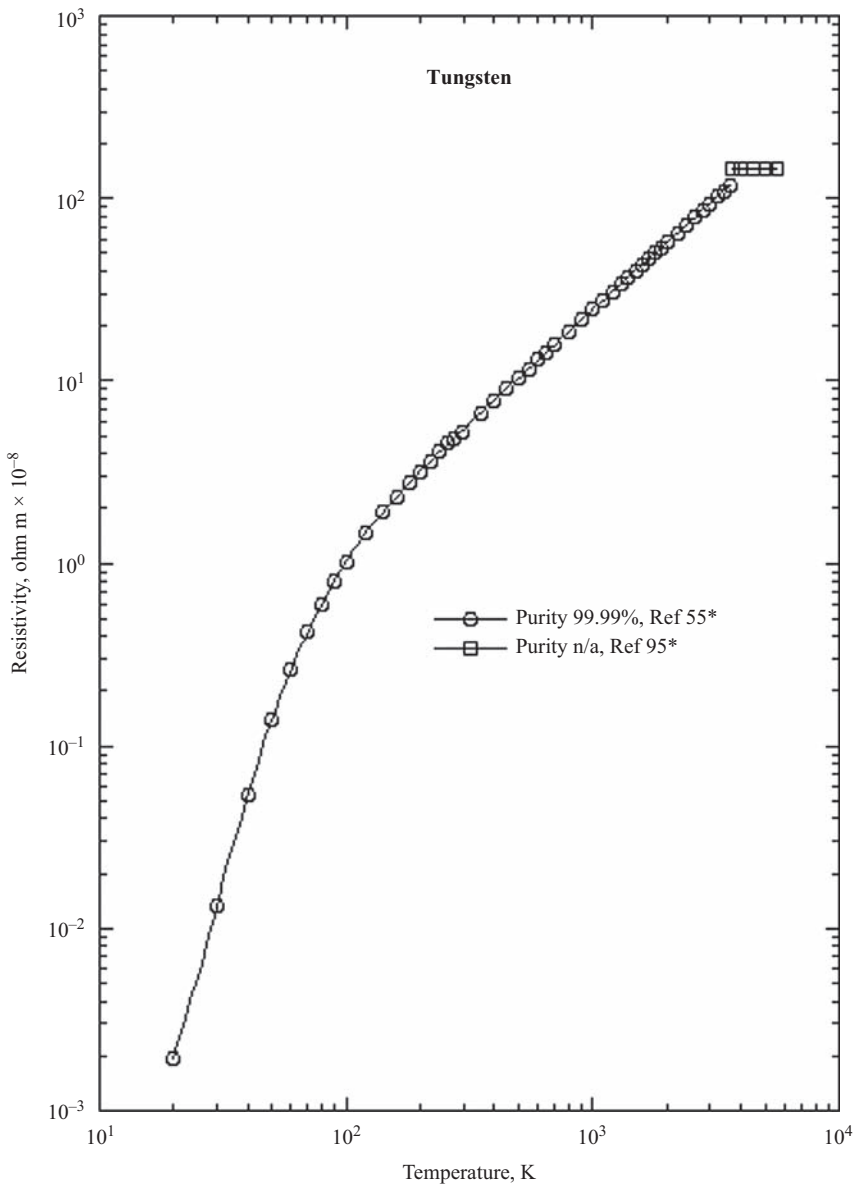




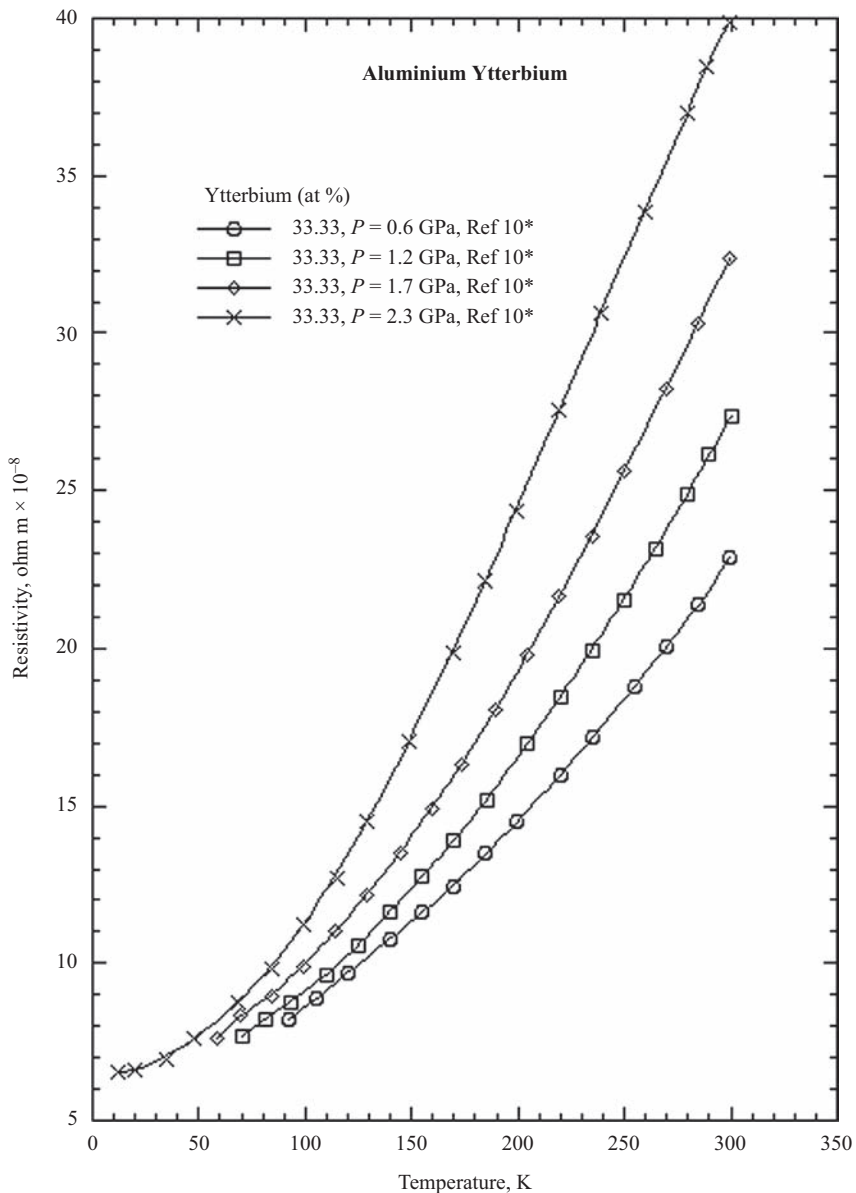


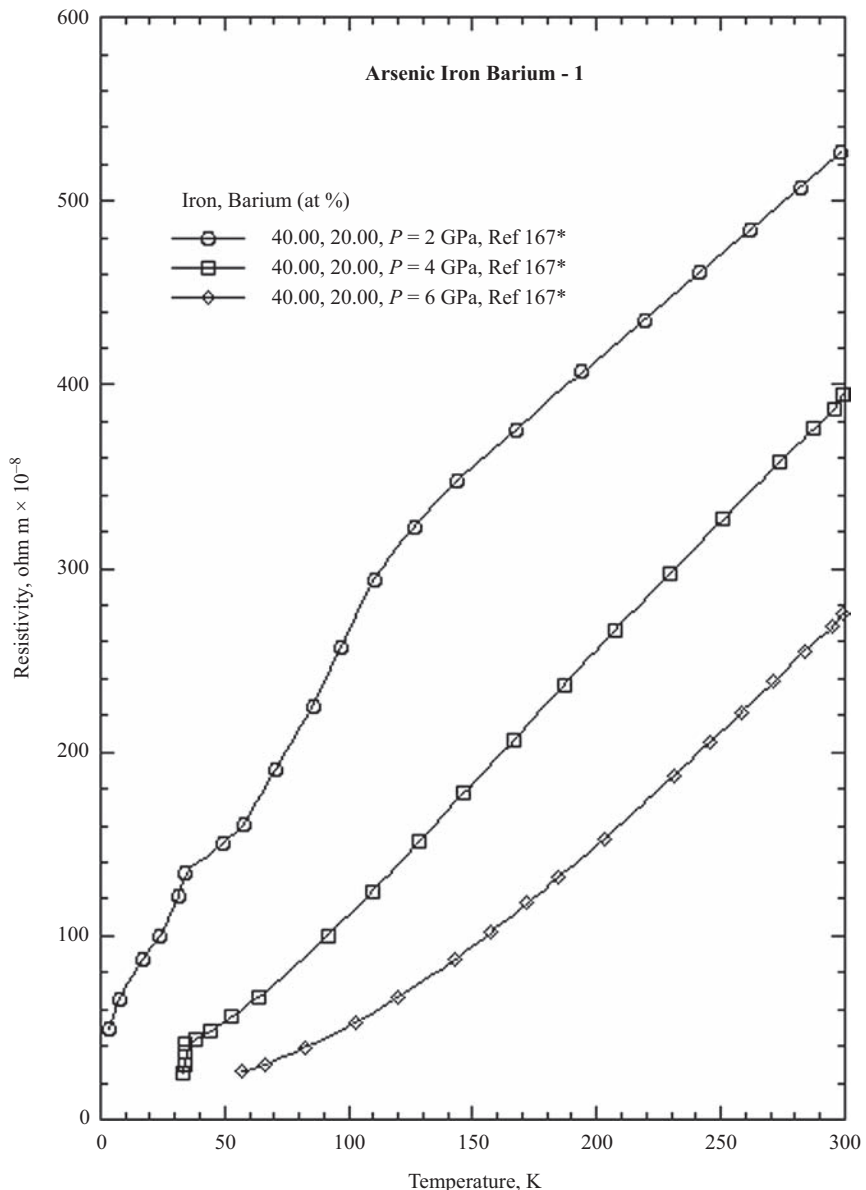


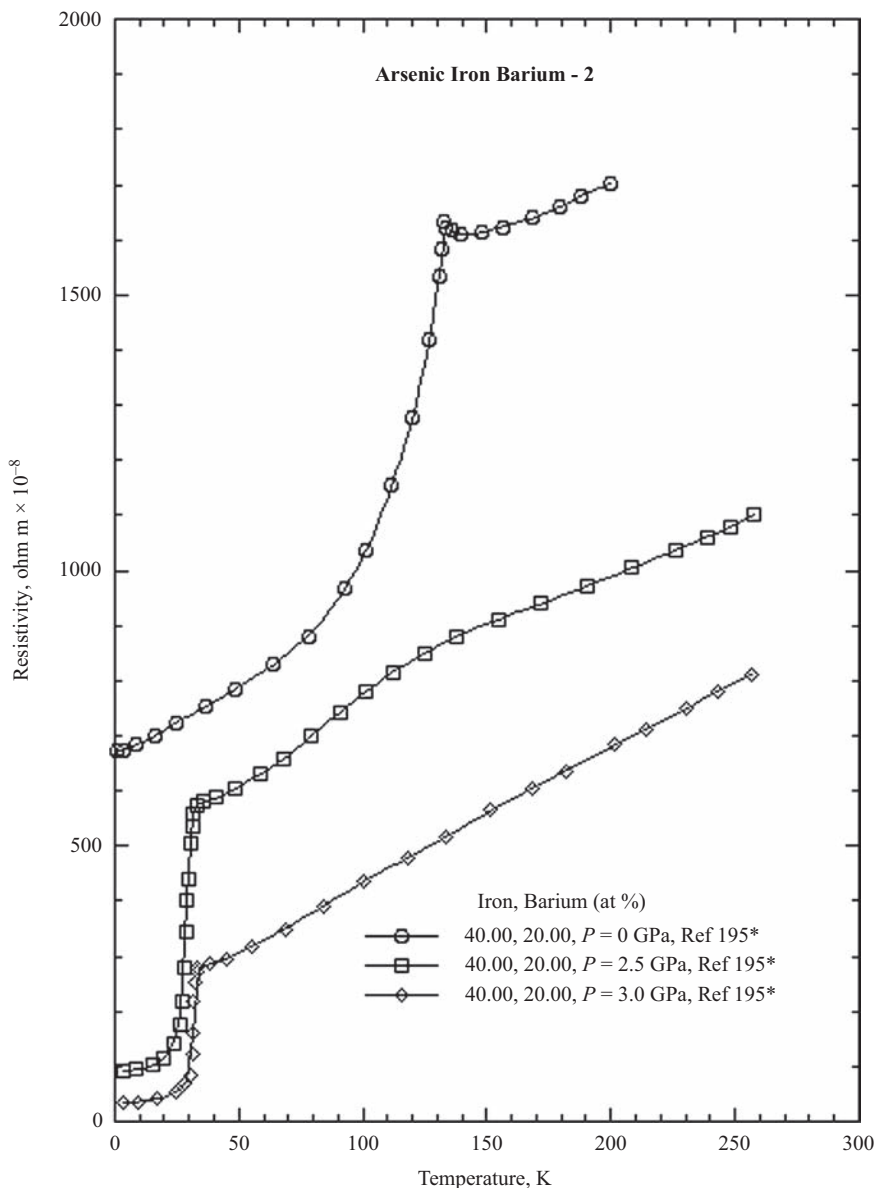


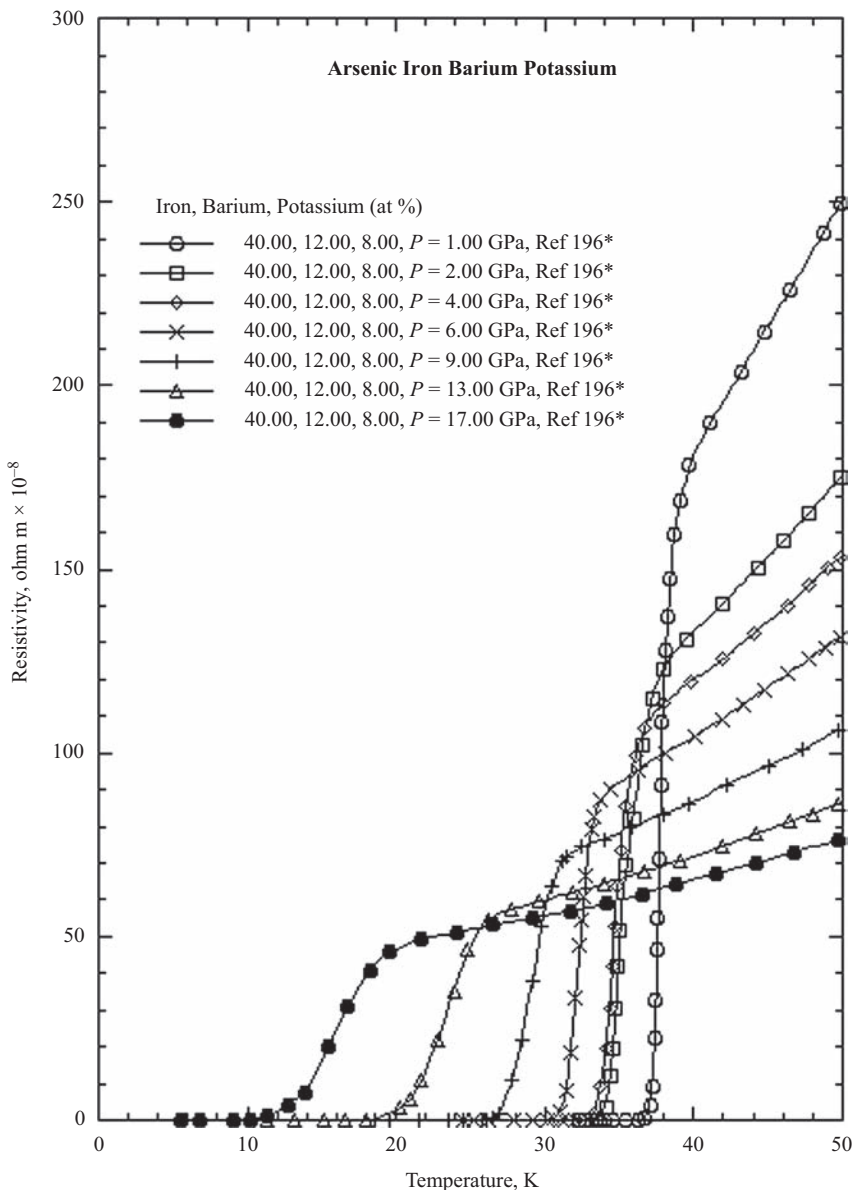


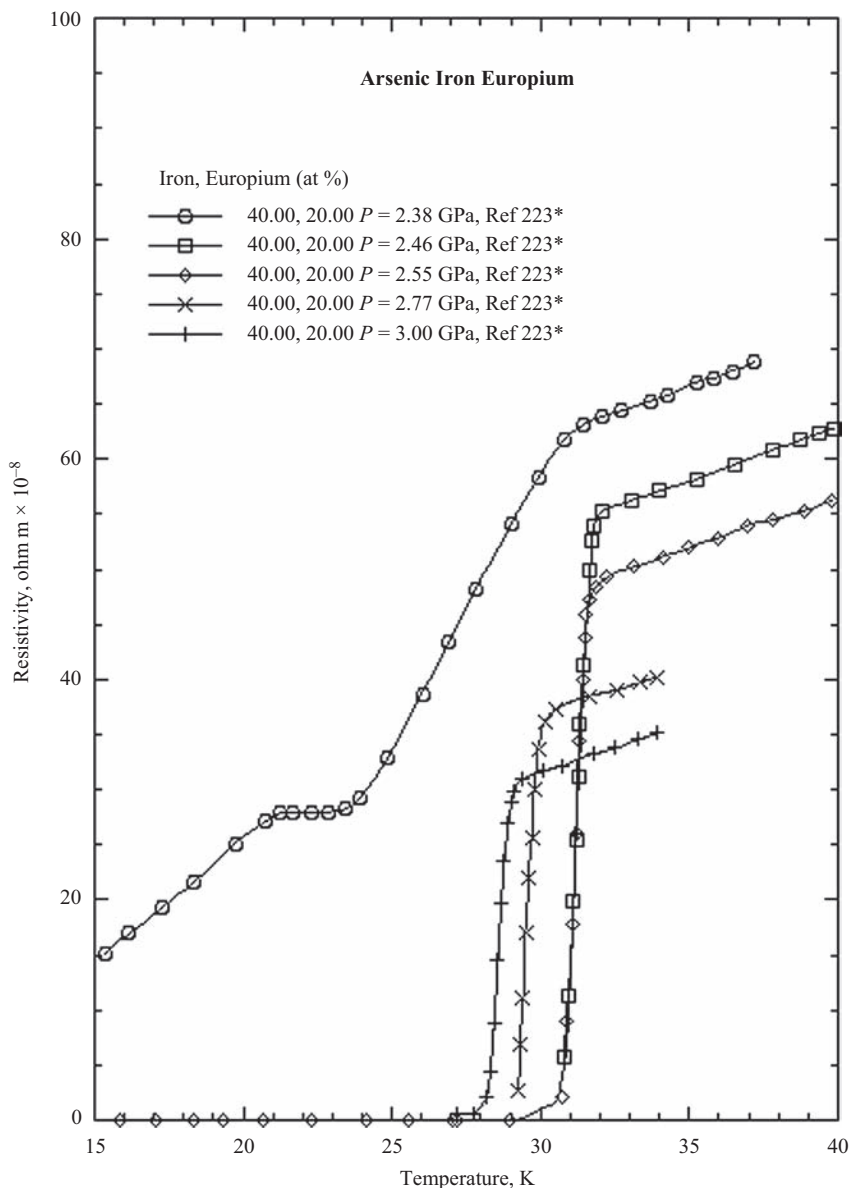
6.2 Electrical resistivity as a function of temperature and pressure

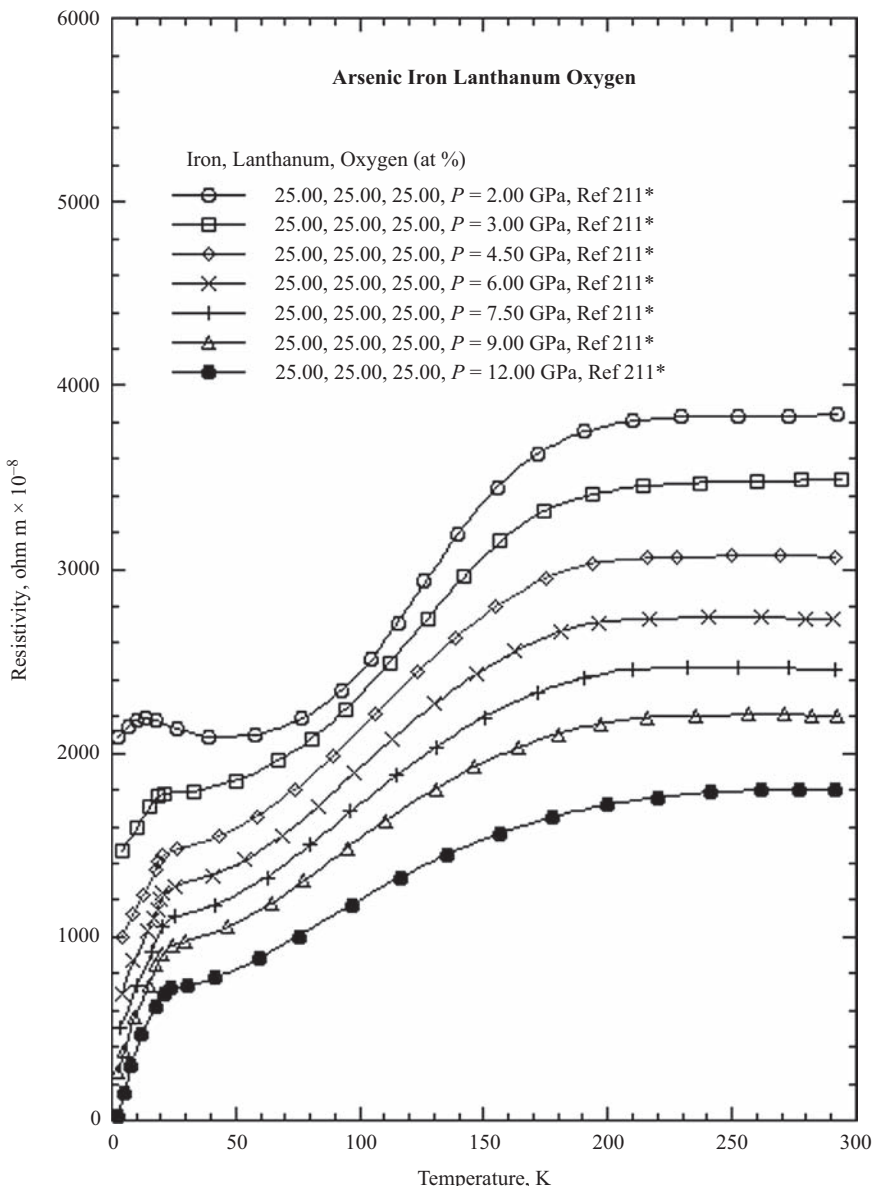


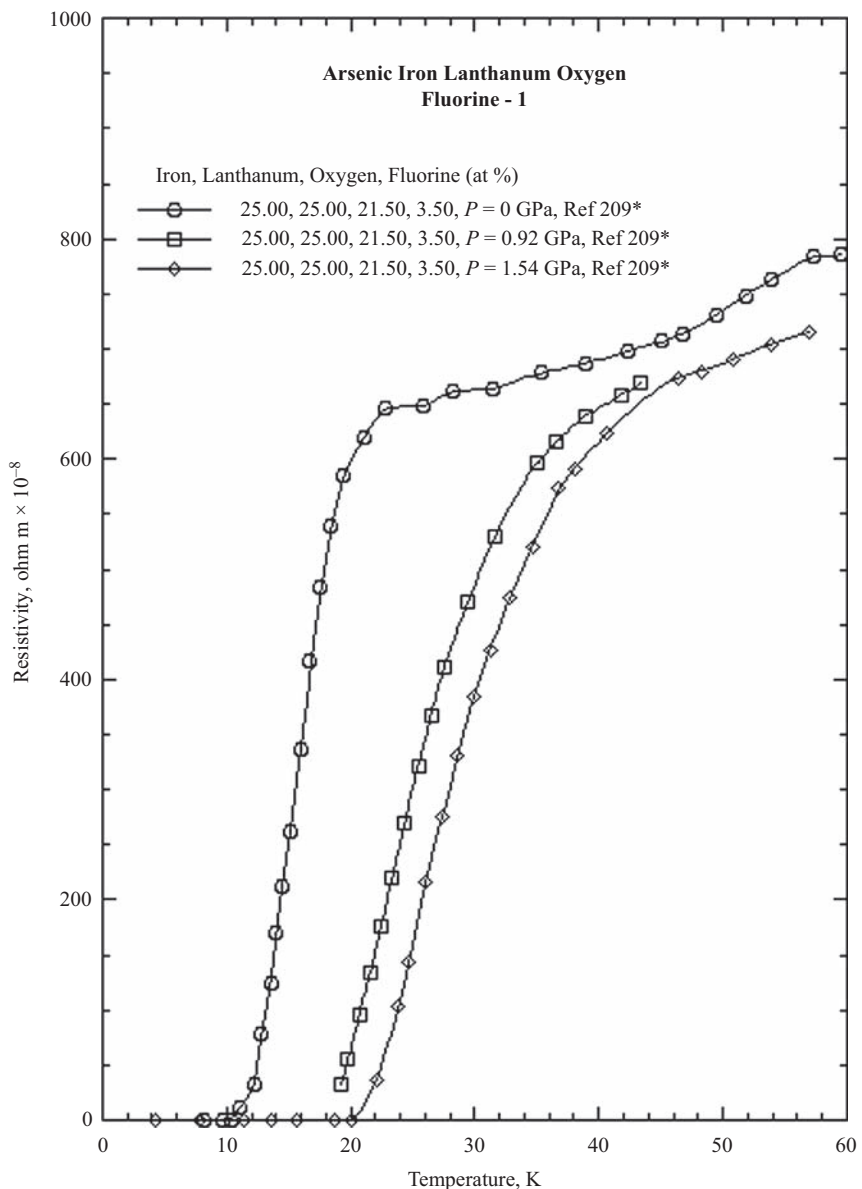


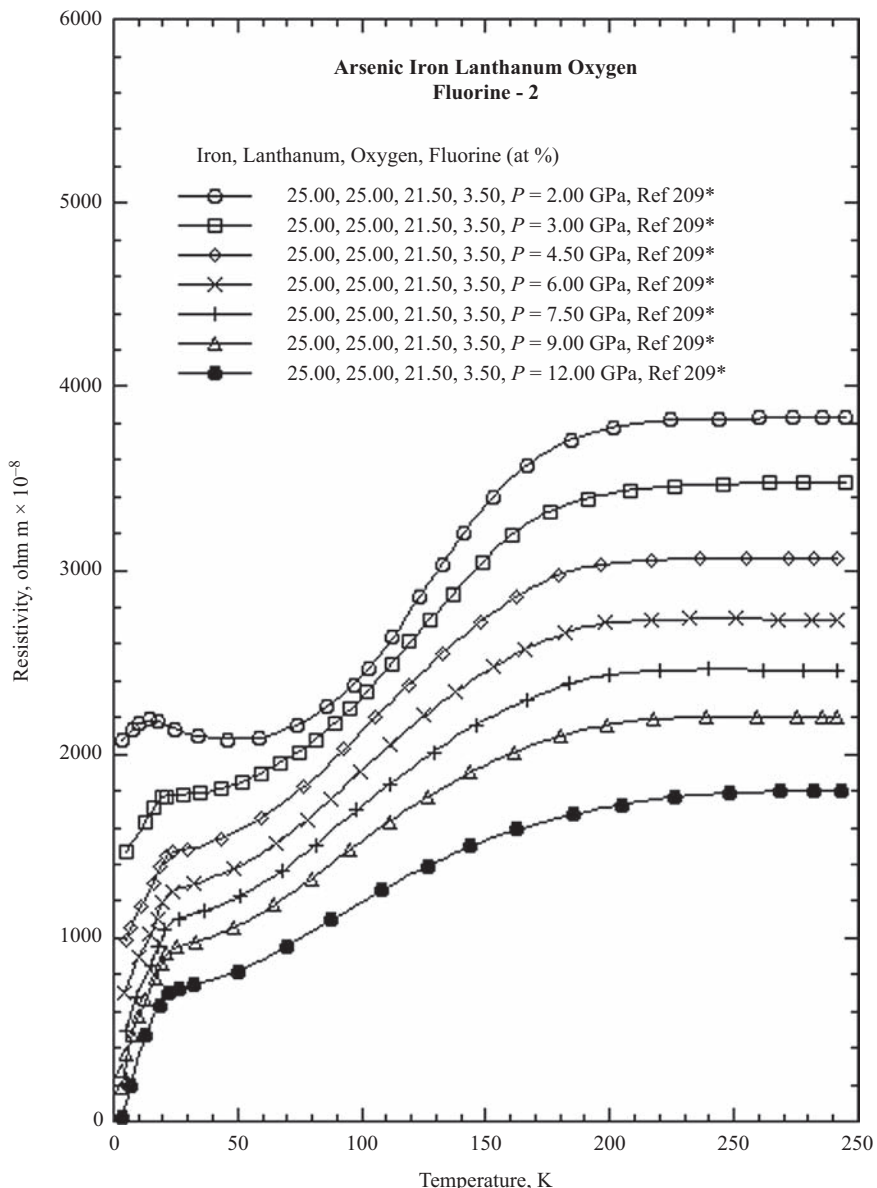


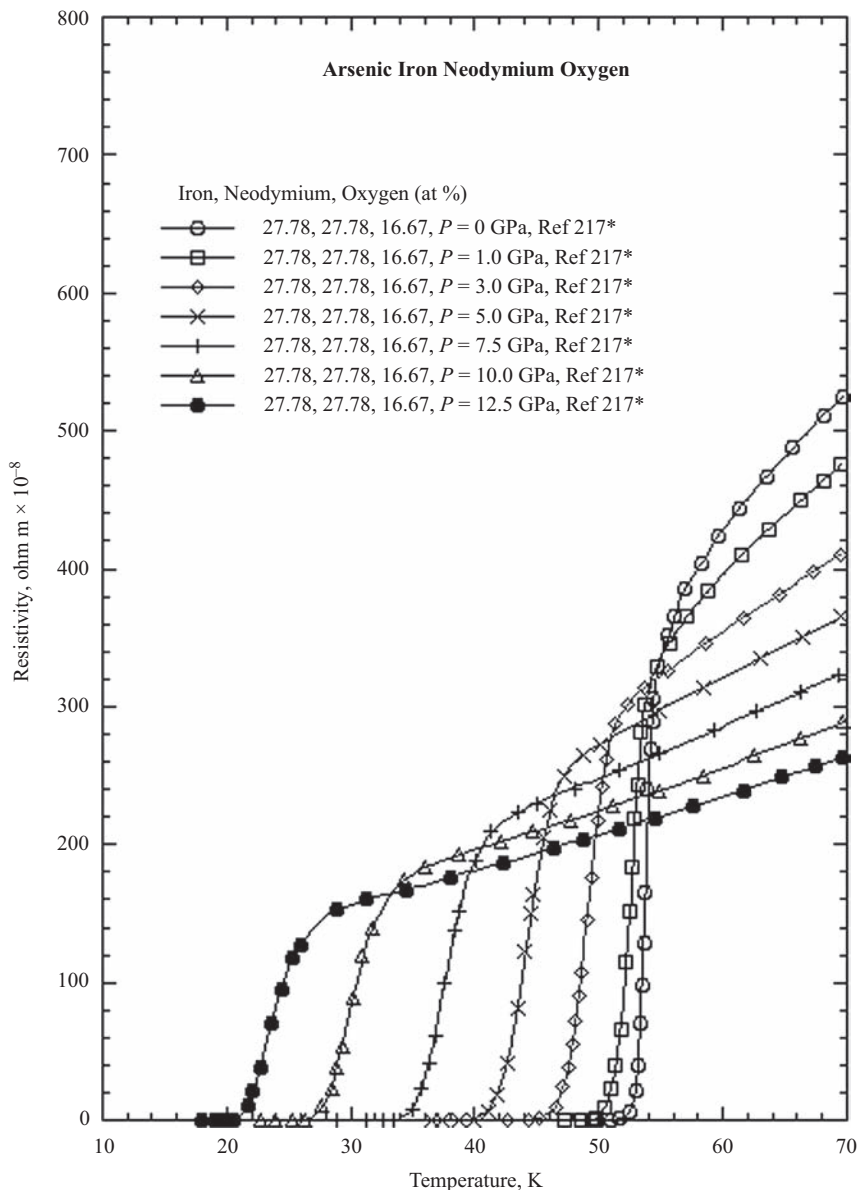


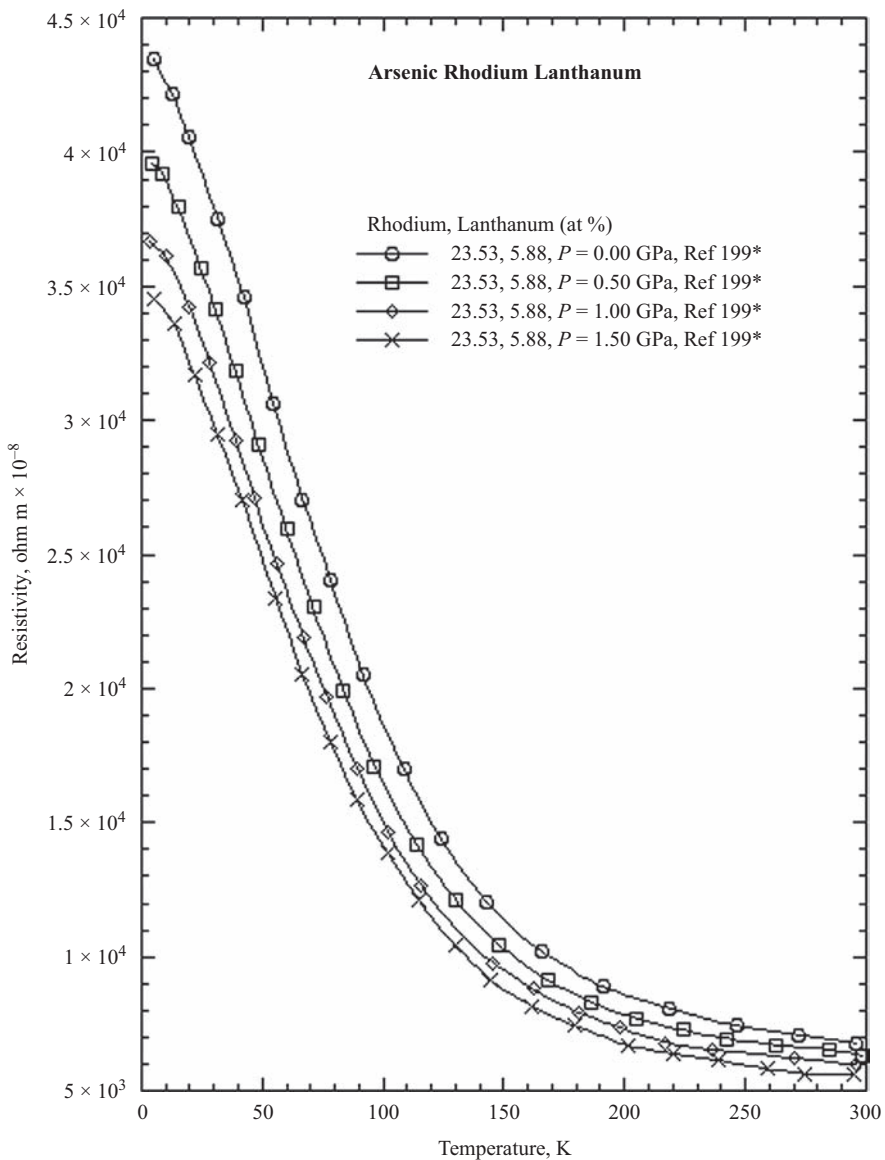


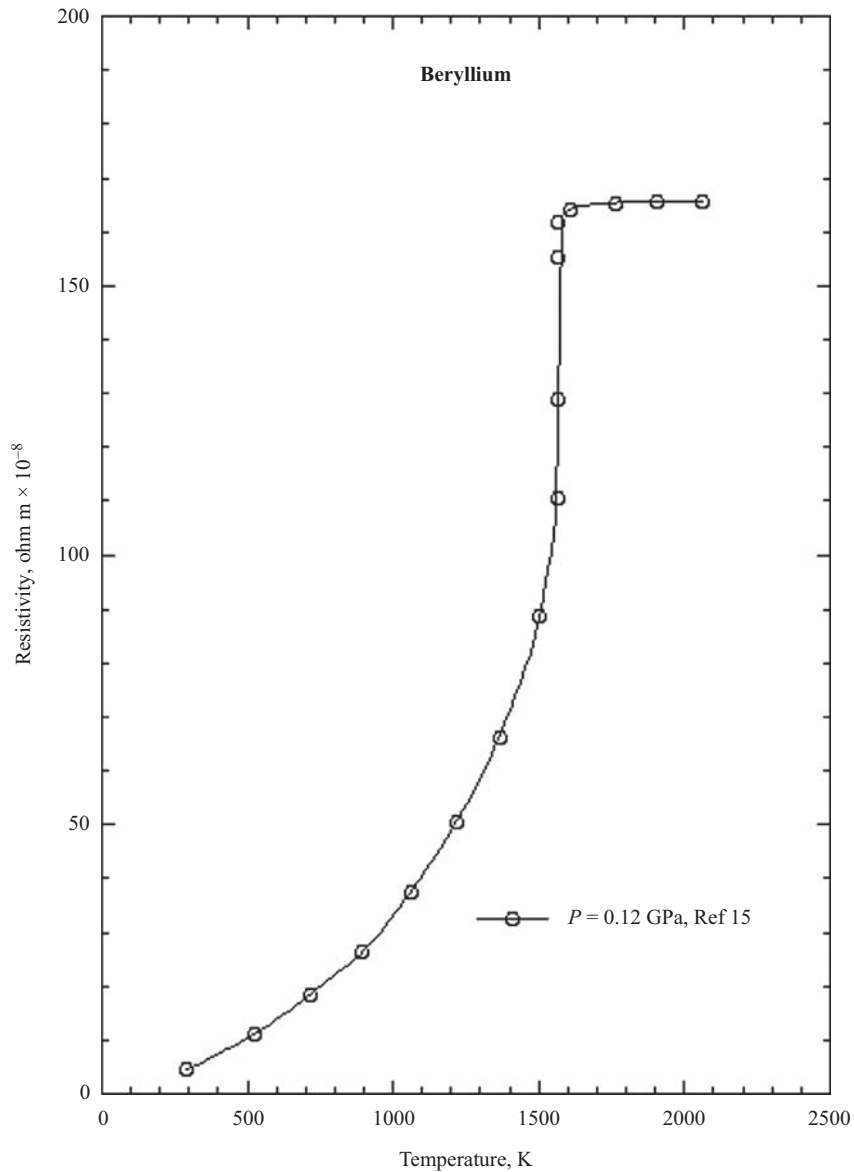


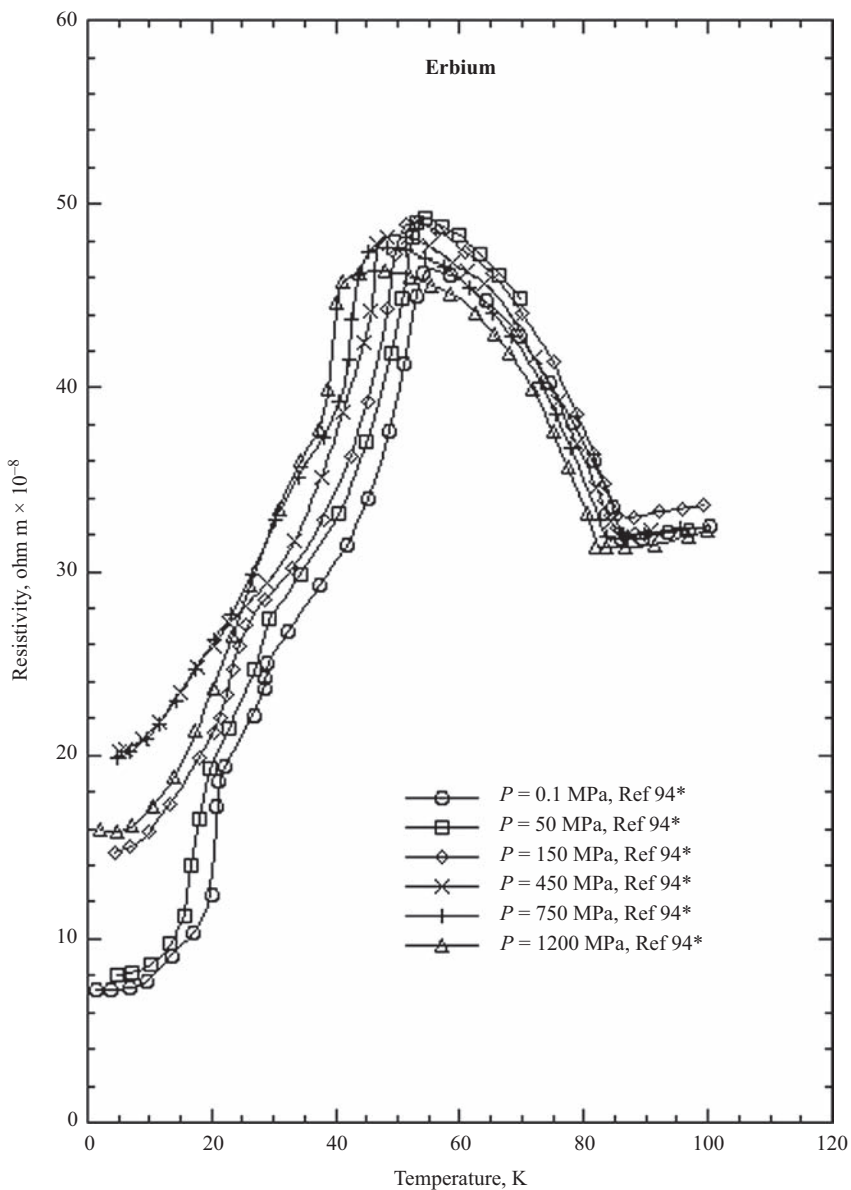


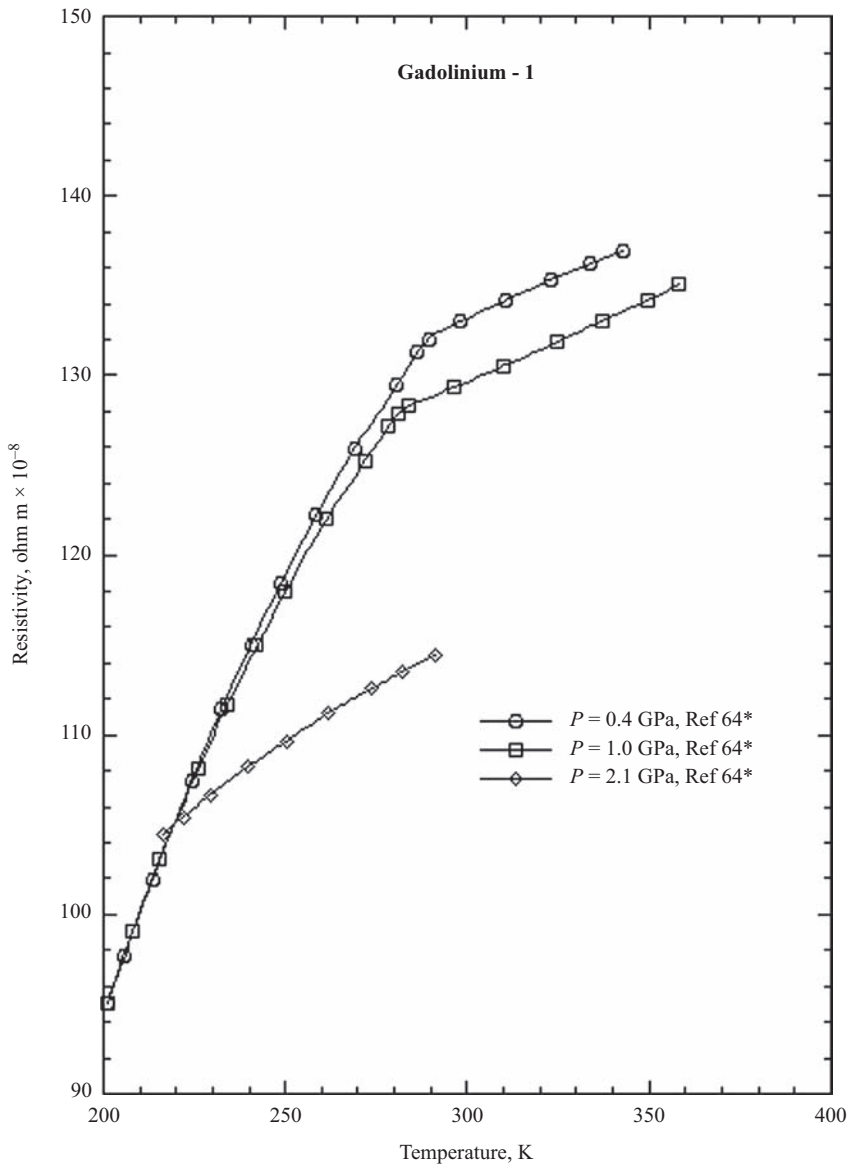


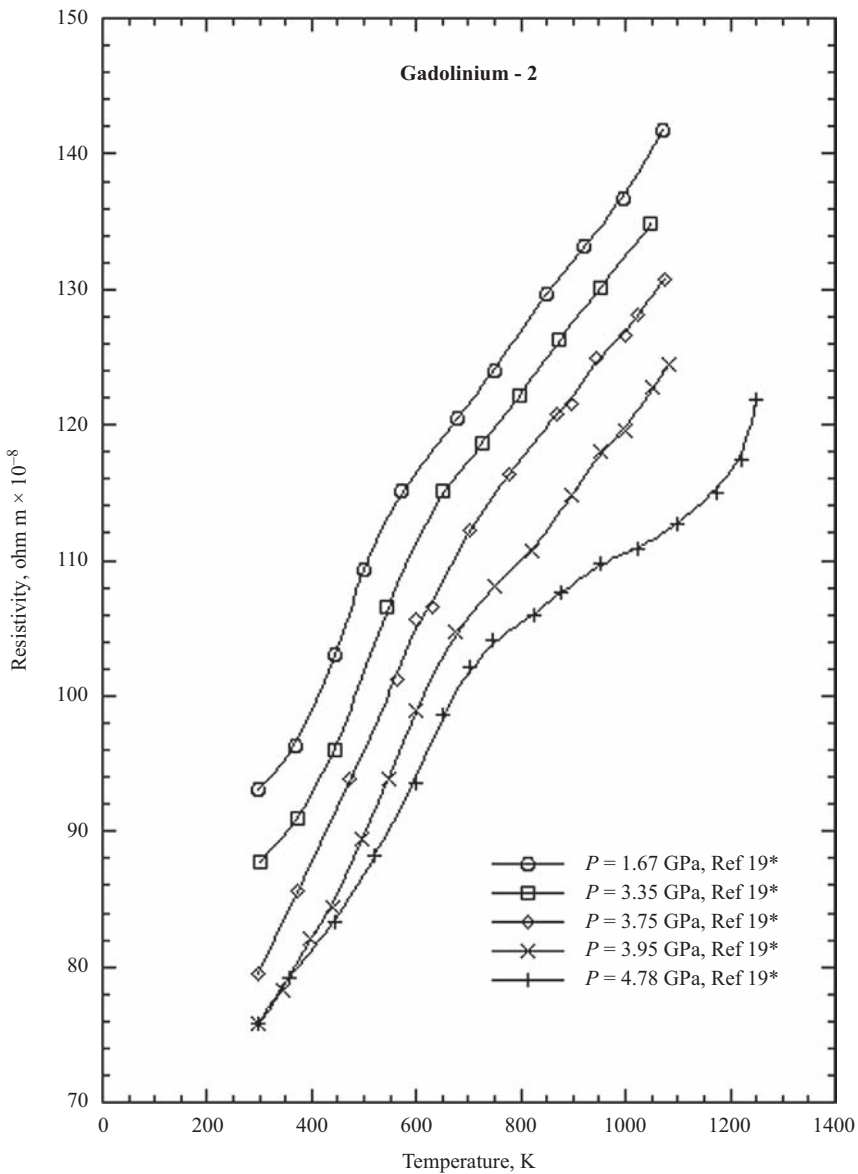


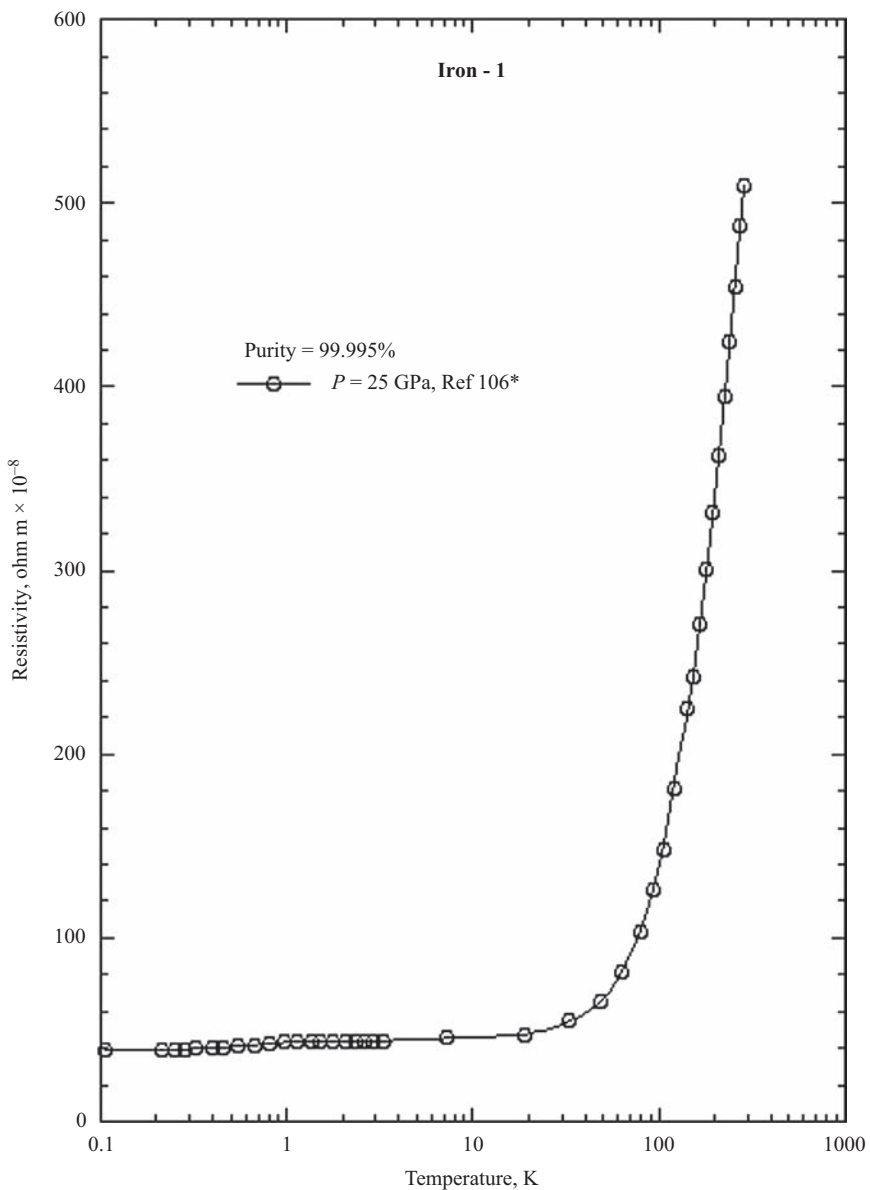


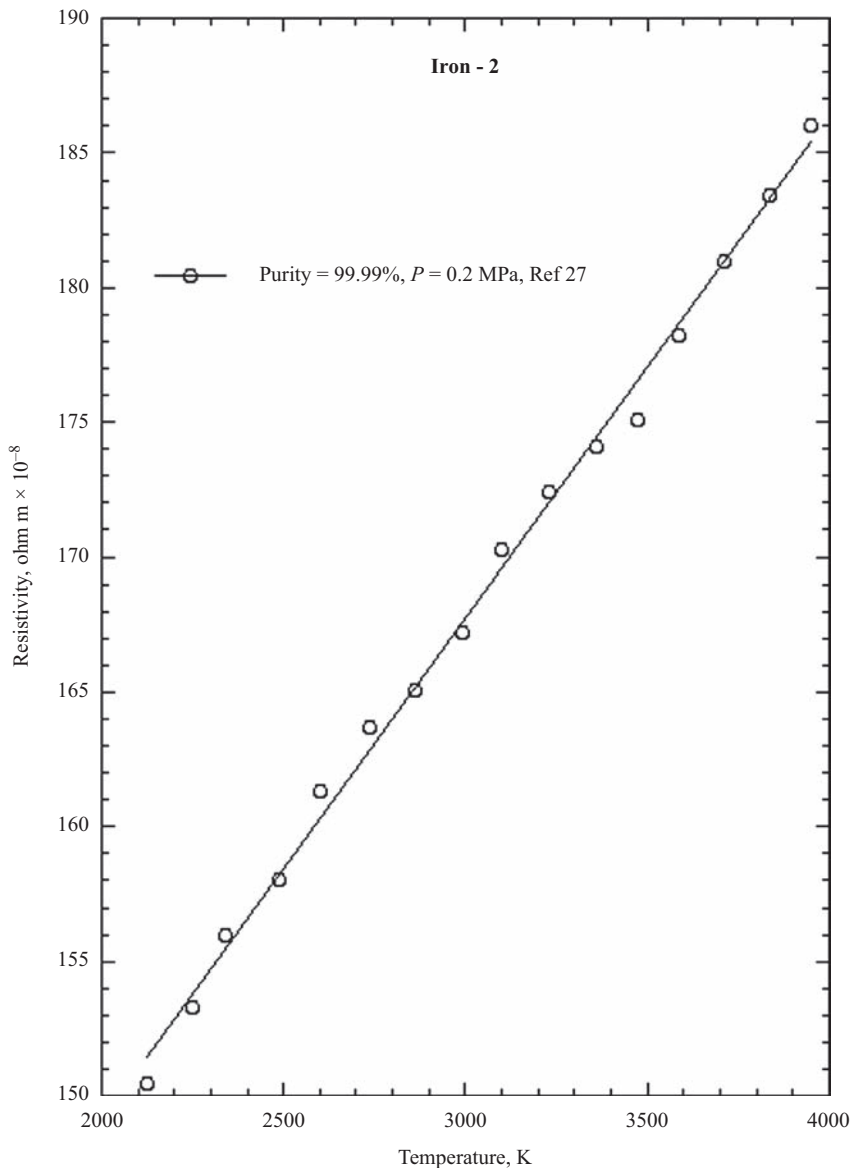


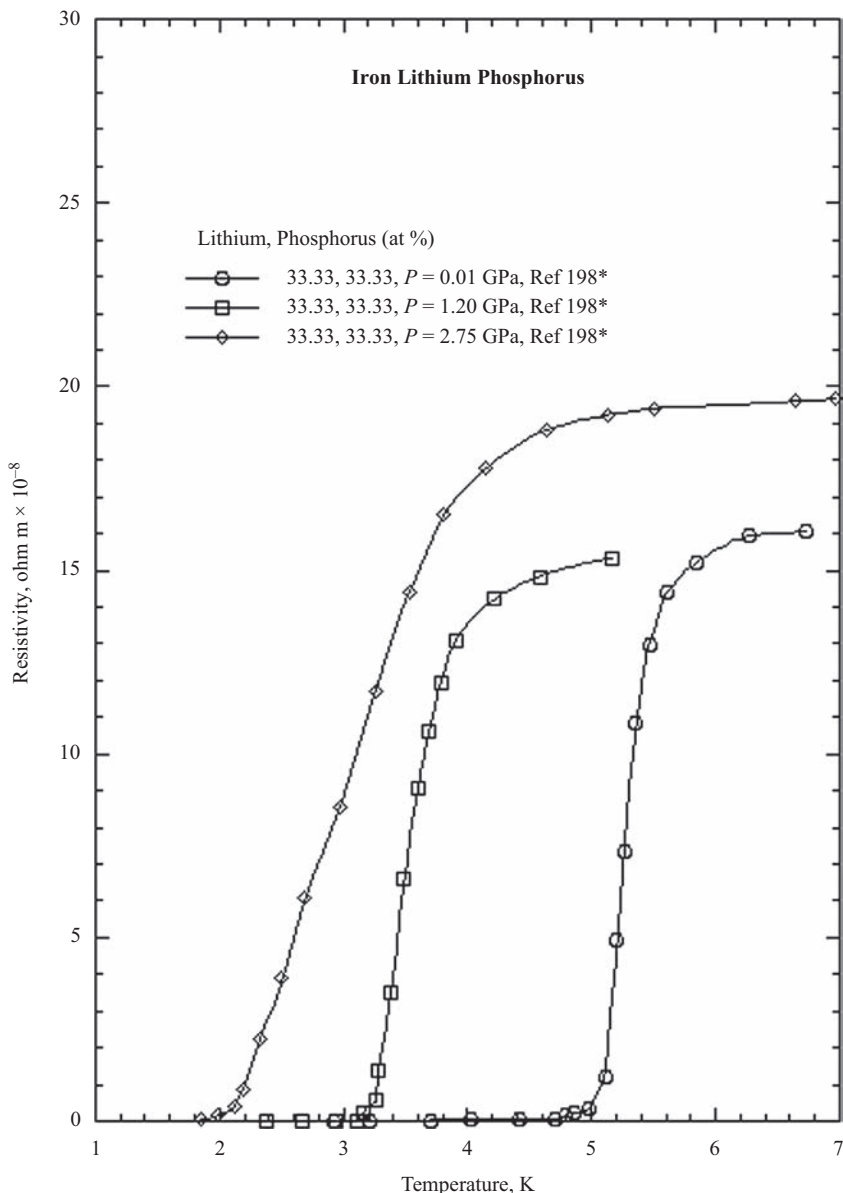


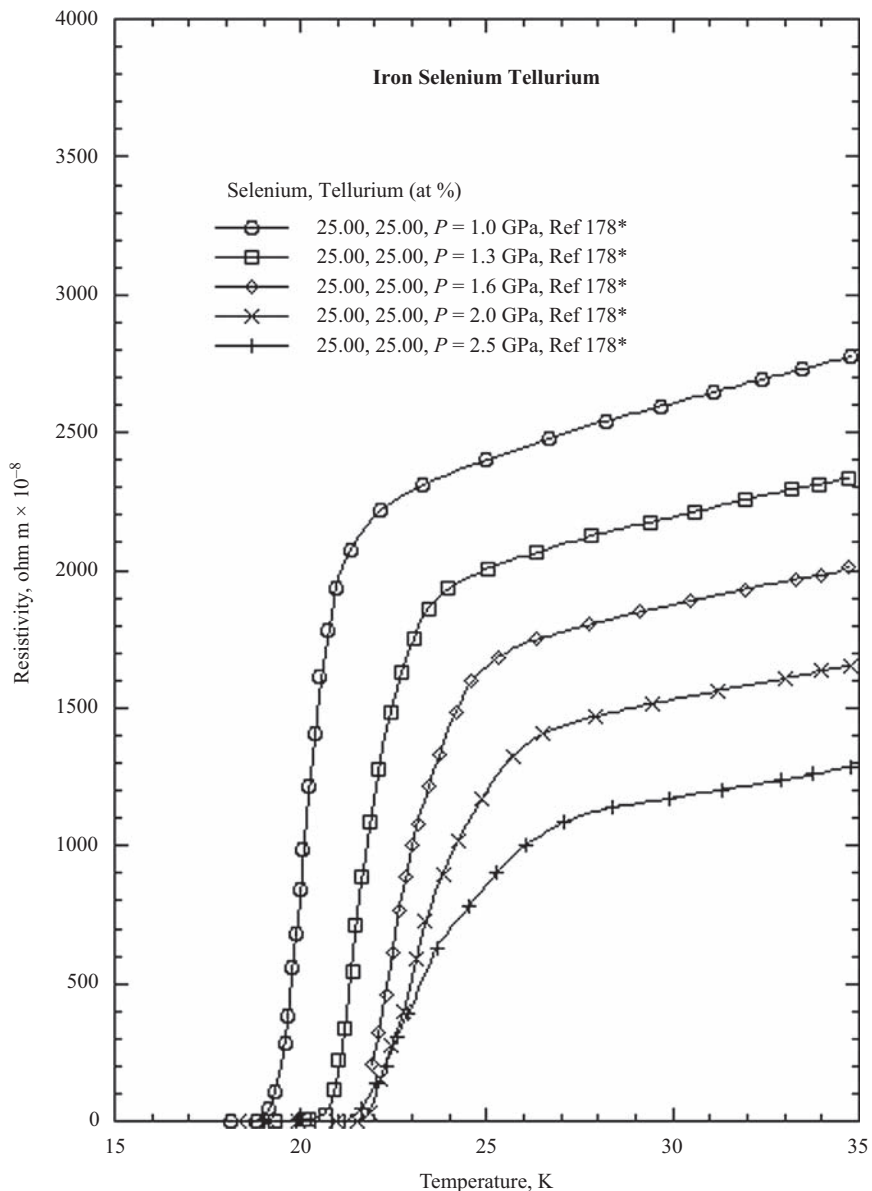


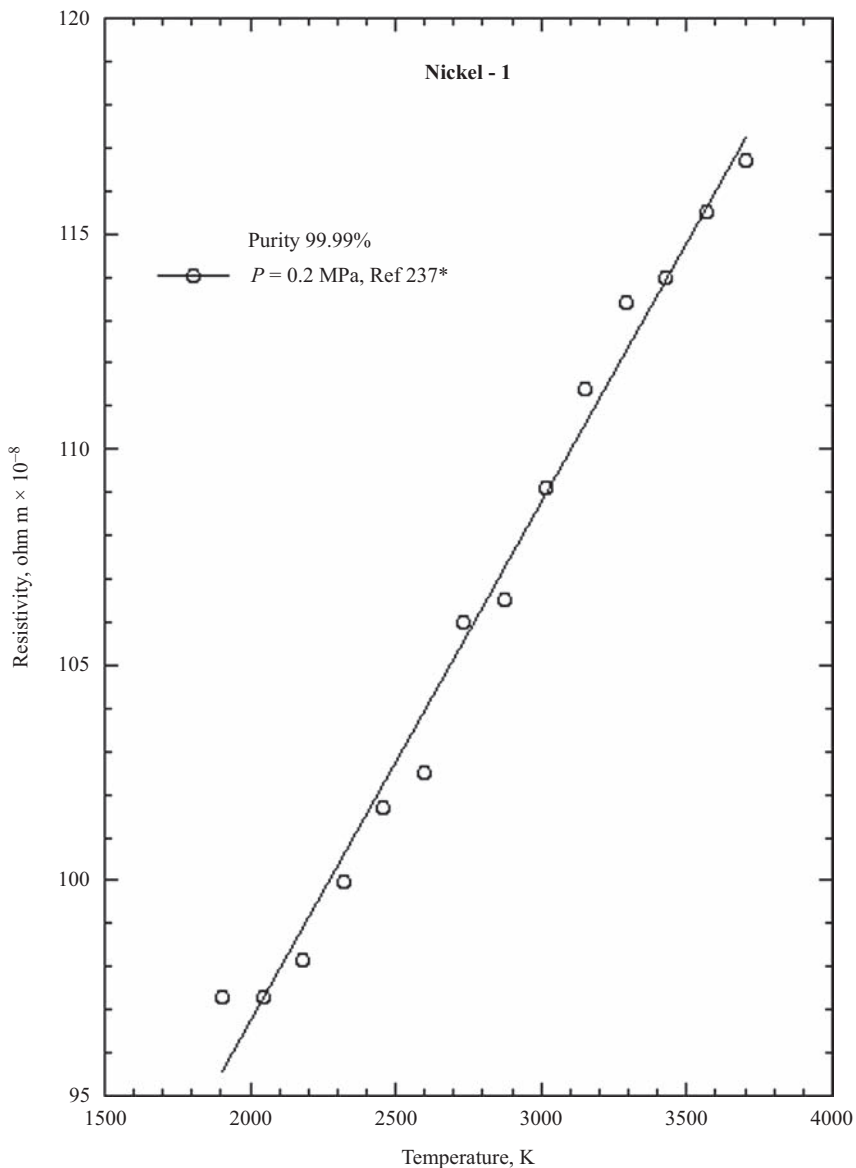


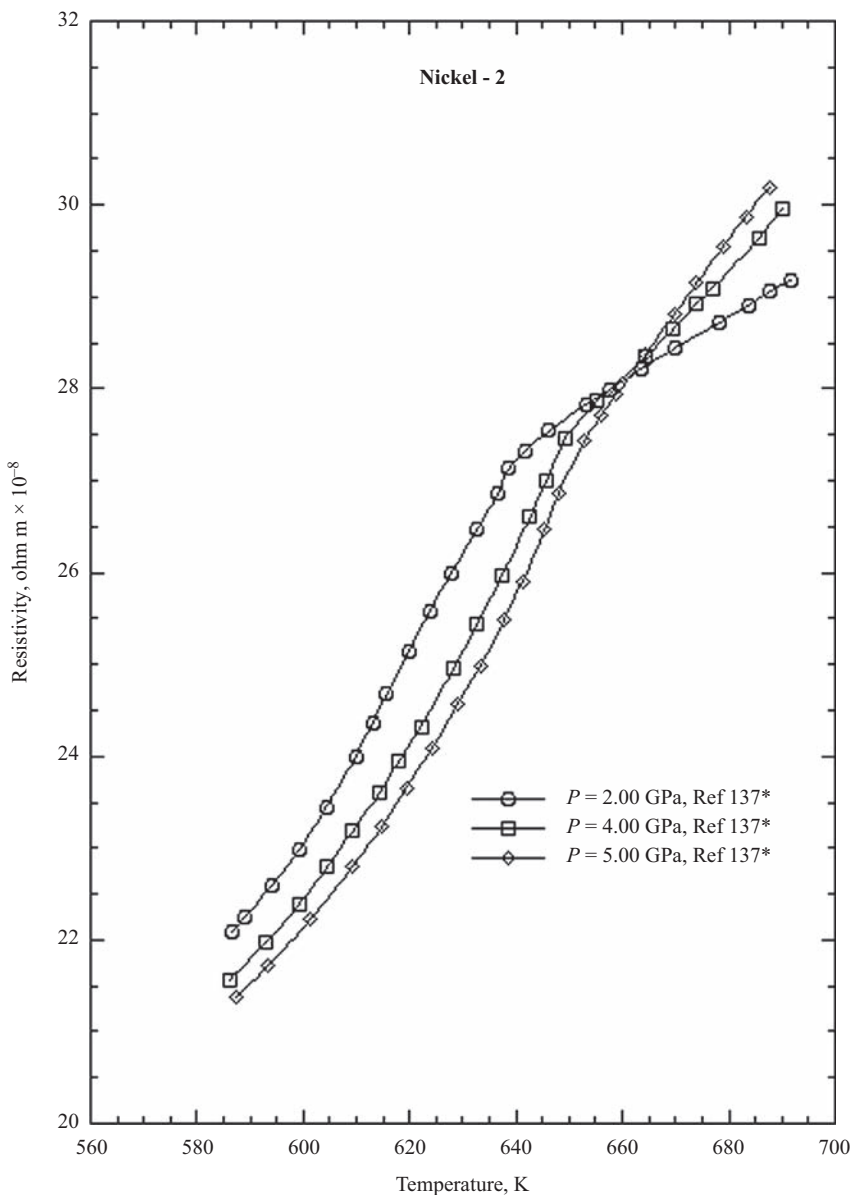


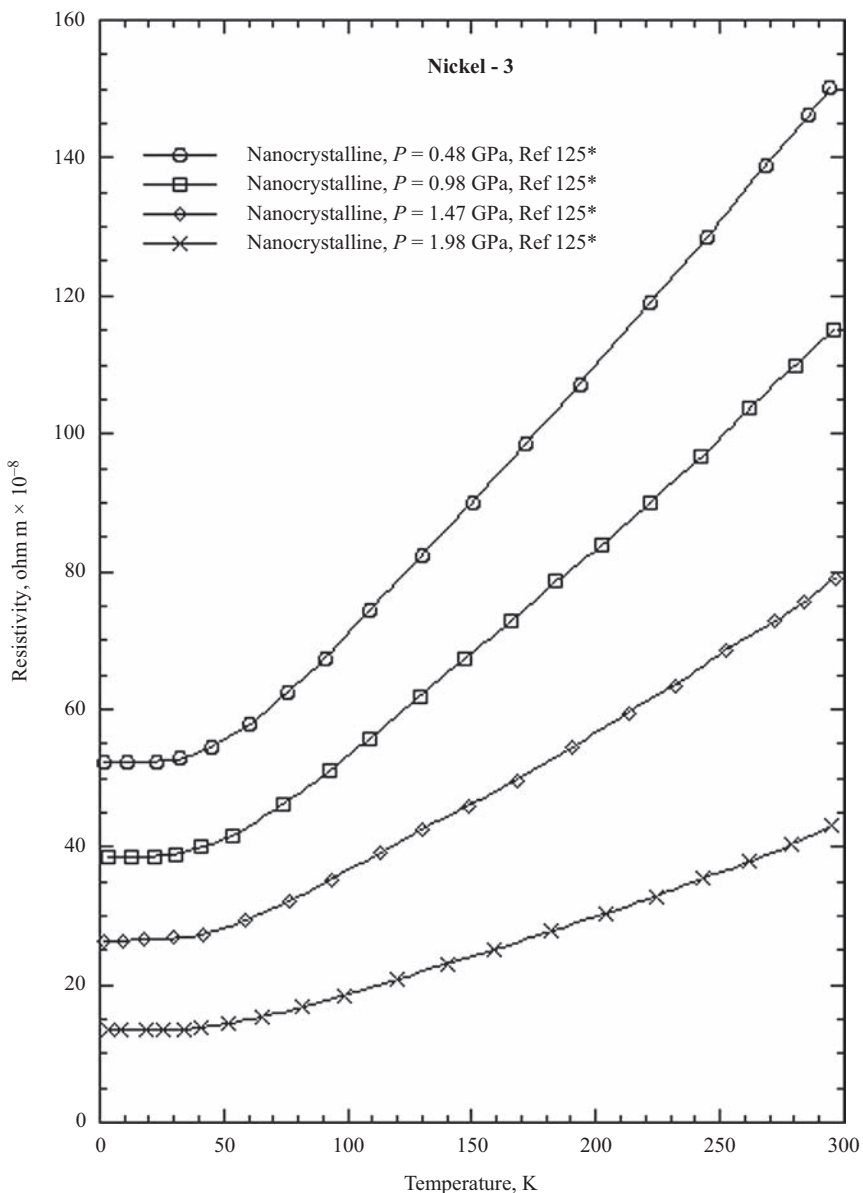


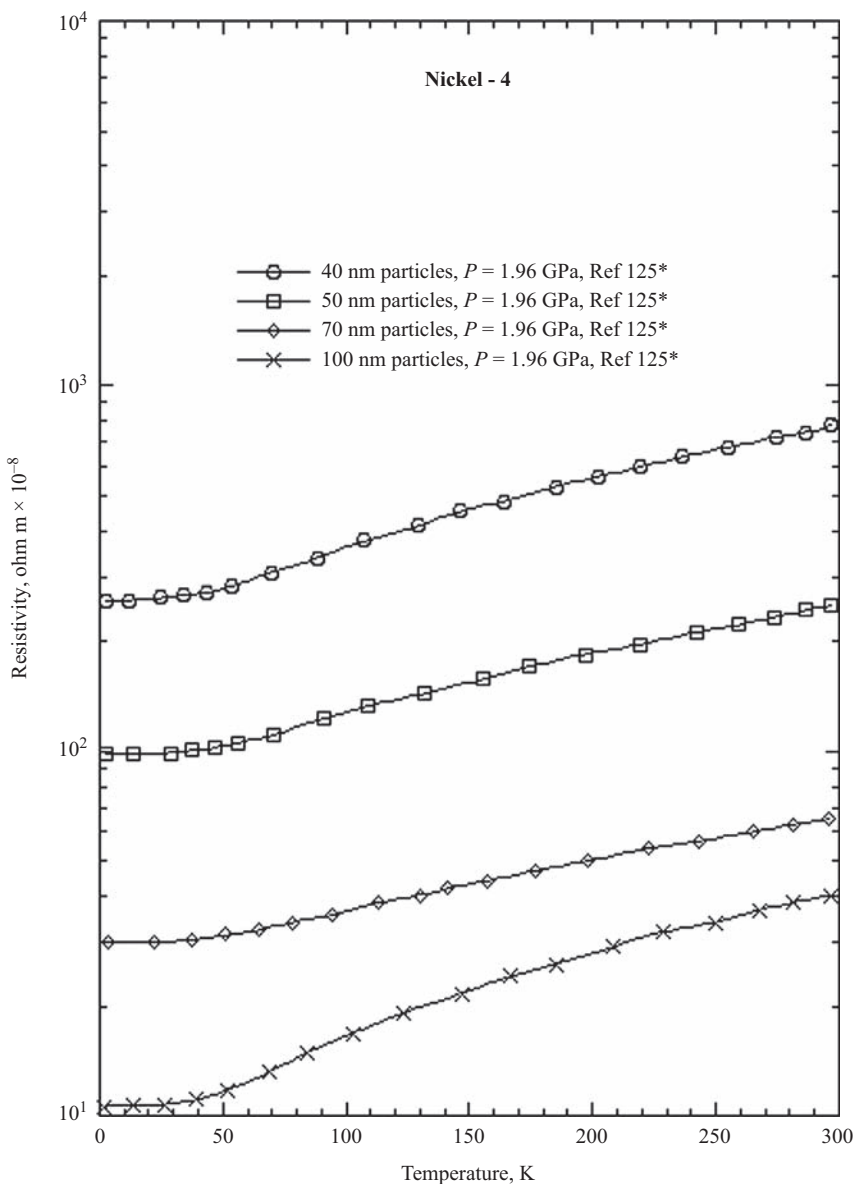


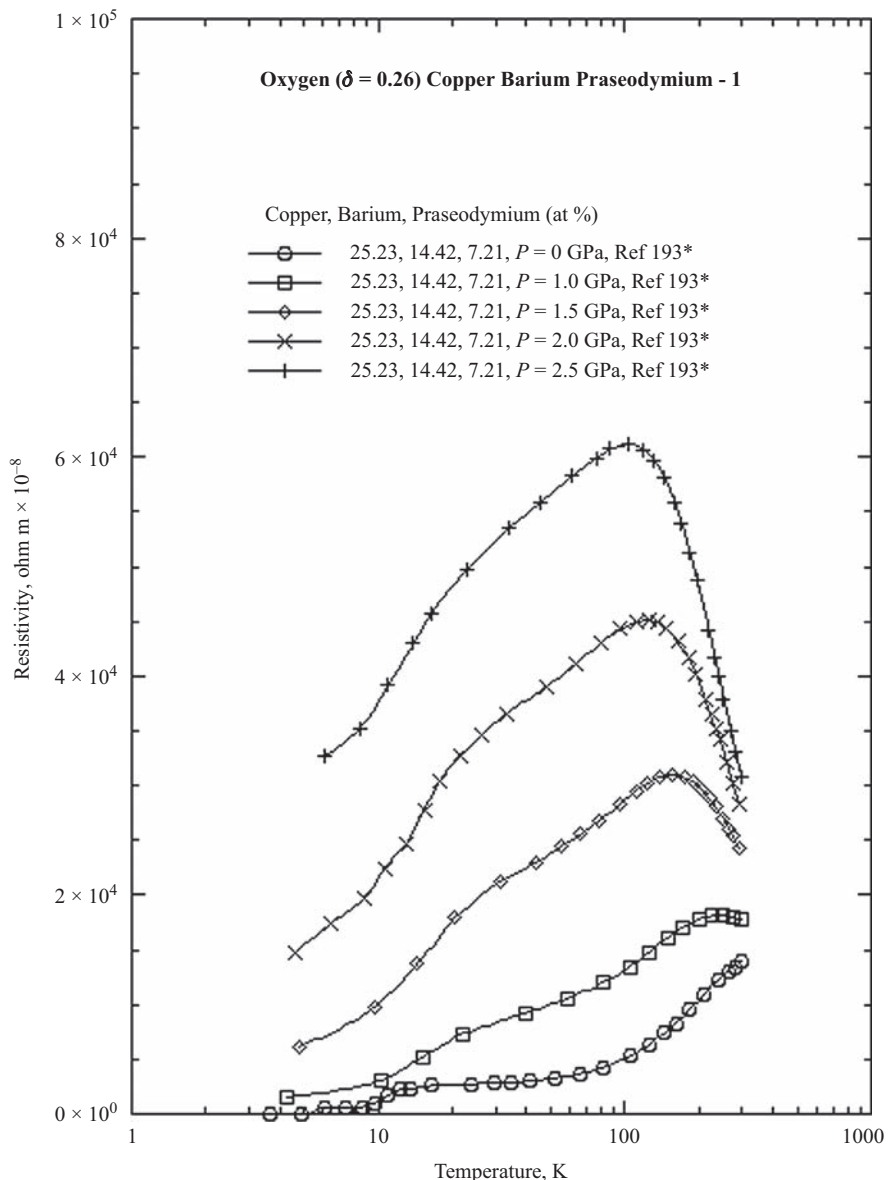


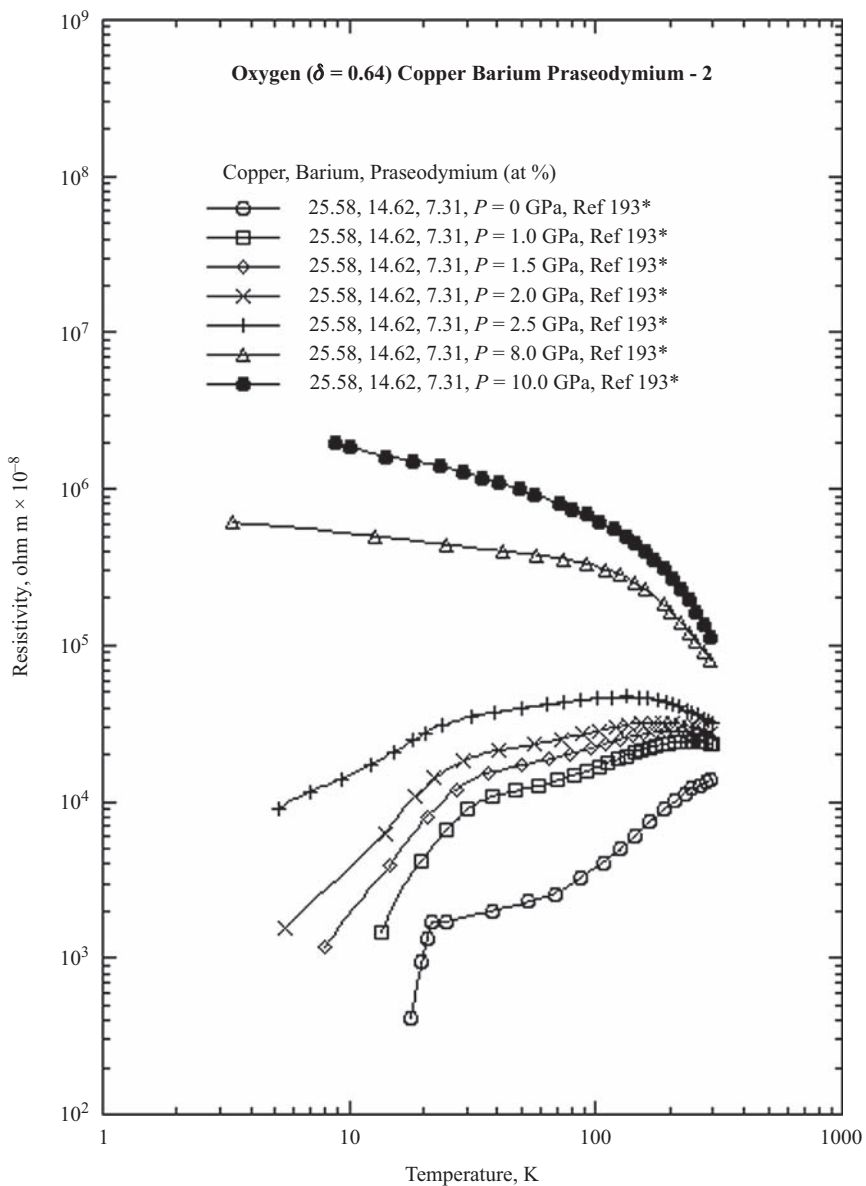


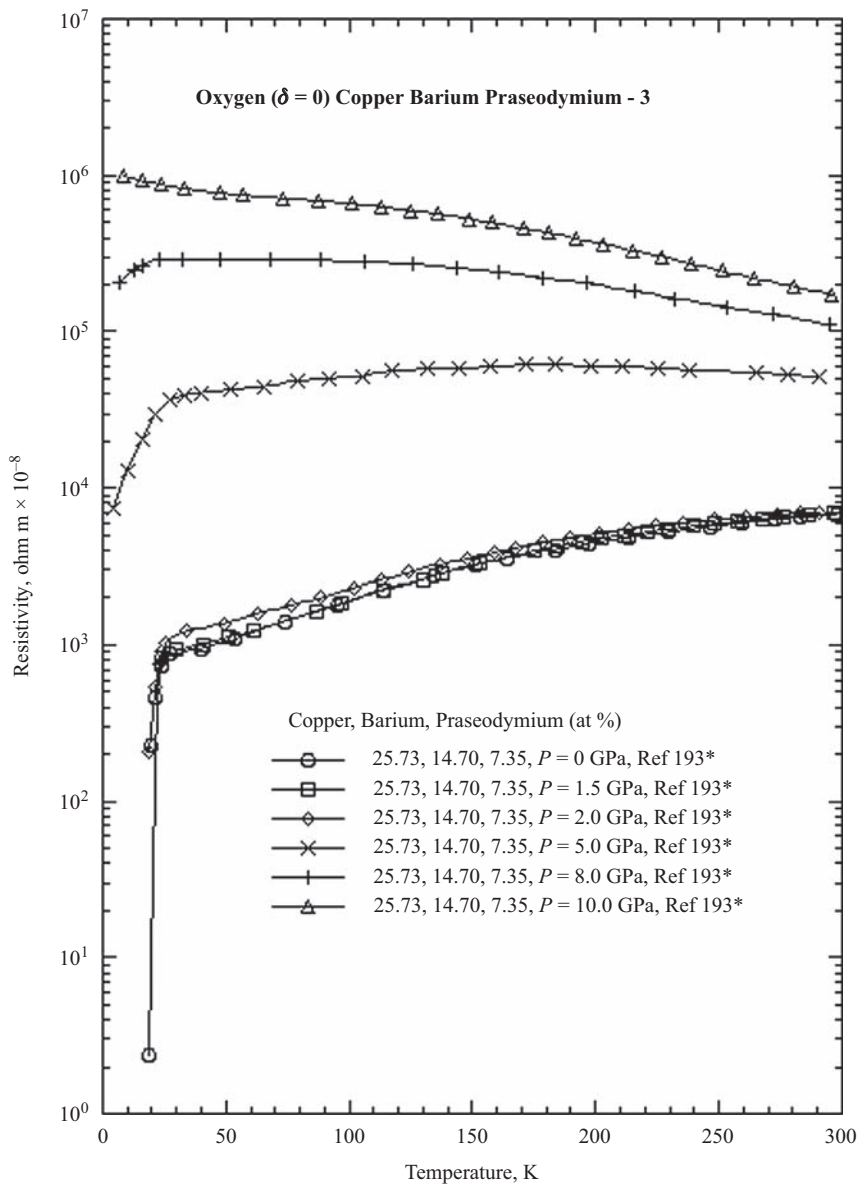


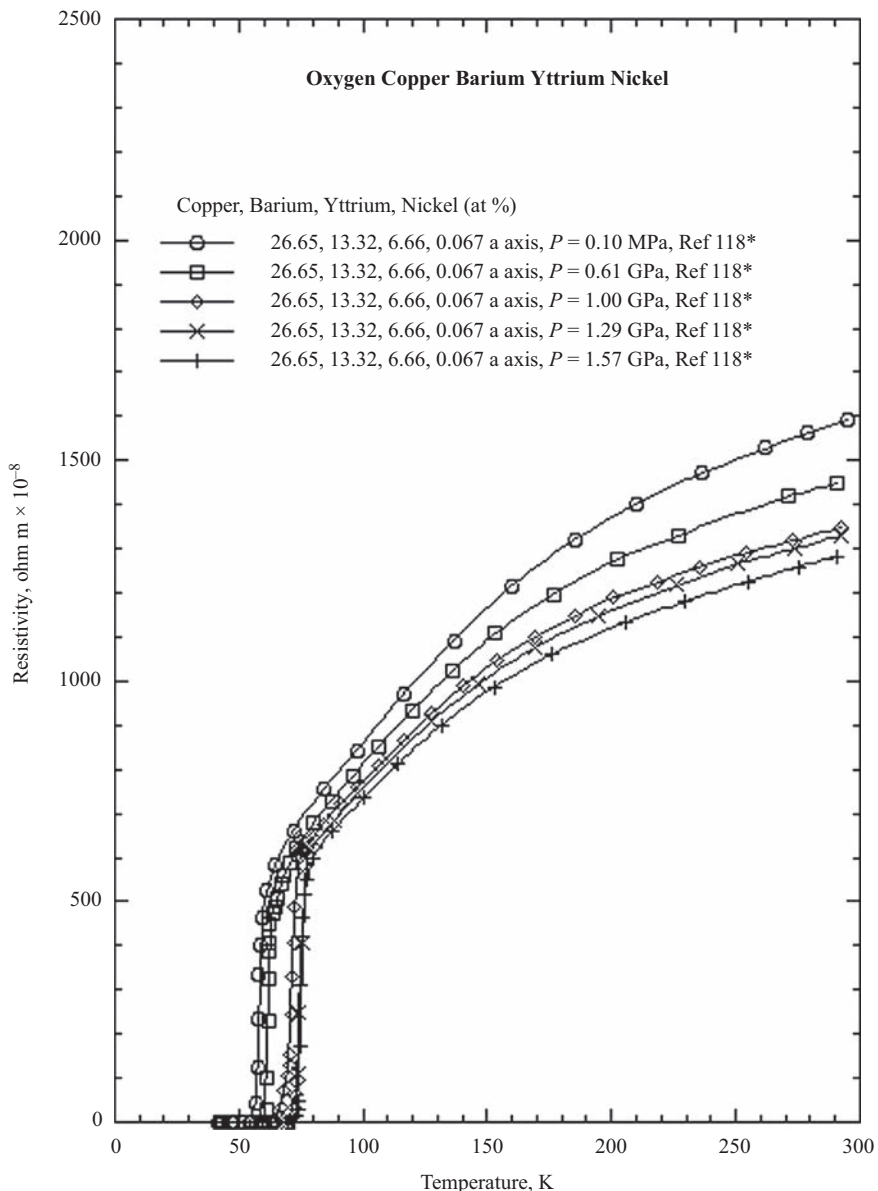


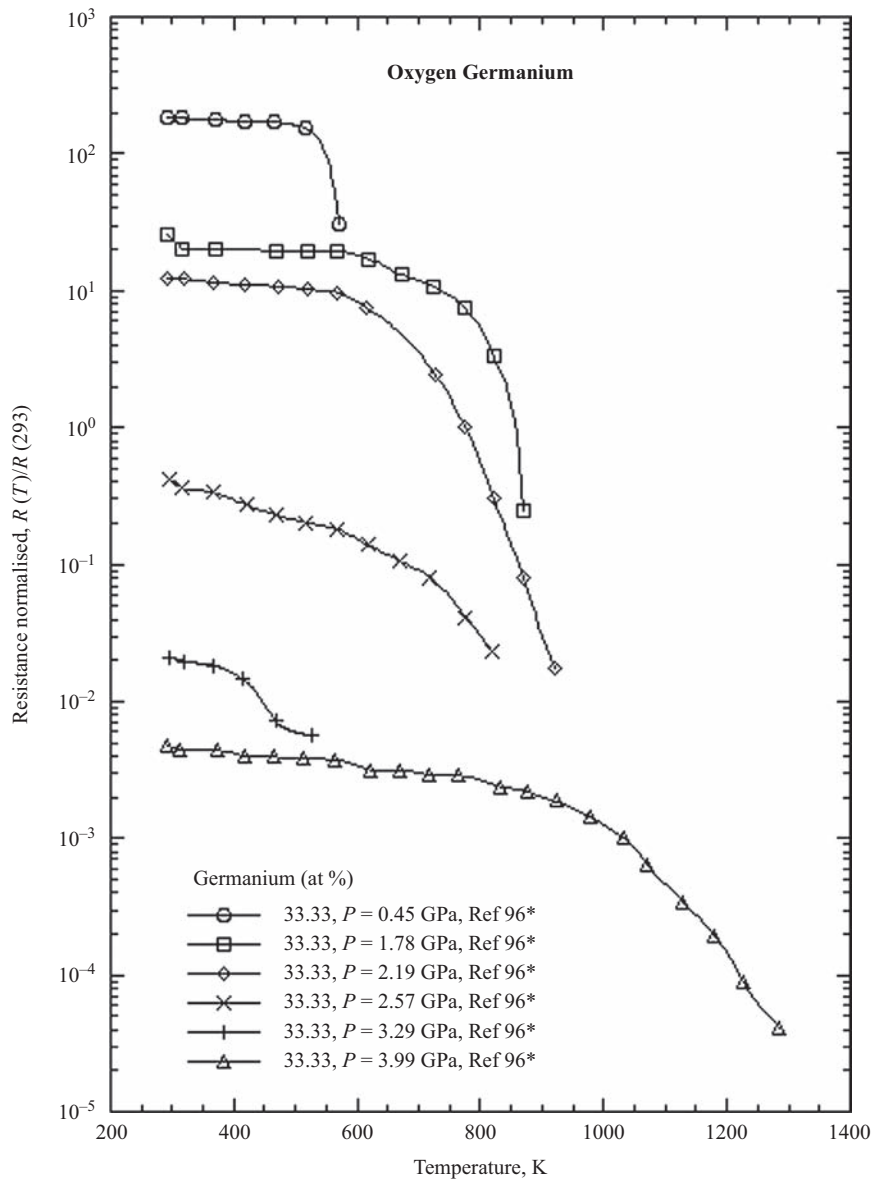


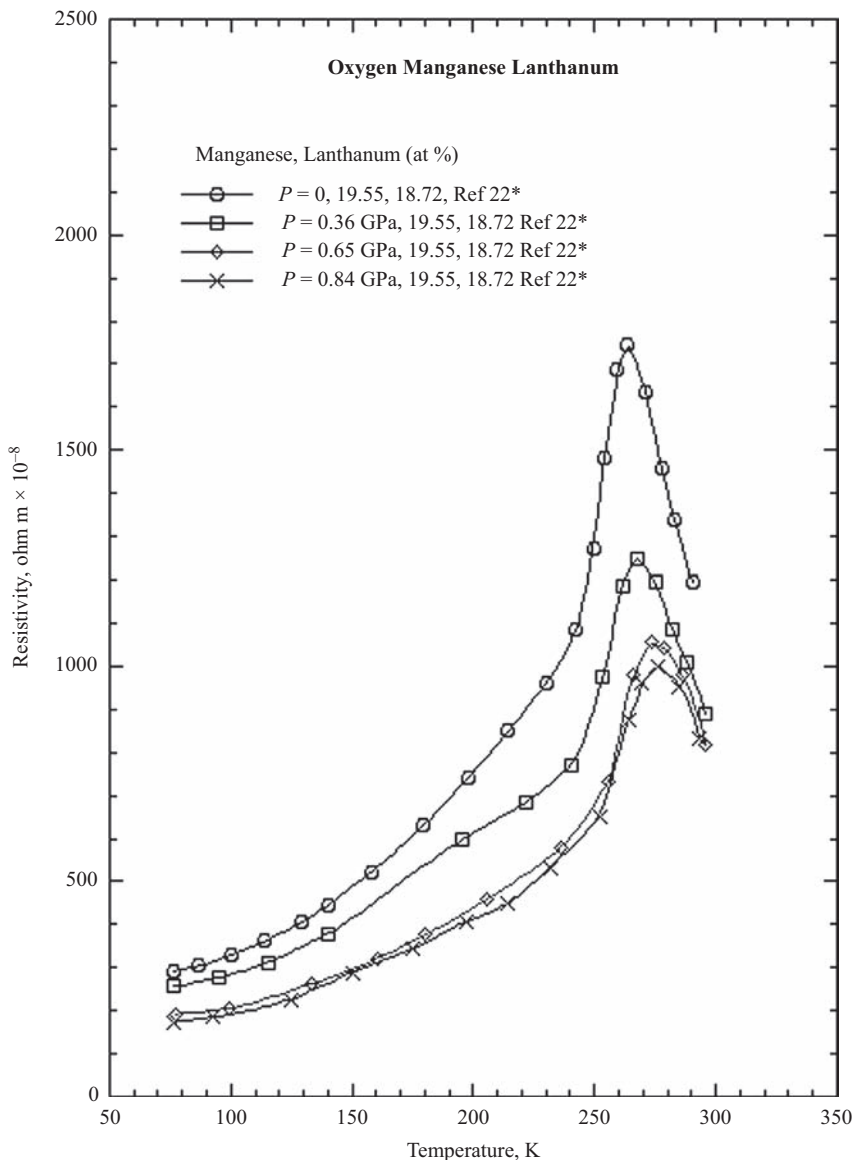


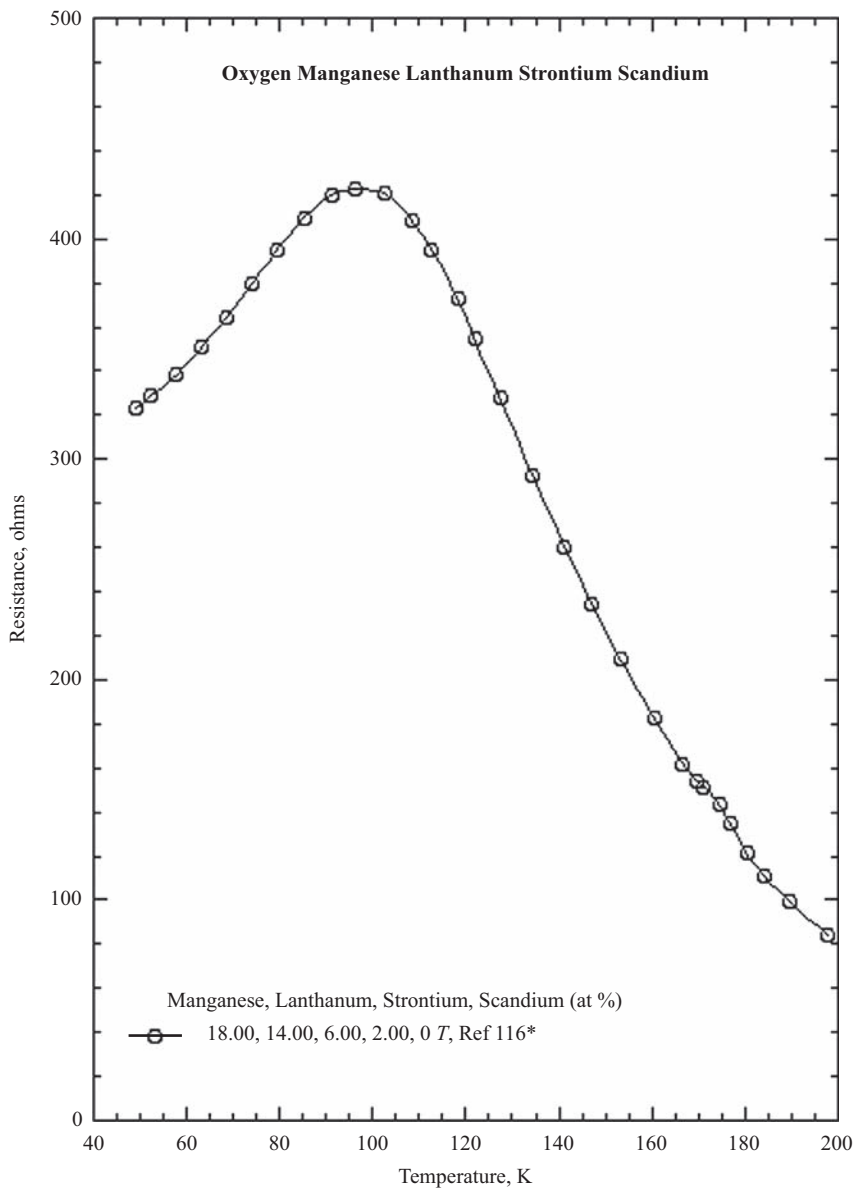


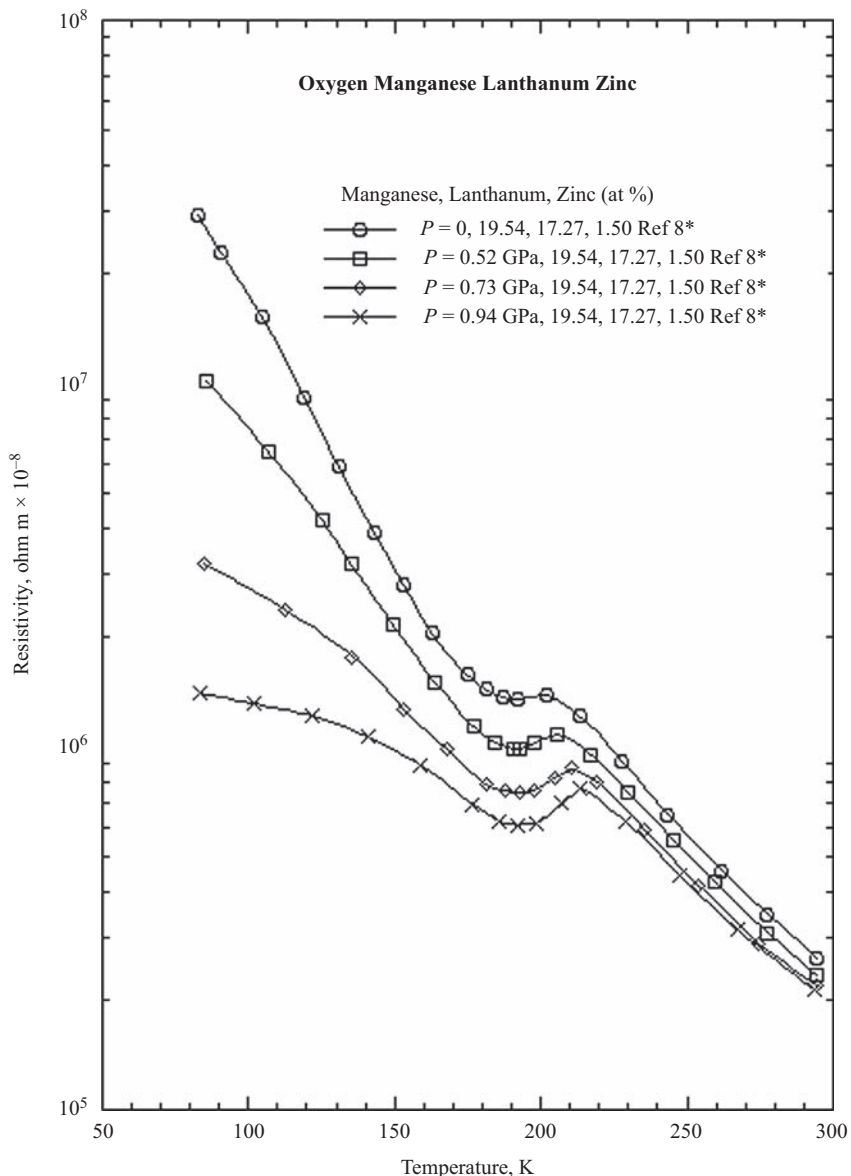


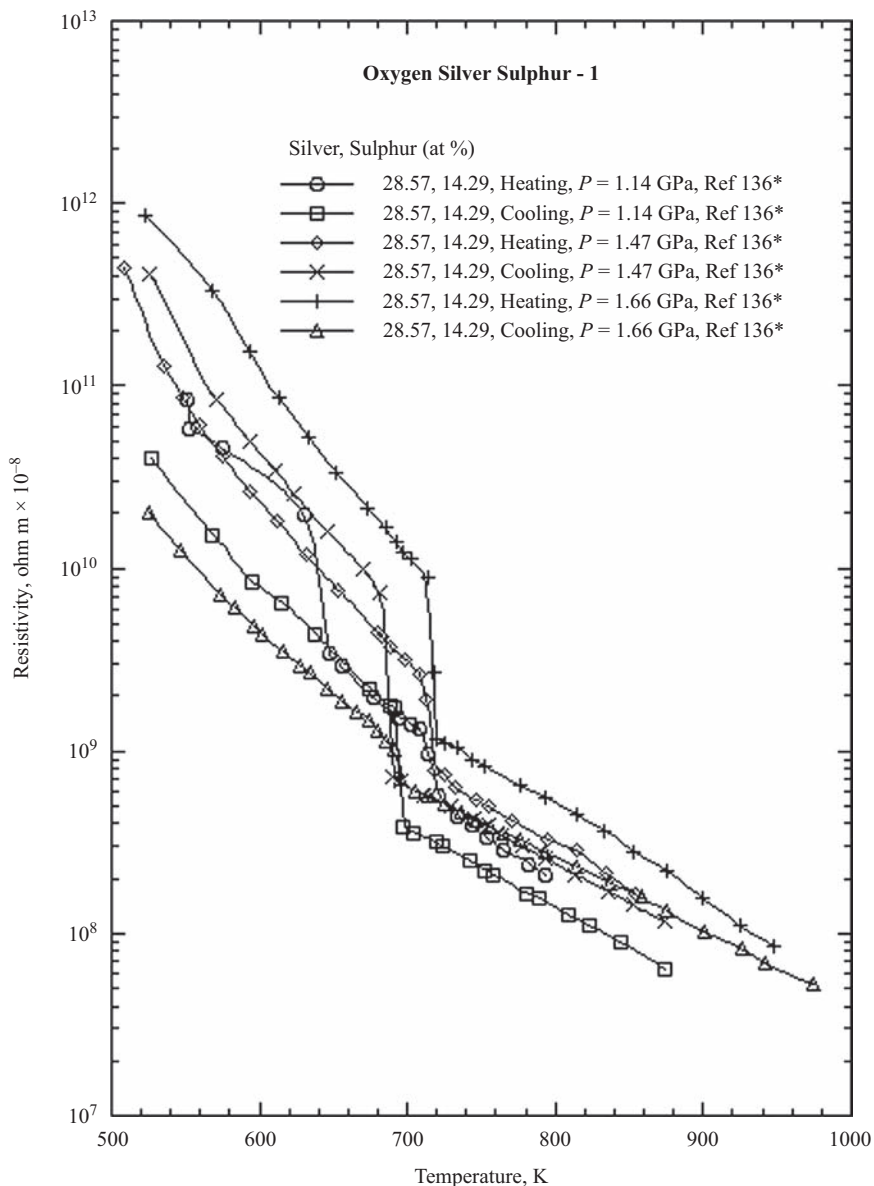


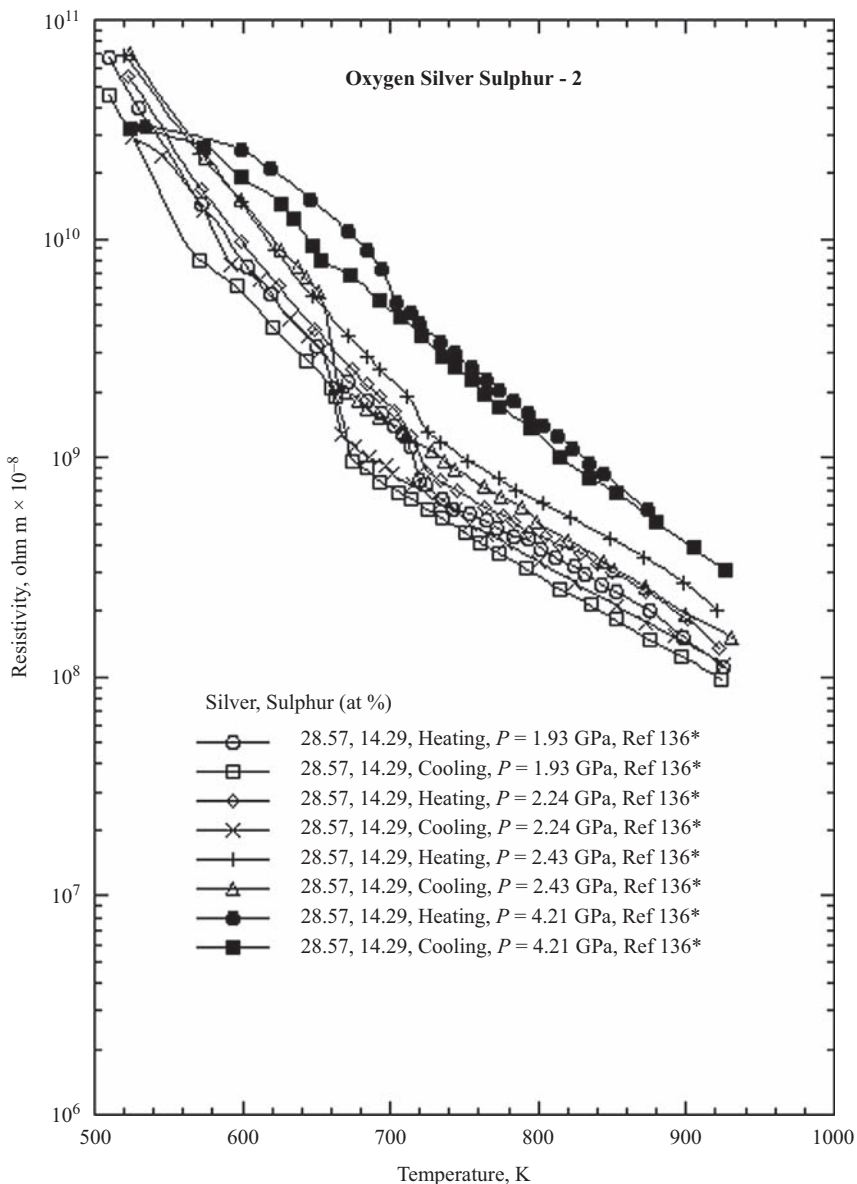


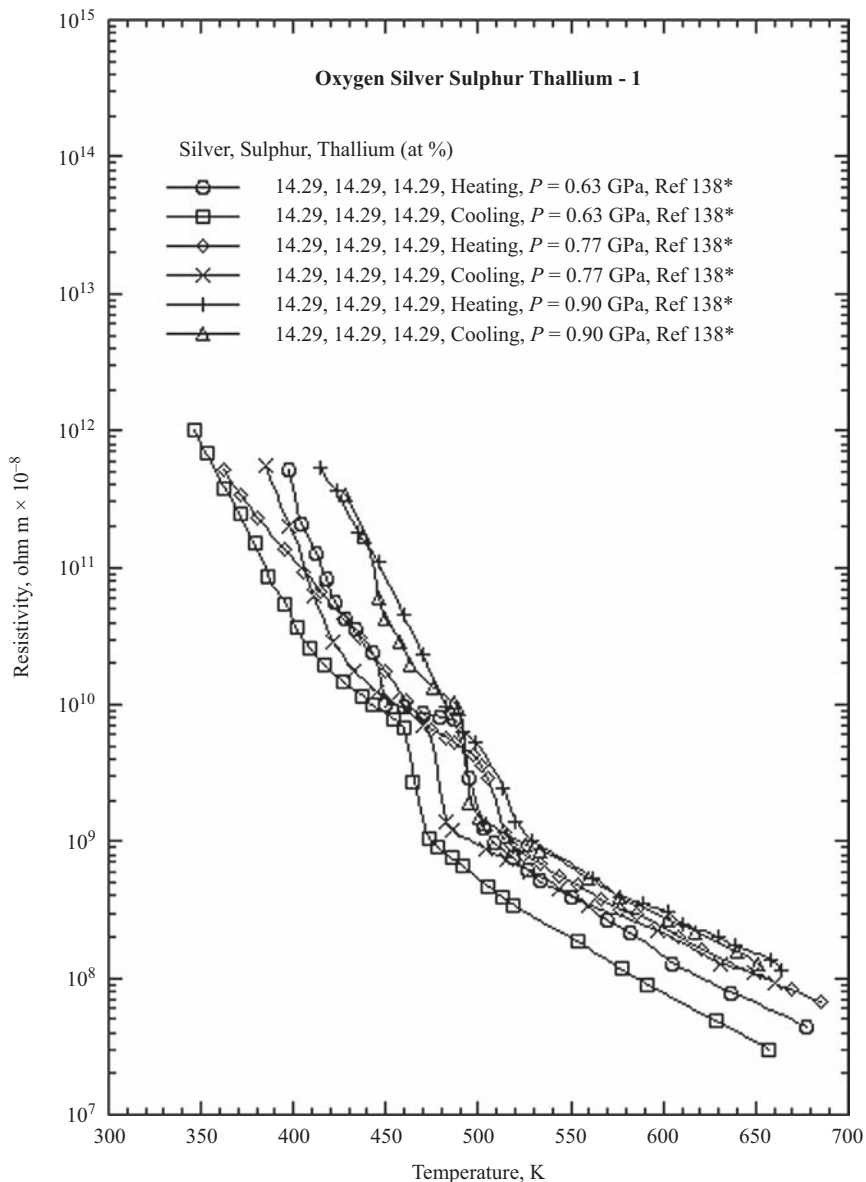


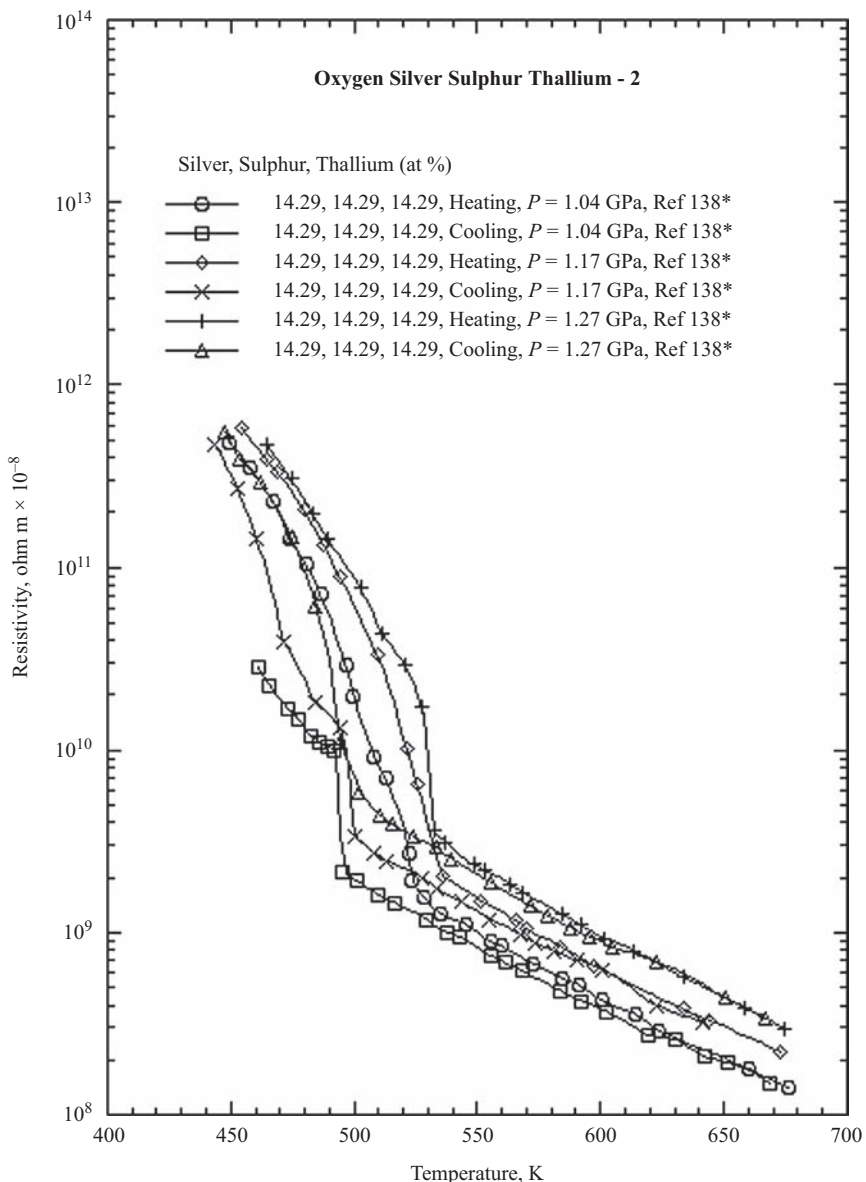


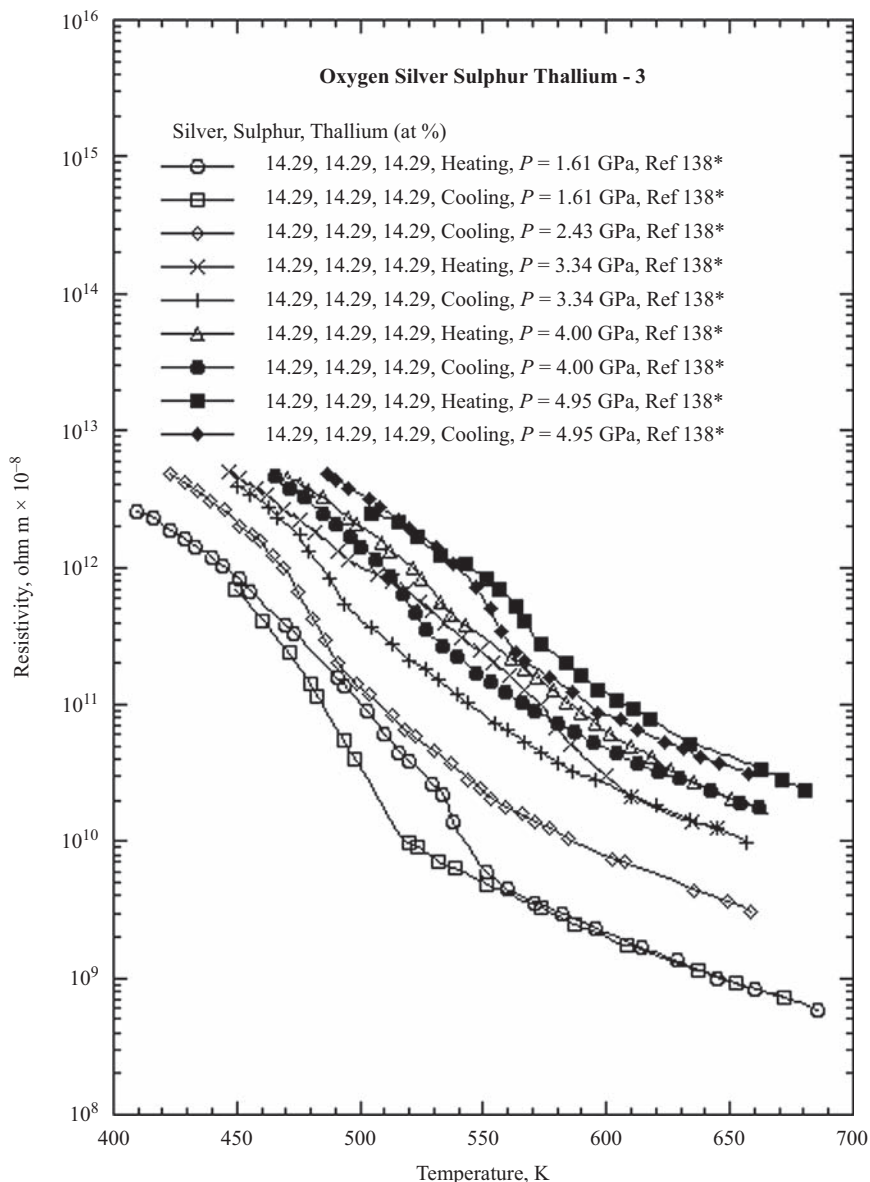


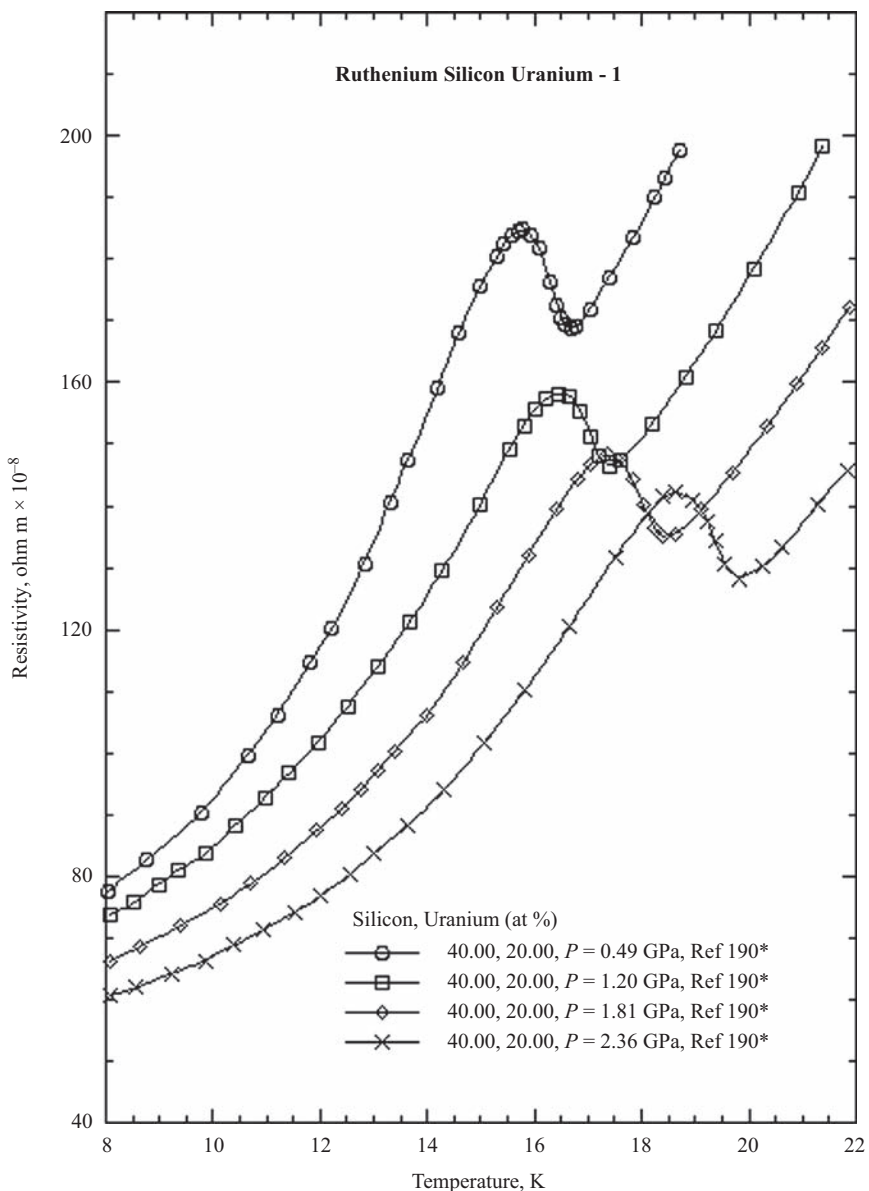


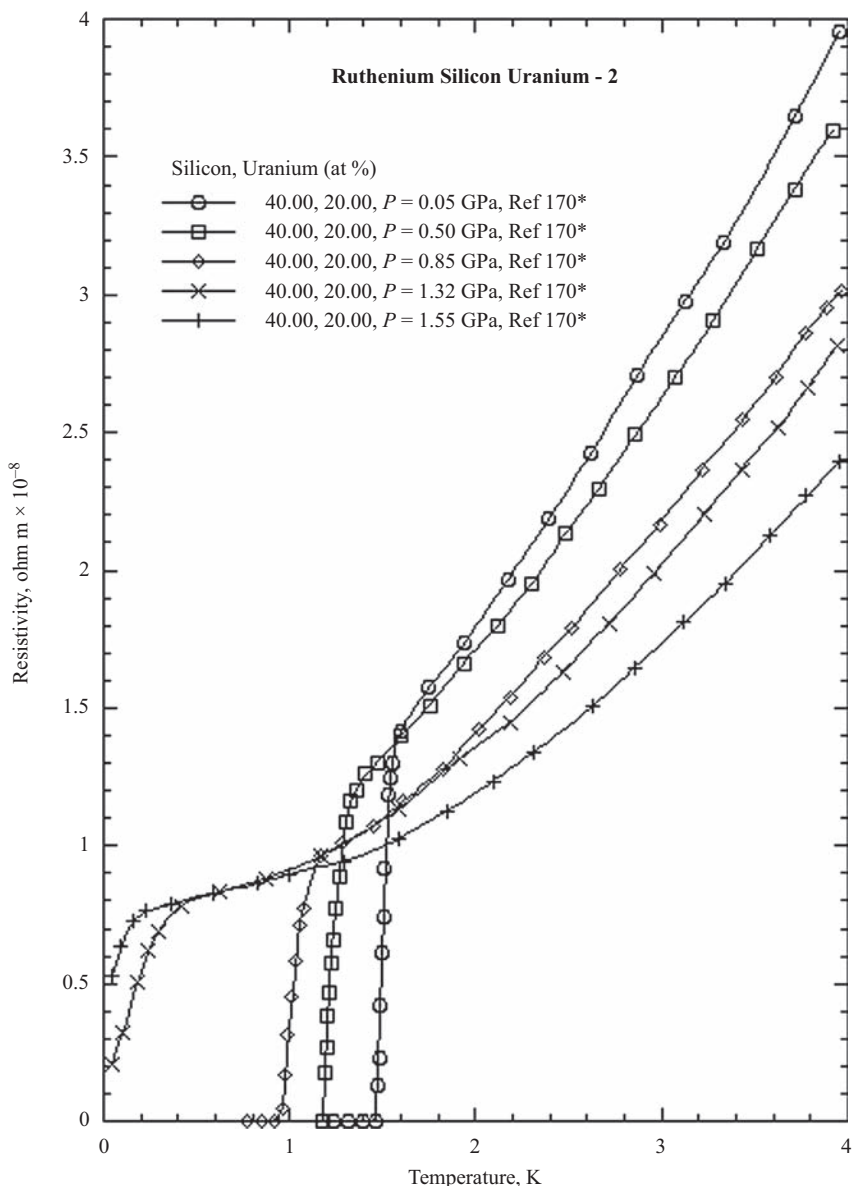


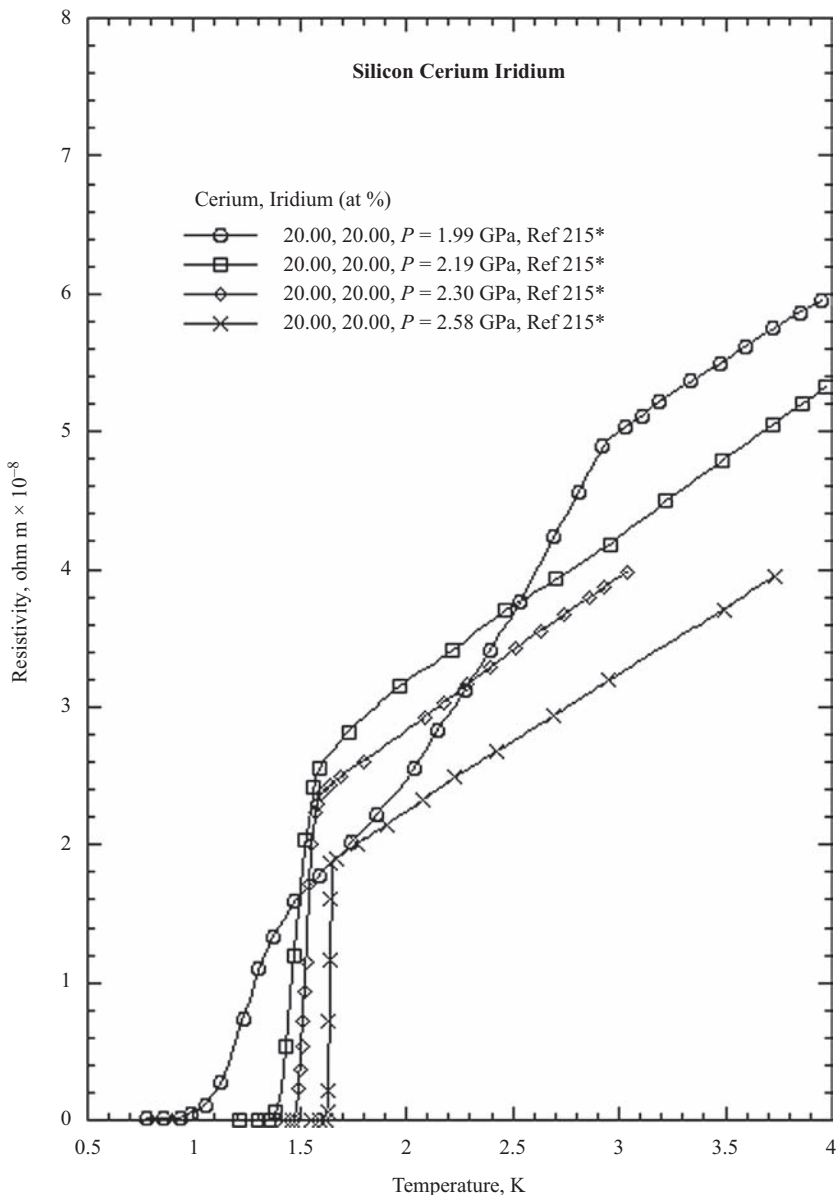


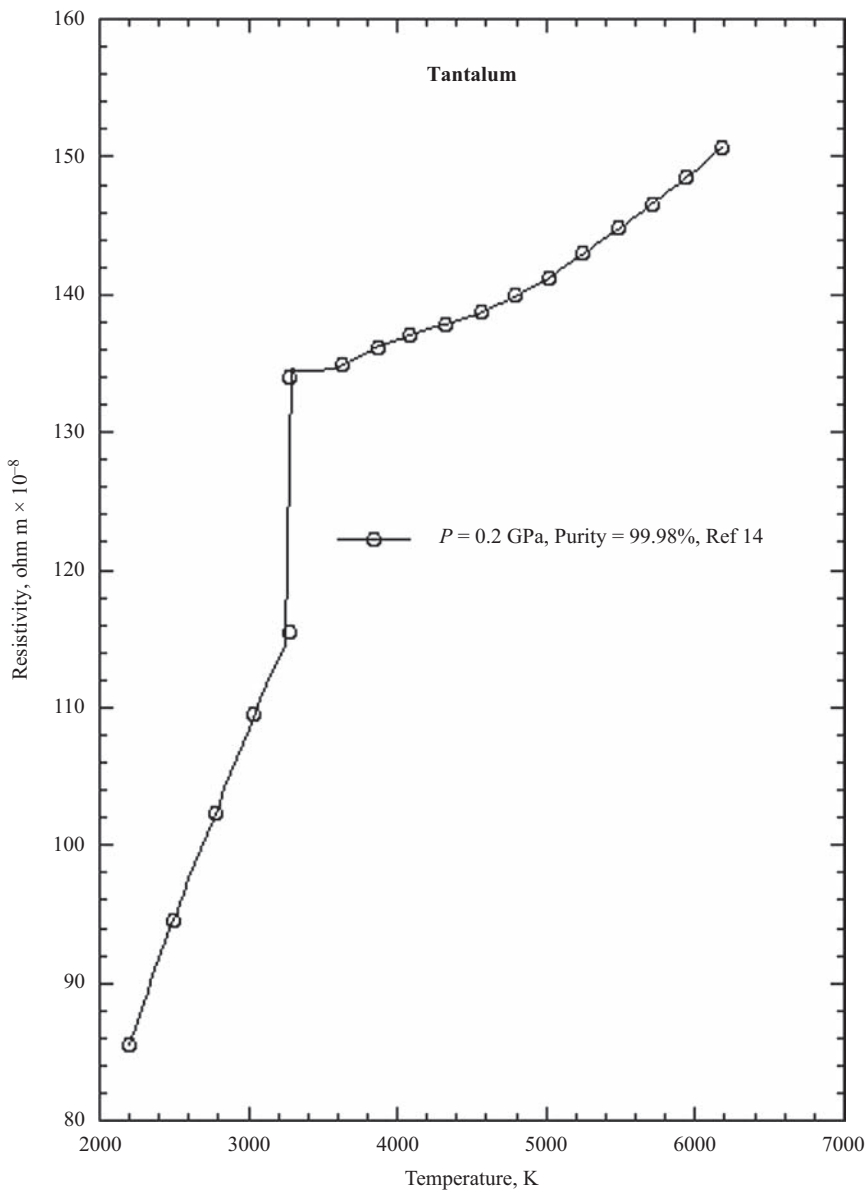


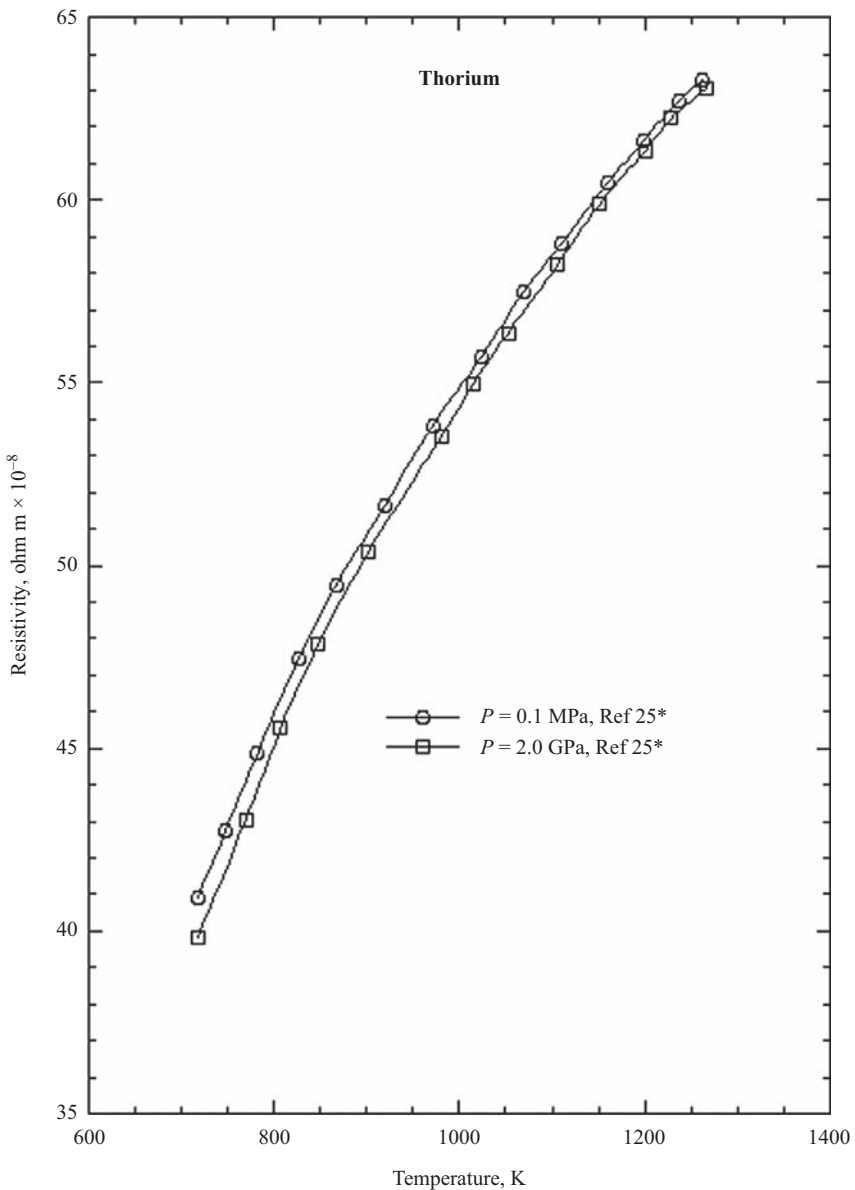


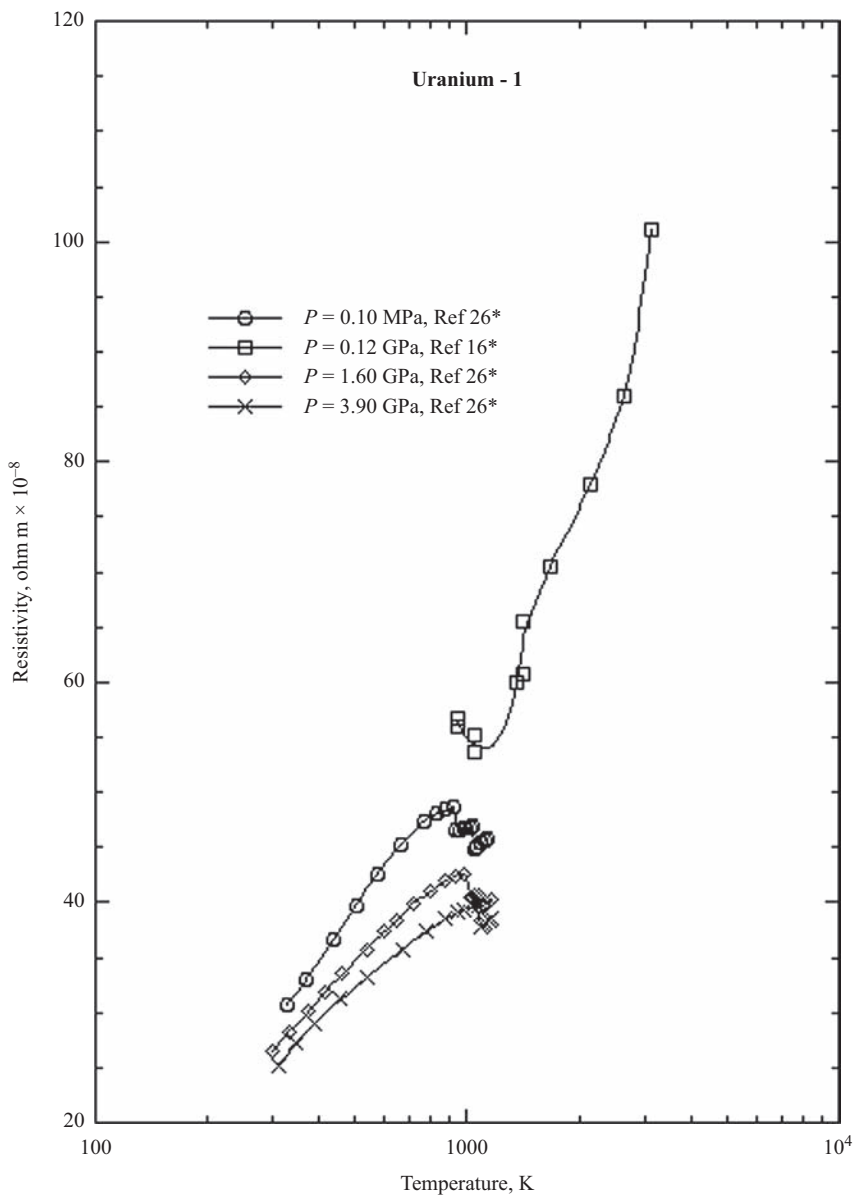


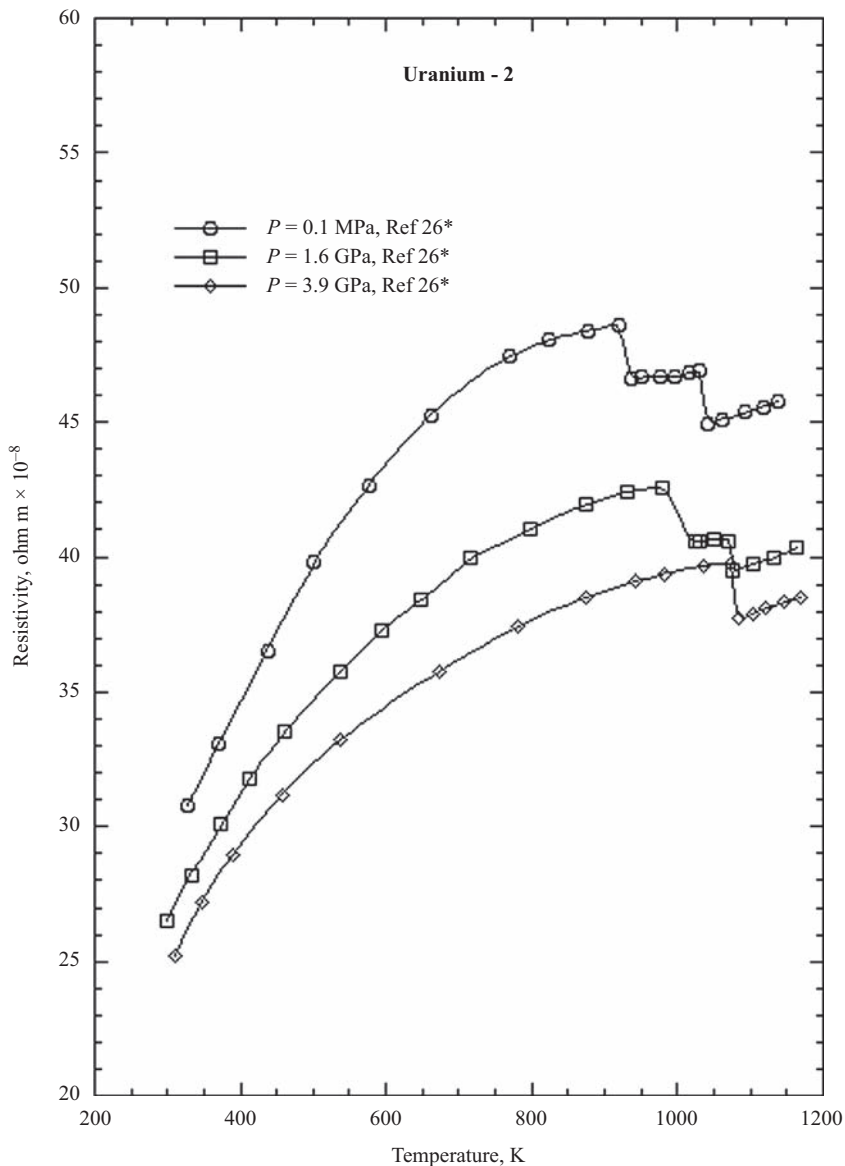


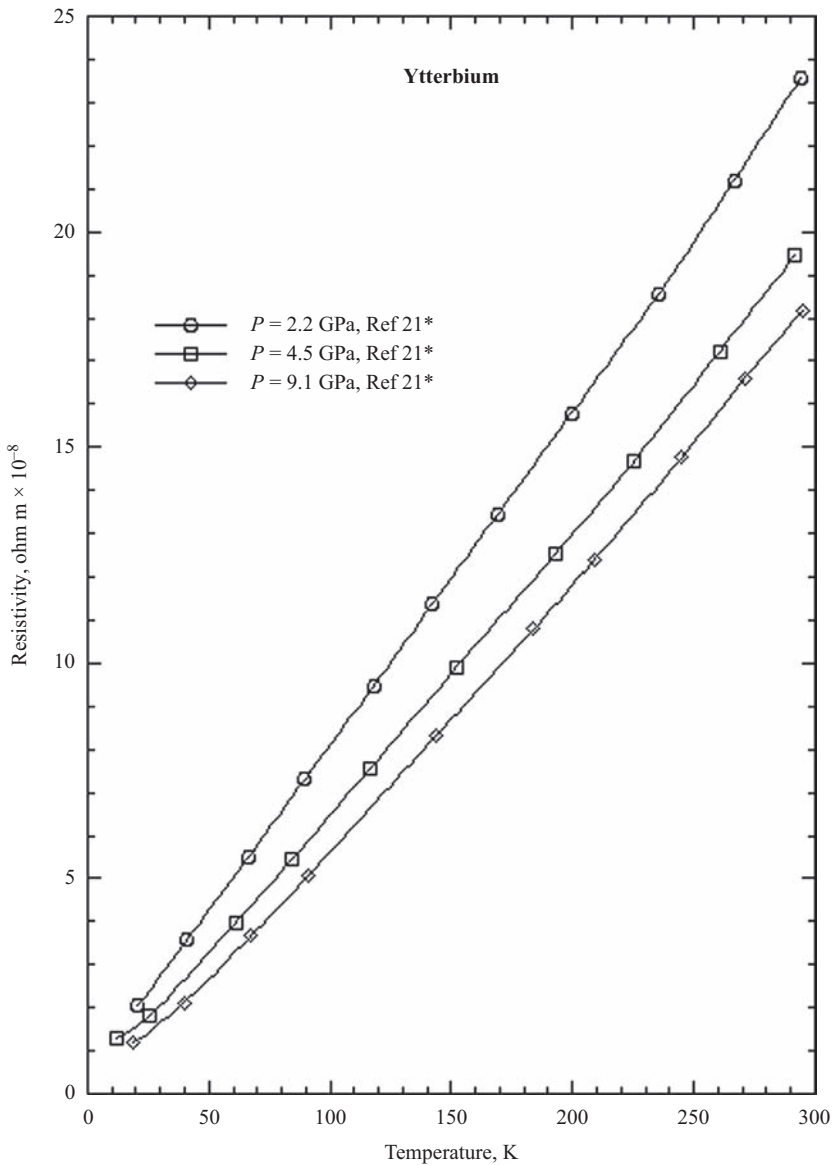


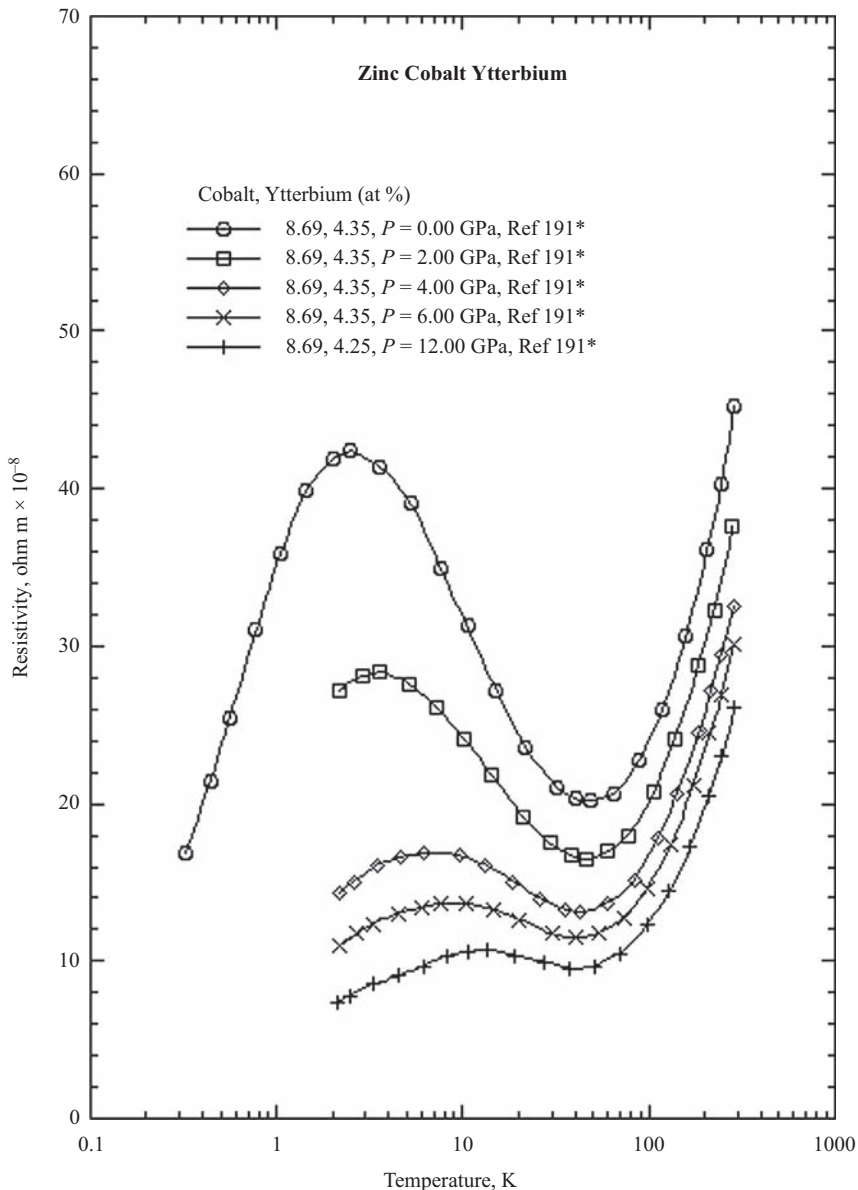


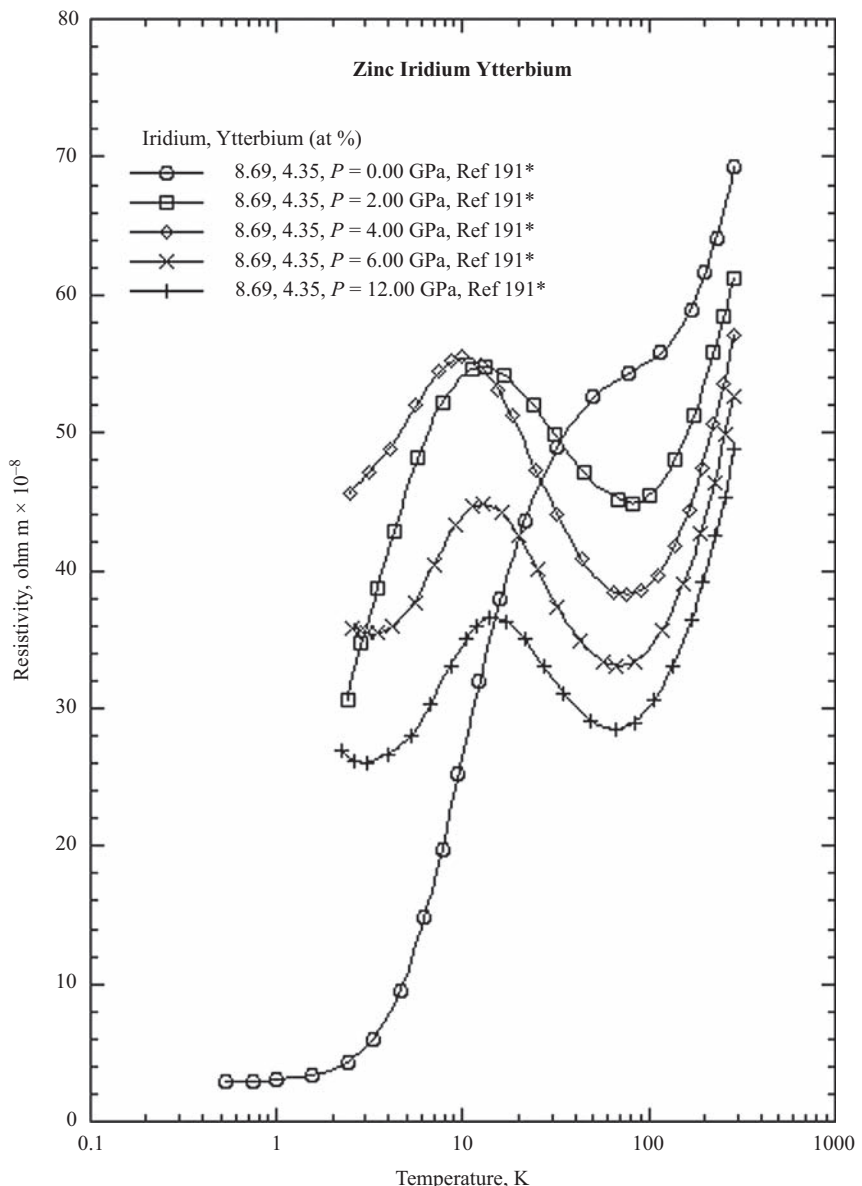


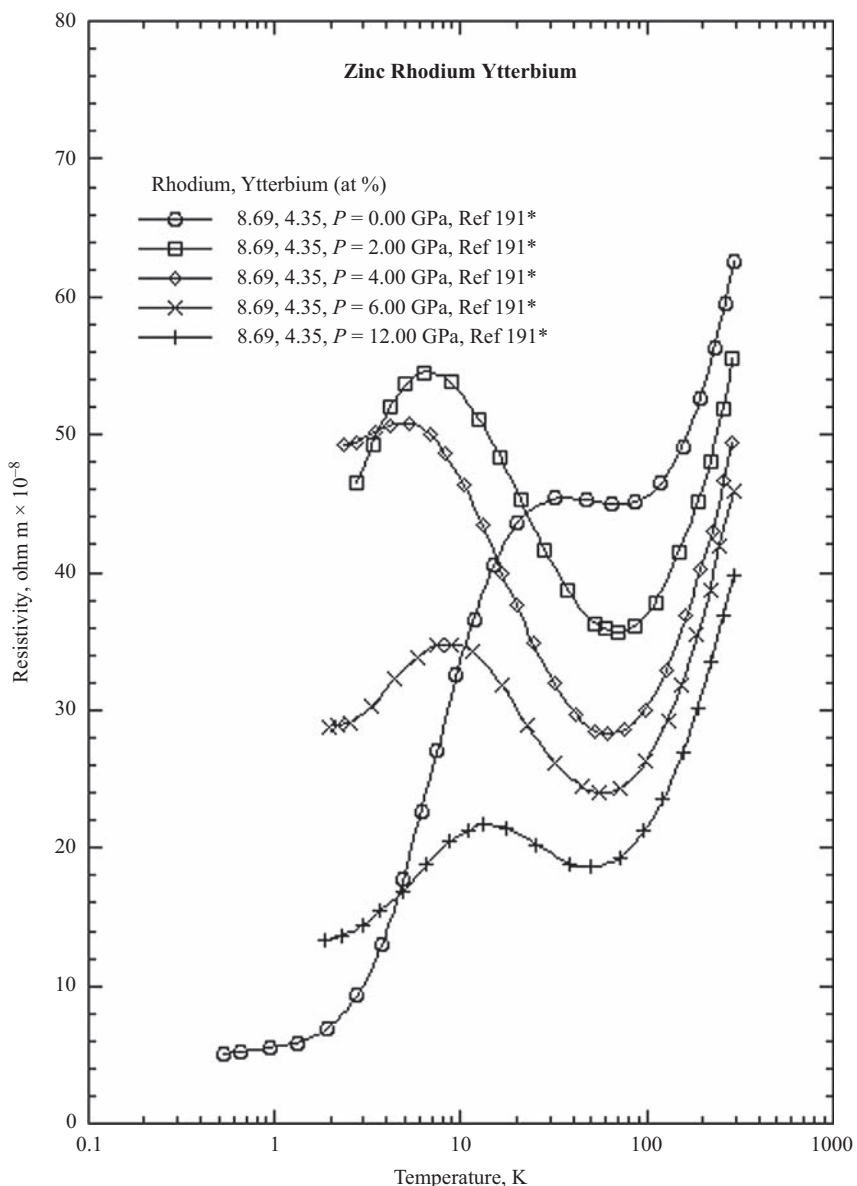


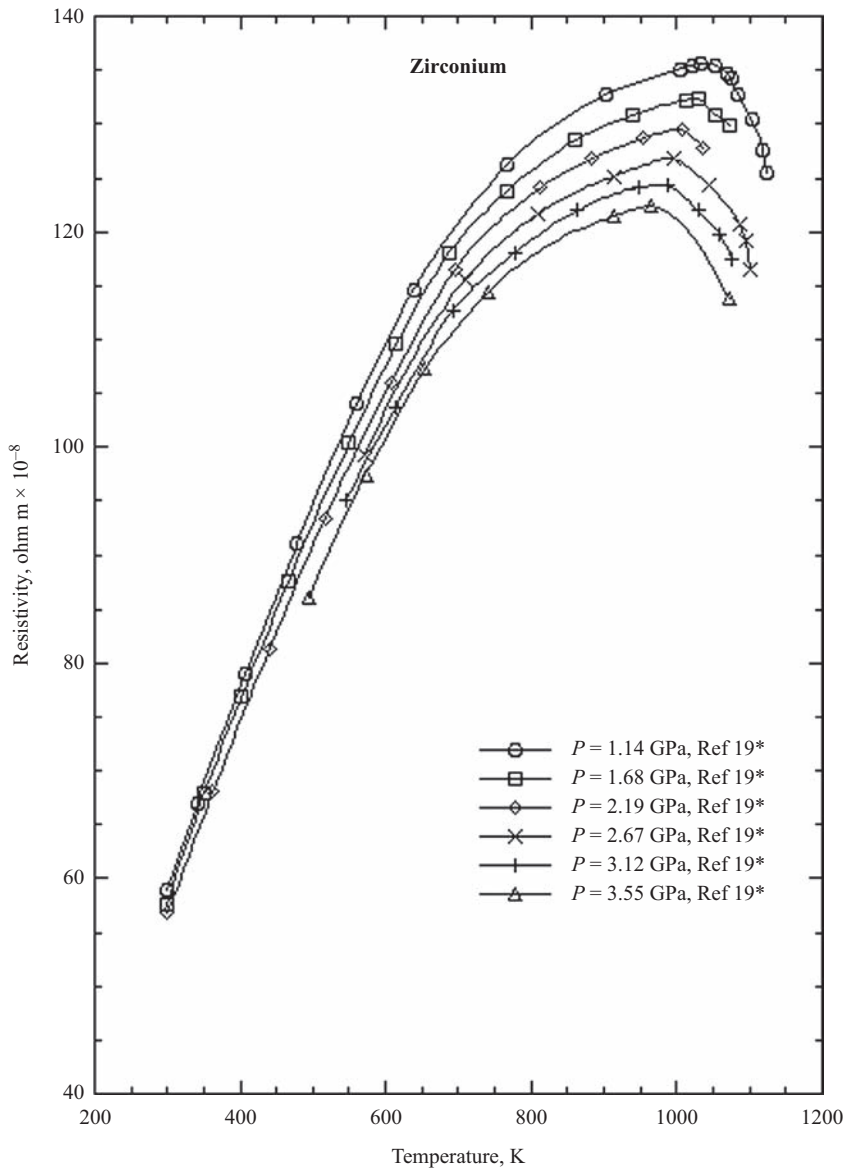




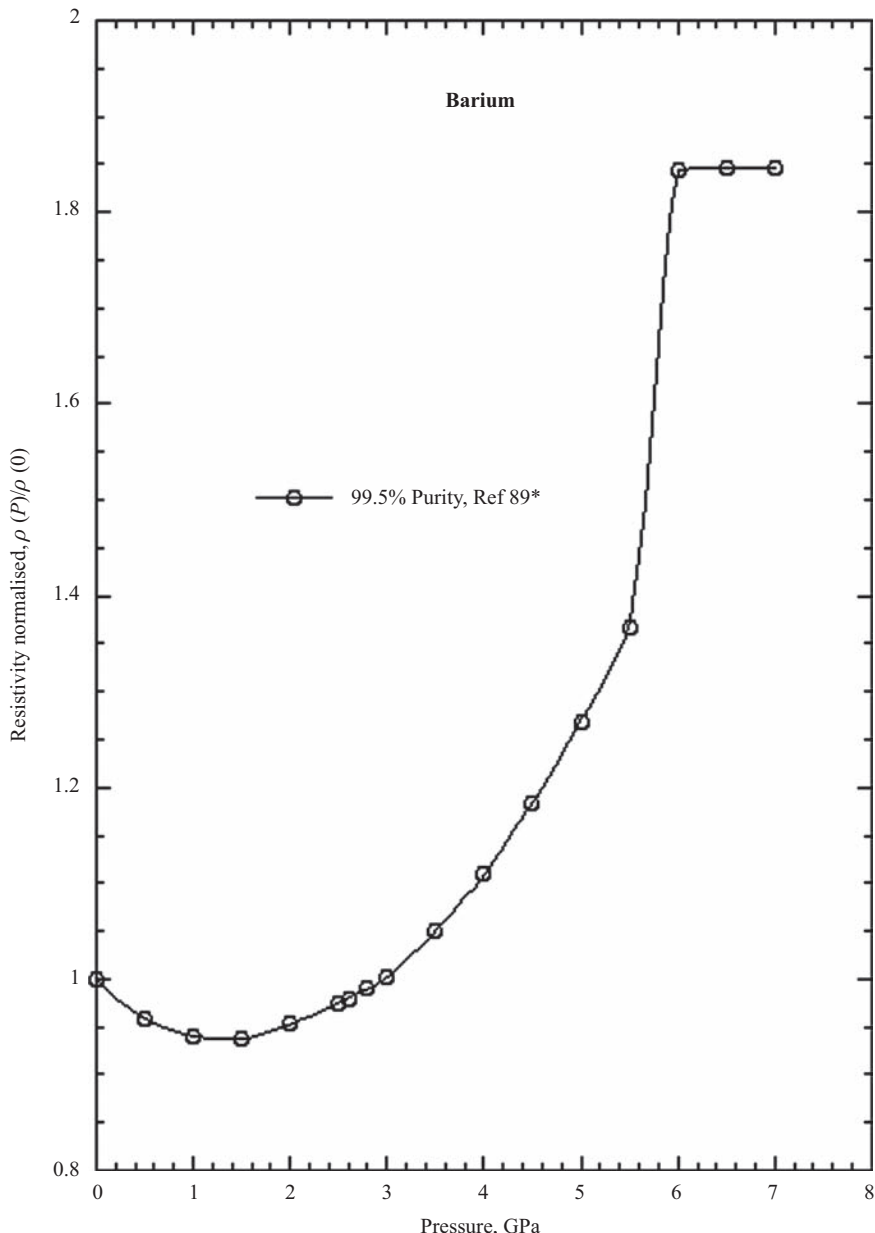


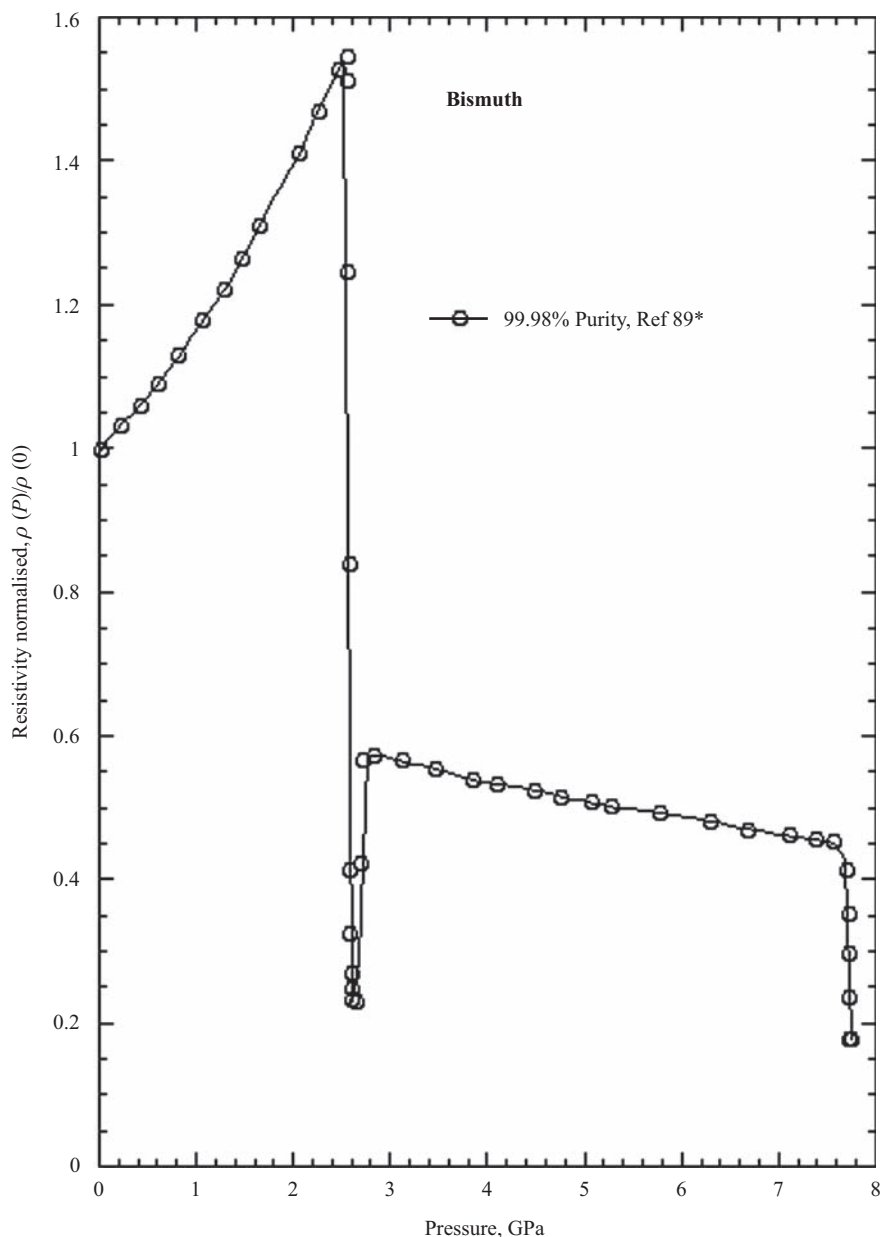


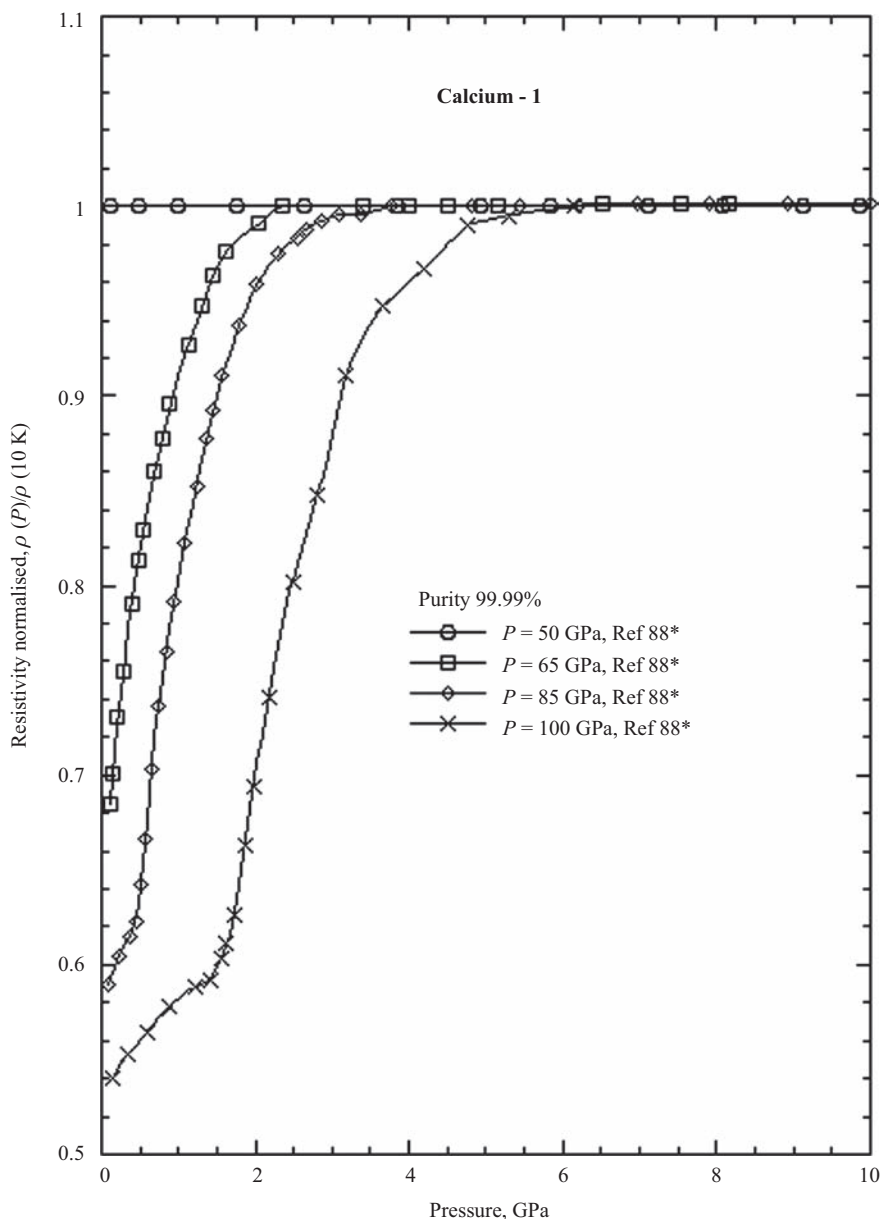


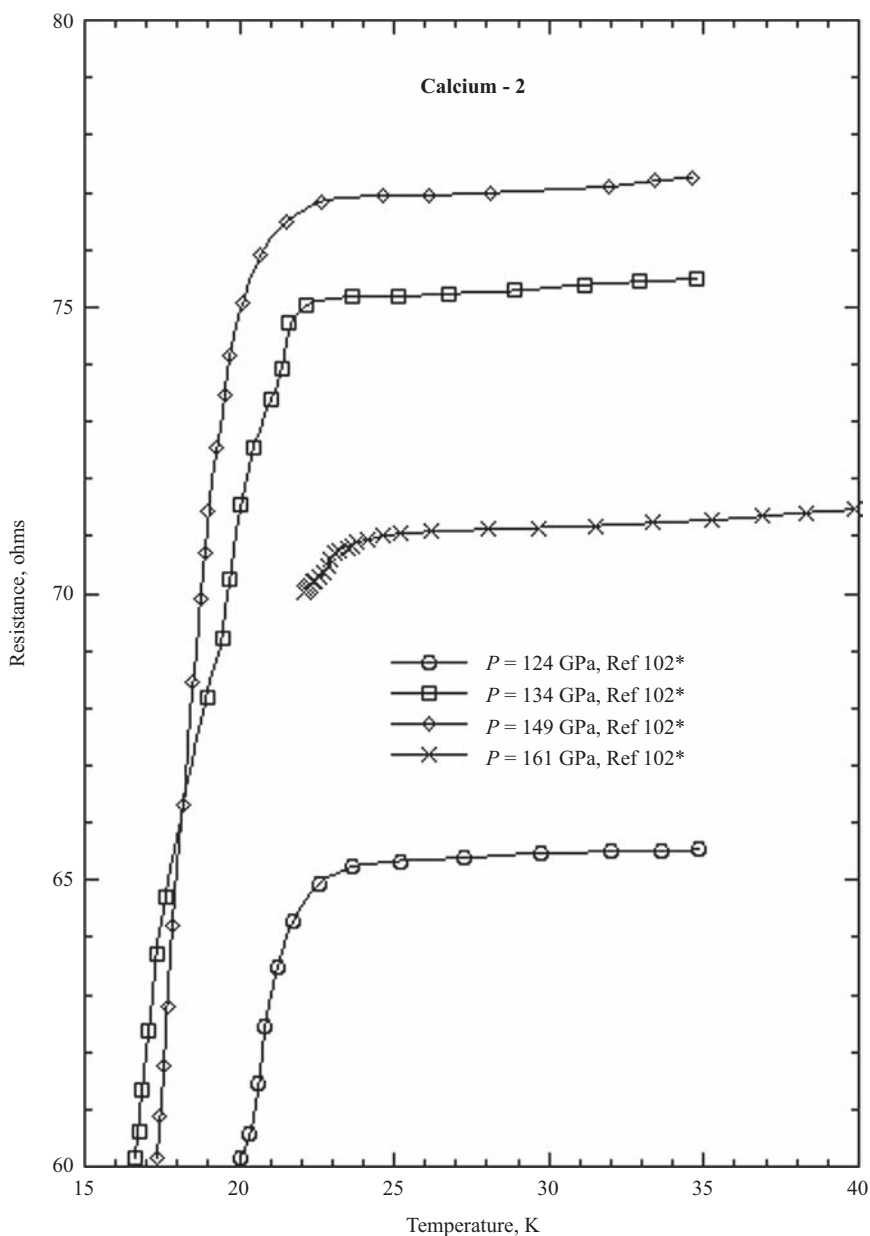


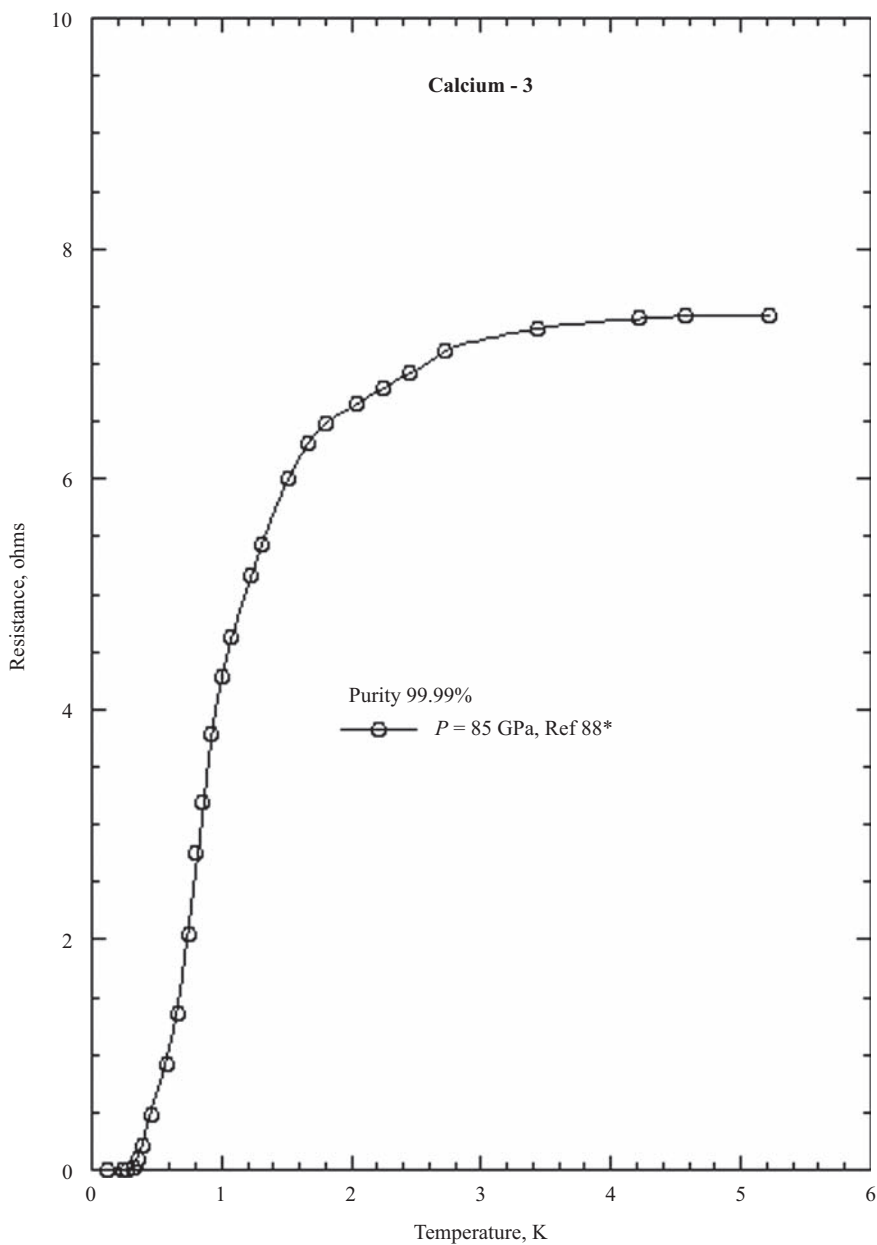
6.3 Resistance measurements as a function of temperature and pressure

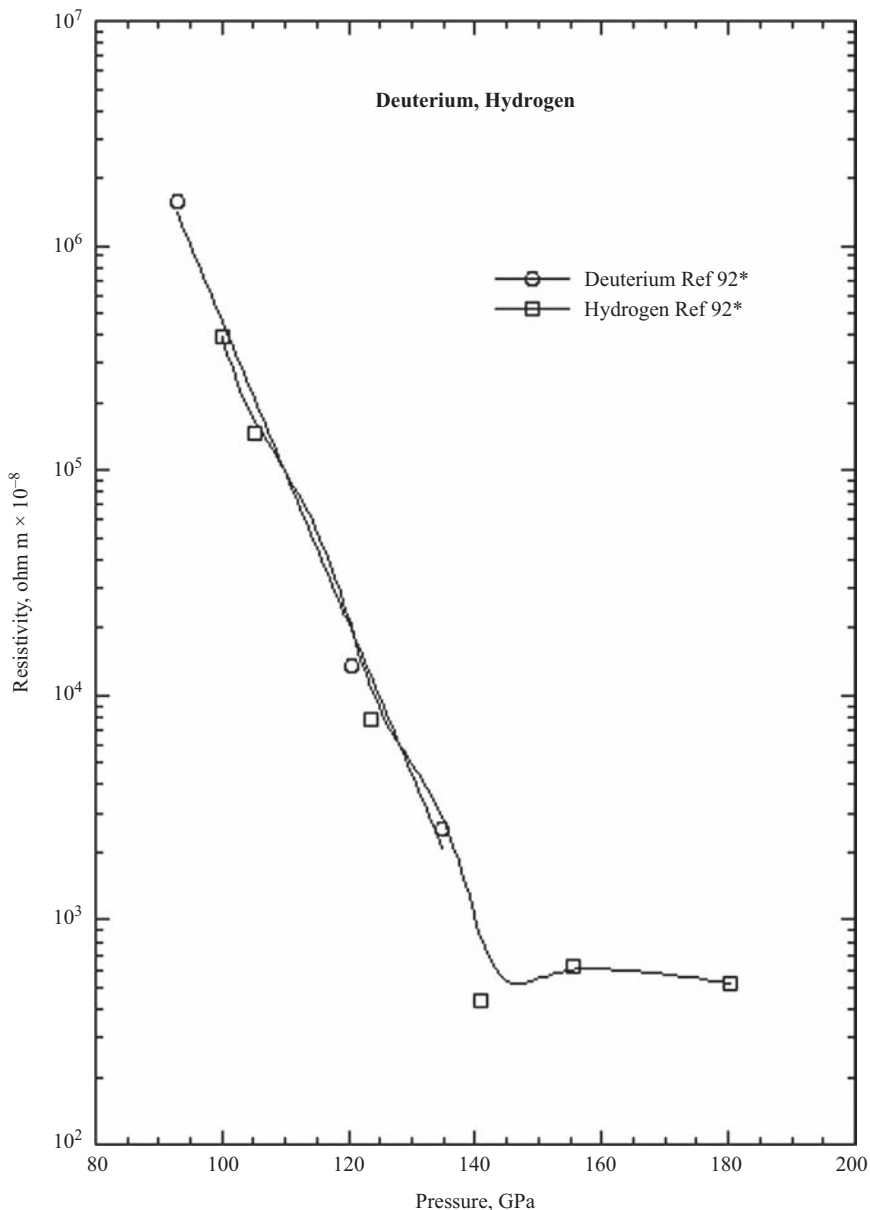


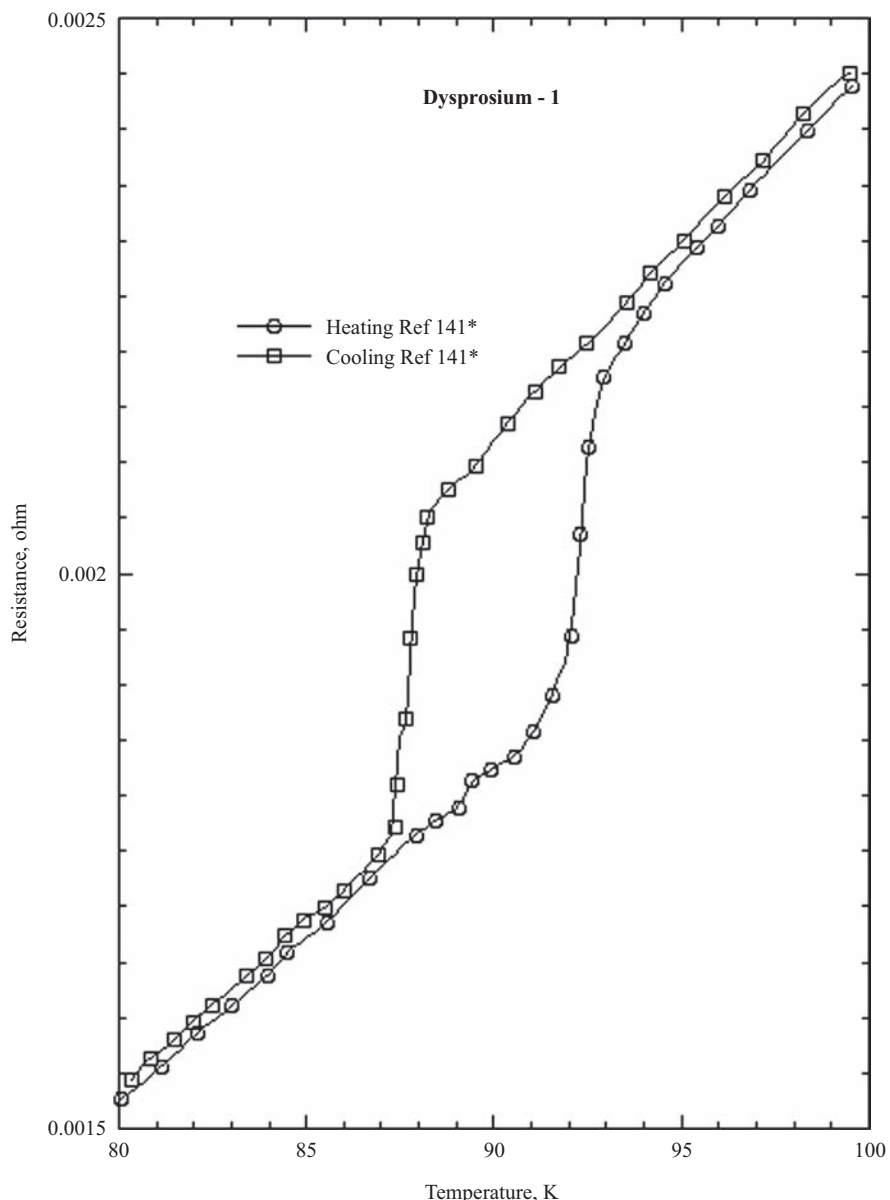


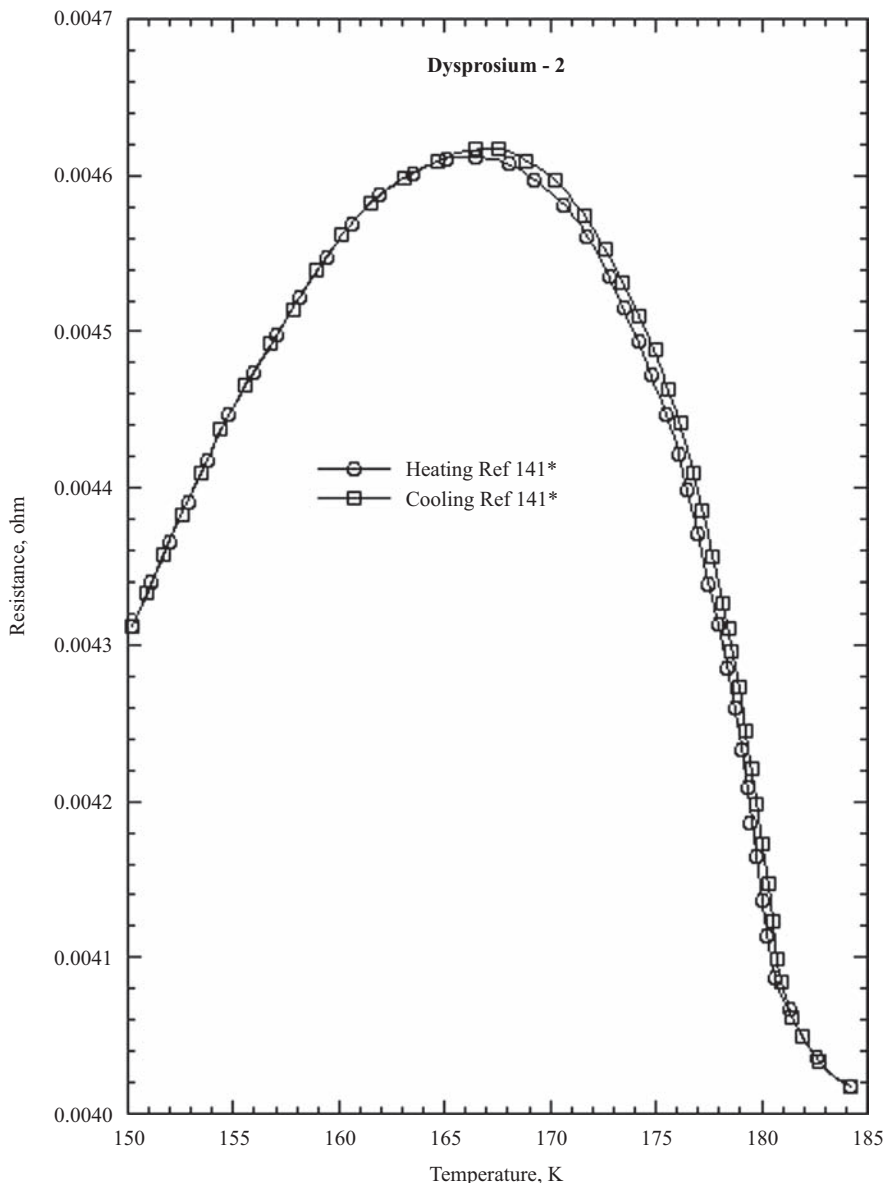


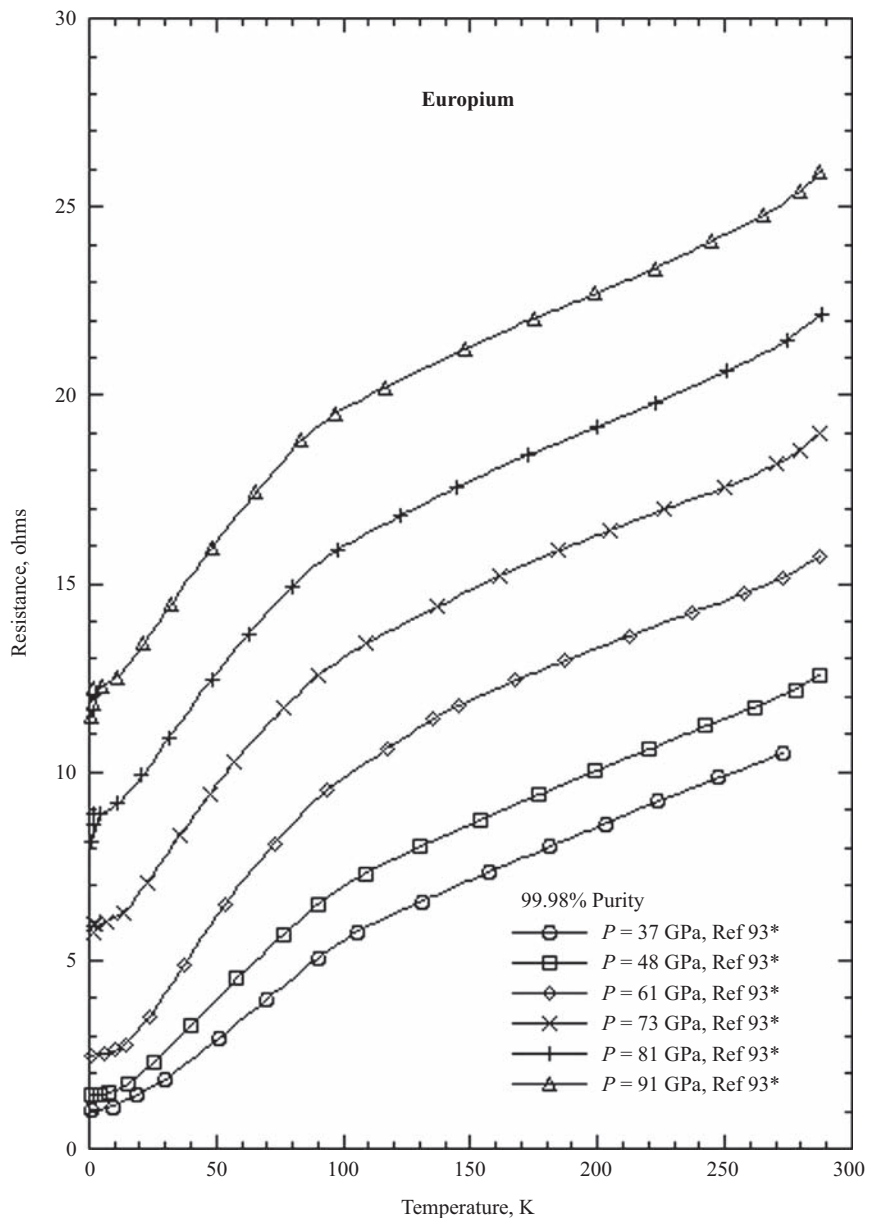


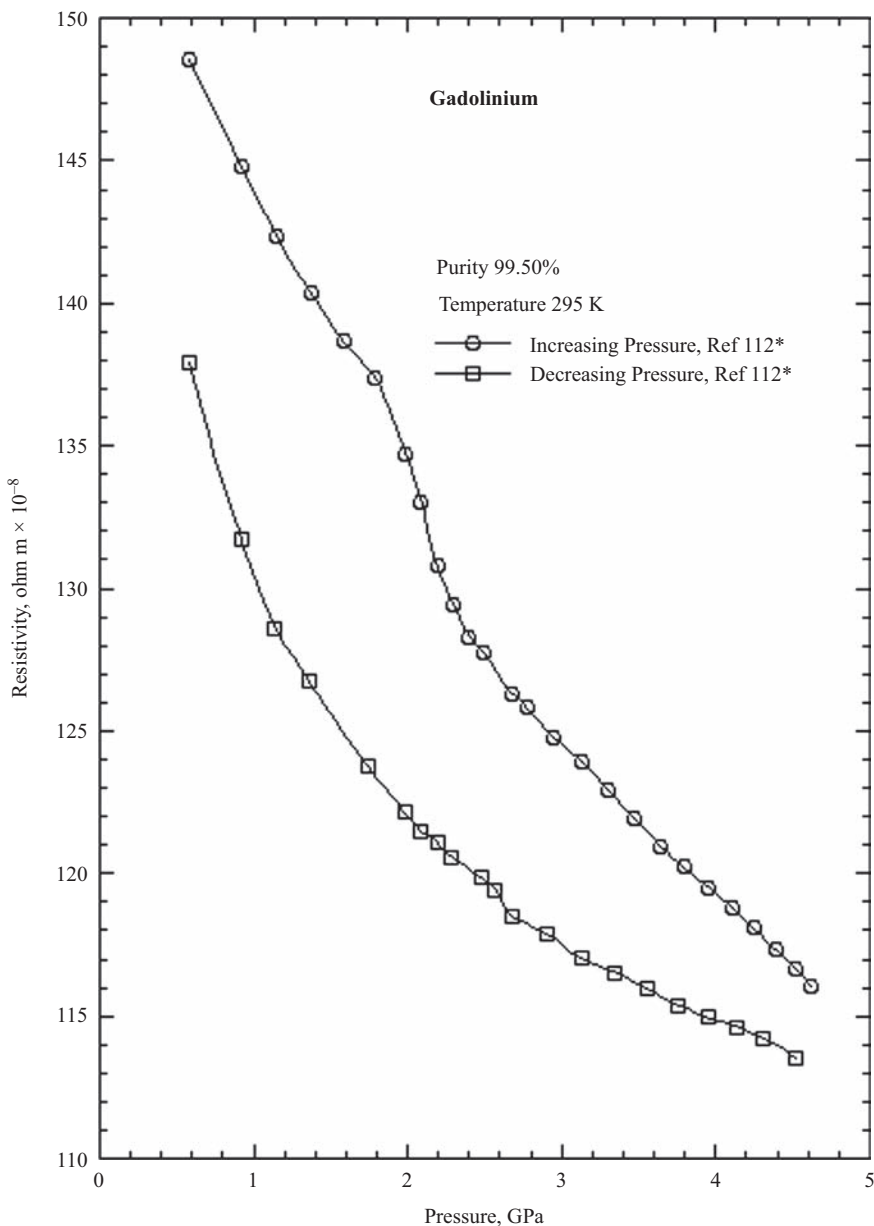


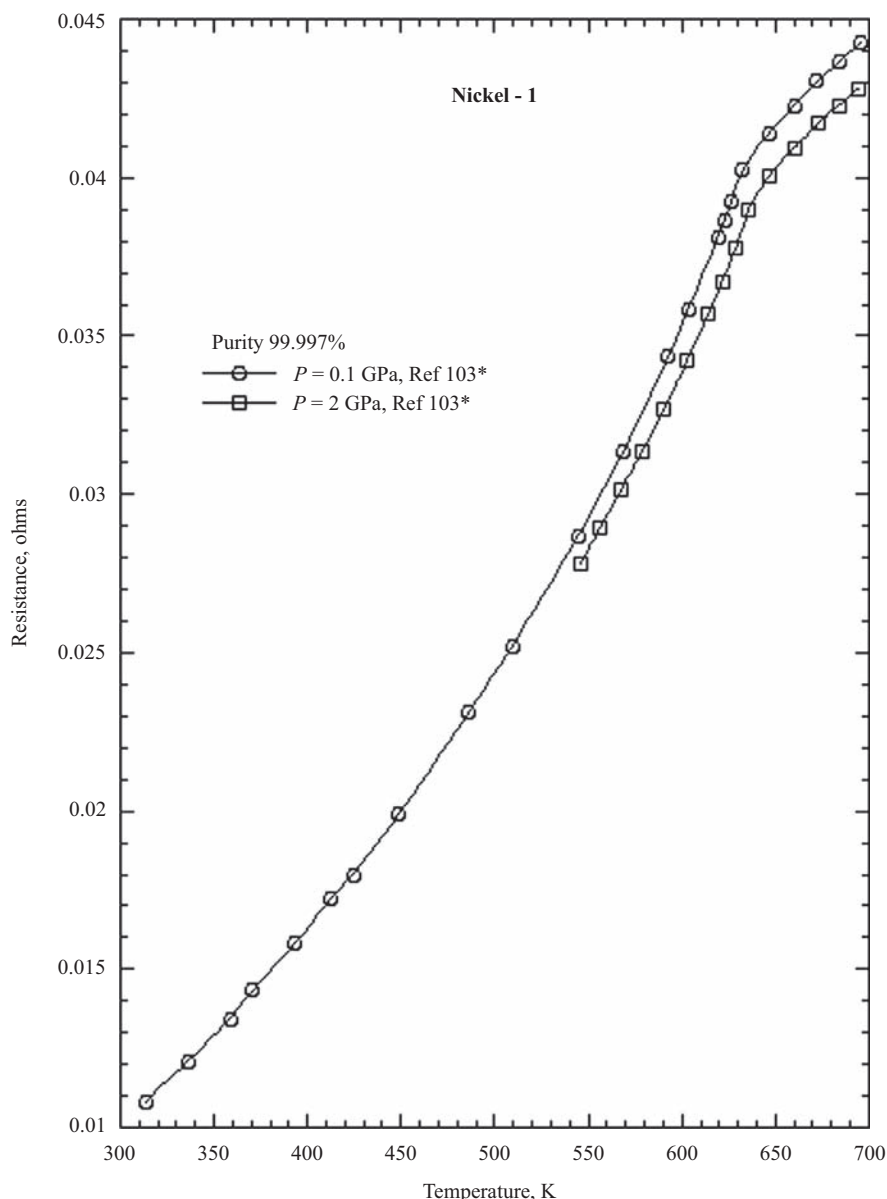


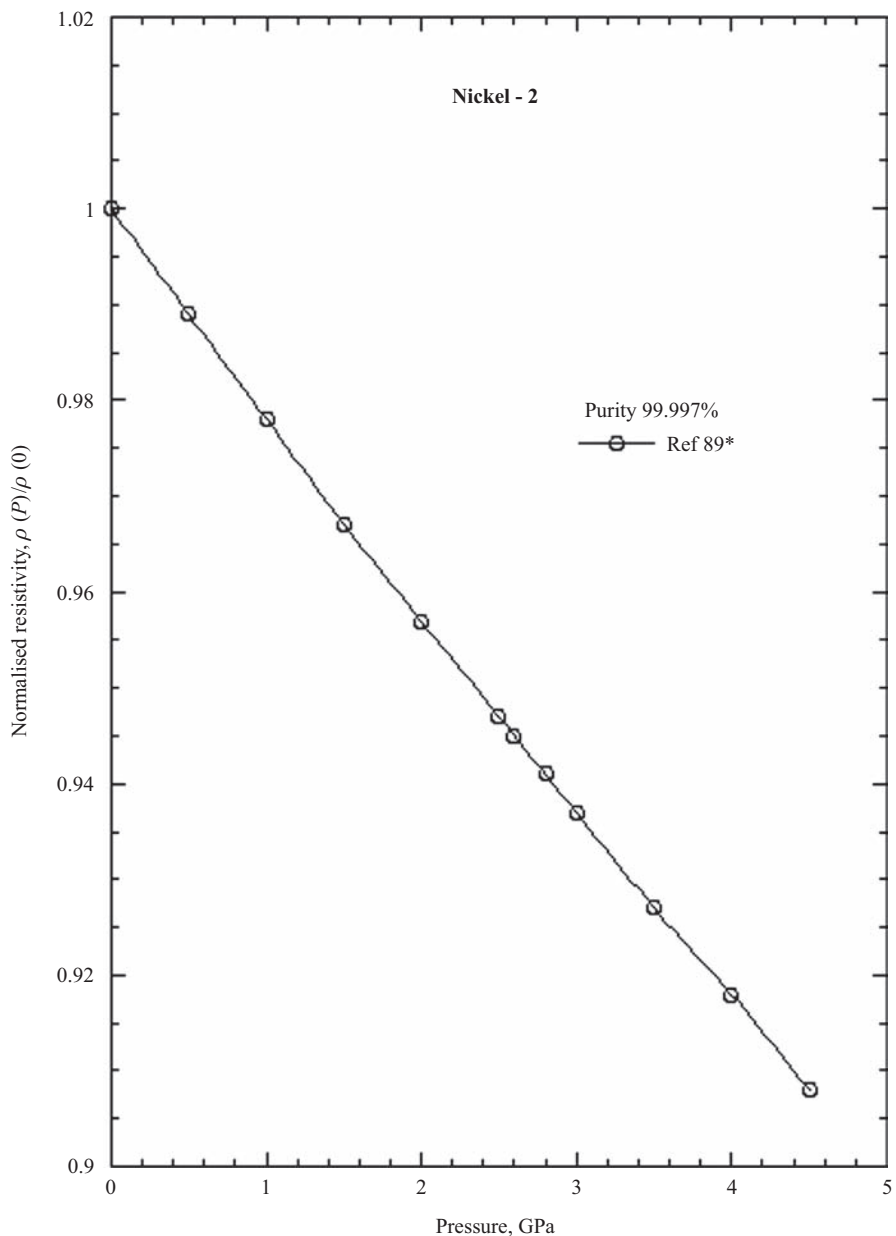


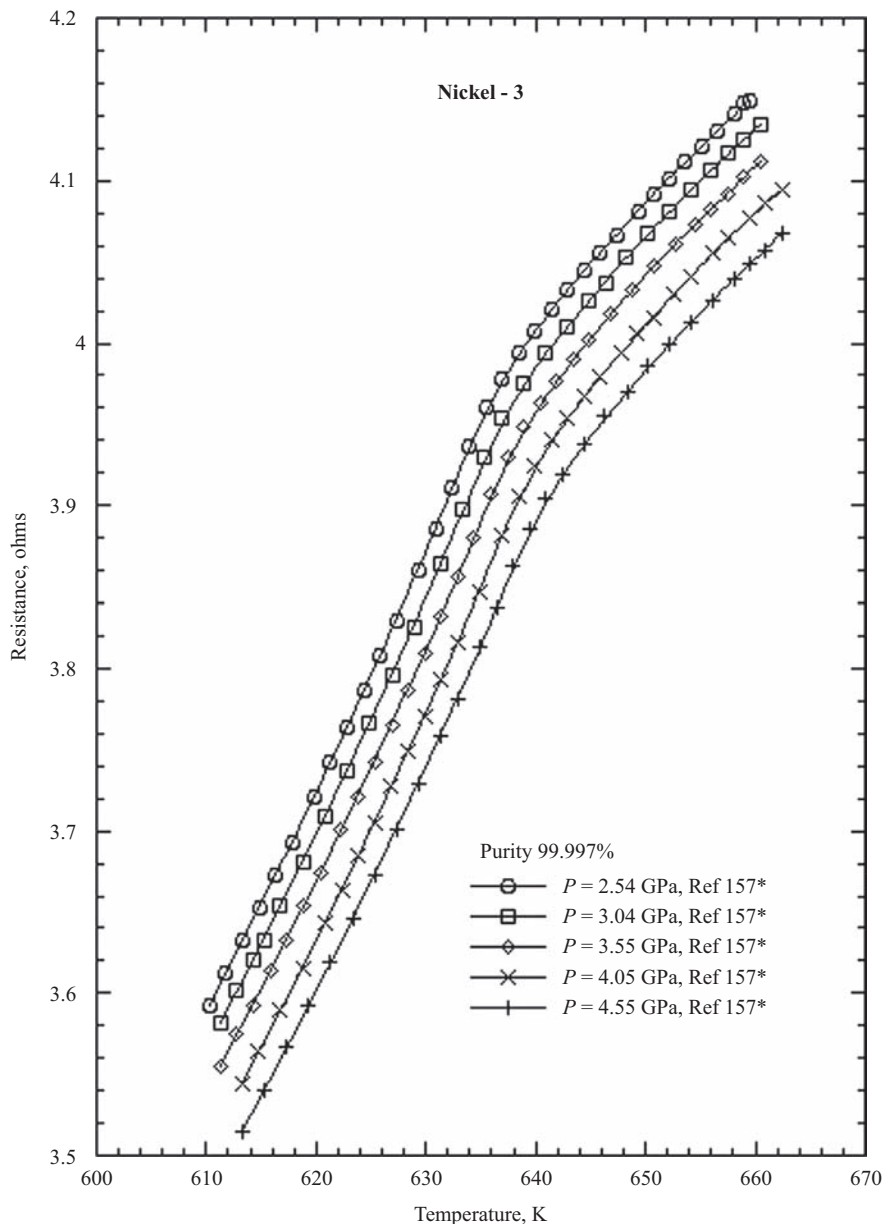


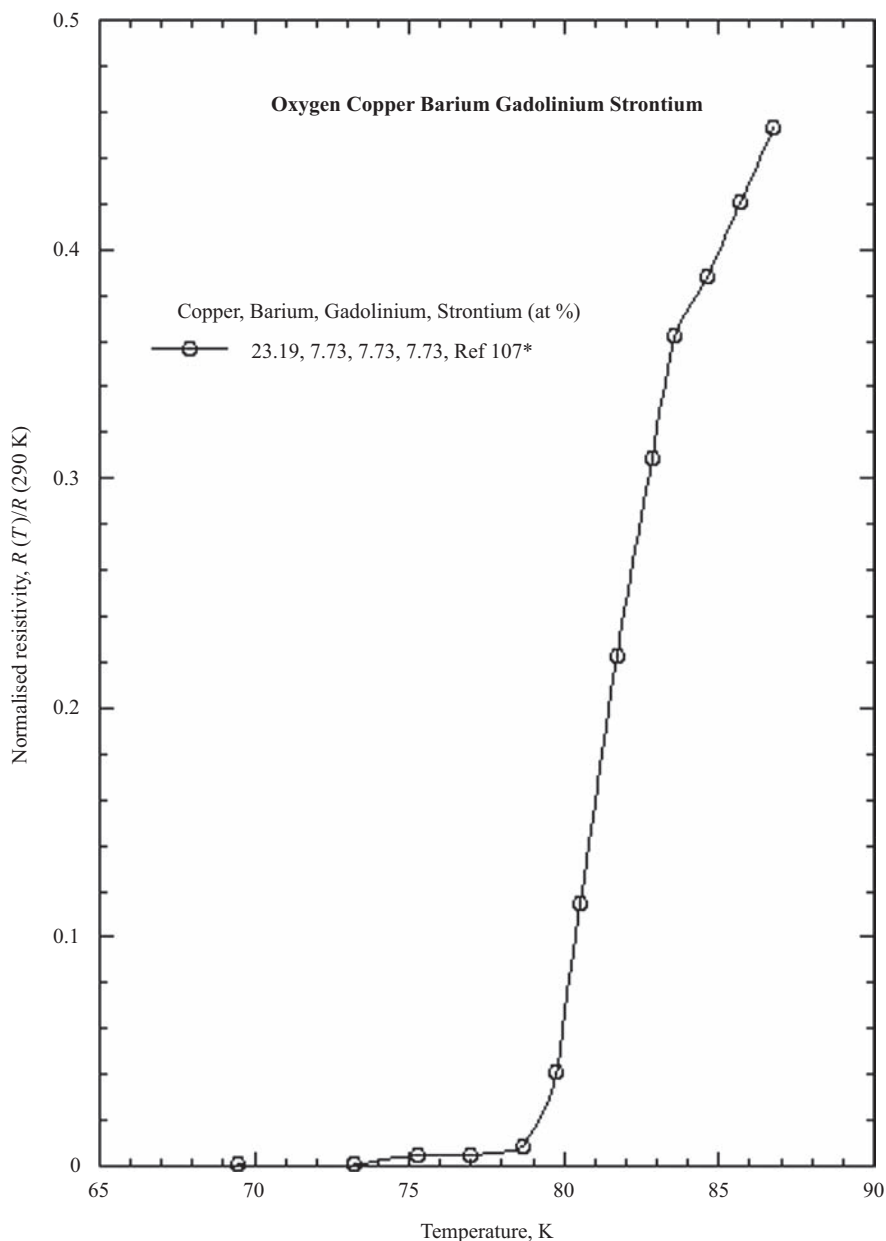


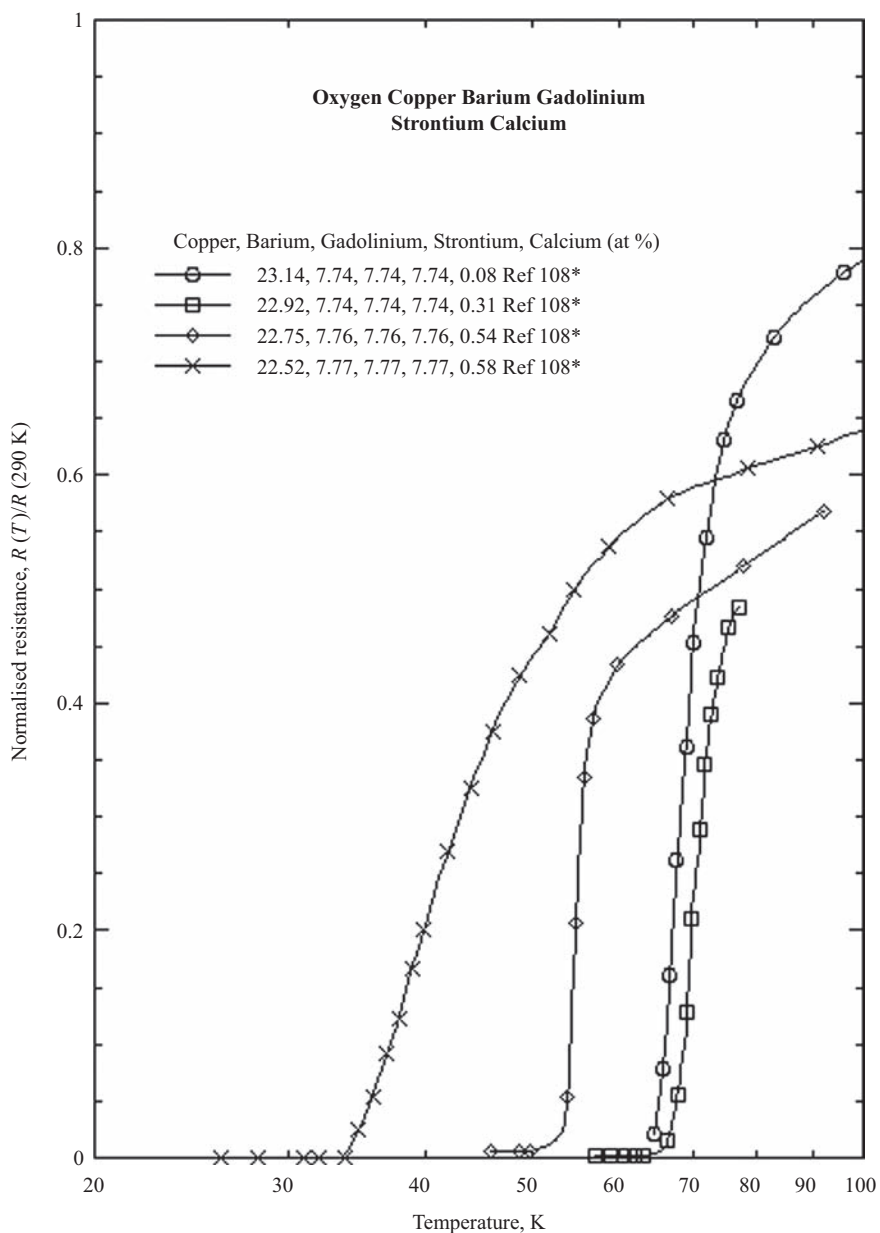


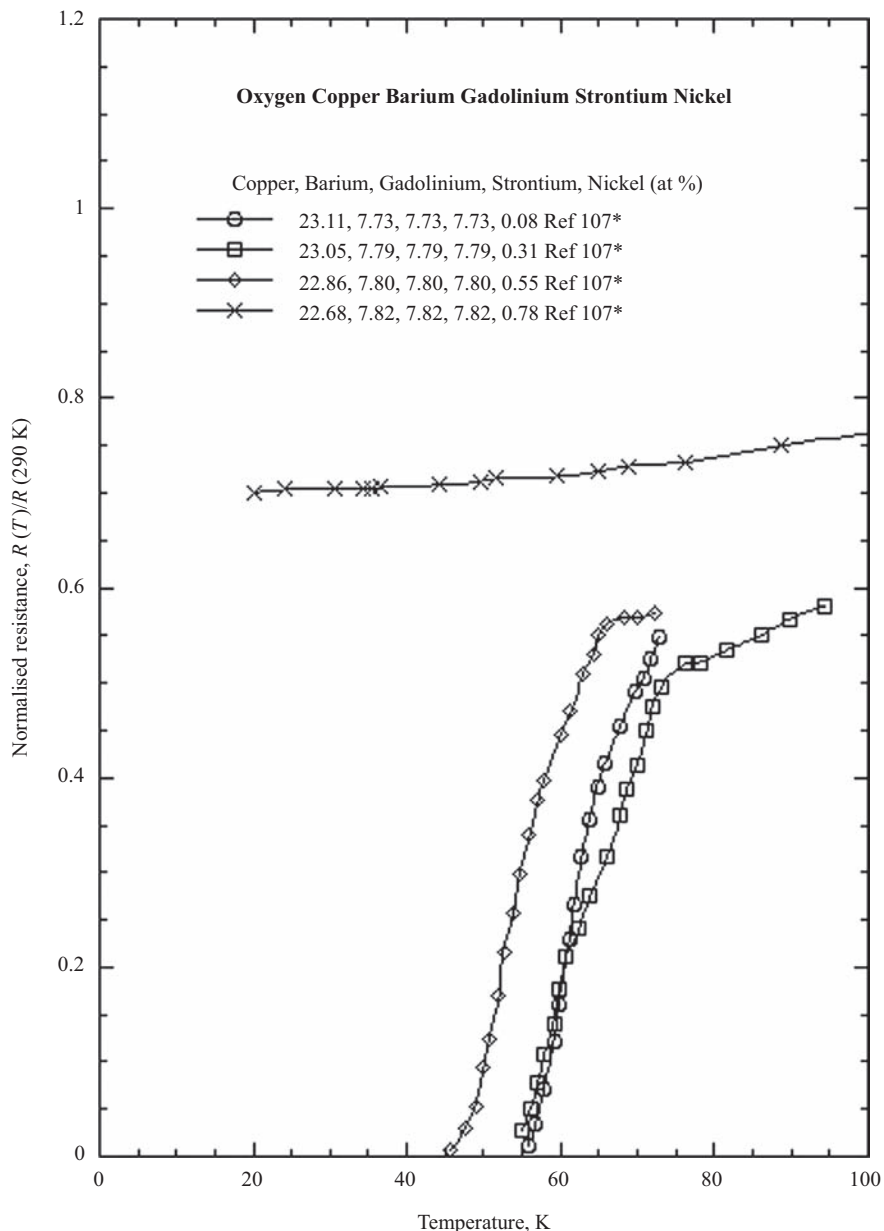


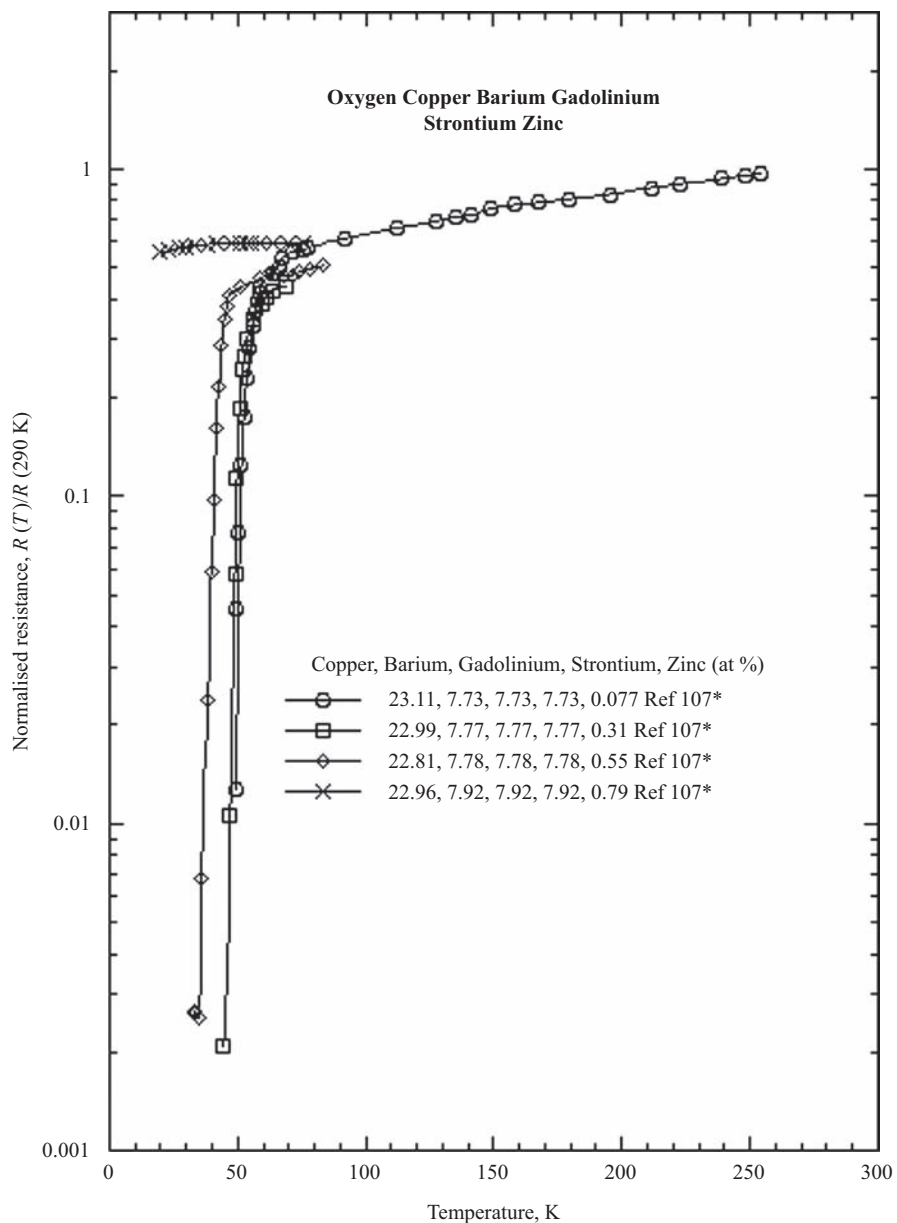


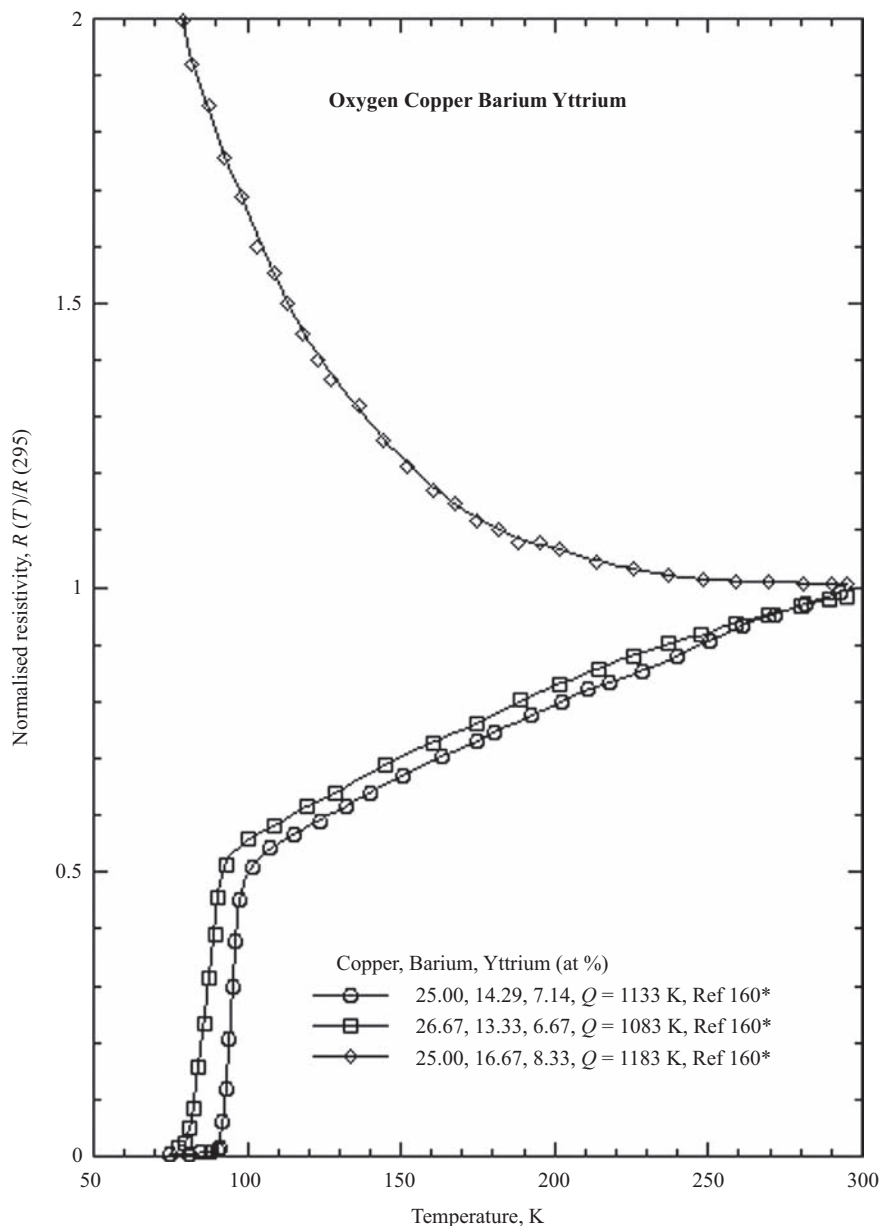


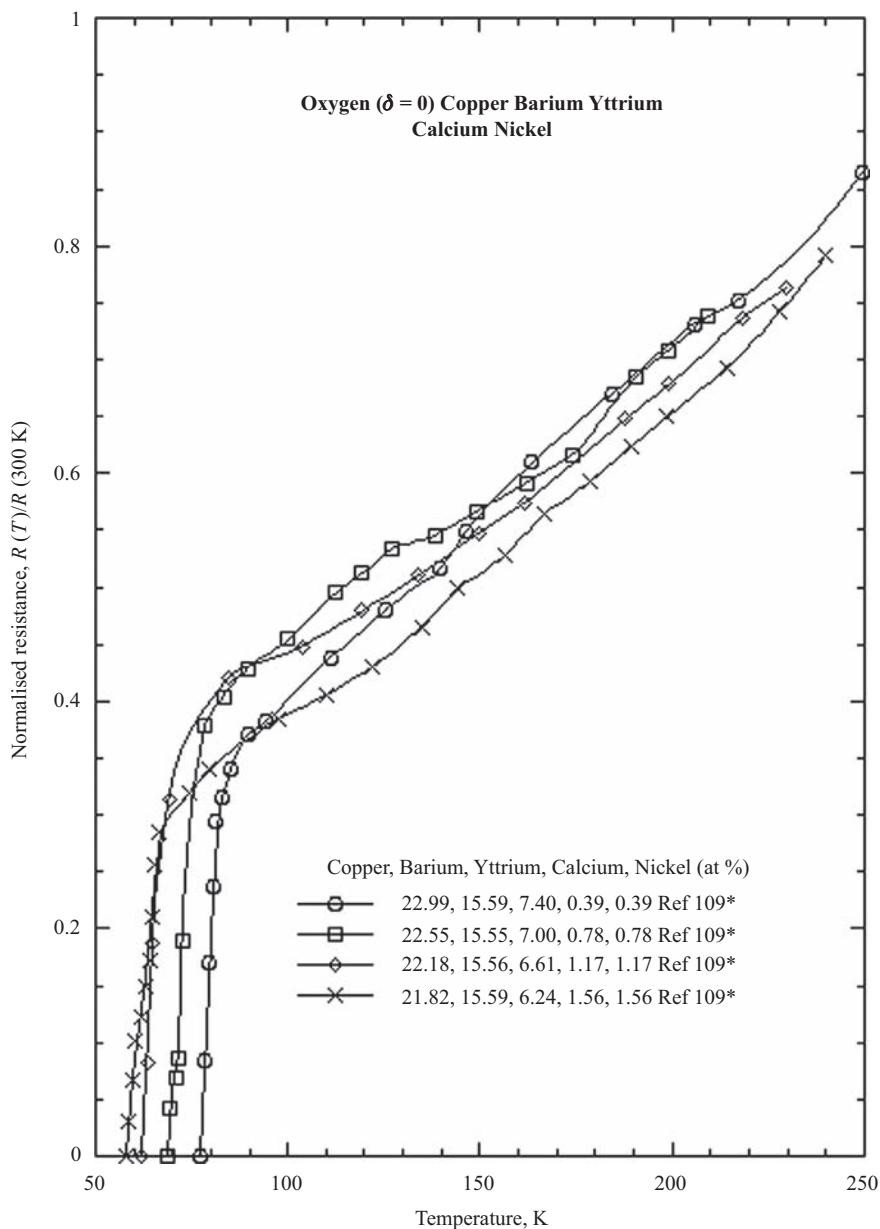


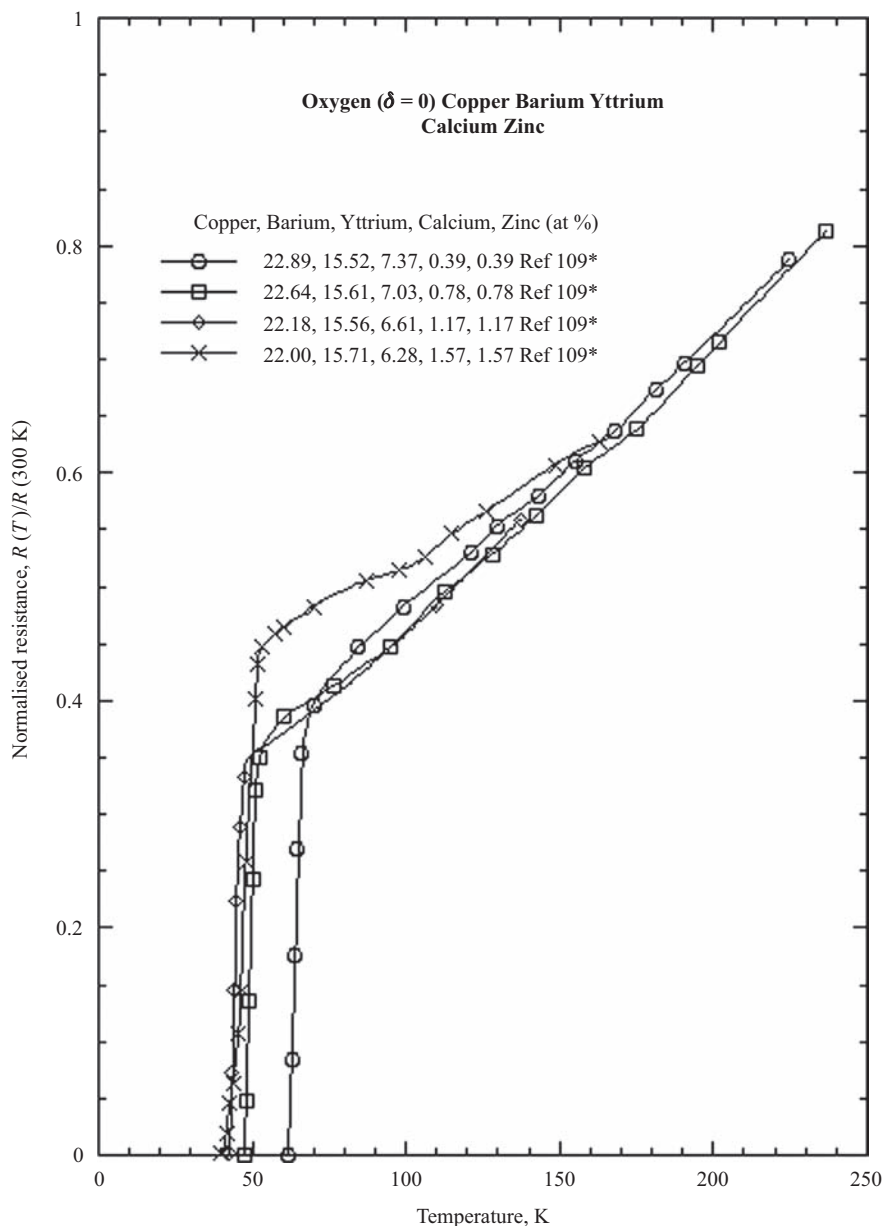


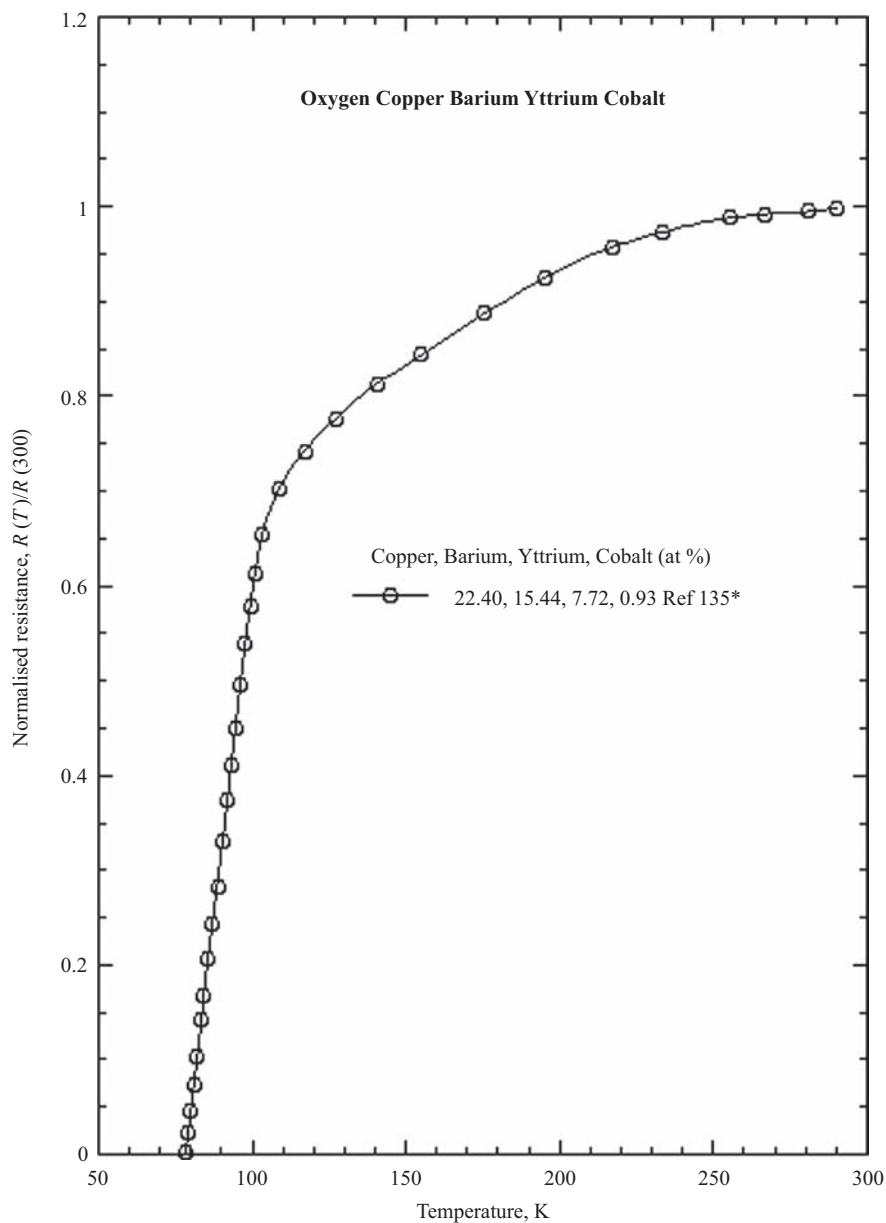


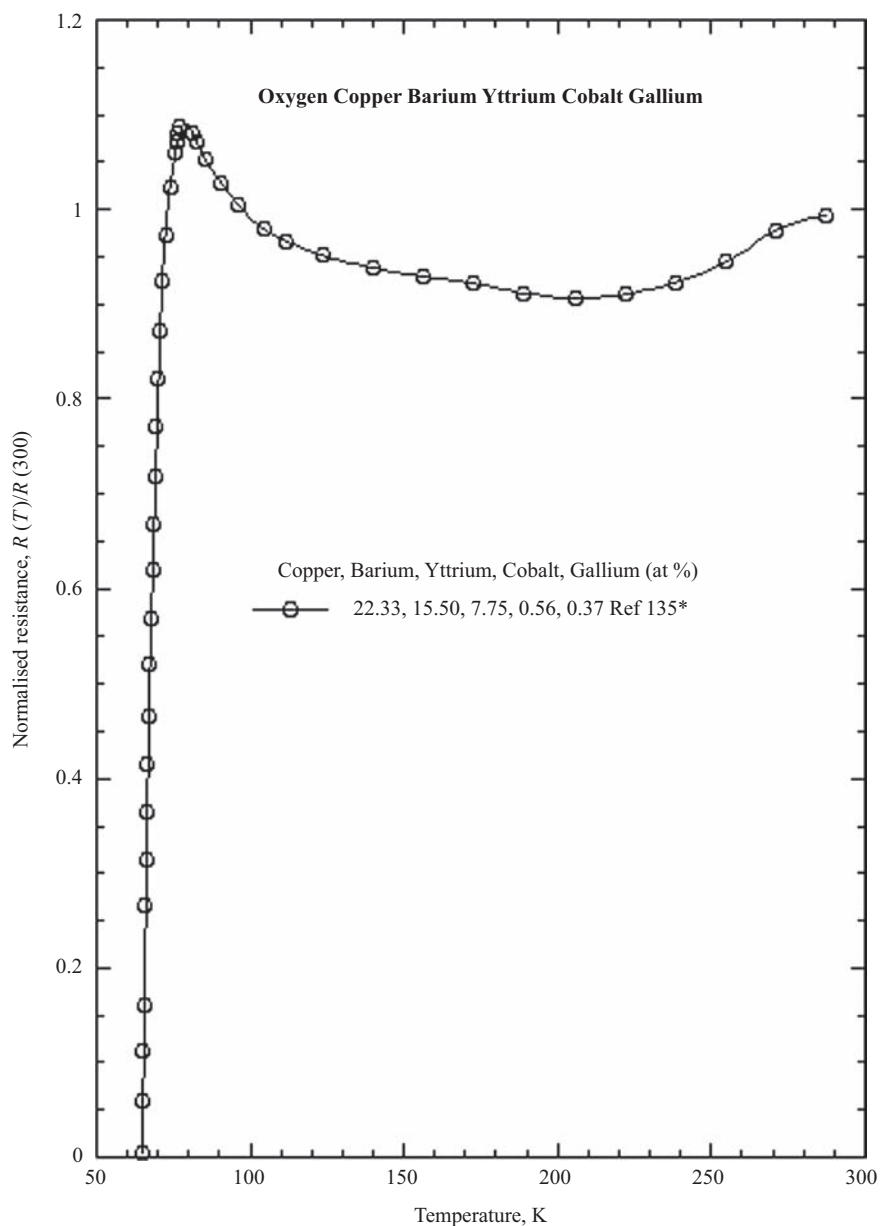


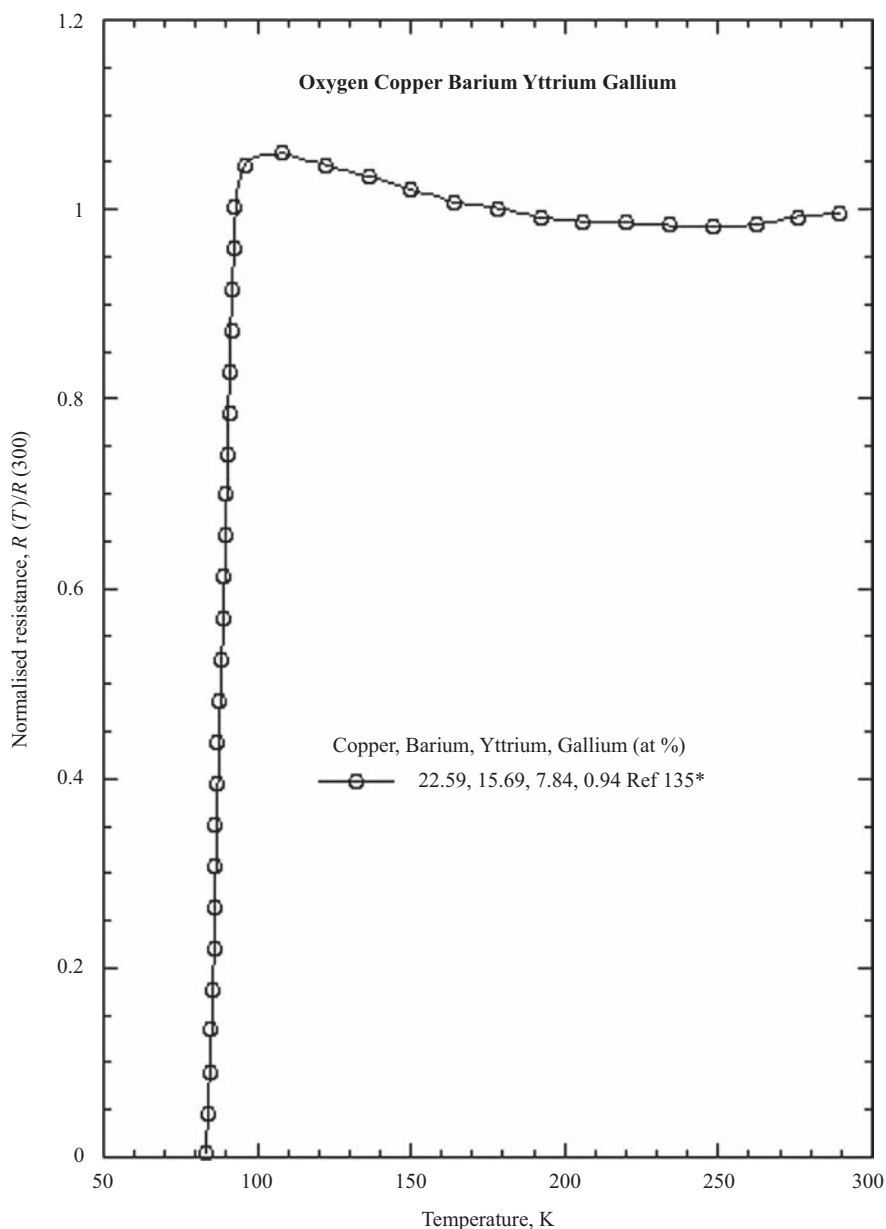


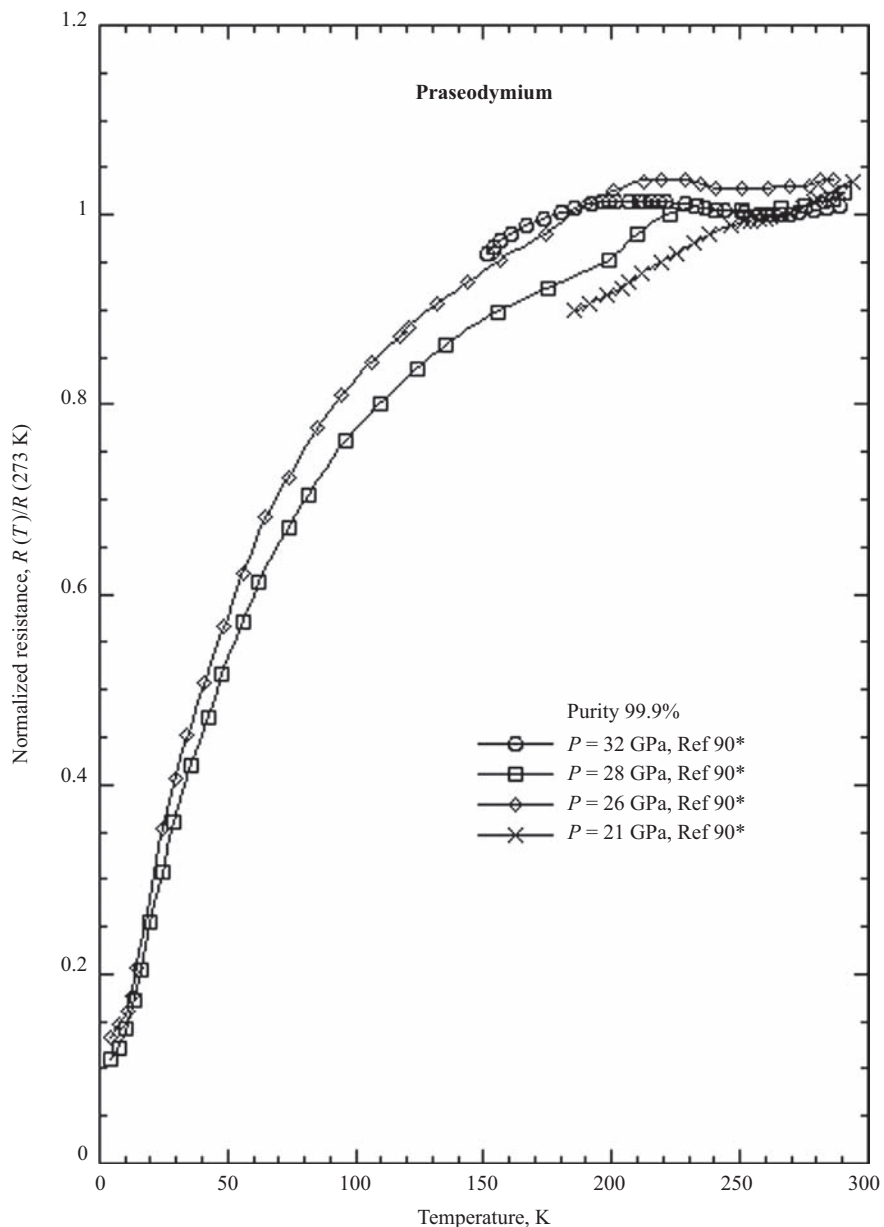


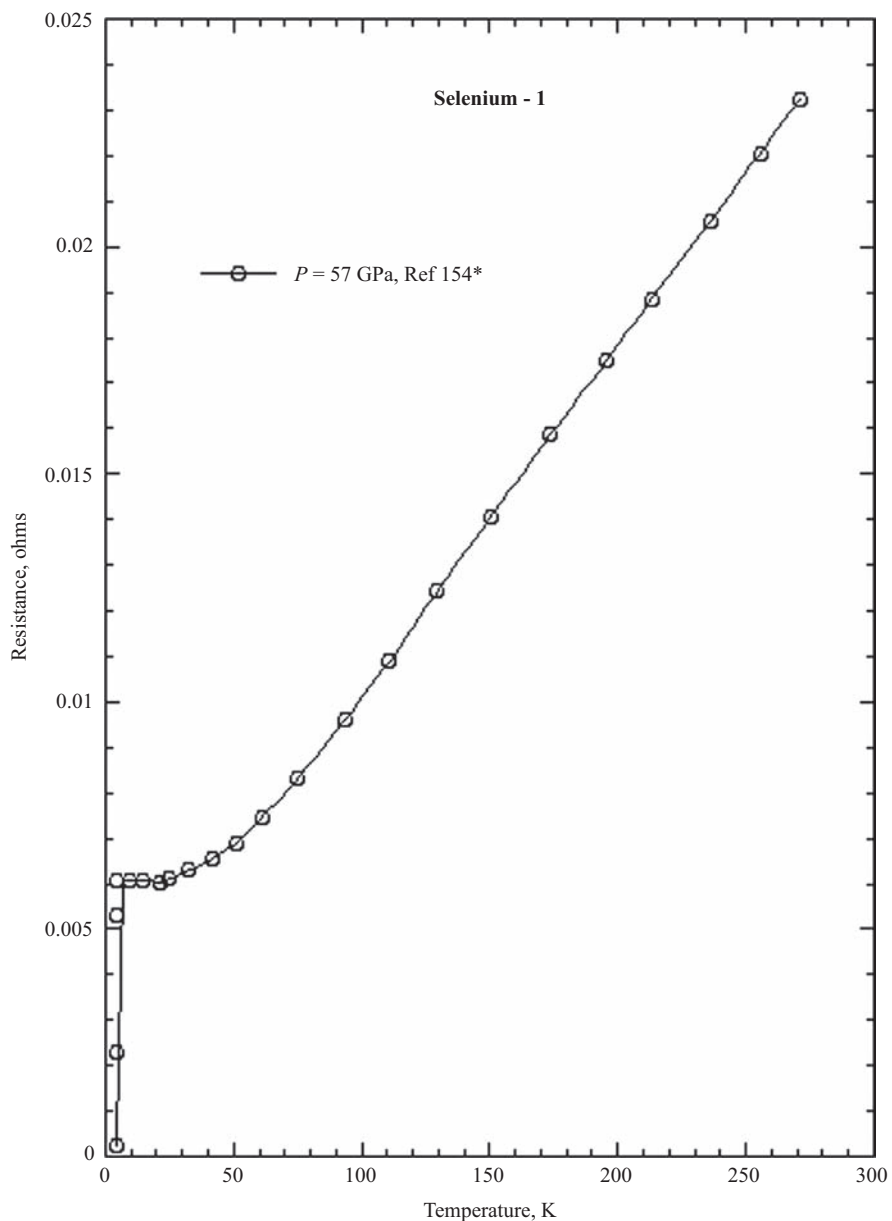


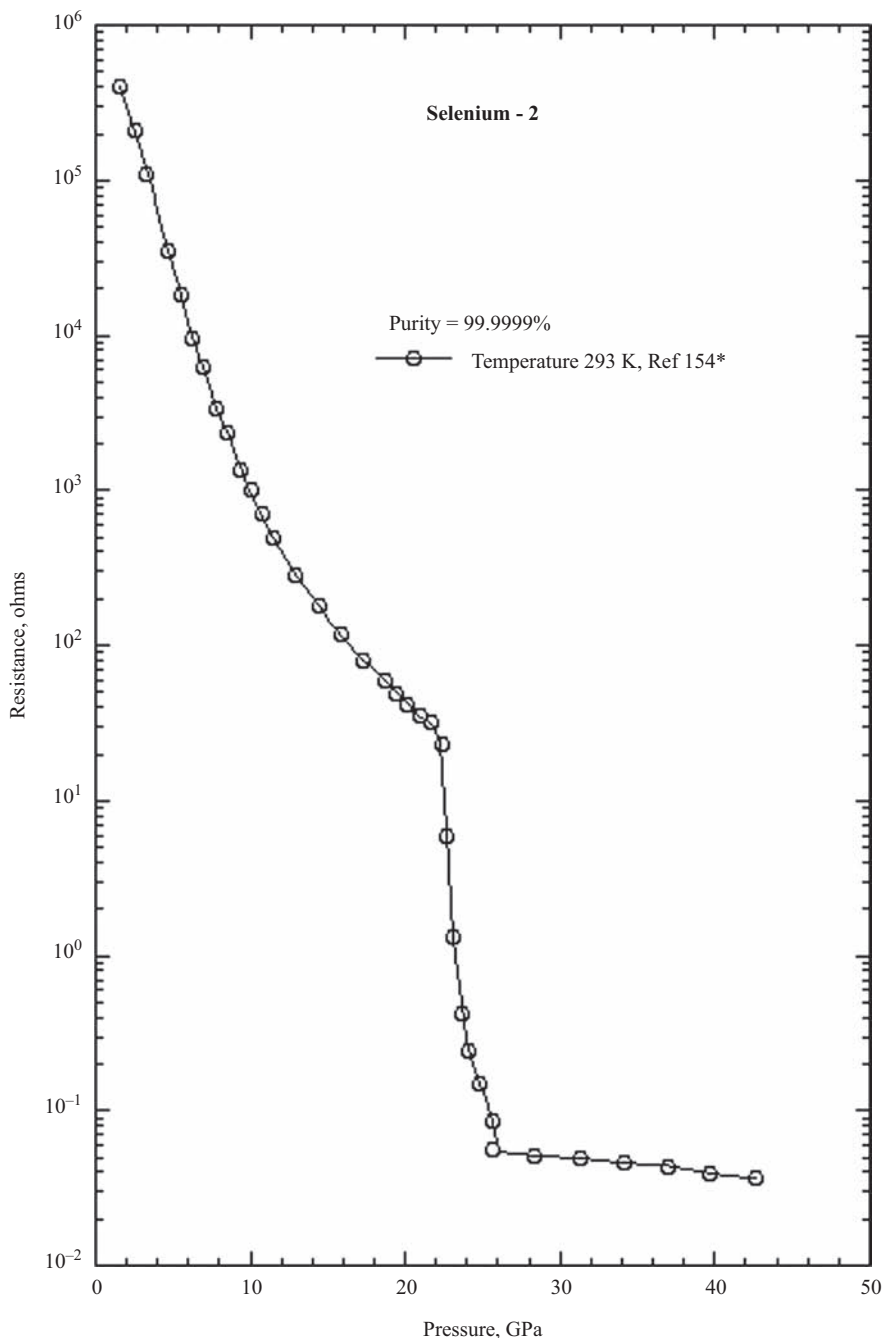


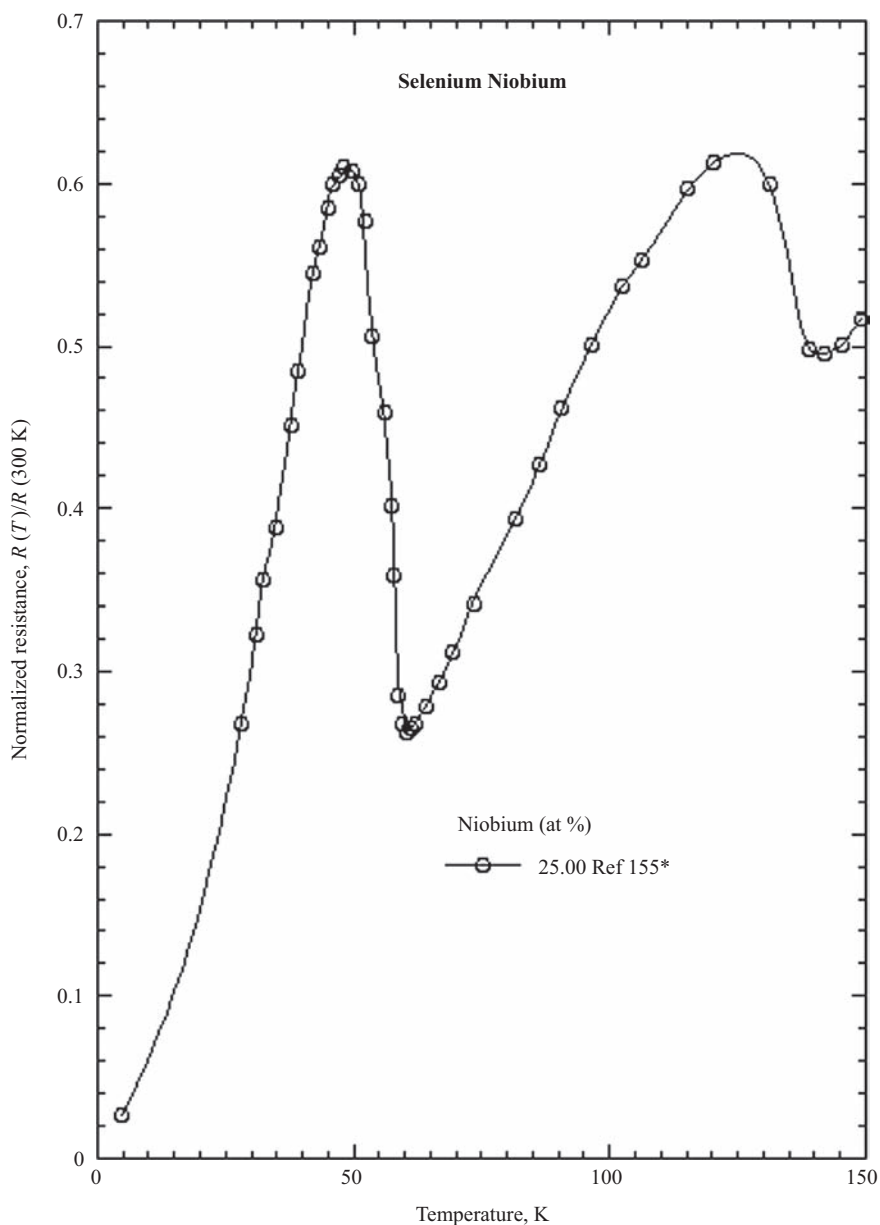


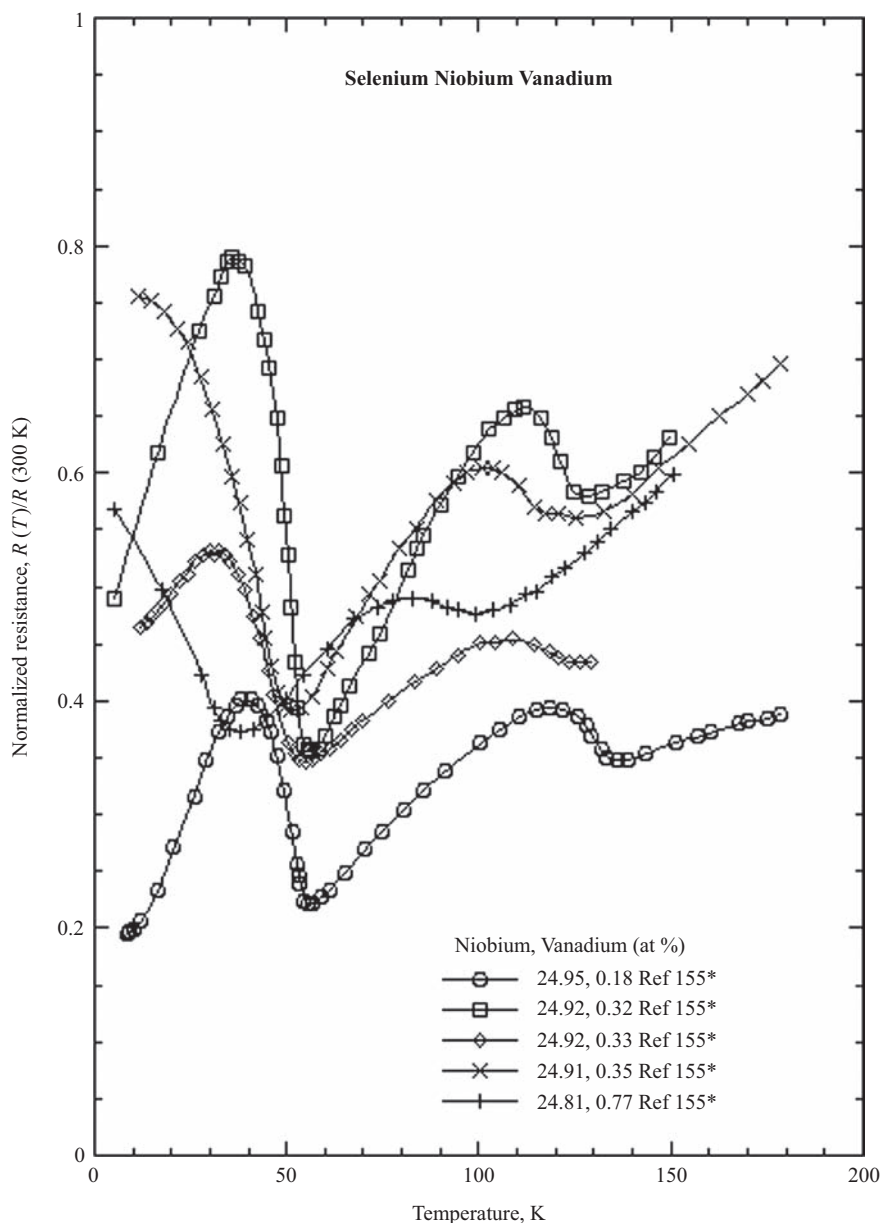


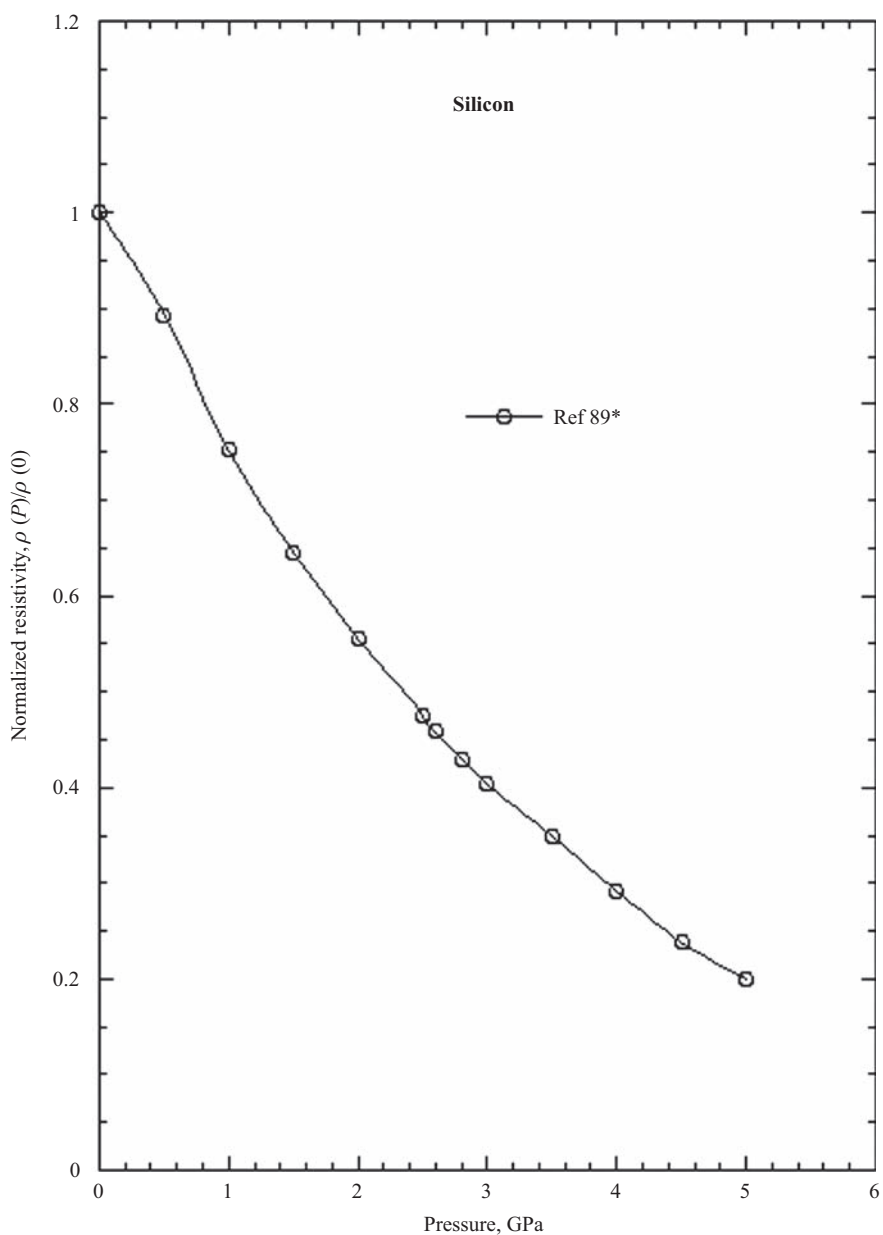


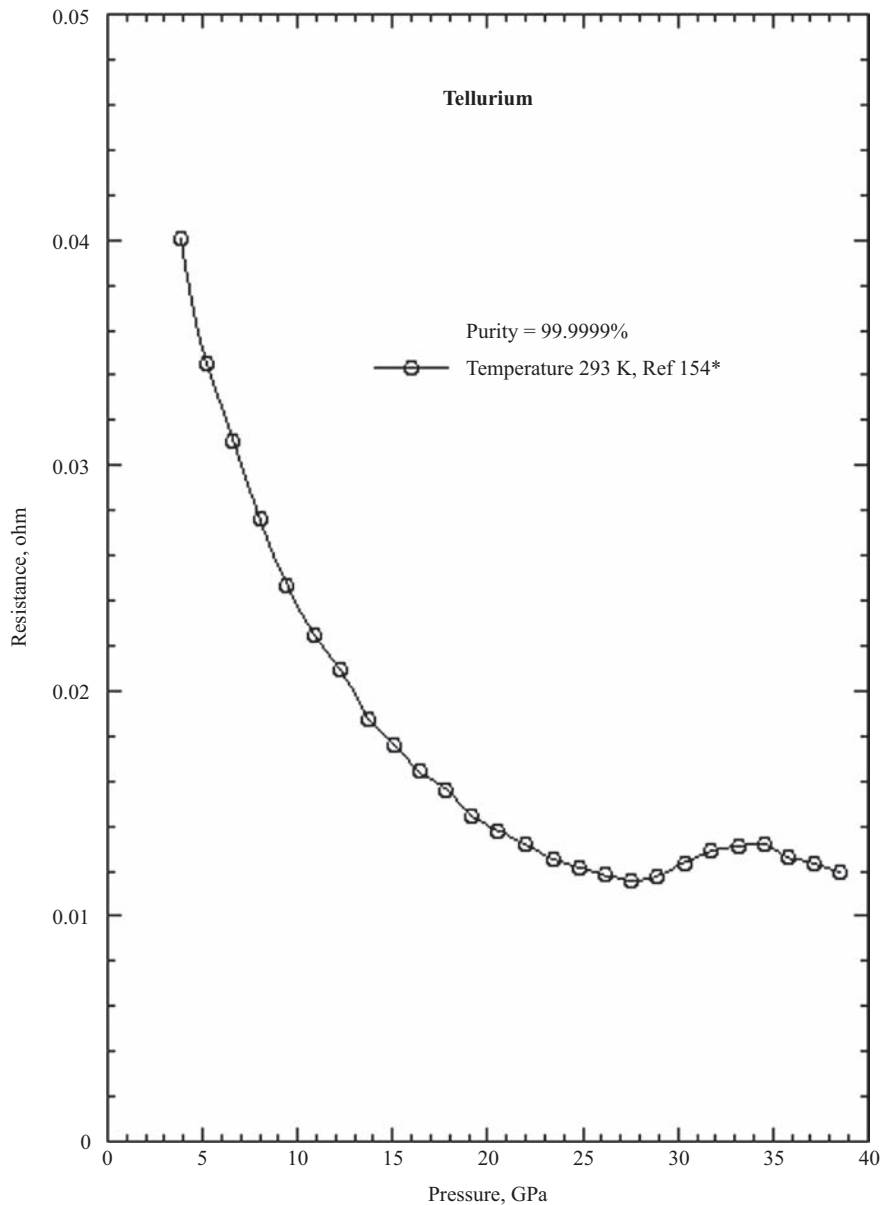


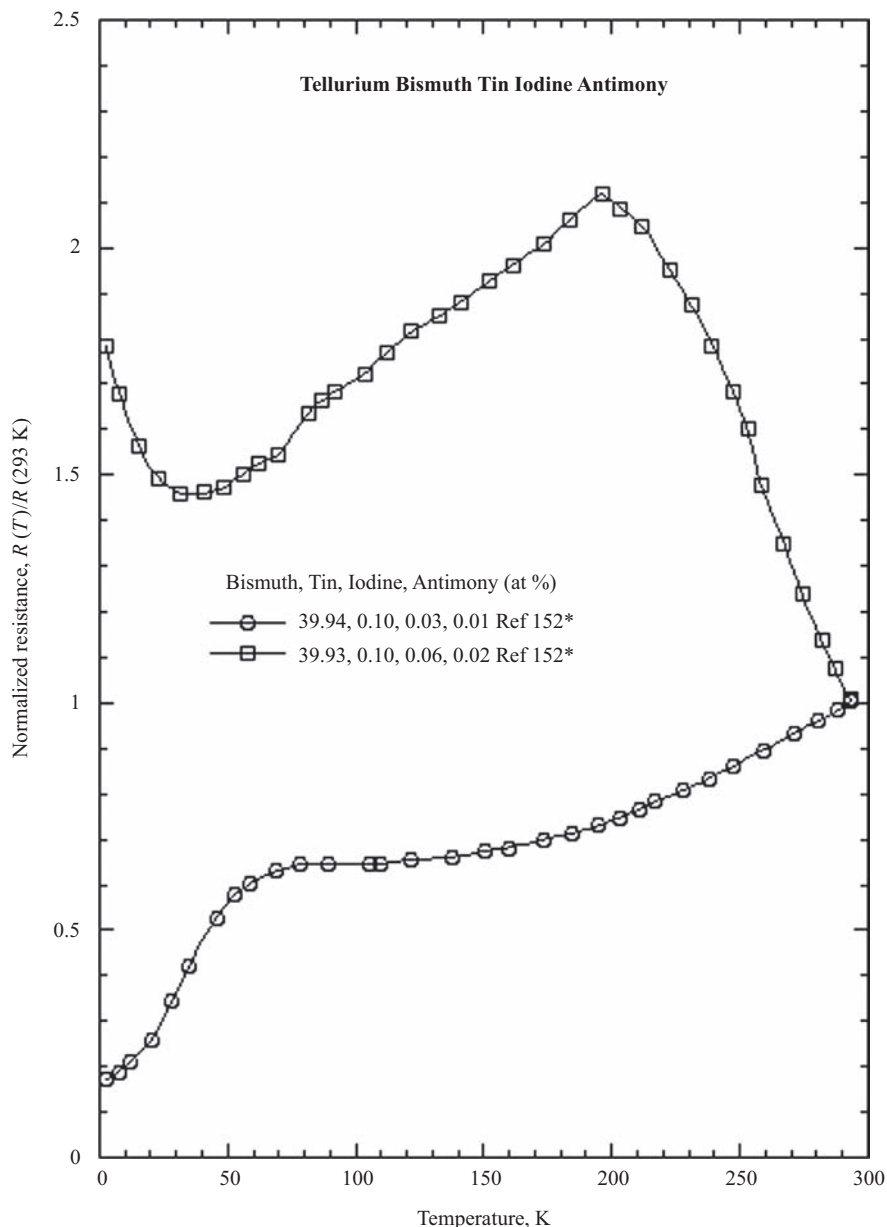


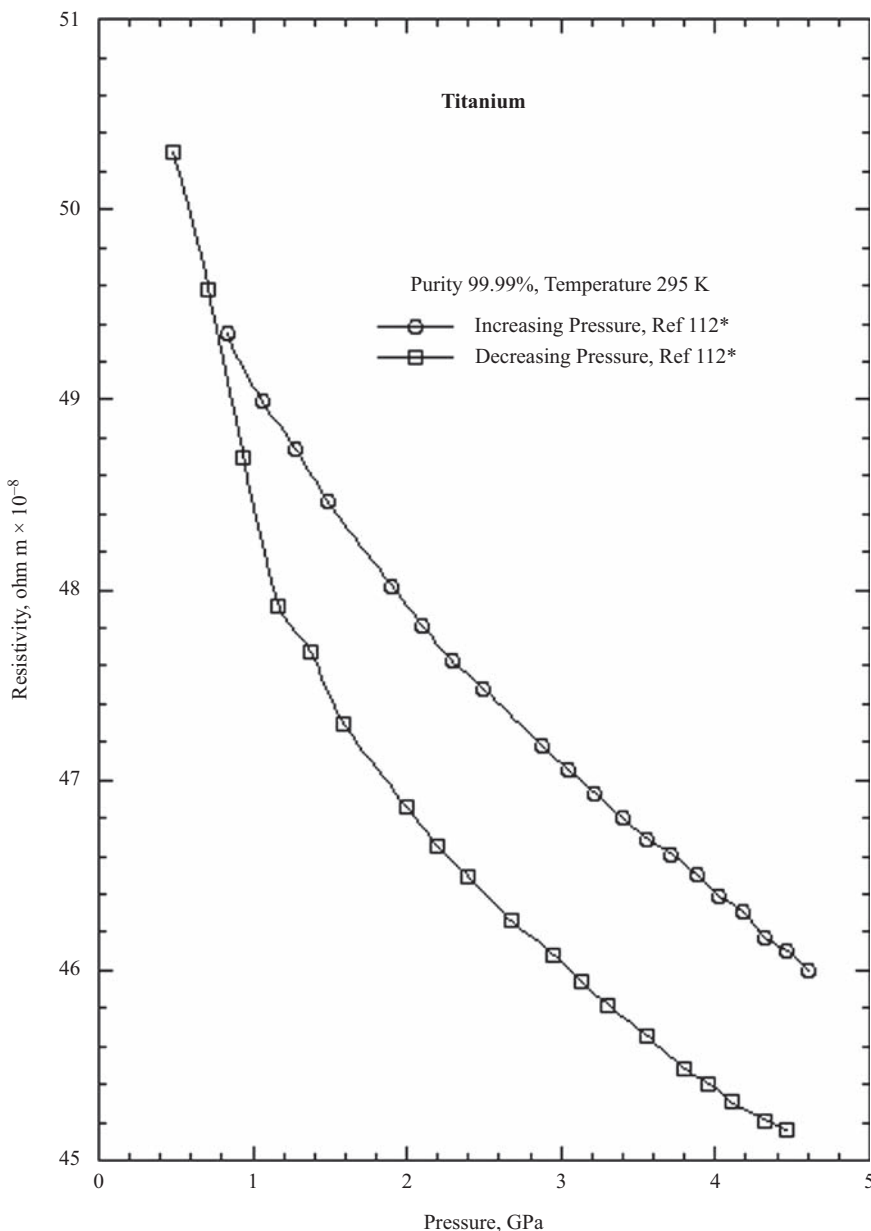


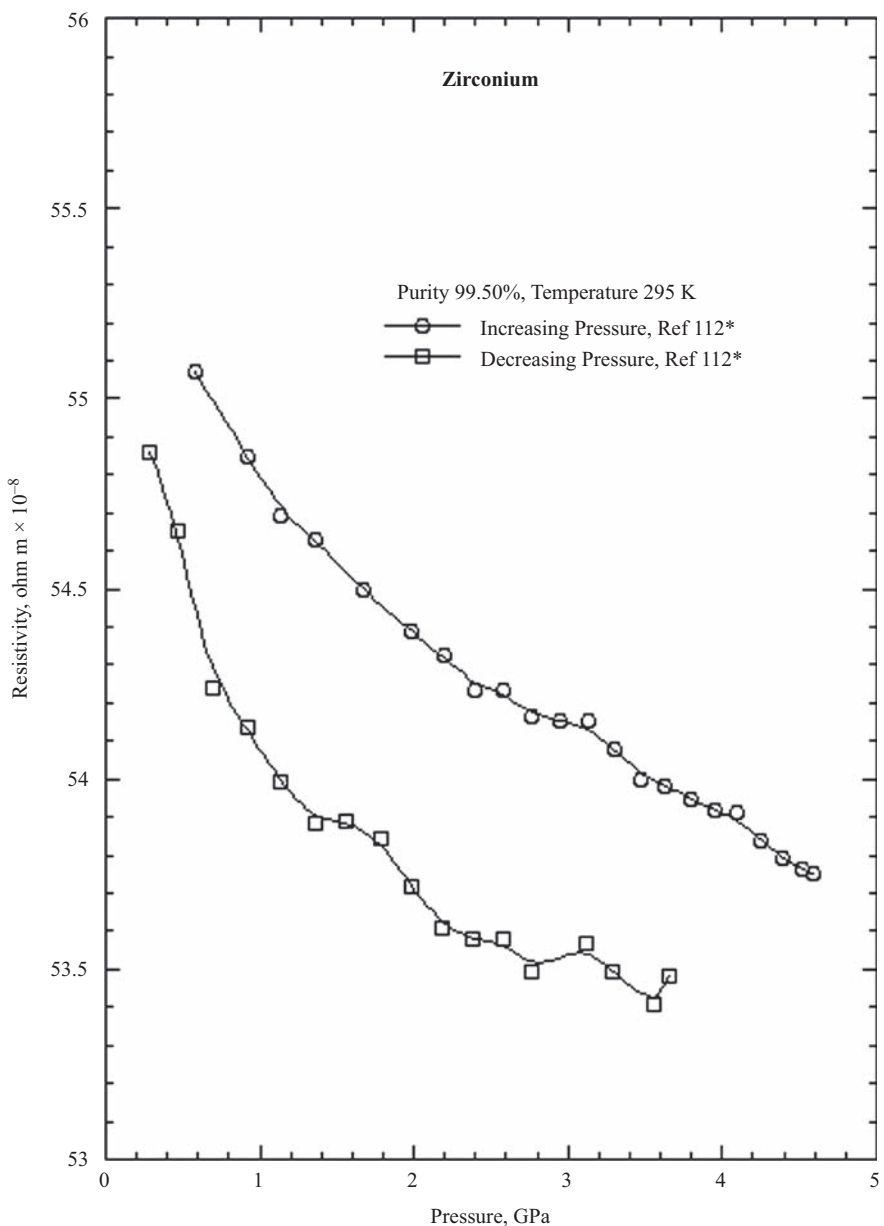












Chapter 7

Resistivity references

- [1] Duijn H.M., van Dijk N.H., de Visser A., Franse J.J.M. ‘The influence of Gd and Ni impurities on the superconducting transition temperature of UPt_3 ’. *Physica B*. 1996, vols 223–4, pp. 44–46
- [2] Okamoto N.L., Koyama T., Kishida K., Tanaka K., Inui H. ‘Crystal structure and thermoelectric properties of chimney-ladder compounds in the Ru_2Si_3 - Mn_4Si_7 pseudobinary system’. *Acta Mater.* 2009, vol. 57, pp. 5036–45
- [3] Kishida K., Ishida A., Koyama T., Harada S., Norihiko I.O., Tanaka K., *et al.* ‘Thermoelectric properties of ternary and Al-containing quaternary $\text{Ru}_{1-x}\text{Re}_x\text{Si}_y$ chimney-ladder compounds’. *Acta Mater.* 2009, vol. 57, pp. 2010–19
- [4] Singh S., Rama N., Sethupathi K., Ramachandra Rao M.S. ‘Correlation between electric transport, optical and magnetic properties of transition metal ion doped ZnO ’. *J. Appl. Phys.* 2009, vol. 103, 07108-D
- [5] Boboridis K. ‘Thermophysical property measurements on niobium and titanium by a microsecond-resolution pulse heating technique using high-speed laser polarimetry and radiation thermometry’. *Int. J. Thermophys.* 2002, vol. 23, pp. 279–91
- [6] Dobrosavljević A.S., Maglić K.D. ‘Heat capacity and electric resistivity of copper research material for calorimetry’. *High Temp. High Press.* 1991, vol. 23, pp. 129–33
- [7] Perović N.Lj., Maglić K.D., Stanimirović A.M. ‘Specific heat capacity and electrical resistivity of nichrome and constantan thermocouple alloys between 300 K and 1500 K’. *5th International Symposium on Temperature and Thermal Measurement in Industry and Science, TEMPMEKO'93*. Amsterdam: Elsevier, 1993, pp. 367–76
- [8] Markovich V., Rozenberg E., Gorodetsky G., Mogilyansky D., Revzin B., Pelleg J. ‘Pressure effect on magnetic and transport properties of Zn doped $\text{La}_{0.91}\text{Mn}_{0.95}\text{O}_3$ manganite’. *J. App. Phys.* 2001, vol. 90, no. 5, pp. 2347–51
- [9] Setton M., Van der Spiegel J. ‘Structural and electrical properties of ZrSi_2 and Zr_2CuSi_4 formed by rapid thermal processing’. *J. App. Phys.* 1991, vol. 70, no. 1, pp. 193–7
- [10] Notatari H., Saiga Y., Kato Y., Iwata K., Katano S., Fujiwara T., *et al.* ‘Effect of pressure on the electrical resistivity of YbAl_2 ’. *J. Phys. Soc. Jpn.* 2007, vol. 76, supp. A, pp. 80–81

- [11] Wu Y.L., Xiong Y.F., Li L.F. ‘Effect of selenium on superconductivity in high-pressure synthesis $\text{Sm}_{1.85}\text{Ce}_{0.15}\text{CuO}_4$ ’. *Physica C*. 2006, vol. 434, pp. 157–60
- [12] Auslender M.I., Rozenberg Kar’kin A.E., Chaudhuri B.K., Gorodetsky G. ‘The nature of the low-temperature minimum of resistivity in ceramic manganites’. *J. Alloy Compd.* 2001, vol. 326, pp. 81–84
- [13] Wang C., Sun Y., Qu Z., Zhang Y. ‘Suppression of superconductivity by the localization of hole carriers in Ti-doped $\text{La}_{1.85}\text{Sr}_{0.15}\text{CuO}_4$ ’. *Phys. Rev. B*. 2006, vol. 73, 144518
- [14] Berthault A., Arles L., Matricon J. ‘High-pressure, high-temperature thermophysical measurements on tantalum and tungsten’. *Int. J. Thermophys.* 1986, vol. 7, pp. 167–79
- [15] Boivineau M., Arlès L., Vermeulen J.M., Thévenin Th. ‘Thermophysical properties of solid and liquid beryllium’. *Int. J. Thermophys.* 1993, vol. 14, pp. 427–39
- [16] Boivineau M., Arlès L., Vermeulen J.M., Thévenin Th. ‘High-pressure thermophysical properties of solid and liquid uranium’. *Physica B*. 1993, vol. 190, pp. 31–39
- [17] Ang R., Sun Y.P., Zhu X.B., Song W.H. ‘Influence of tellurium on the perovskite manganite $\text{La}_{0.5}\text{Ca}_{0.5}\text{MnO}_3$ ’. *Solid State Commun.* 2006, vol. 138, pp. 505–10
- [18] Thévenin Th., Arlès L., Boivineau M., Vermeulen J.M. ‘Thermophysical properties of rhenium’. *Int. J. Thermophys.* 1993, vol. 14, pp. 441–8
- [19] Balog P.S., Secco R.A. ‘High pressure and temperature behaviour of electrical resistivity of hcp metals Ti, Zr and Gd’. *J. Phys. Condens. Matter*. 1999, vol. 11, pp. 1273–87
- [20] Roro K.T., Prinsloo H.L., Alberts H.L. ‘Influence of V and Mn on the electrical transport properties of a Cr + 1.2 at. % Ga alloy’. *J. Alloy Compd.* 2005, vol. 393, pp. 16–25
- [21] Spendeler L., Jaccard D., Sierro J. ‘High pressure transport properties of pure ytterbium in the metallic bcc phase’. *Phys. Lett. A*. 1993, vol. 177, pp. 375–8
- [22] Markovich V., Rozenberg E., Gorodetsky G., Revzin B., Pelleg J., Felner I. ‘Effect of pressure and magnetic field on the resistance of the self-doped manganese perovskite $\text{La}_{0.91}\text{Mn}_{0.95}\text{O}_3$ ’. *Phys. Rev. B*. 2000, vol. 62, pp. 186–90
- [23] Rozenberg E., Auslender M., Felner I., Gorodetsky G. ‘Low-temperature resistivity minimum in ceramic manganites’. *J. App. Phys.* 2000, vol. 88, pp. 2578–82
- [24] Liu X., Xu X., Zhang Y. ‘Effect of Ti dopant on the carrier density collapse in colossal magnetoresistance material $\text{La}_{0.7}\text{Ca}_{0.3}\text{Mn}_{1-y}\text{Ti}_y\text{O}_3$ ’. *Phys. Rev. B*. 2000, vol. 62, pp. 112–19
- [25] Sahu P.Ch., Yousuf M., Govinda Rajan K. ‘Electrical resistivity of thorium up to 10 GPa and 1300 K’. *Physica B*. 1989, vol. 160, pp. 177–82

- [26] Sahu P.Ch., Yousuf M., Govinda Rajan K. ‘Electrical resistivity and phase-transition behaviour of uranium under pressure and temperature’. *Physica B*. 1992, vol. 183, pp. 145–55
- [27] Hixson R.S., Winkler M.A., Hodgdon M.L. ‘Sound speed and thermo-physical properties of liquid iron and nickel’. *Phys. Rev. B*. 1990, vol. 42, pp. 6485–91
- [28] Tripathi R., Awana V.P.S., Panwar N., Bhalla G.L., Habermier H.U., Agarwal S.K., *et al.* ‘Enhanced room temperature coefficient of resistance and magneto-resistance of Ag-added $\text{La}_{0.7}\text{Ca}_{0.3-x}\text{Ba}_x\text{MnO}_3$ composites’. *J. Phys. D: J Appl. Phys.* 2009, vol. 42, 175002
- [29] Das S., Dey T.K. ‘Electrical conductivity and low field magnetoresistance in polycrystalline $\text{La}_{1-x}\text{K}_x\text{MnO}_3$ pellets prepared by pyrophoric method’. *Solid State Communs.* 2005, vol. 134, pp. 837–42
- [30] Maglić K.D., Perović N.Lj., Vuković G.S., Zeković Lj.P. ‘Specific heat and electrical resistivity of niobium measured by subsecond calorimetric technique’. *Int. J. Thermophys.* 1994, vol. 15, pp. 963–72
- [31] Maglić K.D., Pavičić D.Z. ‘Thermal and electrical properties of titanium between 300 and 1900 K’. *Int. J. Thermophys.* 2001, vol. 22, pp. 1833–41
- [32] Pavičić D.Z., Maglić K.D. ‘Specific heat and electrical resistivity of 53% niobium-47% titanium alloy measured by subsecond calorimetric technique’. *Int. J. Thermophys.* 2002, vol. 23, pp. 1319–25
- [33] Shibusaki S., Takahashi Y., Terasaki I. ‘Thermoelectric properties of $\text{LaRh}_{1-x}\text{Ni}_x\text{O}_3$ '. *J. Phys. Condens. Matter.* 2009, vol. 21, pp. 1–4
- [34] Kalyana Lakshmi Y., Venkataiah M., Vithal M., Venugopal Reddy P. ‘Magnetic and electrical behavior of $\text{La}_{1-x}\text{A}_x\text{MnO}_3$ ($\text{A} = \text{Li}, \text{Na}, \text{K}$ and Rb) manganites’. *Physica B*. 2008, vol. 403, pp. 3059–66
- [35] Marcano G. ‘Effect of Mn-doping on the electrical properties of Cu_2GeSe_3 '. *J. Phys. Chem. Solids.* 2005, vol. 66, pp. 2086–9
- [36] Bhatia S.N., Mohapatra N., Kundaliya D., Malik S.K. ‘Transport, magnetic and thermal properties of Pr doped $\text{LaSr}_2\text{Mn}_2\text{O}_7$: a Kondo-type behaviour of resistivity’. *J. Phys. Condens. Matter.* 2006, vol. 18, pp. 7179–92
- [37] Khan N.A., Baber N., Iqbal M.Z., Ul Haq, A. ‘Simple method for direct synthesis $\text{YBa}_2\text{Cu}_4\text{O}_8$ at atmospheric oxygen pressure’. *Appl. Phys. Lett.* 1993, vol. 63, pp. 257–9
- [38] Righini F., Spišiak J., Brussolino G.C., Gualano M. ‘Thermophysical properties by a pulse heating reflectometric technique: niobium 1100 to 2700 K’. *Int. J. Thermophys.* 1999, vol. 20, pp. 1107–16
- [39] Takabatake T., Iga F., Yoshino T., Echizen Y., Katoh K., Kobayashi K., *et al.* ‘Ce and Yb-based Kondo semiconductors’. *J. Magn. Magn. Mater.* 1998, vols 171–81, pp. 277–82
- [40] Ateş A., Yıldırım M., Gürbulak B. ‘Investigation of the electrical properties of Ho-doped InSe single crystal’. *Physica E*. 2004, vol. 21, pp. 85–90
- [41] Vorenkamp T., Koziol Z., de Visser A., Bakker K., Franse J.J.M. ‘Impurity effects in superconducting UPt_3 '. *J. Appl. Phys.* 1991, vol. 69, pp. 5487–9

- [42] Ho C.H., Huang C.E., Wu C.C. ‘Preparation and characterization of Ni-incorporated FeS₂ single crystals’. *J. Cryst. Growth.* 2004, vol. 270, pp. 535–41
- [43] Soni A., Okram G.S. ‘Resistivity and thermopower measurement setups in the temperature range of 5–325 K’. *Rev. Sci. Inst.* 2008, vol. 79, 125103–125103-4
- [44] Wu X.S., Lin J., Liu W.J., Chen W.M., Jin X., Jiang S.S., *et al.* ‘Structure studies of La_{1.85}Sr_{0.15}CuO₄ doped with Mg at high doping level’. *J. Supercond.* 1997, vol. 10, pp. 159–64
- [45] Mori T., Tanaka T. ‘Effect of transition metal doping and carbon doping on thermoelectric properties of YB₆₆ single crystals’. *J. Solid State Chem.* 2006, vol. 179, pp. 2889–94
- [46] Mori T. ‘High temperature thermoelectric properties of B₁₂ icosahedral cluster-containing rare earth boride crystals’. *J. App. Phys.* 2005, vol. 97, pp. 3702–4
- [47] Maglić K.D., Perović N., Vuković G. ‘Specific heat and electric resistivity of molybdenum between 400 and 2500 K’. *High Temp. High Press.* 1997, vol. 29, pp. 97–102
- [48] Okamoto Y., Aruga A., Kasai H., Morimoto J., Miyakawa T., Fujimoto S. ‘Temperature dependence of thermoelectric properties of SiC/B₄C’. *AIP Conference Proceedings 316, Thirteenth International Conference on Thermoelectrics*. Maryland, USA: American Institute of Physics, 1994, pp. 92–95
- [49] Shibusaki S., Kobayashi W., Terasaki I. ‘Mg substitution effects of new thermoelectric Rb oxides’. *2007 International Conference on Thermoelectrics*. Piscataway, USA: Institute of Electrical and Electronics Engineers, 2007, pp. 133–5
- [50] Cabeza O., Barca O., Francesconi G., Bari M.A., Severack C., Muirhead C.M., *et al.* ‘Magnetic and electrical properties of Cr-doped La_{0.7}Ca_{0.3}MnO₃’. *J. Magn. Magn. Mater.* 1999, vols 196–7, pp. 504–5
- [51] Sera M., Sato H., Hiroi M., Kobayashi N. ‘Cu site substitution effect on the Hall coefficient of La_{2-x}Sr_xCuO₄’. *Solid State Commun.* 1994, vol. 90, pp. 803–6
- [52] Radhapiyari L., Phanjoubam S., Sarma H.N.K., Prakash C. ‘Influence of Co²⁺ on the electrical and magnetic properties of Li-Sb ferrites’. *Mater. Letts.* 2000, vol. 44, pp. 65–69
- [53] He T., Huang Q., Ramirez A.P., Wang Y., Regan K.A., Rogado N., *et al.* ‘Superconductivity in the non-oxide Perovskite MgCNi₃’. *Nature* 2001, vol. 411, pp. 54–56
- [54] Koike Y., Okubo T., Fujiwara A., Noji T., Saito Y. ‘Trial of intercalation of Br and Li into Bi₂Sr₂Ca_{n-1}Cu_nO_{2n+4} (n = 1, 2, 3)’. *Solid State Commun.* 1991, vol. 79, pp. 501–5
- [55] White C.K., Minges M.L. ‘Thermophysical properties of some key solids: An update’. *Int. J. Thermophys.* 1997, vol. 18, pp. 1269–327
- [56] Loseva G.V., Ovchinnikov S.G., Balaev A.D., Ivanova N.B., Kiselev N.I. ‘Transition from the Kondo regime to long-range magnetic order in the Fe_xV_{1-x}S system’. *Phys. Solid State*. 2000, vol. 42, pp. 1322–4

- [57] Hasanain S.K., Nadeem M., Shah W.H., Akhtar M.J., Hasan M.M. ‘Effects of iron doping on the transport and magnetic behaviour in $\text{La}_{0.65}\text{Ca}_{0.35}\text{Mn}_{1-y}\text{Fe}_y\text{O}_3$ ’. *J. Phys. Condens. Matter.* 2000, vol. 12, pp. 9007–17
- [58] Young S., Xiaojun X., Yuheng Z. ‘Effects of Fe doping in $\text{La}_{0.67}\text{Sr}_{0.33}\text{CoO}_3$ ’. *Phys. Rev. B.* 2000, vol. 62, pp. 5289–92
- [59] Mhiaoui S., Gasser J.G., Ben Abdellah A. ‘On the thermopower of liquid antimony’. *13th International Conference on Liquid and Amorphous Metals. J. Phy. Conf. Ser.* 2008, vol. 98, pp. 1–9
- [60] Alvarez I., Veiga M.L., Pico C. ‘Structural characterization and electrical behaviour of $\text{LaNi}_{1-x}\text{Sb}_x\text{O}_3$ ($0 \leq x \geq 1/3$) perovskites’. *Solid State Ionics.* 1996, vol. 91, pp. 265–71
- [61] Pan Z.J., Zhang L.T., Wu J.S. ‘Effects of Al doping on the transport performances of CrSi_2 single crystals’. *Scripta Mater.* 2007, vol. 56, pp. 245–8
- [62] Xu G.J., Grivel J.C., Abrahamsen A.B., Chen X.P., Andersen N.H. ‘Structure and superconductivity of double-doped $\text{Mg}_{1-x}(\text{Al}_{0.5}\text{Li}_{0.5})_x\text{B}_2$ ’. *Physica C.* 2003, vol. 399, pp. 8–14
- [63] Xu G.J., Grivel J.C., Abrahamsen A.B., Chen X.P., Andersen N.H. ‘Superconducting properties of Zn and Al double-doped $\text{Mg}_{1-x}(\text{Zn}_{0.5}\text{Al}_{0.5})_x\text{B}_2$ ’. *Physica C.* 2004, vol. 403, pp. 113–18
- [64] Jacobsson P., Sundqvist B. ‘Thermal conductivity and electrical resistivity of gadolinium as functions of pressure and temperature’. *Phys. Rev. B.* 1989, vol. 40, pp. 9541–51
- [65] Larica C., Nunes E., Freitas J.C.C. ‘Low field magnetic studies of some $\text{Gd}_{1-x}\text{La}_x$ alloys’. *J. Phys. Condens. Matter.* 1999, vol. 11, pp. 821–31
- [66] Dudăš J., Feher A., Janoš Š. ‘The temperature hysteresis of the electrical resistance of dysprosium near the order-disorder transition’. *J. Less Common Met.* 1987, vol. 134, pp. L9–11
- [67] Isoda Y., Nagai T., Fujii H., Imai Y., Shinohara Y. ‘Thermoelectric properties of Sb-doped $\text{Mg}_2\text{Si}_{0.5}\text{Sn}_{0.5}$ ’. *25th International Conference on Thermoelectrics.* Piscataway, USA: Institute of Electrical and Electronics Engineers, 2006, pp. 406–10
- [68] Isoda Y., Nagai T., Fujii H., Imai Y., Shinohara Y. ‘The effect of bismuth doping on thermoelectric properties of $\text{Mg}_2\text{Si}_{0.5}\text{Sn}_{0.5}$ ’. *26th International Conference on Thermoelectrics.* Piscataway, USA: Institute of Electrical and Electronics Engineers, 2007, pp. 251–5
- [69] Wang J., Lin Y., Zou H., Pu S., Shi J. ‘Structural transition, electrical and magnetic properties of the B-site Co doped $\text{Sr}_{14}\text{Cu}_{24}\text{O}_{41}$ ’. *J. Phys. Condens. Matter.* 2009, vol. 21, pp. 1–10
- [70] Cao D., Bridges F., Anderson M., Ramirez A.P., Olapinski M., Subramanian M.A., et al. ‘Local distortions in $\text{La}_{0.7}\text{Ca}_{0.3}\text{Mn}_{1-b}\text{A}_b\text{O}_3$ ($\text{A} = \text{Ti}$ and Ga) colossal magnetoresistance samples: Correlations with magnetization and evidence for cluster formation’. *Phys. Rev. B.* 2001, vol. 64, pp. 1–14

- [71] Joshi A.G., Kuberkar D.G., Baldha G.J., Kulkarni R.G. ‘Effect of Mo-Ca substitution on the superconductivity of $\text{GdBa}_2\text{Cu}_3\text{O}_{7-\delta}$ ’. *Physica C*. 1997, vol. 291, pp. 25–33
- [72] Yamaura Y., Takayama-Muromachi E. ‘Enhanced paramagnetism of the 4d itinerant electrons in the rhodium oxide perovskite SrRhO_3 ’. *Phys. Rev. B*. 2001, vol. 64, pp. 1–5
- [73] Yamaura K., Huang Q., Molodovan M., Young D.P., Sato A., Baba Y., et al. ‘High-pressure synthesis, crystal structure determination, and a Ca substitution study of the metallic rhodium oxide NaRh_2O_4 ’. *Chem. Mater.* 2005, vol. 17, pp. 359–65
- [74] Yamaura K., Huang Q., Young D.P., Noguchi Y., Takayama-Muromachi E. ‘Crystal structure and electronic and magnetic properties of the bilayered rhodium oxide $\text{Sr}_3\text{Rh}_2\text{O}_7$ ’. *Phys. Rev. B*. 2002, vol. 66, 134431
- [75] Yamaura K., Huang Q., Young D.P., Takayama-Muromachi E. ‘Crystal structure and magnetic properties of the trilayered perovskite $\text{Sr}_4\text{Rh}_3\text{O}_{10}$: A new member of the strontium rhodate family’. *Chem. Mater.* 2004, vol. 16, pp. 3424–30
- [76] Bathe R., Shinde S.R., Gapecup K.M., Adhi K.P., Patil S.I. ‘Effect of aluminium doping on the magneto-transport properties of $\text{La}_{0.75}\text{Ca}_{0.25}\text{MnO}_3$ ’. *J. Magn. Magn. Mater.* 2003, vol. 256, pp. 425–9
- [77] Assunção M.C. ‘Effect of halogen impurities on the transport properties of selenium glasses’. *J. Non-Cryst. Solids*. 1991, vol. 136, pp. 81–90
- [78] Groń T., Duda A., Krajewski A., Kusz J., Warczewski J., Nikiforov K.G. ‘The electrical conductivity of the strongly defective HgCr_2Se_4 single crystals’. *Radiat. Eff. Defects S.* 2002, vol. 157, pp. 1111–16
- [79] Korn D., Mürer W., Zibold G. ‘Electrical resistivity of amorphous Sn-Cu alloys’. *Phys. Lett.* 1974, vol. 47A, pp. 117–18
- [80] Kleinschmidt P. ‘Electrical conductivity measurements on doped VO_2 single crystals’. *Phys. Lett.* 1974, vol. 47A, pp. 205–6
- [81] Littleton R.T., Jeffries J., Kaeser M.A., Long M., Tritt T.M. ‘High temperature transport probe for thermopower and resistivity measurements’. *1998 Fall Materials Research Society, Symposium Z: Thermoelectric Materials*. Materials Science and Engineering Department, Clemson University, Clemson, SC 29634 USA, 1998
- [82] Yonenaga I., Goto T., Tang X.F., Yamaguchi S. ‘Thermal and electrical properties of Czochralski grown germanium-silicon alloys’. *18th International Conference on Thermoelectrics*. Piscataway, USA: Institute of Electrical and Electronics Engineers, 1999, pp. 436–9
- [83] Kanazawa M., Tsuda N. ‘Logarithmic temperature dependence of resistivity for $\text{Ca}_{0.7}\text{Na}_{0.3}\text{Pd}_3\text{O}_4$ doped with Cu’. *J. Phys. Soc. Jpn.* 2000, vol. 69, pp. 4112–13
- [84] Brahma P., Banerjee S., Chakraborty S., Chakravorty D. ‘Small polaron and bipolaron transport in antimony oxide doped barium hexaferrites’. *J. App. Phys.* 2000, vol. 88, pp. 6526–8

- [85] Peña O., Le Berre F., Padiou J., Marchand T. ‘Single crystal studies of the Chevrel-phase superconductor $\text{La}_x\text{Mo}_6\text{Se}_8$ ’. *J. Solid State Chem.* 1998, vol. 136, pp. 160–6
- [86] Chiodelli G., Massarotti V., Capsomi D., Bini M., Azzoni, C.B., Mozzati M.C., *et al.* ‘Electric and dielectric properties of pure and doped $\text{CaCu}_3\text{Ti}_4\text{O}_{12}$ perovskite materials’. *Solid State Commun.* 2004, vol. 132, pp. 241–6
- [87] Viviani M., Buscaglia V., Buscaglia L., Mitoseriu L., Testino A., Nanni P., *et al.* ‘Analysis of conductivity and PTCR effect in Er-doped BaTiO_3 ceramics’. *J. Eur. Ceram. Soc.* 2004, vol. 34, pp. 1221–5
- [88] Okada S., Shimizu K., Kobayashi T.C., Amaya K., Endo S. ‘Superconductivity of calcium under high pressures’. *J. Phys. Soc. Jpn.* 1996, vol. 65, pp. 1924–6
- [89] Andersson G., Sundqvist B., Bäckström G. ‘A high-pressure cell for electrical resistance measurements at hydrostatic pressures up to 8 GPa: Results for Bi, Ba, Ni and Si’. *J. Appl. Phys.* 1989, vol. 65, pp. 3943–50
- [90] Tateiwa N., Nakagawa A., Fujio K., Kawae T., Takeda K. ‘Pressure-induced valence change in the rare earth metals: The case of praseodymium’. *J. Alloy Compd.* 2006, vols 408–12, pp. 244–7
- [91] Shrivastava V., Jha A.K., Mendiratta R.G. ‘Structural and electrical studies in La-substituted $\text{SrBi}_2\text{Nb}_2\text{O}_9$ ferroelectric ceramics’. *Physica B*. 2006, vol. 371, pp. 337–42
- [92] Weir S.T., Mitchell A.C., Nellis W.J. ‘Metallization of fluid molecular hydrogen at 140 GPa’. *Phys. Rev. Lett.* 1996, vol. 76, pp. 1860–3
- [93] Debessai M., Matsuoka T., Hamlin J.J., Schilling J.S. ‘Pressure-induced superconducting state of europium metal at low temperatures’. *Phys. Rev. Lett.* 2009, vol. 102, 197002
- [94] Ellerby M., McEwen K.A., Bauer E., Hauser R., Jensen J. ‘Pressure-dependent resistivity and magnetoresistivity of erbium’. *Phys. Rev. B*. 2000, vol. 61, pp. 6790–7
- [95] Pottlacher G., Kaschnitz E., Jäger H. ‘Investigations of thermophysical properties of liquid metals with a rapid resistive heating technique’. *J. Non-Cryst Solids*. 1993, vols 156–8, pp. 374–8
- [96] Ault K.M., Secco R.A. ‘High pressure conductivity study of the α -quartz → rutile transformation in GeO_2 ’. *Solid State Commun.* 1996, vol. 98, pp. 449–52
- [97] Makovec D., Ule N., Drofenik M. ‘Positive temperature coefficient of resistivity effect in highly donor-doped barium titanate’. *J. Am. Ceram. Soc.* 2001, vol. 84, pp. 1273–80
- [98] Langhammer H.T., Makovec D., Pu Y., Abicht H.P., Drofenik M. ‘Grain boundary reoxidation of donor-doped barium titanate ceramics’. *J. Eur. Ceram. Soc.* 2006, vol. 26, pp. 2899–2907
- [99] Sasmal K., Lv B., Lorenz B., Guloy A., Chen F., Xue Y.Y., *et al.* ‘Superconducting Fe-based compounds $(\text{A}_{1-x}\text{Sr}_x)\text{Fe}_2\text{As}_2$ with A = K and Cs with transition temperatures up to 37K’. *Phys. Rev. Lett.* 2008, vol. 101, 107007

- [100] Secco E.A., Secco R.A. ‘Cation conductivity in mixed thallium halides’. *Solid State Ionics*. 1999, vol. 118, pp. 37–42
- [101] Nomura T., Kim S.W., Kamihara Y., Hirano M., Sushko P.V., Kato K., *et al.* ‘Crystallographic phase transition and high-T_c superconductivity in LaFeAsO:F’. *Supercond. Sci. Technol.* 2008, vol. 21, 125028
- [102] Yabuuchi T., Matsuoka T., Nakamoto Y., Shimizu K. ‘Superconductivity of Ca exceeding 25 K at megabar pressure’. *J. Phys. Soc. Jpn.* 2006, vol. 75, 083703
- [103] Sundqvist B. ‘Electrical resistance of nickel in the range 300–725 K and 0–2 GPa’. *Phys. Rev. B*. 1988, vol. 38, pp. 283–9
- [104] Okada H., Takahashi H., Takahashi H., Matuishi S., Hirano M., Hosono H. ‘Pressure effect on iron-based superconductors Ca(Fe_{1-x}Co_x)AsF’. *J. Phys. Conf. Ser.* 2010, vol. 200, 012151
- [105] Wang S.F., Dai S.Y., Zhou Y.L., Zhu Y.B., Chen Z.H., Lü H.B., *et al.* ‘Effect of Cd doping on structure and superconductivity in Mg_{0.5}Cd_{0.5}B₂’. *J. Supercond.* 2002, vol. 17, pp. 397–400
- [106] Shimizu K., Kimura T., Furomoto S., Takeda K., Kontani K., Onuki Y., *et al.* ‘Superconductivity in the non-magnetic state of iron under pressure’. *Nature*. 2001, vol. 412, pp. 316–18
- [107] Chong T.V., Ishii O., Kambe S. ‘The study on Zn and Ni substituted GdBaSr Cu₃O_{7-δ} superconductor’. *Physica C*. 2008, vol. 468, pp. 1214–16
- [108] Chong T.V., Kambe S., Ishii O. ‘Effect of Ca doping on the superconducting properties of GdBaSrCu₃O_{7-δ} bulk samples’. *Physica C*. 2009, vol. 469, pp. 985–7
- [109] Gunasekaran R.A., Ganguly J.V., Yakhmi, J.V. ‘Superconducting behaviour of co-doped Y_{1-x}Ca_xBa₂Cu_{3-x}M_xO_{7-δ} (M = Ni or Zn and 0.0 ≤ x ≤ 0.30)’. *Physica C*. 1995, vol. 243, pp. 160–6
- [110] Mori T., Zhang F. ‘Low-temperature magnetism of the compound GdB₁₈Si₅’. *J. Phys. Condens. Matter*. 2002, vol. 14, pp. 11831–6
- [111] Awana V.P.S., Vajpayee A., Mugdol M., Ganesan V., Awasthi A.M., Bhalla G.L., *et al.* ‘Physical property characterization of bulk MgB₂ superconductor’. *Eur. Phys. J. B*. 2008, vol. 62, pp. 281–94
- [112] Balog P.S., Secco R.A. ‘High pressure and temperature behaviour of electrical resistivity of HCP metals Ti, Zr and Gd’. *J. Phys. Condens. Matter*. 1999, vol. 11, pp. 1273–87
- [113] Mugdol M., Sharath Chandra L.S., Ganesan V., Bhalla G.L., Kishan H., Awana V.P.S. ‘Enhanced critical parameters of nanocarbon doped MgB₂ superconductor’. *J. App. Phys.* 2009, vol. 106, 033904
- [114] Ho C.H., Hsich M.H., Huang Y.S. ‘Compensation and carrier conduction in synthetic Fe_{1-x}Ni_xS₂ (0 ≤ x ≤ 0.1) single crystals’. *J. Electrochem. Soc.* 2008, vol. 155, pp. H254–8
- [115] Yen P.C., Huang Y.S., Tiong K.K. ‘The growth and characterization of rhenium-doped WS₂ single crystals’. *J. Phys. Condens. Matter*. 2004, vol. 16, pp. 2171–80

- [116] Yan C., Huang Y., Wang Z., Zhang L., Gao S., Liao C., *et al.* ‘Structural, magnetic and transport properties of Sc-doped $\text{La}_{0.7}\text{Sr}_{0.3}\text{MnO}_3$ ’. *Chinese Sci. Bull.* 2000, vol. 45, pp. 810–14
- [117] Sefat A.S., McGuire M.A., Sales B.C., Jin R., Howe J.Y., Mandrus D. ‘Electronic correlations in the superconductor $\text{LaFeAsO}_{0.89}\text{F}_{0.11}$ with low carrier-density’. *Phys. Rev. B*. 2008, vol. 77, 174503
- [118] Zhou J.S., Goodenough J.B., Dabrowski B. ‘Anomalous transport properties in a $\text{YBa}_2\text{Cu}_4\text{O}_8$ crystal’. *Phys. Rev. B*. 1998, vol. 58, pp. R2956–9
- [119] Xia Y., Ponnambalam V., Bhattacharya S., Pope A.I., Poon S.J., Tritt, T.M. ‘Electrical transport properties of TiCoSb half-Heusler phases that exhibit high resistivity’. *J. Phys. Condens. Matter*. 2001, vol. 13, pp. 1–13
- [120] Ren Z.A., Che G.C., Dong X.L., Yang J., Lu W., Yi W., *et al.* ‘Superconductivity and phase diagram in iron-based arsenic-oxides $\text{ReFeAsO}_{1-\delta}$ ($\text{Re} = \text{rare earth metal}$) without fluorine doping’. *Eur. Phys. Lett.* 2008, vol. 83, 17002
- [121] Pekala K., Pekala M. ‘Low temperature transport properties of nanocrystalline Cu, Fe and Ni’. *Nanostruc. Mater.* 1995, vol. 6, pp. 819–22
- [122] White G.K., Woods S.B. ‘Electrical and thermal resistivity of the transition elements at low temperatures’. *Phil. Trans. R Soc. Lond. A*. 1959, vol. 12, pp. 273–302
- [123] Laubitz M.J., Matsumura T., Kelly P.J. ‘Transport properties of the ferromagnetic metals. II. Nickel’. *Can. J. Phys.* 1976, vol. 54, pp. 92–102
- [124] White G.K. *Experimental Techniques in Low Temperature Physics* (Oxford, Oxford University Press, 1959)
- [125] Okram G.S., Soni A., Rawat R. ‘Anomalous electrical transport behaviour in nanocrystalline nickel’. *Nanotechnology*. 2008, vol. 19, 185711
- [126] Khan N.A., Mumtaz M. ‘Absence of pair-breaking mechanism in $\text{Cu}_{0.5}\text{Tl}_{0.5}\text{Ba}_2\text{Ca}_3\text{Cu}_{4-y}\text{Zn}_y\text{O}_{12-\delta}$ ’. *Phys. Rev. B*. 2008, vol. 77, 054507
- [127] Mori N., Okano H., Furuya A. ‘A comparative study of thermoelectric properties in $(\text{Pr}, \text{Y})\text{Ba}_2\text{Cu}_3\text{O}_7$ and $\text{PrBa}_2\text{Cu}_3\text{O}_7\text{-Ag}$ percolative systems’. *Phys. Stat. Sol. (a)*. 2006, vol. 203, pp. 2828–31
- [128] Mori N., Kameyama T., Enomoto H., Ozaki H., Takano Y., Sekizawa K. ‘Thermoelectric power and resistivity in $\text{Nd}_{2-x}\text{Ce}_x\text{CuO}_4$ system’. *J. Alloy Compd.* 2006, vols 408–12, pp. 1222–5
- [129] Terzieft P., Luck R., Auchet J. ‘Electronic properties of dilute Cr in liquid silver’. *J. Alloy Compd.* 1998, vol. 274, pp. 148–52
- [130] Wenzhong L., Buyin L., Ming F., Zhengwei H. ‘Novel thermistor of Bi-doped $\text{Ba}(\text{Sn}, \text{Sb})\text{O}_3$ with linear negative temperature coefficient’. *Sensor. Actuat.* 2000, vol. 80, pp. 38–41
- [131] McCrone J.E., Tallon J.L., Cooper J.R., MacLaughlin A.C., Attfield J.P., Bernhard C. ‘Magneto-transport properties of doped $\text{RuSr}_2\text{GdCu}_2\text{O}_8$ ’. *Phys. Rev. B*. 2003, vol. 68, 064514
- [132] Chen G.F., Li Z., Wu D., Li G., Hu W.Z., Dong J., *et al.* ‘Superconductivity at 41 K and its competition with spin-density-wave instability in layered $\text{CeO}_{1-x}\text{F}_x\text{FeAs}$ ’. *Phys. Rev. Lett.* 2008, vol. 100, 247002

- [133] Jirák Z., Hejtmánek J., Kníek K., Maryško M. ‘Magnetoresistive behaviour of Cr-doped manganites $\text{Pr}_{0.44}\text{Sr}_{0.56}\text{MnO}_3$ ’. *J. App. Phys.* 2003, vol. 93, pp. 8083–5
- [134] Michiels J., Gschneidner K.A. ‘Electrical properties of yttrium sequisulfide (Y_2S_3) mechanically alloyed with copper, boron and aluminum’. *J. Alloy Compd.* 1997, vol. 347, pp. 9–14
- [135] Dogra A., Rayaprol S., Shah N.A., Kuberkar D.J. ‘Effect of Co – Ga paired substitution on superconductivity in $\text{YBa}_2\text{Cu}_3\text{O}_{7-\delta}$ ’. *Mod. Phys. Lett. B*. 2004, vol. 18, pp. 485–92
- [136] Secco R.A., Secco E.A. ‘Structural and non-structural factors in fast ion conduction in Ag_2SO_4 at high pressure’. *Phys. Rev. B*. 1997, vol. 56, pp. 3099–104
- [137] Yousuf M., Sahu P.C., Rajan G. ‘High-pressure and high-temperature electrical resistivity of ferromagnetic transition metals: Nickel and iron’. *Phys. Rev. B*. 1986, vol. 34, pp. 8086–100
- [138] Secco R.A., Secco E.A. ‘Effect sof pressure on the fast ion conductor AgTlSO_4 ’. *J. Phys. Chem. Solids*. 1995, vol. 56, pp. 1045–51
- [139] Prinz A., Brunthaler G., Ueta Y., Springholz G., Bauer G., Grabecki G., et al. ‘Electron localization in n- $\text{Pb}_{1-x}\text{Eu}_x\text{Te}$ ’. *Phys. Rev. B*. 1999, vol. 59, pp. 983–90
- [140] Viallet V., Marucco J.F., Saint J., Herbst-Ghysel M., Dragoe N. ‘Structural, magnetic and electrical properties of a perovskite containing divalent europium EuZrO_3 ’. *J. Alloy Compd.* 2008, vol. 461, pp. 346–50
- [141] Dudáš J. ‘The influence of the magnetic spin system on electrical resistivity in some rare earth metals’. *Elektrotechn. Čas.* 1994, vol. 45, pp. 310–14
- [142] Jianquan Q., Zhilun G., Yajing W., Longt L. ‘Influence of manganese on PTCR effect in BaTiO_3 -based ceramics doped with Bi_2O_3 vapor’. *Mater. Chem. Phys.* 2002, vol. 73, pp. 97–100
- [143] Fong C.H., Luo J.Y., Yeh K.W., Chen T.K., Huang T.W., Wu P.M., et al. ‘Superconductivity in the PbO-type structure α -FeSe’. *PNAS*. 2008, vol. 105, no. 38, pp. 14262–4
- [144] Ito M., Matsuda T. ‘Thermoelectric properties of non-doped and y-doped SrTiO_3 polycrystals synthesized by polymerized complex process and hot pressing’. *J. Alloy Compd.* 2009, vol. 477, pp. 473–7
- [145] Niimi H., Mihara K., Sakabe Y., Kuwabara M. ‘Influence of Ba/Ti ratio on the positive temperature coefficient of resistivity characteristics of Ca-doped semiconducting BaTiO_3 fired in reducing atmosphere and reoxidized in air’. *J. Am. Ceram. Soc.* 2007, vol. 90, pp. 1817–21
- [146] Okamoto Y., Kato K., Asai K., Morimoto J., Miyakawa T., Aruga A. ‘Thermoelectric characteristics of sintered SiC/Cu semiconductors’. *J. Jpn. Soc. Powder Metall.* 2009, vol. 56, pp. 477–83
- [147] Pulham R.J., Hubberstey P., Hamptonmacher P. ‘Solutions of aluminium in liquid lithium: Electrical resistivity of liquid alloys’. *J. Chem. Soc. Faraday Trans.* 1994, vol. 90, pp. 2753–5

- [148] Inai H., Okamoto Y., Morimoto J. ‘Thermoelectric properties of sintered SiC doped with Ge’. *Mater. Sci. Forum.* 1999, vols 308–11, pp. 659–64
- [149] Okamoto Y., Inai H., Morimoto J. ‘Temperature dependence on the thermoelectric properties of Si doped SiC’. *J. Jpn. Soc. Powder Metall.* 1998, vol. 45, pp. 905–8
- [150] Okamoto Y., Kato K., Morimoto J., Miyakawa T. ‘A study for thermoelectric properties of Ni doped SiC sintered thermoelectric semiconductor’. *16th International Conference on Thermoelectrics*. Piscataway, USA: Institute of Electrical and Electronics Engineers, 1997, pp. 236–9
- [151] Chihib S., Shishikura M., Ino J., Matsumoto S. ‘Electrical and optical properties of CuAlSe₂ grown by iodine chemical vapour transport’. *J. App. Phys.* 1991, vol. 70, pp. 1648–55
- [152] Tahar M.Z., Nemov S.A., Popov D.I., Svechnikova T.E. ‘Transport properties of Sn and SbI₃ doped single crystal p-Bi₂Te₃’. *25th International Conference on Low Temperature Physics. J. Phys. Conf. Ser.* UK: Institute of Physics Publishing Ltd, 2009, vol. 150, 022082
- [153] Wang E., Greenblatt M., El-Idrissi Rachidi I., Canadell E., Whangbo M.H. ‘Anisotropic electronic properties of the diphosphate tungsten bronzes K₂P₈W₂₄O₈₈, K₂P₈W₂₈O₁₀₀ and their substituted compounds’. *J. Solid State Chem.* 1989, vol. 80, pp. 266–75
- [154] Akahama Y., Kobayashi M., Kawamura H. ‘Pressure-induced superconductivity and phase transition in selenium and tellurium’. *Solid State Commun.* 1992, vol. 84, pp. 803–6
- [155] Aronson M.C., Salamon M.B., Christenson K.K., Ghiron K. ‘Effects of doping on the electronic properties of NbSe₃’. *Phys. Rev. B.* 1988, vol. 38, pp. 468–75
- [156] Weller T.E., Ellerby M., Saxena S.S., Smith R.P., Skipper N.T. ‘Superconductivity in the intercalated graphite compounds C₆Yb and C₆Ca’. *Nature Phys.* 2005, vol. 1, pp. 39–41
- [157] Decker D.L., Chen W. ‘High-precision measurement of electrical resistivity of nickel near the ferromagnetic phase transition at high pressure’. *Phys. Rev. B.* 1992, vol. 46, pp. 8237–43
- [158] Leitch A.A., Yu X., Winter S.M., Secco R.A., Dube P.A., Oakley R.T. ‘Structure and property correlations in heavy atom radical conductors’. *J. Am. Chem. Soc.* 2009, vol. 131, pp. 7112–25
- [159] Khan N.A., Irfan M., Nawaz S. ‘Normal pressure synthesis of Mg-doped Cu_{0.5}Tl_{0.5}Ba₂Ca₂Mg₂Cu₅O_{14-δ} superconductor’. *Physica C.* 2007, vol. 455, pp. 63–66
- [160] Khan N.A., Mazhar M., Maqsood A. ‘A novel method for the direct synthesis of the Y₂Ba₄Cu₇O_{15-δ} superconductor’. *Supercond. Sci. Technol.* 2002, vol. 15, pp. 577–80
- [161] Irfan M., Hassan N., Khan N.A. ‘Fluctuation-induced conductivity of five planar Cu_{0.5}Tl_{0.5}Ba₂Ca_{4-x}Mg_xCu₅O_{14-δ} (x = 1, 2) superconductors’. *Physica C.* 2009, vol. 469, pp. 86–90

- [162] Khurram A.A., Khan N.A., Ahadian M.M., Iraji-Zad A. ‘Enhanced inter-plane coupling of Mg doped Cu_{0.5}Tl_{0.5}Ba₂Ca_{2-x}Cu₃O_{10-δ} superconductors: XPS and FTIR studies’. *Physica C*. 2008, vol. 468, pp. 405–10
- [163] Liao C.Z., Dong C., Zeng L.M., He B., Cao W.H., Yang L.H. ‘Crystal structure and physical properties of the new ternary compound MgNi₇B₃’. *J. Alloy Compd.* 2010, vol. 493, pp. 31–34
- [164] Yang J., Shen X.-L., Lu W., Yi W., Li Z.-C., Ren Z.-A., *et al.* ‘Superconductivity in some heavy rare-earth iron arsenide REFeAsO_{1-δ} (RE = Ho, Y, Dy and Tb) compounds’. *New J. Phys.* 2008, vol. 11, 025005
- [165] Nasir N., Melnychenko-Koblyuk N., Grytsiv A., Rogl P., Bauer E., Royanian E., *et al.* ‘Crystal structure and physical properties of EPCo_{4.7}Ge₉ (EP = Sr, Ba, Eu)’. *Intermetallics*. 2009, vol. 17, pp. 471–6
- [166] Zhu Z.D., Sun Y.P., Zhu X.B., Luo X., Wang B.S., Li G., *et al.* ‘Single crystal growth and characterizations of Cu_{0.03}TaS₂ superconductors’. *J. Cryst. Growth*. 2008, vol. 311, pp. 218–21
- [167] Ishikawa F., Eguchi N., Kodama M., Fujimaki K., Einaja M., Ohmura A., *et al.* ‘Zero-resistance superconducting phase in BaFe₂As₂ under high pressure’. *Phys. Rev. B*. 2011, vol. 79, 172506
- [168] Ren Z.A., Wei L., Jie Y., Yi W., Shen X.L., Li Z.C., *et al.* ‘Superconductivity at 55 K in iron-based F-doped layered quaternary compound Sm[O_{1-x}F_x]FeAs’. *Chin. Phys. Lett.* 2008, vol. 25, 2215
- [169] Prakash J., Singh S.J., Patnaik S., Ganguli A.K. ‘Superconductivity at 31.3 K in Yb-doped La(O/F)FeAs superconductors’. *J. Chem. Soc.* 2010, vol. 122, pp. 43–46
- [170] Hassinger E., Matsuda T.D., Knobel G., Taufour V., Aoki D., Flouquet J. ‘Inelastic contribution of the resistivity in the hidden order in URu₂Si₂’. *J. Phys. Conf. Ser.* 2011, vol. 273, 012031
- [171] Baumbach R.E., Hamlin J.J., Janoschek M., Lum I.K., Maple M.B. ‘Magnetic, thermal and transport properties of the actinide based noncentro-symmetric compounds Th₂Fe₁₂P₇ and U₂Fe₁₂P₇’. *J. Phys. Condens. Matter*. 2011, vol. 23, 094222
- [172] Sakai H., Yoshimura K., Ohno H., Kato H., Kambe S., Walstedt R.E., *et al.* ‘Superconductivity in a pyrochlore oxide Cd₂Re₂O₇’. *J. Phys. Condens. Matter*. 2001, vol. 13, pp. L785–90
- [173] Ogino H., Shimizu Y., Ushiyama K., Kawaguchi N., Kishio K., Shimoyama J. ‘Superconductivity above 40 K observed in a new iron arsenide oxide (Fe₂As₂)(Ca₄(Mg, Ti)₃O_y)’. *App. Phys. Exp.* 2010, vol. 3, 063103
- [174] Wikus P., Hertel S.A., Leman S.W., McCarthy K.A., Ojeda S.M., Figueroa-Feliciano E. ‘The electrical resistance and thermal conductivity of Ti 15V-3Cr-3Sn-3Al at cryogenic temperatures’. *Cryogenics*. 2011, vol. 51, pp. 41–44
- [175] Ronning F., Kurita N., Bauer E.D., Scott B.L., Park T., Klimczuk T., *et al.* ‘The first order phase transition and superconductivity in BaNi₂As₂ single crystals’. *J. Phys. Condens. Matter*. 2008, vol. 20, 342203

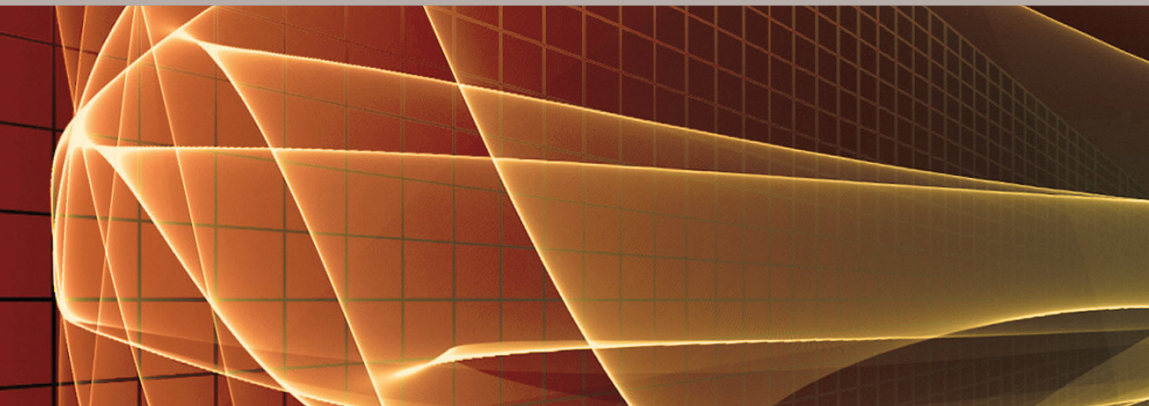
- [176] Tapp J.H., Tang Z., Lv B., Sasmal K., Lorenz B., Chu P.C.W., *et al.* ‘LiFeAs: An intrinsic FeAs-based superconductor with $T_c = 18\text{ K}$ ’. *Phys. Rev. B*. 2008, vol. 78, 060505 (R)
- [177] Tropeano M., Pallecchi I., Cimberle M.R., Ferdeghini C., Lamura G., Vignolo M., *et al.* ‘Transport and superconducting properties of Fe-based superconductors: a comparison between $\text{SmFeAsO}_{1-x}\text{F}_x$ and $\text{Fe}_{1+y}\text{Te}_{1-x}\text{Se}_x$ ’. *Supercond. Sci. Technol.* 2010, vol. 23, 054001
- [178] Horigane K., Takeshita N., Lee C.H., Hiraka H., Yamada K. ‘First investigation of pressure effects on transition from superconductive to metallic phase in $\text{FeSe}_{0.5}\text{Te}_{0.5}$ ’. *J. Phys. Soc. Jpn.* 2009, vol. 78, 063705
- [179] Pandya S., Sherif S., Sharath Chandra L.S., Ganesan V. ‘Resistive broadening in sulphur doped FeTe’. *Supercond. Sci. Technol.* 2010, vol. 23, 075015
- [180] Naren H.R., Tamizhavel A., Ramakrishnan S. ‘Effect of iridium substitution in $\text{Rh}_{17}\text{S}_{15}$ ’. *J. Phys. Conf. Ser.* 2010, vol. 200, 012052
- [181] Ogino H., Katsura Y., Horii S., Kishio, K., Shimoyama J. ‘New iron based arsenide oxides $(\text{Fe}_2\text{As}_2)(\text{Sr}_4\text{M}_2\text{O}_6)$ ($\text{M} = \text{Sc}, \text{Cr}$)’. *Supercond. Sci. Technol.* 2009, vol. 22, 085001
- [182] Matsumura Y., Ogino H., Honi S., Katsura Y., Kishio K., Shimotama H. ‘New series of nickel-based pnictide oxide superconductors $(\text{Ni}_2\text{Pn}_2)(\text{Sr}_4\text{Sc}_2\text{O}_6)$ ($\text{Pn} = \text{P}, \text{As}$)’. *Appl. Phys. Express.* 2009, vol. 2, 063007
- [183] Wu G., Xie Y.L., Chen H., Zhong M., Liu R.H., Shi B.C., *et al.* ‘Superconductivity at 56 K in samarium-doped SrFeAsF’. *J. Phys. Condens. Matter.* 2009, vol. 21, 142203
- [184] Zhu X., Han F., Cheng P., Mu G., Shen B., Fang L., *et al.* ‘Superconductivity in fluoride-arsenide $\text{Sr}_{1-x}\text{La}_x\text{FeAsF}$ compounds’. *EPL*. 2009, vol. 85, 17011
- [185] Luo H., Wang Z., Yang H., Cheng P., Zhu X., Wen H.H. ‘Growth and characterization of $\text{A}_{1-x}\text{K}_x\text{Fe}_2\text{As}_2$ ($\text{A} = \text{Ba}, \text{Sr}$) single crystals with $x = 0 - 0.4$ ’. *Supercond. Sci. Technol.* 2008, vol. 21, 125014
- [186] Anand V.K., Hillier A.D., Adroja D.T., Strydom A.M., Michor H., McEwen K.A., *et al.* ‘Specific heat and μSR study on the noncentrosymmetric superconductor LaRhSi_3 ’. *Phys. Rev. B*. 2011, vol. 83, 064522
- [187] Qi Y., Gao Z., Wang L., Wang D., Zhang X., Ma Y. ‘Superconductivity at 34.7 K in the iron arsenide $\text{Eu}_{0.7}\text{Na}_{0.3}\text{Fe}_2\text{As}_2$ ’. *New J. Phys.* 2008, vol. 10, 123003
- [188] Wu G., Chen H., Wu T., Xie Y.L., Yan Y.J., Lin R.H., *et al.* ‘Different resistivity response to spin-density wave and superconductivity at 20 K in $\text{Ca}_{1-x}\text{Na}_x\text{Fe}_2\text{As}_2$ ’. *J. Phys. Condens. Matter.* 2008, vol. 20, 422201
- [189] Martinella A., Ferretti M., Manfrinetti P., Palenzona A., Tropeano M., Cimberle M.R., *et al.* ‘Synthesis, crystal structure, microstructure, transport and magnetic properties of SmFeAsO and $\text{SmFeAs(O}_{0.95}\text{F}_{0.07}\text{)}$ ’. *Supercond. Sci. Technol.* 2008, vol. 21, 095017
- [190] Jeffries J.R., Butch N.P., Yukich B.T., Maple M.B. ‘The evolution of the ordered states of single-crystal URu_2Si_2 under pressure’. *J. Phys. Condens. Matter.* 2008, vol. 20, 095225

- [191] Mabsubayashi K., Saiga Y., Matsumoto T., Uwatoko Y. ‘Pressure-induced variation of Kondo behaviour on the heavy fermion compounds $\text{YbT}_2\text{Zn}_{20}$ ($T = \text{Co, Rh, Ir}$)’. *J. Phys. Conf. Ser.* 2009, vol. 200, 012112
- [192] Uribe Laverde M.A., Téllez L., Roa-Rojas J. ‘Magnetic, electric and equilibrium properties of $\text{YBa}_2\text{Cu}_{3-x}(\text{PO}_4)_x\text{O}_{7-\delta}$ high temperature superconducting system’. *Mod. Phys. Lett. B* 2009, vol. 23, pp. 807–13
- [193] Ishikawa F., Fukuda K., Hiura Y., Onda Y., Nakayama A., Yamada Y., *et al.* ‘Pressure effects on the electrical resistivity of $\text{Pr}_2\text{Ba}_4\text{Cu}_7\text{O}_{15-\delta}$ oxide superconductor’. *J. Phys. Conf. Ser.* 2009, vol. 150, 052079
- [194] Ren Z.A., Yang J., Lu W., Yi W., Che G.C., Dong X.L., *et al.* ‘Superconductivity at 52 K in iron based F doped layered quarternary compound $\text{Pr}[\text{O}_{1-x}\text{F}_x]\text{FeAs}$ ’. *Mater. Res. Innov.* 2008, vol. 12, pp. 105–6
- [195] Yamazaki T., Takeshita N., Kobayashi R., Saito T., Yamada Y., Kondo K., *et al.* ‘Pressure and K doping induced superconductivity in BaFe_2As_2 ’. *J. Phys. Conf. Ser.* 2011, vol. 273, 012096
- [196] Yamazaki T., Takeshita K., Kondo K., Kobayashi R., Yamada Y., Fukazawa H., *et al.* ‘ ^{75}As -NMR study of the iron pnictide $\text{Ba}_{1-x}\text{K}_x\text{Fe}_2\text{As}_2$ under high pressure’. *J. Phys. Conf. Ser.* 2010, vol. 215, 012041
- [197] Rotter M., Tegel M., Scheißenberg I., Schappacher F.M., Pöttgen R., Deisenhofer J., *et al.* ‘Competition of magnetism and superconductivity in underdoped $(\text{Ba}_{1-x}\text{K}_x)\text{Fe}_2\text{As}_2$ ’. *New J. Phys.* 2009, vol. 11, 025014
- [198] Mydeen K., Lengyel E., Deng Z., Wang X.C., Jin C.Q., Nicklas M. ‘Temperature-pressure phase diagram of the superconducting iron pnictide LiFeP’. *Phys. Rev. B* 2010, vol. 82, 014514
- [199] Arii K., Igawa K., Okada H., Takahashi H., Imai M., Akaishi M., *et al.* ‘Pressure studies in filled skutterudite $\text{La}_{0.8}\text{Rh}_4\text{P}_{12}$ and $\text{LaRh}_4\text{As}_{12}$ ’. *J. Phys. Conf. Ser.* 2009, vol. 150, 052009
- [200] Miyasaka S., Suzuki S., Saijo S., Mikasa Y., Masui T., Tajima S. ‘Resistivity, magnetic susceptibility and specific heat studies in superconductor $\text{LaFePO}_{1-x}\text{F}_x$ ’. *J. Phys. Conf. Ser.* 2009, vol. 150, 052164
- [201] Ogino H., Matsumura Y., Katsura Y., Ushiyama K., Horii S., Kishio K., *et al.* ‘Superconductivity at 17 K in $(\text{Fe}_2\text{P}_2)(\text{Sr}_4\text{Sc}_2\text{O}_6)$: a new superconducting layered pnictide oxide with a thick perovskite oxide layer’. *Supercond. Sci. Technol.* 2009, vol. 23, 075008
- [202] Wang W.C., Liu Q.Q., Lv Y.X., Gao W.B., Yang L.X., Yu R.C., *et al.* ‘The superconductivity at 18 K in LiFeAs system’. *Solid State Commun.* 2008, vol. 148, pp. 538–40
- [203] Chen G.F., Li Z., Wu D., Dong J., Li G., Hu W.Z., *et al.* ‘Element substitution effect in transition metal oxypnictide $\text{Re}(\text{O}_{1-x}\text{F}_x)\text{TAs}$ ($\text{Re} = \text{rare earth, T} = \text{transition metal}$)’. *Chin. Phys. Lett.* 2008, vol. 25, pp. 2235–8
- [204] Ali T., Rupprecht C., Khan R.T., Bauer E., Hilscher G., Michor H. ‘The effect of nitrogen vacancies in $\text{La}_3\text{Ni}_2\text{B}_2\text{N}_{3-\delta}$ ’. *J. Phys. Conf. Ser.* 2010, vol. 200, 012004
- [205] Koyano M., Yamanouchi M. ‘Electronic properties of inhomogeneous Bi-Sb-Ni composite alloys’. *J. Phys. Conf. Ser.* 2009, vol. 150, 052128

- [206] Cao G., Jiang S., Lin X., Wang Cli Y., Ren Z., Tao Q., *et al.* ‘Narrow superconducting window in $\text{LaFe}_{1-x}\text{Ni}_x\text{AsO}$ ’. *Phys. Rev. B*. 2009, vol. 79, 174505
- [207] Prakash J., Singh S.J., Ahmed J., Patnaik S., Ganguli A.K. ‘Compositionally controlled semimetal to superconducting transition in NaF doped LaOFeAs: Enhancement in T_c due to Na-doping’. *Physica C*. 2009, vol. 469, pp. 300–304
- [208] Matsuishi S., Inoue Y., Nomura T., Kamihara Y., Hirano M., Hosono H. ‘Effect of 3d transition metal doping on the superconductivity in quaternary fluoroarsenide CaFeAsF ’. *New J. Phys.* 2009, vol. 11, 025012
- [209] Takahashi H., Okada H., Igawa K., Kamihara Y., Hirano M., Hosono H. ‘Pressure studies of $(\text{La}, \text{Sm})\text{FeAsO}_{1-x}\text{F}_x$ and LaFePO ’. *Physica C*. 2009, vol. 469, pp. 413–17
- [210] Prakash J., Singh S.J., Das D., Patnaik S., Ganguli A.K. ‘New oxypnictide superconductors: $\text{PrOFe}_{1-x}\text{Co}_x\text{As}$ ’. *J. Solid State Chem.* 2010, vol. 183, pp. 338–43
- [211] Okada H., Igawa K., Takahashi H., Kamihara Y., Hirano M., Hosono H., *et al.* ‘Superconductivity under high pressure in LaFeAsO ’. *J. Phys. Soc. Jpn.* 2008, vol. 72, 113712
- [212] Mihalík M., Sečhovský V., Diviš M., Gabáni S., Mihalík M. ‘Superconductivity and physical properties of a LaRhSn single crystal’. *J. Alloy Compd.* 2007, vol. 452, pp. 241–4
- [213] Wu G., Liu R.H., Chen H., Yan Y.J., Wu T., Xie Y.L., *et al.* ‘Transport properties and superconductivity in $\text{Ba}_{1-x}\text{M}_x\text{Fe}_2\text{As}_2$ ($\text{M} = \text{La}$ and K) with double FeAs layers’. *EPL*. 2008, vol. 84, 27010
- [214] Gumeniuk R., Schnelle W., Rosner H., Nicklas M., Leithe-Jasper A., Grin, Y.U. ‘Superconductivity in the platinum germanides $\text{MPt}_4\text{Ge}_{12}$ ($\text{M} = \text{Rare earth or alkaline-earth metal}$) with filled skutterudite structure’. *Phys. Rev. Lett.* 2008, vol. 100, 017002
- [215] Tateiwa N., Haga Y., Matsuda T.D., Ikeda S., Yamamoto E., Okuda Y., *et al.* ‘Large heat capacity jump at the superconducting transition temperature in the non-centrosymmetric superconductor CeIrSi_3 under high pressure’. *J. Phys. Conf. Ser.* 2008, vol. 121, 052001
- [216] Chen G.F., Li Z., Li G., Zhou J., Wu D., Dong J., *et al.* ‘Superconducting properties of Fe-based layered superconductor $\text{LaO}_{0.9}\text{F}_{0.1-\delta}\text{FeAs}$ ’. *Phys. Rev. Lett.* 2008, vol. 101, 057007
- [217] Takeshita N., Iyo A., Eisaki H., Kito H., Ito T. ‘Remarkable suppression of T_c by pressure in NdFeAsO_{1-y} ’. *J. Phys. Soc. Jpn.* 2008, vol. 77, 075003
- [218] Nobori M., Nakano T., Oomi G., Canfield P.C., Cho B.K. ‘Effect of pressure on the superconductivity and magnetism in $\text{HoNi}_2\text{B}_2\text{C}$ ’. *J. Phys. Conf. Ser.* 2010, vol. 200, 012146
- [219] Balamurugan S. ‘Syntheses, magnetic and transport properties of $\text{NbSr}_2(\text{RE}_{1.5}\text{Ce}_{0.5})\text{Cu}_2\text{O}_{10}$; RE = Tb, Ho, Er series’. *Mod. Phys. Lett.* 2010, vol. 24, pp. 1043–57

- [220] Wang L., Gao Z., Qi Y., Zhang X., Wang D., Ma Y. ‘Structural and critical current properties in polycrystalline $\text{SmFeAsO}_{1-x}\text{F}_x$ ’. *Supercond. Sci. Technol.* 2009, vol. 22, 015019
- [221] Yonezawa S., Muraoka Y., Matsushita Y., Hiroi Z. ‘Superconductivity in a pyrochlore-related oxide $\text{KO}_{\text{s}2}\text{O}_6$ ’. *J. Phys. Condens. Matter.* 2004, vol. 16, pp. L9–12
- [222] Ghorbani S.R., Rostamabadi E. ‘The normal state transport properties of $\text{NdBa}_{2-x}\text{La}_x\text{Cu}_3\text{O}_{7-\delta}$: Evidence of localization hole by La’. *Physica C.* 2008, vol. 468, pp. 60–65
- [223] Kurita N., Kimata M., Kodama K., Harada A., Tomita M., Suzuki H.S., et al. ‘High-pressure electrical resistivity measurements of EuFe_2As_2 single crystals’. *J. Phys. Conf. Ser.* 2011, vol. 273, 012098
- [224] Bortolozo A.D., Fisk Z., Sant’anna O.H., Dos Santos C.A.M., Machado A.J.S. ‘Superconductivity in Nb_2InC ’. *Physica C.* 2009, vol. 469, pp. 256–8
- [225] Klemkiene T., Raudonis R., Beganskiene A., Zalga A., Grigoraviciute I., Kareiva A. ‘Scandium and gallium substitution effects in the $(\text{Y}_{1-x}\text{Sc}_x)\text{Ba}_2\text{Cu}_4\text{O}_8$ and $(\text{Y}_{1-x}\text{Sc}_x)\text{Ba}_2\text{Cu}_4\text{O}_8$ superconducting oxides’. *Mater. Chem. Phys.* 2010, vol. 119, pp. 208–13
- [226] Khurram A.A., Ullah A., Khan N. ‘Superconductivity in Co doped $\text{Cu}_{0.5}\text{Tl}_{0.5}\text{Ba}_2(\text{CaM})\text{Cu}_{2.95}\text{Co}_{0.05}\text{O}_{10-\delta}$ ($\text{M} = \text{Mg,Be}$) samples’. *J. Alloy Compd.* 2009, vol. 481, pp. 65–69
- [227] Roumié M., Awad R., Ibrahim I.H., Zein A., Zahraman K., Nsouli B. ‘PIXIE and RBS analysis of Tl-1223 superconducting phase substituted by scandium’. *Nucl. Instrum. Meth. B.* 2008, vol. 266, pp. 133–9
- [228] Rao A., Das A., Chakraborty T., Gahtori B., Agarwal S.K., Sarkar C.K., et al. ‘Electrical and thermal transport properties of $\text{EuBa}_2(\text{Cu}_{1-x}\text{Mn}_x)_3\text{O}_{7-\delta}$ ’. *J. Phys. Condens. Matter.* 2008, vol. 20, 485212
- [229] Chong S.V., Hashimoto S., Yamaguchi H., Kadowaki K. ‘Neodymium-doping induced superconductivity in 1111-SrFeAsF iron-pnictide system’. *J. Supercond. Nov. Magn.* 2010, vol. 23, pp. 1479–84
- [230] Awana V.P.S., Tripathi R., Balamurugan S., Kumar A., Dogra A., Kishan H. ‘Thermal hysteresis in electrical transport of charge ordered $\text{La}_{0.5}\text{Ca}_{0.5}\text{MnO}_3$ manganites’. *J. Alloy Compsd.* 2009, vol. 475, pp. L13–L16
- [231] Mudgel M., Awana V.P.S., Kishan H., Felner I., Alvarez G.A., Bhalla G.L. ‘Superconductivity of various borides: The role of stretched c-parameter’. *J. App. Phys.* 2009, vol. 105, 07E313
- [232] Mudgel M., Awana V.P.S., Lal R., Kishan H., Sharth Chandra L.S., Ganesan V., et al. ‘Anomalous thermoelectric power of the $\text{Mg}_{1-x}\text{Al}_x\text{B}_2$ system with $x = 0.0 – 1.0$ ’. *J. Phys. Condens. Matter.* 2008, vol. 20, 095205
- [233] Layek S., Anand V.K., Hossain Z. ‘Valence fluctuation in $\text{Ce}_2\text{Co}_3\text{Ge}_5$ and crystal field effect in $\text{Pr}_2\text{Co}_3\text{Ge}_5$ ’. *J. Magn. Magn. Mater.* 2009, vol. 321, pp. 3447–52
- [234] Wang P., Stadnik M., Wang C., Cao G.H. ‘Transport, magnetic and ^{57}Fe and ^{155}Gd Mössbauer spectroscopic properties of GdFeAsO and slightly

- overdoped superconductor $\text{Gd}_{0.84}\text{Th}_{0.16}\text{FeAsO}'$. *J. Phys. Condens. Matter.* 2010, vol. 22, 145701
- [235] Yang J.L., Ren W.J., Li D., Hu W.J., Li B., Zhang Z.D. ‘Superconductivity modulated by internal pressure in $\text{Ce}_{1-x}\text{Gd}_x\text{FeAsO}_{0.84}\text{F}_{0.16}$ compounds’. *Supercond. Sci. Technol.* 2010, vol. 23, 025003
- [236] Aghabagheri S., Mohammadizadeh M.R. ‘The bipolaron model in the normal state of Pr-doped $\text{GdBa}_2\text{Cu}_3\text{O}_7$ superconductors’. *Supercond. Sci. Technol.* 2010, vol. 23, 045003



The Handbook of Electrical Resistivity

New materials and pressure effects

This book updates and expands the editor's acclaimed Electrical Resistivity Handbook, bringing together advances in the field over the last two decades. In this period, much has been achieved in the fields of new materials and superconductivity.

This new volume provides a comprehensive compilation of experimental data in graphical form of the resistivity/resistance of over 400 elements, compounds and alloys in three sections. The first section deals with resistivity as a function of temperature, the second section deals with resistivity as a function of temperature and pressure, whilst the third deals with the normalised resistance of materials as a function of temperature and/or pressure.

Gordon Dyos is an experimental physicist whose work spans an enormous variety of subjects, from high-current spark gaps to the measurement of plasma wake concentrations in model atmospheric re-entry missiles, low speed laminar flow wind tunnels and megawatt pulsed arc light sources. He invented the concept and developed the halogen ceramic hob, transpiration cooling of plasma torch nozzles and steel sheet cutting processes using plasma torches. More recently, he has developed a 120kW glow discharge furnace for producing wrought metal from powdered feedstock. In retirement he has worked as a consultant to a plasma torch company and a defence department.

Now in his latter years of retirement he is developing new ideas in novel illumination, a possible plasma transformer and the retro-fitting of a system to de-ice overhead power lines.

ISBN 978-1-84919-149-4



9 781849 191494 ▶

The Institution of Engineering and Technology
www.theiet.org
978-1-84919-149-4